Vol. 270, No. 1, December 15, 1992 ISSN 0003-2670

ANALYTICA CHIMICA ACTA

An international journal devoted to all branches of analytical chemistry

ELSEVIER

ANALYTICA CHIMICA ACTA

Scope. *Analytica Chimica Acta* publishes original papers, preliminary communications and reviews dealing with every aspect of modern analytical chemistry. Reviews are normally written by invitation of the editors, who welcome suggestions for subjects. Preliminary communications of important urgent work can be printed within four months of submission, if the authors are prepared to forego proofs.

Submission of Papers

Americas

Prof. Harry L. Pardue
Department of Chemistry
1393 BRWN Bldg, Purdue University
West Lafayette, IN 47907-1393
USA
Tel:(+1-317) 494 5320
Fax:(+1-317) 496 1200

Computer Techniques

Prof. J.T. Clerc
Universität Bern
Pharmazeutisches Institut
Baltzerstrasse 5, CH-3012 Bern
Switzerland
Tel:(+41-31) 654171
Fax:(+41-31) 654198

Other Papers

Prof. Alan Townshend
Department of Chemistry
The University
Hull HU6 7RX
Great Britain

Tel:(+44-482) 465027
Fax:(+44-482) 466410

Prof. Willem E. van der Linden
Laboratory for Chemical Analysis
Department of Chemical Technology
Twente University of Technology
P.O. Box 217, 7500 AE Enschede
The Netherlands
Tel:(+31-53) 892629
Fax:(+31-53) 356024

Prof. Paul Worsfold
Dept. of Environmental Sciences
University of Plymouth
Plymouth PL4 8AA
Great Britain

Tel:(+44-752) 233006
Fax:(+44-752) 233009

Submission of an article is understood to imply that the article is original and unpublished and is not being considered for publication elsewhere. *Anal. Chim. Acta* accepts papers in English only. There are no page charges. Manuscripts should conform in layout and style to the papers published in this issue. See inside back cover for "Information for Authors".

Publication. *Analytica Chimica Acta* appears in 14 volumes in 1993. The subscription price for 1993 (Vols. 267-280) is Dfl. 4214.00 plus Dfl. 462.00 (p.p.h.) (total approx. US$ 2816.75). *Vibrational Spectroscopy* appears in 2 volumes in 1993. The subscription price for *Vibrational Spectroscopy* (Vols. 4 and 5) is Dfl. 700.00 plus Dfl. 66.00 (p.p.h.) (total approx. US$ 461.50). The price of a combined subscription (*Anal. Chim. Acta* and *Vib. Spectrosc.*) is Dfl. 4592.00 plus Dfl. 528.00 (p.p.h.) (total approx. US$ 3084.25). All earlier volumes (Vols. 1-266) except Vols. 23 and 28 are available at Dfl. 259.50 (US$ 156.25), plus Dfl. 18.00 (US$ 10.75) p.p.h., per volume. The Dutch guilder price is definitive. The U.S. dollar price is subject to exchange-rate fluctuations and is given only as a guide. Subscriptions are accepted on a prepaid basis only, unless different terms have been previously agreed upon.
Our p.p.h. (postage, packing and handling) charge includes surface delivery of all issues, except to subscribers in the U.S.A., Canada, Australia, New Zealand, China, India, Israel, South Africa, Malaysia, Thailand, Singapore, South Korea, Taiwan, Pakistan, Hong Kong, Brazil, Argentina and Mexico, who receive all issues by air delivery (S.A.L.-Surface Air Lifted) at no extra cost. For Japan, air delivery requires 25% additional charge of the normal postage and handling charge; for all other countries airmail and S.A.L. charges are available upon request.

Subscription orders. Subscription orders can be entered only by calendar year and should be sent to: Elsevier Science Publishers B.V., Journals Department, P.O. Box 211, 1000 AE Amsterdam, The Netherlands. Tel: (+31-20) 5803 642, Telex: 18582, Telefax: (+31-20) 5803598, to which requests for sample copies can also be sent. Claims for issues not received should be made within six months of publication of the issues. If not they cannot be honoured free of charge. Readers in the U.S.A. and Canada can contact the following address: Elsevier Science Publishing Co. Inc., Journal Information Center, 655 Avenue of the Americas, New York, NY 10010, U.S.A. Tel: (+1-212) 6333750, Telefax: (+1-212) 6333990, for further information, or a free sample copy of this or any other Elsevier Science Publishers journal.
Advertisements. Advertisement rates are available from the publisher on request.

Detailed "Instructions to Authors" for *Analytica Chimica Acta* was published in Volume 256, No. 2, pp. 373-376. Free reprints of the "Instructions to Authors" of *Analytica Chimica Acta* and *Vibrational Spectroscopy* are available from the Editors or from: Elsevier Science Publishers B.V., P.O. Box 330, 1000 AH Amsterdam, The Netherlands. Telefax: (+31-20) 5862845.

US mailing notice - Analytica Chimica Acta (ISSN 0003-2670) is published biweekly by Elsevier Science Publishers (Molenwerf 1, Postbus 211, 1000 AE Amsterdam). Annual subscription price in the USA US$ 2816.75 (subject to change), including air speed delivery. Second class postage paid at Jamaica, NY 11431. *USA Postmasters*: Send address changes to Anal. Chim. Acta, Publications Expediting, Inc., 200 Meacham Av., Elmont, NY 11003. Airfreight and mailing in the USA by Publication Expediting.

ANALYTICA CHIMICA ACTA

An international journal devoted to all branches of analytical chemistry

(Full texts are incorporated in CJELSEVIER, a file in the Chemical Journals Online database available on STN International; Abstracted, indexed in: Aluminum Abstracts; Anal. Abstr.; Biol. Abstr.; BIOSIS; Chem. Abstr.; Curr. Contents Phys. Chem. Earth Sci.; Engineered Materials Abstracts; Excerpta Medica; Index Med.; Life Sci.; Mass Spectrom. Bull.; Material Business Alerts; Metals Abstracts; Sci. Citation Index)

VOL. 270 NO. 1 CONTENTS DECEMBER 15, 1992

(Continued overleaf)

Contents (continued)

ANALYTICA CHIMICA ACTA
VOL. 270 (1992)

ANALYTICA CHIMICA ACTA

An international journal devoted to all branches of analytical chemistry
Revue internationale consacrée à tous les domaines de la chimie analytique
Internationale Zeitschrift für alle Gebiete der analytischen Chemie

Anal. Chim. Acta, Vol. 270 (1992)

ELSEVIER, Amsterdam–London–New York–Tokyo

0003-2670/92/$05.00

This issue is printed on acid-free paper.

PRINTED IN THE NETHERLANDS

Analytica Chimica Acta, 270 (1992) 1–12
Elsevier Science Publishers B.V., Amsterdam

Evaluation of the enantioselectivity of an ovomucoid and a cellulase chiral stationary phase towards a set of β-blocking agents

C. Vandenbosch and D.L. Massart

Vrije Universiteit Brussel, Pharmaceutical Institute, Laarbeeklaan 103, B-1090 Brussels (Belgium)

W. Lindner

Karl Franzens Universität Graz, Institute of Pharmaceutical Chemistry, A-8010 Graz (Austria)

(Received 13th March 1992; revised manuscript received 18th June 1992)

Abstract

The enantioselectivity of chiral stationary phases (CSP) with ovomucoid and cellulase proteins as chiral selector, towards twenty-four β-blocking agents has been evaluated. On both phases, influences of hydrophobicity, mobile phase modifier content and mobile phase pH on retention behaviour and enantioselectivity were studied. Compounds with a value of the logarithm of the partition coefficient between *n*-octanol and water (log *P*) smaller than 2, are not likely to be enantioseparated on ovomucoid. For the cellulase CSP, a correlation was found between retention behaviour and hydrophobicity. This CSP showed very good enantioselectivity towards the group of compounds studied and a trend in higher separation coefficients for more hydrophobic compounds was observed.

Keywords: Chromatography; β-Blocking agents; Cellulase; Chiral selectors; Chiral stationary phase; Enantioselectivity; Ovomucoid

The group of chiral stationary phases (CSP), includes several proteins which can be used as chiral selectors. α_1 Acid glycoprotein (AGP) [1] and bovine serum albumin (BSA) [2] have been known for several years. The enantiomers of the β-blocking agents bopindolol and the isopropylcarbamatoylisopropylurea derivative of pindolol have been separated on BSA [2]. Besides other groups of compounds, the AGP phase can be used also for the enantioseparation of a number of β-blocking agents [3,4]. More recently, stationary phases with ovomucoid (OVM) and cellulase (CBH I) proteins as chiral discriminator have been described [5–7]. All these proteins are immobilized covalently on to silicagel.

Correspondence to: D.L. Massart, Vrije Universiteit Brussel, Pharmaceutical Institute, Laarbeeklaan 103, B-1090 Brussels (Belgium).

Ovomucoid is a protein obtained from egg-white. Some β-blocking agents (propranolol, pindolol) have been successfully enantioseparated on the OVM phase [5,8]. For a larger group of compounds, a comparison of chromatographic parameters has been made between AGP and OVM columns [8]: in this study the OVM phase was found to be more stable and showed somewhat better resolution and efficiency for most of the compounds studied, however, this trend cannot be generalised and is largely dependent on the structure of the analytes.

Cellulase is an enzyme produced by the fungus *Trichoderma reesei*. A number of β-blocking agents has been separated by means of cellulase

TABLE 1

Evaluation of the OVM CSP under different mobile phase conditions [a]

Compound	log P	MP I			MP II			MP III			MP IV			MP V			MP VI		
		$k'1$	α	f/g	$k'1$	α	f/g	$k'1$	α	f/g	$k'1$	α	f/g	$k'1$	α	f/g	$k'1$	α	f/g
Sotalol (1)	0.28	0	1		0	1		0	1		0.20	1		0.74	1		1.07	1	
Atenolol (2)	0.75	0	1		0	1		0	1		0.17	1		0.68	1		1.09	1	
Nifenalol (3)	1.45	0	1		0	1		0.31	1		1.24	1		2.79	1		7.21	1.09	0.12
Practolol (4)	1.62	0	1		0	1		0	1		0.30	1		0.83	1		1.31	1	
Prenalterol (5)	1.89	0	1		0	1		0	1		0.33	1		0.96	1		1.70	1	
Acebutolol (6)	2.31	0	1		0	1		0.30	1		0.59	1		1.51	1		3.60	1.06	0.05
Metoprolol (7)	2.36	0	1		0	1		0.26	1		0.32	1		1.2	1		3.09	1	
Pindolol (8)	2.42	0.1(S)	1.76		0.4(S)	1.68	0.96	1.51	1.70	1	[b]								
Bunitrolol (9)	2.55	0	1		0.21	1.67	0.73	0.86	1.62	1	3.09	1.68	1	7.16	1.69	1	[b]		
Toliprolol (10)	2.89	0	1		0.25	1		0.65	1		2.86	1.09	0.08	6.51	1		[b]		
Mepindolol (11)	2.95	0	1		0.35	1.23	0.27	1.10	1.20	0.47	[b]								
Oxprenolol (12)	3.2	1.08	1.16	0.31	6.41	1.15	0.33	[b]			[b]								
Carazolol (13)	3.24	1.62	1		5.92	1		[b]			[b]								
Celiprolol (14)	3.3	0	1		0.12	1		0.90	1		2.00	1.09	0.03	2.22(S)	1.08	0.08	6.86	1.16	0.39
Metipranolol (15)	3.33	0	1		0.73	1		2.65	1.10	0.1	[b]								
Alprenolol (16)	3.58	2.40	1		11.7	1		[b]			[b]								
Propranolol (17)	3.66	7.92(S)	1.15	0.61	[b]			[b]			[b]								
Bupranolol (18)	4.11	1.60	1.32	1	[b]			[b]			[b]								
Tertatolol (19)	4.19	> 15																	
Talinolol (20)	4.44	0	1		0.26	1		0.75	1		1.88	1		2.52	1		5.72	1	
Carvedilol (21)	4.66	> 15																	
Isopenbutolol (22)	5.18	> 15																	

[a] MP I: 0.02 M phosphate buffer pH 4.6–ethanol 88/12; MP II: 0.02 M phosphate buffer pH 4.6–ethanol 95/5; MP III: 0.02 M phosphate buffer pH 4.6–ethanol 99/1; MP IV: 0.02 M phosphate buffer pH 5.5–ethanol 99/1; MP V: 0.02 M phosphate buffer pH 6.5–ethanol 95/5; MP VI: 0.02 M phosphate buffer pH 6.5–ethanol 99/1. [b] Not injected due to high retention.

as immobilized chiral selector [7]. The loading capacity on the cellulase CSP was found to be rather low: retention and peak symmetry depend on the concentration when 0.01 nmol or more are injected on column. The influence of different mobile phase compositions has also been studied [7]. It has been demonstrated that the unimmobilised protein has a different conformation at different pH values.

It was noticed that the addition of organic modifier resulted in a decrease of the capacity factors (k') and an increase in enantioselectivity, peak symmetry and efficiency.

Except for the BSA type CSP, the immobilised proteins seem to be rather stable and can be used with high percentages of organic modifier in the mobile phase. AGP, OVM and CBH I are glycoconjugated proteins. The presence of the carbohydrate part might influence the overall stability of the protein.

It is the purpose of this paper to evaluate the enantioselectivity of ovomucoid and cellulase towards twenty-four β-blocking agents and to study the influence of the mobile phase composition on retention behaviour and enantioseparation of the studied compounds. The correlation between retention behaviour and enantioselectivity of OVM and CBH I and the hydrophobicity of the β-blocking agents studied will also be evaluated, as described for AGP previously [3].

EXPERIMENTAL

Apparatus

A Hewlett Packard 1090 liquid chromatograph with diode array detector was used.

The ovomucoid CSP (Ultron ES OVM®, 150 mm × 4.6 mm i.d.) was a gift from G. Tamai [5]. This column was used together with a guard column (Ultron ES OVM-G). The mobile phase flow-rate was 0.8 ml min^{-1}, except when ethanol concentrations of 30% or more were used and column pressure exceeded the prescribed value. The cellulase CSP (100 mm × 2.1 mm i.d.) was a small-bore column and was obtained from C. Pettersson (Uppsala) [7]. The flow-rate of the mobile phase was 0.1 ml min^{-1}. The Novapack® RP 18 column (300 mm × 4 mm i.d.) was obtained from Waters. The commercially available BSA column (Resolvosil®, 150 mm × 4 mm i.d.) was obtained from Macherey Nagel (Düren). This CSP was evaluated in combination with phosphate buffer (pH range 5.0 to 8.0) as mobile phase. The BSA "new generation" was obtained from Allenmark. The mobile phase, used with this column, was ammonium acetate buffer (pH 7.0; 0.1 M)–isopropanol, 95:5.

The mobile phase flow-rate, used with both BSA type columns, was 1 ml min^{-1}. The dead time is measured by determining the retention time where the first deviation from the base-line is observed after injection of isopropanol.

Standards and reagents

The drug compounds were gifts from diverse sources or bought from the respective companies.

Sodium dihydrogenphosphate monohydrate, sodium hydroxide, ammonium acetate and acetic acid were used for the preparation of the mobile phase buffers and were of pro analysis quality. The buffer solutions were prepared with bidistilled water.

Solutions of the drugs (200 μg ml^{-1}) were prepared in the mobile phase. On the ovomucoid column, 10 μl of the drug solutions were injected. On the cellulase CSP, the injection volume was 1 μl.

Temperature

As enantioseparation and retention depend on the temperature, all experiments were performed at a constant oven temperature of 25°C.

RESULTS AND DISCUSSION

The results of the evaluation of ovomucoid and cellulase type CSP for the enantioseparation of β-blocking agents are discussed. For each stationary phase, the influence of the hydrophobicity of the compounds and of the mobile phase composition on the retention behaviour is studied. Further, the effect of hydrophobicity and mobile phase composition on the enantioselectivity is evaluated for each CSP.

Ovomucoid as chiral stationary phase (OVM column)

Table 1 lists the chromatographic results of the evaluation of the OVM column under the different mobile phase conditions. For each compound, the capacity factor of the first eluting enantiomer ($k'1$), the separation factor alpha and the peak : valley ratio f/g [9] are calculated.

Labetalol and nadolol each consist of four stereoisomers and are therefore not mentioned in Table 1: labetalol isomers were resolved in MP (mobile phase) II (Table 1); the stereoisomers of nadolol were (practically baseline) separated in MP IV (Table 1).

Correlation between the retention behaviour and hydrophobicity on OVM

The hydrophobicity of the compounds is expressed as their calculated log P value (Table 1) or as their retention behaviour on RP 18 [3]. The log P value, the logarithm of the partition coefficient between n-octanol and water, was predicted from the structural elements of the compounds [10]. The correlation between the chromatographic retention behaviour and log P has been studied [11,12].

The log k' values of the compounds, obtained on OVM, are plotted against log P and log k'C18 respectively for each mobile phase. The obtained correlation coefficients and their significance are listed in Table 2. Log $k'1$ is the capacity factor of the first eluting peak when a chiral separation was obtained, log $k'2$ is the capacity factor of the second peak. Mobile phase I is not included in Table 2, as data of only 6 compounds were obtained under these conditions: the other compounds were not retained or showed very high k' values (> 15 in Table 1).

Significant correlations are observed in mobile phases with pH values 5.5 and 6.5. In these cases, the correlation coefficients are higher when the independent variable is log k' on RP 18. In Table 2, one observes that the correlation coefficients are slightly smaller when log $k'2$ is the dependent variable. The fact that no correlations were observed in mobile phases II and III must be due to the fact that the net charge of the protein is about zero at pH 4.6 (isoelectric point = 4.3), but it is surprising, since one would expect hydrophobic interactions to be predominant at this pH, and one would then expect rather good correlations.

Correlation between retention behaviour and mobile phase composition

Effect of the percentage organic modifier. In Table 1, a large difference in retention behaviour for the different β-blocking agents can be seen: a

TABLE 2

Correlation between retention behaviour on OVM and hydrophobicity [a]

	log $k'1$ vs. log P (p value)	log $k'2$ vs. log P (p value)	log $k'1$ vs. log k'C18 (p value)	log $k'2$ vs. log k'C18 (p value)
MP II	0.04466	−0.0652	0.1347	0.0169
	(0.9092)	(0.8676)	(0.7297)	(0.9656)
MP III	0.5685	0.4799	0.2721	0.1548
	(0.0864)	(0.1604)	(0.4469)	(0.6695)
MP IV	0.7385	0.7056	0.7755	0.7365
	(0.009)	(0.015)	(0.005)	(0.010)
MP V	0.5898	0.5527	0.7732	0.6934
	(0.056)	(0.078)	(0.005)	(0.018)
MP VI	0.7163	0.7009	0.8662	0.8485
	(0.030)	(0.035)	(0.003)	(0.004)

[a] The correlation coefficients and their significance are given. The p values are calculated by means of the statistical package SPSS/PC [15]. Mobile phase II = 95% phosphate buffer pH 4.6–5% ethanol; mobile phase III = 99% phosphate buffer pH 4.6–1% ethanol; mobile phase IV = 99% phosphate buffer pH 5.5–1% ethanol; mobile phase V = 95% phosphate buffer pH 6.5–5% ethanol; mobile phase VI = 99% phosphate buffer pH 6.5–1% ethanol.

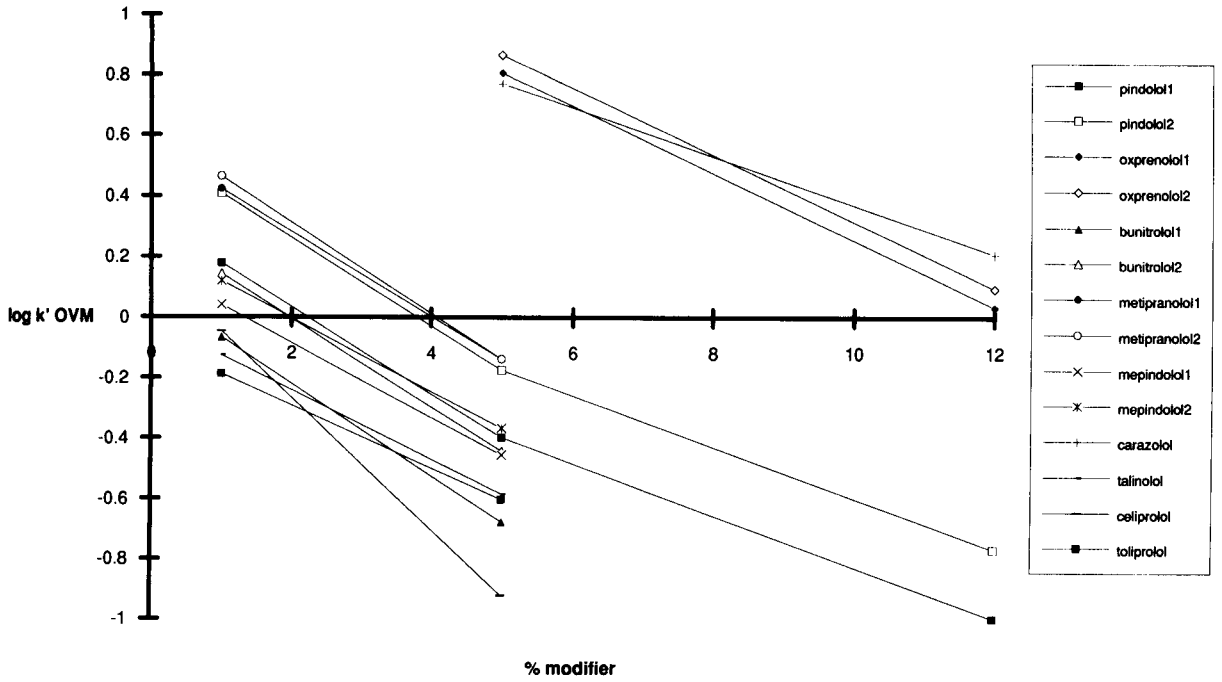

Fig. 1. Influence of the percentage of ethanol on the retention and the enantioseparation of some compounds on ovomucoid CSP. Mobile phase: 0.02 M phosphate buffer pH 4.6 containing different percentages of organic modifier.

number of compounds is not retained using MP I (Table 1, column 2), whereas isopenbutolol, carvedilol and tertatolol did not elute under these mobile phase conditions. However, isopenbutolol enantiomers could be separated by increasing the percentage ethanol of the mobile phase to 50% [pH of the phosphate buffer 4.6; $k'1 = 0.56$ (S isomer elutes first), $\alpha = 1.18$, $f/g = 0.30$]. This indicates that the retention times on the OVM CSP decrease when the ethanol content increases. Similar behaviour could also be observed for other compounds (see Table 1) which is illustrated in Fig. 1.

The relation $\log k' = \text{slope}\ X + \text{intercept}$, where X is the percentage organic modifier, can be calculated for each compound. In achiral, reversed phase type chromatography on CN and C18 and on Chiral AGP, a correlation was found between the slopes and the intercepts of this relation, obtained for each compound [3,13]. This indicates that changing the percentage organic modifier of the mobile phase has a greater influence on the more hydrophobic compounds (the slope of the relationship is larger). For ovomucoid, this correlation can only be found at pH 6.5. This correlation is illustrated in Fig. 2.

Effect of mobile phase pH. Because the isoelectric point of OVM is 4.3, the net charge of the protein is neutral at pH ca. 4.6. This means that electrostatic interactions with other molecules

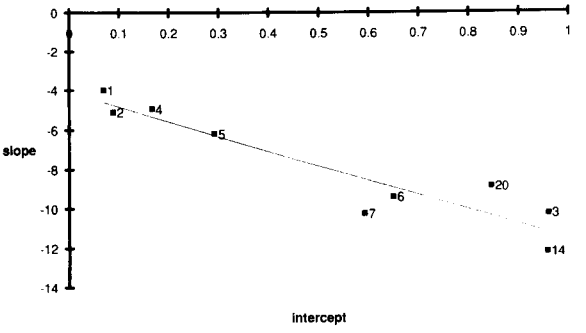

Fig. 2. Correlation between slopes (a) and intercepts (b) of the relation $\log k' = aX + b$ where X is the percentage ethanol, for each compound, at pH 6.5 (for mobile phase conditions and compound numbering see Table 1). Correlation coefficient $r = -0.9383$, $p < 0.001$.

should be minor at this pH, which could be an explanation for the fact that some polar compounds, which show less binding sites for hydrophobic interactions, are barely retained at pH 4.6, especially when relatively high concentrations of ethanol are added to the mobile phase.

In Fig. 3, the log k' values of the compounds on the OVM phase are plotted as a function of pH. The retention time increases to an extent that the more apolar β-blocking agents (with high log P values: see the section *Correlation between the retention behaviour and hydrophobicity on OVM*) are retained too strongly at higher pH values. For more polar compounds, a mobile phase buffer with pH 5.5 or 6.5 is recommended to obtain reasonable retention times. At such higher pH values, the compounds are less dissociated. Talinolol (log $P = 4.44$) and celiprolol (log $P = 3.30$), although more apolar, are not well retained in mobile phases based on phosphate buffer pH 4.6.

In Table 3, the difference in log k' at two mobile phase pH values (with a constant percentage of organic modifier) is divided by the difference in pH. The calculated values are an indication of the influence of mobile phase pH on the retention of the compound. On comparison with RP 18 (Table 3), one observes that changing the

TABLE 3

Influence of pH on the retention behaviour on OVM and CEL and comparison with achiral chromatography [a]

Compound	OVM	CEL	RP18
Metoprolol	0.57	0.48	0.080
Acebutolol	0.57		0.056
Toliprolol	0.71 [b]	0.54	0.14
Sotalol	0.73 [c]	0.48	0.067
Bunitrolol	0.62 [b]		0.069
Prenalterol	0.71 [c]	0.61	0.081
Practolol	0.64 [c]	0.51	0.08
Nifenalol	0.72		0.14
Atenolol	0.81 [c]	0.45	0.08
Talinolol	0.46	0.42	0.05
Celiprolol	0.46	0.44	0.05

[a] The difference in log k' at 2 pH values (with a constant percentage of organic modifier) is divided by the difference in pH. The calculated values are an indication for the influence of mobile phase pH changes on the retention of the compounds. OVM: mobile phase difference: phosphate buffer pH 4.6 and 6.5 (1% ethanol). [b] pH 4.6 and 5.5 (1% ethanol). [c] pH 5.5 and 6.5 (1% ethanol). CEL: mobile phase difference: acetate buffer pH 5.0 and 6.3 (1% isopropanol).

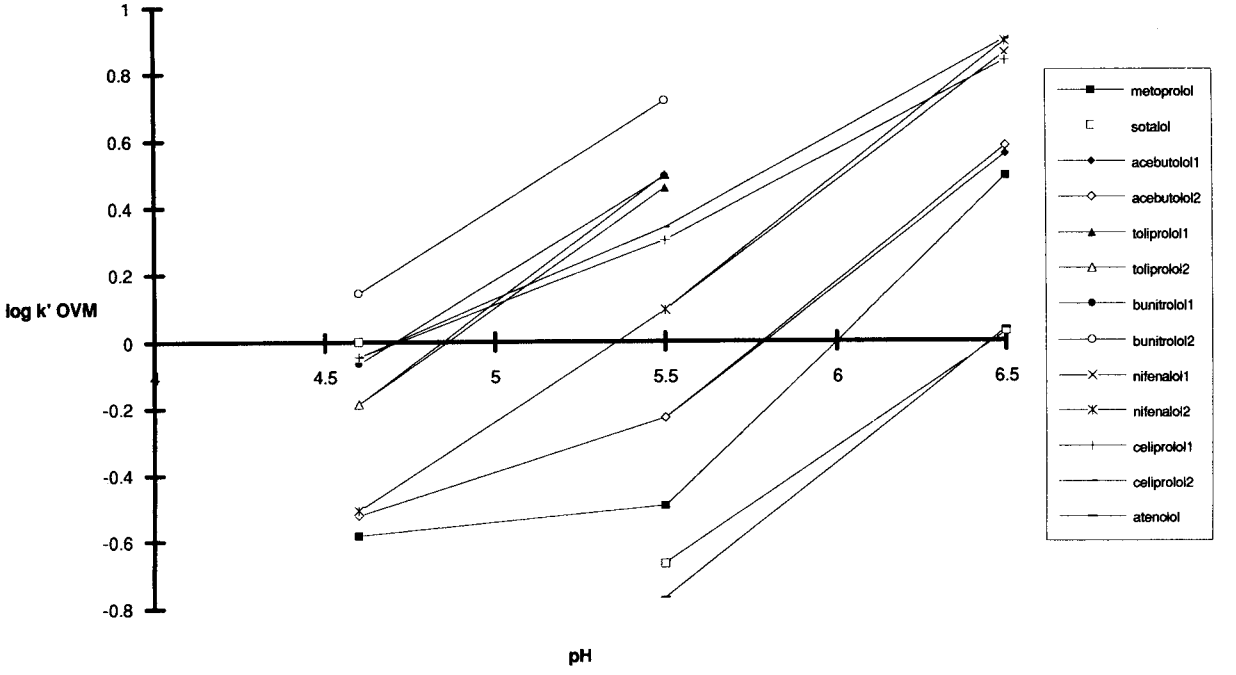

Fig. 3. Influence of the mobile phase pH on the retention and the enantioseparation of some β-blockers on ovomucoid CSP.

pH has much more influence on the retention on OVM, than on RP 18. The same observation has been made for AGP in a previous paper [3]. As for AGP, the difference might be explained by conformational changes in the protein CSPs which exposes more, previously hidden lipophilic contact regions with which the guest molecules can interact. A recent study has shown that conformational changes take place in the low-pH region [6].

Effect of pH, percentage organic modifier and hydrophobicity on enantioseparation

Effect of percentage organic modifier. Figure 1 and Table 1 show that the enantioselectivity is little influenced by the percentage of organic modifier of the mobile phase at pH 4.6. However, metipranolol enantiomers were separated slightly when the ethanol content was changed from 5 to 1%. The same trend was observed for acebutolol, nifenalol and celiprolol enantiomers on lowering the percentage of ethanol at pH 6.5.

Effect of pH. From Table 1, one can also deduce that an increase in the mobile phase pH causes a small increase in enantioselectivity. Some β-blocking agents, which are not enantioseparated at pH 4.6 are (partly) resolved at increased pH of the mobile phase, as also illustrated in Fig. 3. However, synchronously with the increase of stereoselectivity, an increase of plate height and peak asymmetry was observed.

Effect of hydrophobicity. In a previous paper concerning the evaluation of the enantioseparation of β-blockers on AGP [3], it was concluded that sufficiently high retention implies chiral separation in most cases. Therefore, the separation factors alpha (α), obtained on OVM, are plotted as a function of their respective $k'1$ values. The results obtained at pH 4.6 were studied separately (Fig. 4a) because no correlation could be found between retention and hydrophobicity at this pH (see the section *Correlation between the retention behaviour and hydrophobicity on OVM*). Figure 4b represents a plot of the separation factors versus $k'1$ obtained in mobile phases with buffers pH 5.5 and 6.5 in the mobile phase. Clearly (Fig. 4a), it is not necessary that compounds are well retained to obtain enantioseparation; a number of the compounds are well enantioseparated. Increased retention of peak one by increasing the pH of the mobile phase does not necessarily lead to a greater number of enantioseparations as shown in Fig. 4b. Alpha was also plotted as a function of log P. Here, all obtained data were studied in one plot (Fig. 4c). From this plot, one concludes that compounds of the aminopropanol type with log P values less than two are not likely to be enantioseparated on the OVM phase under the mobile phase conditions studied here. Carazolol, metoprolol, tali-

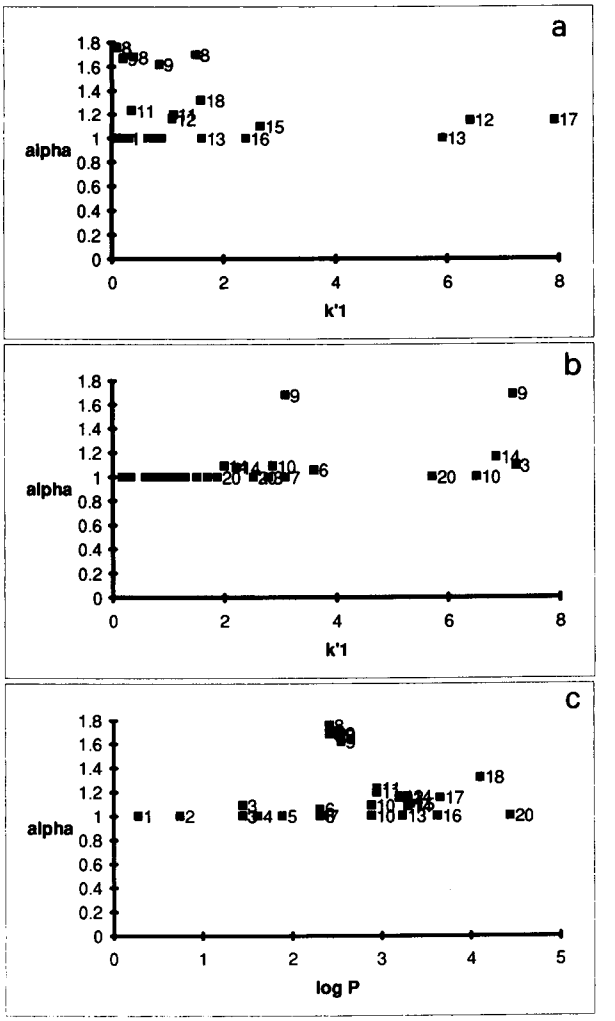

Fig. 4. (a) Correlation between α and $k'1$ (mobile phases with 0.02 M phosphatebuffer pH 4.6), (b) Correlation between α and $k'1$ (mobile phases with 0.02 M phosphatebuffer pH 5.5 and 6.5). (c) Correlation between α and log P (all mobile phases studied here).

nolol and alprenolol however, are not enantioseparated although their log P values are higher than 2.

From Table 1, it is evident that the alpha values of some compounds that are chirally separated with OVM under different mobile phase conditions, remain about the same but their f/g values increase when retention increases. This is illustrated for bunitrolol in Fig. 5.

Due to the poor efficiency of most protein type stationary phases, broad peaks are likely to occur at higher retention times. Thus, compounds such as toliprolol, for which the CSP only shows minor enantioselectivity, will scarcely be enantioseparated by only increasing the retention time but without influencing the stereoselectivity of the chiral stationary phase.

Cellulase as chiral stationary phase (CBH I column)

A number of β-blockers has been separated on the cellulase CSP (alprenolol, metoprolol, propranolol, atenolol, practolol, oxprenolol, pronethalol) [7]. In the context of this study, the applicability of the cellulase CSP for the enantioseparation of additional β-blocking agents, has been evaluated.

Table 4 summarizes the results of the evaluation of the cellulase chiral stationary phase. One notices that most of the β-blocking agents are chirally separated by means of this CSP. The separation of bunitrolol enantiomers is illustrated in Fig. 6. Nadolol and labetalol are not included in Table 4; their isomers were not separated in any of the mobile phases studied here.

Correlation between retention behaviour on the cellulase CSP (CBH I) and hydrophobicity

Just like for AGP [3] and OVM (see the section *Correlation between the retention behaviour and hydrophobicity on OVM*), the relation between retention on CBH I and hydrophobicity, expressed as log k'C18 or log P, has been studied. Table 5 gives the correlation coefficients and

TABLE 4

Evaluation of the cellulase CSP under different mobile phase conditions [a]

Compound	log P	MP I			MP II			MP III		
		$k'1$	α	f/g	$k'1$	α	f/g	$k'1$	α	f/g
Sotalol (1)	0.28	0.19	1	0				0.81	1	0
Atenolol (2)	0.75	0.21	1	0				0.81(R)	1.64	1
Timolol (3)	1.16	[b]						0.83(R)	2.41	1
Nifenalol (4)	1.45	1.89	1.45	1						
Practolol (5)	1.62	0.28	1	0				1.29	1	0
Prenalterol (6)	1.89	0.32	1	0				2	1	0
Acebutolol (7)	2.31	0.79	2.81	1	0.66	2.94	1			
Metoprolol (8)	2.36	0.34	1.69	0.90	0.29	1.81	0.91	1.21	2.11	1
Pindolol (9)	2.42	0.44(R)	1.84	0.97	0.38	1.93	0.97			
Bunitrolol (10)	2.55	0.35	9.7	1	0.29	10.6	1			
Toliprolol (11)	2.89	0.61	1.23	0.42	0.53	1.26	0.39	2.67	1.19	0.74
Mepindolol (12)	2.95	0.50	3.70	1	0.43	3.90	1			
Oxprenolol (13)	3.2	0.53	1.89	1	0.42	2.08	1			
Carazolol (14)	3.24	3.62	1	0						
Celiprolol (15)	3.3	0.47(R)	2.41	1	0.35	2.68	1	1.32	3.82	1
Metipranolol (16)	3.33	1.26	1	0				6.69	1	0
Alprenolol (17)	3.58	0.80	1	0				2.50	1	0
Propranolol (18)	3.66	2.10	3.11	1						
Bupranolol (19)	4.11	0.66	4.57	1						
Tertatolol (20)	4.19	1.09	2.19	1	0.83	2.46	1			
Talinolol (21)	4.44	0.73	1.11	0.05	0.55	1.18	0.09	1.95(+)	1.37	0.86
Isopenbutolol (22)	5.18	1.25(R)	4.74	1	0.96(R)	5.58	1			

[a] MP I: acetate buffer pH 5.0 μ 0.01–0.5% isopropanol; MP II: acetate buffer pH 5.0 μ 0.01–1% isopropanol; MP III: acetate buffer pH 6.3 μ 0.01–1% isopropanol. [b] Could not be determined due to interferences.

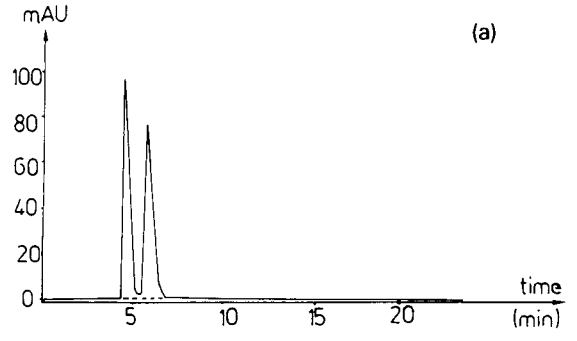

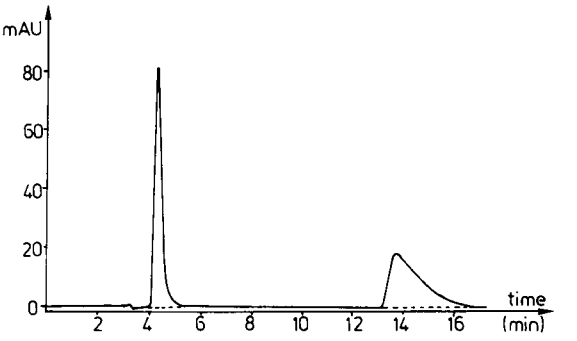

Fig. 6. Enantioseparation of bunitrolol on cellulase. Mobile phase: ammonium acetate buffer pH 5.0 μ 0.01–isopropanol, 99.5:0.5.

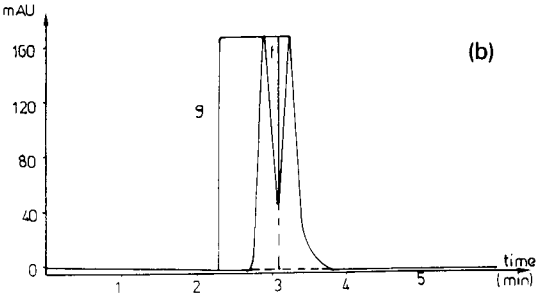

Fig. 5. Separation of bunitrolol on Ovomucoid CSP. (b) Mobile phase II: 5% ethanol–95% 0.02 M phosphate buffer pH 4.6. The calculation of the peak:valley ratio f/g is illustrated. (a) Mobile phase III: 1% ethanol–99% 0.02 M phosphate buffer pH 4.6.

their significance. A significant correlation between retention behaviour on cellulase and hydrophobicity for the two evaluated mobile phases is observed. This is also illustrated in Figs. 7a and b for mobile phase I. In these figures outlying values are obtained for the compounds nifenalol (4) and carazolol (14); a higher correlation is obtained when these two data are excluded (Table 5).

This indicates that hydrophobic interactions probably play an important role in the retention mechanism on the cellulase chiral stationary phase.

Correlation between retention behaviour and mobile phase composition

Effect of organic modifier. In contrast to the ovomucoid phase, information about most β-blocking agents can be obtained with one mobile phase, such as 99.5% acetate buffer pH 5.0, μ 0.01 and 0.5% isopropanol. Only small quantities of organic modifier are needed to elute most of

TABLE 5

Correlation between retention behaviour on cellulase and hydrophobicity [a]

	log k'1 vs. log k'C18 (p value)	log k'2 vs. log k'C18 (p value)	log k'1 vs. log P (p value)	log k'2 vs. log P (p value)
MP I	0.5736 (0.007)	0.6356 (0.002)	0.5659 (0.008)	0.6626 (0.001)
MP I (without 4 and 14)	0.8203 (< 0.001)	0.7163 (< 0.001)	0.8151 (< 0.001)	0.7592 (< 0.001)
MP III	0.7106 (0.048)	0.6899 (0.058)	0.7064 (0.050)	0.8308 (0.011)

[a] The correlation coefficients and their significance are given. Mobile phase I = 0.01 M acetate buffer pH 5–0.5% isopropanol; mobile phase III = 0.01 M acetate buffer pH 6.3–1% isopropanol.

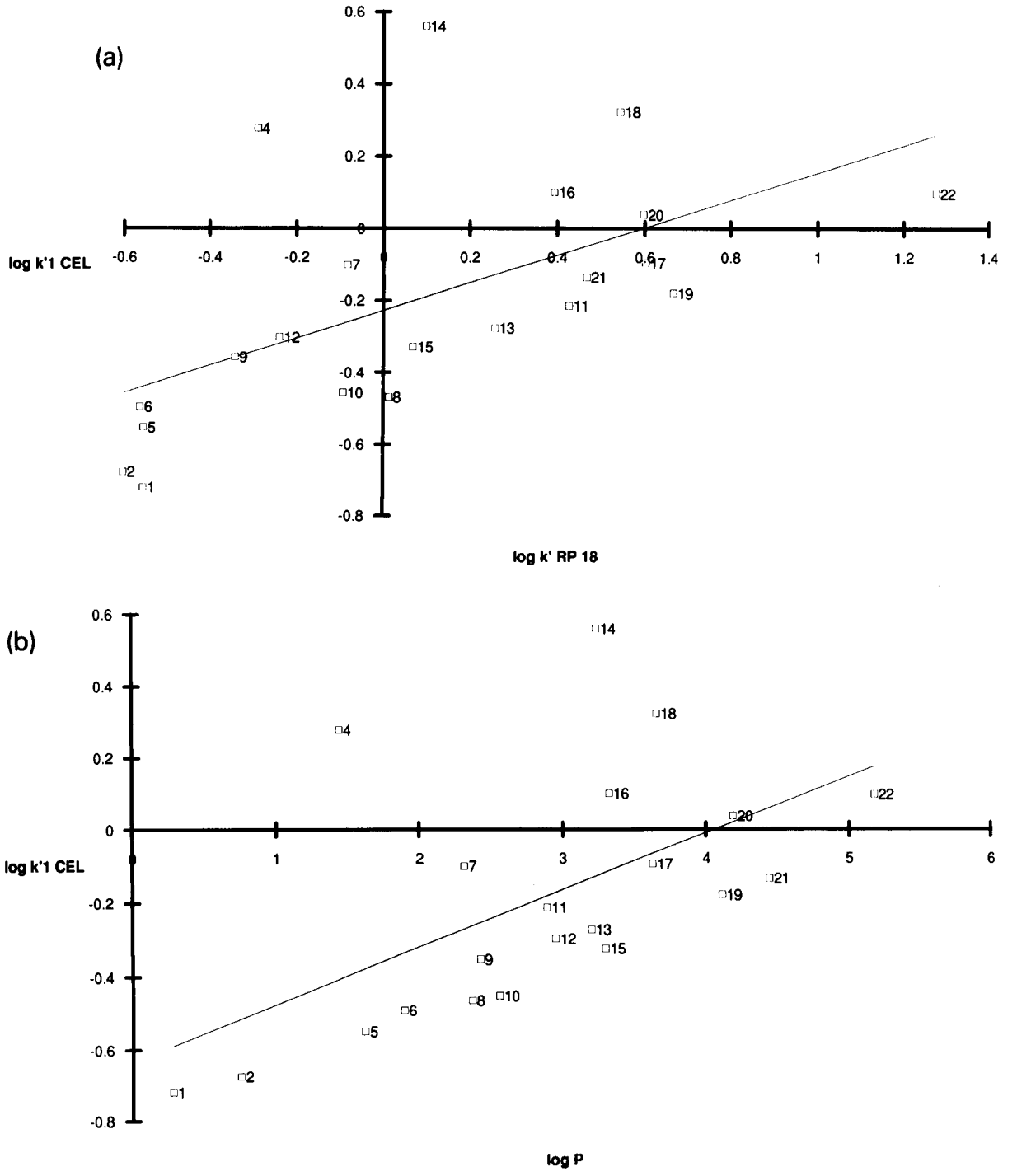

Fig. 7. (a) Correlation between log $k'1$ (ammonium acetate buffer pH 5.0 $\mu = 0.01$ with 0.5% isopropanol in mobile phase) and hydrophobicity (expressed as log k'C18) for cellulase. (b) Correlation between log $k'1$ (ammonium acetate buffer pH 5.0 $\mu = 0.01$ with 0.5% isopropanol in mobile phase) and hydrophobicity (expressed as log P) for cellulase.

the β-blocking agents. An increase of 0.5% isopropanol causes a pronounced decrease in k' on the cellulase column. The cellulase CSP can be used with a mobile phase containing up to 20% isopropanol. Studies were performed on the use of different kinds of organic modifier: no difference in enantioselectivity has been observed [7].

Carvedilol enantiomers were retained too strongly by the CSP in mobile phase I (Table 4). When 15% isopropanol was added to the mobile phase, a large peak with shoulder was observed for carvedilol: the shoulder peak might be an indication for a minor separation of the carvedilol enantiomers.

Alprenolol enantiomers were separated by Marle et al. with $\alpha = 8.3$ [7]. In our experiments, it was not clear whether CBH I is enantioselective for alprenolol or not and probably, alpha was too high so that the second enantiomer was strongly retained under the mobile phase conditions studied here and did not elute in due time without excessive peak broadening. After addition of 10% isopropanol to the mobile phase, a second peak was not observed.

Effect of pH. The retention of the basic compounds increases when the pH of the mobile phase increases ([7] and Table 4). This has been explained in three ways [7]: an increase in negative charge of the protein at higher pH values (isoelectric point = 3.9); a decrease of the degree of dissociation of the aminopropanol type compounds (pK_a values around 8) and a different conformation of the protein at different pH values.

Table 3 illustrates the effect of an increase of the mobile phase pH on the retention behaviour of propanolamine type compounds on cellulase. This effect is calculated as for OVM (see the section *Correlation between retention behaviour and mobile phase*). The same conclusion as for AGP [3] and OVM can be made: retention on chiral stationary phases is much more influenced by pH changes than on classical reversed phase columns.

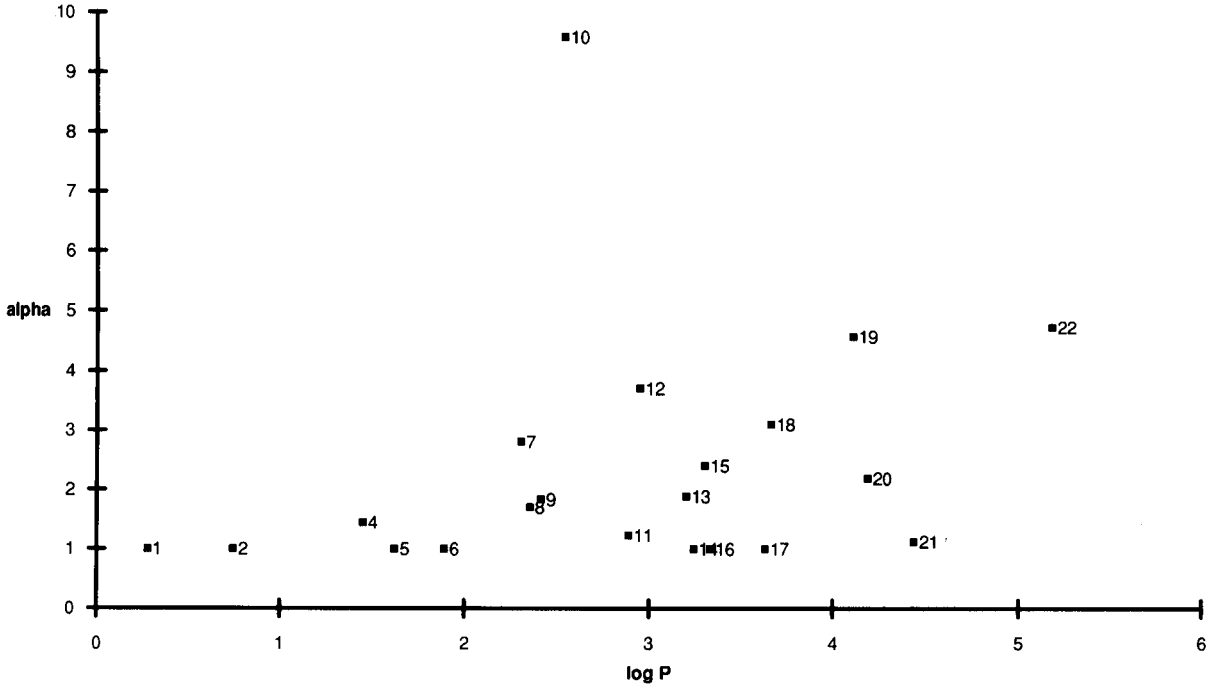

Fig. 8. Enantioselectivity as a function of log P on cellulase (mobile phase: ammonium acetate buffer pH 5.0–0.5% isopropanol).

Effect of hydrophobicity, pH and percentage of organic modifier on enantioseparation

Hydrophobicity. Table 4 shows that the cellulase CSP is enantioselective for most of the β-blocking agents. Figure 8 shows a trend in higher alphas for compounds with higher log P values, i.e., more hydrophobic compounds. This indicates that hydrophobic interactions also play an important role in the chiral discrimination mechanism.

Organic modifier. From Table 4, one can see that the separation factor, alpha, increases slightly when the percentage isopropanol increases. This has also been concluded by Marle et al. [7]. The peak:valley ratio, however, remains the same or decreases at higher percentages of modifier. For most cases, the first eluting enantiomer is practically not retained by the cellulase CSP, whereas the second enantiomer shows high affinity for the stationary phase. This might explain the increase in alpha by increasing the organic modifier content of the mobile phase. This implies that the first eluting enantiomer is barely retained; since the $k'1$ values are very small, high α values were obtained.

pH. An increase in pH leads to higher retention, as described previously. Talinolol becomes well enantioseparated when the pH is increased. In addition, atenolol enantiomers, that were not resolved with MP I and II, are separated at pH 6.3. The detection of the timolol enantiomers is disturbed by the maleate peak observed for MP I and II. At increased pH, retention time is increased and the 2 timolol enantiomers can be easily detected in MP III.

Bovine serum albumin as chiral stationary phase (BSA column)

On the BSA CSP (new generation) enantioseparation of β-blockers was barely observed. The BSA column did not show high affinity for these compounds; they are not well retained. The same observation has been made when using a commercially available BSA phase (Resolvosil®) [14].

Conclusion

Twenty-four β-blocking agents were studied on the ovomucoid and the cellulase chiral stationary phase. Although the β-blockers show similar structural increments with differing lipophilic character, the observed enantioselectivities are quite different.

The ovomucoid phase shows very different affinity for the compounds studied.

An increase in the organic modifier content of the mobile phase leads to smaller k' values on both phases. An increase in the mobile phase pH enhances the retention, an effect which is much more pronounced than on a classical reversed phase type column.

The enantioselectivity is mostly higher for the more hydrophobic compounds, although one observes high enantioselectivities at low retention for ovomucoid at pH 4.6.

The enantioselectivities of AGP, OVM and CBH I were also evaluated for a more diverse set of compounds. The results of these studies will be reported elsewhere.

REFERENCES

1 J. Hermansson, Trends Anal. Chem., 8 (1989) 251.
2 S. Allenmark, J. Liq. Chromatogr., 9 (1986) 425.
3 C. Vandenbosch, T. Hamoir, D.L. Massart and W. Lindner, Chromatographia, 33 (1992) 454.
4 M. Enquist and J. Hermansson, J. Chromatogr., 519 (1990) 285.
5 G. Tamai, M. Edani and H. Imai, Biomed. Chromatogr., 4 (1990) 157.
6 J. Iredale, A.F. Aubry and I. Wainer, Chromatographia, 31 (1991) 329.
7 I. Marle, P. Erlandsson, L. Hansson, R. Isaksson, C. Pettersson and G. Pettersson, J. Chromatogr., 586 (1991) 233.
8 K.M. Kirkland, K.L. Neilson and D.A. McCombs, J. Chromatogr., 545 (1991) 43.
9 P.J. Schoenmakers, Optimization of Chromatographic Selectivity: a Guide to Method Development, Elsevier, Amsterdam, 1986, Ch. 4, p. 121.
10 R.F. Rekker and H.M. de Kort, Eur. J. Med. Chem. – Chim. Ther., 14 (1979) 479.
11 R. Kaliszan, R.W. Blain and R.A. Hartwick, Chromatographia, 25 (1988) 5.
12 A. Kaibara et al., Chem. Pharm. Bull., 39 (1991) 720.
13 T. Hamoir, S. Kokot, K. Douglas and D.L. Massart, J. Chrom. Sci., in press.
14 C. Vandenbosch and D.L. Massart, unpublished results.
15 Manual SPSS/PC Version 1.0, SPSS Inc., Chicago, IL, 1984.

Analytica Chimica Acta, 270 (1992) 13–38
Elsevier Science Publishers B.V., Amsterdam

Mixture designs applied to the study of the liquid chromatographic separation of L-phenylalanine, L-tyrosine and L-tryptophan

Josephine M. Palasota and Stanley N. Deming

Department of Chemistry, University of Houston, 4800 Calhoun Road, Houston, TX 77204-5641 (USA)

(Received 24th April 1992; revised manuscript received 13th July 1992)

Abstract

Mixture designs were used to improve the separation of L-phenylalanine, L-tyrosine and L-tryptophan on a C18 bonded stationary phase. The pH of the mobile phase and retention time of each amino acid were measured for 35 mobile phase formulations containing various concentrations of H_3PO_4, NaH_2PO_4, $NaClO_4$, sodium 1-octanesulfonate and methanol. A non-linear six-parameter model was used to describe the measured pH as a function of the eluent composition with a standard error of estimate of 0.10 pH unit. A different non-linear ten-parameter model was used to describe the measured retention time as a function of eluent composition for each of the three amino acids with a standard error of estimate of 0.08 min. This last model was then used to predict the composition for which the separation would be optimum. The optimum separation was confirmed experimentally.

Keywords: Liquid chromatography; Optimization methods; Mixture design; Phenylalanine; Tryptophan; Tyrosine

The analytical chromatographic separation of amino acids, peptides and proteins has been extensively discussed [1–38]. Techniques such as gas chromatography (GC) [6–9], thin-layer chromatography (TLC) [10–12], ion-exchange chromatography [13–18] and liquid chromatography (LC) [19–37] have been used frequently. As shown by Hancock [38], extensive research has been devoted to improving the efficiency and speed of amino acid analysis in reversed-phase LC (RP-LC).

Over the past several decades, much research has been devoted to the study of achieving optimum separations in chromatography with particular emphasis on finding new ways to locate the global or overall optimum [39–90]. Because the elution order and degree of separation of solutes can be different for different chromatographic conditions [39–45], the possibility of multiple, locally optimum sets of chromatographic conditions exists.

Several theoretical methods [46–50] and empirical methods [51,52] have been utilized for improving chromatographic separations. For example, the sequential simplex technique [53–56] has been used to improve separations in GC [39,57], cation exchange chromatography [58], ion chromatography [59], LC [51,60–63], high-performance TLC [64] and supercritical fluid chromatography [65]. In a series of papers, Laub and Purnell [66–69] presented a systematic "window diagram" approach for separating multi-component samples by GC; window diagrams have also been used for optimizing separations in RP-LC [40–44,70,71]. Other more traditional experimental designs, such as factorial designs [72–74], have

Correspondence to: S.N. Deming, Department of Chemistry, University of Houston, 4800 Calhoun Road, Houston, TX 77204-5641 (USA).

been used for characterizing response surfaces for separations in GC [39,75,76] and LC [71]. Mixture designs [77–80] are becoming increasingly popular for characterizing response surfaces and achieving separations in LC [81–89].

In this work, mixture designs were used to investigate the combined effects of pH, ionic strength (μ), concentration of surface-active ion [ion-interaction reagent (IIR)] and percentage of organic modifier (%M) on the retention behavior and subsequent separation of a mixture of three structurally similar neutral amino acids by RP-LC.

The accepted abbreviations, structures, pK_a values and isoelectric points of phenylalanine, tyrosine and tryptophan are given in Fig. 1. Under the mobile phase conditions used in this work, each amino acid is in equilibrium between the completely protonated form (Fig. 1) and the zwitterionic form. Because the amino acids are structurally similar and have approximately the same pK_a values and isoelectric points, they have similar retention behavior in LC systems; hence it is normally difficult to separate mixtures of them [40–44,90].

MIXTURES

Mixtures (or formulations) consist of two or more components combined in definite propor-

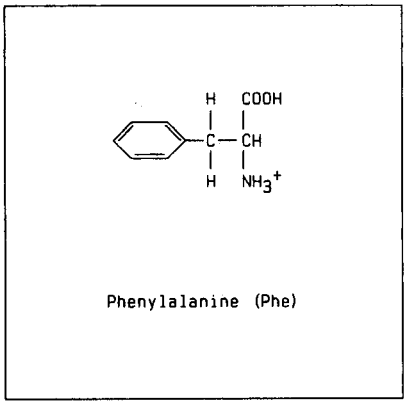

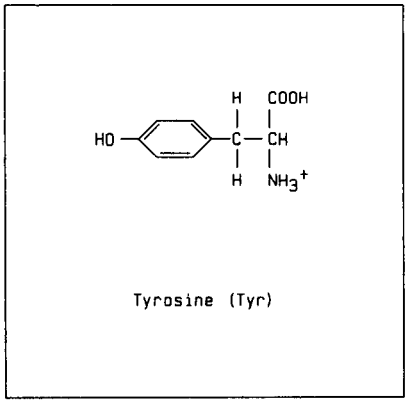

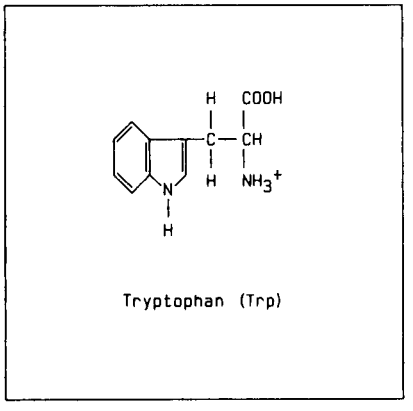

Solute	pK_a	Isoelectric Point
Phe	2.20 9.31	5.50
Tyr	2.17 9.19 10.47	5.70
Trp	2.35 9.33	5.90

Fig. 1. Abbreviations, structures, pK_a values and isoelectric points of phenylalanine, tyrosine and tryptophan. Structures and pK_a values are from [91]; abbreviations and isoelectric points are from [92].

tions such that the sum of their fractions is unity [77–80,88,93–99]. The mathematical expression of this concept is

$$\sum_{i=1}^{n} x_i = x_1 + x_2 + x_3 + \ldots + x_n = 1 \qquad (1)$$

where x_i is the fraction of the ith component in the mixture of n components and is constrained to lie in the range $0 \leqslant x_i \leqslant 1$. The fraction might be expressed as the mole fraction, the mass fraction, the weight fraction or the volume fraction [100]. Alternatively, each x_i in Eqn. 1 might be expressed as a percentage so that the sum of all of the x_i components equals 100% [87].

Because the sum of all the fractions must equal unity (or 100%), only $n - 1$ of the components can be specified independently; the remaining component is a dependent or "slack" variable [101]. Such a system is said to have $n - 1$ degrees of freedom. It is impossible to increase the fraction of one component in the mixture without decreasing the fraction of at least one other component [100,102–105]. Placing one or more equality constraints on a system often leads to a confounded (or confused) interpretation of experimental data. Care must be exercised when assigning component effects to a particular response. In mixtures, for example, an observed change in response could be attributed to the *increase* in one component or to the concomitant *decrease* in one or more of the other components.

The constraint on the mixture space can be understood from a graphical representation of a three-component system. To satisfy the equality constraint of Eqn. 1, experimentation involving three components is restricted to that two-dimensional region on or within the boundaries of the triangle in Fig. 2. Each vertex of the triangle corresponds to a pure component; the left vertex corresponds to pure x_1, the right vertex to pure x_2 and the lower vertex corresponds to pure x_3. True mixtures of all n components lie in the interior of the triangular region; points along the edges correspond to mixtures with only two components.

A move away from a vertex toward the opposite base corresponds to a decrease in the amount

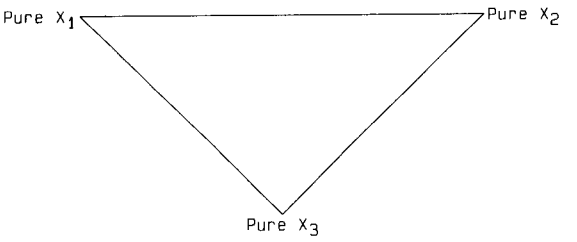

Fig. 2. Graphical representation of the feasible experimental region for a three-component system.

of the vertex component (and a concomitant increase in one or more of the other components). Figure 3 illustrates this concept for each component of a three-component system: each set of parallel dashed lines shows contours of constant composition in that component in 20% increments. For example, in the upper left triangle in Fig. 3, lines drawn parallel to the edge labelled "Percent Pure X_2" correspond to constant amounts of x_1 in the mixture. The percentage of x_1 corresponding to each grid line can be read from the top edge labelled "Percent Pure X_1". Similar sets of lines can be drawn to represent the amounts of x_2 (the upper right triangle in Fig. 3) and x_3 (the lower left triangle in Fig. 3).

The lower right triangle in Fig. 3 shows the diagram obtained from a superposition of the three individual sets of grid lines. This type of "triangular graph paper" is useful for locating a given experiment in the mixture space. As shown by the black dot in the lower right triangle in Fig. 3, for example, an experiment at 20% x_1, 20% x_2 and 60% x_3 is located at the intersection of the three corresponding grid lines.

In practice, mixture designs are often constructed using "pseudo-components" instead of pure components. A pseudo-component is a mixture of pure components, but is generally enriched in one pure component of interest. Thus, for example, in the lower right triangle in Fig. 3, the black dot might represent a pseudo-component mixture rich in pure component x_3; the left and right open circles might represent pseudo component mixtures rich in pure components x_1 and x_2, respectively.

In 1955, Claringbold [106] published the first application of a mixture design, in which a three-

component mixture was used for studying the joint action of hormones in biological systems. Since then, the arrangement of experiments within the constrained mixture space and the subsequent interpretation of the data generated from these experiments are topics that have been developed and expanded [77–79,93–99,101,107–110].

In 1958, Scheffé [98] introduced the simplex-lattice designs. A $\{q,m\}$ lattice has q components, each of which has $m+1$ equally spaced values from 0 to 1 ($x_i = 0, 1/m, 2/m, \ldots, 1$). The lattice represents all possible mixtures with these proportions for each component [77–79,107]. A simple {3,2} simplex-lattice design constructed from pseudo components is shown in the upper left panel of Fig. 4; an expanded view of the design expressed in the pseudo-component percentages is shown in the upper right panel of Fig. 4. This {3,2} design represents one of the simplest of the simplex-lattice designs for three components and requires six experiments (the "design points" shown by black dots). More complex lattice designs have been described [77–79,98,107].

Modified lattice designs are formed by adding one or more experiments to the basic lattice

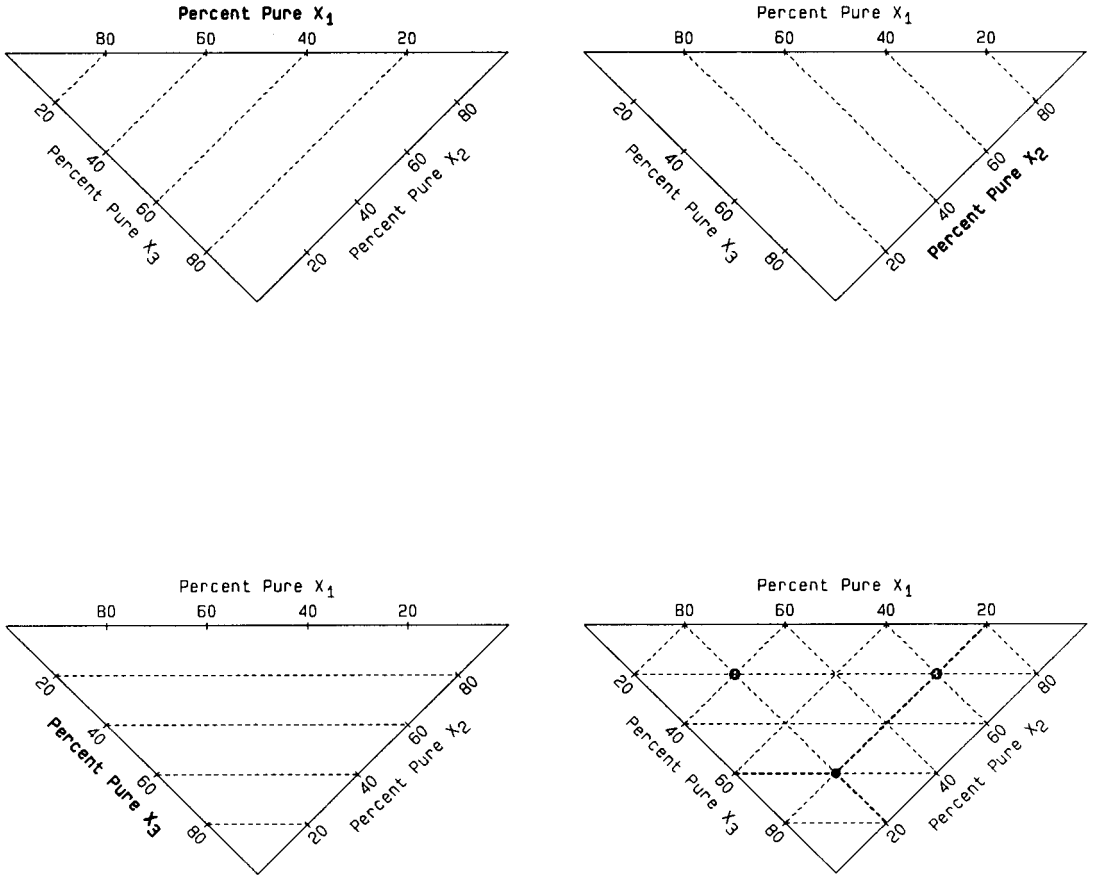

Fig. 3. Graphical representation of the feasible experimental region for a three-component system with parallel dashed lines showing contours of constant composition in 20% increments for x_1 (upper left), x_2 (upper right), x_3 (lower left) and a superposition of x_1, x_2 and x_3 (lower right). The black dot in the lower right figure is an experiment located at the intersection of the three grid lines corresponding to 20% x_1, 20% x_2 and 60% x_3. The black dot is a pseudo-component mixture rich in pure component x_3; the left and right open circles represent pseudo-component mixtures rich in pure components x_1 and x_2, respectively.

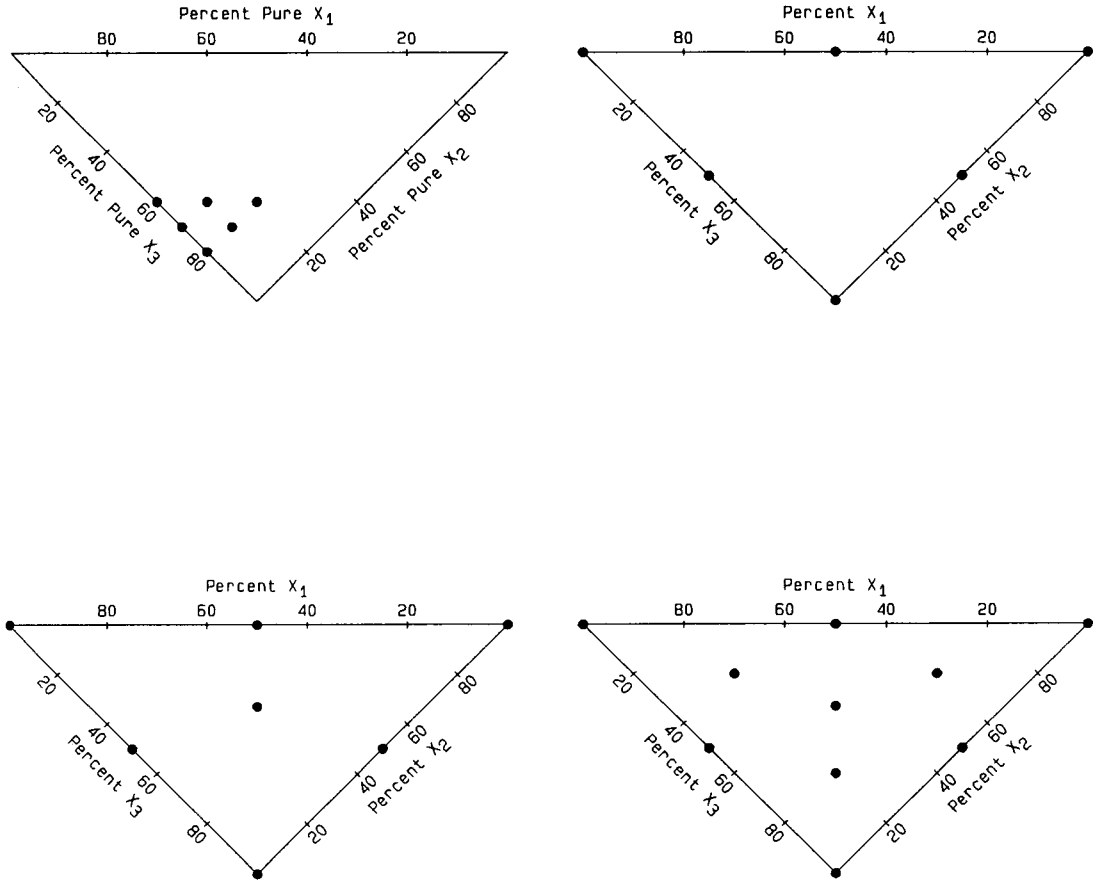

Fig. 4. Upper left: a simple {3,2} simplex-lattice design constructed from pseudo components. Upper right: an expanded view of the {3,2} simplex-lattice design expressed in the pseudo-component percentages. Lower left: a three-component simplex-centroid mixture design. Lower right: a three-component augmented-simplex centroid mixture design.

design. For example, the special-cubic lattice [78,107], or simplex-centroid design [77,99], shown in the lower left panel of Fig. 4, is produced by adding one more experiments at the center of the basic lattice. The added experiment corresponds to a formulation made by mixing one third of each of the three components and represents the only true three-component mixture in the design. The simplex-centroid design can be augmented to include additional experiments located inward from the corners and edges of the simplex. The ten experiments of the three-component augmented simplex-centroid design [77,79,97] are shown in the lower right panel of Fig. 4.

In this work, the basic simplex-lattice design and the augmented simplex-centroid design were used for specifying mobile phase combinations for three-component systems. Pseudo-component mobile phases were used to prepare mixtures.

EXPERIMENTAL

Experimental design

Four three-component mixture designs were used to define a total of 35 mobile phase formulations. For each of the four mixture designs, the first component, x_1, is always H_3PO_4, the second component, x_2, is always NaH_2PO_4 and the third component, x_3, is either $NaClO_4$ or sodium 1-octanesulfonate (NaOSA) or methanol (MeOH).

This assignment of numbers to components is purely arbitrary.

Chromatographic system

The chromatographic system consisted of a computer-controlled BAS-200A LC unit (Bioanalytical Systems, West Lafayette, IN), a 25 cm × 4.6 mm i.d. Spherisorb ODS analytical column having a particle size of 5 μm (Alltech Associates, Deerfield, IL) and a BAS UV-116 external UV–visible variable/dual-wavelength programmable LC detector. The BAS-200A unit was equipped with a temperature-controlled oven, three temperature-controlled mobile phase reservoirs and a Model 7125 syringe-loading sample injector (Rheodyne, Cotati, CA).

Data acquisition

The analog output from the detector was recorded by a Model 281 dual-pen strip-chart recorder (Soltec, Encino, CA) operating at 1 V full-scale and 0.5 in min^{-1}. The analog detector output was also amplified and digitized by a DAS-8 analog-to-digital converter (MetraByte, Taunton, MA) which was interfaced to an IBM personal computer. The analog signal was digitized at a rate of ten data points per second and saved on floppy diskettes. Routines written in Turbo Pascal version 5.0 (Borland International, Scotts Valley, CA) were used to determine retention times. Chromatograms and other illustrations were printed on a Hewlett-Packard (Palo Alto, CA) LaserJet Series III printer equipped with a Plotter-in-a-Cartridge and extended memory (Pacific Data Products, San Diego, CA).

Other instrumentation

pH measurements were made with a glass electrode connected to a Model PBX pH meter, both from Sargent-Welch (Skokie, IL). The calibration of the pH meter was checked with commercially acquired aqueous buffers of known pH and corrected (if necessary) just prior to each measurement. In this work, pH is an apparent pH because of the high MeOH concentration in each of the mobile phases [41,111,112]. Solids used in the preparation of samples and mobile phases were weighed on a Mettler H30 analytical balance (Mettler Instrument, Princeton, NJ).

Chemicals

Distilled water was prepared with a Mega-Pure 1-l all-glass distillation apparatus (Corning, Corning, NY). Methanol (ChromAR, LC grade), H_3PO_4 (AR, 85%) and $NaH_2PO_4 \cdot H_2O$ (granular, AR) were purchased from Mallinckrodt (Paris, KY). 1-Octanesulfonic acid sodium salt (NaOSA, 98%), $NaClO_4$ (99 + %), L-phenylalanine (99%), L-tyrosine (99 + %) and L-tryptophan (99%) were purchased from Aldrich (Milwaukee, WI). Hydrochloric acid (12 M reagent grade, ACS) was obtained from Matheson, Coleman and Bell (Norwood, OH). Aqueous buffers (pH 3 and 7) were obtained from Fisher (Pittsburgh, PA).

Mobile phases

Three solvents were used to prepare the pseudo-component mobile phases: (1) MeOH–H_2O (70 + 30) (70MeOH) was prepared by adding three volumes of water to seven volumes of MeOH; (2) MeOH–H_2O (30 + 70) (30MeOH) was prepared by adding seven volumes of water to three volumes of MeOH; (3) 0.0501 M $NaClO_4$ was prepared by adding 42.9134 g of $NaClO_4$ to 7 l of the previously prepared 70MeOH.

Three sets of three pseudo-component mobile phases were prepared: study A, $x_1 = 0.0515$ M H_3PO_4, $x_2 = 0.0502$ M NaH_2PO_4 and $x_3 = 0.100$ M $NaClO_4$, each prepared in 70MeOH; study B, $x_1 = 0.0515$ M H_3PO_4, $x_2 = 0.0500$ M NaH_2PO_4 and $x_3 = 0.00507$ M NaOSA, each prepared in the 70MeOH containing 0.0501 M $NaClO_4$; studies C and D, $x_1 = 0.0515$ M H_3PO_4, $x_2 = 0.0500$ M NaH_2PO_4 and $x_3 = 30$MeOH, each containing 0.05 M $NaClO_4$ and 0.0025 M NaOSA (the H_3PO_4 and NaH_2PO_4 were prepared in 70MeOH).

A tenth mobile phase, to validate later predicted results, was prepared in 30MeOH and contained 0.10 M $NaClO_4$, 0.05 M H_3PO_4 and 0.0025 M NaH_2PO_4. All other mobile phases were obtained from these pseudo-component solutions using the solvent-mixing capabilities of the liquid chromatograph.

Samples

Concentrated stock solutions containing individual amino acids (ca. 0.01 M Phe, 0.01 M Tyr and 0.004 M Trp) were prepared for a given study by adding the amino acid to a volumetric flask containing the NaH_2PO_4 mobile phase used in that study. Because the amino acids are relatively insoluble (Tyr in particular), 12 M HCl was added dropwise such that its final concentration in the stock solution would be ca. 0.1 M. The mixture was then brought to volume with the NaH_2PO_4 mobile phase. Portions of these concentrated stock solutions were diluted with the NaH_2PO_4 mobile phase to give ca. 4 mM Phe, 2 mM Tyr and 0.3 mM Trp. Samples for the final validation experiment were prepared by a similar method using the final mobile phase. All samples were stored in the flasks in which they were prepared. Because solutions of Trp were found to turn yellow on prolonged exposure to light, flasks containing Trp were wrapped in aluminum foil.

Method

For each experiment, the chromatographic oven and mobile phase temperatures were set at 35°C; 20-μl sample volumes were injected; the detector was operated at 254 nm with an amplifier time constant of 0.1 s and an absorbance range of 0.100 full-scale. Mobile phases were equilibrated with the column for a minimum of 30 minutes at a flow-rate of 1.00 ml min^{-1} before switching to a flow-rate of 1.60 or 2.00 ml min^{-1}. The apparent pH [41, 111, 112] of each mobile phase was measured twice, once just after equilibration and again just before switching to the next mobile phase. Replicate injections of each amino acid in each mobile phase were made to monitor the reproducibility of the LC system and

TABLE 1

Mobile phase composition, mobile phase pH and retention times of Phe, Tyr and Trp for study A (flow-rate = 2.00 ml min^{-1})

Mobile phase composition (%)			Mobile phase pH [a]	Retention time (min)		
0.0515 M H_3PO_4	0.0502 M NaH_2PO_4	0.100 M $NaClO_4$		Phe	Tyr	Trp
100	0	0	2.70	2.380	2.360	2.525
			2.70	2.342	2.352	2.528
			–	2.362 [b]	–	–
50	50	0	3.85	1.607	1.505	1.623
			3.83	1.608	1.507	1.623
0	100	0	5.60	1.617	1.522	1.622
			5.85	1.603	1.528	1.630
60	20	20	3.40	1.605	1.505	1.618
			3.40	1.600	1.507	1.615
20	60	20	4.30	1.615	1.522	1.622
			4.20	1.617	1.518	1.623
			–	–	1.522 [b]	–
33	34	33	3.75	1.580	1.487	1.592
			3.70	1.573	1.488	1.590
50	0	50	2.80	1.545	1.473	1.570
			2.80	1.543	1.473	1.567
0	50	50	5.45	1.608	1.520	1.623
			5.60	1.613	1.522	1.627
20	20	60	3.75	1.575	1.493	1.592
			3.73	1.578	1.488	1.593
0	0	100	5.50	1.622	1.525	1.625
			5.35	1.620	1.523	1.627

[a] Measured once just after equilibration and again just before switching to the next mobile phase. [b] Additional verification of reproducibility.

to improve the precision of the retention time data. A non-linear least-squares program [54] was used for fitting appropriate non-linear models to the set of pH and retention time data in each study. The fitted models were then used to generate plots of the response surface [74, 113]. A grid-search program based on the fitted models was written to search the mixture space with a 5% grid to predict the mobile phase composition which should give the best separation of the three-component sample.

RESULTS AND DISCUSSION

Tables 1–4 list the mobile phase composition, mobile phase pH and retention times of Phe, Tyr and Trp in studies A–D.

Model for pH behavior of the mobile phases

Figure 5 shows pH as a function of composition for the mixture designs used in studies A–D. In each figure, the compositions of the mobile phases are shown by black dots. The average of the two pH measurements is shown beside each dot; replicate pH measurements for a given mobile phase combination never differed by more than 0.25 pH unit (± 0.125 pH unit from the mean). The pooled standard deviation is ± 0.040 pH unit.

In the absence of ionic strength and organic modifier effects, observed pH can be predicted by a combination of four equations derived from fundamental acid–base equilibria [91,112,114–117]:

$$[H^+]^2 = K_w \quad (2)$$

TABLE 2

Mobile phase composition, mobile phase pH and retention times of Phe, Tyr and Trp for study B (flow-rate = 2.00 ml min^{-1})

Mobile phase composition (%)			Mobile phase pH [a]	Retention time (min)		
0.0515 M H_3PO_4	0.0500 M NaH_2PO_4	0.00507 M NaOSA		Phe	Tyr	Trp
100	0	0	2.70	1.580	1.502	1.620
			2.69	1.588	1.508	1.620
50	50	0	3.75	1.577	1.490	1.593
			3.70	1.578	1.495	1.592
0	100	0	5.60	1.618	1.522	1.620
			5.50	1.622	1.527	1.627
60	20	20	3.35	1.590	1.507	1.608
			3.35	1.587	1.508	1.610
20	60	20	4.10	1.580	1.493	1.602
			4.20	1.587	1.493	1.592
33	34	33	3.70	1.600	1.517	1.615
			3.70	1.600	1.515	1.613
50	0	50	2.85	1.588	1.508	1.613
			2.85	1.577	1.500	1.610
			–	–	1.492 [b]	1.598
0	50	50	5.40	1.613	1.520	1.628
			5.50	1.628	1.537	1.630
			–	1.630 [b]	1.523 [b]	–
			–	1.635 [b]	–	–
20	20	60	3.80	1.590	1.503	1.605
			3.70	1.588	1.512	1.610
0	0	100	4.80	1.617	1.530	1.630
			4.70	1.623	1.535	1.635

[a] Measured once just after equilibration and again just before switching to the next mobile phase. [b] Additional verification of reproducibility.

TABLE 3

Mobile phase composition, mobile phase pH and retention times of Phe, Tyr and Trp for study C (flow-rate = 1.60 ml min^{-1})

Mobile phase composition (%)			Mobile phase pH [a]	Retention time (min)		
0.0515 M H_3PO_4	0.0500 M NaH_2PO_4	30MeOH		Phe	Tyr	Trp
100	0	0	2.70	1.950	1.848	1.985
			2.70	1.943	1.852	1.985
50	50	0	3.75	1.982	1.875	2.002
			3.72	1.988	1.878	2.003
0	100	0	5.67	2.012	1.890	2.022
			5.65	2.012	1.895	2.023
60	20	20	3.10	2.058	1.903	2.113
			3.10	2.110	1.947	2.132
20	60	20	3.91	2.070	1.910	2.113
			3.95	2.077	1.913	2.108
33	34	33	3.30	2.122	1.960	2.217
			3.30	2.118	1.932	2.212
50	0	50	2.55	2.262	2.037	2.463
			2.59	2.272	2.028	2.470
0	50	50	4.90	2.167	1.948	2.245
			4.98	2.177	1.923	2.255
20	20	60	3.15	2.245	1.972	2.477
			3.20	2.240	1.965	2.457
0	0	100	4.10	2.402	2.012	2.780
			4.30	2.410	2.015	2.793
			–	2.412 [b]	–	–

[a] Measured once just after equilibration and again just before switching to the next mobile phase. [b] Additional verification of reproducibility.

TABLE 4

Mobile phase composition, mobile phase pH and retention times of Phe, Tyr and Trp for study D (flow-rate = 1.60 ml min^{-1})

Mobile phase composition (%)			Mobile phase pH [a]	Retention time (min)		
0.0515 M H_3PO_4	0.0500 M NaH_2PO_4	30MeOH		Phe	Tyr	Trp
40	0	60	2.50	2.355	2.042	2.652
			2.50	2.352	2.048	2.658
30	10	60	2.80	2.312	2.018	2.562
			2.80	2.305	2.047	2.615
			–	–	–	2.552 [b]
20	20	60	3.10	2.235	1.988	2.462
			3.10	2.273	1.982	2.453
30	0	70	2.50	2.487	2.135	2.960
			2.50	2.493	2.107	2.942
20	10	70	2.90	2.475	2.092	2.853
			2.90	2.403	2.048	2.780
20	0	80	2.55	2.675	2.195	3.395
			2.60	2.682	2.185	3.310

[a] Measured once just after equilibration and again just before switching to the next mobile phase. [b] Additional verification of reproducibility.

$$[H^+]^3 + K_{a1}[H^+]^2 - (K_{a1}C_{HA} + K_w)[H^+] - K_wK_{a1} = 0 \quad (3)$$

$$[H^+]^2 = (K_{a1}K_{a2}C_A + K_wK_{a1})/(C_A + K_{a1}) \quad (4)$$

$$[H^+]^2 + (C_A + K_{a1})[H^+] - K_{a1}C_{HA} = 0 \quad (5)$$

In each equation, $[H^+]$ is the hydrogen ion concentration, K_w is the autoprotolysis constant of water, K_{a1} is the first acid dissociation constant of H_3PO_4, K_{a2} is the second acid dissociation constant of H_3PO_4, C_{HA} is the analytical or total concentration of H_3PO_4 in the mobile phase and C_A is the analytical or total concentration of NaH_2PO_4 in the mobile phase.

Equations 2–5 each represent one of four situations. Equation 2 is used when the mobile phase contains no added acidic or basic compounds and applies to those mobile phases at the lower vertex for studies A–C in Fig. 5. Equation 3 is used when the mobile phase contains H_3PO_4 but not NaH_2PO_4 and applies to those mobile phases along the left edge of each triangle for studies A–D in Fig. 5. Equation 4 is used when the mobile phase contains NaH_2PO_4 but not H_3PO_4

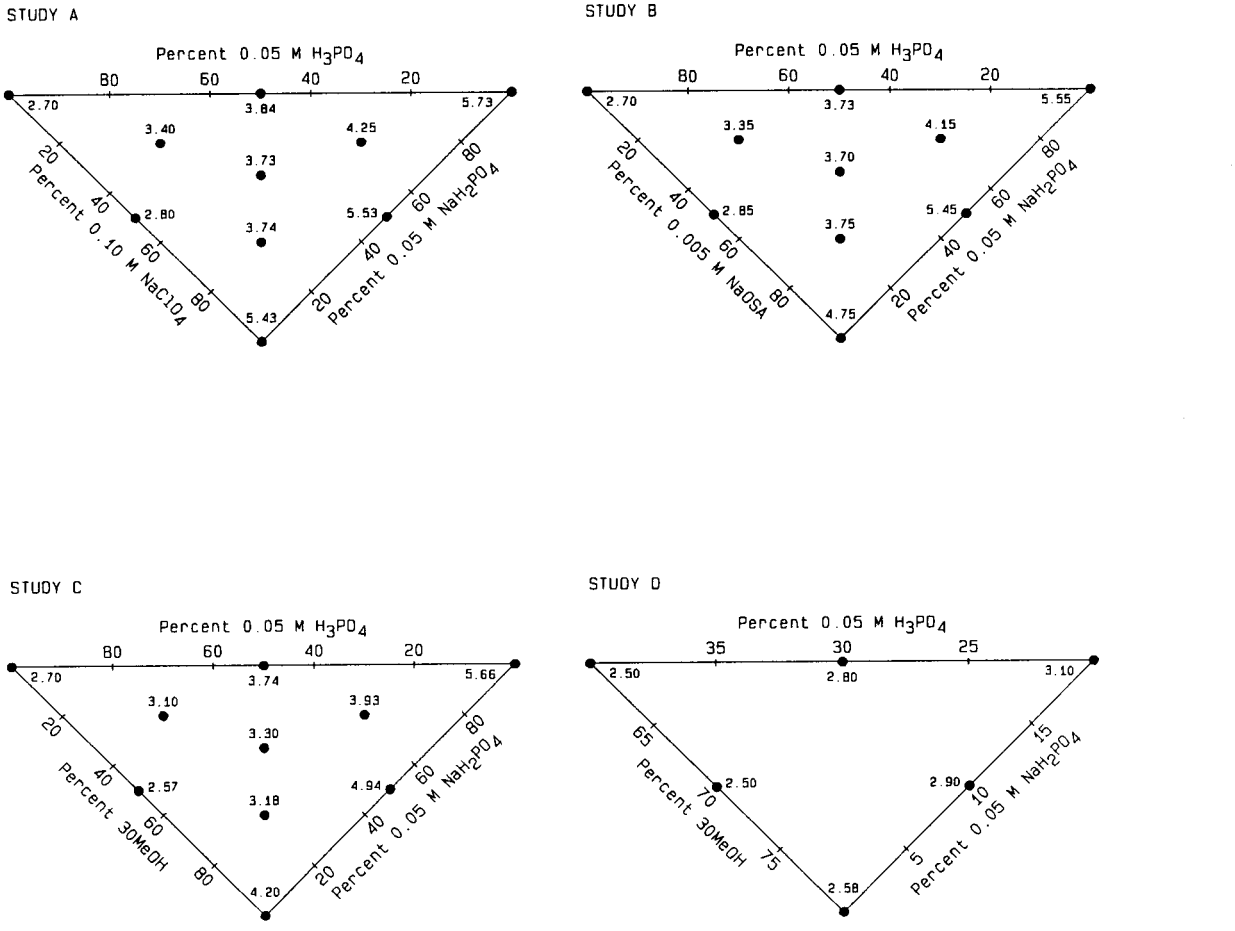

Fig. 5. Three-component mixture designs showing pseudo-component mobile phases, mobile phase combinations investigated and the average pH of each mobile phase combination. Study A: pseudo-component mobile phases of 0.05 M H_3PO_4, 0.10 M $NaClO_4$ and 0.05 M NaH_2PO_4 prepared in 70MeOH. Study B: pseudo-component mobile phases of 0.05 M H_3PO_4, 0.005 M NaOSA and 0.05 M NaH_2PO_4 prepared in a 70MeOH solution of 0.0501 M $NaClO_4$. Studies C and D: pseudo-component mobile phases of 0.05 M H_3PO_4, 30MeOH and 0.05 M NaH_2PO_4 containing 0.05 M $NaClO_4$ and 0.0025 M NaOSA (the H_3PO_4 and NaH_2PO_4 were prepared in 70MeOH).

and applies to those mobile phases along the right edge of each triangle for studies A–C in Fig. 5. Equation 5 is used when the mobile phase contains both H_3PO_4 and NaH_2PO_4 and applies to all other mobile phases.

Solutes in aqueous solutions containing an inert inorganic salt tend to be more dissociated (smaller pK) than in solutions containing no additional salt [91, 115]. Solutes in aqueous solutions containing an organic modifier tend to be less dissociated than in solutions containing no organic modifier [112]. To account for the effects of increased salt concentration and added organic modifier, Eqns. 2–5 were modified empirically:

$$[H^+]^2 = K_w^* \quad (6)$$

$$[H^+]^3 + K_{a1}^*[H^+]^2 - (K_{a1}^* C_{HA} + K_w^*)[H^+] - K_w^* K_{a1}^* = 0 \quad (7)$$

$$[H^+]^2 = (K_{a1}^* K_{a2}^* C_A + K_w^* K_{a1}^*)/(C_A + K_{a1}^*) \quad (8)$$

$$[H^+]^2 + (C_A + K_{a1}^*)[H^+] - K_{a1}^* C_{HA} = 0 \quad (9)$$

where

$$K_w^* = K_w \times 10^{-\beta} \quad (10)$$

$$K_{a1}^* = K_{a1} \times 10^{-\beta} \quad (11)$$

and

$$K_{a2}^* = K_{a2} \times 10^{-\beta} \quad (12)$$

In Eqns. 10–12, K_w^* is the apparent autoprotolysis constant of water, K_{a1}^* is the apparent first acid dissociation constant of H_3PO_4, K_{a2}^* is the apparent second acid dissociation constant of H_3PO_4 and β is an offset defined by the empirical equation

$$\beta = \beta_{NaClO_4}[NaClO_4] + \beta_{NaOSA}[NaOSA] + \beta_{MeOH}(\%MeOH) \quad (13)$$

where β_{NaClO_4} is an effect of $NaClO_4$ (presumably an ionic strength effect), β_{NaOSA} is an effect of NaOSA (presumably another ionic strength effect) and β_{MeOH} is an effect of MeOH (presumably an organic modifier effect). If the resulting value of β in Eqn. 13 is positive, then each K^* calculated from Eqns. 10–12 will be smaller than its corresponding K value; if the value of β is negative, then each K^* will be larger than its corresponding K value. The parameters K_w, K_{a1}, K_{a2}, β_{NaClO_4}, β_{NaOSA} and β_{MeOH} are the adjustable parameters of the pH model.

TABLE 5

Parameter estimates and diagnostic statistics for Eqns. 7–9 fitted to the combined pH data in Tables 1–4

Parameter estimates [a]		Diagnostic statistics	
pK_{a1}	2.2440 (2.148)	SS_r	0.5646
pK_{a2}	5.7728 (7.199)	s_r	0.09700
pK_w	15.6074 (14.000)	R^2	0.9978
β_{NaClO_4}	−2.6454		
β_{NaOSA}	−3.8306		
β_{MeOH}	0.02370		

[a] Numbers in parentheses are from [91].

When the mixture contains neither H_3PO_4 nor NaH_2PO_4, the only theoretical source of H^+ is from the autoprotolysis of water. Because the prediction of pH for unbuffered systems is notoriously difficult (for example, it is difficult to account for the variable and usually unknown concentration of dissolved CO_2 [115]), the three mobile phases containing neither H_3PO_4 nor NaH_2PO_4 were not used to fit the pH model.

Regression analysis for the pH model

Table 5 lists non-linear least-squares parameter estimates for pK_{a1}, pK_{a2}, pK_w, β_{NaClO_4}, β_{NaOSA} and β_{MeOH} for the pH model represented by Eqns. 7–9 fitted to the combined pH data in Tables 1–4. Numbers in parentheses are literature values for pK_{a1}, pK_{a2} and pK_w.

Diagnostic statistics are also listed in Table 5. The standard error of estimate, s_r (the standard deviation of the experimental points about the fitted model), indicates that the measured pH has an agreement with the fitted model of approximately ± 0.10 pH unit, consistent with the generally accepted precision of pH measurements [91]. The coefficient of multiple determination, R^2, indicates that the six-parameter model accounts for almost 99.8% of the variability in the data set. Hence the current model is considered to give an adequate prediction of pH as a function of mobile phase composition. The good agreement between calculated and literature values for pK_w, pK_{a1} and pK_{a2} is reasonable given the small

uncertainties in measured pH [73,117] and the restriction of Eqn. 13 to first-order terms only.

Observed and predicted pH behavior of the mobile phases

The fitted model is shown in Fig. 6 for studies A–D. The design points are shown by black dots (see also Fig. 5).

Fig. 7 contains four plots that correspond to the four panels in Fig. 6. Each of the four plots in Fig. 7 contains lines that radiate from the vertex that contains no H_3PO_4 and no NaH_2PO_4; this vertex corresponds to the lower vertex in studies A–C and to an imaginary vertex in study D (see the upper left panel in Fig. 4 for reference). Each of the radiating lines shows pH as a function of composition for a constant (but different) H_3PO_4/NaH_2PO_4 ratio. The lighter lines toward the left in each plot are rich in H_3PO_4 and poor in NaH_2PO_4; the darker lines toward the right are rich in the conjugate base and poor in the conjugate acid. The single line at the back of each plot shows pH as a function of increasing percentage of NaH_2PO_4 (or as a function of

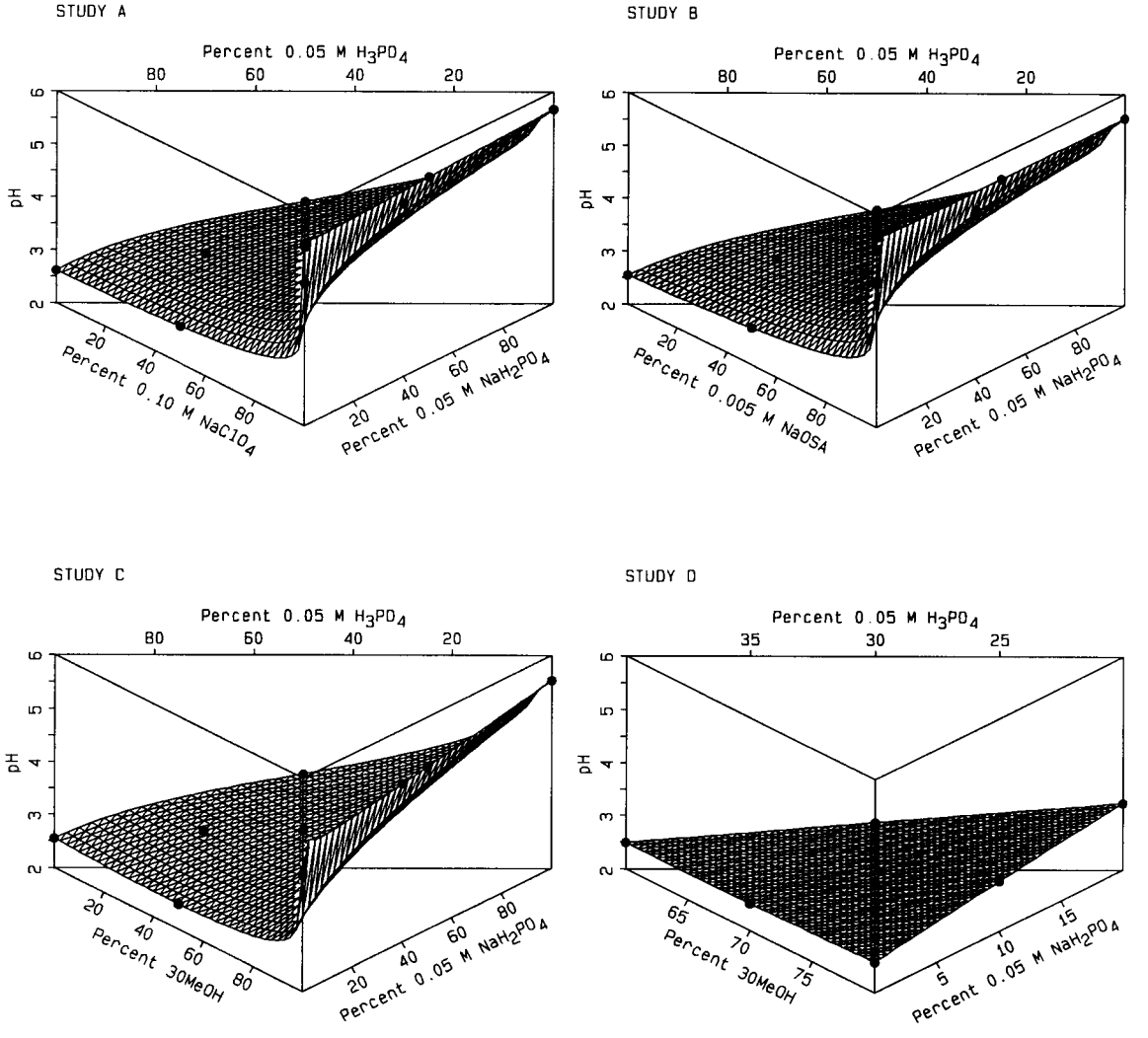

Fig. 6. Three-dimensional response surface plots of pH as a function of mobile phase composition for studies A–D.

decreasing H_3PO_4) in the absence of added component x_3. All of these lines follow the contours shown in Fig. 6.

Fig. 8 is another view of the information contained in Figs. 5–7. Note that the percentage of component x_3 decreases from left to right along the horizontal axis in each presentation. Careful inspection shows that the left sides of the graphs in Fig. 8 correspond to the lower vertexes in Figs. 5–7. Hence the views in Fig. 8 are those which would be seen if the observer were located to the right of the plots in Figs. 6 and 7 looking "west" parallel to the x_1 axis: the percentage of x_3 is seen increasing to the left and the pH is increasing upward from this view. Each line in Fig. 8 shows pH vs. decreasing x_3 at a constant H_3PO_4/NaH_2PO_4 ratio and corresponds to a line in Fig. 7. The darker lines in each graph represent lower H_3PO_4/NaH_2PO_4 ratios close to the observer; lighter lines represent higher H_3PO_4/NaH_2PO_4 ratios far from the observer. In studies C and D in Fig. 8, as the percentage of

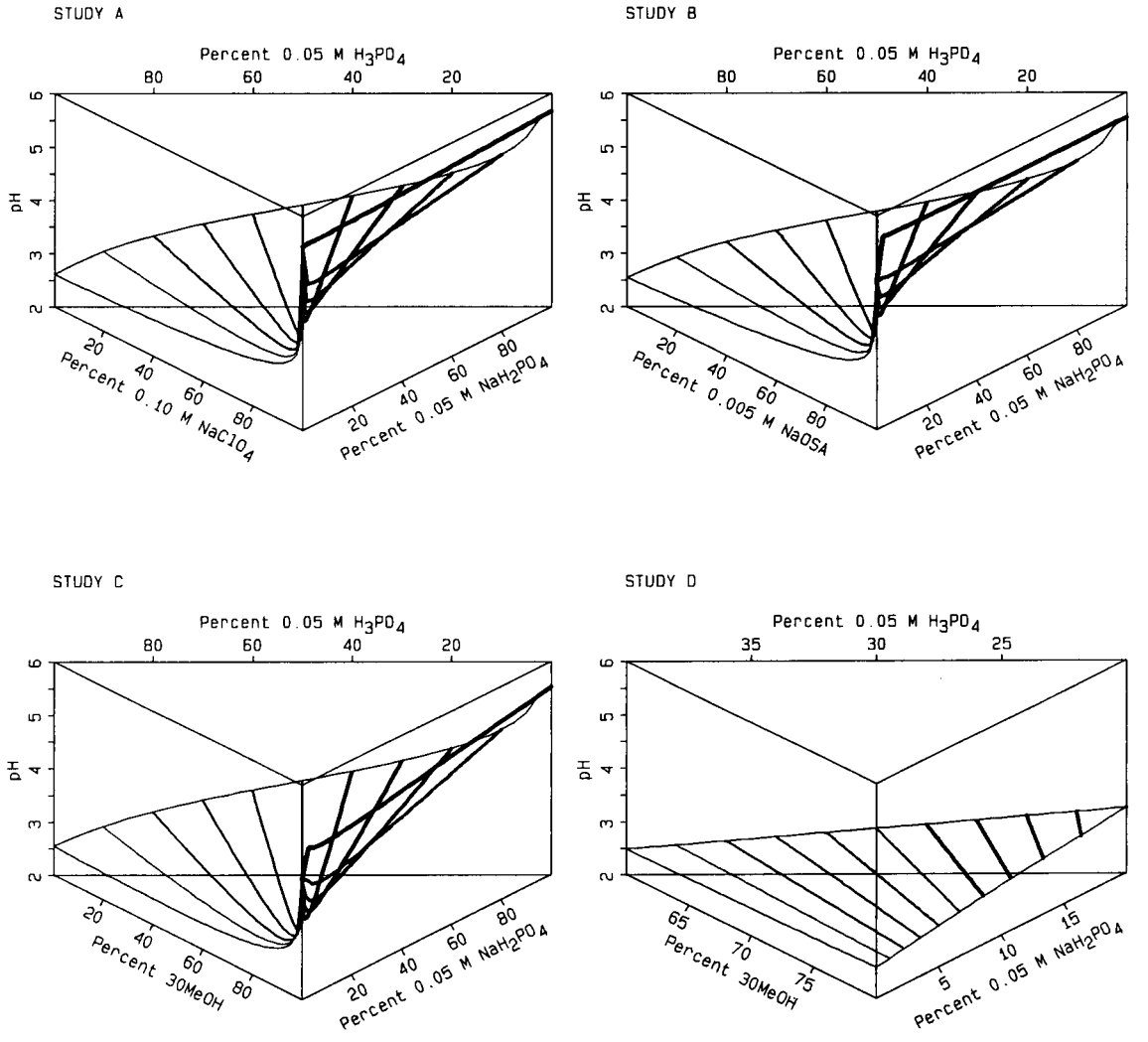

Fig. 7. Three-dimensional plots of pH as a function of mobile phase composition for studies A–D showing lines which radiate from the vertex that contains no H_3PO_4 and no NaH_2PO_4. Mobile phases along each line contain a constant (but different) H_3PO_4/NaH_2PO_4 ratio.

30MeOH increases (and the percentage of 70MeOH decreases), the absolute percentage of methanol in the mixture decreases; this is shown by the extra horizontal axes in panels C and D in Fig. 8.

In study A shown in Fig. 8, as the amount of added $NaClO_4$ increases (to the left) and the total amount of H_3PO_4 and NaH_2PO_4 decreases, the pH decreases slightly except for those conditions when there is little or no conjugate base. This is consistent with the general chemical observation that solutes in aqueous solution containing an inert inorganic salt tend to be more dissociated than in solutions containing no additional salt [91, 115]. In study B, the effect is smaller: the concentration of added 0.005 M NaOSA is only one twentieth that of the 0.10 M $NaClO_4$.

In study C in Fig. 8, as the amount of methanol increases (to the right), the pH increases. Changes in the concentration of organic modifier in a solution can have significant effects on the dissociation constants of ionizable solutes [91,112,115]. Weak acids such as H_3PO_4 in solutions containing increased amounts of organic modifier will have dissociation constants that are smaller than those found for the same solute under more aqueous conditions [112]. Hence the measured

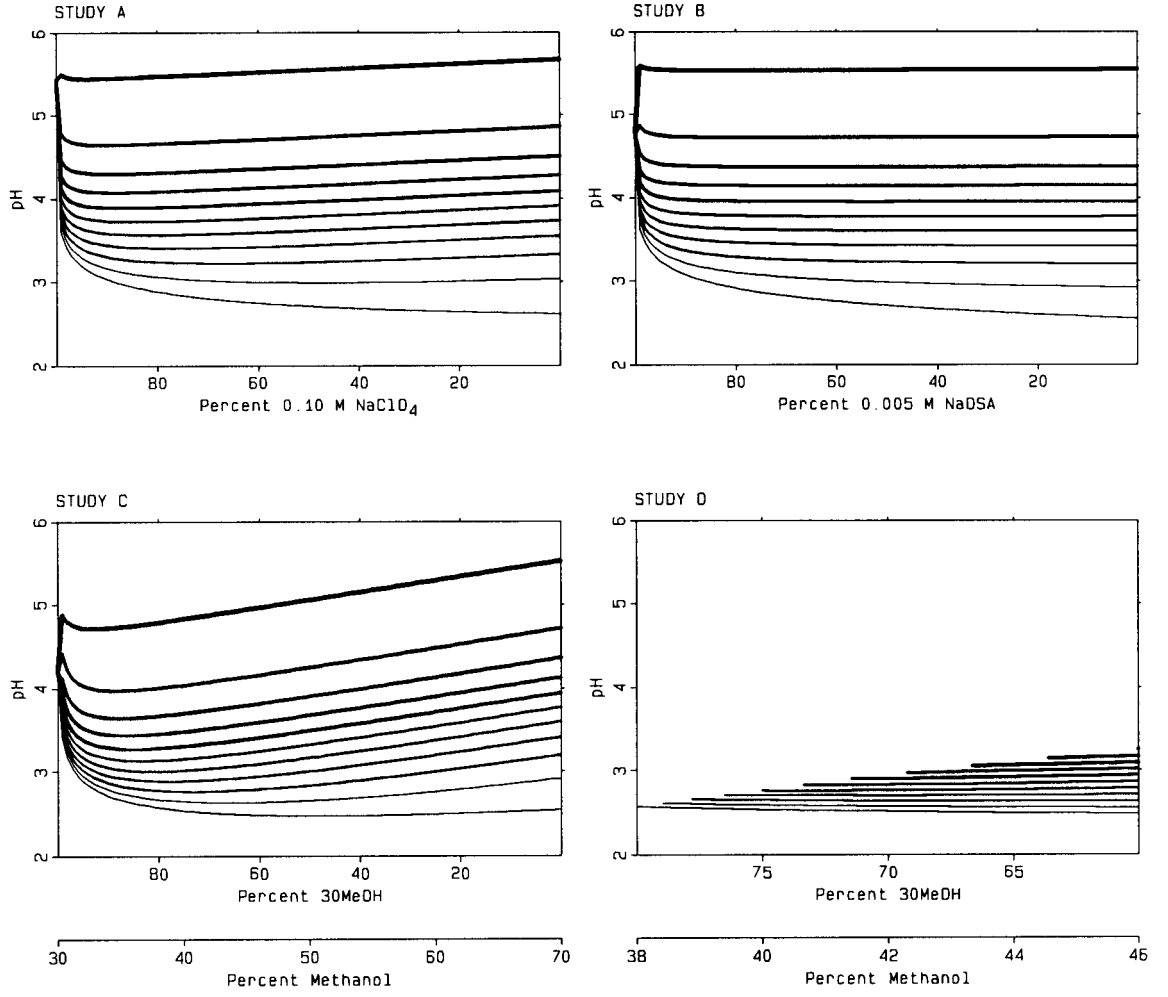

Fig. 8. Alternative two-dimensional view of Fig. 7 (see text for discussion).

pH of these less aqueous solutions will be higher than it would be under more aqueous conditions. Study D shows the same effects over a more restricted domain of composition.

Model for retention behavior of Phe, Tyr and Trp

The chromatographic retention behavior of amino acids is often affected by the pH, the ionic strength, the concentration of IIR and the amount of organic modifier in the mobile phase [38].

Effect of mobile phase pH. At low pH, Phe, Tyr and Trp will exist partially in the conjugate acid form (fully protonated with a single positive charge) and partially in the conjugate base form (zwitterionic, doubly charged but neutral). At moderate ionic strength, the observed chromatographic retention time as a function of hydrogen ion concentration can be described by the relationship

$$t_r = f_{(H_2A^+)} t_{(H_2A^+)} + f_{HA} t_{HA} \quad (14)$$

where t_r is the observed chromatographic retention time of the amino acid, $f_{(H_2A^+)}$ is the fraction of amino acid in the fully protonated form, $t_{(H_2A^+)}$ is the retention time of the fully protonated amino acid, f_{HA} is the fraction of amino acid in the zwitterionic form and t_{HA} is the retention time of the zwitterionic amino acid [40,42,118].

The fraction of the protonated form of the amino acid is, by definition,

$$f_{(H_2A^+)} = [H_2A^+]/([H_2A^+] + [HA]) \quad (15)$$

and the fraction of the zwitterionic form of the amino acid is

$$f_{HA} = [HA]/([H_2A^+] + [HA]) \quad (16)$$

Multiplying both the numerator and the denominator of Eqns. 15 and 16 by the quantity $[H^+]/[H_2A^+]$ gives Eqns. 17 and 18, respectively:

$$f_{(H_2A^+)} = \frac{[H^+]}{[H^+] + [H^+][HA]/[H_2A^+]} \quad (17)$$

$$f_{HA} = \frac{[H^+][HA]/[H_2A^+]}{[H^+] + [H^+][HA]/[H_2A^+]} \quad (18)$$

Because the quantity $[H^+][HA]/[H_2A^+]$ is the amino acid's first acid dissociation constant, K_{a1},

$$f_{(H_2A^+)} = [H^+]/([H^+] + K_{a1}) \quad (19)$$

and

$$f_{HA} = K_{a1}/([H^+] + K_{a1}) \quad (20)$$

By experimentally measuring the retention time of a solute at three or more levels of mobile phase pH, Eqns. 14, 19 and 20 can be used to estimate values of pK_{a1}, $t_{(H_2A^+)}$ and t_{HA} for that solute.

Effect of mobile phase ionic strength. Changes in the chromatographic retention of solutes as a function of ionic strength can be described by the addition of a semi-empirical linear term to Eqn. 14:

$$t_r = f_{(H_2A^+)} t_{(H_2A^+)} + f_{HA} t_{HA} + \beta_1 \mu^{-1} \quad (21)$$

where β_1 is a measure of the effect of the mobile phase ionic strength and μ is the ionic strength of the mobile phase [91,112,114–116]. In this work, the ionic strength of the mobile phase is determined from the equation

$$\mu = 0.5(2[NaClO_4] + 2[NaOSA] + 2[NaH_2PO_4] + 2[H^+]) \quad (22)$$

where $NaClO_4$ and NaOSA are assumed to be completely ionized and $[H^+]$ is predicted from fitted Eqns. 7–9 ($[OH^-]$ in these acidic solutions is negligible). The NaH_2PO_4 is assumed to ionize into Na^+ and $H_2PO_4^-$ ions; further dissociation or hydrolysis of the $H_2PO_4^-$ ion is assumed to be negligible [91].

The third term in Eqn. 21 accounts for large relative changes in the ionic strength of the eluent [119]. At moderate to high ionic strengths, the retention time is relatively insensitive to changes in ionic strength of the mobile phase. As the ionic strength approaches zero, however, the retention time becomes more sensitive to changes in ionic strength, as reflected in the reciprocal ionic strength term in Eqn. 21, which for positive values of β_1 becomes hyperbolically larger at lower ionic strengths.

Effect of IIR concentration. Previous work [44,118] has demonstrated that the retention be-

havior of charged solutes in the presence of a charged IIR can be described adequately by the addition of a semi-empirical linear term to Eqn. 21:

$$t_r = f_{(H_2A^+)}t_{(H_2A^+)} + f_{HA}t_{HA} + \beta_1\mu^{-1} + f_{(H_2A^+)}\beta_2[IIR]^{\beta_3} \quad (23)$$

where [IIR] is the concentration of IIR in the mobile phase and β_2 and β_3 ($0 < \beta_3 < 1$) are parameters of the Freundlich adsorption isotherm [120,121]. A positive value of β_2 indicates that the presence of IIR increases the retention of the injected solute and a negative value for β_2 indicates that the presence of IIR decreases the retention of the injected solute. The quantity $f_{(H_2A^+)}$ appears in the last term because only the positively charged fraction of the amino acid will encounter charge–charge interactions with the negatively charged IIR.

Effect of organic modifier concentration. Organic modifiers have been shown to influence both solute and solvent dissociation constants and produce changes in the selectivity and retention of a given solute [44,90,112,122–126]. This effect can be described by including a semi-empirical multiplicative non-linear exponential term [44,123] in Eqn. 23:

$$t_r = \left\{f_{(H_2A^+)}t_{(H_2A^+)} + f_{HA}t_{HA} + \beta_1\mu^{-1} + f_{(H_2A^+)}\beta_2[IIR]^{\beta_3}\right\}e^{-\beta_4(\%M)} \quad (24)$$

where β_4 is a measure of the effect of the added organic modifier and %M is the percentage of organic modifier (in this instance MeOH) in the mobile phase. A positive value of β_4 indicates that the presence of organic modifier decreases the retention of the injected solute.

Regression analysis for the retention model

Table 6 lists one set of parameter estimates [$t_{(H_2PHE^+)}$, t_{HPHE}, $t_{(H_2TYR^+)}$, t_{HTYR}, $t_{(H_2TRP^+)}$, t_{HTRP}, β_1, β_2, β_3 and β_4] corresponding to a minimum sum of squares of residuals (SS_r) for Eqn. 24 fitted to the combined retention data for Phe, Tyr and Trp in Tables 1–4. For these calculations, the pK_{a1} of Phe, Tyr and Trp were held constant at the literature values of 2.20, 2.17 and 2.35, respectively [91] [the data corresponding to 100% (v/v) of 30MeOH in study C were omitted from the regression analysis calculations because a mixture of the three solutes produced an unexplained fourth peak when this mobile phase was used; the data at 20% (v/v) H_3PO_4–80% (v/v) 30MeOH in study D were also omitted because they produced residuals that were much larger than the other residuals and thus represented outliers that could not be accounted for with the existing model]. Also listed in Table 6 are the standard error of estimate for the experimental points, s_r, and the coefficient of multiple determination, R^2.

TABLE 6

Parameter estimates and diagnostic statistics for Eqn. 24 fitted to the combined retention data for Phe, Tyr and Trp in Tables 1–4

Parameter estimates [a]		Diagnostic statistics	
$t_{(H_2PHE^+)}$	2.6525	SS_r	1.1439
t_{HPHE}	3.0466	s_r	0.07525
$t_{(H_2TYR^+)}$	2.1187	R^2	0.9988
t_{HTYR}	2.8448		
$t_{(H_2TRP^+)}$	3.4325		
t_{HTRP}	3.0755		
β_1	0.004395		
β_2	42.7158		
β_3	0.7740		
β_4	0.006411		

[a] For these calculations, the pK_{a1} of Phe, Tyr, and Trp were held constant at the literature values of 2.20, 2.17, and 2.35, respectively [91].

Equations 25–27 show the three separate non-linear models that can be written from the parameter estimates in Table 6:

$$t_r = \left\{f_{(H_2PHE^+)}t_{(H_2PHE^+)} + f_{HPHE}t_{HPHE} + \beta_1\mu^{-1} + f_{(H_2PHE^+)}\beta_2[IIR]^{\beta_3}\right\}e^{-\beta_4(\%M)} \quad (25)$$

$$t_r = \left\{f_{(H_2TYR^+)}t_{(H_2TYR^+)} + f_{HTYR}t_{HTYR} + \beta_1\mu^{-1} + f_{(H_2TYR^+)}\beta_2[IIR]^{\beta_3}\right\}e^{-\beta_4(\%M)} \quad (26)$$

$$t_r = \left\{f_{(H_2TRP^+)}t_{(H_2TRP^+)} + f_{HTRP}t_{HTRP} + \beta_1\mu^{-1} + f_{(H_2TRP^+)}\beta_2[IIR]^{\beta_3}\right\}e^{-\beta_4(\%M)} \quad (27)$$

For these models, $f_{(H_2PHE^+)}$, $f_{(H_2TYR^+)}$ and $f_{(H_2TRP^+)}$ are the fractions of the fully protonated forms of Phe, Tyr and Trp, respectively; $t_{(H_2PHE^+}$, $t_{(H_2TYR^+)}$ and $t_{(H_2TRP^+)}$ are the retention times of the fully protonated forms of Phe, Tyr and Trp, respectively; f_{HPHE}, f_{HTYR} and f_{HTRP} are the fractions of the zwitterionic forms of Phe, Tyr and Trp, respectively; t_{HPHE}, t_{HTYR} and t_{HTRP} are the retention times of the zwitterionic forms of Phe, Tyr and Trp, respectively; and β_1, β_2, β_3 and β_4 are the salt, surfactant and organic modifier effects common to each model.

Unlike $t_{(H_2A^+)}$ and t_{HA}, which depend on the identity of the individual solute, β_1, β_2, β_3 and β_4 are parameters that depend only on the mobile phase composition and, therefore, apply to all solutes. The positive parameter estimates for β_1, β_2, β_3 and β_4 indicate that the greater the ionic strength of the mobile phase, the shorter is the retention time of the injected solute; the greater the concentration of oppositely charged NaOSA in the mobile phase, the longer is the retention time of the injected solute; and the greater the concentration of MeOH in the mobile

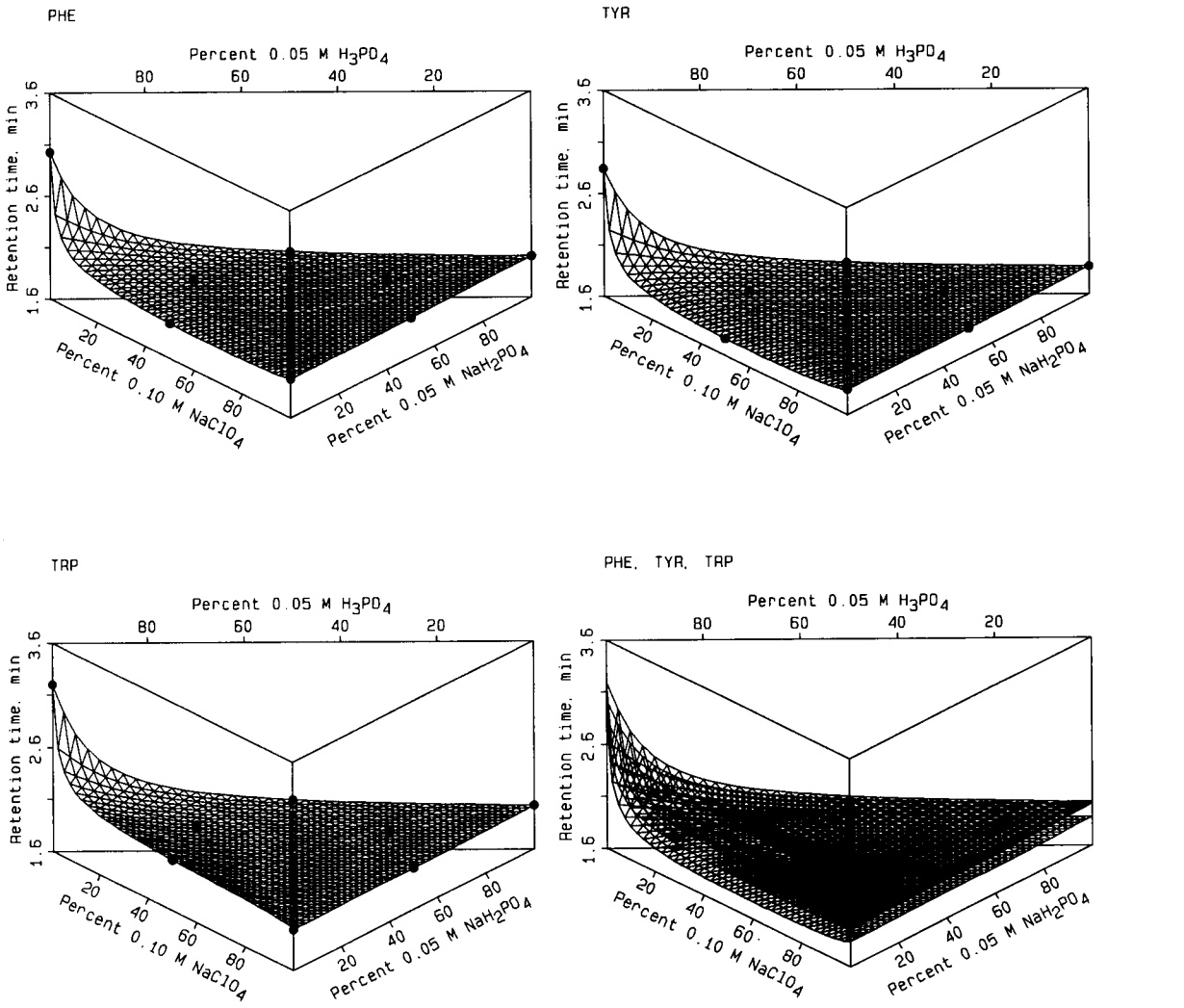

Fig. 9. Three-dimensional response surface plots of retention time of Phe, Tyr and Trp as a function of mobile phase composition for study A. A superposition of the three individual surfaces is shown in the lower right figure.

phase, the shorter is the retention time of the injected solute.

The standard error of estimate (the standard deviation of residuals) is ± 0.08 min, or ca. 5 s. Hence the standard deviation of differences in retention times is expected to be $\pm(\sqrt{2})(0.08) = \pm 0.11$ min, or ca. 7 s [91]. The coefficient of multiple determination indicates that the ten-parameter model accounts for almost 99.9% of the variability in the data set. Thus, Eqn. 24 gives a statistically adequate prediction of the retention behavior of Phe, Tyr and Trp with respect to changes in the pH (governed primarily by the concentrations of H_3PO_4 and NaH_2PO_4), the concentration of $NaClO_4$, the concentration of NaOSA and the percentage of MeOH in the mobile phase.

Observed and predicted retention behavior of Phe, Tyr and Trp

Three-dimensional response surface plots of retention time for Phe, Tyr and Trp as a function

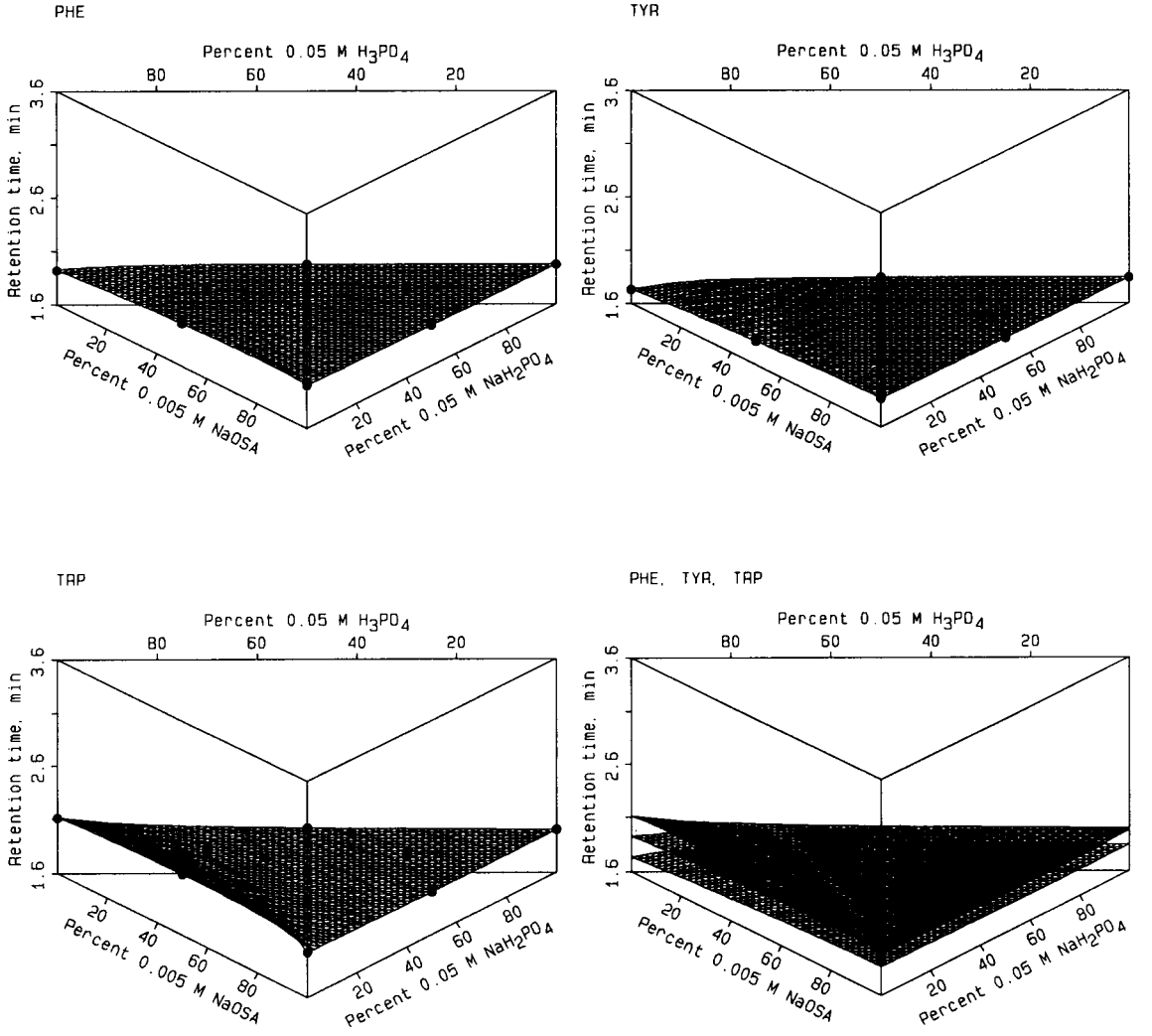

Fig. 10. Three-dimensional response surface plots of retention time of Phe, Tyr and Trp as a function of mobile phase composition for study B. A superposition of the three individual surfaces is shown in the lower right figure.

of mixture composition are shown in Figs. 9–12. Each figure also contains a superposition of all three response surfaces.

Study A. The overall shape of each response surface in Figure 9 can be attributed to changes in the ionic strength of the mobile phases. Along the right wall of each triangle, the pH of the mobile phase is relatively constant (see Fig. 5) and the ionic strength varies from ca. 0.05 M (at 100% 0.05 M NaH_2PO_4) to ca. 0.10 M (at 100% 0.10 M $NaClO_4$). Moving from the right wall toward the opposite left vertex, the ionic strength of the mobile phase is greatly decreased (to ca. 0.01 M) as the ionic $NaClO_4$ and NaH_2PO_4 are depleted and only the partially dissociated 0.05 M H_3PO_4 is present. This decrease in ionic strength results in greatly increased solute retention as predicted by Eqn. 21 [122].

Previous work [40–42,111,125,127] has demonstrated that the retention time of weak acids and weak bases should behave sigmoidally as a function of the pH of the mobile phase. In this study,

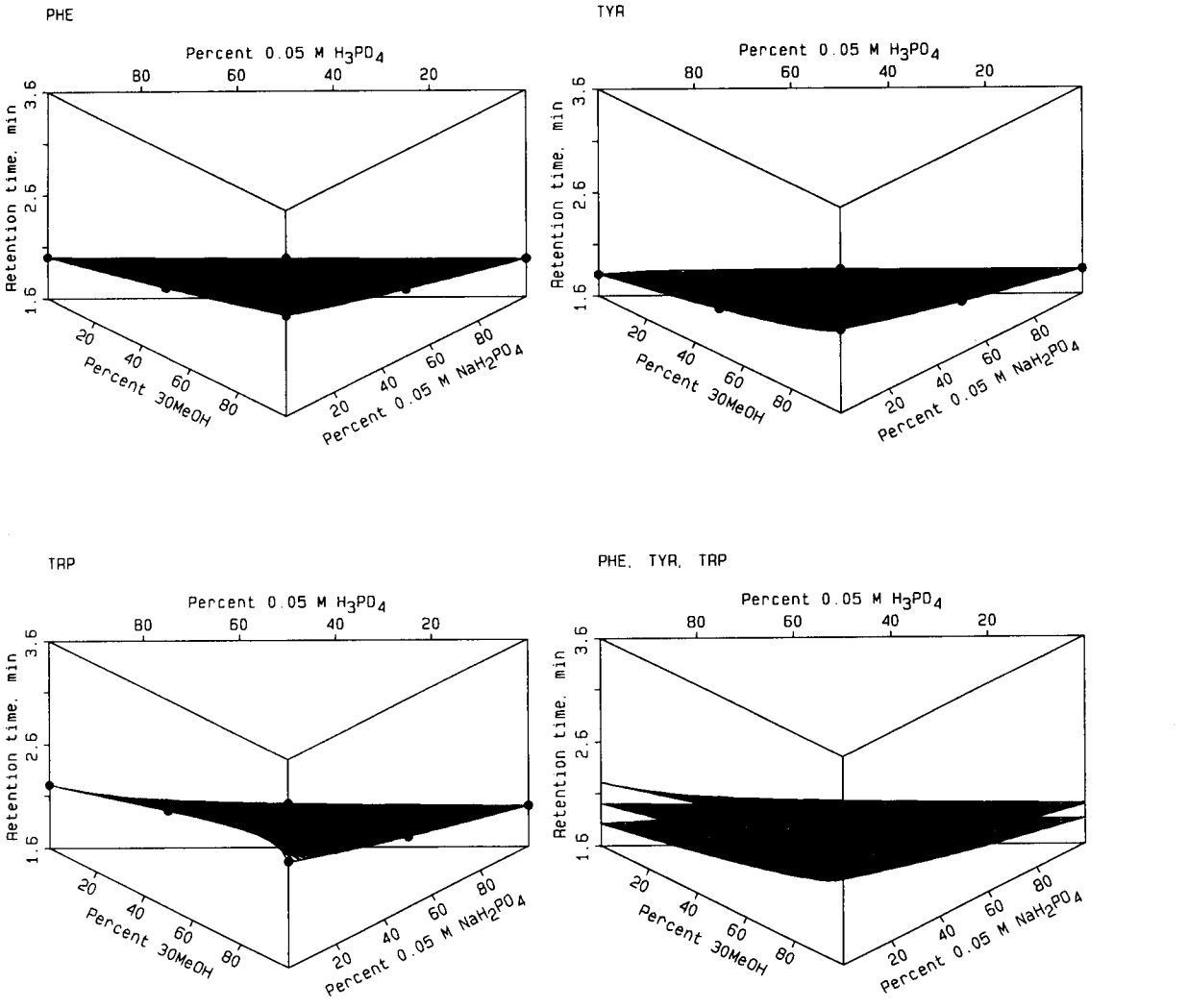

Fig. 11. Three-dimensional response surface plots of retention time of Phe, Tyr and Trp as a function of mobile phase composition for study C. A superposition of the three individual surfaces is shown in the lower right figure.

however, the expected effect of pH has been masked by the dominating effect of ionic strength over most of the experimental domain.

As shown by the superposition of the three response surfaces in the lower right panel of Fig. 9, variation in the concentrations of the three pseudo-component mobile phases in this study has very little effect on the separation of a mixture of Phe, Tyr and Trp; this is confirmed in the upper left panel of Fig. 13, which shows chromatograms of a sample containing Phe, Tyr and Trp for the various eluent mixtures. However, these chromatograms do clearly demonstrate the effect of ionic strength on peak shape: moving away from the right edge toward the opposite vertex, the shape of the solute peak remains sharp with little evidence of band broadening or tailing until the NaH_2PO_4 and $NaClO_4$ have been completely depleted from the mobile phase (at 100% 0.05 M H_3PO_4) where the solutes elute as a broad band that has obvious tailing.

Study B. In Fig. 10, there is little change in solute retention as a function of composition. The presence of 0.05 M $NaClO_4$ in each of the

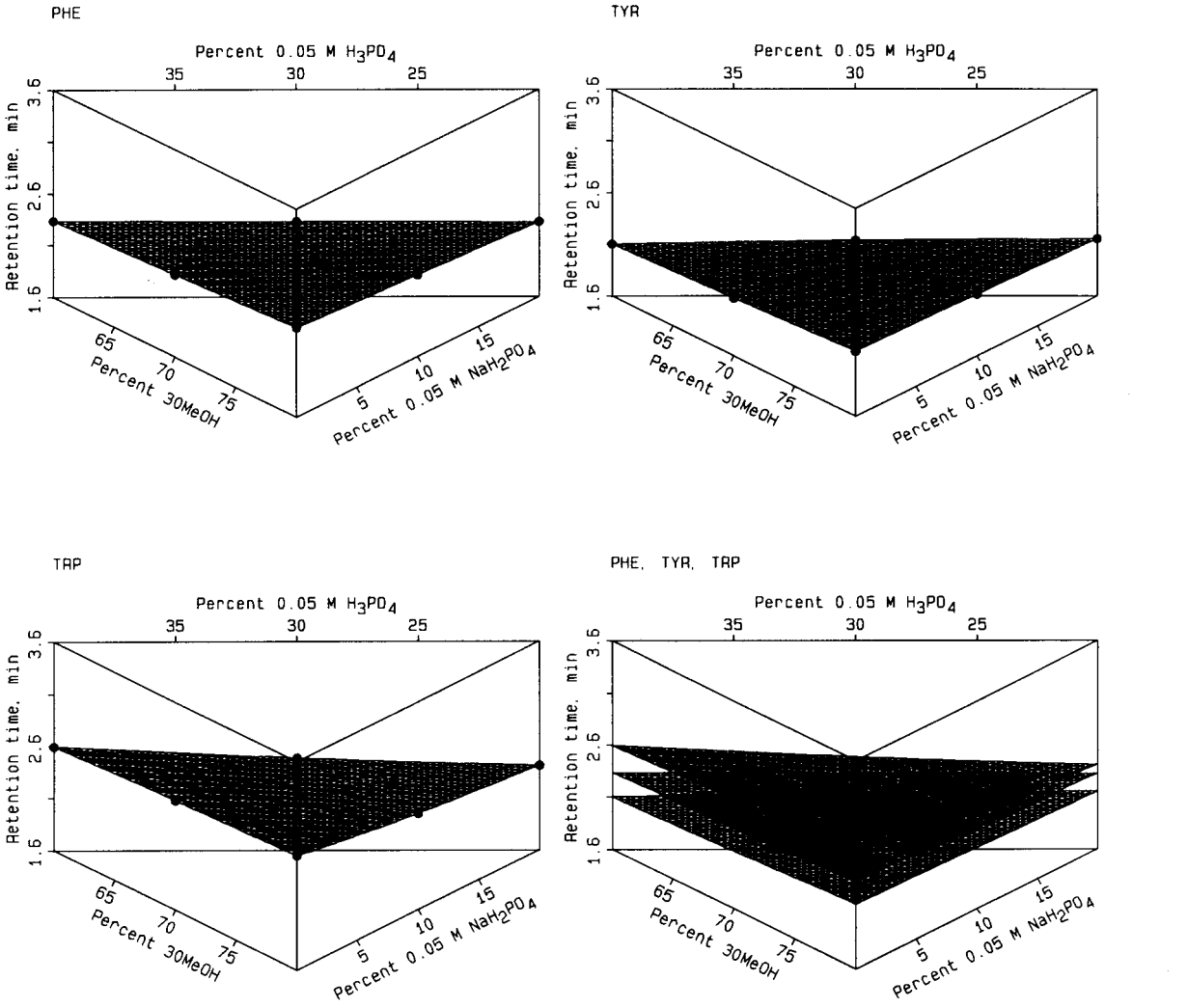

Fig. 12. Three-dimensional response surface plots of retention time of Phe, Tyr and Trp as a function of mobile phase composition for study D. A superposition of the three individual surfaces is shown in the lower right figure.

pseudo-component mobile phases in study B attenuates the ionic strength effect observed in study A.

Previous investigators have shown that surface-active ions have very little or no effect on the retention behavior of zwitterionic solutes [118]: the electrostatic forces that normally exist between a singly charged IIR and a zwitterionic solute are negligible, presumably because of the cancelling effects of the attracted positively charged amine group and the repelled negatively charged carboxylate group [118]. Hence NaOSA should have a minimal effect on the retention time of the zwitterionic form of the amino acids.

Along the right wall of each triangle in Fig. 10, the solutes have a greater tendency to exist in their zwitterionic form. At the opposite left vertex and a lower pH, the solutes Phe, Tyr and Trp have a greater tendency to exist in the fully protonated, positively charged form and are expected to be retained more strongly on the column by the presence of the oppositely charged OSA^- ion [24,122,125,126,128–135]. In this study, however, any effect of NaOSA seems to have been suppressed, probably by the high salt content of the mobile phases.

The superposition of the three response surfaces in the lower right panel of Fig. 10 predicts

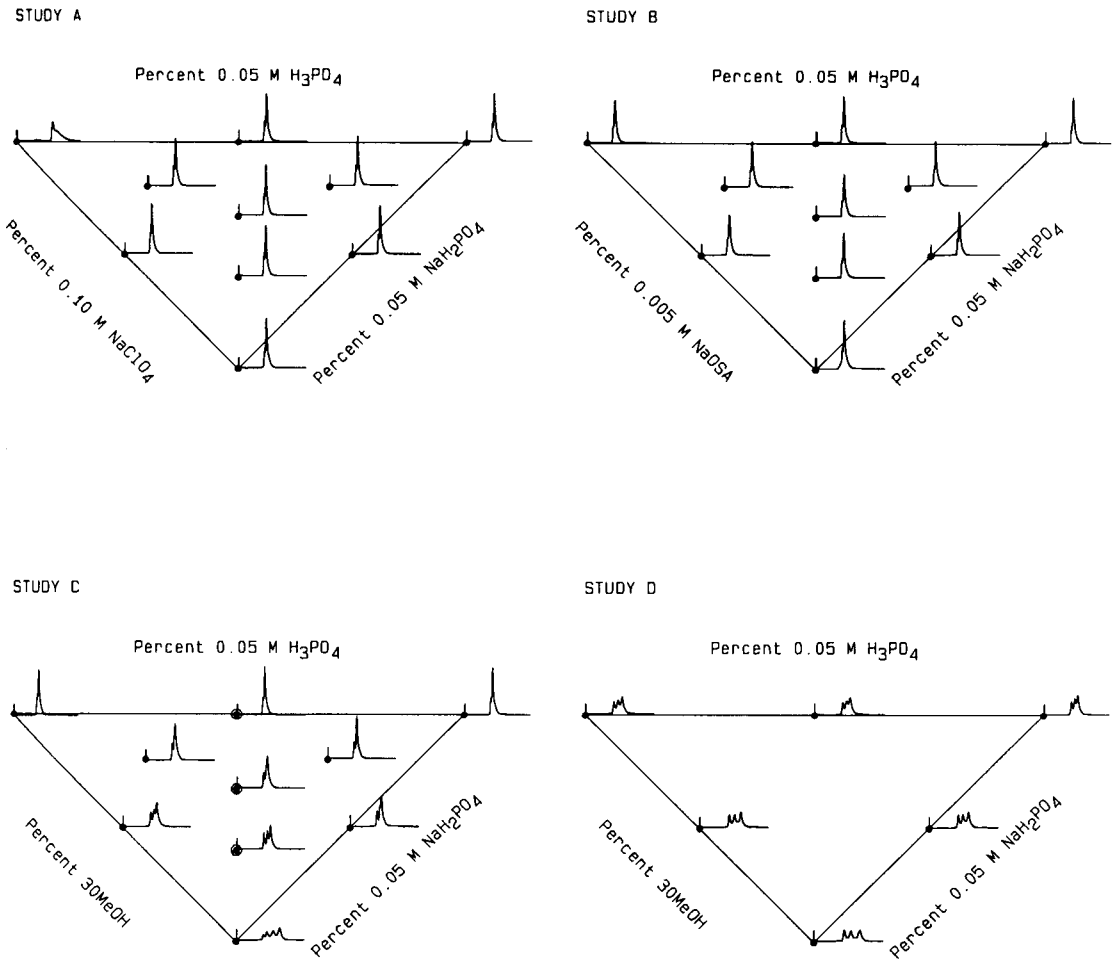

Fig. 13. Typical chromatograms of a mixture of Phe, Tyr and Trp from studies A–D.

an improved separation of a mixture of Phe, Tyr and Trp in the region of high H_3PO_4 concentration. As shown by the chromatograms in the upper right panel of Fig. 13, any improvement still does not result in a useable separation.

Study C. Fig. 11 illustrates the effect of organic modifier on the retention behavior of Phe, Tyr and Trp [44,90,122–126]. This effect can be observed by moving from the back wall of each triangle toward the front vertex: as the concentration of organic modifier decreases (30MeOH replaces 70MeOH), all three solutes show an increase in retention time.

The superposition of the three response surfaces in the lower right panel of Fig. 11 predicts an improved separation of Phe, Tyr and Trp in the region of ca. 60–80% 30MeOH where the sandwich of surfaces is the widest. As shown by

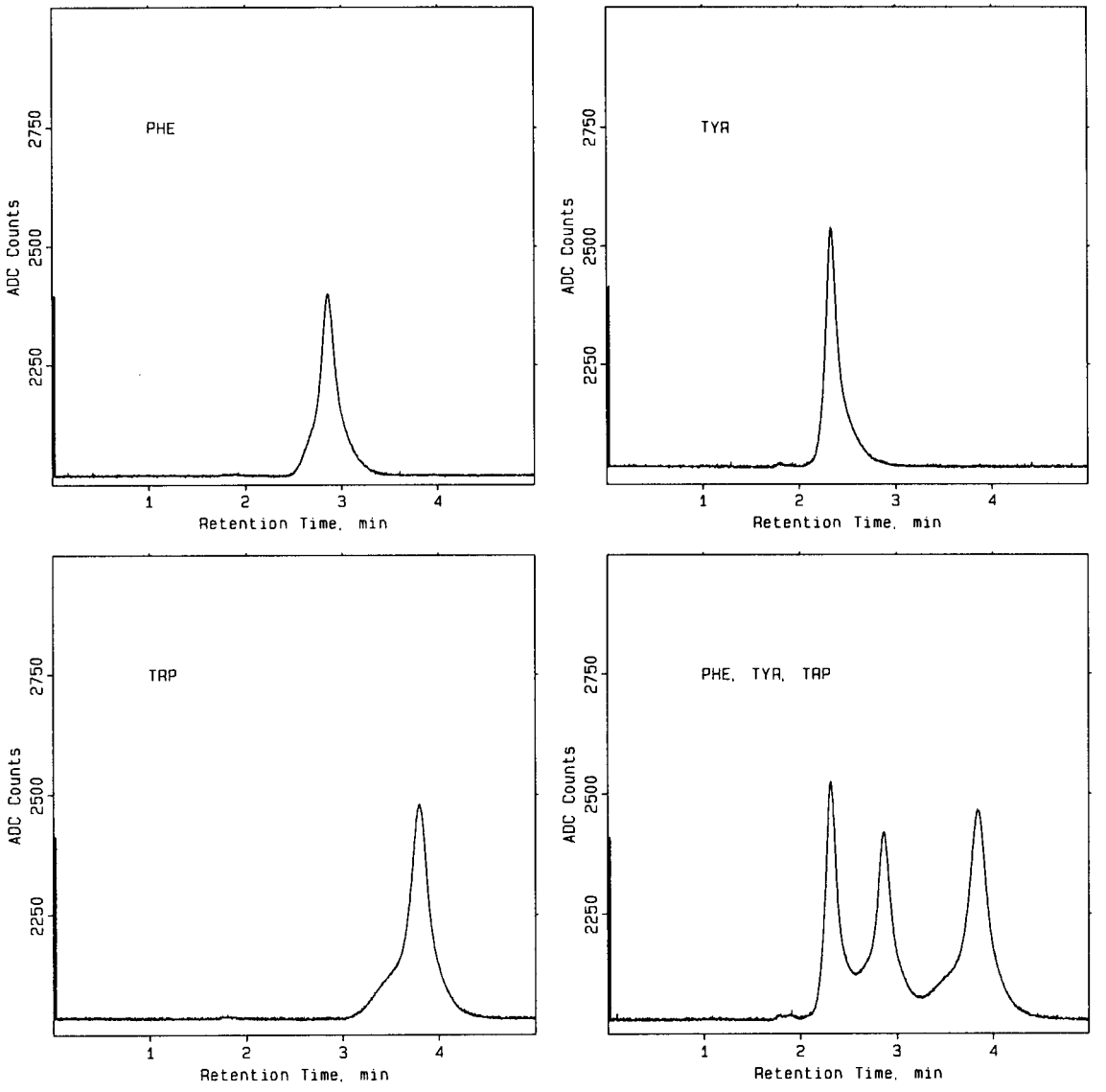

Fig. 14. Chromatograms of Phe, Tyr and Trp and a mixture of Phe, Tyr and Trp. Mobile phase: 30MeOH, 0.0515 M H_3PO_4, 0.00251 M NaH_2PO_4 and 0.100 M $NaClO_4$. Average pH = 2.13. Flow-rate = 1.60 ml min^{-1}.

the actual chromatograms in the lower left panel of Fig. 13, this is the region of greatest chromatographic separation.

The importance of MeOH is particularly evident in the differences among the three chromatograms at those mobile phases containing a constant 1:1 ratio of H_3PO_4 to NaH_2PO_4 (those marked with open circles). Under these conditions of ca. constant pH, a decrease in the overall MeOH concentration in the mobile phase (increase in 30MeOH and decrease in 70MeOH) results in increased resolution of the three solute components [44,90,122–126].

Study D. Fig. 12 predicts a good separation of all three solutes over the restricted domain of organic modifier composition. Chromatograms are shown in the lower right panel of Fig. 13. All six chromatograms confirm the feasibility of effecting a separation over this region of factor space. The best separations appear at lower pH (region of the left side) and decreased organic modifier content (region of the lower vertex).

Grid-search optimization

A grid-search program was written to evaluate the pH and retention time models and predict the mobile phase composition which would give an optimum separation of Phe, Tyr and Trp. The search was carried out at all possible combinations of 21 levels of each of the five factors (H_3PO_4, NaH_2PO_4, $NaClO_4$, NaOSA and MeOH) investigated in this work. The minimum, maximum and predicted optimum concentrations of each of the factors in this 21^5 grid [72–74] are provided in Table 7.

TABLE 7

Minimum, maximum and optimum concentrations of each of the five factors in the 21^5 grid-search experiment

Factor	Concentration [a]		
	Minimum	Maximum	Optimum
[$NaClO_4$]	0.0000	0.1000	0.1000
[NaOSA]	0.0000	0.0050	0.0000
%MeOH	30.0000	70.0000	30.0000
[H_3PO_4]	0.0000	0.0500	0.0500
[NaH_2PO_4]	0.0000	0.0500	0.0025

[a] The concentration of MeOH is expressed as a percentage; all other concentrations are expressed in units of molarity.

TABLE 8

Predicted and actual mobile phase pH and retention times for the 21^5 grid-search experiment (flow-rate = 1.60 ml min^{-1})

Parameter	Predicted result	Actual result
pH	1.3895	2.15
		2.10
$t_{R_{Trp}}$ (min)	2.8282	3.772
		3.780
$t_{R_{Phe}}$ (min)	2.2573	2.962
		2.833
		2.840
$t_{R_{Tyr}}$ (min)	1.8586	2.305
		2.272

Chromatograms of each of the individual solutes plus a mixture of the three solutes are shown in Fig. 14. The corresponding predicted and actual mobile phase pH and retention times are given in Table 8.

Conclusion

The development and validation of retention models for application to RP-LC systems have been described on several occasions recently [136–138]. This work has demonstrated the systematic application of classical mixture designs to improve the separation of a mixture of structurally similar amino acids by RP-LC. This approach to improved chromatographic separation is advantageous because mobile phase preparation is minimized: only pseudo-component mobile phases need to be prepared by the analyst; these can then be mixed in various proportions to make up the other mobile phases. One problem with mixture designs, however, is the confounding of factor effects: it is not possible to determine the effect of one factor at a single level of all of the other factors in the system. Hence, in such constrained systems, the overall effect of a single factor cannot be established with absolute certainty.

This work was supported by Grant Number 003652-108 from the Advanced Technology Program, Texas Higher Education Coordinating

Board, Division of Research Programs, and Grant Number CR-817552 from the United States Environmental Protection Agency. The authors thank Dr. Frederick H. Walters for helpful discussions at the beginning of this project and Dr. Stephen L. Morgan for suggestions on programming the non-linear pH model.

REFERENCES

1 J. Rosmus and Z. Deyl, Chromatogr. Rev., 13 (1971) 163.
2 J. Rosmus and Z. Deyl, J. Chromatogr., 70 (1972) 221.
3 Z. Deyl, J. Chromatogr., 127 (1976) 91.
4 R. Pfeifer, R. Karol, J. Korpi, R. Burgoyne and D. McCourt, Am. Lab., 15 (3) (1983) 78.
5 E. Grushka and R.P.W. Scott, Anal. Chem., 45 (1973) 1626.
6 C.W. Gehrke, H. Nakamoto and R.W. Zumwalt, J. Chromatogr., 45 (1969) 24.
7 C.W. Gehrke and H. Takeda, J. Chromatogr., 76 (1973) 63.
8 H. Lindley and P.C. Davis, J. Chromatogr., 100 (1974) 117.
9 O. Grahl-Nielsen, J. Chromatogr., 93 (1974) 229.
10 Z. Deyl and J. Rosmus, J. Chromatogr., 20 (1965) 514.
11 J.P. Zanetta, G. Vincendon, P. Mandel and G. Gombos, J. Chromatogr., 51 (1970) 441.
12 N. Seiler and M. Wiechmann, Fresenius' Z. Anal. Chem., 220 (1966) 109.
13 D.H. Spackman, W.H. Stein and S. Moore, Anal. Chem., 30 (1958) 1190.
14 P.B. Hamilton, Anal. Chem., 35 (1963) 2055.
15 S. Moore, D.H. Spackman and W.H. Stein, Anal. Chem., 30 (1958) 1185.
16 J.R. Cronin and P.E. Hare, Anal. Biochem., 81 (1977) 151.
17 M. Roth and A. Hampaï, J. Chromatogr., 83 (1973) 353.
18 S. Udenfriend, S. Stein, P. Böhlen, W. Dairman, W. Leimgruber and M. Weigele, Science, 178 (1972) 871.
19 E.J. Kikta, Jr., and E. Grushka, J. Chromatogr., 135 (1977) 367.
20 G.W.-K. Fong and E. Grushka, J. Chromatogr., 142 (1977) 299.
21 G.W.-K. Fong and E. Grushka, Anal. Chem., 50 (1978) 1154.
22 M.T.W. Hearn and B. Grego, J. Chromatogr., 203 (1981) 349.
23 M.T.W. Hearn, W.S. Hancock and C.A. Bishop, J. Chromatogr., 157 (1978) 337.
24 M.T.W. Hearn, B. Grego and W.S. Hancock, J. Chromatogr., 185 (1979) 429.
25 C.A. Bishop, W.S. Hancock, S.O. Brennan, R.W. Carrell and M.T.W. Hearn, J. Liq. Chromatogr., 4 (1981) 599.
26 D.J. Pietrzyk and C.-H. Chu, Anal. Chem., 49 (1977) 860.
27 E. Bayer, E. Grom, B. Kaltenegger and R. Uhmann, Anal. Chem., 48 (1976) 1106.
28 D.W. Hill, F.H. Walters, T.D. Wilson and J.D. Stuart, Anal. Chem., 51 (1979) 1338.
29 M.K. Radjai and R.T. Hatch, J. Chromatogr., 196 (1980) 319.
30 H. Engelhardt, J. Asshauer, U. Neue and N. Weigand, Anal. Chem., 46 (1974) 336.
31 R. Schuster, Anal. Chem., 52 (1980) 617.
32 A. Haag and K. Langer, Chromatographia, 7 (1974) 659.
33 S. Einarsson, B. Josefsson and S. Lagerkvist, J. Chromatogr., 282 (1983) 609.
34 Y. Tapuhi, D.E. Schmidt, W. Lindner and B.L. Karger, Anal. Biochem., 115 (1981) 123.
35 L. Dou and I.S. Krull, Anal. Chem., 62 (1990) 2599.
36 E.C. Huang and J.D. Henion, Anal. Chem., 63 (1991) 732.
37 S. Levin and E. Grushka, Anal. Chem., 57 (1985) 1830.
38 W.S. Hancock (Ed.), CRC Handbook of LC for the Separation of Amino Acids, Peptides and Proteins, Vol. I, CRC, Boca Raton, FL, 1984.
39 S.L. Morgan and S.N. Deming, J. Chromatogr., 112 (1975) 267.
40 S.N. Deming and M.L.H. Turoff, Anal. Chem., 50 (1978) 546.
41 W.P. Price, Jr., and S.N. Deming, Anal. Chim. Acta, 108 (1979) 227.
42 W.P. Price, Jr., R. Edens, D.L. Hendrix and S.N. Deming, Anal. Biochem., 93 (1979) 233.
43 B. Sachok, R.C. Kong and S.N. Deming, J. Chromatogr., 199 (1980) 317.
44 B. Sachok, J.J. Stranahan and S.N. Deming, Anal. Chem., 53 (1981) 70.
45 S.L. Morgan and S.N. Deming, Sep. Purif. Methods, 5 (1976) 333.
46 R.S. Swingle and L.B. Rogers, Anal. Chem., 44 (1972) 1415.
47 J.C. Giddings, Anal. Chem., 32 (1960) 1707.
48 T.B. Rooney and W. Aznavourian, Anal. Chem., 36 (1964) 2112.
49 B.O. Ayers, R.J. Loyd and D.D. DeFord, Anal. Chem., 33 (1961) 986.
50 E. Grushka, Anal. Chem., 42 (1970) 1142.
51 V. Svoboda, J. Chromatogr., 201 (1980) 241.
52 S. Turina, M. Trbojević and M. Kaštelan-Macan, Anal. Chem., 46 (1974) 988.
53 W. Spendley, G.R. Hext and F.R. Himsworth, Technometrics, 4 (1962) 441.
54 J.A. Nelder and R. Mead, Comput. J., 7 (1965) 308.
55 S.N. Deming and L.R. Parker, Jr., CRC Crit. Rev. Anal. Chem., 7 (1978) 187.
56 S.N. Deming and S.L. Morgan, Anal. Chim. Acta, 150 (1983) 183.
57 J. Holderith, T. Tóth and A. Váradi, J. Chromatogr., 119 (1976) 215.
58 R. Smits, C. Vanroelen and D.L. Massart, Fresenius' Z. Anal. Chem., 273 (1975) 1.

59 T. Sundén, M. Lindgren and A. Cedergren, Anal. Chem., 55 (1983) 2.
60 M.L. Rainey and W.C. Purdy, Anal. Chim. Acta, 93 (1977) 211.
61 M.W. Watson and P.W. Carr, Anal. Chem., 51 (1979) 1835.
62 J.C. Berridge, J. Chromatogr., 244 (1982) 1.
63 J.C. Berridge, J. Chromatogr., 485 (1989) 3.
64 B.M.J. De Spiegeleer, P.H.M. De Moerloose and G.A.S. Slegers, Anal. Chem., 59 (1987) 62.
65 J.A. Crow and J.P. Foley, Anal. Chem., 62 (1990) 378.
66 R.J. Laub and J.H. Purnell, J. Chromatogr., 112 (1975) 71.
67 R.J. Laub and J.H. Purnell, Anal. Chem., 48 (1976) 799.
68 R.J. Laub and J.H. Purnell, Anal. Chem., 48 (1976) 1720.
69 R.J. Laub, J.H. Purnell and P.S. Williams, J. Chromatogr., 134 (1977) 249.
70 J.J. Stranahan, S.N. Deming and B. Sachok, J. Chromatogr., 202 (1980) 233.
71 J.S. Kiel, S.L. Morgan and R.K. Abramson, J. Chromatogr., 485 (1989) 585.
72 G.E.P. Box, W.G. Hunter and J.S. Hunter, Statistics for Experimenters: an Introduction to Design, Data Analysis and Model Building, Wiley, New York, 1978.
73 S.N. Deming and S.L. Morgan, Experimental Design: a Chemometric Approach, Elsevier, Amsterdam, 1987.
74 G.E.P. Box, Biometrics, 10 (1954) 16.
75 S.L. Morgan and C.A. Jacques, J. Chromatogr. Sci., 16 (1978) 500.
76 Q.S. Wang, C.S. Zhu, B.W. Yan and H.B. Chen, Chromatographia, 31 (1991) 173.
77 J.A. Cornell, Experiments with Mixtures: Designs, Models and the Analysis of Mixture Data, Wiley, New York, 2nd edn., 1990.
78 V.L. Anderson and R.A. McLean, Design of Experiments: a Realistic Approach, Dekker, New York, 1974.
79 A.I. Khuri and J.A. Cornell, Response Surfaces: Designs and Analyses, Dekker, New York, 1987.
80 D.A. Doornbos, A.K. Smilde, J.H. de Boer and C.A.A. Duineveld, in E.J. Karjalainen (Ed.), Scientific Computing and Automation (Europe) 1990, Elsevier, Amsterdam, 1990, p. 85.
81 J.L. Glajch, J.J. Kirkland and K.M. Squire, J. Chromatogr., 199 (1980) 57.
82 J.L. Glajch, J.J. Kirkland and L.R. Snyder, J. Chromatogr., 238 (1982) 269.
83 M. De Smet, G. Hoogewijs, M. Puttemans and D.L. Massart, Anal. Chem., 56 (1984) 2662.
84 D.P. Herman, H.A.H. Billiet and L. de Galan, Anal. Chem., 58 (1986) 2999.
85 P.M.J. Coenegracht, A.K. Smilde, H.J. Metting and D.A. Doornbos, J. Chromatogr., 485 (1989) 195.
86 H.J. Issaq, Am. Lab., 15 (2) (1983) 41.
87 J.L. Glajch and J.J. KirKland, J. Chromatogr., 485 (1989) 51.
88 G. Mazerolles, D. Mathieu, R. Phan-Tan-Luu and A.M. Siouffi, J. Chromatogr., 485 (1989) 433.
89 A.K. Smilde, P.M.J. Coenegracht, C.H.P. Bruins and D.A. Doornbos, J. Chromatogr., 485 (1989) 169.
90 A. Bartha, G. Vigh and J. Ståhlberg, J. Chromatogr., 485 (1989) 403.
91 D.C. Harris, Quantitative Chemical Analysis, Freeman, New York, 3rd edn., 1991.
92 J. McMurry, Organic Chemistry, Brooks/Cole, Monterey, 1984.
93 R.D. Snee, CHEMTECH, 9 (1979) 702.
94 J.S. Murty and M.N. Das, Ann. Math. Stat., 39 (1968) 1517.
95 R.D. Snee, J. Qual. Technol., 3 (1971) 159.
96 R.A. McLean and V.L. Anderson, Technometrics, 8 (1966) 447.
97 J.A. Cornell, Technometrics, 15 (1973) 437.
98 H. Scheffé, J.R. Statist. Soc., Ser. B, 20 (1958) 344.
99 H. Scheffé, J.R. Statist. Soc., Ser. B, 25 (1963) 235.
100 F. Riedo and E. sz. Kováts, J. Chromatogr., 239 (1982) 1.
101 R.D. Snee, Technometrics, 15 (1973) 517.
102 L.R. Snyder and J.L. Glajch, J. Chromatogr., 214 (1981) 1.
103 J.L. Glajch and L.R. Snyder, J. Chromatogr., 214 (1981) 21.
104 L.R. Snyder, J.L. Glajch and J.J. KirKland, J. Chromatogr., 218 (1981) 299.
105 D.R. Cox, Biometrika, 58 (1971) 155.
106 P.J. Claringbold, Biometrics, 11 (1955) 174.
107 J.W. Gorman and J.E. Hinman, Technometrics, 4 (1962) 463.
108 N.R. Draper and W. Lawrence, J.R. Statist. Soc., Ser. B, 27 (1965) 450.
109 N.R. Draper and W.E. Lawrence, J.R. Statist. Soc., Ser. B, 27 (1965) 473.
110 W.O. Thompson and R.H. Myers, Technometrics, 10 (1968) 739.
111 B.A. Bidlingmeyer, J. Chromatogr. Sci., 18 (1980) 525.
112 H.A. Laitinen and W.E. Harris, Chemical Analysis. An Advanced Text and Reference, McGraw-Hill, New York, 2nd edn., 1975.
113 G.E.P. Box and P.V. Youle, Biometrics, 11 (1955) 287.
114 J.S. Fritz and G.H. Schenk, Quantitative Analytical Chemistry, Allyn and Bacon, Boston, 4th edn., 1979.
115 R.W. Ramette, Chemical Equilibrium and Analysis, Addison-Wesley, Reading, MA, 1981.
116 J.H. Kennedy, Analytical Chemistry: Principles, Saunders College, New York, 2nd edn., 1990.
117 H. Freiser and Q. Fernando, Ionic Equilibria in Analytical Chemistry, Wiley, New York, 1963.
118 R.C. Kong, B. Sachok and S.N. Deming, J. Chromatogr., 199 (1980) 307.
119 B.A. Bidlingmeyer and F.V. Warren, Jr., Anal. Chem., 54 (1982) 2351.
120 G.W. Castellan, Physical Chemistry, Addison-Wesley, Reading, MA, 3rd edn., 1983.
121 I.N. Levine, Physical Chemistry, McGraw-Hill, New York, 3rd edn., 1988.
122 E. Tomlinson, in W.S. Hancock (Ed.), CRC Handbook of

LC for the Separation of Amino Acids, Peptides and Proteins, Vol. I, CRC, Boca Raton, FL, 1984, p. 129.
123 P. Jandera and H. Engelhardt, Chromatographia, 13 (1980) 18.
124 R.M. McCormick and B.L. Karger, J. Chromatogr., 199 (1980) 259.
125 J.L.M. van de Venne, J.L.H.M. Hendrikx and R.S. Deelder, J. Chromatogr., 167 (1978) 1.
126 J.H. Knox and J. Jurand, J. Chromatogr., 125 (1976) 89.
127 C. Horváth, W. Melander and I. Molnár, Anal. Chem., 49 (1977) 142.
128 B.A. Bidlingmeyer, S.N. Deming, W.P. Price, Jr., B. Sachok and M. Petrusek, J. Chromatogr., 186 (1979) 419.
129 D.P. Wittmer, N.O. Nuessle and W.G. Haney, Jr., Anal. Chem., 47 (1975) 1422.
130 S.P. Sood, L.E. Sartori, D.P. Wittmer and W.G. Haney, Anal. Chem., 48 (1976) 796.
131 J.C. Kraak, K.M. Jonker and J.F.K. Huber, J. Chromatogr., 142 (1977) 671.
132 R.S. Deelder, H.A.J. Linssen, A.P. Konijnendijk and J.L.M. van de Venne, J. Chromatogr., 185 (1979) 241.
133 J.H. Knox and R.A. Hartwick, J. Chromatogr., 204 (1981) 3.
134 E. Tomlinson, T.M. Jefferies and C.M. Riley, J. Chromatogr., 159 (1978) 315.
135 C. Horvath, W. Melander, I. Molnar and P. Molnar, Anal. Chem., 49 (1977) 2295.
136 R.M.L. Marques and P.J. Schoenmakers, J. Chromatogr., 592 (1992) 157.
137 J.A. Lewis, D.C. Lommen, W.D. Raddatz, J.W. Dolan and L.R. Snyder, J. Chromatogr., 592 (1992) 183.
138 J.A. Lewis, J.W. Dolan and L.R. Snyder, J. Chromatogr., 592 (1992) 197.

Analytica Chimica Acta, 270 (1992) 39–44
Elsevier Science Publishers B.V., Amsterdam

Sensitive determination of ethacrynic acid in urine samples by reversed-phase liquid chromatography with ultraviolet detection using solid-phase extraction techniques for sample clean-up

Pilar Campíns-Falcó, Rosa Herráez-Hernández and Adela Sevillano-Cabeza

Departamento de Química Analítica, Facultad de Química, Universidad de Valencia, Burjassot (Valencia) (Spain)

(Received 9th July 1992)

Abstract

A rapid method is described for the identification and determination of ethacrynic acid in human urine samples by liquid chromatography with UV detection, the retention time of the analyte being 4.9 min. The samples were previously conditioned using C_{18} solid-phase extraction columns and chromatographed on an HP-LiChrospher RP C_{18} column (5 μm; 125 mm × 4 mm i.d.) with gradient elution with acetonitrile–acetate buffer (pH 4). The detector was set at 275 nm and furosemide was used as an internal standard. The procedure was applied to the determination of ethacrynic acid at concentrations of 0.01–10 μg ml^{-1} and the limit of detection was 6 ng ml^{-1}.

Keywords: Liquid chromatography; UV–Visible spectrophotometry; Doping; Ethacrynic acid; Extraction; Pharmaceuticals; Urine

Ethacrynic acid is a high-ceiling diuretic, primarily used in the treatment of oedema when a rapid and potent diuretic action is required. It has been used in sports in attempts to evade drug testing and to reduce body weight in sports that involve weight categories.

Spectrophotometric [1], polarographic [2], volumetric [3] and chromatographic methods [4] are available for the determination of ethacrynic acid in pharmaceutical preparations. However, only a few procedures have been described for its determination in biological samples, and most of these involve gas chromatography (GC).

Stüber et al. [5] proposed a procedure for the determination of this diuretic in plasma based on extraction with diethyl ether and derivatization with pentafluorobenzyl bromide, followed by mass spectrometric (MS) detection. This assay can be applied in the ng ml^{-1}–μg ml^{-1} range, and the limit of detection was between 10 and 20 ng ml^{-1} in guinea pig plasma. Sullivan and Fox [6] reported an assay for the determination of ethacrynic acid and its cysteine derivative in small plasma samples. The analyte was separated from the biological matrix with butyl chloride and then derivatized with trimethylpentane. An electron-capture detector was utilized. This assay can be applied to the determination of ethacrynic acid in the range 1–50 ng μl^{-1}. Recently, Singh et al. [7] compared GC–MS and liquid chromatography (LC) with UV detection for the determination of some acidic drugs, including ethacrynic acid, in the plasma and urine of horses. The drugs were extracted from the samples with dichloromethane

Correspondence to: P. Campíns-Falcó, Departamento de Química Analítica, Facultad de Química, Universidad de Valencia, Burjassot (Valencia) (Spain).

and, after evaporation, the residues were dissolved in the mobile phase for LC analysis, or derivatized with bis(trimethylsilyl)trifluoroacetamide before GC determination. In the latter system, samples containing low levels of drugs can be concentrated to increase the sensitivity; however, concentrated samples may contain interfering peaks when analysed by LC.

Although GC usually provides good sensitivity it may not be possible to analyse large numbers of samples owing to the cost involved [7]. Moreover, the time taken for analysis is higher as prior derivatization of the sample is required. This paper describes a rapid method for the determination of ethacrynic acid in human urine samples by LC with UV detection, as an alternative to GC procedures. The mobile phase composition was optimized to obtain a suitable sensitivity for both detection and determination purposes. Sensitive methods are required in detecting ethacrynic acid because of its illegitimate use in sports [7,8], and also in quantification procedures because, owing to its pharmacokinetic behaviour, its concentrations in urine samples are usually low [9].

EXPERIMENTAL

Apparatus

A Hewlett-Packard Model 1040A liquid chromatograph, equipped with a diode-array UV detector linked to a data system (Hewlett-Packard Chem Station) was used for data acquisition and storage. The system was coupled to a quaternary pump (Hewlett-Packard 1050 Series) with a 25-μl sample loop injector.

The column was an HP-LiChrospher 100 RP 18 (5 μm; 125 mm $\times$ 4 mm i.d.). Signal detection was set between 200 and 400 nm every 640 ms, and all the assays were performed at room temperature.

Reagents

All the reagents were of analytical-reagent grade except methanol and acetonitrile, which were of LC grade (Scharlau). Water was distilled, deionized and filtered through 0.45-μm nylon membranes (Teknokroma). Ethacrynic acid and internal standard (furosemide) stock solutions were prepared by dissolving pure ethacrynic acid (Sigma) and furosemide (Lasa) in methanol. Propylamine hydrochloride (Fluka), sodium acetate (Panreac) and acetic acid (Probus) were also used.

Standard solutions

Stock standard solutions of ethacrynic acid and the internal standard (2 mg ml^{-1}) were prepared by dissolving 50 mg of the pure compound in 25 ml of methanol. These solutions were stored in the dark at 2°C. Working standard solutions were prepared daily by dilution of these stock standard solutions with the appropriate volumes of methanol.

Mobile phase

An acetate buffer–acetonitrile gradient, with an increasing acetonitrile content from 20% at 0 min to 60% at min 6, was used as the mobile phase. The acetate buffer was prepared by dissolving 2 g of sodium acetate in 500 ml of distilled, deionized water, after the addition of 0.7 ml of propylamine hydrochloride. The pH was adjusted to 4 adding the minimum amount of concentrated acetic acid. The solution was prepared daily, filtered through a 0.45-μm nylon membrane and degassed with helium before use. The flow-rate was set at 1 ml min^{-1}. The chromatographic signal was monitored at 275 nm.

Sample treatment

Extra-Sep C_{18} solid-phase extraction columns, 200 mg in 3 ml (Teknokroma), for sample treatment were previously conditioned with 1.0 ml of methanol followed by 0.5 ml of distilled water. A 300-μl volume of a methanolic solution of the internal standard (1 μg ml^{-1}) was added to 2.0 ml of urine samples. The samples were then drawn through the columns and washed with 0.5 ml of distilled water to eliminate the biological matrix. The analyte and the internal standard were eluted from the column with 0.5 ml of methanol and the extracts were evaporated to dryness with a stream of nitrogen. The residues were reconstituted with 300 μl of methanol. The resulting solutions were finally filtered through

15-mm 0.45-μm nylon filters (Teknokroma) and 5 μl were injected into the column.

Recovery studies

Free urine samples (2.0 ml) were spiked with ethacrynic acid standard solutions to give different concentrations in the range 0.01–10 μg ml^{-1}. These samples were subjected to the previously described extraction procedure. The percentage of drug recovered for a particular extraction was calculated by comparing the peak-area ratio of ethacrynic acid to internal standard in the spiked samples with the peak-area ratio obtained for the direct injection of 5 μl of methanolic solutions containing an equivalent amount of drugs. Each concentration was assayed in duplicate.

Preparation of standards for calibration

Standards for calibration were prepared by spiking 2.0 ml of urine samples with the appropriate volumes of ethacrynic acid methanolic solution to give different concentrations in the range 0.01–10.0 μg ml^{-1}. These samples were extracted and chromatographed as described above. Peak-area ratios of ethacrynic acid to furosemide were plotted against ethacrynic acid concentration, and the resulting calibration graph was used to calculate the ethacrynic acid concentration in unknown samples.

RESULTS AND DISCUSSION

Acetonitrile–phosphoric acid mixtures are reportedly the most common eluents for the LC identification or determination of ethacrynic acid. However, it was found that with a mobile phase consisting of acetonitrile–0.05 M phosphate buffer with different pH values in the range 3–5, the ethacrynic acid peak is asymmetric and its intensity is low. Therefore, the limits of detection obtained are usually high, and many LC procedures that use phosphate buffers in the mobile phase do not provide adequate sensitivity for screening proposes [9,10].

In a previous test for screening of diuretics using an HP-Hypersil ODS-C_{18} analytical column (5 μm; 250 mm × 4 mm i.d.), it was demonstrated

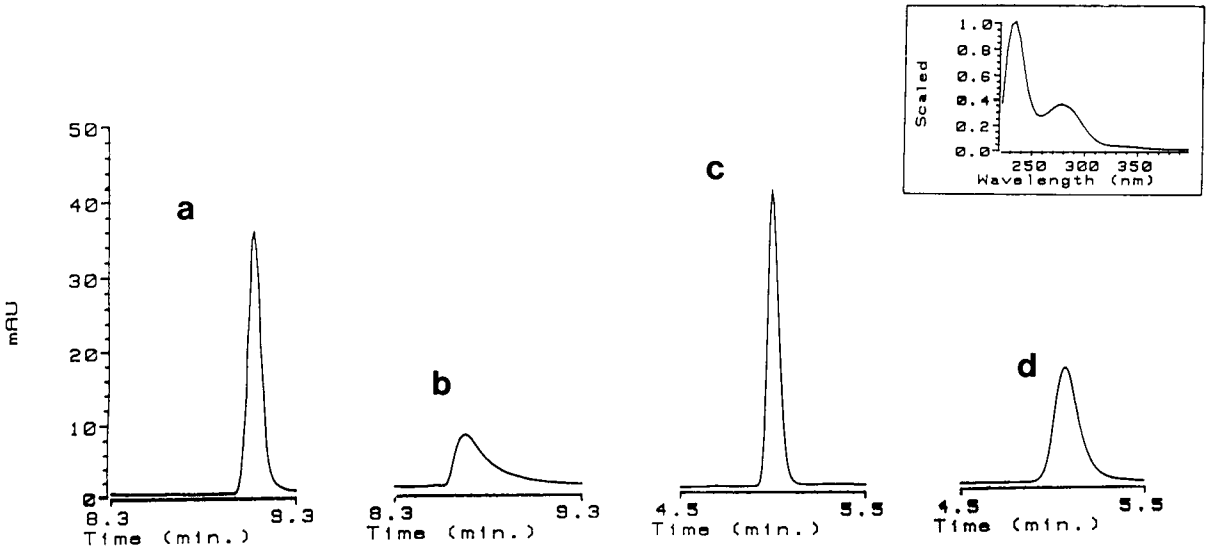

Fig. 1. Chromatograms obtained at 275 nm for ethacrynic acid in different chromatographic systems: in an HP-Hypersil ODS column with a mobile phase of (a) acetonitrile–0.05 M phosphate buffer (pH 3) and (b) acetonitrile–0.05 M acetate buffer (pH 4); and in an HP-LiChrospher RP C_{18} column with a mobile phase of acetonitrile–0.05 M acetate buffer (pH 4) with (c) gradient elution and (d) isocratic elution (30 + 70). Inset: normalized UV spectrum of ethacrynic acid.

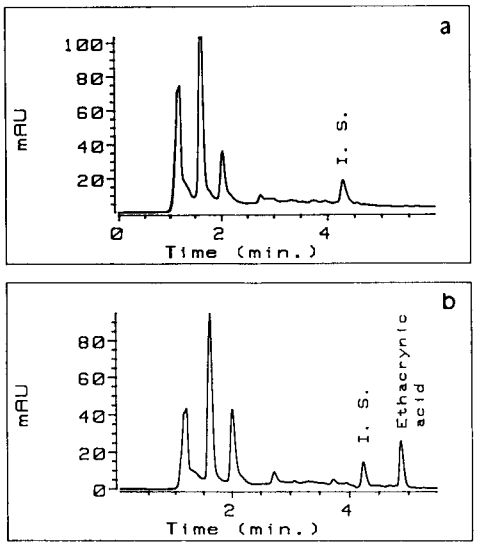

Fig. 2. Chromatograms at 275 nm of (a) blank and (b) urine sample spiked with 7.5 μg ml^{-1} of ethacrynic acid. The peak at 4.3 min corresponds to the internal standard (I.S.).

that with a mobile phase consisting of acetonitrile–acetate buffer, the chromatographic response of the more acidic compounds, such as ethacrynic acid ($pK_a = 3.5$), is increased [8], as can be seen in Fig. 1a. This figure also shows the UV spectrum of the analyte. Although wavelengths under 250 nm cannot be utilized, owing to the absorption characteristics of the acetate buffer, the sensitivity is significantly improved as the resulting peaks for ethacrynic acid were symmetrical and narrow (see Fig. 1).

TABLE 1

Recovery of ethacrynic acid at the different concentrations tested

Ethacrynic acid concentration (μg ml^{-1})	Recovery (%)
0.01	90.84
0.10	86.89
0.50	86.82
1.00	83.83
5.00	89.91
10.00	86.93
	Mean: 87 ± 4

Different gradient elution conditions were tested in order to obtain a suitable sensitivity for detecting or determining ethacrynic acid, using a LiChrospher 100 RP 18 (5 μm; 125 mm × 4 mm i.d.) column. The best results were obtained with a mobile phase consisting of acetonitrile–0.05 M acetate buffer (pH 4). The elution profile was also optimized to obtain an appropriate resolution in a short time of analysis. Chromatographic signals obtained for ethacrynic acid using isocratic conditions are less intense than those obtained in the gradient elution mode, as can be seen in Fig. 1.

TABLE 2

Analytical properties of the different chromatographic methods proposed for ethacrynic acid

Sample	Chromatographic separation	Detection	Mobile phase composition	Volume of sample (ml)	Limit of detection (μg ml^{-1})	Ref.
Human plasma	GC	MS	Helium	1.0	0.01–0.02	5
Guinea pig plasma	GC	Electron-capture	Methane–argon	0.020	< 1	6
Horse urine	GC	MS	–	1.0	0.020–0.050	7
Horse urine	LC	UV, 235 nm	Acetonitrile–0.05 M phosphate buffer	0.050	0.050–0.150	7
Human urine	LC	UV, 230 nm	Acetonitrile–0.05 M phosphate buffer (pH 3)	2.0	0.02	8
Human urine	LC	UV, 275 nm	Acetonitrile–0.05 M acetate buffer (pH 4)	2.0	0.006	This work

The employment of solid-phase extraction columns for sample treatment provides clean extracts of the drug for analysis and the recoveries of ethacrynic acid and the internal standard are greater than those obtained for the same samples using a conventional liquid–liquid extraction procedure [11]. Moreover, the chromatograms obtained show fewer background peaks (and their intensity is low) than those obtained with liquid–liquid extraction under acidic conditions, this medium being necessary to obtain suitable recoveries of the analyte [10].

Figure 2 shows chromatograms of (a) blank and (b) spiked urine samples. Under the working conditions, ethacrynic acid and the internal standard are eluted at 4.9 and 4.3 min, respectively, whereas the endogenous compounds are primarily eluted within 3 min. By comparing Fig. 2a and b it can be seen that with the proposed sample treatment and the elution conditions, the chromatograms are free from endogenous compounds which may interfere with the identification or determination of ethacrynic acid.

The extraction recoveries for the different ethacrynic concentrations tested with a C_{18} packing are given in Table 1. The efficiency and precision obtained in the sample clean-up step are adequate, with mean recoveries for ethacrynic acid of $87 \pm 4\%$ ($n = 12$) in the concentration range 0.01–10.0 $\mu g\ ml^{-1}$. For the internal standard the mean recovery obtained was $91 \pm 5\%$ ($n = 11$), similar to the value obtained for the analyte.

The calibration graphs obtained were linear over the working range 0.01–10.0 $\mu g\ ml^{-1}$, the intercept being essentially zero. The mean correlation coefficient was 0.9998. The limit of detection (for a signal-to-noise ratio of 3) corresponds to an ethacrynic acid concentration in urine of 6 $ng\ ml^{-1}$. In Table 2 this value and the limits of detection obtained with different assays previously reported for ethacrynic acid are compared. As can be seen, the sensitivity obtained with the proposed procedure is comparable to that obtained when utilizing GC procedures [5–7]. For LC procedures, the sensitivity is clearly improved when, with the same sample treatment, acetate buffer is used instead of phosphate buffer in the eluent. Although the amount of drug detected is similar in both procedures, the limit of detection in urine samples obtained with the proposed procedure is lower than that reported by Singh et al. [7]. This can be explained by the volume of sample and the eluent composition utilized. Moreover, the sensitivity cannot be increased by concentrating the sample, owing to the interference of endogenous compounds. With the sample clean-up and elution conditions used here, the samples can be concentrated without any interference from endogenous compounds. The injection of volumes of samples greater than 5 μl for chromatography is not suitable because of the increase in the background noise.

In Table 3 the results obtained for different urine samples spiked with ethacrynic acid are

TABLE 3

Precision and accuracy of the determination of ethacrynic acid in urine

Subject No.	Concentration added ($\mu g\ ml^{-1}$)	Concentration determined ($\mu g\ ml^{-1}$)	Mean value ($\mu g\ ml^{-1}$)
1	0.50	0.44	0.48 ± 0.04
		0.52	
		0.49	
	2.50	2.32	2.6 ± 0.2
		2.59	
		2.78	
	7.50	6.90	7.2 ± 0.3
		7.31	
		7.50	
2	0.50	0.51	0.51 ± 0.05
		0.47	
		0.56	
	2.50	2.55	2.57 ± 0.02
		2.58	
		2.57	
	7.50	7.02	7.3 ± 0.5
		7.10	
		7.89	
3	0.50	0.55	0.51 ± 0.05
		0.47	
		0.44	
	2.50	2.56	2.57 ± 0.02
		2.54	
		2.45	
	7.50	7.34	7.3 ± 0.5
		7.76	
		7.68	

summarized. The measured concentrations are close to the actual concentrations in all instances. It can be concluded that the method is both accurate and precise, with relative standard deviations ranging between 1% and 10% for concentrations of 2.50 and 0.50 μg ml^{-1}, respectively.

Conclusion

An LC system for the identification and determination of ethacrynic acid in urine samples has been developed. The chromatographic conditions were optimized to obtain a sensitivity comparable to that provided by GC procedures. The assay is very rapid as no prior derivatization of the analyte is required. Moreover, the use of solid-phase extraction columns saves time in the sample preparation step and provides high recoveries of the analyte.

The authors are grateful to the DGICYT for financial support for the realization of Project PB 88-0495.

REFERENCES

1 V. Cavrini, D. Bonazzi, A.M. Di Pietra and R. Gatti, Analyst, 114 (1989) 1307.
2 G. Shen, X. Shi and R. Yu, Yaoxue Xuebao, 22 (1987) 841.
3 S.R. Shukla, I.C. Shukla and V.N. Pathak, East. Pharm., 26 (1983) 129.
4 R.J. Yarwood, W.D. Moore and J.H. Collett, J. Pharm. Sci., 74 (1985) 220.
5 W. Stüber, E. Mutschler and D. Steinbach, J. Chromatogr., 227 (1982) 193.
6 W.R. Sullivan and K.E. Fox, J. Chromatogr., 452 (1988) 396.
7 A.S. Singh, Y. Jang, U. Mishra and K. Granley, J. Chromatogr., 568 (1991) 351.
8 R. Herráez-Hernández, P. Campíns-Falcó and A. Sevillano-Cabeza, J. Liq. Chromatogr., in press.
9 R.O. Fullinfaw, R.W. Burry and R.F.W. Moulds, J. Chromatogr., 415 (1987) 347.
10 S.F. Cooper, R. Massé and R. Dugal, J. Chromatogr., 489 (1989) 65.
11 P. Campíns-Falcó, R. Herráez-Hernández and A. Sevillano-Cabeza, J. Liq. Chromatogr., 14 (1991) 3575.

Analytica Chimica Acta, 270 (1992) 45–53
Elsevier Science Publishers B.V., Amsterdam

Liquid chromatographic and spectrofluorimetric determination of aspartame and glutamate in foodstuffs following fluorescamine fluorigenic labelling

F. García Sánchez and A. Aguilar Gallardo

Department of Analytical Chemistry, Faculty of Sciences, University of Málaga, 29071 Málaga (Spain)

(Received 13th April 1992)

Abstract

A spectrofluorimetric method for determining aspartame (AS) and sodium glutamate (GL) based on labelling with fluorescamine (FC) was developed. Mixtures of AS and GL were analysed by isodifferential synchronous derivative spectrofluorimetry. R.S.D.s of 6.4% and 3.0% were obtained by the individual methods. Detection limits of 0.03 and 0.1 μg ml^{-1} were obtained for AS and GL, respectively. On the basis of the FC derivatization procedure, a liquid chromatographic method to determine AS and GL was developed. R.S.D.s of 0.62 and 0.34% were obtained with fluorimetric detection and 2.26 and 3.14% with photometric detection at 395 nm. Detection limits were 0.04 and 0.02 μg ml^{-1} (spectrofluorimetric detection) and 0.2 and 0.1 μg ml^{-1} (spectrophotometric detection) for AS and GL, respectively. These methods were applied to the determination of AS in carbonated soft drinks and GL analyses in commercial dried soups.

Keywords: Fluorimetry; Liquid chromatography; Aspartame; Foods; Glutamate

Aspartame, a dipeptide (*N*-L-α-aspartyl-L-phenylalanine 1-methyl ester), has a sweetening power 180 times that of sucrose [1]. It is often used as substitute for saccharin in foods and as a sweetener in carbonated drinks. It is synthesized from L-aspartic acid and L-phenylalanine [2]. Although aspartame is not toxic, high concentrations may cause illness and so the aspartame content in foods is controlled by the health authorities in many countries. Methods for the determination of aspartame in foods are generally based on gas chromatography [3] and liquid chromatography (LC) [4–7].

L-Glutamic acid enhances flavours and the sodium salt is widely used as a food additive. Although about 500 000 metric tons of glutamate are consumed annually, high doses may be toxic and the World Health Organization sets a limit of 120 mg kg^{-1} body weight as the maximum daily dose [8]. The Association of Official Analytical Chemists recommends potentiometric titration of the previously ion-exchanged monosodium glutamate [9]. Spectrophotometric [10], spectrofluorimetric [11] and chromatographic methods [12–14] have also been described.

In this work, the optimum experimental conditions were investigated for the spectrofluorimetric determination of aspartame and glutamate based on fluorophore generation by derivatization with fluorescamine (FC). Reversed-phase LC determination of AS and GL with precolumn derivatization was also carried out and applied to real samples.

Correspondence to: F. García Sánchez, Department of Analytical Chemistry, Faculty of Sciences, University of Málaga, 29071 Málaga (Spain).

EXPERIMENTAL

Apparatus

The spectra (range 250–600 nm) were obtained at room temperature with a Perkin-Elmer LS-50 luminescence spectrometer, fitted with a xenon lamp (9.9 W) pulsed at line frequency, 1×1 cm fused-silica cells and a R928 Hamamatsu photomultiplier. Slit widths were set at 5/5 nm. The emission spectra were not corrected for non-linear instrumental response.

The LC equipment included a Merck–Hitachi L-6200 pump. Injections were made with a Merck–Hitachi AS-4000 autosampler. A Merck–Hitachi L-4250 UV–visible detector was also used. The analogue signals were converted into digital signals by a Merck–Hitachi D-6000 interface. Integration was made with a PC/AT computer and the instrumental parameters were controlled by Merck–Hitachi HM software. A Spherisorb S5 ODS-2 reversed-phase column (200×4.6 mm i.d. 5 μm particle size) and a Spherisorb S5 ODS-2 precolumn (60×4.6 mm i.d.; 5 μm particle size) was used; the mobile phase was buffer (pH 9)–acetonitrile–methanol at a flow-rate of 0.5 ml min^{-1}.

Sequential spectra of eluted peaks were recovered with a Model ABI-1000S diode-array detector (Applied Biosystems). The data obtained with this system were processed and analysed by means of Labcal software (Galactic, Salem, NH).

The LS-50 spectrofluorimeter was used as a detector on-line with the UV–visible or diode-array spectrophotometer.

Reagents

Aqueous stock standard solutions of the L-aspartyl-L-phenylalanine methyl ester (Aldrich) (5.91×10^{-3} M) and monosodium L-glutamate (Aldrich) (3.59×10^{-3} M) were prepared weekly. Working standard solutions were prepared from these by appropriate dilution.

Analytical-reagent-grade fluorescamine {4-phenylspiro[furan-2(3*H*),1′-phthalan]-3,3′-dione} was obtained from Aldrich and was dissolved in acetone (1 mg ml^{-1}).

Phosphate buffer solution (0.2 M) and sodium borate–HCl buffer solution (0.2 M) were prepared from potassium and sodium salts (Merck), respectively.

All solvents were of analytical-reagent grade (Merck) and demineralized water was used throughout. LC mobile phases were of Lichrosolv gradient grade (Merck).

Spectrofluorimetric method

In 10-ml volumetric flasks were placed the appropriate volumes containing mixtures of AS and GL with concentrations between 0.1 and 1 μg ml^{-1}, 1 ml of FC (3.4×10^{-3} M) and 2 ml of buffer solution (pH 9). The solution was then diluted with water. The synchronous first-derivative spectra were recorded at $\Delta\lambda = 90$ nm for AS and $\Delta\lambda = 85$ nm for GL.

The relative fluorescence intensity (RFI) and the derivative values (expressed in cm) were converted into units of concentration by applying the corresponding regression equations or calibration graphs.

LC method

Aliquots of 15–300 μl of aqueous standard solutions of AS and GL (10 μg ml^{-1}) were introduced in a 1.5-ml flask and 150 μl of a 3.4×10^{-3} M acetone solution of FC and 300 μl of pH 9 buffer solution were added. The mixture was diluted to 1.5 ml and shaken for 10 s.

Volumes of 10 μl of this solution were injected into the chromatograph and eluted with pH 9 buffer–acetonitrile–methanol (50 + 25 + 25, v/v/v) at a flow-rate of 0.5 ml min^{-1}. Two detectors on-line (UV–visible and spectrofluorimetric) set at 395 and 395/482 nm, respectively, gave the peaks corresponding to GL and AS at $t_R = 3.12$ and 4.14 min, respectively, for UV–visible detection and at 3.5 and 4.5 min, respectively, for fluorimetric detection.

RESULTS AND DISCUSSION

Because of their amine character, AS and GL react with FC to form two fluorophores whose spectra are very similar. Figure 1 shows the excitation and emission spectra of the FC derivatives of AS and GL under the final experimental con-

ditions. As expected, the spectral parameters for both compounds are similar. Each compound was characterized by its well resolved excitation maximum and its single emission peak, at 393/483 and 397/482 nm for AS and GL, respectively.

The operating parameters for the individual compounds can be optimized to give one analytical method for each. However, as this work shows, the spectra of both compounds overlap considerably and this precludes the use of normal spectrofluorimetry to determine the individual compounds in mixtures. Consequently, after fixing the individual optimum conditions for determining AS and GL, a new set of conditions was selected to obtain good emission signals for each compound before carrying out the analysis of mixtures of AS and GL.

As a fluorigenic reagent for amino compounds, FC lacks selectivity, which emphasizes the need for more detailed information about the effect of the main reaction conditions so that the fluorescence yield might be improved to permit the selective analysis of mixtures of fluorophores with FC.

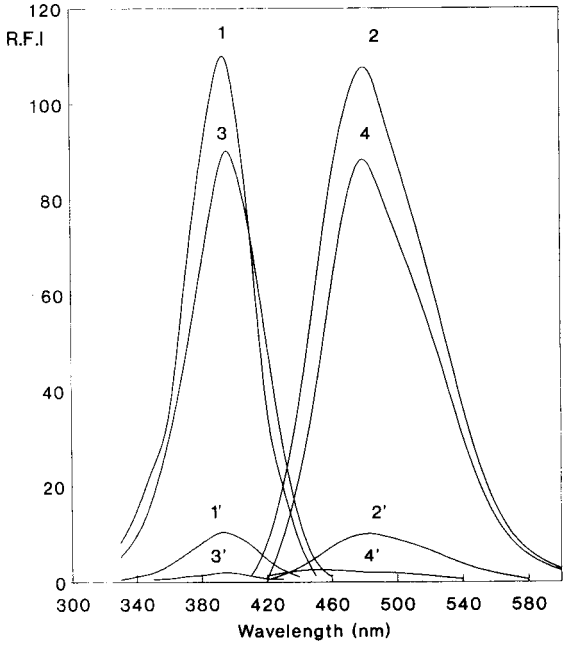

Fig. 1. Excitation and emission spectra of FC derivatives of (1, 2) AS and (3, 4) GL and the respective blank solutions (1'-4'). [AS] = 2.5 μg ml^{-1}, pH 7.5; [GL] = 2.5 μg ml^{-1}, pH 9.0.

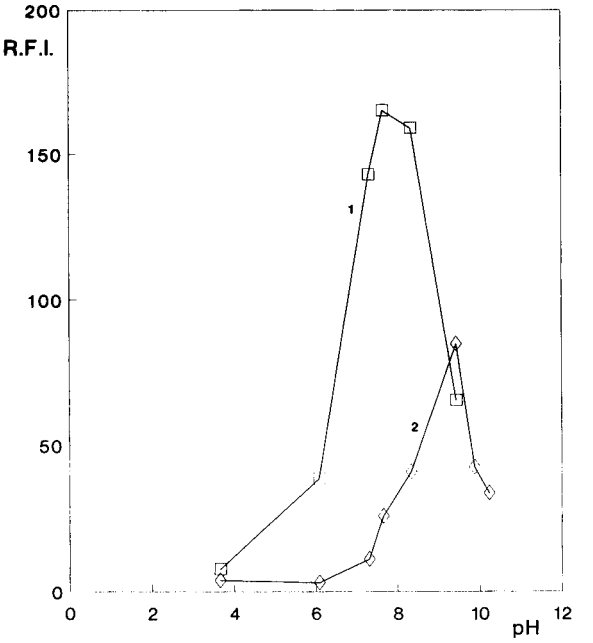

Fig. 2. Influence of pH on the relative fluorescence intensity of (1) AS and (2) GL. [AS] = [GL] = 5 μg ml^{-1}; [FC] = 3.6 × 10^{-4} M.

Influence of reaction variables

The effect of pH on fluorescence intensity was explored by carrying out several assays of solutions that contained 5 μg ml^{-1} AS or GL and 2 ml of different buffer solutions that covered the pH range 3.8–10, together with 1 ml of FC standard solution.

The results in Fig. 2 show that the maximum fluorescence for the AS fluorophore occurred at pH 7.5 and that of GL at pH 9. In both instances, the narrow range in which the fluorescence intensity was maximum suggests that careful control of the solution pH is required. On the other hand, to obtain good yields in the labelling reactions of mixtures of both compounds, the pH setting must be a compromise and in this work pH 9 appeared to be the optimum.

FC reacts very quickly with primary amines ($t_{1/2}$ = 100–500 ms), but frequently a great excess of FC is needed to produce good thermodynamic

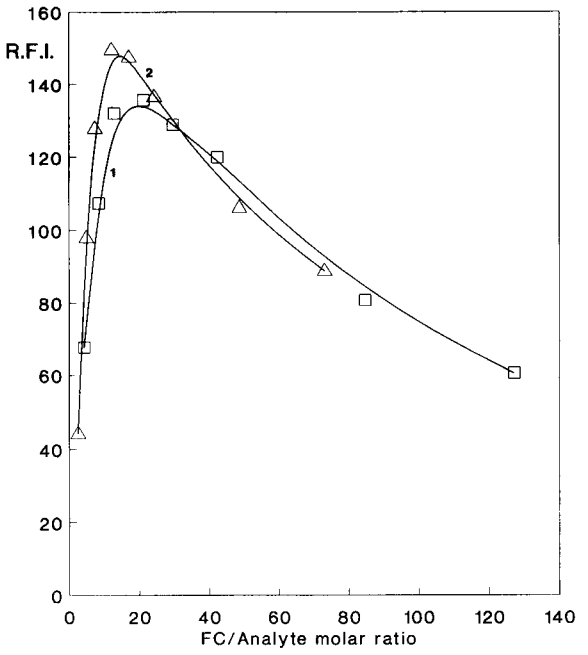

Fig. 3. Influence of the FC/analyte molar ratio on the relative fluorescence intensity of (1) AS (pH 7.5) and (2) GL (pH 9.0).

equilibrium conditions, as described previously [15].

The effect of FC concentration on fluorophore formation was observed by measuring the fluorescence intensity for each compound at different FC/analyte molar ratios, while all other experimental conditions were kept constant at the optimum values. Figure 3 shows that maximum response was obtained when the FC/analyte molar ratio was within the range 12:1–20:1; in subsequent work a ratio of 15:1 was employed for the individual determinations of AS and GL. For the simultaneous determination of the two compounds a molar ratio of 25:1 was selected.

Influence of instrumental parameters

Spectrofluorimetric method. The synchronous scanning first-derivative fluorimetric approach takes advantage of the band-narrowing effect of synchronous scanning to maximize the first-derivative amplitudes. In this way, better sensitivity may be obtained, especially if the normal spectra show broad profiles and, on the other hand, improved selectivity in multi-component analyses was obtained when the graphical method of plotting isodifferential amplitude measurements was used.

The wavelength scanning interval ($\lambda_{em} - \lambda_{ex} = \Delta\lambda$), a critical parameter for spectral shape, was optimized by using the sequential recovery of synchronous spectral data with newly modified software. The best results were obtained at $\Delta\lambda$ = 90 and $\Delta\lambda$ = 85 nm for AS and GL, respectively.

As can be seen in Fig. 1, the excitation/emission spectra of AS and GL overlap. However, as shown in Fig. 4, the first derivatives of the synchronous spectra corresponding to the same component at different concentrations have values of zero on the ordinate scale (differential fluorescence). This so-called isodifferential point indicates that the contribution of this component to the overall derivative signal is zero, as discussed earlier, and consequently the amplitudes of the derivative spectra from this wavelength to the break with the experimental derivative curve of the mixture are independent of this component.

Figure 4 also shows that the isodifferential points corresponding to the AS and GL series are located at 393 and 397 nm, respectively.

LC Method. Optimization of LC parameters was performed by seeking the separation of the peaks corresponding to GL and AS derivatives, allowing separate peak integration. Figure 5 shows the contour plot of 500 spectra collected during

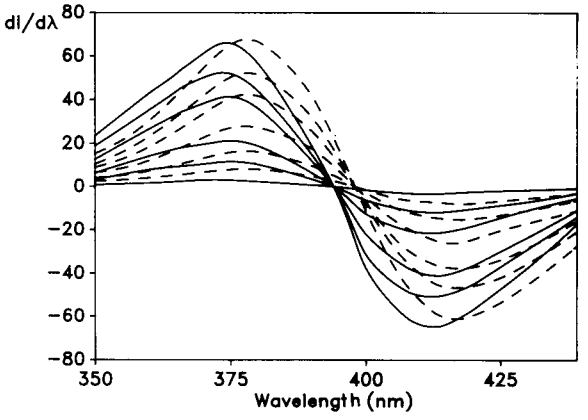

Fig. 4. Synchronous first-derivative spectra of (solid lines) AS and (dashed lines) GL at several different concentrations. [AS] = [GL] = 0.1, 0.3, 0.5, 0.8 and 1.0 μg ml^{-1}.

chromatographic elution using a time interval in the events programme of the diode-array detector of 0.03 spectra per minute.

Three peaks are detected at $t_R = 3.20$, 4.00 and 4.25 min, arising from GL, hydrolysed FC and AS, respectively, with the UV–visible detector set at 395 nm. Peak purity analysis [16] shows that both 3.20 and 4.25 min are retention times at

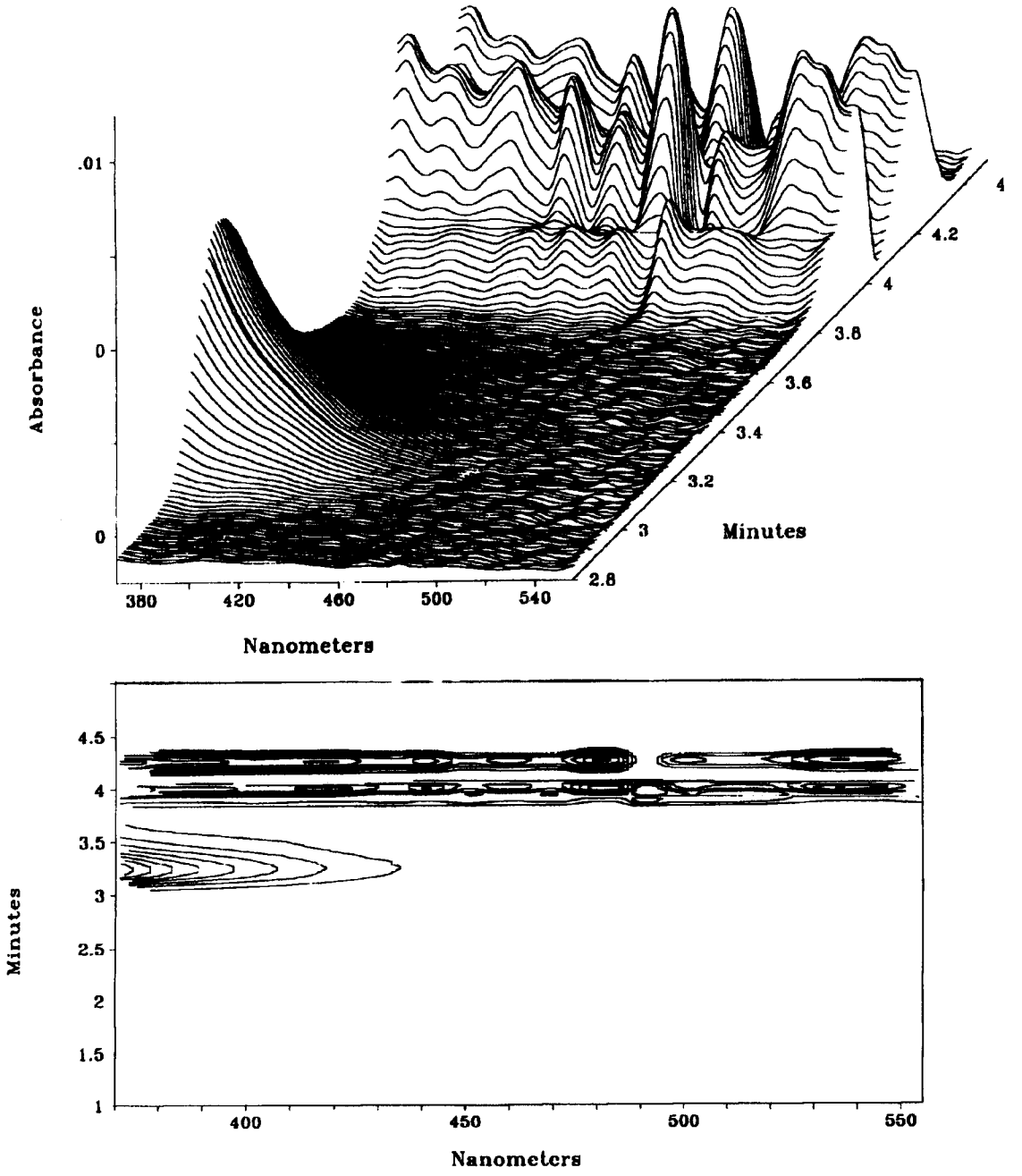

Fig. 5. Three-dimensional and contour plot of the chromatographic elution of 1 μg ml^{-1} AS and 1 μg ml^{-1} GL after derivatization with FC.

which eluted AS and GL virtually pure (purity = 0.996 for both). In comparison with these values, near to unity, the purity index of the peak at t_R = 4.00 min is 0.44.

It should be pointed out that because the detectors are connected in series, some delay in t_R from one to other detector signal is produced.

Spectrofluorimetric detection at λ_{exc} = 395 and λ_{em} = 482 nm shows only two peaks at 3.5 and 4.5 min corresponding to GL and AS derivatives of FC, respectively.

Quantitative analysis

Spectrofluorimetric method. Calibration graphs were constructed by analysing a series of samples of known AS and GL concentrations. Studies with solutions of AS and GL alone established that the concentrations of AS and GL correlated well with the synchronous derivative signals. The detector response was linear over the concentration range 0.1–1 μg ml^{-1}. The equations obtained by least-squares treatment were

$$DS^1 = 58.3[AS] + 3.16 \quad r = 0.990 \ (n = 5)$$

and

$$DS^1 = 49.7[GL] + 3.37 \quad r = 0.994 \ (n = 5)$$

for AS and GL, respectively, where DS^1 is the first-derivative signal, in arbitrary units.

To evaluate the reproducibility of the individual methods, a series of six solutions with concentrations of 0.5 μg ml^{-1} were prepared. The results are given in Table 1.

LC method. The detector reponse was linear over the concentration range 0.1–2 μg ml^{-1} for spectrofluorimetric and 1–4 μg ml^{-1} spectrophotometric detection. The equations obtained by least-squares treatment were as follows:

spectrofluorimetric detection:

$$A = 150.2[GL] + 99.2 \quad r = 0.999 \ (n = 5)$$
$$A = 121.9[AS] + 100.9 \quad r = 0.999 \ (n = 5)$$

spectrophotometric detection:

$$A = 2625[GL] - 1656 \quad r = 0.991 \ (n = 4)$$
$$A = 1391[AS] - 441 \quad r = 0.985 \ (n = 4)$$

where A is area under the peak, in arbitrary units, and concentrations are in μg ml^{-1}.

The standard deviations of the LC methods were calculated from three determinations at each of six different concentrations covering the calibration range. The six standard deviations obtained were averaged; this value is taken as the standard deviation of the method, and is used to calculate limiting values.

Table 1 also gives other analytical figures of merit of the methods. The detection limit, $C_L(k = 3)$, and determination limit, C_Q (k = 10), are reported as recommended by IUPAC [17].

Comparison of the methods

The spectrofluorimetric methods for the determination of AS and GL were compared with the corresponding methods using LC (y) and spectrofluorimetric (x) detection, by regression analysis [18]. The values of slope (a), intercept (b) and correlation coefficient (r) (n = 8) for GL are a = 1.0032, b = 0.0273 and r = 0.9979 and for AS are a = 0.9967, b = 0.0198 and r = 0.9992, showing excellent agreement and the absence of any systematic error.

TABLE 1

Analytical parameters of the proposed methods

Method	C_L (μg ml^{-1}) [a]		C_Q (μg ml^{-1}) [a]		t_R (min) [a]		Error (%) [b]		R.S.D. (%) [c]	
	AS	GL	AS	GL	AS	GL	AS	GL	AS	GL
Synchronous first-derivative spectrofluorimetry	0.03	0.10	0.11	0.34	–	–	6.4	3.4	6.38	3.00
LC– spectrofluorimetric detection	0.04	0.02	0.14	0.08	4.5	3.5	1.5	0.9	0.62	0.34
LC– spectrophotometric detection	0.22	0.10	0.72	0.35	4.1	3.1	6.3	8.7	2.26	3.14

[a] For definitions, see text. [b] Error = $100t \cdot$ S.D./$\bar{x}$. [c] For six determinations of 0.5 μg ml^{-1}.

TABLE 2

Spectrofluorimetric interference study at 0.5 μg ml^{-1} AS and at 0.5 μg ml^{-1} GL

Interferent	AS : interferent wt. ratio	Recovery (%) (first deriv.)	GL : interferent wt. ratio	Recovery (%) (first-deriv.)
Dulcin	1:5	83.8	1:5	86.8
			1:10	112.6
Sodium cyclamate	1:5	83.6	1:5	89.6
			1:10	114.2
Saccharin	1:10	79.0	1:10	76.0
			1:20	88.4
Ascorbic acid	1:10	89.4	1:10	86.8
	1:20	92.0		
Methyl paraben	1:10	90.8	1:10	72.8
	1:20	114.8	1:20	88.0
Benzoic acid	1:10	90.8	1:10	82.6
	1:20	112.0	1:20	86.2
Nicotinamide	1:10	84.8	1:10	75.2
	1:20	84.8	1:20	81.6

TABLE 3

Spectrofluorimetric analysis of binary mixtures of AS and GL

AS : GL wt. ratio	AS			GL		
	Taken (μg ml^{-1})	Found (μg ml^{-1})	Error (%)	Taken (μg ml^{-1})	Found (μg ml^{-1})	Error (%)
1:10	0.5	0.5	0	–	–	–
1:15	0.5	0.47	−6	–	–	–
1:5	1.0	0.89	−11	–	–	–
1:1	–	–	–	0.5	0.48	3.7
2:1	–	–	–	0.5	0.46	8.0
5:1	–	–	–	0.5	0.47	6.0

Interference study

The effects of other food additives on the determination of 0.5 μg ml^{-1} AS and 0.5 μg ml^{-1} GL by the first-derivative synchronous method were studied. The results, summarized in Table 2, show that good recoveries of AS and GL were obtained at interferent to analyte ratios below 1:20.

In general, the errors were negative and only methyl paraben and benzoic acid in the determination of AS and sodium cyclamate and dulcin in the determination of GL interfered positively, at interferent to analyte ratios higher than 10:1. Because the amounts of interferent assayed were fairly high, the interferences are probably spectral (inner filter effect).

The results obtained in the determination of each food additive in binary mixtures for differ-

TABLE 4

Spectrofluorimetric determination of AS in carbonated soft drinks

Sample No.	Synchronous first derivative		
	Added (μg ml^{-1})	Found (μg ml^{-1}) [a]	Mean recovery (%) [a]
1	0.00	–	–
	0.20	0.16 ± 0.01	80 ± 8
	0.50	0.48 ± 0.07	97 ± 4
	0.80	0.64 ± 0.04	82 ± 2
2	0.00	–	–
	0.20	0.17 ± 0.03	86 ± 4
	0.50	0.43 ± 0.03	86 ± 7
	0.80	0.66 ± 0.01	83 ± 1
3	0.00	–	–
	0.20	0.15 ± 0.03	75 ± 3
	0.50	0.42 ± 0.02	83 ± 2
	0.80	0.69 ± 0.02	86 ± 3

[a] Mean ± S.D. (n = 3).

TABLE 5

LC analysis of spiked binary mixtures of GL and AS in dried soups

GL			AS		
Added (μg ml^{-1})	Mean recovery [a] (%)	R.S.D. [a] (%)	Added (μg ml^{-1})	Mean recovery [a] (%)	R.S.D. [a] (%)
0	6.3	0.01	–	–	–
1	85.5	1.32	–	–	–
2	79.0	1.22	–	–	–
1	84.7	3.45	1	94.2	2.29
1	102.1	1.27	0.5	79.3	3.81

[a] $n = 3$.

TABLE 6

LC analysis of spiked binary mixtures of GL and AS in carbonated soft drinks

GL			AS		
Added (μg ml^{-1})	Mean recovery [a] (%)	R.S.D. [a] (%)	Added (μg ml^{-1})	Mean recovery [a] (%)	R.S.D. [a] (%)
–	–	–	0.2	100.6	1.60
–	–	–	0.5	107.9	2.14
–	–	–	0.8	109.1	1.16
1	88.1	0.65	0.5	107.7	1.02
1	98.8	1.93	1	96.2	0.30

[a] $n = 3$.

TABLE 7

Determination of monosodium glutamate in dried soup

Method	Volume (μl) [a]	Found (μg ml^{-1}) [b]	Glutamate (μg ml^{-1} soup) [c]	Glutamate (g kg^{-1} soup) [d]
Spectrofluorimetric	10	0.09 ± 0.02	9.33 ± 2.51	1.50 ± 0.42
LC	10	0.06 ± 0.01	6.30 ± 0.70	1.04 ± 0.11

[a] Aliquot of final solution taken for analysis (see text). [b] Concentration of GL in final solution (mean ± S.D., $n = 3$). [c] Concentration of GL in original soup solution (mean ± S.D., $n = 3$). [d] Concentration of GL in original dried soup (mean ± S.D., $n = 3$).

ent AS/GL ratios are given in Table 3. It can be seen that the reported method gave satisfactory results for the binary mixtures tested.

Determination of AS in carbonated beverages and of GL in dried soups

The usefulness of the methods developed in this work was evaluated by applying the methods to the determination of AS in carbonated drinks and to that of GL samples of commercial powdered soups.

Sample preparation of carbonated drinks was simple; they were degassed by immersion in an ultrasonic bath before analysis.

The samples of commercial dehydrated and homogenized soup were mixed with demineralized water (3 g in 500 ml) and agitated vigorously. The solutions were filtered through Whatman No. 1 filter-paper, then 25 ml were dialysed for 24 h at room temperature against 1000 ml of deionized water. The dialysed solution was concentrated to 25 ml in a rotary vacuum evaporator. Aliquots of the remaining solution were taken for analysis.

Table 4 gives the results obtained by applying the spectrofluorimetric procedure to the determination of AS in carbonated soft drinks, and Tables 5 and 6 those for the LC determination of

GL and AS in dried soups and soft drinks by LC. The results obtained demonstrate the effectiveness of the proposed methods in determining the analytes assayed in these type of samples.

Table 7 presents the results obtained in the determination of endogenous GL in dried soups by applying the spectrofluorimetric and LC methods. The results show that the spectrofluorimetric procedure reports a higher concentration than the LC method, probably because of the more pronounced effect of the concomitants in the matrix on the overall fluorimetric signal. However, both procedures give comparable results.

The authors thank the Comisión Interministerial de Ciencia y Tecnología (Project PB89-0543) for supporting this study.

REFERENCES

1 M.R. Cloninger and R.E. Baldwin, J. Food Sci., 39 (1974) 347.
2 G.E. Inglett, Food Technol., 35(3) (1981) 37.
3 I. Furda, P.D. Malizia, M.G. Kolor and P.J. Vernieri, J. Agric. Food Chem., 32 (1975) 340.
4 B.B. Woodward, G.P. Heffelfinger and D.I. Ruggles, J. Assoc. Off. Anal. Chem., 62 (1979) 1011.
5 T.A. Tyler, J. Assoc. Off. Anal. Chem., 67 (1984) 745.
6 N.G. Webb and D.D. Beckman, J. Assoc. Anal. Chem., 67 (1984) 510.
7 M. Nishigima, M. Kanmuri, Y. Waturi and Y. Kimura, Shokuhin Eiseigaku, 17 (1976) 78.
8 Toxicological Evaluation of Certain Food Additives and Contaminants, 29th Meeting of the Joint FAO/WHO Expert Committee Food Additives, World Health Organization, Geneva, 1987.
9 E. Fernandez-Flores, A.R. Johnson and V.H. Blomquist, J. Assoc. Off. Anal. Chem., 52 (1969) 744.
10 V.D. Yanchuk and V.V. Petrenko, Farmatsiya, 37(1) (1988) 73.
11 E.D. Coppola, S.N. Christie and J.G. Hanna, J. Assoc. Off. Anal. Chem., 58 (1975) 58.
12 P. Sporns, J. Assoc. Off. Anal. Chem., 65 (1982) 567.
13 A.T. Rhys Williams and S.A. Winfield, Analyst 107 (1982) 1092.
14 H.J. Keller, K.Q. Do, M. Zollinger, K.M. Winterhalter and M. Cuenod, Anal. Biochem., 166 (1987) 431.
15 J.A.F. de Silva and N. Stronjny, Anal. Chem., 47 (1975) 714.
16 G. Webster, Int. Lab. News, December (1991).
17 IUPAC, Spectrochim. Acta, Part B, 33 (1978) 241.
18 J.C. Miller and J.N. Miller, Statistics for Analytical Chemistry, Horwood, Chichester, 2nd edn., 1988.

Analytica Chimica Acta, 270 (1992) 55–61
Elsevier Science Publishers B.V., Amsterdam

Determination of metal ions as EDTA complexes by reversed-phase ion-pair liquid chromatography

Jen-Fon Jen and Chih-Shih Chen

Department of Chemistry, National Chung-Hsing University, Taichung 40217 (Taiwan)

(Received 10th March 1992; revised manuscript received 25th June 1992)

Abstract

A reversed-phase ion-pair liquid chromatographic method was developed for the determination of metal ions in aqueous solution. Metal ions were first chelated with EDTA, followed by injection into the chromatographic system. A reversed-phase C_8 column was used to separate the chelate ions with an eluent consisting of acetonitrile–water mixture (8 + 92, v/v) containing 0.002 M tetrabutylammonium as the counter ion. UV detection at 242 nm was applied. Factors affecting the ion-pair formation and the chromatographic separation were studied. This method can be applied to the determination of metal ions such as Pb, Ni, Cd, Fe and Cu. The linear dynamic range is larger than two orders of magnitude, the detection limit is at the ng ml^{-1} level and the R.S.D. is ca. 3% at mid-calibration range. The method has been successfully used in metal analysis of electroplating waste water. The results are comparable to those of atomic absorption spectrometry.

Keywords: Ion chromatography; Liquid chromatography; EDTA complexes; Metal ions

In recent years there has been continuing interest in the liquid chromatographic (LC) determination of metal ions with reversed-phase columns and chelating agents [1–11]. As an alternative to traditional spectroscopic methods and electrochemical methods, such methods have the advantages of accomplishing detection and separations at the same time and being free from interferences, especially in multi-element analysis or trace metal analysis of samples with complicated matrices. Commonly used chelating agents include dithizone [1], dithiocarbamates [1–7], β-diketones [1,8], and quinolin-8-ol [1,9–11]. Applications of these reagents are often limited to a specific system, and they sometimes cannot be used with various metal ions. Ethylenediaminetetraacetic acid (EDTA) [12] is as an excellent chelating agent which is able to form sufficiently stable chelates with 62 different metals [13]. As the combination ratio of EDTA with metal ions is 1 : 1, the chelates are always negatively charged, regardless of the charge on the metal ions [12]. This might be the reason why it has never been employed in metal analysis determinations using reversed-phase LC. Several studies [14–16] have shown it to be a successful chelating agent for metal determinations by ion-exchange chromatography. The advantages include high flexibility and ease of handling.

Recently, an alternative to conventional ion-exchange chromatography for the separation of inorganic anions has been developed [17–21]. This method combines the use of reversed-phase columns and ion-pair reagents, which has the advantage of easy control of the anion-exchange capacity. In this method, a dynamic anion-exchange bed was created by the sorption of a hydrophobic cation (from an ion-pairing reagent)

Correspondence to: Jen-Fon Jen, Department of Chemistry, National Chung-Hsing University, Taichung 40217 (Taiwan).

in the eluent on the stationary phase of a reversed-phase column [22]. This method makes it possible to separate anionic chelates by reversed-phase ion-pair LC.

Parkes et al. [23] used a reversed-phase C_8 column to determine nitrilotriacetic acid via copper chelates and ion-pair LC. Venezky and Ruzinski [24] and Dai and Hilz [25] also used an ODS column for the determination of EDTA based on the formation of a stable metal–EDTA complex. However, to the authors' knowledge, there have been no previous reports on the determination of metal ions using this method.

In this study, a reversed-phase LC procedure based on the combination of EDTA chelation and ion-pair formation was developed for the determination of metals. Metals were first chelated with EDTA, followed by separation with a C_8 column and eluent with acetonitrile–water containing tetrabutylammonium (TBA) ion as the ion-pairing agent. Ion pairs were formed directly inside the column and UV detection was applied.

To evaluate the applicability of the proposed method, in addition to the chromatographic behaviour, detection limits, linear dynamic detection range and repeatability were studied through the separation of several metal ions.

EXPERIMENTAL

Apparatus

The chromatograph used was a Gilson system including two Model 302.5 SC single-piston pumps, a Model 811 dynamic 1.5-ml mixer, a Model 802C manometric module and a Holochrome·UV detector with a 20-μl flow cell. The detection wavelength was set at 242 nm. A reversed-phase Supelcosil LC-8 column (25 cm × 4.6 mm i.d., particle size 3 μm) was used for all separations. A Rheodyne Model 7125 injector with a 20-μl external loop was used for sample introduction. A Hewlett-Packard HP-3390A integrator was used to obtain the chromatograms and perform data calculations. In order to verify the LC results, the samples were also analysed with a Hitachi Model Z-8100 polarized Zeeman effect atomic absorption spectrometer using the relevant hollow-cathode lamps with wavelengths and slit widths as recommended for the metals of interest.

Reagents

The water used for the preparation of all solutions and eluents was distilled and deionized. Stock standard solutions of Pb(II), Ni(II), Fe(III), Cu(II), Cd(II), Cr(III) and Co(II) were prepared from ACS reagent grade chemicals. Fresh working standard solutions of low concentration were prepared daily by dilution of the stock standard solutions with water. Na_2EDTA was obtained from Merck and tetrabutylammonium hydroxide from J.T. Baker. LC eluents were prepared from HPLC-grade methanol and acetonitrile (Mallinckrodt) and tetrabutylammonium hydroxide, followed by pH adjustment with 5×10^{-3} M sulphuric acid. All eluents were filtered through a 0.45-μm PVDF membrane filter and degassed ultrasonically before use.

RESULTS AND DISCUSSION

To establish the optimum chromatographic system, factors that affect the formation of chelates and ion pairs and the retention behaviour, such as pH of the sample medium and eluent, concentrations of EDTA and TBA and the composition of eluent, were studied.

Metal chelate formation and UV detection

As metal ions were precolumn chelated with EDTA, the LC separation and UV detection will depend on the extent of chelation. Chelation between metal ions and EDTA has been discussed elsewhere [12]. The solution pH and the EDTA concentration are the most important factors in the chelation reaction. A higher pH favours complex formation, but there is a risk of hydroxide precipitation. Different metal species will exist in solution as a function of pH and EDTA concentration. Hence the pH should be controlled in the sample preparation and in the eluent. In a multi-element sample, competition of chelate formation among different metal ions will occur. Priority of formation depends on the mag-

nitude of the formation constants of individual chelates. During a multi-element separation, adequate addition of EDTA is necessary to ensure complete chelation of all metals. Sometimes, certain metals can be intentionally excluded from complexation by controlling the pH of solution or the EDTA content. This is one of the flexible characteristics of the use of EDTA in chromatography. To ensure complete chelation, a precolumn chelation was substituted for in-line chelation as the sample preparation.

In order to obtain the highest detectability, the wavelength is best set at that of maximum absorbance (λ_{max}). EDTA does not absorb above the cut-off wavelength of the eluent. When ion paired with the TBA ion, the λ_{max} of the complex is unchanged. Table 1 shows the λ_{max} values for several metal complexes. The data indicate that λ_{max} is different for each complex. Hence the wavelength selection is flexible for optimum detection. Undesired absorption signals could be eliminated by changing the detection wavelength.

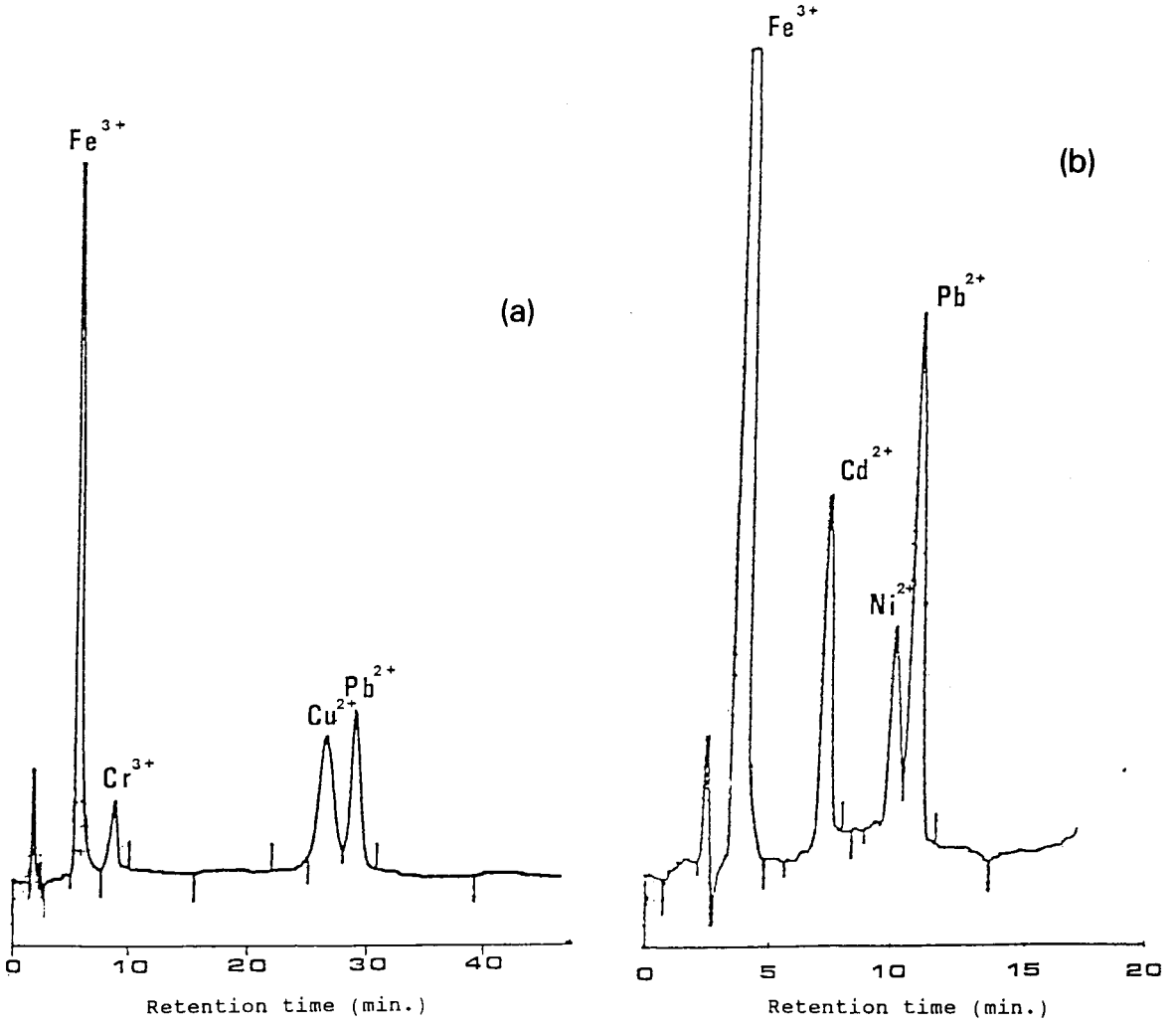

Fig. 1. Chromatograms of metal–EDTA complexes under the optimum conditions. (a) Eluent acetonitrile–water (8 + 92, v/v) containing 0.0004 M TBA at pH 4.0, with an RP-C_8 column for 20 μg ml^{-1} Pb^{2+}, 10 μg ml^{-1} Cu^{2+}, 8 μg ml^{-1} Fe^{3+} and 10 μg ml^{-1} Cr^{3+}. (b) Eluent, acetonitrile–water (8 + 92, v/v) containing 0.01 M TBA at pH 4.0, with an RP-C_8 column for 15 μg ml^{-1} Pb^{2+}, 30 μg ml^{-1} Fe^{3+}, 3 μg ml^{-1} Ni^{2+} and 3 μg ml^{-1} Cd^{2+}.

TABLE 1

λ_{max} values of metal–EDTA complexes

Sample	λ_{max} (nm)	ϵ [a] (l mol^{-1} cm^{-1})	Absorbance [b]	Concentration (M) [b]
Pb^{2+}–EDTA	242	9.95×10^{3}	0.995	1×10^{-4}
Fe^{2+}–EDTA [c]	258	8.65×10^{3}	0.865	1×10^{-4}
Fe^{3+}–EDTA	257	9.77×10^{3}	0.977	1×10^{-4}
Cu^{2+}–EDTA	258	3.16×10^{3}	0.316	1×10^{-4}
Ni^{2+}–EDTA	219	1.90×10^{3}	1.901	1×10^{-3}
Cd^{2+}–EDTA	– [d]			1×10^{-3}
Co^{2+}–EDTA	222	2.46×10^{3}	2.082	8.5×10^{-4}
Cr^{3+}–EDTA	303	2.52×10^{2}	0.242	9.6×10^{-4}
	393	67.64	0.068	
	541	98.75	0.095	
EDTA	– [d]			1×10^{-3}

[a] Molar absorbtivity. [b] In acetonitrile–water (5+95, v/v) at pH 4.0. [c] Fe^{2+}–EDTA is oxidized to Fe^{3+}–EDTA immediately if dissolved oxygen is present in the sample solution. [d] No absorption peak above 210 nm.

It might even improve the apparent resolution of a separation. Moreover, programmed wavelength selection would give the best chromatogram. However, in most multi-element analyses, a single wavelength is generally selected to detect all species. In the present studies, a detection wavelength of 242 nm was used throughout.

Chromatographic behaviour

The ion interaction model is suitable for the interpretation of the retention mechanism in ion-pair chromatography. With the sorption of the ion-pair reagent on the stationary phase, a dynamic ion-exchange bed was formed. Various papers [26,27] have discussed different separation schemes for this. Retention behaviour should follow the charged interaction and the electrostatic action law, that is, the higher the charge of the analyte ion, the greater is the interaction between the analyte ion and the bed. For different ions of the same charge, the larger the ionic radius, the more strongly attracted is the ion to the bed. Because the complexation of metal ion with EDTA is in a 1:1 ratio regardless of the charge on the cation, the complex usually has a charge of $n-4$ (where n is the charge on the cation). Hence metal ions with higher charge will be eluted faster. The capacity factors (k') of metal ions determined by the proposed method generally follow this trend. Figure 1 shows chromatograms of several metal chelates obtained by the proposed method. In Fig. 1a the higher charged iron(III) and chromium(III) ions were eluted faster than the copper(II) and lead ions. Figure 1b shows the chromatogram of some heavy metal ions which are always present in industrial waste water.

Effect of pH. In the determination of multicharged ions, the retention behaviour can be adjusted by pH control. However, the eluent pH should be adjusted carefully as it will affect the stability of the metal–EDTA complexes. With a

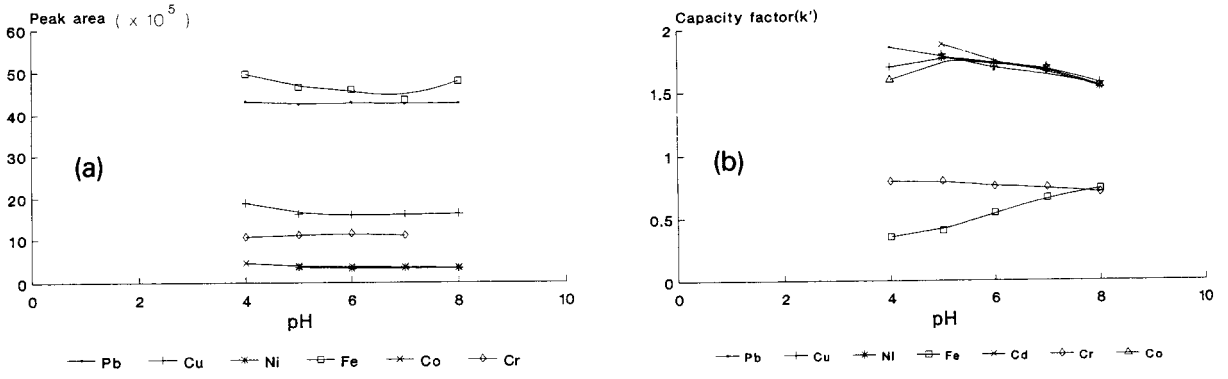

Fig. 2. (a) Effect of pH on peak area. Eluent, acetonitrile–water (24 + 76, v/v) containing 0.002 M TBA; flow-rate, 1.0 ml min^{-1}. ● = Pb; + = Cu; * = Ni; □ = Fe; × = Co; ◇ = Cr. Concentration of Pb, Cu, Ni, Fe(III) and Co = 0.001 M; Cr(III) = 0.00096 M. (b) Effect of pH on capacity factor (k'). Eluent and flow-rate as in (a). ● = Pb; + = Cu; * = Ni; □ = Fe; × = Cd; ◇ = Cr; △ = Co. Concentrations of Pb, Cu, Ni, Fe(III), Cd and Co = 0.001 M; Cr(III) = 0.00096 M, in 0.002 M EDTA solution.

higher pH, there is a risk of hydroxide formation. However, the influence of pH depends on the solubility product of the metal hydroxide. Figure 2a shows this influence in the pH range studied. The quantitative detection seems not be affected by pH in the range 4–8. This implies that the complexes are stable at natural water pH, and the proposed method can be applied directly to analyses for aqueous metal ions. The retention behaviour of metals was also influenced by pH, as shown in Fig. 2b. The capacity factor of Fe^{3+} increases significantly as the pH changes from 4 to 8, that of Pb^{2+} decreases more rapidly and those of Cu^{2+}, Ni^{2+} and Cd^{2+} decrease more slowly. The retention mechanism cannot give an adequate explanation for this divergent behaviour.

Effect of ion-pair reagent. The sorption of TBA offers dynamic ion-exchange sites. Hence the retention of metal–EDTA complexes is directly related to the surface charge arising from the absorbed cations. An adsorption equilibrium is established between the eluent and the surface of the stationary phase. With the ion-exchange mechanism, the retention increases with increasing amount of TBA adsorbed until the surface is saturated. However, the results of this work show that k' increases with increasing amount of TBA in the low concentration range, levels off and then decreases at higher concentrations (Figure 3a). This indicates the existence of another force that competes with the ion–ion interaction. As the interaction between the analyte and eluent (maybe TBA^+ in the eluent) is stronger than that between the analyte and ion-exchange sites, k' decreases. Figure 3b demonstrates the influence of TBA on detection. As the TBA concentration increases above 0.01 M, the detection signal does not change. This implies that the formation of a real ion-pair species did not reach equilibrium during elution. This is consistent with the ion-exchange mechanism.

An interesting phenomenon occurs when TBA^+ is in a lower concentration range, where different metal chelates have increased or decreased signals.

Effect of organic modifier. The in situ formed neutral ion pair will adsorb firmly on the surface of a reversed-phase column owing to the large size of the ion pair. Therefore, an organic modifier in the eluent is needed to compete with the TBA or ion pairs in the adsorption equilibria in order to control the elution rate. From considerations of viscosity and dielectric constant, acetonitrile was selected as the organic modifier (rather than methanol) throughout all the studies. The k' value decreases rapidly as the acetonitrile content increases, but the resolution also becomes worse. However, no significant change in the detectability was observed. Therefore, appropriate adjust-

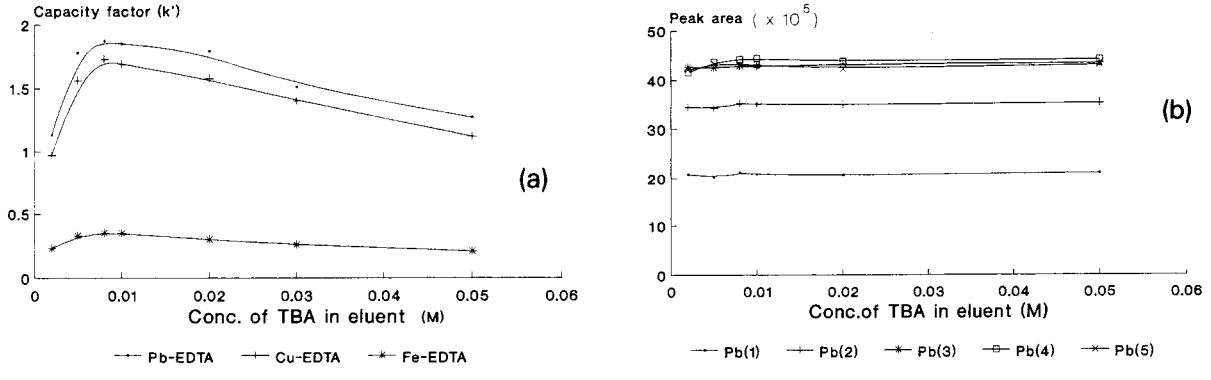

Fig. 3. (a) Effect of TBA concentration on capacity factor (k'). Eluent, acetonitrile–water (24 + 76, v/v) containing 0.002 M TBA, pH = 4; flow-rate, 1.0 ml min^{-1}. ● = Pb–EDTA; + = Cu–EDTA; * = Fe–EDTA. Concentration of complexes = 0.001 M. (b) Effect of TBA concentration on peak area. Eluent and flow-rate as in (a). Pb concentration = 0.001 M. EDTA concentration: ● = 0.005; + = 0.0008; * = 0.001; □ = 0.0015; × = 0.002 M.

ment of the organic modifier and ion-pair reagent in the eluent is necessary for optimum chromatographic elution.

Metal ion determination. Owing to the flexible characteristics of EDTA and ion-pair reagents in chromatography, optimum conditions should be established for the separation of target metal ions. Figure 1a and b demonstrate the analyses of a mixture of Pb^{2+}, Cu^{2+}, Ni^{2+}, Cd^{2+} and Fe^{3+} under the optimum experimental conditions. All the metals give sharp and symmetric peaks.

The analytical results obtained from an electroplating waste water sample utilizing the proposed LC method were compared with those using the atomic absorption spectrometric (AAS) method (Table 2). In general, they are in good agreement. The results obtained with the LC method are lower than those with the AAS method. This might be expected because of the inherent differentiation between species of the same metal by the chromatographic technique.

Calibration and detection limits. In order to test the applicability of the method to trace analysis, calibration graphs were constructed for the six metals over a range of concentrations. The results are summarized in Table 3. Linear relationships are found between the peak areas and the amounts injected for all the metals with correlation coefficients all above 0.999. The reproducibility was examined with five replicate injections of 20 μl of 0.001 M of each metal ion. Peak areas were measured and the relative standard deviation was calculated. The detection limits listed in Table 3 were calculated from three times the average background noise level. The values fall near the ng ml^{-1} level.

TABLE 3

Linear dynamic ranges and detection limits for metal–EDTA complexes

Metal	Linear range [a] ($\mu g\ ml^{-1}$)	Detection limit [b] ($\mu g\ ml^{-1}$)
Pb^{2+}	4.0–650	12
Fe^{3+}	0.5–200	1.4
Cu^{2+}	3.0–650	66
Ni^{2+}	1.2–200	1.4
Cd^{2+}	2.0–500	3.5
Cr^{3+}	0.5– 40	20

[a] Correlation coefficient at least 0.999 ($n = 5$). [b] Signal-to-noise ratio ≈ 3.

Conclusion

The developed LC method combines the advantage of using EDTA in sample preparation and an ion-pair reagent in chromatography. The system is extremely flexible as the concentrations of EDTA, TBA and acetonitrile and the pH and detector wavelength can all be adjusted to optimize the conditions for a given situation. This study indicates that the proposed LC method can be an alternative to traditional spectroscopic and electrochemical methods in the determination of metal ions in water.

The authors acknowledge gratefully financial support from the National Science Council of the Republic of China, under the grant contract number NSC 79-0208-M-005-25.

TABLE 2

Comparison of LC and AAS results

Metal	LC ($\mu g\ ml^{-1}$)	R.S.D. (%) [a]	AAS [b] ($\mu g\ ml^{-1}$)	R.S.D. (%) [a]
Pb^{2+}	30.0	1.7	30.2	1.1
Cu^{2+}	14.1	1.2	14.3	0.8
Fe^{3+}	12.3	1.9	12.9	3.3
Cr^{3+}	15.1	0.2	15.1	1.2

[a] For five consecutive analyses of the same solution. [b] The wavelength used for Pb determination was 283.3 nm, for Cu 324.8 nm, for Fe 248.3 nm and for Cr 359.3 nm.

REFERENCES

1 B.R. Willeford and V. Hans, J. Chromatogr., 251 (1982) 61.
2 J.N. King and J.S. Fritz, Anal. Chem., 59 (1987) 703.
3 J.N. King and J.S. Fritz, Anal. Chem., 57 (1985) 1016.
4 A.M. Bond and G.G. Wallace, Anal. Chem., 54 (1982) 1706.
5 A.M. Bond and G.G. Wallace, Anal. Chem., 55 (1983) 718.
6 A.M. Bond and G.G. Wallace, Anal. Chem., 56 (1984) 2085.
7 K.P. O'Riordan, G. Heneghan and G.G. Wallace, Anal. Chem., 57 (1985) 1354.

8 R.C. Gurira and P.W. Carr, J. Chromatogr. Sci., 20 (1982) 461.
9 C.-W. Whang, L.-C. Wu and L.-C. Chou, Proc. Natl. Sci. Counc. ROC (A), 11 (1987) 363.
10 L.H.J. Lajunen, E. Eijrvi and T. Kenakkala, Analyst, 109 (1984) 699.
11 R.D. Gupta, G.S. Manku, A.N. Bhat and B.D. Jain, Aust. J. Chem., 23 (1970) 1387.
12 D.A. Skoog and D.M. West, Fundamentals of Analytical Chemistry, Saunders, New York, 1982, pp. 283–284.
13 J.A. Dean, Lange's Handbook of Chemistry, McGraw-Hill, New York, 7th edn., Table 5–15, pp. 5-55–5-56.
14 G.J. Nickless, J. Chromatogr., 313 (1985) 129.
15 D.M. Fraley, D. Yates and S.E. Manahan, Anal. Chem., 51 (1979) 2225.
16 K. Hayakawa, T. Sawada, K. Shimbo and M. Miyazaki, Anal. Chem., 59 (1987) 2241.
17 K. Ito, Y. Ariyoshi, F. Tanabiki and H. Sunahara, Anal. Chem., 63 (1991) 273.
18 I. Ziad and D.J. Pietrzyk, Anal. Chem., 54 (1982) 2601.
19 R.M. Cassidy and S. Elchuk, Anal. Chem., 54 (1982) 1558.
20 A. Berthod, I. Girard and C. Gonnet, Anal. Chem., 58 (1986) 1356.
21 T. Okada, Anal. Chem., 60 (1988) 1511.
22 B.A. Bidlingmeyer, C.T. Santasania and F.V. Warren, Anal. Chem., 59 (1987) 1843.
23 D.G. Parkes, M.G. Caruso and J.E. Spradling, III, Anal. Chem., 53 (1981) 2154.
24 D.L. Venezky and W.E. Rudzinski, Anal. Chem., 56 (1984) 315.
25 J. Dai and G.R. Hilz, Anal. Chem., 60 (1988) 301.
26 D. Shea and W.A. MacCrehan, Anal. Chem., 60 (1988) 1449.
27 Z.M. Shakhsher and W.R. Seitz, Anal. Chem., 62 (1990) 1758.

Analytica Chimica Acta, 270 (1992) 63–78
Elsevier Science Publishers B.V., Amsterdam

Evaluation of gel permeation chromatographic techniques and diode-array UV detection for the characterization of biotechnological fermentation substrates and broths

György Marko-Varga

Department of Analytical Chemistry, University of Lund, Box 124, S-221 00 Lund (Sweden)

Damià Barceló

Department of Environmental Chemistry (CID–CSIC), Consejo Superior de Investigaciones Cientificas, Jordi Girona 18–26, E-08034 Barcelona (Spain)

(Received 6th March 1992; revised manuscript received 7th July 1992)

Abstract

Gel permeation chromatography (GPC) was used for the analysis and characterization of fermentation substrates and broths. Chemical or enzymatic hydrolysis of wood and waste waters from the pulp industry were used as the substrate in ethanol fermentations. Sample pretreatment was carried out by liquid–liquid extraction with dichloromethane and water. The two phases were subjected to analysis by organic and aqueous GPC using a polymer-based GPC column, a silica support and a GPC column with dichloromethane, water and water-miscible tetrahydrofuran as the mobile phases, respectively. Diode-array UV spectrophotometric detection (DAD) of substrates and broths was utilized for characterization complementary to the GPC separations. The DAD method will give UV absorption spectra for different samples providing unique fingerprints for the specific compounds present.

Keywords: Gel permeation chromatography; Liquid chromatography; UV–Visible spectrophotometry; Fermentation; Sulphite liquor; Waters; Wood

In the search for alternative energy sources, great efforts have been made to find solutions through chemical or biochemical processes. Waste waters from the pulp industry and/or fast-growing energy woods containing large amounts of sugars derived from lignocellulose fractions are potentially inexpensive carbon sources as the substrate for ethanol production, through fermentation.

To be able to optimize and increase the ethanol yield for the overall fermentation process, the investigation and characterization of fermentation substrates and broths processed under various conditions is needed. The hydrolysis of wood and waste water from the pulp industry is effected either chemically or enzymatically. It will produce a complex mixture containing a wide variety of compounds, e.g., lignin and its hydrolysis products, which yields phenol and phenol derivatives, humic substances and browning reaction components that are more or less toxic to the yeast in the fermentation process. Moreover, during the fermentation step, the level of toxic compounds may vary widely owing to the metabolism in the fermenter.

Ethanol, an important organic solvent, can be

Correspondence to: G. Marko-Varga, Department of Analytical Chemistry, University of Lund, Box 124, S-221 00 Lund (Sweden).

produced by fermentation processes and is utilized in the chemical industry as a raw material or as an alternative engine fuel. In oil crises, interest in the biotechnological production of ethanol to be used as an alternative energy source increases. Different sources have been utilized in order to find cheap substrates with a high production yield of ethanol, e.g., prehydrolysates of aspen and pine woods [1], cane molasses [2], sugar cane bagasse [3], corn syrup [4] and lignocellulose materials [5–7].

Plant biomass, i.e., lignocellulose materials such as industrial waste waters, agricultural residues and wood, are considered to be the most abundant renewable resource available for fermentation to produce liquid fuels, for fibre and paper manufacture or as chemical feedstocks. These sources contain large amounts of poly-, oligo-, di- and monosaccharides that can be used as the carbon source in fermentation processes. Lignocellulose materials have great potential for utilization, covering about 95% of the world biomass [8].

The determination of carbohydrates in lignocellulose substrates is fused with considerable problems and errors when using ligand-exchange liquid chromatographic separation with refractive index detection [9,10]. The chromatographic peaks are not only due to sugar, but also contain other interfering compounds, giving rise to faults in the evaluations [11]. These are reasons why an investigation of the characterization of the different substrates and broths with regard to the lignin and decomposition compounds in these samples is of great importance. There is also a lack of knowledge about the composition of the fermentation broth during the run of the process and consequently the information obtained can be used as a strategy to improve the fermentation conditions, resulting in higher yields.

This paper reports the characterization of fermentation substrates by three types of gel permeation chromatographic (GPC) separations (two organic- and an aqueous-based separation). Three different hydrolysates originating from various hydrolysis treatments were investigated: acid-hydrolysed pine wood, fermentation substrates and broths from steam-treated, enzymatically hydrolysed soft wood (*Salix caprea*) (EH) and chemically hydrolysed waste water from the pulp industry (spent sulphite liquor, SSL). These sources were used as substrates and fermented using bakers' yeast (*Saccharomyces cerevisiae*). GPC was utilized for the characterization of lignin and its breakdown products with regard to the molecular mass distribution. Three different GPC column materials were used for the separation of the fermented and unfermented hydrolysates. The separation columns used were both silica and polymer based with dichloromethane (water-immiscible organic solvent), tetrahydrofuran (water-miscible organic solvent) and water containing 5% of methanol as the mobile phases. Analyses were carried out by liquid chromatography (LC) with UV detection. The different samples were also characterized using computer-coupled UV diode-array detection (UV-DAD). These spectra can be used as a fingerprint for the composition in the various samples during the fermentation process and/or for qualitative evaluation in combination with a second LC system [12].

EXPERIMENTAL

Apparatus

The chromatographic apparatus consists of an LC pump (Model 400; Applied Biosystems, Foster City, CA) using an injector (Model 6020; Rheodyne, Cotati, CA) and a Varian UV–visible spectrophotometric detector (Vari-Chrom; Varian, Sunnyvale, CA) and a diode-array UV detector (Chrom-A-Scope; Barspec, Rehovot, Israel) coupled with a recorder (Model 2210; Pharmacia, Uppsala, Sweden). HPLC-grade methanol, dichloromethane, acetonitrile, tetrahydrofuran and HPLC-grade water (Carlo Erba, Milan) were used in the LC mobile phase. The mixtures of the eluents were degassed in an ultrasonic bath prior to use.

Columns

The analytical GPC columns used were as follows: (1) a Zorbax PSM 60 S (Rockland Technologies through Chrompack, Middelburg, Netherlands) stainless-steel column (250 × 6.2

mm i.d.) with a molecular mass operating range of 100–10 000 with water containing 5% of methanol as the organic modifier as the mobile phase; (2) a Bio-Beads SX-12 (Bio-Rad Labs., Richmond, CA) stainless-steel column (450 × 10 mm i.d.) with dichloromethane as the mobile phase with molecular mass exclusion above 400; and (3) Phenogel (Phenomenex, Ramuko, Palos Verdes, CA, USA) with a molecular mass operating range up to 1000 with tetrahydrofuran as the mobile phase.

Hydrolysis

The three different substrates were enzyme-hydrolysed willow (EH), acid-hydrolysed pine and spent sulphite liquor (SSL), and were prepared as follows.

Wood from fast-growing willow (*Salix caprea*) was oven dried with a final composition of 23% hemicellulose, 36.8% cellulose, 20.7% lignin and 19.5% remainder [13,14]. The hydrolysis of the wood was effected by a two-stage steam pretreatment at 220°C at a pressure of 24 bar for 10 min as described by Eklund et al. [13,14]. The condensate from the first pretreatment containing the hemicellulose fraction was mixed with the enzyme-hydrolysed cellulose in the second pretreatment step. The enzymes used were a mixture of cellulase from *Trichoderma reesei* (Celluclast 2L, Novo, Denmark) and cellulase from *Aspergillus niger* (Novozyme, Novo) [13]. This hydrolysate was then a clear, dark-brown solution used as the substrate for the fermentation.

Wood from pine was hydrolysed in two steps. The first-stage hydrolysis, producing the hemicellulose fraction, was effected at 160°C with a liquid-to-solid ratio of 3:1, SO_2(g) equivalent to an acid concentration of 2.5% H_2SO_4 on dry wood substance for 30 min [15]. The hydrolysate was then passed through a plug-flow reactor at 160°C whereafter the substrate contained 24.5 g l^{-1} glucose, 20.1 g l^{-1} xylose, 7.3 g l^{-1} galactose, 5.9 g l^{-1} arabinose and 37.5 g l^{-1} mannose [15]. The second stage of hydrolysis was applied to the solid cellulose remaining from the first stage at 230°C for 0.7 min with an acid-to-wood ratio of 0.7%, which is equivalent to an acid concentration of 0.2% H_2SO_4 in solution. This hydrolysate contained ca. 202 g l^{-1} glucose and 10.4 g l^{-1} 5-hydroxymethylfurfural (5-HMF) [15].

With spent sulphite liquor substrate and broths, the substrate is a sodium-based technical substrate from the pulp industry. Softwood was hydrolysed by boiling in Na_2SO_3 and the addition of SO_2(g). The hydrolysis yields solid cellulose, used for paper production, and SSL, a soluble fraction containing the hemicellulose, parts of the lignin, sugars and reactive intermediates and extractives [16].

Fermentation conditions

EH and SSL were both incubated in a slowly stirred beaker (100 ml), thermostated at 30°C, sealed with a rubber seal and incubated with *Saccharomyces cerevisiae* (140 g l^{-1} wet weight), 0.25% (w/v) yeast extract (Difco) and 0.025% (w/v) ammonium sulphite. The substrates were pretreated by adjusting the pH to 6.0 with sodium hydroxide and the addition of fermentation nutrients as described [5,16].

Sample preparation

Samples were taken from the fermenter after 0, 1, 3 and 24 h and denoted (a2), (a3), (a4), (b2), (b3) and (b4), respectively, with samples (a) originating from SSL fermentation and samples (b) from the EH fermentation. The substrates at the beginning, before fermentation ($t = 0$ h), are denoted (a1), (b1), (c1) and (c2) for SSL, EH and pine samples, respectively. The pine samples were investigated only as substrates. The samples were subsequently diluted 50–100-fold with mobile phase and filtered through a Millex HV (Millipore) sterile filter to remove particulate contaminants in the samples, then frozen until analysis. The samples were then injected directly into the LC system.

Extraction procedures

A 1-ml volume of 100-fold diluted fermentation substrates and broths was extracted with 1 ml of dichloromethane by shaking for 1 h. This resulted in three phases: an organic, an aqueous and an intermediate phase between the organic and aqueous phases. The volumetric ratios between the three phases varied for all the samples,

but the intermediate phase was the smallest for unfermented substrates, independent of their source.

RESULTS AND DISCUSSION

Nature of the chemically and enzymatically hydrolysed lignocellulose substrates

Lignocellulose was hydrolysed chemically by acid or by the use of steam pretreatment in combination with enzymes (cellulases, see Experimental). The substrates originate from either wood, *Salix candera* or pine, or waste water from the pulp industry (SSL), which is a by-product from the sulphite pulping process containing hemicellulose with various levels of lignocellulose, oligosaccharides and various monosaccharides [6,16,17]. In this characterization study water-soluble and more non-polar structured lignin and lignin breakdown products (aromatic monomers) present in the substrates and broths during different times in an ethanol fermentation were investigated. The substrates differ not only in their origins but also in the cellulose part in the wood hydrolysates. In this respect, free hexoses are utilized as the carbon source in the fermentation while the cellulose fraction from the pulp industry is used for paper production and is subsequently not present as sugar monomers in the SSL substrate.

The vigour of the hydrolysis also leads to differences in the various substrates. Chemical treatment with acid (sulphuric acid) is considered to be a more severe method of hydrolysis resulting in a substrate with a more complex composition, whereas enzymatic hydrolysis using cellobiases is considered to be milder, yielding a substrate with less spread of the breakdown products from the lignin. SSL is in some ways comparable

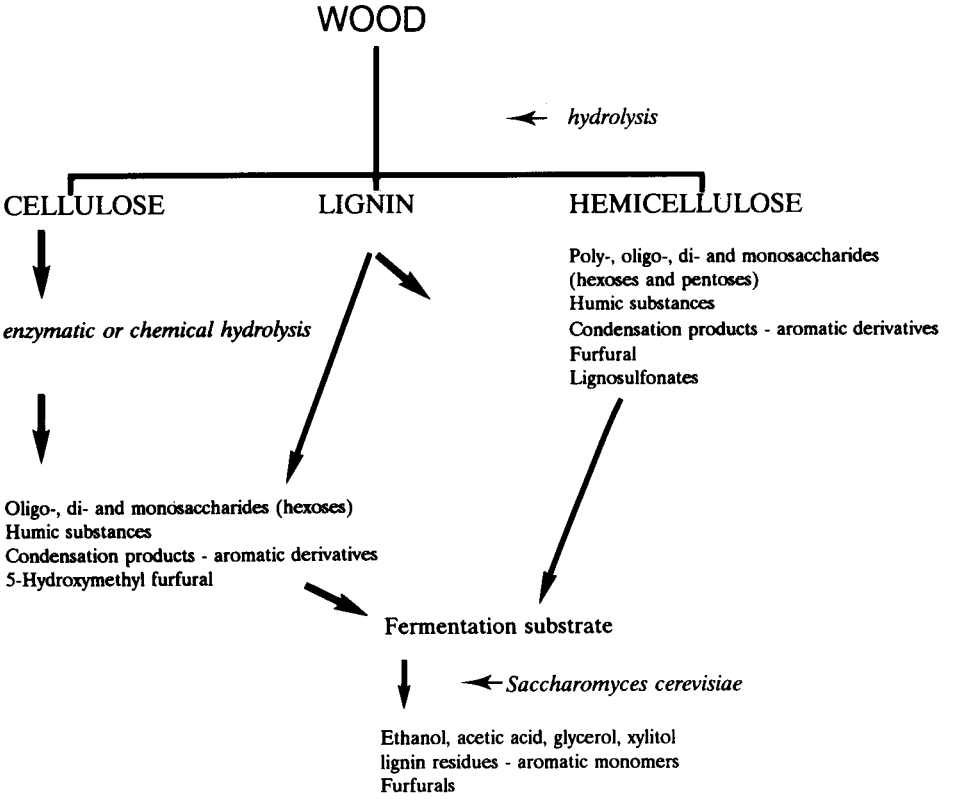

Fig. 1. Scheme of hydrolysis and fermentation of lignocellulose.

to these two and other wood hydrolysates [18,19]. The breakdown scheme of the lignocellulose hydrolysates is illustrated in Fig. 1. Lignocellulose does not show a uniform composition, but consists of a diverse mixture of low-, medium- and high-molecular-mass compounds. The three main constituents are lignin, cellulose and hemicellulose (see Fig. 1). Lignin is a complex, highly branched, irregular, three-dimensional aromatic organic polymer composed of phenylpropane subunits including coumaryl, guaiacyl and syringyl groups. These moieties are covalently linked together by a variety of bonds, mainly with β-aryl ether bonds of the lignin polymer monomers [20]. Lignin also contains extractives, consisting of a large number of organic compounds that can be extracted partly with water but totally with an organic solvent. Often, sophisticated instrumentation is needed, e.g., infrared or proton or carbon-13 nuclear magnetic resonance spectrometry [21,22], to assign the structure of lignin, which has not yet been completely elucidated.

The hemicellulose fraction contains soluble sugars, e.g., non-cellulosic polysaccharides [23], cellobiose and both pentose and hexose monosaccharides [24], easily dissolved lignin and lignin decomposition products and also uronic acids and their derivatives, condensation products and furfurals and humic substances. Cellulose contains hydroglucose units of β-D-glucose units linked together by 1–4-glucosidic linkages forming the glucanic polymer chains. Lignin more strongly bound to cellulose chains will be dissolved in this hydrolysate fraction.

Delignification of wood can be advantageous in some instances, but problems arise because decomposition of the hemicellulose may occur [23]. These three groups (cellulose, hemicellulose and lignin) are all high-molecular-mass compounds. Medium- and low-molecular-mass compounds in the substrates and broths are degradation and condensation products of lignin, cellulose and hemicellulose.

The hydrolysates from both chemical and enzymatic hydrolysis form a complex mixture consisting of a wide variety of compounds present in the substrates used in the fermentation process, many of which are toxic and act as inhibitors of the process itself. Other compounds known to be produced in wood hydrolysates are the humic substances [25,26], which are dark-brown, colloidal and amorphous compounds of very complex composition. Defined structures of these humic substances are unknown but hypothetical structures of humic acid with polyaromatic structures exhibiting hydroxy, carboxy, carbonyl, amino and quinone groups have been proposed by Ailen et al. [27]. Humic and fulvic acids, which are polymers of hydroxybenzoic acids and hydroxyphenols, are the major constituents [25]. Humic substances behave like polyelectrolytes and are known in nature to function as large poly ion exchangers with a large capacity to bind, e.g., metal ions, amino acids, peptides, proteins and aliphatic and aromatic compounds [28].

Condensation products are known to be formed in microbial growth media especially in one of the hydrolysis steps when high temperatures are used at acidic pH. Maillard or browning reactions are also known to occur, involving amines, amino acids and proteins that react with sugars, aldehydes and ketones to form these condensation products and contribute to the dark-brown colour of the media [29,30].

The level of organic solvents in the fermentation broth will increase owing to the ethanol and minor amounts of methanol produced, which will result in a varying composition of the soluble part of the broth. Compounds such as lignin, phenolic derivatives, humic substances and browning reaction components and cello- and xylo-oligomers with more hydrophobic characteristics will dissolve in the more apolar solution. This has been found to be the case in studies of lignin decomposition with oxygen in aqueous alkaline ethanol samples [31].

Liquid–liquid extraction

The SSL, EH and the pine acid hydrolysates were subjected to liquid–liquid extraction (see Experimental). The aqueous samples were mixed with dichloromethane, resulting in a phase separation between the organic and aqueous phases. A third intermediate phase appeared between the two phases. Addition of different salts was tried to eliminate this, but it was not completely

successful and consequently abandoned. The volume of this intermediate phase varied in both substrates and broths, perhaps depending on their composition. One factor that varies strongly between the samples is the ethanol content, which might be an explanation for the variation in volumes of this phase.

The alcohol concentration (ethanol and small amounts of methanol) will increase throughout the fermentation with time, increasing the solubility of more hydrophobic components in the broths, e.g., aromatic polymers and apolar aromatic breakdown products. The increase in alcohol levels is typically exponential for the first 2–3 h and then levels off with a small increase to the end of the fermentation (24 h).

The aromatic structure of lignin and its decomposition products and fragments consists of chromophores that strongly absorb in the UV region (190–380 nm), making them suitable for analyses with UV detection [8]. Owing to the lack of phenolic reference compounds available, the columns were calibrated with benzene homologues and benzene derivatives. The retention volumes obtained on the three GPC columns are given in Table 1.

Gel permeation chromatographic separations

Analyses for lignin and humic substances and their biodegradation is not an easy task. Various techniques have been used, e.g., UV-spectrophotometry to investigate characteristic absorption bands from residual free lignin [8], preparative reversed-phase (RP) chromatography with photodiode-array detection of fulvic substances in river waters [32], analytical RP separation for tracing phenolics in the decomposition of organic matter in soil [33] and normal-phase solid-phase extraction followed by capillary gas chromatography with flame ionization detection [34]. Phenols and aromatic hydrocarbons isolated from biomass and benzoic derivatives in wheat extracts were determined by gas chromatography with mass spectrometric and Fourier transform infrared spectrometric detection [35], whereas GPC separations were applied to biomass products [36], wheat straw extracts [37], Kraft lignin [38] and dioxane lignin [39].

TABLE 1

Retention volumes (ml) of reference compounds on three GPC columns [a]

Analyte	Column		
	Phenogel	SX-12	Zorbax
Phenol	10.0	14.2	5.8
o-Cresol	8.4	14.0	5.9
Benzaldehyde	11.3	14.5	6.0
Naphthalene	9.4	13.2	5.1
Anthracene	9.1	12.6	4.9
Chrysene	9.0	12.8	4.8

[a] For experimental conditions, see Experimental.

The distribution of high- and low-molecular-mass components from the organic and aqueous phases of the liquid–liquid extraction (see Experimental) was investigated by organic and aqueous GPC separations for the three types of hydrolysates (pine hydrolysates, SSL and EH) and the two types of broths (SSL and EH) using UV detection at 280 nm. The broths were removed from the fermenter after 1, 3 and 24 h. The resulting chromatograms of the dichloromethane-extracted phase from the four substrates and six broths are shown in Figs. 2–4. SSL shows a molecular mass distribution of compounds resulting in five main peaks in the raw substrate (see Fig. 2, a1, $t = 0$ h). The first peak in the chromatograms of the SSL fermentation (Fig. 2, a1–a4) represents compound(s) with molecular masses around 400 or higher, since they correspond to compounds with the retention time of total exclusion. This fraction, possibly lignin polymers, remains more or less constant throughout the fermentation, as illustrated in the four chromatograms in Fig. 2. The second peak in the chromatograms (Fig. 2) seems to increase during the first hour (see Fig. 2, chromatograms a2 and a3), whereafter the component is probably consumed in the process, the peak returning to the level of the start of the fermentation ($t = 0$ h), while the third peak increases and remains high until the end of the process. The components corresponding to the last two peaks are almost totally metabolized after 3 h (see Fig. 2, chromatograms a2 and a3). The distributions of components in the broth after 3 h and after 24 h are

very similar (see Fig. 2, chromatograms a3 and a4), the only difference being that the peak heights of these fractions have decreased to the end. There are differences in the resulting DAD UV spectra of the different substrates and broths of SSL, as shown in Fig. 5, proving the variation in composition of the substrate during the process. Both substrate and broth samples absorb from 225 to 380 nm with two peak maxima at 230 and 280 nm, respectively. The ratio of these two maxima (peak-height ratio) increases from 0.8 to 1.9 over 24 h.

The steam-treated enzyme hydrolysate shows minor high-molecular-mass aromatic fragments

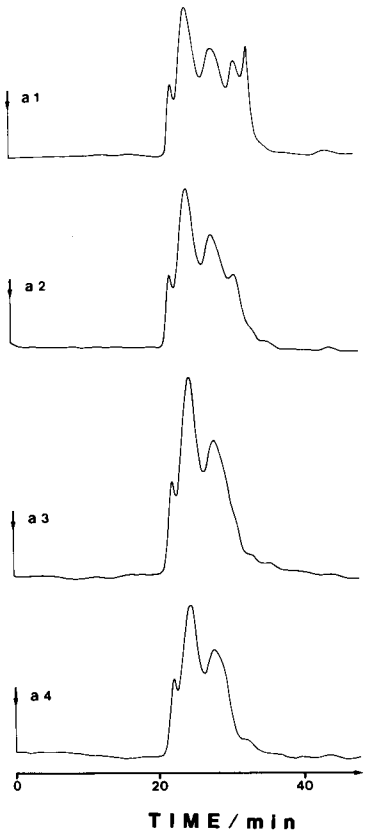

Fig. 2. Chromatograms of the organic phase of the (liquid–liquid extraction) spent sulphite liquor (SSL) diluted 100-fold using a Bio-Beads SX-12 GPC column with dichloromethane as the mobile phase. UV detection at 280 nm (attenuation 0.1 a.u.f.s.); flow-rate, 0.5 ml min^{-1}; injection, volume 20 μl. (a1) Substrate at $t = 0$ h; (a2) broth at $t = 1$ h; (a3) broth at $t = 3$ h; (a4) broth at $t = 24$ h.

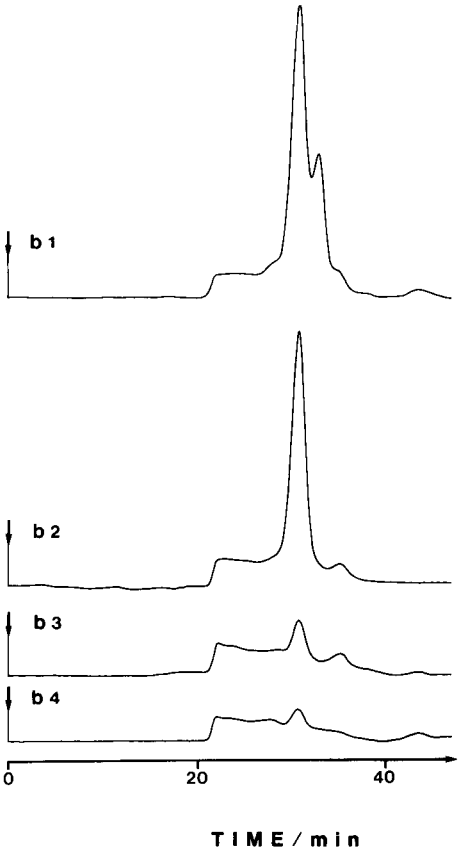

Fig. 3. Chromatograms of the organic phase of the (liquid–liquid extraction) enzyme-hydrolysed willow (EH) samples diluted 100-fold. Conditions as in Fig. 2. (b1) Substrate at $t = 0$ h; (b2) broth at $t = 1$ h; (b3) broth at $t = 3$ h; (b4) broth at $t = 24$ h.

(see Fig. 3, chromatograms b1–b4). There are two major peaks in the hydrolysate corresponding to the retention time of aromatic monomers. The first of these two peaks decreases during the first hour (see Fig. 3) while the second peak decreases to about one tenth of its original height after 24 h. The component corresponding to the second peak is decomposed very fast; it can hardly be traced after 1 h of fermentation. The spectra of the EH samples (see Fig. 6) appear very similar to those for SSL, the only difference being that the ratio of the characteristic bands at 230 and 280 nm does not shift during the process.

The GPC separations of the two pine hydrolysates are illustrated in Fig. 4. The first hemicel-

lulose fraction contains some minor high-molecular-mass fractions while two major peaks appear at the end of the chromatogram, corresponding to monomeric phenolics. The enzymatically hydrolysed cellulose fraction (see Fig. 4, chromatogram c2) also contains minor fractions of high-molecular-mass components whereafter one large peak appears in the chromatogram corresponding to the same retention time as for the first peak of the hemicellulose fraction (see Fig. 4). The DAD UV spectra of the two substrates are almost identical, the hemicellulose having a sharper absorption peak around 280 nm compared with the cellulose hydrolysate (see Fig. 7).

The organic phases of the four different substrate extracts show minor differences in the distribution of compounds depending on the type of

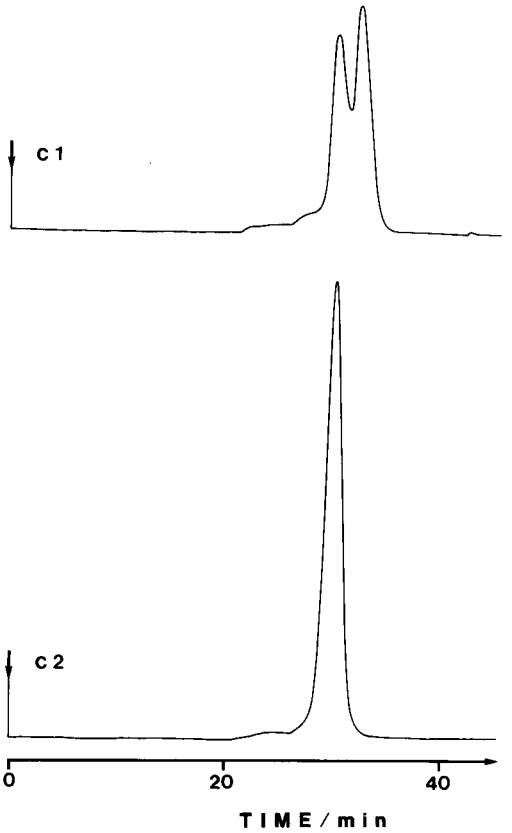

Fig. 4. Chromatograms of the organic phase of the (liquid–liquid extraction) acid-hydrolysed pine samples diluted 100-fold. Conditions as in Fig. 2. (c1) Hemicellulose substrate, (c2) cellulose substrate.

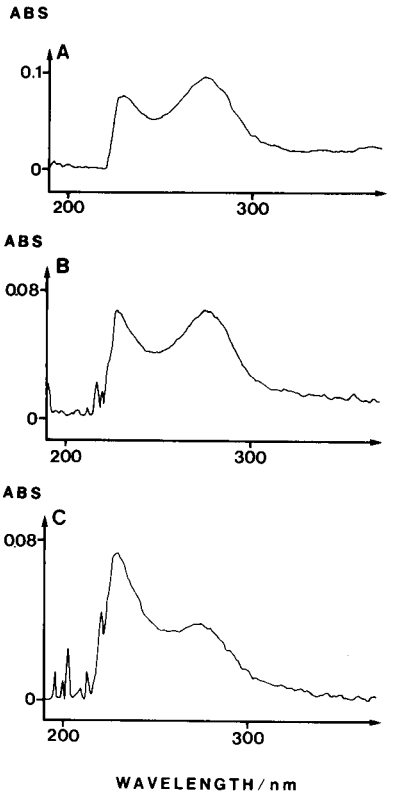

Fig. 5. Diode-array UV spectra of the organic phase of the (liquid–liquid extraction) spent sulphite liquor (SSL) diluted 1000-fold in a flow-injection analysis system using dichloromethane as the eluent and an injection volume of 20 μl. (A) Substrate at $t = 0$ h; (B) broth at $t = 3$ h; (C) broth at $t = 24$ h.

hydrolysis treatment and the origin of the wood. There is also a difference in substrate composition between SSL and EH broths in the presence of lignin components that are not consumed or degraded in SSL as in EH to the end of the fermentation. Hydrolysis of the cellulose by catalysis with cellulase enzymes produces less lignins and derivatives because the hydrolysis of the various types of cellulases is selective [40–42]. This is not the case with chemical hydrolysis, which often takes place at high temperature and at extreme pH values and yields a more complex matrix.

The aqueous extracted fractions of both substrates and broths were found to contain major amounts of the lignin polymers and their decomposition products. The levels of poly-, oligo- and

monomers of aromatics, e.g., phenols, phenol derivatives, aromatic acids, alcohols and aldehydes, are high in these types of samples [43,44]. The amounts of high-molecular-mass compounds vary strongly in the aqueous phase for SSL during the fermentation (see Fig. 8, chromatograms a1–a4), illustrated by the first peak in the chromatograms. This variation was found to be just the opposite in the organic phase for SSL, where it was almost constant throughout the fermentation. The two eluted peaks in the middle of the chromatograms have changed after 1 h (see Fig. 8, chromatogram a2) of fermentation whereafter they return to the levels similar to that of the starting point after 3 h, remaining constant until the end of the process. The last peak in the separation remains more or less constant throughout the 24 h. The DAD UV spectra corresponding to the starting substrate and to the end of the process (24 h), shown in Fig. 9, vary only slightly in broadness and heights of the absorption bands of the two spectra, which is in accordance with the chromatographic separation (see Fig. 8, chromatograms a1 and a4). The peak maximum at 210 nm is broader for the substrate ($t = 0$ h) than for the broth ($t = 24$ h). The characteristic peak maximum for lignin compounds at 280 nm at the start is also higher than in the fermented broth.

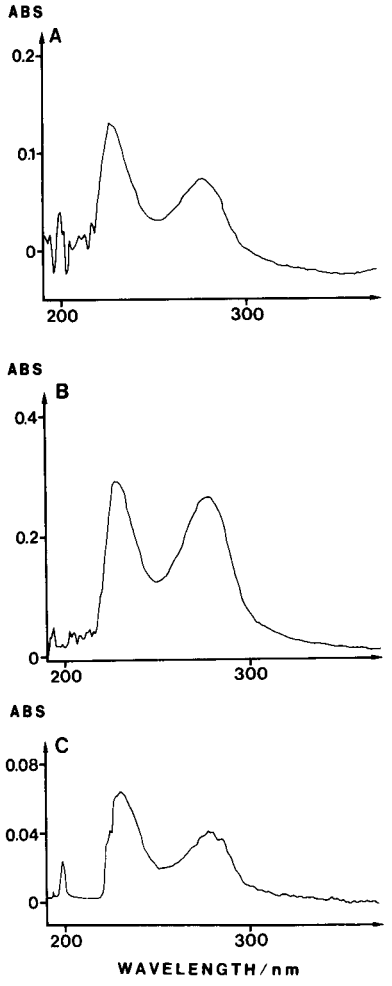

Fig. 6. Diode-array UV spectra of the organic phase of the (liquid–liquid extraction) enzyme-hydrolysed willow (EH) samples diluted 1000-fold. Conditions as in Fig. 5. (A) Substrate at $t = 0$ h; (B) broth at $t = 3$ h; (C) broth at $t = 24$ h.

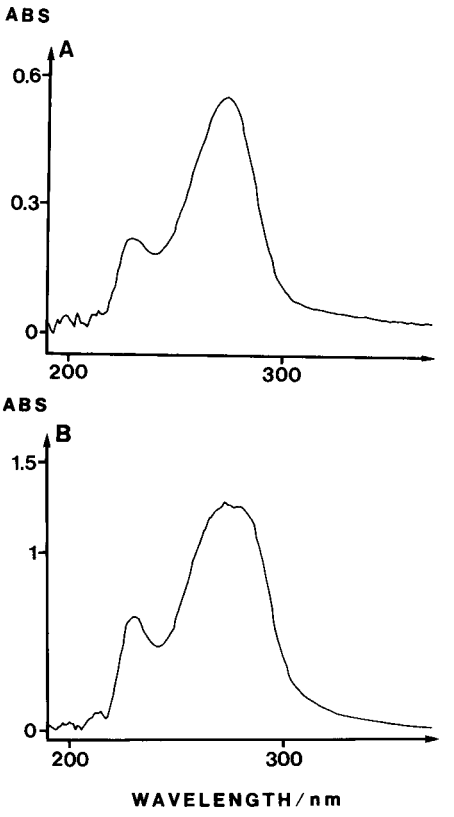

Fig. 7. Diode-array UV spectra of the organic phase of the (liquid–liquid extraction) acid-hydrolysed pine samples diluted 1000-fold. Conditions as in Fig. 5. (A) Hemicellulose substrate; (B) cellulose substrate.

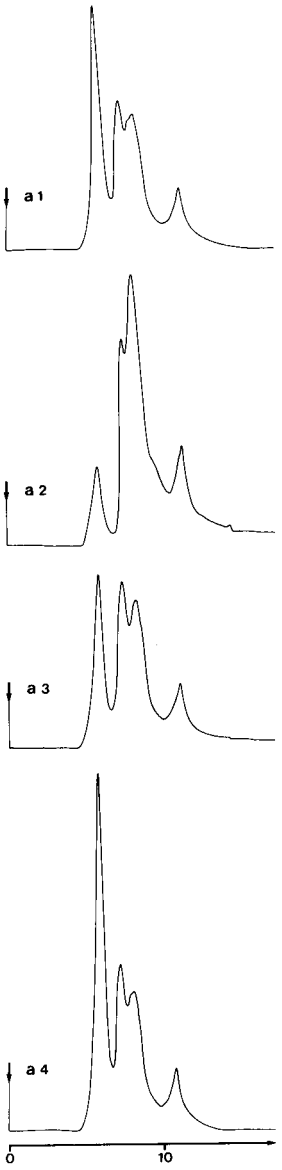

Fig. 8. Chromatograms of the aqueous phase of the (liquid–liquid extraction) spent sulphite liquor (SSL) diluted 500-fold using a Zorbax PSM 60 GPC column with water containing 5% methanol as the mobile phase with UV detection at 280 nm (attenuation 1.0 a.u.f.s.). Flow-rate, 0.5 ml min^{-1}, injection volume, 20 μl. (a1) Substrate at $t = 0$ h; (a2) broth at $t = 1$ h; (a3) broth at $t = 3$ h; (a4) broth at $t = 24$ h.

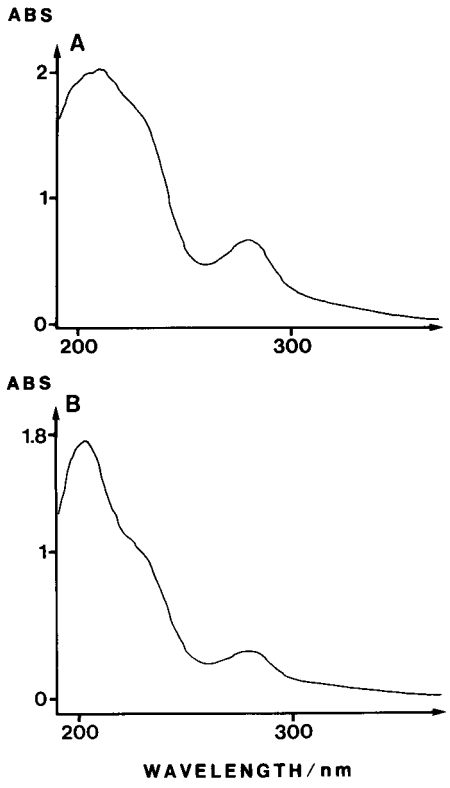

Fig. 9. Diode-array UV spectra of the aqueous phase of the (liquid–liquid extraction) spent sulphite liquor (SSL) diluted 1000-fold analysed in a flow-injection system using water as the eluent with an injection volume of 20 μl. (A) Substrate at $t = 0$ h; (B) broth at $t = 24$ h.

It can be seen by comparing the two chromatograms in Fig. 8 (chromatogram a1) and Fig. 10 (chromatogram b1) that the enzyme-hydrolysed willow substrate is much "cleaner" and has a less complex composition than SSL. The aqueous phase of the liquid extract of the willow substrate contains a small fraction eluting at the beginning of the chromatogram, whereafter a major peak appears as shown in Fig. 10. The chromatogram also contains small fractions that correspond to the elution time of aromatic monomers. The broth (Fig. 10, chromatogram b2) consists of almost the same molecular mass distribution of components as for the starting broth, with one exception. A large peak appears at the very end of the separation. The capacity factor (k') of this element(s) far exceeds the k' value of

NaCl, the smallest molecule separated. Consequently, it is assumed that this peak corresponds to compound(s) produced in the process that have a high affinity for the silica surface of the support. The retention is therefore not only due to size exclusion. An interesting observation is that the DAD UV spectra of the substrate and broth are very similar (see Fig. 11), although the chromatograms are very different. The only difference in the DAD UV spectra of the substrate and broth is in the total absorbance value, where the substrate diluted 500-fold and the broth 3000-fold resulted in almost the same total absorption, as shown in Fig. 11. This difference in absorbance values partly explains the large peak at the end of the chromatogram of the broth (Fig. 10, chromatogram b2).

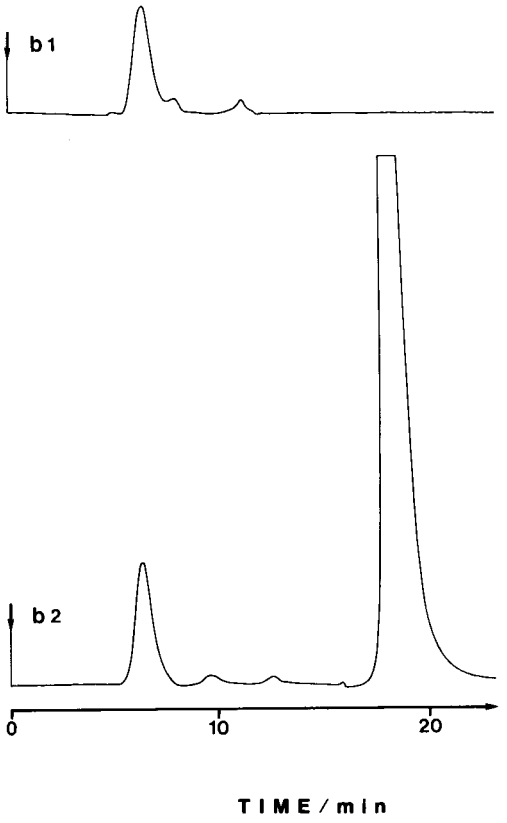

Fig. 10. Chromatograms of the aqueous phase of the (liquid–liquid extraction) enzyme-hydrolysed willow (EH) samples diluted 500-fold. Attenuation 0.5 a.u.f.s.; other conditions as in Fig. 8. (b1) Substrate at $t = 0$ h; (b2) broth at $t = 1$ h.

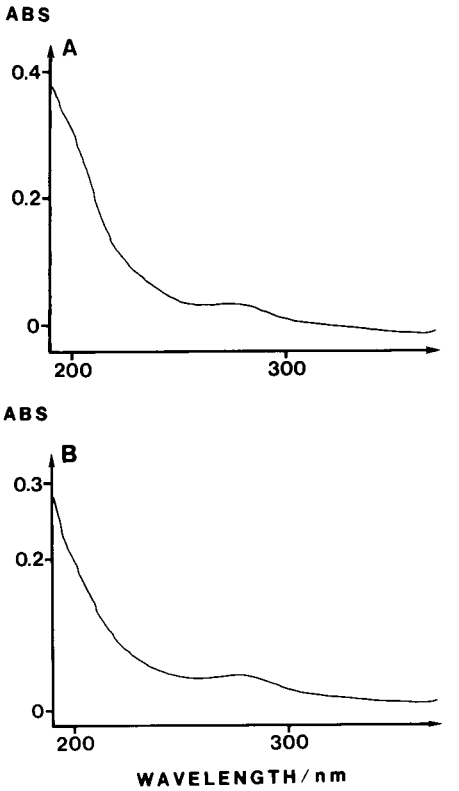

Fig. 11. Diode-array UV spectra of the aqueous phase of the (liquid–liquid extraction) enzyme-hydrolysed willow (EH). Conditions as in Fig. 9. (A) Substrate sample diluted 1000-fold at $t = 0$ h; (B) broth diluted 3000-fold at $t = 1$ h.

The aqueous phase of the pine hemicellulose hydrolysate shows a separation consisting of three major peaks with the first two eluting in the middle of the operating molecular mass range of the column (see Fig. 12, chromatogram c1). The third major fraction of the substrate has a retention time similar to those of degraded aromatic monomers from lignin.

The composition of the cellulose hydrolysate is illustrated in Fig. 12, chromatogram c2. A negative peak is seen in the beginning of the chromatogram corresponding to k' values of larger molecules. It is assumed that the eluted salt or matrix components, and possibly analyte(s) present in the sample, cause a refractive index effect in the UV flow cell, resulting in this negative dip. The substrate contains only one major peak.

The DAD UV spectra of the two pine substrates are shown in Fig. 13. They look very similar but the cellulose hydrolysate shows a higher absorption than the hemicellulose hydrolysate at 280 nm. Just like in the organic phase, there are major differences in lignin content in the various samples in the aqueous phase. However, the spectra for the SSL and pine hydrolysates have bands that are more similar than EH, which exhibits an absorption over almost the whole UV region (190–350 nm).

The liquid–liquid (dichloromethane–water) extraction of the samples gave an additional intermediate phase. After organic and aqueous GPC separations, the total content of the samples was investigated by using water-miscible tetrahydrofuran as the mobile phase, in which the samples were totally soluble, with a Phenogel GPC separation column. It was found that the flow-rate

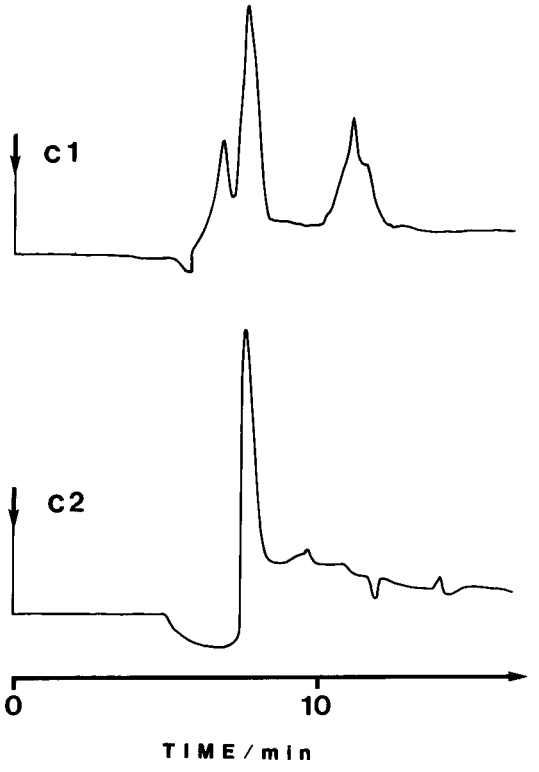

Fig. 12. Chromatograms of the aqueous phase of the (liquid–liquid extraction) acid-hydrolysed pine samples diluted 500-fold. Conditions as in Fig. 8. (c1) Hemicellulose substrate; (c2) cellulose substrate.

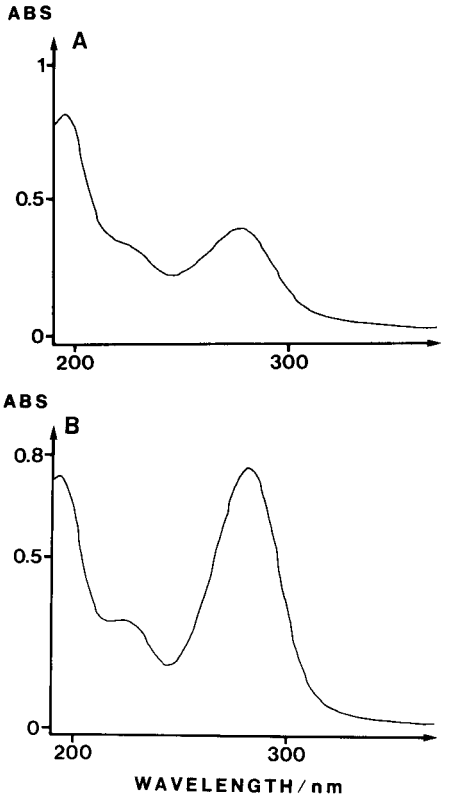

Fig. 13. Diode-array UV spectra of the aqueous phase of the (liquid–liquid extraction) acid-hydrolysed pine diluted 3000-fold. Conditions as in Fig. 9. (A) Hemicellulose substrate; (B) cellulose substrate.

influences the separation factor of some benzenes owing to the poor resolution of the column. The variations in the resolution of benzene, naphthalene, coronene, anthracene and chrysene at various flow-rates are shown in Fig. 14. The resolution of the benzenes is poor at 2 and 1 ml min^{-1} (see Fig. 14a and b). The resolution is improved by using a flow-rate of 0.35 ml min^{-1}, but this resulted in a larger band-broadening and a longer analysis time. The separation becomes worse again on going to lower flow-rates. Resolution between chrysene–anthracene and naphthalene–coronene could not be obtained at any of the flow-rates investigated.

The resulting chromatograms of SSL, EH and the two Canadian hydrolysates and broths using a flow-rate of 0.4 ml min^{-1} are shown in Figs. 15–17. There is no significant difference between

the SSL samples at the beginning, during (chromatograms not shown) and at the end of the fermentation (see Fig. 15). The EH samples show some variation during the fermentation. This can be seen in Fig. 16, where chromatogram b1 is at the start ($t = 0$ h) and b3 after 3 h of fermentation. There are more smaller fractions produced in the process with time. The chromatogram at the end ($t = 24$ h) was almost identical with chromatogram b3. The pine hydrolysates did not show large differences in this GPC separation using tetrahydrofuran as the mobile phase. The hemicellulose and cellulose hydrolysates contain many components. This is to be expected, as a lot of soluble lignin derivatives are present in the first hemicellulose fraction. Lignin polymers more tightly bound to the cellulose can only be dissolved by higher temperatures in combination with the addition of acid. This is just what is done with the cellulose of the pine. The result is that both hydrolysates seem to have a similar composition of lignin polymers and their corresponding breakdown products.

It is difficult to draw any real conclusions from the separations made on the Phenogel column regarding the content of aromatic poly-, oligo- and monomers present in the intermediate phase, not only because of the poor resolution, of the column but also because of the difficulties in evaluating the third intermediate phase with the help of the chromatograms from the organic and aqueous phases in the other two GPC systems. The reason is that it is difficult to transform the resolution efficiencies of each column because of the lack of appropriate standards.

Conclusions

Characterization of fermentation substrates and broths can be achieved by combining chromatograms from organic and aqueous GPC separations with DAD UV spectra. Lignin, its breakdown products and derivatives were found to be present in both the organic and aqueous phases in all four substrates and six fermented broths studied. It can be concluded that these chromatographically interfering components are present during the whole fermentation process, thus requiring the use of certain sample pretreatment

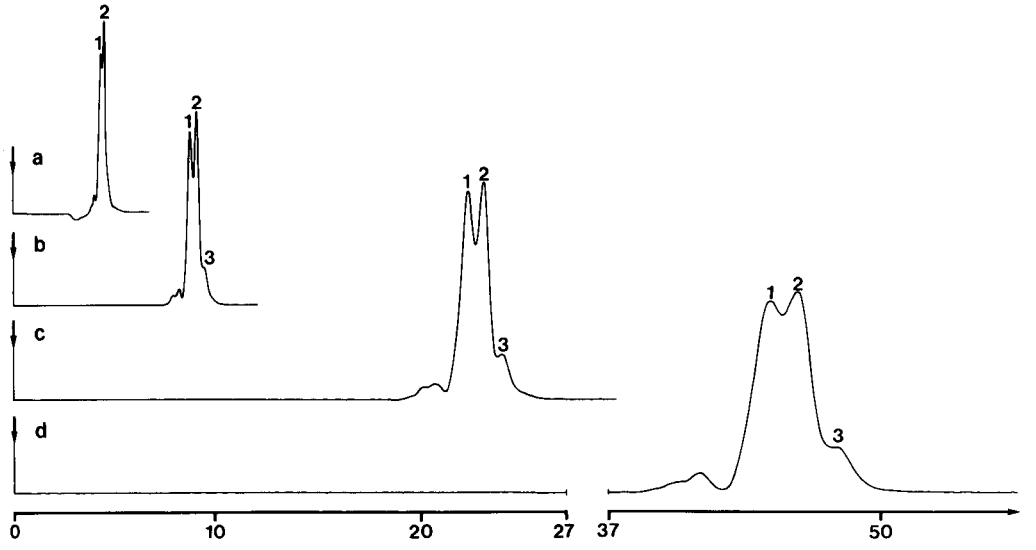

Fig. 14. Resulting chromatograms of the flow dependence of the Phenogel column using terahydrofuran as the mobile phase. Attenuation 0.5 a.u.f.s.; all other conditions as in Fig. 8. (a) 2 ml min^{-1}; peak 1 = chrysene, anthracene; peak 2 = naphthalene, coronene and benzene. (b) 1 ml min^{-1}; peak 1 = chrysene, anthracene; peak 2 = naphthalene, coronene; peak 3 = benzene. (c) 0.35 ml min^{-1}; peak 1 = chrysene, anthracene; peak 2 = naphthalene, coronene; peak 3 = benzene. (d) 0.1 ml min^{-1}; peak 1 = chrysene, anthracene; peak 2 = naphthalene, coronene; peak 3 = benzene.

steps when components other than these aromatic derivatives are being analysed. These lignin compounds might otherwise cause severe interferences in the chromatographic separations. This is particularly true when aqueous mixtures of mobile phases are used owing to the poor solubility of many of the interferents, leading to precipitation on the chromatographic support. This was obvious in a reversed-phase LC separation applied to Ebro river waste water [45], where 75% of acetonitrile had to be added to be able to desorb lignin polymers bound to the stationary phase in the analytical column.

Further qualitative work with these types of biotechnological fermentation samples for analyses for phenolics and breakdown products from lignin is in progress and our preliminary results have shown the presence of these type of phenolics and aldehydes [11].

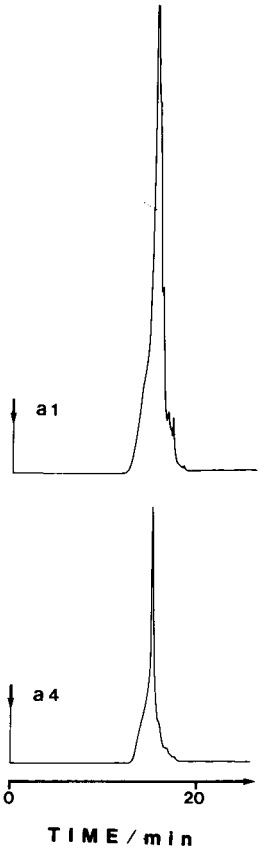

Fig. 15. Separations of spent sulphite liquor (SSL) diluted 1000-fold using a Phenogel GPC column with tertahydrofuran as the mobile phase. Flow-rate, 0.4 ml min^{-1}; all other conditions as in Fig. 8. (a1) Substrate at $t = 0$ h; (a4) broth at $t = 24$ h.

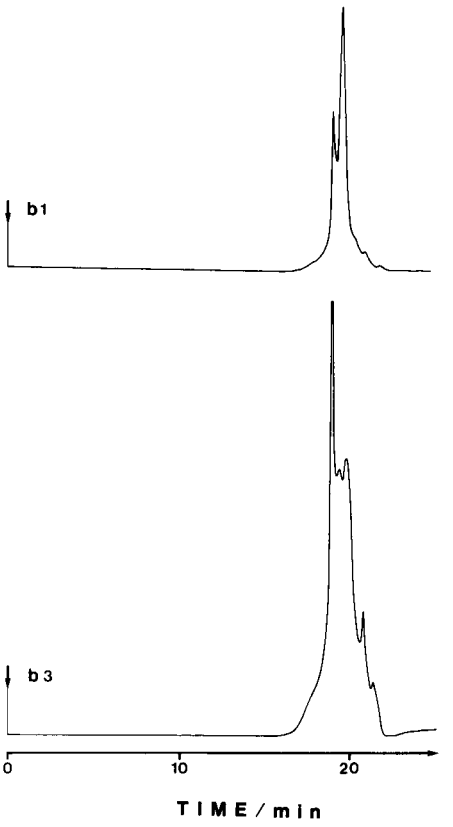

Fig. 16. Separations of enzyme-hydrolysed pine samples diluted 500-fold. Conditions as in Fig. 15. (b1) Substrate at $t = 0$ h; (b3) broth at $t = 3$ h.

LC–mass spectrometric analysis of lignin breakdown products will help to solve problems encountered with the determination of sugars co-eluting in ligand-exchange separations in carbohydrate analysis [46]. Another important reason for determining phenolics and derivatives is that biochemical mechanistic studies can be made by investigating the potential inhibitory effect of these compounds [47,48] on the process, as little is known about the content and the effect of these inhibitors.

Funding for this work was obtained from the Swedish Board for Technical Development

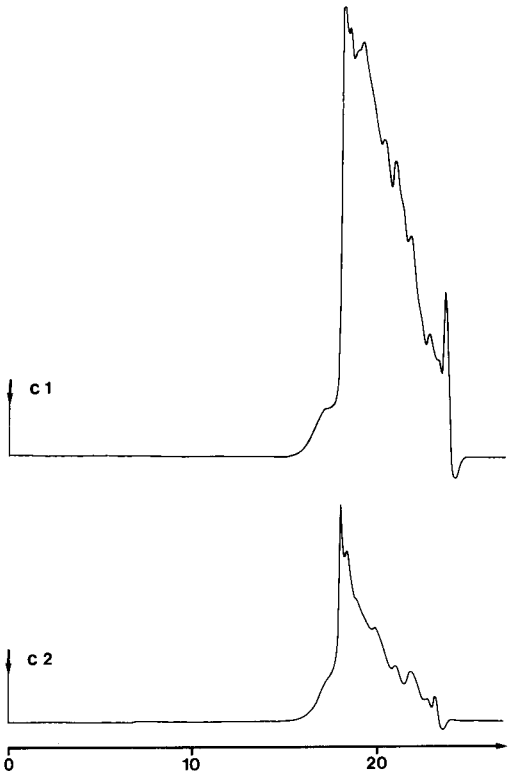

Fig. 17. Separations of acid-hydrolysed pine diluted 1000-fold. Conditions as in Fig. 15. (c1) Hemicellulose substrate, (c2) cellulose substrate.

(STU), the Swedish Institute and Craaford Stiftelsen. Mr. Alexander Rappensberger is gratefully acknowledged for the help with the figures. The steam-treated hydrolysate was a gift from M. Galbe and R. Eklund, Department of Chemical Engineering, University of Lund, Sweden, the spent sulphite liquor from Modo, Örnsköldsvik, Sweden, and the two Canadian hydrolysates from A. O'Boyle and D. Good, Bio-Hol Developments, Ontario, Canada. The fermentation samples were a gift from Mr. T. Lindén, Department of Technical Microbiology University of Lund. The authors also thank Miss Lisbeth Olsson, Department of Technical Microbiology, University of Lund, for constructive discussions concerning this work.

REFERENCES

1 S.R. Parekh and M. Wayman, Process Biochem., 6 (1987) 25.
2 S.G. Patil and B.G. Patil, Enzyme Microb. Technol., 11 (1989) 38.
3 S.P. Oliver and P.J. du Toit, Biotechnol. Bioeng., 28 (1986) 684.
4 A.F. Pomes, J. Am. Chem. Soc Brew. Chem., 38 (1980) 67.
5 T. Lindén and B. Hahn-Hägerdal, Enzyme Microb. Technol., 11 (1989) 583.
6 T. Lindén and B. Hahn-Hägerdal, Appl. Environ. Microbiol., 58 (1992) 1661.
7 T. Lindén and B. Hahn-Hägerdal, Enzyme Microb. Technol., in press.
8 H. Janshekar and A. Fiechter, in A. Fiechter (Ed.), Advances in Biochemical Engineering/Biotechnology, Springer, Berlin, 1983, p. 53.
9 G. Marko-Varga, E. Domínguez, B. Hahn-Hägerdal, L. Gorton, H. Irth, G.J. De Jong, R.W. Frei and U.A.Th. Brinkman, J. Chromatogr., 523 (1990) 173.
10 G. Marko-Varga, E. Domínguez, B. Hahn-Hägerdal and L. Gorton, J. Chromatogr., 506 (1990) 423.
11 G. Marko-Varga, G. Durand and D. Barceló, unpublished results.
12 A.L. Pometto and D.L. Crawford, Methods Enzymol., 161B (1988) 183.
13 R. Eklund, M. Galbe and G. Zacchi, J. Wood Chem. Technol., 8 (1988) 379.
14 R. Eklund, M. Galbe and G. Zacchi, in M. Matsuoka (Ed.), VIII International Symposium on Alcoholic Fuels, New Energy and Industrial Technology Development Organization, Tokyo, 1988, p. 101.
15 J.E. Fein, D. Potts, D. Good, M. Beavan, A. O'Boyle, D. Dahlgren, M.J. Beck and R.L. Griffith, in IGT Conference on Energy from Biomass and Wastes XV, p. 269.
16 T. Lindén and B. Hahn-Hägerdal, Biotechnol. Tech., 3 (1989) 189.
17 L. Olsson, T. Lindén and B. Hahn-Hägerdal, Appl. Biochem. Biotechnol., 34/35 (1992) 359.
18 P.A. Pfeifer, G. Bonn and O. Bobleter, Biotechnol. Lett., 6 (1984) 541.
19 A.V. Tran and R.P. Chambers, Enzyme Microb. Technol., 8 (1986) 439.
20 R.L. Crawford (Ed.), Lignin Biodegradation and Transformation, Wiley, New York, 1981.
21 M.D. Rahman and J.M. Pepper, J. Wood Chem. Technol., 8 (1988) 313.
22 R. McElroy and K. Lai, J. Wood Chem. Technol., 8 (1988) 313.
23 H.J. Wenzl, The Chemical Technology of Wood, Academic, New York, London, 1970.
24 F. Tjerneld, I. Persson, P.-Å. Albertsson and B. Hahn-Hägerdal, Biotechnol. Bioeng., 15 (1985) 40.
25 H.L. Bonn, M. McNeal and G.A. O'Connor (Eds.), Soil Chemistry, Wiley, New York, 1979.

26 T.A. Clark and K.L. Mackie, J. Chem. Technol. Biotechnol., 34 (1984) 101.
27 G.R. Ailen, D.M. McKnight, R.L. Warstaw and P. MacCarthy (Eds.), Humic Substances in Soil and Water Geochemistry: Isolation and Characterisation, Wiley, New York, 1985.
28 G.G. Choudry (Ed.), Humic Substances, Gordon and Breach, New York, 1984.
29 N.A. Eskin, H.M. Handerson and R.J. Townsend, Biochemistry of Food, Academic, New York, 1971.
30 L.C. Maillard, C.R. Acad. Sci., 154 (1912) 66.
31 C. Hagström-Näsi and E. Sjöström, J. Wood Chem. Technol., 8 (1988) 299.
32 F.Y. Saleh, W.A. Ong and D.Y. Chang, Anal. Chem., 61 (1989) 2792.
33 R.D. Hartley and H. Buchan, J. Chromatogr., 180 (1979) 139.
34 C. Brage and K. Sjöström, J. Chromatogr., 538 (1991) 303.
35 H.J. Chavas das Neves and E.M. Monteiro Gaspar, J. High Resolut. Chromatogr., 13 (1990) 550.
36 E. Burtscher, O. Bobleter, W. Schweld, R. Concin and H. Binder, J. Chromatogr., 390 (1987) 401.
37 G.C. Galletti and G. Chiavari, J. Chromatogr., 536 (1991) 303.
38 S.S. Kelley, W.G. Glasser and T.C. Ward, J. Wood Chem. Technol., 8 (1988) 341.
39 C. Hagström-Näsi and E. Engvall, Holzforschung, 41 (1987) 39.
40 T.M. Wood and V. Garcia-Campayo, Biodegradation, 1 (1990) 147.
41 T.W. Jeffries, Biodegradation, 1 (1990) 163.
42 T.M. Enari and M-L. Niku-Paavolaa, CRC Crit. Rev. Biotechnol., 5 (1986) 67.
43 J. Buchert, K. Niemelä, J. Puls and K. Poutanen, Process Biochem. Int., 10 (1990) 176.
44 G.E. Achladas, J. Chromatogr., 542 (1991) 263.
45 G. Marko-Varga and D. Barceló, Chromatographia, (1992) 34 (1992) 146.
46 G. Marko-Varga, L. Gorton, E. Domínguez and D. Barceló, Chromatographia, submitted for publication.
47 J. Buchert and K. Niemelä, J. Biotechnol., 18 (1991) 1.
48 N. Banerjee, R. Bhatnager and L. Viwanathan, Enzyme Microb. Technol., 3 (1981) 24.

Analytica Chimica Acta, 270 (1992) 79–86
Elsevier Science Publishers B.V., Amsterdam

Preconcentration of chromium, copper and manganese from sea water on pretreated solid materials for determination by atomic absorption spectrometry

F. Baffi, A.M. Cardinale and R. Bruzzone

Istituto di Chimica Generale, Cattedra di Chimica Analitica, Università di Genova, Viale Benedetto XV 3, 16132 Genova (Italy)

(Received 20th March 1992; revised manuscript received 10th June 1992)

Abstract

A systematic study of the use in "batch equilibration" of pretreated solid Chelex-100 and Lewatit TP 207 (H^+ form) for the preconcentration of Cr(III), Cu(II) and Mn(II) dissolved in sea water is presented. The preparation of the resin and the suggested procedure are useful because sea water can be treated immediately after sampling, which is very important with regard to speciation analysis. A comparison between Chelex-100 and Lewatit TP 207 resins showed that the macroporous Lewatit TP 207 is able to recover both the colloidal form and the free dissolved ionic form of Cr(III). For Cu(II) the use of both exchangers on two sea water subsamples will give useful information, whereas for Mn(II) the choice of Chelex-100 or Lewatit TP 207 is immaterial.

Keywords: Atomic absorption spectrometry; Sample preparation; Chromium; Copper; Manganese; Preconcentration; Sea water

The determination of the total concentrations of heavy metals and more especially their speciation analysis in sea water are very important with regard to their toxicity and their biogeochemical cycles in the marine environment [1].

Because of the low concentrations of these metals in sea water, a prior preconcentration step is usually required. Many procedures have been suggested, but the most common is the use of Chelex-100. Riley and Taylor [2] carried out the first study on this resin, reporting the recoveries of numerous species. They also developed an on-column preconcentration procedure for Cu, Zn, Cd, Ni and Co from sea water. Florence and Batley [3] criticized this use of Chelex-100 because the resin in the H^+ form could chelate heavy metals only after the passage of about 1 l of sea water, which causes a loss of about 10%. They suggested a column pretreatment with sodium acetate solution in order to obtain the first effluent at pH 7.1 [4]. They pointed out that Chelex-100 is not suitable for capturing metals adsorbed on organic and inorganic colloids, so that for a total content determination, pretreatment of the sample is necessary.

Kingston et al. [5] studied the interferences from the salt matrix eluted at the same time as the heavy metals. The problem became important when sophisticated instrumental techniques such as electrothermal atomic absorption spectrometry (AAS) were used. They proposed the use of a Chelex-100 column (100–200 mesh) in the ammonium form. The most interesting aspect is the selective elution of the salt matrix using 1 M

Correspondence to: F. Baffi, Istituto di Chimica Generale, Cattedra di Chimica Analitica, Università di Genova, Viale Benedetto XV 3, 16132 Genova (Italy).

ammonium acetate, followed by elution of the heavy metals with 2.5 M HNO_3, in order to determine metals by electrothermal AAS.

The utilization of Chelex-100 was studied, comparing various preconcentration procedures, by Boniforti et al. [6]. They used the method proposed by Kingston et al. [5], the preconcentration step being carried out in batch followed by on-column elution. The possible use of Chelex-100 to characterize chemical classes of metals in sea water was discussed in a study for Cd [7]. The aim was to obtain an exchanger able to give the minimum alteration of a sea water system in the preconcentration phase. This procedure, although satisfactory for Cd, as the blank values were very low, was not satisfactory for other metals. Further tests were carried out [8] to utilize Chelex-100 in the H^+ form and in batch equilibration. The utilization of the H^+ form when used in a column was previously criticized by Florence and Batley [4]. The present procedure utilizes the buffer capacity of sea water to retain the metals by the resin through prolonged contact between the two phases.

The aim of this study was to develop a simple, rapid and accurate procedure for the preconcentration of Cr(III), Cu(II) and Mn(II) from sea water. Chelex-100 and the Lewatit TP 207 ion exchanger, a weakly complexing and macroporous resin, both in the H^+ form, were used. As far as is known, the ion exchanger Lewatit TP 207 has never been used with a sea-water matrix. To characterize sea-water samples in terms of bioavailability, the possibility of the simultaneous use of both exchangers is considered.

EXPERIMENTAL

Samples

Samples of coastal sea water, previously homogenized, were filtered through a 0.40-μm Nuclepore filter in a nitrogen atmosphere using a pressure difference of about 40 kPa. The subsamples were immediately treated with the resin in order to effect the preconcentration.

The standard sea water CASS-2 (National Research Council of Canada, Sea Water Reference Materials), used in order to test the method, attained a pH of 6–7 with addition of about 1.80 g l^{-1} of Na_2CO_3.

Instrumentation

A Varian AA 300 atomic absorption spectrometer with GTA graphite furnace, Model 96 autosampler and IBM computer were used for the determination of metals in the eluate. A Varian Model 400 atomic absorption spectrometer with a Zeeman-effect background corrector was also used for Cu and Cr. The standard addition method was used to determine metal concentrations in each sample.

Reagents

Nitric acid (65%), hydrochloric acid (37%), sodium carbonate (Suprapur, Merck), sodium hydroxide (20%), hydrochloric acid (37%) (RPE, Carlo Erba) and 1000 mg l^{-1} standard solutions (Merck) were used.

Materials

Containers, micropipette tips and other laboratory materials were made of polythene or polystyrene. The filtration apparatus was made of polycarbonate (Sartorius, Model SM165.10); 60-μm nylon filters and 0.40-μm Nuclepore filters were used.

Cleaning procedure

Before use, the containers, filtration apparatus and micropipette tips were treated with HCl (1 + 1) for 1 h, washed with high-purity water [obtained from a Milli-Q system (Waters)], dried at 40°C, washed with Freon TF and stored in polythene bags.

Nylon filters were washed with NaOH (1 + 1) and deionized and Milli-Q-purified water. Nuclepore filters were washed with HCl (1 + 1) and deionized and Milli-Q-purified water.

All chemical procedures were carried out in a hood with a laminar vertical flow, using polythene gloves.

Exchangers

Chelex-100 (Na^+ form) (Bio-Rad Laboratories), 50–100 mesh, and Lewatit TP 207 (Na^+ form) (Bayer), 50 mesh, were used.

Preparation of exchangers in H^+ form

Two different methods for the preparation of the exchangers, one rapid and the other slow, have been carried out. According to the rapid procedure: 10 g of the exchangers were equilibrated for 24 h with 500 ml of 2 M HCl and washed with Milli-Q-purified water (500 ml for 2 h) to pH 5.5, which became stable after 30 h, then dried at 40°C and stored. According to the slow procedure: a 10-g amount of Na^+-form exchanger was equilibrated with 500 ml of 2 M HCl for 24 h. Each day for three days, three washings with Milli-Q-purified water were made. During the next 25 days, only one washing (500 ml) was made each day to ensure the diffusion of the excess of the H^+ ions from the interior of the microporous resin. At the end of these washings the pH was 5.5 and it was always the same after 60 h.

Capacity experiments with resins in H^+ form

Experiments were carried out in batch equilibration by varying the ratio of sea water volume to dried resin weight. Each exchanger (0.15 g) was used with sea water volumes increasing from 100 to 800 ml in the same kind of container. The contact time was 30 h.

RESULTS AND DISCUSSION

The first stocks of exchangers (Chel 1 and Lew 1) were prepared with the rapid procedure.

pH controls in capacity experiments

The final pH values, evaluated after 30 h, were already reached within a maximum of 2 h [8], ensuring that the resin–sea water contact time was sufficient for chelation or exchange.

The pH values obtained with different volumes of sea water are reported in Fig. 1. With Chelex-100 resin a pH value of 5.5 is obtained using a volume between 100 and 200 ml; at this pH chelation can occur [3]. It seems that Lewatit TP 207 is able to retain metallic ions (by ion exchange or complexing, according to the producer) at pH 4.5, corresponding to a volume of 100 ml. For both Chelex-100 and Lewatit TP 207, the pH values exhibit only a small variation on changing the volumes of sea water in the range 200–400 ml.

Capacity experiments

Capacity experiments were carried out with Chel 1 or Lew 1 in order to verify the behaviour

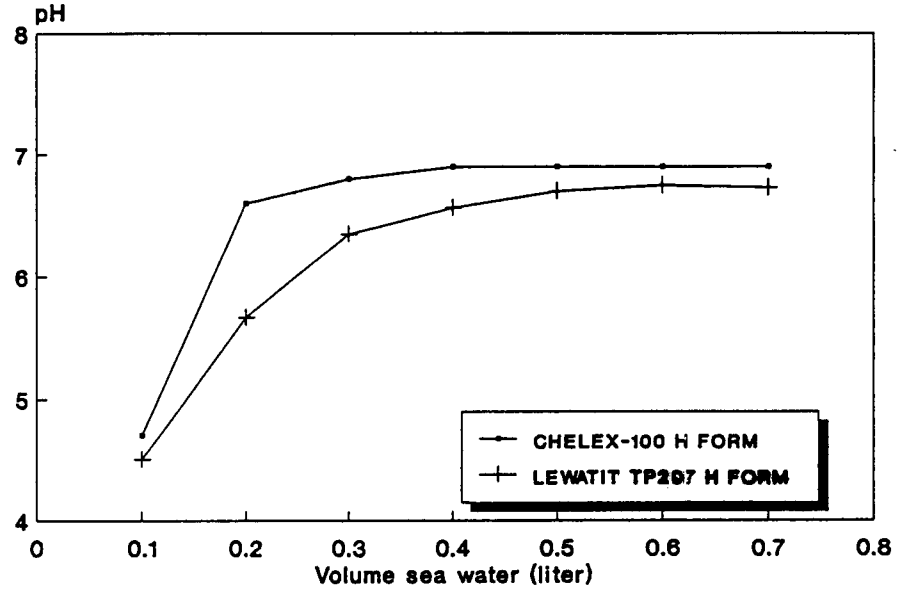

Fig. 1. pH values obtained with different volumes of sea water after 30-h batch equilibration with 0.15 g of (•) Chelex-100 (Chel 1) and (+) Lewatit TP 207 (Lew 1) resins in the H^+ form.

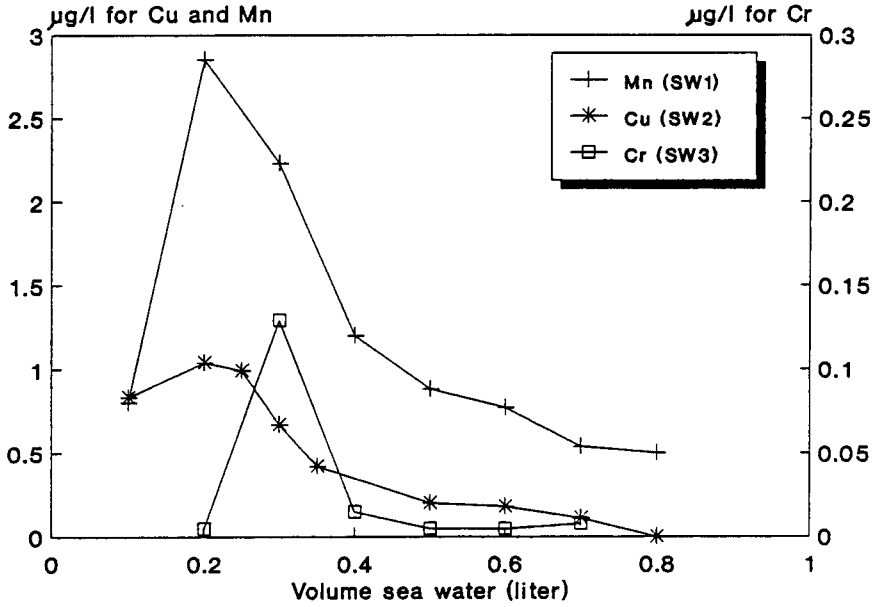

Fig. 2. Capacity curves for (□) Cr(III), (*) Cu(II) and (+) Mn(II) ($\mu g\ l^{-1}$ vs. sea water volume) for different samples [(+) SW1; (*) SW2; (□) SW3] using 0.15 g Chelex-100 (Chel 1), H^+ form. Blank values for 0.15 g of resin: 5.0 ng, 17.0 ng and at the detection limit for Cr, Cu and Mn, respectively.

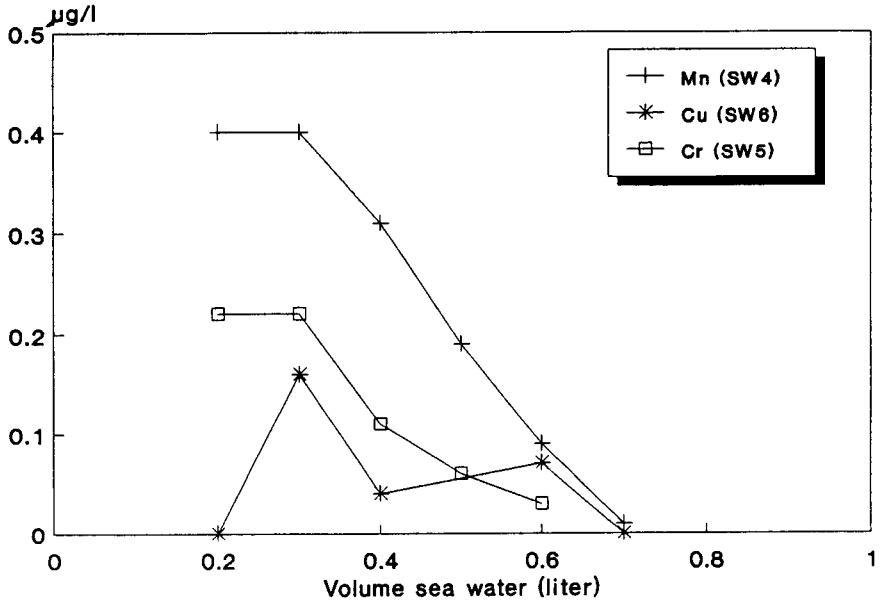

Fig. 3. Capacity curves for (□) Cr(III), (*) Cu(II) and (+) Mn(II) ($\mu g\ l^{-1}$ vs. sea water volume) for different samples [(+) SW4; (□) SW5; (*) SW6] using 0.15 g Lewatit TP 207 (Lew 1), H^+ form. Blank values for 0.15 g of resin: at the detection limit, 40 ng and 10 ng for Cr, Cu and Mn, respectively.

TABLE 1

Results obtained with 300 ml of coastal sea water standard CASS-2 with 0.15 g of Chelex-100 resin (Chel 1) [a]

Metal	Found ($\mu g\ l^{-1}$)	Certified ($\mu g\ l^{-1}$)
Cu	0.648 ± 0.019	0.675 ± 0.039
Cr	0.020 ± 0.010	0.121 ± 0.016
Mn	1.86 ± 0.45	1.99 ± 0.15

[a] All results are averages for three subsamples. The blank values were 0.056 ± 0.024 $\mu g\ l^{-1}$, 0.017 ± 0.009 $\mu g\ l^{-1}$ and below the detection limit for Cu, Cr and Mn respectively. Detection limits: $3s$ on the blank value.

of the exchangers with respect to analysis under real conditions and in order to evaluate the optimum ratio of sea water volume to dried resin weight. The action of acidic pH predominates at low ratios and matrix effects at high ratios.

Different samples of coastal sea water (SW1–SW6) were used in order to simulate various situations and avoid systematic errors.

Figures 2 and 3 show the curves obtained (metal concentrations vs. sea water volume) for Cr, Cu and Mn with Chelex-100 (SW1–SW3) and Lewatit TP 207 (SW4–SW6), respectively. The presence of a maximum between 200 and 400 ml of sea water presumably depends on two different parameters that have opposite effects: the increase in pH and the effect of the saline matrix (35‰ salinity). The information obtainable from these kinds of curves may be very useful in establishing the optimum ratio of sea water volume to resin weight. This is very important because the non-H^+ form of the resin shows a very different capacity.

Previous results obtained for the exchangers in "sea water" form [7,8], plotted as concentration ($\mu g\ l^{-1}$) versus sample volume, exhibit a rapidly decreasing capacity, eventually reaching a constant value. This behaviour can be ascribed to the already attained equilibrium between the resin and the saline matrix.

Selection of procedure with Chel 1 and Lew 1 exchangers

On the basis of the results obtained, the following preconcentration procedure for Cr(III), Cu(II) and Mn(II) was carried out with standard sea water CASS-2.

Preconcentration was effected by a batch equilibration procedure using 0.15 g of exchanger and an exactly measured volume of about 300 ml of sea water in a 500-ml container. The samples attained a pH of 6–7 with addition of about 1.80 g l^{-1} of Na_2CO_3. The water and the exchanger remained in contact for 30 h on a shaking plate.

The exchanger was separated by decantation or filtration through a 60-μm nylon filter, washed with 100 ml of Milli-Q-purified water, dried at 40°C for 24 h and stored. For elution the exchanger was then transferred into a 50-ml container and eluted after remaining in contact with 2 ml of 1 M HNO_3 for 1 h. Table 1 gives the results obtained. This procedure was not applied to Lewatit TP 207 resin because it seemed to be

TABLE 2

Concentrations of Cr, Cu and Mn in sea water ($\mu g\ l^{-1}$) obtained by preconcentration with (A) Chelex-100 and (B) Lewatit TP 207 [a]

Sample	Cr ($\mu g\ l^{-1}$)		Cu ($\mu g\ l^{-1}$)		Mn ($\mu g\ l^{-1}$)	
	A	B	A	B	A	B
SW7	0.016 ± 0.002	0.028 ± 0.001	0.049 ± 0.053	0.145 ± 0.001	0.149 ± 0.012	0.145 ± 0.02
SW8	0.380 ± 0.017	0.430 ± 0.001	1.76 ± 0.02	0.620 ± 0.005	–	–
SW9	0.031 ± 0.022	0.048 ± 0.003	0.545 ± 0.040	0.022 ± 0.038	0.177 ± 0.048	0.168 ± 0.065
SW10	0.171 ± 0.022	0.150 ± 0.040	0.407 ± 0.003	0.081 ± 0.001	1.11 ± 0.03	1.12 ± 0.12
SW11	0.006 ± 0.001	0.024 ± 0.004	0.255 ± 0.080	0.108 ± 0.012	0.349 ± 0.040	0.354 ± 0.041

[a] A ratio of 300 ml of sea water to 0.15 g of resin was used. All results are averages for three subsamples. Blank values for Lewatit TP 207: below detection limit, 0.164 ± 0.05 $\mu g\ l^{-1}$ and 0.034 ± 0.07 $\mu g\ l^{-1}$ for Cr, Cu and Mn, respectively. Blank values for Chelex-100: 0.056 ± 0.024 $\mu g\ l^{-1}$, 0.017 ± 0.039 $\mu g\ l^{-1}$ and below detection limit for Cu, Cr and Mn, respectively. Detection limits: $3s$ on the blank values.

capable of retaining only the ionic and weakly bonded species.

The results show that Cu and Mn concentrations are in good agreement with the certified values whereas for Cr a recovery of only 16% was obtained. This percentage is in good agreement with the literature data [3–11] considering Cr speciation analysis. Labile Cr(III) amounts to 10% and 16% of total Cr [9–11].

Comparison between the two exchangers

The procedure suggested above was applied using both Chel 1 and Lew 1 resins to preconcentrate Cr(III), Cu(II) and Mn(II) from two subsamples of the same sample using five different sample waters (SW7–SW11). The results obtained are given in Table 2.

Lewatit TP 207, except for the SW12 sample, is able to retain Cr(III) better than Chelex-100 (obviously, on changing the sea water sample, the percentage of metal retained by the two resins changes). This behaviour can be attributed to the penetration of some colloidal particles [on which Cr(III) is absorbed] into the macroporous resin [4].

In contrast, except for the SW7 sample, the amount of Cu(II) retained by Chelex-100 resin is always greater than that retained by Lewatit TP 207. This result is in agreement with literature data for Cu speciation analysis. In fact, this element is present to only a minor extent in a weakly bound or ionic species [12]. Lewatit TP 207 resin probably retains only these species whereas Chelex-100 is also able to exchange the complexed forms.

For Mn a no significant difference was observed between the behaviour of the two resins and it is concluded that Mn(II) does not pose problems regarding its absorption on colloids or strong complex formation.

Standardized and slow procedure for preparation of H^+-form resins and pH control

On the basis of the previous promising results, the preparation of the H^+ form of Chelex-100 and the pH control were standardized (Chel 2). The aim of this procedure was to shift the maximum capacity towards smaller volumes of samples, for 0.15 g of exchanger. This possibility minimizes the influence of salinity on the resin

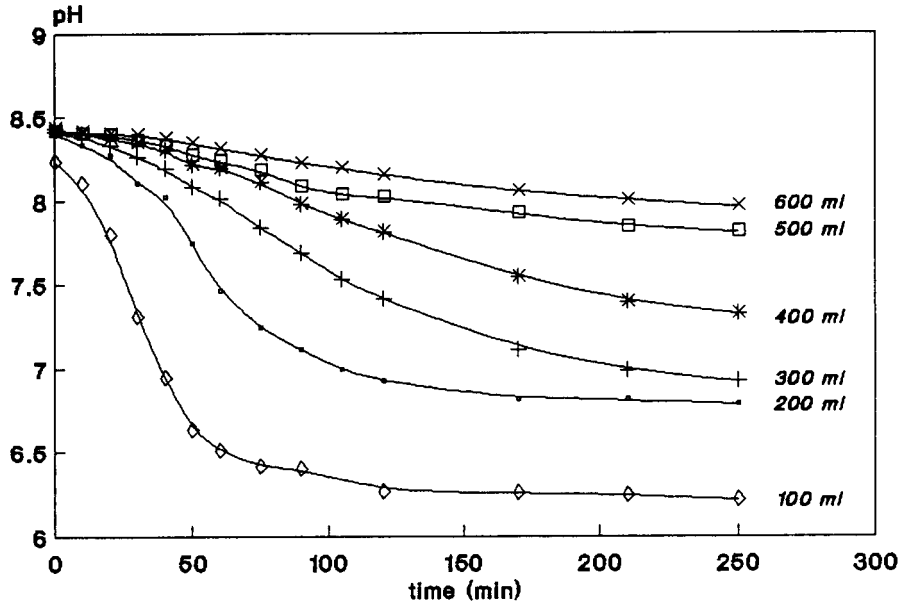

Fig. 4. pH values obtained with different volumes of sea water vs. time in batch equilibration with 0.15 g of Chelex-100 (Chel 2), H^+ form.

performance. Moreover stocks of resin with reproducible behaviour can be obtained. In fact, a rapid wash could result in a poor performance of the resin. Its microporosity caused the retention of H^+ ions with a reduction in the capacity for metals and in the buffer effect for the sea water.

Further, capacity experiments were carried out to improve the preconcentration procedure for each metal. The determination of Mn(II) in sea water was studied at low, medium and high concentration levels. From the results in the literature [13] it seems that Mn(II) is in the ionic or weakly complexed form.

pH control. This was effected with sea water samples (35‰ salinity) by varying the ratio of sea water volume to dried resin weight. The pH was measured from the beginning of the "batch equilibration" procedure until the pH values were constant. In this way it is possible to characterize the stock of resin.

In Fig. 4 typical pH trends for Chelex-100 (Chel 2) are shown. In comparison with the curves in Fig. 1 and those previously published [8], the pH values appear to be higher for the same volumes of sea water. This result is due to the slow and accurate washing procedure. The standardized procedure for the preparation of the H^+-form resin ensures a better and reproducible performance of the resin. This procedure may be even more satisfactory for the macroporous Lewatit TP 207.

Capacity experiments. Chel 2 was used for the determination of Mn(II) in sea water. Typical results are shown in Fig. 5 for three different sea water samples: SW12 (offshore), SW13 (coastal) and SW14. The last sample was obtained from SW13 with addition of 20 $\mu g\ l^{-1}$ of Mn(II).

The results show, as expected, that the optimum sea water volume (100 ml) is smaller than the previous volume (300 ml) for 0.15 g of resin. In fact, after a rapid washing, the volume of sea water necessary to obtain the required buffer effect for H^+ ions is higher. The possible use of a smaller volume of sea water is very important in minimizing possible effects of the saline matrix.

A control experiment was done with the standard sea water CASS-2. An Mn(II) concentration of $2.08 \pm 0.25\ \mu g\ l^{-1}$ was obtained compared with the certified value of $1.99 \pm 0.15\ \mu g\ l^{-1}$. Moreover, the result obtained for SW14 con-

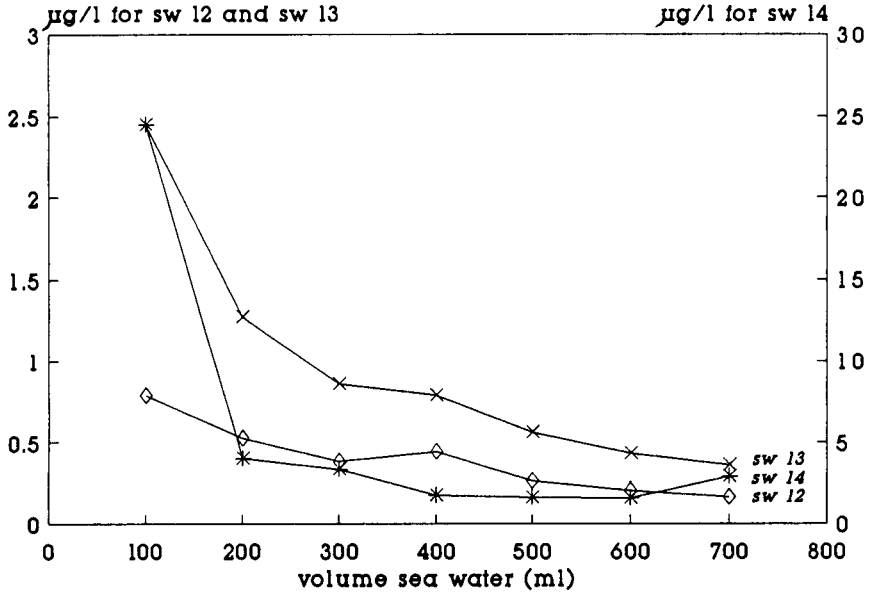

Fig. 5. Capacity curves for Mn(II) ($\mu g\ l^{-1}$ vs. sea water volume) for three samples, (◇) SW12 (coastal), (×) SW13 (offshore) and (*) SW14 [SW13 + 20 $\mu g\ l^{-1}$ Mn(II)] using 0.15 g of Chelex-100 (Chel 2), H^+ form. Blank value at the detection limit.

firmed the efficiency of the resin, again for higher contents of Mn(II).

The capacity curves were measured to determine the concentration of Ni in coastal sea water. The preliminary results confirmed the optimum ratio of 100 ml of sea water to 0.15 g of Chel 2 resin and the possibility of the simultaneous accurate determination of more metals.

Conclusions

On the basis of the results obtained, Chelex-100 and/or Lewatit TP 207 resin in the H^+ form can be recommended for the preconcentration of Cr(III), Cu(II) and Mn(II) from sea water. The advantages are as follows: easily standardized preparation procedure for the resins; use of pH control to verify the performance of the resin; low blank values; the possibility of preparing for oceanographic cruises, containers with the exchangers of the same stocks for preconcentration *in situ* of sea water, immediately after sampling with minimum contamination; minimization of matrix effects, using 0.15 g of resin with a well know sea water volume (ca. 100 ml in the batch equilibration with a contact time of 30 h for Mn). The preliminary results for Ni confirm the possibility of the simultaneous determination of more metals.

Regarding the utilization of the two exchangers Chelex-100 and Lewatit TP 207 on the same sample the following can be suggested: for the determination of Cr(III), the use of Lewatit TP 207, which gives more useful information on the bioavailable species, and in fact probably this exchanger also retains colloidal species; for the determination of Cu(II), the use of both resins, which gives information about the speciation, Lewatit 207 probably retaining only the ionic and weakly bound species whereas Chelex-100 also binds the strongly bonded species; and for the determination of Mn(II), the choice of the exchanger seems to be immaterial.

The results obtained with Chel 1 and Lew 1 will be more reliable when using resins prepared according to the standardized procedure.

This paper is a contribution from the Gruppo di Ricerca Oceanologica Genova (GRO-G). This work was supported by a financial contribution from the Ministero Pubblica Istruzione, Fondi 40%.

REFERENCES

1 J. Buffle, Complexation Reactions in Aquatic Systems, an Analytical Approach, Horwood, Chichester, 1988, p. 1.
2 J.P. Riley and D. Taylor, Anal. Chim. Acta, 40 (1968) 479.
3 T.M. Florence and G.E. Batley, Talanta, 22 (1975) 201.
4 T.M. Florence and G.E. Batley, Talanta, 23 (1976) 179.
5 H.M. Kingston, I.L. Barnes, T.J. Brady and T.C. Rains, Anal. Chem., 50 (1978) 2064.
6 R. Boniforti, R. Ferraroli, P. Frigieri, D. Heltai and G. Queirazza, Anal. Chim. Acta, 162 (1984) 33.
7 F. Baffi, R. Frache and A. Dadone, Ann. Chim. (Rome), 74 (1984) 385.
8 F. Baffi and A. Cardinale, Int. J. Environ. Anal. Chem., 41 (1990) 15.
9 G.E. Batley and J.P. Matousek, Anal. Chem., 52 (1980) 1570.
10 E. Nakayama, T. Kuwamoto, H. Tokoro and T. Fujinga, Anal. Chim. Acta, 131 (1981) 247.
11 F. Ahern, J.M. Eckert and N.C. Payne, Anal. Chim. Acta, 175 (1985) 147.
12 C.M.G. van den Berg, Mar. Chem., 14 (1984) 201.
13 T.M. Florence, Talanta, 29 (1982) 345.

Analytica Chimica Acta, 270 (1992) 87–93
Elsevier Science Publishers B.V., Amsterdam

Liquid–liquid extraction separation of thallium(I) with cryptand 222 and erythrosin

Mayuri N. Gandhi and Shripad M. Khopkar

Centre for Environmental Science and Engineering, Indian Institute of Technology, Bombay 400 076 (India)

(Received 10th January 1992; revised manuscript received 30th April 1992)

Abstract

Thallium(I) was quantitatively extracted, at pH 6.5, with 1×10^{-3} M cryptand 222 in chloroform with 1×10^{-3} M erythrosin as the counterion. From the organic phase it was stripped with 0.1 M sulphuric acid and was determined by atomic absorption spectrometry at 276.8 nm. The composition of extracted species for thallium(I): cryptand 222: erythrosin was 1 : 1 : 1. The separation of thallium(I) from several elements, and its determination in spiked sediments, was possible.

Keywords: Atomic absorption spectrometry; Cryptands; Erythrosin; Extraction; Liquid–liquid extraction; Thallium

Attempts have been made to use benzo-15-crown-5 [1], 18-crown-6 [2], dibenzo-24-crown-8 [3] and 12-crown-4 [4] for the liquid–liquid extraction of thallium(I) with picrate. With 12-crown-4 or 15-crown-5 the extraction was not quantitative. The separation was feasible with dibenzo-18-crown-6 [5], and dicyclohexano-18-crown-6 was used for the extraction of the anionic chlorocomplex of thallium(III) [6]. The cation K(18-crown-6)$^+$ was used for extraction of TlI_4^- [7], and the aza analogue of 18-crown-6 was also used [8]. However systematic investigations of such extraction of thallium with cryptands except evaluation of stability constants [9], are lacking. Such studies are reported in this paper. The structures of the cryptands studied are shown in Fig. 1.

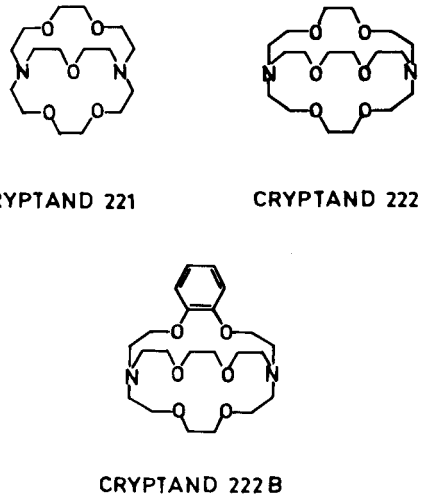

Fig. 1. Different types of cryptands.

EXPERIMENTAL

Apparatus and reagents

A Model GBC 902 atomic absorption spectrometer (GBC, Dandenong), Orion microproces-

Correspondence to: M.N. Gandhi, Regional Sophisticated Instrumentation Centre, Indian Institute of Technology, Bombay 400076 (India).

sor 901 ion analyser (Orion, Cambridge, MA). Wrist action flask shaker (Toshniwal, Bombay). The cryptands were supplied by Merck (Darmstadt).

The stock solution of thallium(I) was prepared by dissolving 1.123 g of thallium(I) sulphate into one litre of distilled water, containing 1% sulphuric acid. It contained 0.998 mg ml^{-1} thallium(I) on standardisation [10]. A solution containing 10 μg ml^{-1} of thallium(I) was prepared by appropriate dilution. Aqueous solution of erythrosin (Aldrich Milwaukee, WI) was used.

General procedure

To an aliquot of solution containing 50 μg of thallium(I), was added erythrosin solution so that its concentration was 1×10^{-3} M in a total volume of 10 ml. The pH of the solution was adjusted to 6.5 with 0.01 M sulphuric acid or tetramethylammonium hydroxide. Then the solution

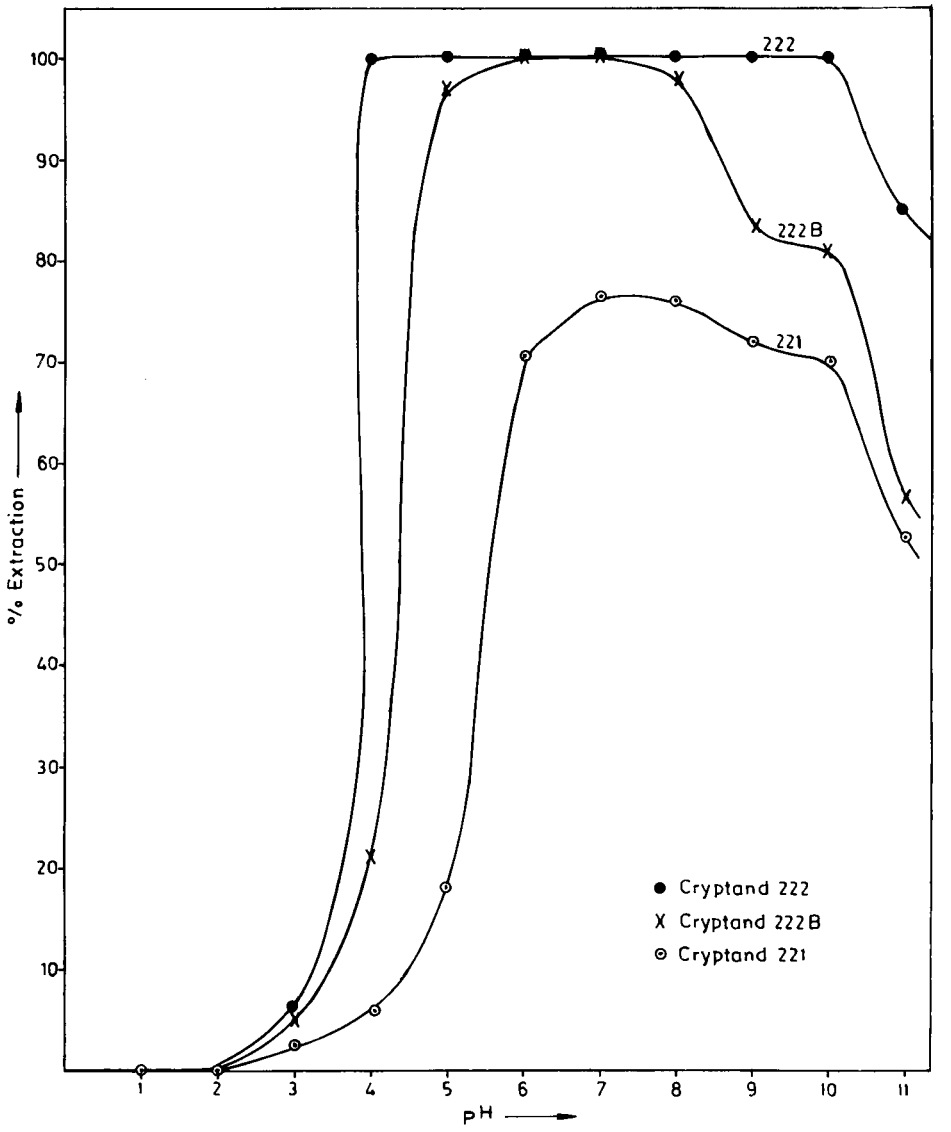

Fig. 2. Extraction of thallium(I) as a function of pH.

was transferred into a separating funnel. A volume of 10 ml of 1×10^{-3} M cryptand 222 in chloroform was added and the mixture was shaken by using a wrist action flask shaker for ca. 5 min. The two phases were allowed to settle and separate. From the organic phase thallium(I) was stripped with 10 ml of 0.1 M sulphuric acid and was determined by atomic absorption spectrometry (AAS) at 276.8 nm with an air–acetylene flame.

RESULTS AND DISCUSSION

Extraction as function of pH

Thallium(I) was extracted between pH 1–12 with 1×10^{-3} M solutions of cryptands 221, 222 and 222B in chloroform with 1×10^{-3} M of erythrosin as the counterion. The extraction was quantitative at pH 4–10 with cryptand 222 and at pH 6–8 with cryptand 222B. It was poor with cryptand 221 (Fig. 2).

Extraction with varying concentrations of cryptand 222

Thallium(I) was extracted with varying concentrations ($0.01–5 \times 10^{-3}$ M) of cryptand 222 in chloroform. Since extraction was quantitative above 0.75×10^{-3} M, solutions of 1×10^{-3} M cryptand 222 in chloroform were used throughout (Table 1).

Extraction with various counterions

Thallium(I) was extracted at pH 6.5 with 1×10^{-3} M of cryptand 222 in the presence of 1×10^{-3} M of various counterions. The extraction was quantitative with rose bengal, erythrosin, bromothymol blue and picric acid, but it was poor with fluorescein. Erythrosin was preferred as the counterion as it has a higher molar volume and a planar structure favouring extensive ion-pair formation (Table 2).

TABLE 1

Extraction as a function of cryptand 222 concentration

Cryptand concentration (10^{-3} M)	Percentage extraction	Distribution ratio (D)
0.010	10.0	0.11
0.025	22.7	0.29
0.050	40.0	0.66
0.075	45.4	0.83
0.10	53.3	1.13
0.25	75.0	3.0
0.50	96.0	24.0
0.75–5.0	100.0	∞

TABLE 2

Extraction with various counterions

Counterion concentration (10^{-3} M)	Percentage extraction	Distribution ratio (D)
Erythrosin	100.0	∞
Eosin	65.7	1.48
Rose bengal	100.0	∞
Fluorescein	4.9	0.05
Bromothymol blue	100.0	∞
Picric acid	100.0	∞
Tropeolin OO	97.0	32.3
Metanil yellow	97.0	32.7
2,4-Dinitrophenol	87.2	3.83
Tetraphenyl borate	75.3	3.04

Extraction with varying concentrations of erythrosin

Thallium(I) was extracted with 1×10^{-3} M of cryptand 222 in chloroform with $0.01–3 \times 10^{-3}$ M of erythrosin. The extraction was 50% with 0.1×10^{-3} M, but was quantitative with 1×10^{-3} M of erythrosin (Table 3).

Effect of solvents

Thallium(I) was extracted at pH 6.5 with 1×10^{-3} M of erythrosin and 1×10^{-3} M of cryptand

TABLE 3

Extraction as a function of erythrosin concentration

Erythrosin concentration (10^{-3} M)	Percentage extraction	Distribution ratio (D)
0.10	10.1	0.11
0.025	22.0	0.25
0.05	36.1	0.56
0.06	43.0	0.75
0.10	56.3	1.29
0.25	79.2	3.82
0.5	89.0	8.14
1.0–3.0	100.0	∞

TABLE 4

Extraction with varying solvents

Solvent	Dielectric constant (ϵ)	Percentage extraction	Distribution ratio (D)
Cyclohexane	2.00	7.2	0.07
Benzene	2.28	5.0	0.05
Toluene	2.30	7.5	0.08
Xylene	2.38	9.6	0.10
Carbon tetrachloride	2.24	1.0	0.01
Chloroform	4.80	100.0	∞
1,2-Dichloroethane	10.50	98.1	52
Dichloromethane	9.08	99.9	5000
Nitrobenzene	34.8	100.0	∞
n-Hexane	1.90	7.8	0.08
Chlorobenzene	5.7	36.0	0.56

222 in various solvents. Dichloromethane, dichloroethane, nitrobenzene and chloroform offered quantitative extraction while others were poor extractants. Chloroform was preferred as it not only offered better phase separation, but also favoured extensive ion-pair formation due to its high dielectric constant (Table 4).

TABLE 5

Effect of stripping acids

Stripping acid	Percentage extraction		
	0.10 M	0.50 M	1–6 M
$HClO_4$	87.2	99.8	100.0
HNO_3	78.0	99.9	100.0
H_2SO_4	99.9	99.8	100.0
CH_3COOH	66.0	92.8	100.0

Effect of stripping agents

After extraction thallium(I) was stripped with 0.1–6 M of various mineral acids. All the acids in the concentration range 0.5–6 M were effective. 0.1 M sulphuric acid (Table 5) was preferred as the common stripping agent.

Effect of metal ion concentration

When other factors were kept constant and concentration of thallium was varied, 1.5–15 μg

TABLE 6

Maximum tolerable amounts of diverse ions at the extraction of thallium [a]

Ion	Added as	Amount [b] (μg)	Ion	Added as	Amount (μg)
Li^+	Li_2SO_4	300	Ga^{3+}	$Ga(NO_3)_3$	100
Na^+	Na_2SO_4	300	In^{3+}	$In_2(SO_4)_3$	75
K^+	K_2SO_4	300	Sn(IV)	$Sn(SO_4)_2$	200
Rb^+	$RbNO_3$	300	Pb^{2+}	$Pb_2(CH_3COO)_2$	150
Cs^+	$CsNO_3$	250	As(III)	$As_2(SO_4)_3$	200
Be^{2+}	$Be(NO_3)_2 \cdot 6H_2O$	200	Sb(III)	$Sb(NO_3)_3$	250
Mg^{2+}	$MgSO_4 \cdot 7H_2O$	150	Bi(III)	$Bi(NO_3)_3$	150
Ca^{2+}	$Ca(NO_3)_2$	150	Se(IV)	Na_2SeO_3	250
Sr^{2+}	$Sr(NO_3)_2$	200	Te(IV)	Na_2TeO_3	200
Ba^{2+}	$Ba(NO_3)_2$	300	Ce^{3+}	$Ce(NO_3)_3 \cdot 6H_2O$	300
Cr(VI)	$K_2Cr_2O_7$	300	UO_2^{2+}	$UO_2(NO_3)_2 \cdot 6H_2O$	250
Mn^{2+}	$Mn(NO_3)_2$	200	Th(IV)	$Th(NO_3)_4 \cdot 4H_2O$	200
Fe^{3+}	$Fe(SO_4)_3 \cdot 7H_2O$	200	MoO_4^{6-}	$(NH_4)_6Mo_7O_{24} \cdot 4H_2O$	300
Co^{2+}	$CoSO_4$	200	VO_3^-	$(NH_4)VO_3$	250
Ni^{2+}	$NiSO_4 \cdot 2H_2O$	200	Cl^-	HCl	500
Cu^{2+}	$CuSO_4 \cdot 5H_2O$	200	Br^-	HBr	500
Zn^{2+}	$ZnSO_4 \cdot 7H_2O$	150	ClO_4^-	$HClO_4$	500
Cd^{2+}	$3CdSO_4 \cdot 8H_2O$	200	PO_4^{3-}	H_3PO_4	500
Hg^{2+}	$Hg(NO_3)_2$	300	NO_2^-	$NaNO_2$	300
Zr(IV)	$Zr(NO_3)_4 \cdot 5H_2O$	50	NO_3^-	HNO_3	500
Hf(IV)	$Hf(SO_4)_2 \cdot 4H_2O$	50	SO_4^{2-}	H_2SO_4	500
Al^{3+}	$Al_2(SO_4)_3 \cdot 24H_2O$	250			

[a] Tl(I): 15 μg. [b] 500 μg was maximum amount tested.

ml^{-1} of thallium was quantitatively extracted. The linear calibration range for AAS was 15–65 $\mu g\ ml^{-1}$ while the 3σ detection limit was 0.35 $\mu g\ ml^{-1}$ of thallium. The method was reproducible with a relative standard deviation of 1.82% ($n = 6$) and the concentration of thallium employed was 50 μg per 10 ml of solution.

Period of equilibration

Thallium(I) was extracted over various periods of equilibration ranging from 1 to 20 min. The extraction was quantitative after 2 min.

Nature of extracted species

The nature of the extracted species was ascertained from the plot of log[D] versus log[cryptand 222] with 1×10^{-3} M erythrosin and plot of log[D] versus log[erythrosin] with 1×10^{-3} M cryptand 222, where D is the distribution ratio. The corresponding slopes were 1.0 and 1.1, hence the probable composition of its extracted species is thallium : cryptand : erythrosin = 1 : 1 : 1.

Effect of diverse ions

The maximum tolerable amounts of various ions are shown in Table 6. Hafnium, zirconium, gallium and indium interfered most strongly.

TABLE 7

Separation from multicomponent mixtures

Sample No.	Ions	Amount taken (μg)	pH	Cryptand concentration (M)	Cryptand	Counter-ion [a]	Solvent	Stripping acid, concentration (M)	Ref.
1	Pb^{2+}	25	3.5	5×10^{-4}	222B	a	Toluene	HCl, 1	11
	Tl(I)	25	4.0	1×10^{-3}	222	b	$CHCl_3$	H_2SO_4, 0.1	–
	Mn^{2+}	15	5.5	2.5×10^{-3}	221	b	$CHCl_3$	$HClO_4$, 0.5	12
	Zn^{2+}	50	Unextracted						–
2	Cd^{2+}	10	6.5	3×10^{-4}	221	d	Benzene	H_2SO_4, 0.1	13
	Tl(I)	10	4.0	1×10^{-3}	222	b	$CHCl_3$	H_2SO_4, 0.1	–
	Mn^{2+}	15	5.5	2.5×10^{-3}	221	b	$CHCl_3$	$HClO_4$, 0.5	12
	Cr(VI)	20	Unextracted						–
3	Tl(I)	25	6.5	1×10^{-3}	222	c	$CHCl_3$	H_2SO_4, 0.1	–
	Cu^{2+}	10	5.5	3×10^{-4}	222	b	CH_2Cl_2	$HClO_4$, 0.5	14
	Ni^{2+}	25	7.5	2.5×10^{-3}	222	b	CH_2Cl_2	HCl, 4	15
	Zn^{2+}	50	Unextracted						–
4	Cd^{2+}	10	6.5	3×10^{-4}	221	d	Benzene	H_2SO_4, 0.1	13
	Tl(I)	10	6.5	1×10^{-3}	222	b	$CHCl_3$	H_2SO_4, 0.1	–
	Co^{2+}	25	6.0	5×10^{-3}	222	b	CH_2Cl_2	HCl, 4	16
	V(V)	30	Unextracted						–
5	Tl(I)	25	4.0	1×10^{-3}	222	b	$CHCl_3$	H_2SO_4, 0.1	–
	Mn^{2+}	15	5.5	2.5×10^{-3}	221	b	$CHCl_3$	$HClO_4$, 0.5	12
	Ni^{2+}	25	7.5	5×10^{-3}	222	b	CH_2Cl_2	HCl, 4	15
	Cr(VI)	20	Unextracted						–
6	Tl(I)	50	4.0	1×10^{-3}	222	b	$CHCl_3$	H_2SO_4, 0.1	–
	Mn^{2+}	15	5.5	2.5×10^{-3}	221	b	$CHCl_3$	$HClO_4$, 0.5	12
	Co^{2+}	25	6.0	5×10^{-3}	222	b	CH_2Cl_2	HCl, 4	16
	Cs^{+}	30	Unextracted						–
7	Pb^{2+}	25	3.5	5×10^{-4}	222B	a	Toluene	HCl, 1	11
	Cd^{2+}	10	6.5	3×10^{-4}	221	d	Benzene	H_2SO_4, 0.1	13
	Tl(I)	10	4.0	1×10^{-3}	222	b	$CHCl_3$	H_2SO_4, 0.1	–
	Mn^{2+}	10	5.5	2.5×10^{-3}	221	b	$CHCl_3$	$HClO_4$, 0.5	12
	Te(IV)	50	Unextracted						–

[a] a, eosin; b, erythrosin; c, picric acid; d, rose bengal.

Separation from multicomponent mixtures

The various separations of thallium from associated elements were effected using the known extraction conditions for other elements with different cryptands. An advantage of difference in pH, reagent concentration, solvent or nature of cryptand was fully exploited to develop such separations (Table 7).

Lead, thallium(I), manganese(II) and zinc were separated by extracting lead with cryptand 222B at pH 3.5, thallium(I) with cryptand 222 at pH 4.0, manganese(II) [12] with cryptand 221 at pH 5.5, while zinc was not extracted.

A mixture of cadmium, thallium(I), manganese(II) and chromium(VI) was separated by extracting cadmium with cryptand 221 at pH 6.5 [13], thallium(I) with cryptand 222 at pH 4.0, manganese(II) [12] with cryptand 221 at pH 5.5, while chromium(VI) was not extracted.

A mixture of thallium(I), copper(II), nickel and zinc was separated by extracting thallium(I) with cryptand 222 at pH 6.5, copper(II) with cryptand 222 at pH 5.5 [14], nickel [15] with cryptand 222 at pH 7.5, while zinc was not extracted.

Cadmium, thallium(I), cobalt(II) and vanadium(V) were separated by extracting cadmium [13] with cryptand 221 at pH 6.5, thallium(I) with cryptand 222 at pH 6.5, cobalt(II) [16] with cryptand 222 at pH 6.0 while vanadium(V) was not extracted.

Thallium(I), manganese(II), nickel and chromium(VI) were separated by extracting thallium (I) with cryptand 222 at pH 4.0, manganese(II) [12] with cryptand 221 at pH 5.5, nickel with cryptand 222 at pH 7.5, while chromium(VI) was not extracted.

The mixture of thallium(I), manganese(II), cobalt(II) and ceasium was separated by extracting thallium(I) with cryptand 222 at pH 4.0, manganese(II) [12] with cryptand 221 at pH 5.5, cobalt(II) [16] with cryptand 222 at pH 6.0, while caesium was not extracted.

The mixture of lead, cadmium, thallium(I), manganese(II) and tellurium(VI) was separated by extracting lead(II) with cryptand 222B at pH 3.5, cadmium [13] with cryptand 221 at pH 6.5, thallium(I) with cryptand 222 at pH 4.0, manganese(II) [12] with cryptand 221 at pH 5.5, while tellurium(VI) was not extracted.

In these separations species were stripped from the organic phase with the appropriate mineral acids prior to determination by AAS (Table 7).

TABLE 8

Determination of thallium(I) added to a marine sediment

Sample No.	Amount spiked μg	Amount found μg	Thallium(I) spike recovered (%)
1	0	0	–
2	10	9.9	99.0
3	25	25.0	100.0
4	35	34.0	98.1
5	50	49.0	98.0

Analysis of marine sediments

The amount of thallium in marine sediments does not exceed 40 $\mu g\ g^{-1}$. The technique of spiking [17], therefore, was used. Five different concentrations of thallium(I) were added and from the spiked and unspiked samples thallium(I) was extracted with cryptand 222 and determined as above. The results were satisfactory (Table 8), although no thallium was found in the unspiked sediment.

The proposed method is simple, rapid and selective. It was possible to separate thallium(I) from various mixtures in just half an hour. The separation from lead, cadmium, zinc, cobalt(II), nickel, manganese(II) and chromium(VI) is of significance as they are associated in aquatic environment. The separation from lead, selenium-(IV) and tellurium(IV) is useful as they are associated in minerals. The separation from caesium, lead(II) and vanadium(V) is of interest for separation from nuclear waste.

REFERENCES

1 T. Maeda, K. Kimura and T. Shono, Z. Anal. Chem., 298 (1979) 363.

2 Y. Takada and H. Goto, Bull. Chem. Soc. Jpn., 52 (1979) 1920.

3 Y. Takeda, Bull. Chem. Soc. Jpn., 52 (1979) 2501.
4 Y. Takeda, M. Nemoto and S. Fujiwara, Bull. Chem. Soc. Jpn., 55 (1982) 3438.
5 T. Sekine, H. Wakabayashi and Y. Hasagawa, Bull. Chem. Soc. Jpn., 51 (1978) 645.
6 H. Koshima and H. Onishi, Analyst, 111 (1986) 1261.
7 R.G. Vibhute and S.M. Khopkar, Anal. Chim. Acta, 222 (1989) 215.
8 M.K. Beklemishev, L.J. Gorodilova, N.I. Shevtsov, L.M. Kardivarenko and N.M. Kuz'min, Zh. Anal. Chim., 44 (1989) 1058.
9 B. Dietrich, Inclusion Compd., 2 (1984) 337.
10 F.J. Welcher, The Analytical Use of Ethylenediaminetetracetic Acid, Van Nostrand, London, 1958 p. 182.
11 M.N. Gandhi and S.M. Khopkar, Ind. J. Chem., 30A (1991) 706.
12 M.N. Gandhi and S.M. Khopkar, Anal. Sci., 8 (1992) 233.
13 M.N. Gandhi and S.M. Khopkar, Chem. Anal. (Warsaw), in press.
14 M.N. Gandhi and S.M. Khopkar, Mikrochim. Acta, in press.
15 M.N. Gandhi and S.M. Khopkar, Bull. Chem. Soc. Jpn., in press.
16 M.N. Gandhi and S.M. Khopkar, J. Chem. Sci., in press.
17 R.A. Horn, Chemistry of the Environment, Wiley, New York, 1978.

a Chimica Acta, 270 (1992) 95–99
Science Publishers B.V., Amsterdam

Synergic extraction of tervalent lanthanoids with 2-thenoyltrifluoroacetone and ethylenediamine as a neutral bidentate ligand

Shigeto Nakamura [1] and Nobuo Suzuki

Department of Chemistry, Faculty of Science, Tohoku University, Aoba-ku, Sendai, Miyagi 980 (Japan)

(Received 1st June 1992)

Abstract

The synergic extraction of tervalent lanthanoids [Ln(III)], La, Nd, Tb and Yb, with 2-thenoyltrifluoroacetone (Htta) and ethylenediamine (en) in benzene was investigated. The partition coefficient of en between benzene and aqueous phase was determined as $10^{-3.46}$. The synergic enhancement was observed at pH > 7.2, and was attributed to the formation of the adduct $Ln(tta)_3en$. The adduct formation constant, $\beta_{s,1}$, increases with increase of atomic number of Ln(III).

Keywords: Extraction; Lanthanoids

most synergic extractions of tervalent lanoids [Ln(III)] with an acidic chelating agent in the presence of a neutral unidentate d, such as tributylphosphate, it has been ed out that the synergic enhancement de- es with increasing atomic number of Ln(III) We have found, on the contrary, that the gic enhancement increases with increase in tomic number of Ln(III) when a bidentate ocyclic amine is used as the neutral donor forming the adduct LnA_3S. This peculiar ncy has been observed in the limited comions of β-diketones, such as hexafluoroacetylacetone, pivaloyltrifluoroacetone and 2-thenoyltrifluoroacetone (Htta), with a neutral bidentate ligand, such as 1,10-phenanthroline (phen) and 2,2′-bipyridine (bpy) [2–5]. Since these neutral ligands have nitrogens as donor atoms in the aromatic ring structure, it was suspected that this tendency might be a rare phenomenon observed only in systems involving a neutral ligand having a heterocyclic ring structure and may be attributed to a specific interaction such as back-donation between the central metal and the neutral ligand. To discuss in detail this interesting tendency, it is necessary to study a synergic extraction system involving a simple neutral bidentate ligand. Ethylenediamine (en) is an aliphatic amine having a simple bidentate structure and has often been used in coordination chemistry. It is strange, however, that en has not been used in liquid–liquid extraction chemistry.

In this work, the synergic extraction of Ln(III) with Htta and en in benzene was investigated. The adduct formation constant for en was deter-

pondence to: N. Suzuki, Department of Chemistry, Fac- Science, Tohoku University, Aoba-ku, Sendai, Miyagi apan).
ent address: Institute for Advanced Materials Process- Tohoku University, Aoba-ku, Sendai, Miyagi 980 an).

mined and compared with those for other bidentate ligands, i.e., phen and bpy.

EXPERIMENTAL

Materials

Radioisotopes, ^{140}La, ^{147}Nd, ^{160}Tb, ^{169}Yb, used as tracers, were produced by the neutron irradiation of each oxide or nitrate in the nuclear reactor (JRR-4) of the Japan Atomic Research Institute at a thermal neutron flux of 5.5×10^{13} n cm^{-2} s^{-1} for 6 h. The irradiated sample was dissolved in hydrochloric acid. Htta was purified by vacuum sublimation. Ethylenediamine was shaken with sodium hydroxide pellets and distilled before use. Benzene was purified by a standard method. Unless stated otherwise, the reagents used were of guaranteed reagent grade.

Partition coefficient of ethylenediamine

It is necessary to determine the partition coefficient of en to calculate the equilibrium concentration of en. No data on the partition coefficient of en have been reported. Ethylenediamine stock solution was prepared by dissolution in degassed water. A 50-cm^3 volume of a 0.04–0.1 M en solution was adjusted to pH > 12 by the addition of sodium hydroxide and shaken with 120 cm^3 of benzene for 30 min at 25°C. After centrifugation, the distributed en in the benzene phase (100 cm^3) was stripped into 10 cm^3 portion of 0.001 M hydrochloric acid. The concentration of en was determined by back-titration with 0.001 M sodium hydroxide.

The partition coefficient (P_S) is calculated from the following equation:

$$P_S = \frac{C_o}{C_{init} - C_o V_{org}/V_{aq}} \quad (1)$$

where C_{init} and C_o are the initial concentration of en in the aqueous phase and the equilibrium concentration of en in the organic phase, respectively, and V_{org} and V_{aq} are the volumes of the organic and aqueous phase, respectively.

Synergic extraction of Ln(III)

An aqueous solution (6 cm^3) containing 10^{-5} M Ln(III) labelled with its radioisotope, 10^{-3}–10^{-1} M en as a neutral ligand and 0.01 M citrate was placed in a 30-cm^3 extraction vial with a ground-glass stopper. The ionic strength in the aqueous phase was adjusted to 1 M with hydrochloric acid and sodium hydroxide. An equal volume of a benzene solution containing 10^{-5}–10^{-2} M Htta was added to the aqueous phase and the vial was shaken for 1–3 h at 25°C. After centrifugation, an aliquot was taken from each phase and the γ-activity was measured with an NaI(Tl) well-type scintillation detector connected with a single-channel analyser. The distribution ratio of Ln(III) was obtained as the radioactivity ratio. The pH of the aqueous phase was adjusted with 10^{-3}–10^{-2} M piperazine-*N*,*N*′-bis(2-ethanesulphonic acid), boric acid–sodium hydroxide solution, and the equilibrium pH after shaking was measured with a glass electrode.

Theoretical

The extraction equilibrium of a triply charged cation M^{3+} with a chelating extractant HA is expressed as

$$M^{3+} + 3\overline{HA} \rightleftharpoons \overline{MA_3} + 3H^+$$

where the horizontal bar over the species denotes the organic phase.

The distribution ratio (D_0) of M^{3+} with HA in the presence of a complexing agent, C^{z-}, forming a water-soluble complex can be expressed as follows:

$$D_0 = \frac{[\overline{MA_3}]}{[M^{3+}] + \Sigma[MA_n^{3-n}] + \Sigma[MC_y^{3-zy}]}$$

$$= \frac{P_M \beta_3 [A^-]^3}{1 + \Sigma\beta_n [A^-]^n + \Sigma\beta_{c,y}[C^{z-}]^y}$$

where A^- denotes the chelating anion in the aqueous phase, P_M is the partition coefficient of MA_3, and β_n and $\beta_{c,y}$ are the overall formation constants of MA_n^{3-n} and MC_y^{3-zy}, respectively.

When a neutral ligand, S, is added to this system, the distribution ratio (D) can be expressed as

$$D = \frac{[\overline{MA_3}] + \Sigma[\overline{MA_3S_m}]}{[M^{3+}] + \Sigma[MA_n^{3-n}] + \Sigma[MC_y^{3-zy}]}$$

$$= \frac{P_M\beta_3[A^-]^3\left(1 + \Sigma\beta_{s,m}[\bar{S}]^m\right)}{1 + \Sigma\beta_n[A^-]^n + \Sigma\beta_{c,y}[C^{z-}]^y} \quad (4)$$

where $\beta_{s,m}$ is the adduct formation constant in the organic phase corresponding to the following equilibrium:

$$\overline{MA_3} + m\bar{S} \rightleftharpoons \overline{MA_3S_m} \quad (5)$$

From Eqns. 3 and 4, the following equation is obtained:

$$D/D_0 = 1 + \Sigma\beta_{s,m}[\bar{S}]^m \quad (6)$$

If MA_3S_m is the dominant species in the organic phase, D/D_0 will depend on the mth power of the equilibrium concentration of S in the organic phase.

RESULTS AND DISCUSSION

Effect of tta anion concentration

First we examined the synergic extraction of Ln(III) with Htta and en at pH 5, but in contrast to the other neutral bidentate ligands investigated previously [2–5], no synergic enhancement with en was observed at this pH. This may be attributed to very low concentration of the neutral en in the organic phase under this condition, because the partition coefficient of en is small and the acid dissociation constants of the protonated en are very small, i.e., log $K_{H_2S} = -7.10$ and log $K_{HS} = -9.89$ [6]. The synergic extraction of Ln(III) with Htta and en was therefore carried out in a higher pH region, i.e., pH 7.2–8.8, in the presence of citrate to prevent the hydrolysis of Ln(III). Considering the possibility of decomposition of Htta in an alkaline medium, experiments at pH > 9 are not recommended.

The effect of tta anion concentration in the aqueous phase on the distribution ratio of Tb(III) is shown in Fig. 1. The equilibrium concentration

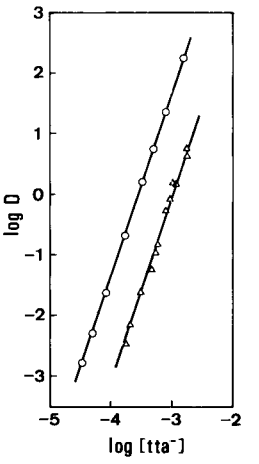

Fig. 1. Effect of tta$^-$ concentration in the aqueous phase the distribution ratio of Tb(III) in the presence of 0.01 citrate. △ = Htta alone, pH 7.2–8.8; ○ = Htta–5.1×10^{-2} en, pH 7.8.

of tta anion in the aqueous phase was calcula from the following equation;

$$[A^-] = \frac{C_{HA}}{(P_{HA} + 1)[H^+]/K_{HA} + 1}$$

where C_{HA} is the initial concentration of H and K_{HA} and P_{HA} are the acid dissociation c stant and the partition coefficient of Htta, resp tively. The literature values of K_{HA} and P were adopted, i.e., log $K_{HA} = -6.23$ [7] a log $P_{HA} = 1.62$ [8]. The plots of the extraction Tb(III) with 10^{-5}–10^{-2} M Htta alone at 7.2–8.8 in the presence of 0.01 M citrate giv straight line with a slope of 3.0. In this pH regi the term $\Sigma\beta_{c,y}[C^{z-}]^y$ in Eqn. 3 may be consta because almost all the citrate is present in completely dissociated form (citrate)$^{3-}$, as p dicted from the acid dissociation constants citric acid, i.e., log $K_{H_3C} = -2.85$, log K_{H_2} -4.35 and log $K_{HC} = -5.82$ [9]. Thus, the m extraction equilibrium expressed by Eqn. 2 confirmed in the presence of citrate. On addit of 5.1×10^{-2} M en to this system, the distri tion ratio of Tb(III) increases, and the plots a straight line, also with a slope of 3.0, as sh in Fig. 1. This indicates that the extracted spe also has three tta anions, i.e., Tb(tta)$_3$(en)$_m$ the presence of en. Considering the predomin

ɔecies of en in this pH region, Hen^+ or H_2en^{2+}, ıere was a possibility of the ion-pair extraction f a higher tta complex such as $Tb(tta)_4^-$ with a rotonated en cation, but the experimental re-ılts showed no evidence of such an ion-pair ɛtraction under the present conditions.

Effect of en concentration

The synergic extraction of 10^{-3} M Htta and ırious concentrations of en in the presence of trate was carried out, and the plots of log D/D_0 gainst log $[\overline{en}]$ are shown in Fig. 2. The equilib-um concentration of en in the benzene phase is ılculated by the following equation;

$$\bar{5}] = \frac{C_S}{1 + \frac{1}{P_S}\left\{1 + \frac{[H^+]}{K_{HS}}\left(1 + \frac{[H^+]}{K_{H_2S}}\right)\right\}} \quad (8)$$

here C_S is the initial concentration of en and P_S the partition coefficient of en. K_{H_2S} and K_{HS} ere taken from the literature [6] and P_S was ɔtained in this experiment as log $P_S = -3.46$, om the distribution ratio of en at pH > 12, here neutral en is predominant in the aqueous hase. The plots for La, Nd, Tb and Yb give raight lines with slopes of 1.0. This indicates ıat the mole ratio of the neutral chelate to en in ıe adduct formed in the organic phase is 1:1, ɛ., the adduct is $Ln(tta)_3en$.

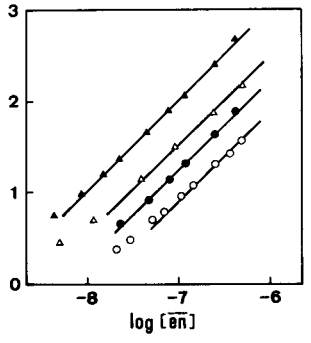

g. 2. Effect of the equilibrium concentration of en in ben-ne on the synergic enhancement of Ln(III) with Htta and ı. $[Htta]_{init} = 10^{-3}$ M. ○ = La, 5×10^{-3} M citrate, pH 8.1; = Nd, 1×10^{-2} M citrate, pH 8.0; △ = Tb, 1×10^{-2} M trate, pH 8.0; ▲ = Yb, 1×10^{-2} M citrate, pH 7.9.

TABLE 1

Adduct formation constants ($\beta_{s,1}$) in Ln(III)–Htta–en,–phen and –bpy systems

Ln	Log $\beta_{s,1}$		
	en	phen [a]	bpy [b]
La	7.87	8.65	5.36
Nd	8.24	9.39	5.95
Tb	8.54	9.92	6.46
Yb	9.04	9.99	6.54

[a] Ref. 5. [b] Ref. 4.

Comparison of adduct formation constants

The values of $\beta_{s,1}$ are given in Table 1 together with those for phen and bpy. The $\beta_{s,1}$ values increase with increasing atomic number of Ln(III). This is the opposite order observed in the most synergic extraction systems involving a neutral unidentate ligand, but is similar to the trend in synergic systems involving bpy or phen as a neutral bidentate ligand [2–5]. This shows that the present trend can be observed in synergic extractions involving a neutral bidentate ligand, irrespective of the fundamental structure, such as an aliphatic amine or a heterocyclic amine.

A large $\beta_{s,1}$ value is observed even with a simple bidentate amine such as en; the $\beta_{s,1}$ values for en are larger than those for bpy but are smaller by one order of magnitude than those for phen. The larger $\beta_{s,1}$ for en than bpy can simply be understood by comparing the acid dissociation constant as a simple measure of basicity of the neutral ligand, that is, log K_{HS} for bpy is -4.50 [10], and this value must be compared with the corresponding value for en, -9.89. The $\beta_{s,1}$ value for en is smaller than that for phen. This cannot simply be explained by their basicities, because the acid dissociation constant of protonated en is smaller than that of phen (log $K_{HS} = -5.04$ [10]). To understand the difference in the $\beta_{s,1}$ values obtained with different types of bidentate neutral ligands for the given lanthanoid(III), a further systematic study using other bidentate ligands having different functional groups must be carried out.

In conclusion, the addition of en as a simple neutral bidentate ligand enhances the extraction of lanthanoids by forming the adduct, $Ln(tta)_3en$,

e adduct formation constant is large and ıes with increase in the atomic number of). This interesting tendency observed in ic extraction systems containing a neutral ıte ligand of an aliphatic amine as well as a cyclic amine suggests a new possibility for ing the selectivity of synergic liquid–liquid ion.

ENCES

larcus and A.S. Kertes, Ion Exchange and Solvent action of Metal Complexes, Vol. 6, Wiley–Intersci-, London, 1969, p. 815.

2 S. Nakamura and N. Suzuki, Inorg. Chim. Acta, 114 (1986) 101.
3 S. Nakamura and N. Suzuki, Polyhedron, 5 (1986) 1805.
4 S. Nakamura and N. Suzuki, Polyhedron, 7 (1988) 155.
5 S. Nakamura and N. Suzuki, Bull. Chem. Soc. Jpn, submitted for publication.
6 R. Griesser and H. Sigel, Inorg. Chem., 9 (1970) 1238.
7 J.C. Reid and M. Calvine, J. Am. Chem. Soc., 72 (1950) 2948.
8 T. Wakahayashi, S. Oki, T. Omori and N. Suzuki, J. Inorg. Nucl. Chem., 26 (1964) 2255.
9 A.K. Grzybowski, S.S. Tate and S.P. Datta, J. Chem. Soc. A, (1970) 241.
10 S. Nakamura, H. Imura and N. Suzuki, Inorg. Chim. Acta, 110 (1985) 101.

Chimica Acta, 270 (1992) 101–106
Science Publishers B.V., Amsterdam

quential simplex optimization in a constrained simplex mixture space in liquid chromatography

A. Palasota, Iphigenia Leonidou, Josephine M. Palasota, Hui-Li Chang and Stanley N. Deming

Department of Chemistry, University of Houston, Houston, TX 77204-5641 (USA)

(Received 18th April 1992; revised manuscript received 10th July 1992)

Abstract

The sequential simplex method is used in a constrained simplex mixture space to optimize the liquid chromatographic separation of five neutral organic solutes: uracil, phenol, acetophenone, methylbenzoate, and toluene. The mobile phase composition is varied while column temperature, mobile phase flow-rate, and sample concentration are held constant. The chromatographic response function and the total analysis time are used in an overall desirability function to direct the progress of the sequential simplex optimization.

Keywords: Liquid chromatography; Optimization methods; Desirability functions; Organic solutes; Sequential simplex optimization

sequential simplex method of optimiza- as introduced by Spendley et al. [1] and ed by Nelder and Mead [2] as an efficient tive to the effective classical factorial de- ethod of *ev*olutionary *op*eration (EVOP) he sequential simplex is a local hill-climb- orithm that moves a geometric figure of vertexes through a k-dimensional factor oward a region that will produce an im- response. Several authors have reported ccessful application of the simplex algo- to the optimization of chromatographic ions [5–30]. The geometric distribution of + 1 vertexes in the k-dimensional factor lefines the sequential simplex figure.

rmulation or mixture is defined as a com- n of two or more components such that n of all fractions in the formulation equals 100%) [31–40]. Because of this equality int, only $k - 1$ components of the mixture can be specified independently. For example, consider a three-component mixture of acetonitrile (ACN), water (H_2O), and methanol (MeOH) represented by the simplex mixture design in the upper panel of Fig. 1: because %ACN + %H_2O + %MeOH = 100%, the concentration of only two of the three components (e.g., ACN and MeOH) can be specified independently; the third component (H_2O) serves as a slack or makeup variable [41]. The geometric distribution of the k pure-component vertexes in the $k - 1$ independent dimensions of the shaded constrained factor space defines the simplex mixture figure (lower panel of Fig. 1).

If the goal is to optimize the composition of the mobile phase mixture, then it is possible to use the sequential simplex method of optimization inside the constrained simplex mixture space. In this work, we demonstrate the use of the variable-size sequential simplex method [2] for determining the mobile phase composition that results in an improved separation of five neutral organic solutes commonly used as test standards in reversed-phase liquid chromatographic (LC)

dence to: S.N. Deming, Department of Chemistry, y of Houston, 4800 Calhoun Road, Houston, TX 41 (USA).

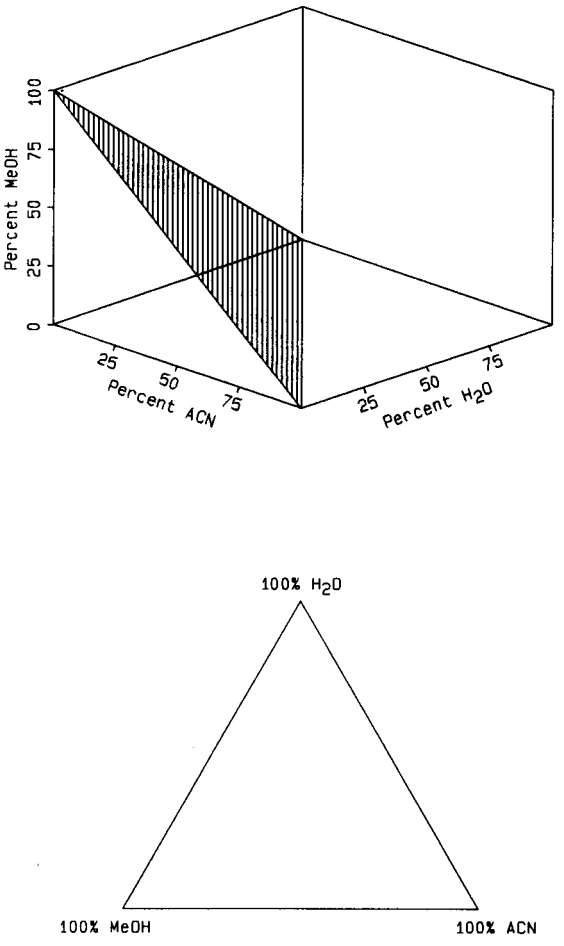

Fig. 1. A three-component mixture space of acetonitrile (ACN), water (H_2O), and methanol (MeOH).

separations. The three components of the mobile phase are ACN, MeOH, and H_2O. Because only two of the three mobile phase components can be specified independently, the factor space is two-dimensional and a three-vertex sequential simplex is used to optimize the composition of ACN and MeOH; the magnitude of the third component (H_2O) is calculated by difference.

EXPERIMENTAL

Instrumentation

The liquid chromatographic system consisted of a Model M-6000A solvent delivery system (Waters, Milford, MA), a Model 7125 six injector (Rheodyne, Cotati, CA), a Model U ultraviolet detector (Bioanalytical Systems, Lafayette, IN) fixed at 254 nm, and a 25 cm mm i.d. Accusphere ODS analytical column W Scientific, Folsom, CA). The detector a fier time constant was set at 0.1 s and 2 sample volumes were injected. The column allowed to equilibrate at 1.0 ml min^{-1} for 3(prior to initial sample injection. The m phases and column were at ambient temper and the mobile phase flow-rate was 1.0 ml m

The analog output from the detector recorded by a Model 255/MM (Linear In ments, Reno, NV) strip-chart recorder and si taneously digitized by a laboratory com (IBM). Chromatograms were plotted on a L Jet Series III printer (Hewlett-Packard, Palo CA) equipped with a Plotter-in-a-Cartridge hancement and a 4-Mbyte memory upg (Pacific Data, San Diego, CA).

Mobile phase and sample preparation

Mobile phases were prepared by adding grade methanol (Mallinckrodt, ChromAR, I KY) and LC-grade acetonitrile (EM Sci Gibbstown, NJ) to a 500-ml volumetric flask a graduated cylinder. The flask was dilute volume with distilled water. The distilled was prepared with a Mega-Pure 1-l all glass lation apparatus (Corning, Corning, NY).

The sample mixture of 0.1106 mM uracil drich, Milwaukee, WI), 2.127 mM phenol drich), 0.0943 mM acetophenone (Aldrich), mM methylbenzoate (Aldrich), and 7.811 toluene (Aldrich) was prepared in a mobile containing 33% (v/v) MeOH, 33% (v/v) and 34% (v/v) H_2O.

Chromatographic response function

The dual objectives of the chromatogr method reported here are complete solute re tion and short analysis time. The chron graphic response function (CRF) [42] is used quantitative measure of the first objectiv general

$$\mathrm{CRF} = \sum_{i=1}^{n-1} \ln(f/g)$$

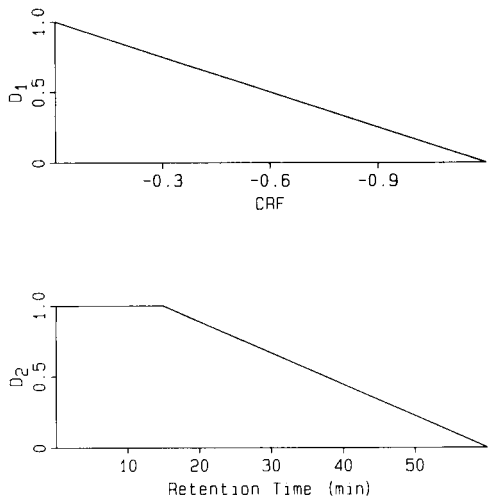

Fig. 2. Mapping of the individual desirability functions associated with this study. $D_1 = 1.0 + \mathrm{CRF}/1.2$; $D_2 = 1.0$ up to 15 min; $D_2 = 1.0 + (15.0 - \mathrm{time})/45.0$ beyond 15 min.

where f is the depth of the valley below a straight line connecting the ith pair of adjacent peak maxima, g is the height of the straight line above the baseline at the valley between the peaks [42], and n is the number of components in the sample. The logarithm of the peak separation (f/g) for all $n-1$ pairs of adjacent peaks is used so that the CRF will be more sensitive to highly overlapped peaks and less sensitive to those peaks that are better resolved [42].

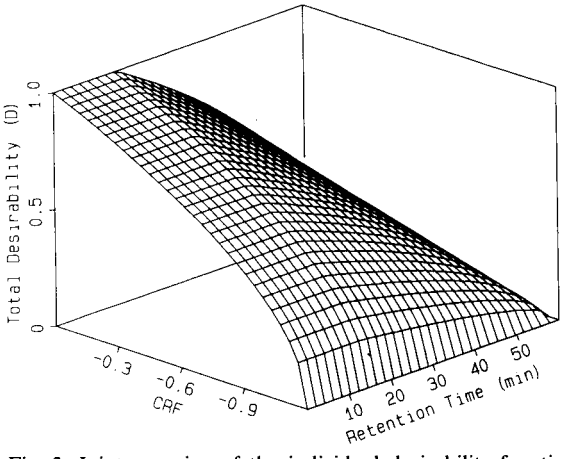

Fig. 3. Joint mapping of the individual desirability functions into a total desirability.

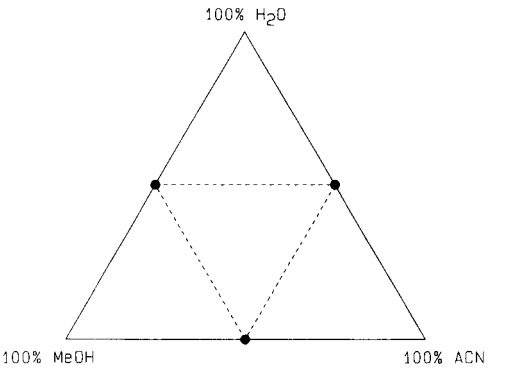

Fig. 4. The selected initial sequential simplex (solid dot connected by dashed lines) for optimizing the five-componen system.

Desirability functions

As Harrington has pointed out, "in nearly al situations requiring human judgement, one i faced with a multiplicity of measures which mus be balanced one against the other, weighted i accordance with their relative importance, com promised where these measures are mutually op posing, and variously manipulated to achieve a optimum judgement. If by some means the sev eral properties could be measured in consisten units, or, even better, could be expressed as num bers on a dimensionless scale, then the arithmeti operations intended to combine these measure becomes feasible" [43].

Multiple responses in sequential simplex opti mization can be combined into a dimensionles

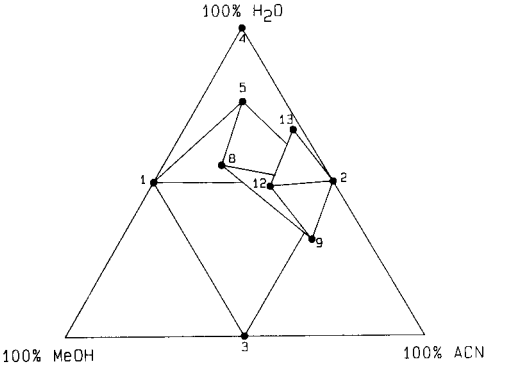

Fig. 5. Progression of the simplex for the five-componer system.

easure of performance termed an overall desir-
ility function [43–46]

$$= (D_1 \cdot D_2 \cdot \ldots D_m)^{1/m} \quad (2)$$

here D is the overall desirability associated with given chromatogram, and D_1 to D_m are the sirabilities of the first to mth responses. If an dividual response is totally undesirable, its de-ability function is assigned a value of zero; if an dividual response is totally desirable, its desirability function is assigned a value of one. If an individual response is at some intermediate level, its desirability is assigned a value between zero and one.

The mth root of the product of the individual desirabilities is used to calculate the overall desirability, D, so that poor desirability in any one response will have a large influence on the overall desirability. The mappings of responses into the desirability functions used in this study are

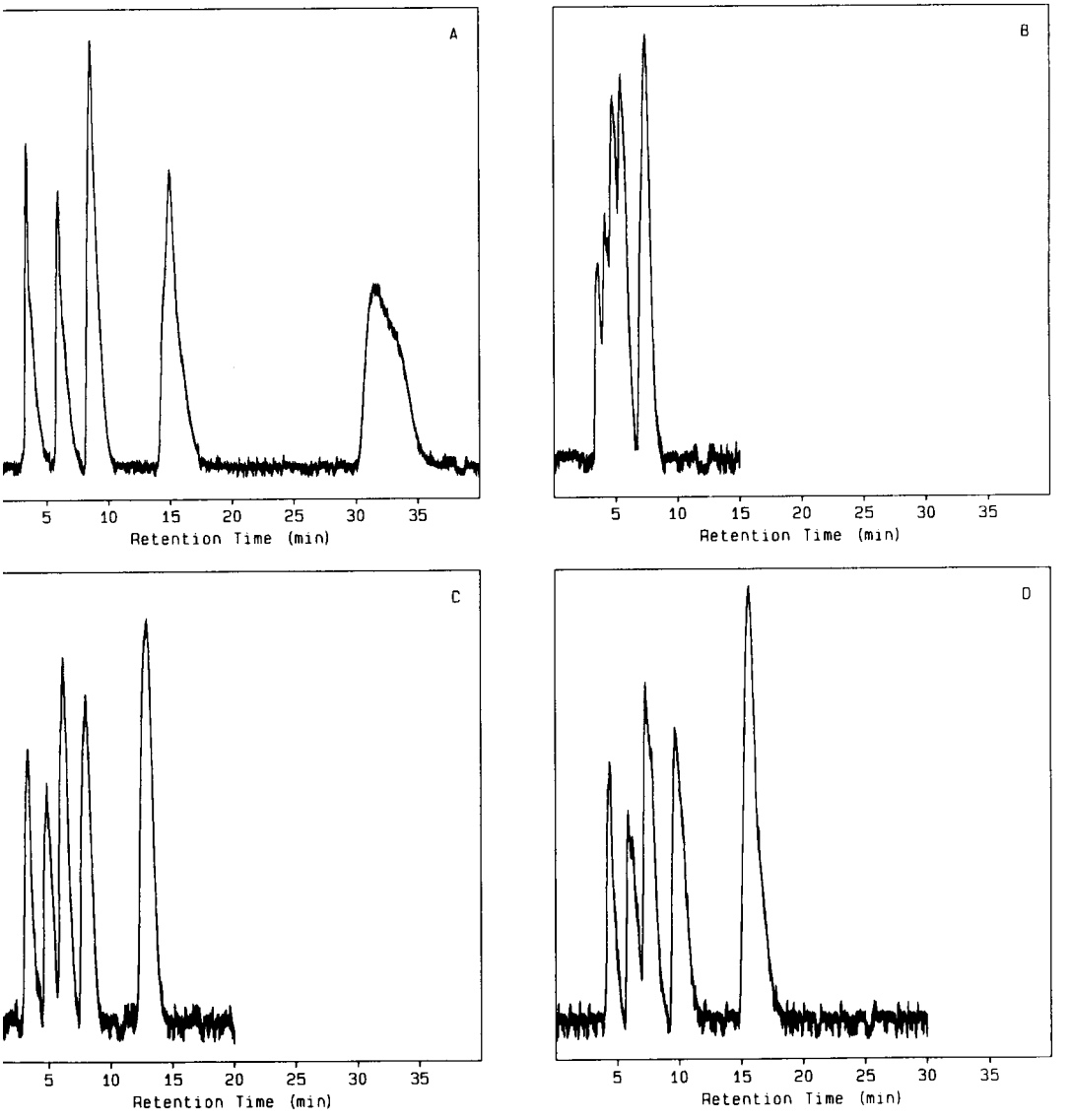

. 6. Chromatograms corresponding to (A) vertex 1, (B) vertex 9, (C) vertex 2, and (D) vertex 12.

Fig. 2. As the CRF [42] becomes more the desirability D_1 (a measure of the eparation) decreases. As the overall re- time increases, the desirability D_2 (a of the total analysis time) remains con- unity until 15 min and then decreases to 0 min.

it mapping of the individual responses tal desirability is shown in Fig. 3. When is zero and the overall retention time is 15 min, the overall desirability is maxi- decrease in CRF and/or increase in etention time beyond 15 min produces a in the overall desirability.

sequential simplex

itial sequential simplex is shown by the s connected by dashed lines in Fig. 4. ction of any vertex in this initial simplex lt in the recommendation of an experi- 100% of one of the three components of ure. The next iteration of the sequential will recommend an experiment outside ined mixture space; consequently the will begin to contract [11–13].

AND DISCUSSION

rogress of the sequential simplex opti- of the three-component eluent is illus- Fig. 5. The search for best solute resolu- short analysis time was terminated after es (a total of 9 experiments, see Table of the 13 vertexes suggested experiments he constrained mixture space and were ed boundary violations. These are not Fig. 5.

natograms generated at several of the either showed poor separation of the ponent solute or an extremely long total time. As examples, we show the chro- ns corresponding to vertex 1 [MeOH– + 1, v/v) mobile phase] and vertex 9 ·ACN–H_2O (15.6 + 53.1 + 31.3, v/v/v) hase] in panels A and B of Fig. 6, respec- ecause both good resolution and short ime are desired, the overall response for omatogram is poor.

TABLE 1

Mobile phase compositions and responses

Vertex	Simplex move [a]	Mobile phase composition (%)			Total desirability
		MeOH	ACN	H_2O	
1	I	50.0	0.0	50.0	0.79
2	I	0.0	50.0	50.0	0.96
3	I	50.0	50.0	0.0	0.00
4	R–3	0.0	0.0	100.0	0.00
5	C_R	12.5	12.5	75.0	0.00
6	R–1	–	–	–	BV [b]
7	C_R	–	–	–	BV [b]
8	C_W	28.1	15.6	56.3	0.00
9	R–5	15.6	53.1	31.3	0.00
10	R–8	–	–	–	BV [b]
11	C_R	–	–	–	BV [b]
12	C_W	18.0	33.6	48.4	0.93
13	R–9	2.3	30.5	67.2	0.66

[a] I = initial simplex; R – x = reflection by rejecting vertex x; C_R = subsequent contraction on the reflection side; C_W = subsequent contraction back on the side of the rejected vertex. [b] BV = boundary violation.

The chromatograms that resulted in the best overall desirability are shown in panels C and D of Fig. 6. Vertex 2 [ACN–H_2O (1 + 1, v/v) mobile phase], panel C, gave the best response (the largest overall desirability). Each pair of adjacent peaks is baseline-resolved with the exception of peaks two and three; the total analysis time is less than 15 min. Consequently, the total desirability is nearly maximal. Vertex 12 [MeOH–ACN–H_2O (18.0 + 33.6 + 48.4, v/v/v) mobile phase], panel D, gave the next-to-the-best response. Each pair of adjacent peaks is baseline-resolved with the exception of peaks two and three, but the analysis time is slightly greater than 15 min.

Conclusion

The results of this study indicate that sequential simplex optimization can be applied successfully to the development of mobile phase formulations for reversed-phase liquid chromatographic separations. Desirability functions are shown to be an effective tool for multiple-response optimization.

The authors thank H.T. Gramann, III for computer programming. This work was supported by

the Advanced Technology Program, Texas Higher Education Coordinating Board, Division of Research Programs, grant number 003652-108 and by the U.S. Environmental Protection Agency, project number CR-817552. Notice: although the research described in this paper was funded in part by the U.S. Environmental Protection Agency, it has not been subject to Agency review and therefore does not necessarily reflect the views of the Agency. No official endorsement should be inferred. Mention of trade names or commercial products does not constitute endorsement or recommendation for use.

REFERENCES

1 W. Spendley, G.R. Hext and F.R. Himsworth, Technometrics, 4 (1962) 441.
2 J.A. Nelder and R. Mead, Comput. J., 7 (1965) 308.
3 G.E.P. Box, Appl. Stat., 6 (1957) 81.
4 G.E.P. Box and N.R. Draper, Evolutionary Operation, Wiley, New York, 1969.
5 J.A. Crow and J.P. Foley, Anal. Chem., 62 (1990) 378.
6 J.W. Dolan and L.R. Snyder, J. Chromatogr. Sci., 28 (1990) 379.
7 J.L. Glajch and L.R. Snyder (Eds.), Computer Assisted Method Development for High-Performance Liquid Chromatography, Elsevier, Amsterdam, 1990.
8 S.R. Goode, J.J. Gemmill and B.E. Watt, J. Anal. At. Spectrom., 5 (1990) 483.
9 S.N. Deming, J.M. Palasota, J. Lee and L. Sun, J. Chromatogr., 485 (1989) 15.
10 J.C. Berridge, J. Chromatogr., 485 (1989) 3.
11 F.H. Walters, L.R. Parker, Jr., S.L. Morgan and S.N. Deming, Sequential Simplex Optimization, CRC Press, Boca Raton, FL, 1991.
12 J.C. Berridge, Techniques for the Automated Optimization of HPLC Separations, Wiley, New York, 1985.
13 P.J. Schoenmakers, Optimization of Chromatographic Selectivity, Elsevier, Amsterdam, 1986.
14 M.R. Detaevernier, L. Dryon and D.L. Massart, J. Chromatogr., 128 (1976) 204.
15 M.L. Rainey and W.C. Purdy, Anal. Chim. Acta, 93 (1977) 211.
16 J.C. Berridge, Anal. Proc. (London), 19 (1982) 472
17 J.C. Berridge, J. Chromatogr., 244 (1982) 1.
18 J.C. Berridge, Chromatographia, 16 (1982) 172.
19 J.C. Berridge, Anal. Proc. (London), 20 (1983) 29.
20 D.L. Dunn and R.E. Thompson, J. Chromatogr., 26
264.
21 E.J. Knudson and K.J. Siebert, J. Am. Soc. Brew.
41 (1983) 51.
22 J.H. Nickel and S.N. Deming, LC, Liq. Chromatogr
Mag., 1 (1983) 414.
23 J.C. Berridge, Analyst (London), 109 (1984) 291.
24 J.C. Berridge and E.G. Morrisey, J. Chromatog
(1984) 69.
25 R. Cela, C.G. Barroso, C. Viseras and J.A. Perez
mante, Anal. Chim. Acta, 191 (1986) 283.
26 C.E. Goewie, J. Liq. Chromatogr., 9 (1986) 1431.
27 A.P. Halfpenny and P.R. Brown, J. Liq. Chroma
(1986) 2585.
28 F. Vlacil and V. Hamplova, Collect. Czech. Chem
mun., 51 (1986) 45.
29 F.H. Walters and G. Gomez, Anal. Lett., 19 (198
30 S. Ghodbane and G. Guiochon, Chromatograp
(1988) 53.
31 J.A. Cornell, Experiments with Mixtures: Designs,
and the Analysis of Mixture Data, Wiley, New Yo
ed., 1990
32 V.L. Anderson and R.A. McLean, Design of Exper
A Realistic Approach, Marcel Dekker, New York,
33 A.I. Khuri and J.A. Cornell, Response Surfaces:
and Analyses, Marcel Dekker, New York, 1987.
34 R.D. Snee, CHEMTECH, 9 (1979) 702.
35 J.S. Murty and M.N. Das, Ann. Math. Stat., 39
1517.
36 R.D. Snee, J. Qual. Technol., 3 (1971) 159.
37 R.A. McLean and V.L. Anderson, Technometrics,
447.
38 J.A. Cornell, Technometrics, 15 (1973) 437.
39 H. Scheffé, J. Roy. Stat. Soc. Ser. B, 20 (1958) 344
40 H. Scheffé, J. Roy. Stat. Soc. Ser. B, 25 (1963) 235
41 R.D. Snee, Technometrics, 15 (1973) 517.
42 S.L. Morgan and S.N. Deming, J. Chromatogr., 11
267.
43 E.C. Harrington, Jr., Ind. Qual. Control, 21 (1965)
44 L.A. Zadeh, CHEMTECH, 17 (1987) 340.
45 L.A. Zadeh, Inf. Control, 8 (1965) 338.
46 R. Smits, C. Vanroelen and D.L. Massart, Freser
Anal. Chem., 273 (1975) 1.

Analytica Chimica Acta, 270 (1992) 107–113
Elsevier Science Publishers B.V., Amsterdam

Expert system for the determination of the analytical strategy in a laboratory for elemental analysis

Part 1. Project definition

B. van den Bogaert
Laboratory for Analytical Chemistry, University of Amsterdam, Amsterdam (Netherlands)

J.B.W. Morsink
Koninklijke / Shell-Laboratorium, Amsterdam (Shell Research B.V.), Amsterdam (Netherlands)

H.C. Smit
Laboratory for Analytical Chemistry, University of Amsterdam, Amsterdam (Netherlands)

(Received 3rd September 1991)

Abstract

In an analytical laboratory where the expertise and the instrumentation to apply a variety of techniques for the determination of elemental compositions are present, establishing the strategy that has to be followed in order to solve a specific analytical problem is a crucial activity. To determine which techniques should be used and which procedures should be followed as well as their order of execution, requires the synthesis of the possibilities and requirements of the different techniques with respect to the properties of the material to be investigated and the client's demand. As the first step towards an expert system for the analytical technical aspects of this task, the structure of the knowledge domain has been investigated. It is concluded that an overall system can be built incrementally by constructing subsystems for the different techniques and putting these together in a general framework. The structure of the knowledge is found to be the same for all techniques and the development of one subsystem is therefore expected to ease the development of following subsystems. The development of such a subsystem for x-ray fluorescence spectrometry, is described in Part 2.

Keywords: Expert system; Artificial intelligence; Elemental analysis

In this article the first stage of a project for the development of an expert system for the determination of the analytical strategy in a laboratory for elemental analysis is described. The main activity in this stage has been the investigation of the structure of the knowledge domain in order to make a planning for the actual development Our practical experience with the resulting planning is described in Part 2 [1].

As part of the framework of artificial intelligence (AI), the idea of programming intelligenc has been around since the beginning of the computer age. The concept of expert systems ha forced a breakthrough in the wall of scepticisr that has always surrounded AI. Exactly wher this success has come from is hard to tell, bu

Correspondence to: H.C. Smit, Laboratory for Analytical Chemistry, University of Amsterdam, Nieuwe Achtergracht 166, 1018 WV Amsterdam (Netherlands).

everal factors can be mentioned that have aided n giving credibility to the claim that expert-sys-em technology really works. AI started out by ying to build general problem solvers but did ot succeed. Later on it turned to the building of pecific problem solvers and did succeed report-dly. For these specific problem solvers the name xpert systems was coined. Other factors that ave contributed to the above-mentioned credi-ility are the significant increase of computer ower that has taken place since the early years f AI and, maybe most important, the fact that ne concept of expert systems can be translated nto marketable products in the form of expert ystem development tools. The enthusiasm that ook the place of the scepticism spread out over ne analytical community during the 80's. Several ublications appeared in literature [2–10], in hich the principles of expert systems were intro-uced, a review of current work was given, often promising future was outlined and sometimes eneral lessons from the authors' experience in xpert-system development were taught.

The lab on which our work is focused, i.e. the lemental analysis group at the Koninklijke/ hell-Laboratorium, Amsterdam (Netherlands), ad several motives to get involved in expert ystems. The principal motive was to consolidate he available knowledge, since loss of expertise, aused by the departure of an expert, proved to e a structural problem. Related to this consoli-ation was the need to document the knowledge n an accessible way, for instruction and refer-nce purposes. As long as the expert is still avail-ble, an expert system will relieve him from some f his work, allowing more efficient use of the ab's human resources. The fourth motive was the ossibility for improvement in the performance of he tasks to be implemented, by being more com-lete and more consistent than the experts them-elves. Another important aspect was the poten-ial spin-off from the development process con-isting of better insight into the operation of the aboratory and an overview of weak spots in the vailable knowledge.

All these motives are mentioned primarily to tress their consequence for the nature of the xpert-system development project. This project will be focused on knowledge available in the form of expertise of the laboratory staff. This knowledge will have to be extracted from the staff and, in contrast to e.g. textbook knowledge, it is unlikely to be structured. Furthermore, it may very well be rather site specific.

KNOWLEDGE DOMAIN

Context

The crucial step in the development of an expert system is the exact definition of the knowledge that should be implemented. Knowledge itself is elusive, but the more tangible concept of a task can be used to identify a domain of knowledge. In other words, a knowledge domain is the body of knowledge required to perform a task. This definition can be considered a limitation, discarding the general applicability of knowledge by tying it down to a specific application, but it is necessary in order to restrict the objective of a development project to manageable proportions. Thus the first stage in our project is to make an inventory of the tasks that are performed in the analytical laboratory. An extensive inventory has not been made. What is presented here is meant to give the context of the task that has been selected.

One of many ways to describe an analytical laboratory is as a place where analytical problems are solved. In this problem solving, analysis is of course the central activity and most conventional programming efforts have been concerned with supporting this activity. This has lead to applications like instrument control, data acquisition and data processing. Analysis is, however, just one link in a chain of activities (Fig. 1). Analysis cannot be performed efficiently without prior determination of the strategy and the results should be evaluated before being reported to the client. In the lab under observation the strategy determination is especially important, because the lab forms part of a large industrial research facility in which many different and often unique analytical problems arise. Furthermore, the lab has a broad range of state-of-the-art instrumentation and techniques available for solving these problems.

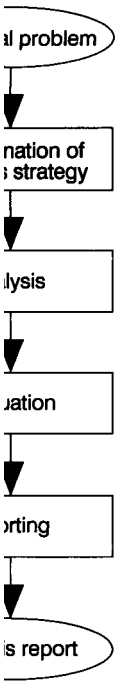

line of analytical problem solving.

the conventional programming para-
notion of this chain of activities in
problem solving has led to the idea of
y information management systems, i.e.
ng of the flow of samples and data to
at for each activity all the information
at hand. In the expert-system perspec-
is no focus on the analysis activity or
mation flow. One can think of expert
or all the activities in the problem solv-
nalysis just as much as for the determi-
the analysis strategy or for the evalua-
nalysis results. For the present project
rmination of the analysis strategy has
sen as the task for an expert system.

terization

mplexity of the task of determining the
strategy may be characterized by the
f possible problems and the amount of
olutions. The latter is determined by the
nd the scope of the techniques involved.
l chemistry consists of a multitude of
s and procedures and a typical analyti-

cal laboratory has a considerable number of these available for use. Every technique has its specific capabilities and requirements, but can usually be configured to solve a much wider range of problems. The more expertise there is on each technique, the more problems can be tackled by each of them and the more overlap the various techniques have.

When the composition of the flow of incoming problems is rather static, as in a factory product-control lab, the total number of solutions becomes less significant. In that case problem solving passes from planning and configuring into classification and the strategy determination reduces to recognizing a problem as belonging to some standard solution. When the composition of the flow is dynamic, as in the central analytical lab of a research centre, the chance that a standard solution will suffice will be small.

Input and output

The main input of the strategy-determination task is the analytical problem to be solved. In this context we do not identify this problem with the physical sample of material to be investigated, but rather with the information that is available on that sample, such as the properties of the material and the client's demands. In laboratory practice the analytical problem is not the only input for the task of strategy determination. The current logistics also play an important role, i.e. the workload for each technique and the availability and capabilities of the staff members. Here we focus on the analytical technical aspect of the strategy determination, which takes the analytical problem as input. The information contained in an analytical problem is outlined below.

Analytical problem
- specimen data
  - basic properties
    - amount
    - physical form
      - aggregation state
      - form, e.g. powder
    - matrix, i.e. presence and/or concentration
      - molecular

  - elemental
- derived properties
  - handling properties, e.g. solubility
  - sample type, e.g. catalyst
- chemical background, e.g. "from the top of a distillation column"
- client's demands (overall, or for each analyte)
  - qualitative/quantitative analysis
  - precision and accuracy
  - deadline
  - available budget

Not only the values of the elements in the above outline are of importance for the strategy determination, but also the relative weight of these values determined by the reliability in case of the physical and chemical a priori information and by the importance in case of the demand issues. Furthermore, most of the time not all of the information outlined above will be explicitly asked for, which also causes weight-factor variation. When the values of certain information elements are derived from more general information such as sample type, they are in fact only assumed and should have a weight that is less than that of values that have been acquired directly.

The output of the strategy determination is of course the analysis strategy, which is used here to indicate the planning of the techniques that should be used and the order in which they should be used, the sample-preparation procedures to follow and the configuration of the individual techniques. Hirayama et al. [11] describe a system with very much the same objective, using the term planning instead of strategy. Related topics are covered in literature under the names of both planning and method selection. These publications deal with systems that involve one technique that needs to be configured, e.g. liquid chromatography [12–15] or atomic absorption spectrometry [16].

Internal structure

The task of strategy determination has now been defined by its input and output, i.e. it has been described from the outside. For the development of an expert system we need a description from the inside. For this purpose we have

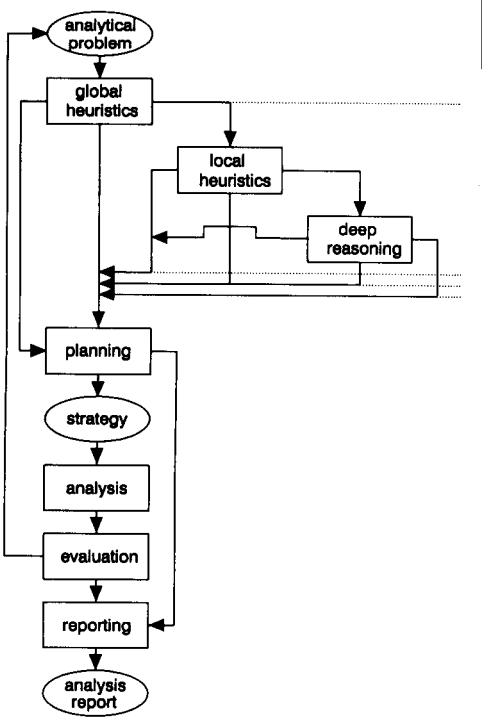

Fig. 2. Model of knowledge involved in strategy de tion.

built a simple model of the structure problem-solving process and the knowled volved. This model is depicted in Fig. 2, w in fact an expanded version of Fig. 1. Th task box has been opened up revealing a ture of actions at a lower level. Moreove arrows have been added, one pointing bac the evaluation to the input and one for shortcut from the strategy determination porting. The structure of local heuristics an reasoning represents the reasoning for on nique. The dashed lines indicate that in fac techniques are connected in parallel to the heuristics and planning.

When an analytical problem enters the l first treated with what have been called heuristics. A problem may enter via the h the lab, the sample administration or one technique experts. Which way it will be d mainly on the familiarity of the client wi organization and the facilities of the lab. one of these persons can apply some

cs, but the sample administration knows
olies the largest set. These global heuris-
tain basic knowledge of the possibilities of
ilable techniques and classification rules
ıpon experience with determining strate-
r instance, if a specimen is gaseous, the
ieuristics can conclude that no technique
ble. Global heuristics can give three kinds
ut. They can conclude that the analytical
ı can be solved by the lab (middle arrow),
annot be solved by the lab (left arrow) or
y do not have the knowledge to tell (right

ıe latter case the possibilities for solving
lytical problem will have to be evaluated
l for all relevant techniques by the respec-
hnique experts. At the technique level the
e is analogous to the global level. A tech-
xpert will first work with his ready knowl-
his technique, which we will call local
cs. At this level an expert may conclude
technique can solve the problem or part
iddle arrow), that it cannot (left arrow) or
ready knowledge is insufficient so he
be conclusive (right arrow). When his
nowledge has failed he can turn to deep
ıg, i.e. collect information from books and
es and make some calculations. A tech-
pert performing deep reasoning can again
e that his technique can be used, that it
be used or that he cannot tell for sure
it can or cannot be used. The latter
that the possibilities of evaluating that
ıe a priori are exhausted. The only way
find out what can be achieved with the
ıe is to try it out in practice, i.e. explo-
nalysis or research has to be performed.
al reasoning has been depicted for one
ıe, whereas in practice it may be active
ral. Which technique experts are called
r a certain problem is determined by the
euristics.

ocal reasoning is related to the reasoning
nvolved in the actual analysis (Fig. 3). In
lysis stage the parameters in the configu-
f the technique, or instrument, and the
preparation procedure are optimized by
back the evaluated measurement data.

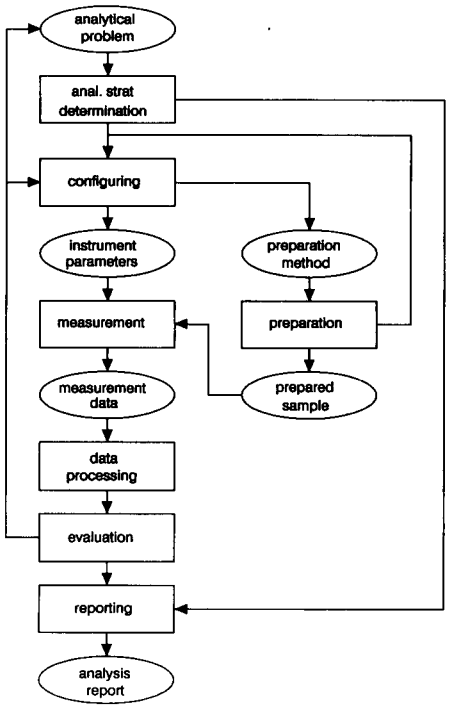

Fig. 3. Model of reasoning during analysis.

The optimization cycle has to be started with a first guess of these parameters. In the local reasoning for the strategy determination this optimization is performed a priori, by using expectations of measurement results instead of real measurements. These expectations require models of the measurement process and the sample preparation. The difference between heuristics and deep reasoning is primarily the degree of complexity of the models used. Local heuristics and deep reasoning are the extremes of how a problem is dealt with at one technique locally. They have been identified separately though in practice there is a gradual transition from one to the other. The outcome of the local reasoning may be used as the first guess in the optimization process during the analysis. The concept of optimization suggests the use of formal methods, such as SIMPLEX. We believe that these methods are not suited for implementing the a priori optimization, because the response will not usually be predicted numerically, which makes it difficult to define an optimization criterion.

The result from applying the global heuristics and the different local heuristics and deep reasoning is a list of possibilities of all the relevant techniques regarding the solution of the analytical problem. More or less as a by-product, information has been generated on how the techniques have to be configured in order to realize the listed possibilities. Subsequently formulating a strategy on the basis of these data is a matter of planning. Sometimes planning is trivial, e.g. when no technique has the necessary potential or when the analytical problem has been recognized as identical to one that has been solved before, but typically it is a complex process that has to take into account the overlap and the interdependence of techniques. In practice, planning also includes balancing the budget to the cost of the possible solutions, and weighing laboratory logistics against the effort needed for each solution. When the planning requires research to be done the determination of the analysis strategy becomes a cyclic process, because there will be a feed-back of the results of the research to the analytical problem.

DEVELOPMENT PLANNING

Implementing all of the reasoning involved in the strategy determination is a large and complex job and it would not be wise to try and achieve it all at once. The model of strategy determination (Fig. 2) suggests several possibilities for restricting the domain and reducing the complexity. One could implement only the global reasoning, i.e. global heuristics and planning, but because of its lack of depth the resulting system would be rather static and not able to cope with the diversity of problems to be solved in practice. Our choice has been to start with the reasoning for one technique, both local heuristics and deep reasoning, embedded in as much of the global reasoning as is necessary to make use of the results of the local reasoning. The planning part of this embedding global reasoning will be only rudimentary, since balancing the possibilities of different techniques is the kernel of planning and in the first instance there will be only one technique to deal with. When another technique is added, the reasoning may be extended accordingly, will have a large effect on the nature planning part. We expect that the experie implementing one technique will ease the opment of modules for additional tech since the internal structure is the same techniques. In developing the system and i systems we further restrict ourselves by fc on the analytical technical aspects of the s determination and taking into account laboratory logistics nor matters of budget.

DISCUSSION

An important aspect of the presented m its linearity, i.e. it is not cyclic. In the mo technique experts are only reconsulted wh amount of information on the analytical p has increased because of explorative resea practice, however, bottlenecks in the pl stage may require a technique expert th already been consulted to reconsider his sions. This touches on the matter of aut e.g. who decides if a technique expert may with local heuristics or should go over t reasoning. The linear model represents th situation in which the technique experts use all the available information and al knowledge in order to come to conclusion minimal uncertainty.

The model has been drawn with a s laboratory for elemental analysis in mind, consider it to have a wider applicability, all for elemental analysis, but also for anal a whole.

From the point of view of consolidating edge the strategy determination task seem a suitable candidate for implementation, b knowledge of all techniques is essential fo ing a correct assessment of the possibilit each problem that needs to be solved. A motive has been the possibility for improv An expert-system that brings together di fields of expertise might represent the ide ference of experts in which all argumen come up and be properly balanced.

Conclusion

On the basis of a simple linear model of the knowledge domain, an approach for the development of an expert system for the determination of the analytical strategy in a laboratory for elemental analysis has been planned. An overall system will be constructed of separately developed technique subsystems attached to a global framework. The subsystems are expected to be similarly structured. The construction will be started with the development of one such technique subsystem. This development will be covered in the next part of this publication. The focus will be on the analytical technical aspect of the strategy.

We gratefully acknowledge the financial support of the Koninklijke/ Shell-Laboratorium, Amsterdam (Shell Research B.V.), Amsterdam, Netherlands.

REFERENCES

1 B. van den Bogaert, J.B.W. Morsink and H.C. Smit, Anal. Chim. Acta, 270 (1992) 115.
2 R.E. Dessy, Anal. Chem., 56 (1984) 1200.
3 R.E. Dessy, Anal. Chem., 56 (1984) 1312.
4 S.A. Borman, Anal. Chem., 58 (1986) 1192.
5 M. Withers, Chem. Br., (1986) 697.
6 J. Klaessens and G. Kateman, Fresenius' Z. Anal. Chem. 326 (1987) 203.
7 G.J. Kleywegt, Lab. Microcomp., 6(2) (1987) 74.
8 T.P Bridge, M.H. Williams and A.F. Fell, Chem. Br. (1987) 1085.
9 A.P. Wade, S.R. Crouch and D. Betteridge, Trends Anal Chem., 7 (1988) 358.
10 A.R. de Monchy, A.R. Forster, J.R. Arreteig, L. Le and S.N. Deming, Anal. Chem., 60 (1988) 1355.
11 H. Hirayama, R. Wohlsen and C. Brede, ACS Symp. Ser. 408 (1989) 200.
12 D. Goulder, T. Blaffert, A. Blokland, L. Buydens, A Chhabra, A. Cleland, N. Dunand, H. Hindriks, G. Kateman, H. van Leeuwen, D. Massart, M. Mulholland, G Musch, P. Naish, A. Peeters, G. Postma, P. Schoenmakers M. de Smet, B. Vandeginste and J. Vink, Chromatographia, 26 (1988) 237.
13 L. Buydens, A. Peeters and D.L. Massart, Chemom. Intell Lab. Syst., 5 (1988) 73.
14 M.A. Tischler and E.A. Fox, Comput. Chem., 11 (1987 235.
15 H. Gunasingham, B. Srinivasan and A.L. Ananda, Anal Chim. Acta, 182 (1986) 193.
16 W.R. Browett and N.J. Stillman, Prog. Anal. Spectrosc., 1 (1989) 72.

Analytica Chimica Acta, 270 (1992) 115–130
Elsevier Science Publishers B.V., Amsterdam

Expert system for the determination of the analytical strategy in a laboratory for elemental analysis

Part 2. Development of an x-ray fluorescence subsystem [1]

B. van den Bogaert
Laboratory for Analytical Chemistry, University of Amsterdam, Amsterdam (Netherlands)

J.B.W. Morsink
Koninklijke / Shell-Laboratorium, Amsterdam (Shell Research B.V.), Amsterdam (Netherlands)

H.C. Smit
Laboratory for Analytical Chemistry, University of Amsterdam, Amsterdam (Netherlands)

(Received 3rd September 1991)

Abstract

In this article, the second in a series on the development of an expert system for the determination of the analytical strategy in a laboratory for elemental analysis, the construction of a subsystem for x-ray fluorescence (XRF) spectrometry is described. An intuitive approach was followed for the knowledge acquisition, consisting of prototyping, based on prior analysis. The knowledge has been elicited primarily by interviewing an XRF expert. The analysis resulted in a hierarchical model of the knowledge in combination with a breadth-first strategy, which is a refinement of the model described in the first article in this series. The refined model has been implemented using the tool Nexpert Object. The implementation is not strictly a subsystem, but also contains the model structure of the overall strategy determination task. The current system is site specific with regard to the actual knowledge content, but the structure has a wider applicability. The expert system is focused on sample preparation and does not consider the measurement process in detail. The available expertise, being based on practice where a priori information may be supplemented with experimental data, was found to be unsuitable for the purpose of the expert system, which is to rely on a priori information only.

Keywords: Expert system; X-ray fluorescene; Artificial intelligence; Elemental analysis

The work described here is part of a project for the development of an expert system for the determination of the analytical strategy in a laboratory for elemental analysis, i.e. the selection of the techniques to be applied in the solution of a certain problem. This strategy determination is a complex task requiring a lot of knowledge, because of the complexity of the matrices in which elements have to be analyzed, the number of techniques and sample preparations that may be used, and the number and complexity of the interferences that may occur in the measurement process.

Correspondence to: H.C. Smit, Laboratory for Analytical Chemistry, University of Amsterdam, Nieuwe Achtergracht 166, 1018 WV Amsterdam (Netherlands).

[1] For Part 1, see Ref. 1.

In the exploration stage of this project an inventory of the knowledge that would be required for this system led to the conclusion that an overall system could be built by putting together subsystems for the individual techniques [1]. Each subsystem has to evaluate the possibilities of the respective technique: whether it can or cannot be used to solve the problem or part of it. In the ideal case, a subsystem also produces the required experimental setup, i.e. sample preparation method, instrument configuration and measurement conditions. In the development of each subsystem the future use as part of an overall system has to be taken into account.

Systems having these capacities will be of interest to the sample administration, the technique expert, the experts on other techniques and the management, in other words to all of the laboratory staff. Of course outsiders, and clients of the laboratory in particular, are also potential users of these systems, but the systems will not be developed especially to accommodate such use.

For a first subsystem the x-ray fluorescence (XRF) technique was selected. This selection has been made primarily on practical grounds. XRF is one of the working-horses in the element analytical laboratory for which the overall system is being developed (Koninklijke/Shell-Laboratorium, Amsterdam). Furthermore, in this lab some experience in developing an expert system for XRF had already been gathered. The reason to focus on XRF at that time was the imminent departure of the senior XRF expert. Further arguments in favour of XRF are that it is a well-established technique and knowledge concerning it is considered to be mature. The senior XRF specialist can be considered a reliable source of expertise to draw from. As a model for the relevant expertise, a priori optimization of the experimental setup has been proposed [1].

For quantitative applications, however, XRF is not the transparent technique one might have expected it to be, despite its maturity and the low number of characteristic lines per element compared to e.g. inductively coupled plasma optical emission spectrometry (ICP-OES). The reason for the complexity in quantification is the occurrence of matrix effects. Handling matrix effects, by tuning the sample preparation and the measurement procedure, is the central issue in practical XRF work. Matrix effects may therefore be expected to play an important role in the expert system as well. Further complexity of the XRF domain is caused by the fact that XRF may be used to analyze most of the periodic system, covering large concentration ranges, in a wide variety of samples.

The XRF expertise in the element analytical laboratory is based on practical experience, which limits the scope of the available expertise and thereby the scope of the expert system, since we wish to restrict ourselves primarily to the expert as the source of knowledge for the system. There are two aspects to this limitation. One is that the problems the lab is confronted with, however diverse they may be, will not completely cover the vast range of problems that may in principle be solved by XRF. The other is that XRF will not be used to solve all of the incoming problems, since it has to compete with other available techniques. Both the nature of the incoming problems and the collection of techniques present, make the available expertise site specific. The expert system based on this expertise will inevitably be site specific as well, but this concerns only the actual knowledge content. The structure of the system may well have a wider applicability.

SYSTEM DEVELOPMENT

In this section, after an evaluation of some options for knowledge acquisition, the approach followed and the tools used are described. The knowledge acquisition approaches that have been evaluated are rapid prototyping, KADS and self-learning expert systems.

Knowledge acquisition

Expert systems have often been described as the first public success in the field of artificial intelligence (AI) [2]. This description follows from a technical view of the matter, in which the techniques of representing and manipulating bodies of knowledge are considered the quintessence of expert systems and little attention is paid to

the bodies of knowledge. Knowledge acquisition, the compilation of these bodies, is often referred to as the bottleneck of expert-system development.

Rapid prototyping. From a technical point of view, a logical way of building an expert system is by prototyping, in which implementations are used directly to model knowledge. When the implementation works, the model is correct. When it does not work, it is replaced by another implementation. Prototyping is of course nothing new and it has not been designed specifically for expert-system development. It is just the most intuitive and direct approach to writing any program, an approach one normally would not rely on, out of fear for unstructured, unintelligible and unmaintainable programs. In expert-system literature this fear is much smaller. Building an expert system is like a new way of programming, heuristic instead of algorithmic or declarative instead of procedural, using intelligible and maintainable code, viz. the knowledge itself. In this view a lack of structure is the remaining risk of prototyping.

KADS. We wanted to use a more formal approach to knowledge acquisition, but we found KADS (Knowledge Acquisition Documentation and Structuring), the only formal method described in literature [3–5], difficult to work with. It forms a world on its own, difficult to penetrate, using a jargon whose merits did not always become clear to us. We felt that using KADS would introduce too much overhead for our project, because of the time needed to get familiar with it, and because it is aimed at acquisition from zero level. Furthermore, KADS had not yet been fully completed when we studied it. Instead of providing a smooth transition from raw knowledge to implementation, a cyclic incremental development process was still required. How different this would be from prototyping was not discussed. In an interview with Wielinga, one of the fathers of KADS, our objections matched those of others [6].

Self-learning expert systems. The use of a self-learning expert system was suggested by the fact that all incoming analytical problems are recorded in the sample administration. Self-learning systems require a collection of cases for training and preferably another set of cases for testing. One might expect both sets to be easily compiled from the records of the sample administration. We rejected the self-learning approach for several reasons. First of all, the records contained only limited information. We observed that the actual decisions had been made on considerations outside the scope of the recording. Secondly, even if the information would be complete, founding the expert system only on prior cases might result in a system that lacks the desired flexibility. Incoming problems may well be unique, and without considering some level of abstraction between problem and solution, the knowledge represented by the case will also be unique and of limited applicability. To achieve real flexibility of a self-learning system for our purposes a very large artificially generated training set would have to be used. This would bring us into a vicious circle, because in order to prudently construct such a set one needs good insight into the knowledge that needs to be contained in it. Having obtained such insight it is more direct to explicitly program it into an expert system then to use it to instruct a self-learning mechanism.

Approach followed

We have developed the expert system by prototyping. In order to minimize the risk of a lack of structure in the resulting system, we have made an analysis before starting the implementation. The analysis has been made intuitively, not in any formal way, but our intuition had been educated by studying the KADS documentation and some other publications [7,8].

Our sources of knowledge have been interviews with and observations of the XRF expert, literature study, observations of meetings of all technique experts and interviews with the sample administrator, in this order of importance. All recording of interviews and observations has been done by making notes, not by audio or videotaping. The interviews were informal. Interview hints in literature [9] gave us a better idea of our own activities, but were not so different from our own intuitive approach that they really changed it. In the interviews with the XRF expert the technique was the central issue, next to fictitious what–if

situations and real cases. The literature studied did not consist of articles on current research, but rather of textbooks on the general principles of XRF analysis [10–12]. A review of current research in the field served as an indication of the status of the practical use of XRF in the lab [13], confirming that this use is restricted to the application level.

Knowledge acquisition can be regarded as learning, and learning is a not a linear process. The more you learn, the better you realize how little you know, let alone how little you knew before. One will often have to revise and refine earlier beliefs. Therefore the description of the practical work given below should not be taken as strictly chronological.

We started by making a list of the concepts and the terminology that are in use in the XRF knowledge domain. For variables, all possible values were specified. The objective was to turn the list into a closed world of references and explanations like a kind of encyclopedia of the domain. In the first instance we tried to make the list as complete as possible. Later on, we aimed specifically at the concepts that appeared to be relevant to the specific expertise needed in our expert system. After a first stage of collecting primarily factual information we started to focus on causal relations. We first collected direct consequences of certain values of variables; after that, we focused on complex consequences, i.e. when a pattern of variable values determines the result instead of a single variable. In interviews with the XRF expert this was done by creating a simple situation which was subsequently complicated step by step. For complex consequences we tried to describe the interactions on an abstract level in order to make our observations as general as possible. Next we tried to create a hierarchical organisation of the concepts, assuming that every concept has or may be assigned a limited scope. The resulting hierarchy was used to make a selection for the first implementation of the expert system. This also implied a choice of the level of knowledge representation and a decision about what was going to be inferred and what calculated, retrieved from database or asked from the user. During the implementation the latest version of the expert system was tested with existing material as well as new analytical problems.

Tools

For the implementation of the expert system we decided to use a commercially available tool, because we felt that building our own tool from scratch using a programming language would only distract from the most important and most interesting aspect of our project: the gathering, structuring and coding of knowledge. We did not perform an extensive evaluation of existing tools in order to find the one most suited for our purposes, assuming that to a certain extent any tool would do, a notion also found in literature [14]. One tool may ease the implementation whereas another tool complicates it, but this seems to be a subjective, programmer-dependent matter. To stay on the safe side we chose a sophisticated tool, the expert-system development environment Nexpert Object (Neuron Data). Furthermore, there was already some experience with Nexpert within Shell and the reviews were positive.

We used a workstation, a VAXstation 3200 from Digital Equipment with an 8-Mbyte memory, a high-resolution colour screen, running under the VMS/VWS operating system, with corresponding Nexpert version 1.1 software. We also used Nexpert for some time on a PC-AT (8 MHz, 2-Mbyte extended memory, EGA), but on this platform the performance of the development environment was not acceptable. If the move from PC to workstation would not have been possible, we would probably have turned to another, less demanding and therefore maybe less sophisticated tool.

We coded the knowledge base (KB) in a general ASCII editor, because we found this easier and more direct, giving more control over the contents and the lay-out of the KB. We did not use any run-time software on the workstation. Instead we chose to supplement the development environment with some user interface functions by linking our own routines to the Nexpert kernel. Though Nexpert itself is written in C, we coded our own routines using VAX Fortran, because the Fortran compiler was available and

```
sample information
      - physical form
            - aggregation state
            - available amount
            - dimensions
      - element matrix
            - elements present
            - concentration estimate of these elements
      - component matrix
            - presence of e.g. silica
            - abundance of the components
      - chemical properties
            - inertia towards several polymer foils
            - volatility
client's demand
      - primary
            - elements to be analyzed
            - precision of the analysis
            - fate of the sample
      - secondary
            - loosening the primary demands
inference control
      - decision in case of uncertainty
session control
administrative information
      - sample administration code
      - short description of the problem
```

Fig. 1. Outline of the input of the XRF expert system.

because we already knew Fortran and were not familiar with C.

In the knowledge-acquisition phase we have made use of some general-purpose PC software. Our most important tool has been Framework (Ashton-Tate). We used Framework to order and structure knowledge fragments and to experiment with numerical models using database information in spreadsheet calculations. Framework can, however, create textual structures only and often during expert-system development the need arose to make graphical structures like flow charts. For this purpose we used Freelance (Lotus Development). For tentative structures, however, paper and pencil remained the most suited tools, since changes in structure generally require a total reconstruction of the computer drawing and a new sketch is made more easily.

RESULTS

In this section, the current expert system itself, not a numerical evaluation of its capabilities, is presented as the result of the research. The expert system is described from several points of

Start of session
A list of old sessions is displayed
Enter the code of the analysis request that is going to be examined:
1
A session record of this request exists. Recording this session will override. Do you want to record?
False
You can enter a short description of the sample or the analytical problem to be processed:
spent-cat
What is the aggregation state of the sample?
solid
Does the sample have the form of a fine powder?
True
The periodic system input window is displayed. Inference resumes when the user indicates the end of editing by selecting "ok" or "cancel". In this example the final state of the editor window is as in fig. 4.
Does the sample contain silica as a major component?
True
Does the sample contain siliconcarbide?
False
How many grams of sample are available for analysis?
5
The amount of metals (not counting Al) is critical. Is there over 4%m metals in the sample?
True
The result of the session is displayed. For this example the result is displayed in fig. 5.
End of session

Fig. 2. Annotated transcription of a session with the XRF expert system. Annotations are in italics.

```
***** sample.small

It has been established that the sample should
stay intact. Therefore the entire sample has to
fit into one of the containers that are used to
introduce samples into the spectrometer. These
containers have a more or less cylindrical shape
with a diameter of about 30 mm and a length of
about 50mm.

Answering 'True' to this question will make the
expert system conclude that it is worthwile to
evaluate the possibilities of XRF for the
analytical problem at hand. Because only direct
introduction of the sample is possible these
possibilities will be limited to semi-quantitative
analysis.

Answering 'False' will terminate the evaluation of
analytical possibilities; XRF cannot be used.

Answering 'Notknown' will result in unpredictable
behaviour of the expert system, because the system
is based on two-state, not three-state logic.
```

Fig. 3. An example help file. The file is linked to the knowledge base item "sample.small" and will be displayed when the user requests more information when the expert system asks the question: "Is the sample less than 30 mm in diameter?".

view. We start by giving a short functional description of the system, without evaluating it. The evaluation will take place in the discussion. After the functional description, we describe the system from the outside, i.e. its user interface. Then we turn to the system's inside. First we will describe, in an abstract way, the inference model that forms the basis of the knowledge base, then we will describe how this model is actually used in the knowledge base. In a separate paragraph the problem of handling diverse levels of detail in the input is discussed. The results section ends with some notes on the documentation and the portability of the expert system program.

Functional description

The system asks the user for information on the incoming analytical problem. This is outlined in Fig. 1, which is not an exhaustive listing of all possible input; each session will have its own set of inputs. Note that the system takes neither

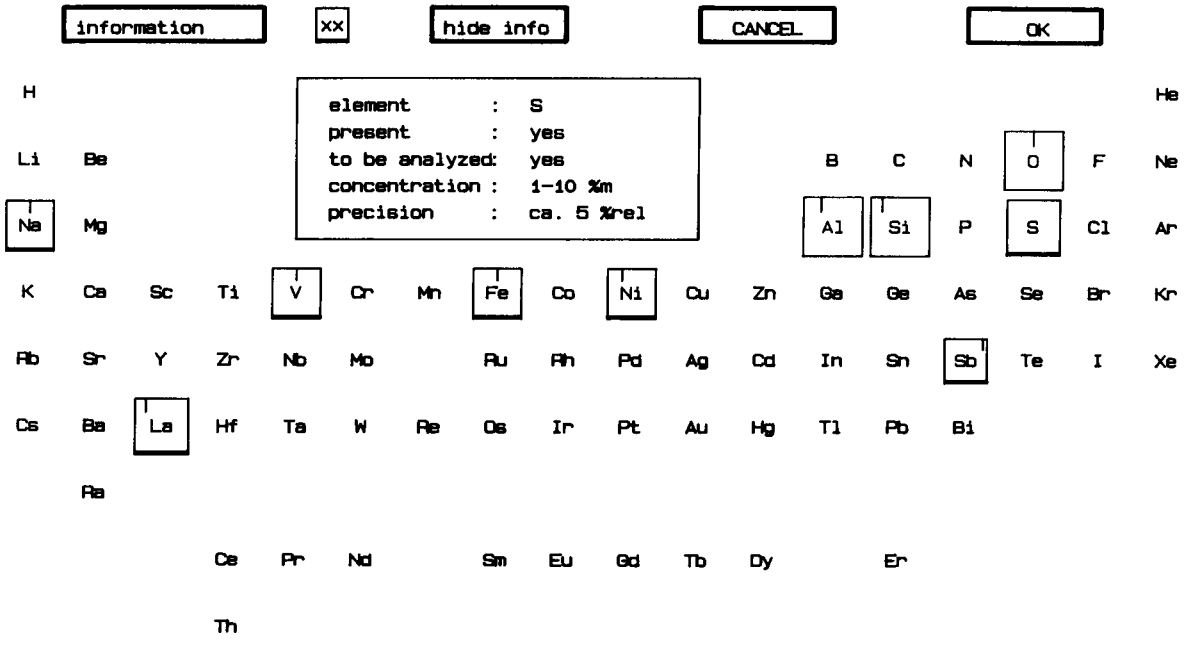

Fig. 4. An example of the appearance of the periodic system editor window. On the computer screen the symbols for Na, S, V, Fe, Ni, Sb and La are displayed in red indicating that these elements should be analyzed, those for Al, Si and O in blue, indicating that they are present but do not need to be analyzed and all others in black. The size of an element box is proportional to the order of magnitude of the element's concentration. The left/right position of the indicator along the top edge is proportional to the location of a concentration estimate within its order of magnitude. The width of the bottom edge is inversely proportional to the desired precision. Elements that are not displayed are not contained in the expert system.

deadline nor budget as input. On the basis of the information supplied, which is assumed to be complete and correct, and element data retrieved from a small database, it decides if XRF can be used to solve the problem or part of it, and what sample preparations are needed. No advice on the experimental setup beyond the sample preparations is generated. The results of the inference are reported to the user. The behaviour of the system is illustrated with an annotated transcription of a session (Fig. 2).

User interface

The system has two ways of collecting its input from the user: individual questions and a batch editor. The system contains scores of questions that can be asked by means of the standard Nexpert question window. In practice not all of these questions will be used during a single session, though some of them will return in every session. For each question there is a corresponding file with additional information on the question and possible answers (an example is given in Fig. 3). The display of these files is used as a substitute for Nexpert's explain facility, which we find cryptic and unusable. The best method for the user to inspect the context of a question is to inspect the rule network. This is a very useful and flexible function of the Nexpert development environment in which the structure and the current status of the inference, as far as it is rule based, can be visualized.

A batch editor has been written especially for this expert system. It draws the periodic system of the elements on the screen in which four general element properties can be edited by using the mouse pointer (Fig. 4). The status of the elements, i.e. the values of their properties, is visualized by using graphical attributes such as colour and size of the icons by which they are depicted. This graphical representation always gives all information at once. The user can also choose for a textual representation of the element status, but this will only be displayed for one element at a time, on top of the periodic system. This editor has been developed to ease the input of the large amounts of element-related data that are typical for the description of element analytical problems. Entering these data via Nexpert's standard question routines during testing of early implementations made us realize that it is a problem that forms an essential part of the overall problem to be tackled.

```
Report on analysis request 1.00

XRF can help you solve the analytical problem.
The best it can do is listed below.

Using bead introduction, the following elements
can be analyzed with a precision of 3%rel:
      Na
      S
      V
      Fe
      Ni

When the sample is pressed with cellulose,
the following elements can be analyzed
with a precision of 10%rel:
      Sb
      La

End of report
```

Fig. 5. The report of the example session described in the text.

The output of the system, the report (see Fig. 5), is generated as a text file outside Nexpert, using Fortran, and displayed by a standard Nexpert function. The Nexpert development environment has no reporting facilities. When its inference on a knowledge base has come to an end this fact is reported and that is it. To inspect what the inference has produced one has to actively use the possibilities for inspecting the status of the inference. Other output of the system takes place in background. Every session will by default be recorded, resulting in a Nexpert journal file containing the answers to the questions that have been asked, a database in Nexpert database format with the data that has been entered via the special editor, and an update of the database in Nexpert database format of the recorded sessions. To embed the journaling into the knowledge base required some Fortran programming. All these files are readable, but not specifically meant to be read. The information in these files may be used as defaults in later sessions, which is of general use to reduce the amount of input effort, but which has been designed originally to

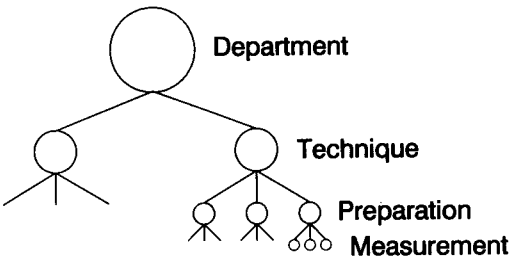

Fig. 6. The hierarchy of the laboratory organization to which the inference model corresponds that is used by the expert system.

allow simple evaluation of (minor) changes in the specification of a certain problem. Furthermore, after a period of expert-system use, the files will consitute a library of cases that may be used to evaluate the system.

Inference model

The expert system is built on the basis of a breadth-first search through a hierarchical model of the knowledge domain. The model can be seen as an organisational hierarchy of the laboratory (Fig. 6). Each level in the model corresponds to a level of detail in both the description of a problem and the solution to that problem; for a detailed solution one needs detailed information. The levels are chosen in such a way that the available information allows the selection of a best solution, disregarding levels with more detail. This best solution then has to prove that it still is the right choice on the next level of detail. When it fails, it is discarded and replaced by the next best solution. When it is partially successful the next best is selected in parallel in order to achieve success where the best has failed. When the inference is started on a low level of detail of problem and solution, it will come to an optimal solution by successively optimizing levels of increasing detail.

This model is a refinement of the model we proposed during project definition [1]. The latter model recognized different units of expertise: global heuristics, local heuristics, deep reasoning and planning. In the refined model we have introduced some other terms. Global heuristics may be identified with a combination of the department and the technique level of the new model, local heuristics with the sample preparation level and deep reasoning with the measurement level. For planning there is no such analogon. In the refined model, planning is made into an integral part of the overall procedure. This means that planning is no longer strictly a global task, but is also present in the subsystem. The removal of a separate planning is based on practical experience with implementation of the unrefined model. To rely on planning means that the inference is allowed to generate a large amount of data which the planning should condense into a single conclusion. Since the generated information is of a technical nature, i.e. related to the expert system and not directly to reality, planning also becomes a purely technical matter which turns out to be difficult to control.

In fact, the model covers the entire strategy determination task, not just the XRF knowledge domain. Developing the overall expert-system technique by using this model is no longer a matter of building individual technique systems. Each technique should be added directly to the existing system.

Implementation of the inference model

Part of the knowledge base is used for session control and does not represent domain knowledge. We will not consider that part here.

The inference model has been implemented on three levels: department, technique and XRF sample preparation. The XRF measurement process is treated differently. The three levels are implemented by using classes. The department and the technique classes each contain two objects, the XRF preparation class contains four. Only the preparation level is a full implementation of the model. The four methods contained in the preparation class cover the vast majority of the problems that might need to be solved. The department and the technique level are used to create a closed logical world and as the basis for future extensions. This will be described below.

At the department level, the inference selects the best candidate solution simply on the value of the sample aggregation state. The element-analysis lab does not handle gaseous samples and this

Name	fusible	stand	bead	pel	abs	noxrf
Ag	False	False		15	1	False
Al	True	True	500	30	6	False
Ar	False	False			1	True

Fig. 7. An extract from the XRF database in Nexpert's database format. fusible = goes into bead quantitatively; stand = bead technique developed; bead = optimum detection limit in standard bead; pel = as bead for cellulose pellet; abs = absorption factor when measured in He; noxrf = XRF principally impossible.

selection works out as a kind of input control. For gaseous samples, the user is referred to the gas-analysis lab at Koninklijke/Shell-Laboratorium, Amsterdam. The two objects that are present in the department class are therefore the element-analysis lab and the gas-analysis lab.

On the technique level, ICP-OES is used as the complement to XRF in much the same way. When the system would be extended with ICP knowledge, the two techniques would have to compete seriously on this level. In the absence of such knowledge XRF takes what he wants and gives ICP what he does not like. The selection of XRF is based on aggregation state, handling properties, physical form, the elements to be analyzed and the overall precision demand for the analysis. If the sample is an aqueous solution, the inference immediately concludes that ICP should be used; if it is a non-aqueous liquid, the inference gives the user the opportunity to demand that XRF is selected. When it turns out on further levels that XRF cannot solve the problem or that it can only solve part of it, ICP is not

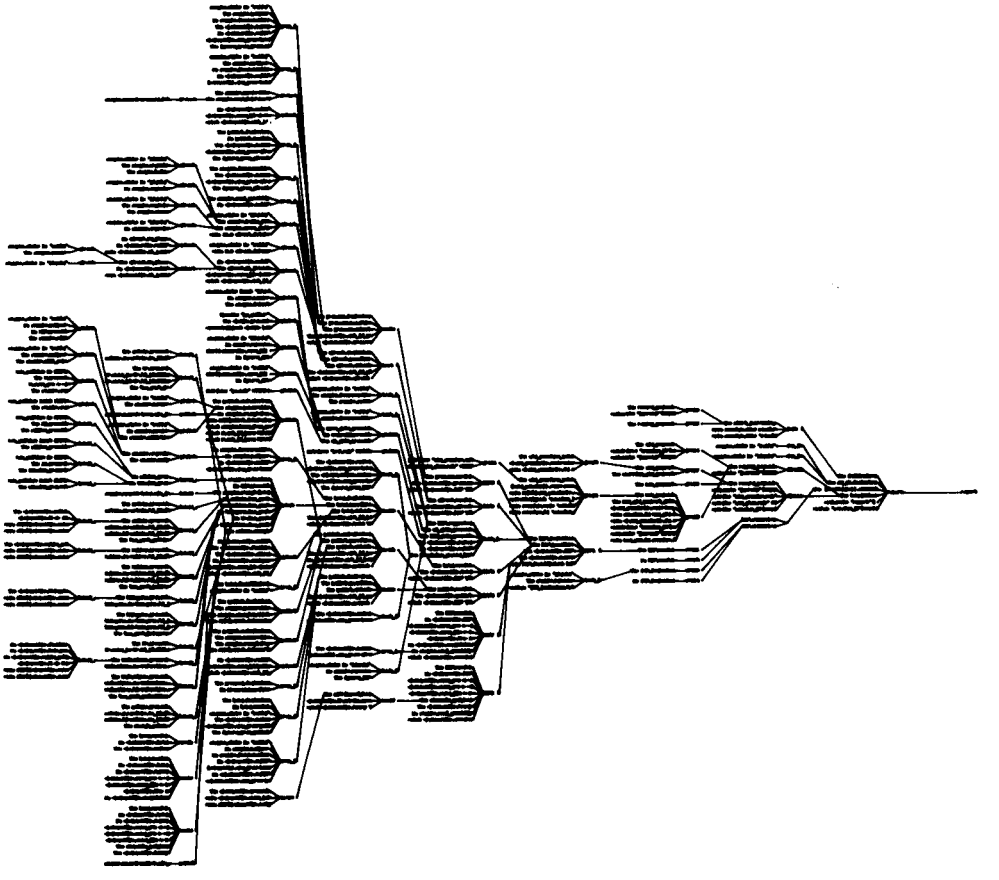

Fig. 8. The rule net generated by Nexpert with a "full left extend" on the ultimate goal of the inference process, i.e. "report". This net does not contain all rules. The rules are not readable, because the size of the figure is reduced to give the overview. In practice, only a small, readable part of the net will be displayed on the screen.

selected as the next best option, because at the moment this is useless since there is no knowledge available on ICP. Instead, XRF's incapacity is mentioned in the end report to the user.

At the XRF preparation level, there is true competition between the candidate solutions, i.e. there is knowledge available on all objects in the preparation class. Preparations may also be selected in parallel. Together, the four sample preparations present in the knowledge base cover the vast majority of the problems that may need to be tackled by XRF. The criteria in their evaluation are: the desired precision of analysis, physical form, amount, composition, chemical properties and handling properties. The desired precision gets the highest priority in the evaluation.

The next level of inference is the lowest in the knowledge base, the measurement level. The information that is decisive on this level is the expected concentration of the elements present. Ideally, this information would be used to create a measurement configuration that is optimal with respect to the detection limit. For reasons explained in the discussion this optimization is not implemented in the current expert system. Instead, for each element to be analyzed an estimate of the optimum detection limit is retrieved from an external database (see Fig. 7 for an impression of this database). The estimates depend on the sample preparation. For two preparations the values are fixed and taken directly from the database. For the other two they are calculated on the basis of database values. The calculations take into account the amount of sample introduced and possible absorption caused by measuring in a helium atmosphere instead of in vacuo. The reasoning on the measurement level succeeds when the estimated concentrations of at least some of the elements to be analyzed are found to be higher than their respective detection limits.

The inference model is implemented basically using a backwards-chaining rule network. An impression of this network is given in Fig. 8. In addition to the rules, the knowledge base makes extensive use of Nexpert's so-called metaslots to trace the values of variables during inference. This cannot be visualized in the rule network. No use is made of forwards chaining. In our experience forward chaining does not lead to a converging process, since it lacks the goal orientation of backward chaining. The process of selection and rejection of a solution on a certain inference level is programmed by using two properties for the solutions, one for the initial selection and one for the confirmation or rejection. Nexpert's "reset hypothesis" option, which is intended for implementation of non-monotonous reasoning, did not satisfy for this purpose.

Dealing with diverse amounts of detail in the input

The amount of detail in the specification of an analytical problem may differ considerably. A concentration estimate may in practice be given as a numeric value, e.g. "4.5 % (m/m)", but also as an indication, e.g. "several mass per cents", or "bulk". These representations may be present together in one analytical problem description. A normal numerical representation does not satisfy here and neither does an order of magnitude indication. We have chosen for an intermediate representation: orders of magnitude for rough concentration estimates and a subdivision of each order for the specification of detailed concentration preknowledge. Each concentration estimate thus represented is translated internally into a value expressed in $\mu g\ g^{-1}$, the smallest unit used in XRF practice in the lab of our observations. The specification detail is translated into a window around this value. This window functions only in the background and is not something the user has to work with.

All numerical considerations in the knowledge base using estimated element concentrations have been formulated in accordance with this approach. Some considerations that were present in the analysis of the knowledge domain could not be represented in the knowledge base in this way, e.g. non-standard dilution factors in sample preparation are not accounted for, since the dilution effect is smaller than can be represented by the data.

A special evaluator of numerical tests has been constructed. Each normal evaluation of the form

if value > limit then o.k.

Slot name	Purpose
element.fusible	True if the element will remain in the sample quantitatively during the fusion process in which the bead is formed.
XRF.indicated	True if XRF promises to give the best possibilities for solving the analytical problem

Fig. 9. An extract from the knowledge base documentation. The purpose list.

is replaced by a set of evaluations

if low bound > limit then o.k.
if high bound < limit then not o.k.
if low bound < limit,
and high bound > limit then consult user for o.k.

in which low and high bounds refer to the precision window that has been set around each value that is related to element concentration estimates. A similar set of evaluations exists for the other test operators. These sets of evaluations require calculations to be performed once with the low bounds of all values and once with the high bounds. The principle is only useful for simple calculations like additions, multiplications and divisions. In complex calculations, such as the calculation of matrix effects, the inclusion of low bounds only would not necessarily result in the low bound to the result. For this and other reasons, which will be discussed later, the current knowledge base does not contain such complex calculations.

Documentation

We have provided the system with a manual and technical documentation. The manual provides some Nexpert essentials and a description of the purpose and the philosophy of the added features. Writing the technical documentation for the Fortran routines was straightforward, but for the knowledge base it turned out to be more complicated. The documentation we have written consists of three pieces, an extensively commented knowledge-base source listing, a list of the meaning of each knowledge-base slot given a certain value (Fig. 9) and a list of the structural context of each slot (Fig. 10). The explanation of the terminology used in the latter list gives insight into the construction of the knowledge base and is therefore listed in full in the appendix to this article.

Program portability

The expert system consists of a knowledge base running on an extended version of the Nexpert Object development environment under UIS on a VAXstation with high-resolution colour graphics, i.e. the development version is the only existing version. The system may be turned into a runtime by linking the extensions to the Nexpert Object graphical runtime. However, the portability will remain limited, since the extensions are written in VAX Fortran, using constructs that are not standard Fortran77 and make extensive use of the possibilities of the UIS graphical routines and of the graphical capabilities of the workstation screen.

Slot name	Source	Strategy	Triggered by	Use
Purpose				
element.fusible	db	side	XRF.indicated	exp
XRF.indicated	inf	hypo		exp

Fig. 10. An extract from the knowledge base documentation. The structural context list. An explanation of the terms used can be found in the text.

DISCUSSION

Capabilities and limitations of the expert system

The expert system makes knowledge on preparation and measurement level available on the computer and allows it to be put to use for all of the laboratory staff, relieving the XRF expert. We expect that the inference model will work for other techniques as well and that the implementation of the model will be similar for each technique. Therefore we assume that the extension of the expert system in breadth by adding other techniques may be accomplished rather quickly. The knowledge on the other techniques does not need to be deeper than that on XRF in the current system, to create something that may be of use for the entire lab. The system as it is does not give advice on the experimental setup and it does not contain knowledge on element interactions in the measurement process. This will be discussed in detail in the next section.

Problems with deep reasoning

In practice, element interactions in the measurement process determine the experimental setup ultimately used in analysis. These interactions, as well as the setup, have been left out of the expert system, because the available expertise was found to be unsuitable, and substitution of this expertise by a theoretical approach proved to be problematic. There is a common factor which is the fundamental problem of deep reasoning for a priori purposes: the uncertainty of the input. To elucidate this the nature of the expertise and the theoretical approach will be described in more detail.

The nature of the expertise. The expert is aware of many element interactions and their consequences upon analyzability and experimental setup. This information may be quantitative, but in that case it will usually be highly specific, being based on problems that actually have been solved, or it may be qualitative, being based on theory and generalizations of practical experience. When the expert system has to be able to do more than recognizing incoming problems as being identical to old ones, it has to be based on the general information from the expert. This information can typically be described as heuristic rules of the form

if element combination **then** problem

The element combinations found were always bivariate, e.g. Cr and V, or Pb and As. Generalizations of the type "a light element in a heavy matrix" are often made. The element combinations can usually be given some detail as in "X next to Y, where X is low compared to Y". The description of the resulting problem is e.g. "I can hardly see element X", "I will not achieve my usual detection limit for element X", or "The detection limit for element X will no longer be 50 $\mu g\ g^{-1}$, but rather several hundreds or maybe 1000". An important aspect of these problems is that they are not necessarily insuperable. In fact, in most cases the expert will rely upon his skills in exploiting the possibilities of his technique to overcome potential problems and will simply try to perform the analysis. The function of the heuristics is rather to create an alertness for practical problems than to prevent from turning to practice altogether. They may be used to come to a first guess of the measurement conditions, but not to provide reliable estimates of the ultimately attainable results. We have found these heuristics to be too fragmentary and too vague to be used in the expert system. They lack conclusiveness in the a priori evaluation of XRF possibilities.

There are several reasons why the expert does not a priori evaluate potential problems with the amount of detail that is required for the expert system. First of all, the element interactions are too complex to expect anyone to oversee them all. The expert too has to rely on simplifications, but a simplified description can still be correct for its own purposes. It is the purpose of the knowledge in which the expert differs from the expert system. The system cannot perform experimental work and therefore has to come as far as possible on the basis of a priori information. The expert can rely on experiments for additional information and is therefore free to find an optimum between exhaustive a priori evaluation and experimentation. The location of the optimum is in first instance determined by the available a priori

information, but will always be a subjective matter. Our XRF expert, for instance, is a man of practice, for whom the optimum tends to be on the practical side. The nature of the technique is an important factor in this; the easier the experiment, the more likely one is to turn to it.

Alternatives for the available expertise. Our model for the expertise on the measurement level, the a priori optimization of the experimental setup, proved to be insufficient, in essence because the expert is not tied to a priori information like the expert system is. We assume that the model may still be used to emulate this expertise. There are two options for performing the required optimization. One of these is to rely on the expert's knowledge on practical optimization, the other is to use a formal optimization approach. We prefer the formal approach, because there is evidence that it performs better than a human expert in multivariate domains [15]. A formal approach can in principle be complete in its considerations of element interactions, whereas the approach founded on expertise would require some simplification of the optimization problem.

Both approaches need a routine that simulates XRF measurement data on the basis of a tentative measurement configuration and the expected sample composition. For the knowledge-based approach this simulation has to result in spectra, i.e. the visual representation of the data the expert is used to work with. Part of the expertise will be in the interpretation of these spectra with respect to the optimization, e.g. in the criterion needed to evaluate the test "Is the line free?" and in estimating detection limits. The formal approach requires that the simulation yields detection limits. In order to achieve this, the available data processing methods have to be incorporated in the simulation routine. Maybe routines in existing data-processing software can be isolated and used.

Note that the concept of precision has not been mentioned in this context. Precision may be included in the optimization, but in the current knowledge base the concept is present at the level of sample preparations, because in practice standard precision values are used for the sample preparations. When an optimization routine is to be a deepening of the current system with respect to detectability only, this situation can persist, otherwise the inference on the sample preparation level has to be reconsidered. A similar argument can be used for the consideration of deadline and budget.

The big difference between simulations and real measurements is of course that simulations will not provide any missing information, they merely transform the information that is put in. For a fundamental approach, based on a model of the physics that underlie XRF, the input should be numeric. In practice, however, the available concentration information is approximate and the optimization has to be able to translate this information for the simulation. The expert is used to optimizing on the basis of real data, not on approximate simulated data. When the expert system is to be based on his approach it will need additional knowledge, consisting of experience with the data simulation.

The formal approach requires a measure of uncertainty, which might be attained by simulating the data for different combinations of concentration estimates. For each element the estimates used in this approach could be the centre and the bounds of the window within which the concentration is expected. The problem of this approach is the increase of the amount of possible combinations as P^N, where P is the number of levels considered, and N the number of elements present. Therefore a large number of calculations will be required for every point of the response surface on which the optimization takes place. Even if this is not prohibitive, one has to decide how to use the resulting uncertainty in the optimization. When a response surface has an optimum for a certain experimental setup, this may be obscured by the uncertainty. Furthermore, the uncertainty may have a minimum for some setup, but this does not necessarily coincide with a response optimum. To find a prudent path through the response surface in the presence of uncertainty would be a research topic in itself.

We have not really embarked on solving the problems outlined above, because that would be beyond the original scope of our project, which

was to implement existing knowledge on XRF, not to extend it.

Implementation

We are rather disappointed in the implementation advantage that is brought about by the use of a special expert-system development tool, viz. Nexpert. By using an ordinary general-purpose procedural language we might have obtained the same results with less trouble. A large part of the trouble has been in the separation of knowledge and inference engine, as is described in the exposition below. A critical discussion of this and other aspects of the difference between classical and expert-system programming which corresponds to our experiences can be found in Ref. 16.

Languages such as Pascal, Fortran and C are linearly structured; the program statements are executed in the order in which they are written down. The linear structure is only affected by jumps, e.g. in loops or calls. These jumps constitute a kind of metalevel in the program. They direct the execution from one point in the linear structure to another, or from one linear structure to another. For expert systems the situation is quite different. The knowledge base can be considered a program written in the language stated by the inference engine. The structure of this program is no longer linear. The order of execution of the program statements is controlled by the inference engine. For this purpose the inference engine maintains an agenda, a list of things that have to be done ordered by priority. The way in which this agenda is followed reminds of the execution of a classical program. One might say that a classical program is its own agenda, whereas a knowledge base only implies an agenda.

The realization of the agenda is controlled by the strategy of the inference engine. In simple expert system development tools (shells) the strategy is fixed and simple, but in Nexpert it can be controlled in many ways both statically and dynamically, i.e. both before and during a knowledge base consultation. The static control is located in the strategy section of a knowledge base; the dynamic control may be present throughout the production section. Unfortunately, it is not possible in Nexpert to make the agenda visible. This means that the procedural aspects of a knowledge base can only be observed directly by running the expert system, which makes them difficult to control.

In our hands all Nexpert's cleverly contrived strategy options could not be put to efficient use. The workings of simple test knowledge bases containing some advanced feature could mostly be elicited with some effort, but the effects of these features on larger knowledge bases often became incomprehensible. In general, Nexpert's advanced features, e.g. "reset hypothesis", had the inclination to do something different from what we needed. In our experience it takes less time to program around this by using the most basic means, i.e. primarily ordinary backwards chaining, then to try and change the knowledge base in a such a way that the feature may be used. As a result we have used only very little of Nexpert's inference functions, viz. backwards chaining and inheritance in conjunction with metaslots.

For practical purposes the rules in a backwards-chaining structure can be viewed as subroutines that are called by the name of their conclusions. The metaslots do not have a direct analogon like that, but are used similarly. In this view an important aspect of these routines is that they share all information. Because of this it is difficult to create a closed logical world, since every variable that is introduced for local purposes may create an open end somewhere else in the knowledge base. Keeping the world of an expert system closed in a sensible way has been recognized as a crucial factor in its success [17].

In our experience, pieces of knowledge cannot be coded into an expert system in some neutral form that allows flexible use. The terminology used in a piece of code should at least agree with the rest of the knowledge base, but even then the pieces cannot be put to work when they are not formulated within a strategy to arrive at some goal. Therefore it will not be simple to update or otherwise modify a knowledge base for someone who does not know the internal structure and terminology of the system, not even for the expert, though to change small facts such as detec-

tion limits will be easy. More in general, the gain in transparency of the expert system that results from using the special expert-system techniques and the concomitant gain in ease of updating is difficult to be established objectively.

Knowledge acquisition

The most difficult aspect of knowledge acquisition turned out to be explicitness. We found that we could easily absorb the knowledge we encountered without having to make it explicit. By the natural process of learning, things started to fall into position in a mental model, creating an understanding of what had been learnt. The transformation of the mental model into an external model, in other words making the knowledge explicit, is not a process that can be formalized into a recipe which guarantees results. It is typically a task to be performed by an analytical or scientific mind. The idea of making a list of concepts, extending this from facts to relations and using this as the basis for creating a hierarchical model could only serve as a tool and did not by itself lead to results.

Conclusion

As part of a project for the development of an expert system for the determination of the analytical strategy in a laboratory for elemental analysis, an expert system has been developed that evaluates the possibilities of XRF for a given analytical problem.

An intuitive approach was followed for the knowledge acquisition, consisting of prototyping, based on prior analysis. The knowledge has been elicited primarily by interviewing an XRF expert. The approach was found to be sufficient. The analysis resulted in a hierarchical model of the knowledge in combination with a breadth-first strategy, which is a refinement of the model described in Part 1 [1].

The refined model has been implemented by using the tool Nexpert Object, using only the basic functions of the tool, such as backwards-chaining production rules. More complex functions were found to complicate rather than to facilitate the programming.

The implementation is not strictly a subsystem, but also contains the model structure of the overall strategy-determination task. The current system is site specific with regard to the actual knowledge content, but the structure has a wider applicability. Development of additional technique subsystems will be facilitated by using the same knowledge model and by complying with the existing structure. Extension and updating of the system requires insight in the expert system program.

The expert system does not contain deep reasoning, i.e. it does not consider matrix effects in the measurement, and it does not give information on the optimal experimental setup. The available expertise, being based on practice, where a priori information may be supplemented with experimental data, was found to be unsuitable for the purpose of the expert system, which is to rely on a priori information only.

We gratefully acknowledge the financial support by the Koninklijke/ Shell-Laboratorium, Amsterdam (KSLA) (Shell Research B.V.), Amsterdam, Netherlands, for the work described in this article. We thank Jan Vogel (KSLA), the XRF specialist in our investigations, for his cooperation, and Watze Mandema (KSLA) and Hans Boelens (University of Amsterdam) for valuable discussion.

APPENDIX

Explanation of terms used in the documentation of the XRF expert system

The possible sources from which the Nexpert inference engine can draw the value of the slot are:

user	the person that is consulting the expert system;
inf	inference, i.e. induction from other information;
def	default, i.e. the internal database of the knowledge base;
.../def	initial value;
calc	calculation;
db	external database.

The different strategies that are being followed by the expert system written for the Nexpert environment to tap the above-mentioned information sources are:

- exec — by execution of an external routine;
- hypo — by making it the hypothesis of a rule, i.e. part of an inference chain;
- inh — objects in a class are put into a subclass, taking all their properties and the corresponding values with them; this move is triggered by the hypothesis of the rule in which it takes place; this hypothesis is stated in the next column;
- local — a slot that is used only within a construct within a rule;
- meta — metaslot;
- side — as a side effect of a rule, whose hypothesis is used as a trigger; this hypo is stated in the next column.

The 'use' column indicates the reason why a slot is present in the Nexpert knowledge base. When the field is empty the slot is used autonomously.

- trigger — when a slot is never used in the knowledge base in an other function than as the trigger for other slots;
- combi — as trigger, but also used autonomously.

The 'purpose' column specifies what is implemented with the slots.

- prog — programming aspects that do not belong to the field of expertise of the system;
- exp — part of the expertise in the domain of the system;
- exp! — approximation of part of the expertise;
- imp — no real part of the expertise, but needed for implementing it.

REFERENCES

1 B. van den Bogaert, J.B.W. Morsink and H.C. Smit, Anal. Chim. Acta, 270 (1992) 107.
2 B.G. Buchanan et al., in F. Hayes-Roth, D. Waterman and D. Lenat (Eds.), Building Expert Systems, Addison-Wesley, Reading, MA, 1983.
3 J. Breuker and B. Wielinga, in M. van Someren and G. Schreiber (Eds.), Proceedings NAIC88 Amsterdam, University of Amsterdam, Amsterdam, 1988, p. 24.
4 G. Schreiber, B. Bredeweg, M. Davoodi and B. Wielinga, Towards a design methodology for KBS, Report of Esprit project P1098: knowledge acquisition in formal domains, Dep. of Social Science Informatics, University of Amsterdam, Amsterdam, 1987.
5 J. Breuker, B. Wielinga, M. van Someren, R. de Hoog, G. Schreiber, P. de Greef, B. Bredeweg, J. Wielemaker, J.P. Billault, M. Davoodi and S. Hayward, Model-driven knowledge acquisition: interpretation models, Report of Esprit project P1098: knowledge acquisition in formal domains, Dep. of Social Science Informatics, University of Amsterdam, Amsterdam, 1987.
6 J. Thiemann, Kennissystemen, 3(3) (1989) 3.
7 N. Shadbolt, Expert Syst. User, 4(10) (1988) 22.
8 T. Rajan, Expert Syst. User, 5(5) (1989) 18.
9 M. Davies and S. Hakiel, Expert Syst., 5(1) (1988) 42.
10 L.S. Birks, X-Ray Spectrochemical Analysis, Wiley-Interscience, New York, 2nd ed., 1969.
11 R. Jenkins and J.L. De Vries, Quantitative XRF, MacMillan, London, 2nd ed., 1970.
12 E.P. Bertin, Introduction to X-ray Spectrometric Analysis, Plenum, New York, 1978.
13 A.A. Markowicz and R.E. Van Grieken, Anal. Chem., 60 (1988) 28R.
14 Expert Syst. User, 4(2) (1988) 12.
15 J.W. Elling, L.J. de Koning, F.A. Pinkse, N.M.M. Nibbering and H.C. Smit, Anal. Chem. 61 (1989) 330.
16 Expert Syst. User, 6(3) (1990) 16.
17 M.Z. Bell, J. Oper. Res. Soc., 36 (1985) 613.

Analytica Chimica Acta, 270 (1992) 131–136
Elsevier Science Publishers B.V., Amsterdam

Biosensor for the determination of L-lysine

E. Vrbová and M. Marek

Department of Biochemistry and Microbiology, Institute of Chemical Technology, 166 28 Prague (Czechoslovakia)

E. Ralys

Fermentas, Association for Science and Production, Vilnius (Lithuania)

(Received 22nd November 1991; revised manuscript received 20th July 1992)

Abstract

A biosensor for the determination of L-lysine was prepared, consisting of a Clark-type oxygen sensor and a convenient support with an immobilized enzyme system fixed to its surface. L-Lysine-α-oxidase was co-immobilized with catalase via the Ugi reaction using glutaraldehyde and cyclohexyl isocyanide either on a partially hydrolysed nylon net or on the preactivated or native collagen membrane. The consumption of oxygen was detected by the oxygen sensor. Hydrogen peroxide was decomposed by catalase to increase the sample throughout. The enzyme electrode prepared was tested from the viewpoint of its substrate specificity, pH and temperature effect on the enzyme activity and characterized by the specific and relative activity of the immobilized enzyme system. The linear range of biosensor response to the substrate was 6.7×10^{-6}–6.7×10^{-4} M; the apparent Michaelis constant (1.3 mM) and the stability of biosensor were also determined. The enzyme electrode was used for the determination of L-lysine in wheat extracts.

Keywords: Biosensors; Enzymatic methods; Enzyme electrodes; Lysine; Wheat

The accurate and rapid determination of L-lysine is of great interest owing to its importance in human alimentation. In addition to photometric methods which employ the enzyme lysine aminotransferase [1–7], L-lysine decarboxylase [8] and L-lysine-α-oxidase [9,10], numerous biosensors have been developed for the specific determination of L-lysine. Potentiometric detection was used when either lysine decarboxylase [11–15] or microorganisms containing it [16] were immobilized on a CO_2 sensor. Amperometric measurement of the oxygen uptake with the enzyme electrode coupled with lysine oxidase has been described [15,17–20]. L-Lysine-α-oxidase catalyses the oxidation of L-lysine [21] to α-keto-ε-aminocaproate, ammonia and hydrogen peroxide. Cyclization of α-keto-ε-aminocaproate to the intramolecular dehydrated form Δ^1-piperidine-2-carboxylate proceeds spontaneously. In this work, the preparation of an enzyme electrode for L-lysine based on L-lysine-α-oxidase and catalase co-immobilized covalently either on a nylon net [22] or on a collagen membrane [23] is described.

Correspondence to: E. Vrbová, Department of Biochemistry and Microbiology, Institute of Chemical Technology, Technicka 5, 166 28 Prague (Czechoslovakia).

EXPERIMENTAL

Materials

Lysine oxidase (LysOD, L-lysine-α-oxidase, E.C. 1.4.3.14, from *Trichoderma* sp., 22 IU mg^{-1} protein) (Fermentas, Lithuania) was used undiluted. Catalase (Cat) (H_2O_2:H_2O_2 oxidoreductase, E.C. 1.11.1.6, from beef liver, 80 640 IU mg^{-1} of suspension) (Reanal, Hungary) was used

in the form of an undiluted crystalline suspension.

Glutaraldehyde (Koch Light, Colnbrook, UK) was applied as a 5.0% aqueous solution, cyclohexyl isocyanide (CHIC) (Fluka, Buchs, Switzerland) was used in the form of the undiluted liquid. Other chemicals were of analytical-reagent grade from Lachema (Brno).

The nylon net used (UHELON 63; Rempo, Prague) has a mesh of 3969 cm^{-2} with a thickness of 100 μm. The collagen membrane used (Cutizin, Jilemnice, Czechoslovakia) was 100 μm thick.

Co-immobilization of lysine oxidase and catalase on a nylon net

The nylon net was partially hydrolysed with 25% hydrochloric acid for 1 s, then thoroughly washed with distilled water and dried in air. A 10-μl volume of lysine oxidase in solution (500 IU ml^{-1} enzyme) was applied to the hydrolysed surface, then 2.5 μl of catalase suspension, 2.5 μl of glutaraldehyde solution and 1 μl of CHIC were added [22] and incubated for 2–7 days at 4°C. The nylon net with the bound enzyme system was thoroughly washed with 0.1 M potassium phosphate buffer (pH 7.5), which was also used for its storage at 4°C.

Co-immobilization of lysine oxidase and catalase on a collagen membrane

The collagen membrane, either native or activated by 24-h treatment with 6 M urea [23] was wetted with 0.1 M potassium phosphate buffer (pH 7.5). A 10-μl volume of lysine oxidase, 2.5 μl of catalase suspension, 2.5 μl of glutaraldehyde solution and 1 μl of CHIC were applied to the surface. For comparison purposes lysine oxidase and catalase were also co-immobilized in the absence of CHIC. Further processing and storage were as described above.

Preparation of enzyme electrodes and determination of L-lysine

The carrier with co-immobilized enzymes was fixed on the tip of a Clark-type oxygen sensor (0.8 mm cathode) (Chemoprojekt, Czechoslovakia) and inserted into a thermostated (30°C), stirred reaction vessel (1.5 ml). A 1.4-ml volume of 0.1 M potassium buffer (pH 7.5), saturated with atmospheric oxygen, was pipetted into the vessel and the reaction was triggered by the addition of 100 μl of L-lysine in suitable concentrations, or the other amino acids for the determination of the substrate specificity. The enzyme electrode response was measured with a nanoammeter having a stabilized source of direct polarized voltage and a signal derivative device (Chemoprojekt). Both the single signal and its derivatives were monitored by means of a TZ 4200 chart recorder (Laboratory Instruments, Prague).

Characterization of the prepared electrode

The dependence of the activity of co-immobilized enzymes on the pH of the reaction medium was determined in the same way as the determination of L-lysine, but the buffer pH ranged from 4.5 to 10 (limiting values of pH were adjusted by means of phosphoric acid or potassium hydroxide) and 100 μl of 0.1 M L-lysine solution were used.

The effect of temperature on the activity of the above enzyme systems was measured in an analogous way in an excess of substrate (100 μl of 0.1 M L-lysine) at pH 7.5 in the temperature range 23–50°C. After each pH or temperature change the system was allowed to stabilize for 10 min.

Preparation of wheat extracts from young plants

A 2-g amount of fresh material was washed thoroughly with distilled water and inactivated with steam for 5 min, homogenized and extracted with 80% ethanol. The extract was filtered and then evaporated at 50°C. The residue was dissolved in a 2.5% solution of trichloroacetic acid (3.0 ml) and the amounts of free amino acids were determined with an amino acid analyser (Mikrotechna, Prague) [24]. For the L-lysine determination by means of the biosensor, the evaporation residue was dissolved in distilled water (2.0 ml).

RESULTS AND DISCUSSION

Biosensors for the determination of L-lysine were prepared according to methods described

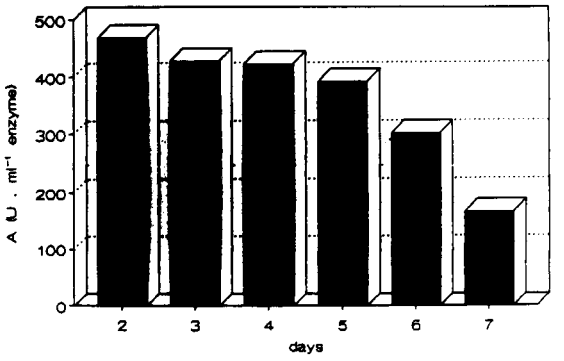

Fig. 1. Dependence of activity of lysine oxidase–catalase on the immobilization time. A = Specific activity of lysine oxidase co-immobilized on nylon net.

previously [22,23,25]. Lysine oxidase and catalase were covalently co-immobilized either on a nylon net activated by partial hydrolysis with hydrochloric acid or on a native and activated collagen membrane. The effect of CHIC and the duration of immobilization on the enzyme activity is shown in Figs. 1 and 2. The maximum activity of lysine oxidase co-immobilized on the net was reached after 2 days (468 IU ml^{-1} enzyme); in contrast, the activity on the protein carrier after the same period was very low in three cases (18 IU ml^{-1} on average) and the maximum activity was reached after 4 days (320 IU ml^{-1} on average). No significant differences between a modified and a native

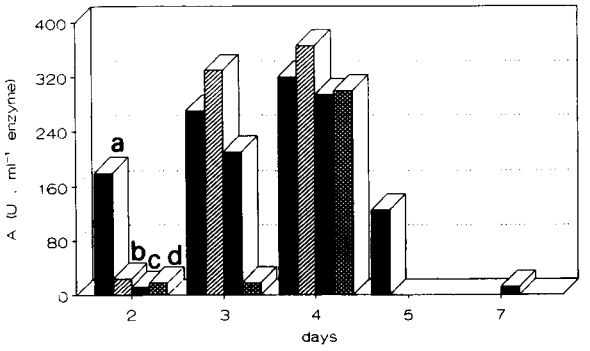

Fig. 2. Effect of the carrier, CHIC and immobilization time on activity of lysine oxidase–catalase co-immobilized on collagen membrane. A = Specific activity of lysine oxidase; a = activated collagen membrane with CHIC; b = activated collagen membrane without CHIC; c = native collagen membrane with CHIC; d = native collagen membrane without CHIC.

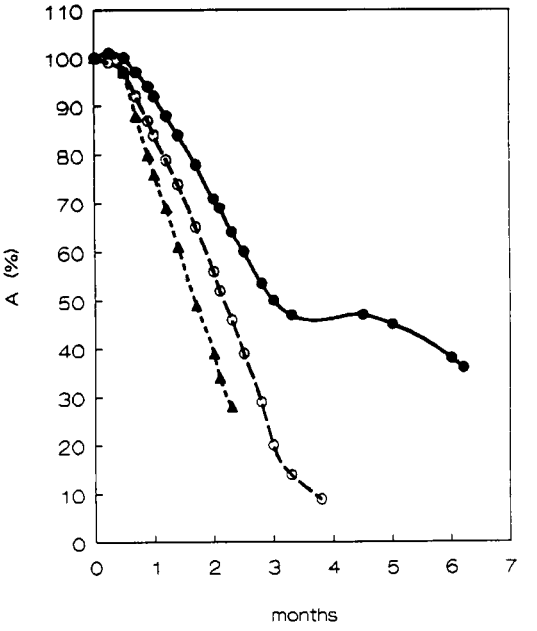

Fig. 3. Stability of biosensor. A = Relative activity. Lysine oxidase–catalase co-immobilized on (●) nylon net with CHIC; (○) collagen membrane with CHIC; (▲) collagen membrane without CHIC.

(original) collagen membrane were found. The presence of CHIC had, in agreement with previous work [22], a mild stabilizing effect (Fig. 3).

The biosensors prepared were characterized by the effect of pH on the activity of enzymes (Fig. 4). The optimum pH was 7.5; 90–100% of the enzyme activity was retained over a relatively wide range of pH (6.5–9.6). The shapes of the pH curves were not influenced by the type of carrier applied and were shifted toward the acid range compared with the pH optimum of the free enzyme (8.0–9.0).

Measurements of the effect of temperature on the enzyme electrode signal showed the same maximum value of activity for both enzyme conjugates (at 45°C, Fig. 5).

From the calibration graphs (rate of oxygen consumption in the reaction mixture), the linear range of the biosensor with respect to the substrate concentration (L-lysine) was found in the extend over two orders of magnitude (Fig. 6) with a lower limit of determination of 6.7×10^{-6} M in the reaction vessel, i.e., 1×10^{-4} M in the in-

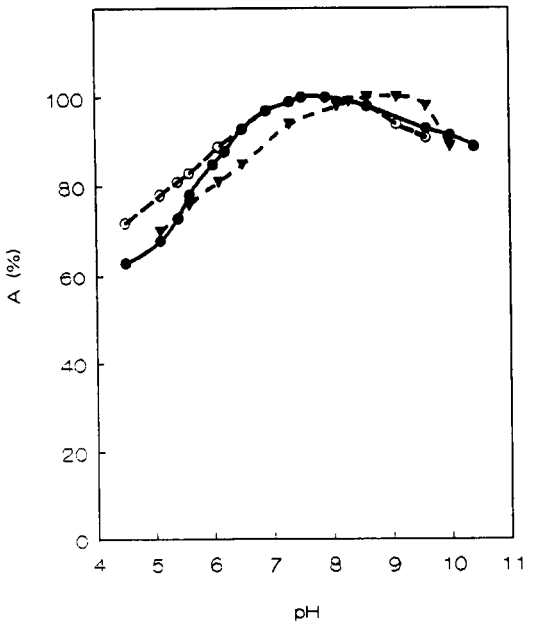

Fig. 4. Effect of pH on enzyme activity. A = Relative activity; ▼ = free lysine oxidase; ● = lysine oxidase–catalase on nylon net; ○ = lysine oxidase–catalase on collagen membrane.

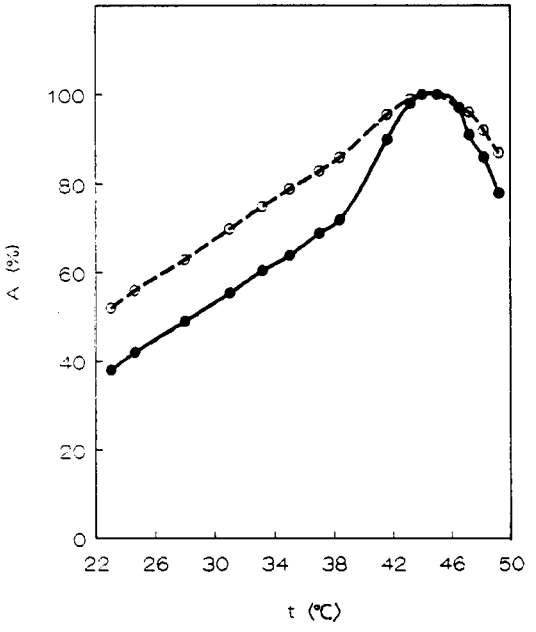

Fig. 5. Effect of temperature on biosensor response. A = relative activity; ● = lysine oxidase–catalase on nylon net; ○ = lysine oxidase–catalase on collagen membrane.

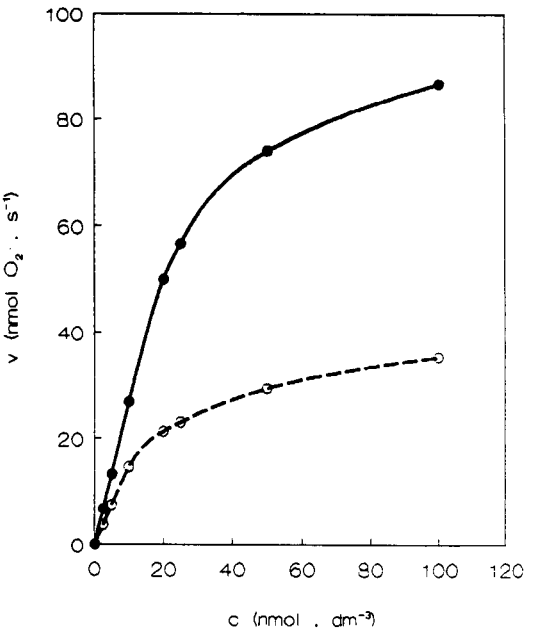

Fig. 6. Calibration graphs. v = Rate of oxygen depletion; c = concentration of L-lysine in sample; ● = lysine oxidase–catalase on nylon net; ○ = lysine oxidase–catalase on collagen membrane.

jected sample, and an upper limit of 6.7×10^{-4} M L-lysine in the vessel, i.e., 1×10^{-2} M in the sample. The values of the apparent Michaelis constant, $K_{M(app)}$, determined using the Gauss–Newton method of non-linear regression from the calibration graphs, were 1.33 and 1.30 mM for enzymes immobilized on the nylon net and collagen membrane, respectively. These values are comparable to the K_M value for the free enzyme (3.0 mM) [26]. A suprisingly low K_M was reported by Kusakabe et al. [21], $K_M = 4.0 \times 10^{-2}$ mM.

The substrate specificity was determined. All common L-amino acids and more unsual ones (citrulin and ornithine) were tested as possible substrates. In some instances, when the optically active L-form was not available, the racemic mixtures of an suitable amino acid were tested. The results are given in Table 1.

Responses were observed only to L- and DL-lysine and DL-ornithine, L-arginine and L-cysteine. For these substances their relative rates of oxidation were measured and compared with values

TABLE 1

Substrate specificity of lysine oxidase

Substrate	Relative rate of oxidation		$K_{M(app)}$ (mM)
	Co-immobilized LysOD/Cat	Free LysOD	
L-Lysine	100	100	1.33
DL-Lysine	90	89.4	2.11
DL-Ornithine	16	17	1.82
L-Arginine	11.5	9.2	1.52
L-Cysteine	11.5	9.2	5.19

determined with the free enzyme. Apparent Michaelis constants were calculated from the calibration graphs as mentioned above (Fig. 7).

The narrow substrate specificity observed permitted the determination of L-lysine in wheat extracts from young plants. Reproducibility was tested by repeated 100-μl injections of wheat extract samples in the reaction vessel; mean values for sets of ten injections are given in Table 2. The maximum standard deviations were found to be 1.2 μg g^{-1} of fresh material and the relative

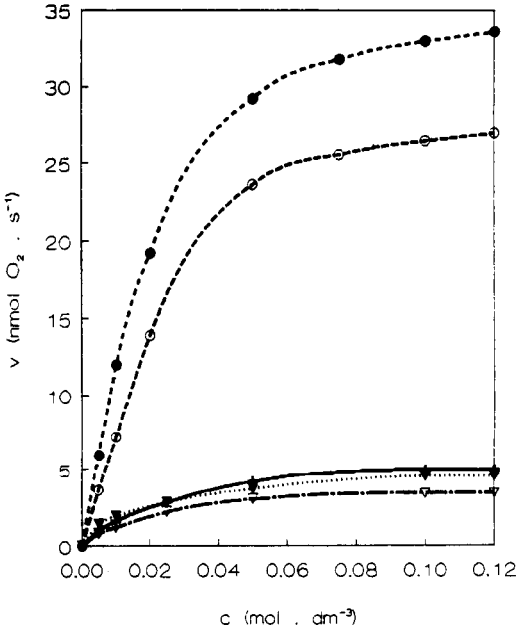

Fig. 7. Substrate specificity of co-immobilized lysine oxidase–catalase. v = Rate of oxygen depletion; c = concentration of substrate in sample; ● = L-lysine; ○ = DL-lysine; + = DL-ornithine; ▼ = L-cysteine; ▽ = L-arginine.

TABLE 2

Determination of free L-lysine in wheat extracts of young plants; comparison of the L-lysine biosensor and the amino acid analyser [a]

Sample No.	L-Lysine (μg g^{-1} fresh material)	
	Biosensor	Amino acid analyser
1	40.0	41.1
2	84.6	82.5
3	63.7	64.2
4	63.6	64.4

[a] Equation of the linear regression was found to be $y = 1.075x - 4.497$ ($r = 0.9997$, $n = 4$), where y and x are the concentrations determined using the biosensor and the amino acid analyser, respectively.

standard deviations were less than 1.6% for all samples. The results were in agreement with the values obtained with the amino acid analyser (Table 2) and with literature data [27,28].

Investigating the stability of enzyme electrodes (Fig. 3), 20 assays daily on average were carried out within 1 month. After this time period the biosensors were tested every week (20 assays as a minimum) and after 3 months they were used and tested only occasionally. Within 6 months about 800 analyses were performed and the activities had decreased to 50% (nylon net) and 20% (collagen membrane) of their initial values.

Biosensors prepared by co-immobilization of lysine oxidase and catalase on the collagen membrane in the absence of CHIC showed a decrease in enzyme activity during 3 months. If the enzyme conjugates immediately after the immobilization procedure were stored at 4°C in 0.1 M potassium phosphate buffer (pH 7.5) and were not used for determination, they retained a high enzyme activity regardless of the type of carrier and the presence of CHIC. After 9 months the average decrease in enzyme activity was 5% and after 12 months it was 10%. Co-immobilized catalase permitted a considerable shortening of the time between two assays (ca. 70 s depending on the L-lysine concentration to be determined) owing to a faster baseline stabilization. After washing out of the reaction vessel the response time interval was only 5 s (Table 3).

TABLE 3

Effect of co-immobilized catalase on the biosensor characterization

Parameter	LysOD/Cat	LysOD
Time interval per analysis (s)	70	120
Response time (s)	5	5–8
Activity after 6 months (%)	50	20

Considering the simple immobilization technique, the attainability of an oxygen sensor, the narrow substrate specificity, the determination rate and the relatively high stability of the prepared enzyme electrodes, they are suitable for routine determinations of L-lysine during cultivation processes, in the food industry and in agricultural production and even for the determination of L-lysine in blood plasma or serum.

REFERENCES

1 K. Soda, T. Hirasawa and T. Fukumura, Anal. Biochem., 87 (1978) 283.
2 K. Soda, T. Hirasawa and T. Yagi, Jpn. Pat., 79 24 691 (1979).
3 Y. Kurimura, N. Makiguchi and T. Yagi, Jpn. Pat., 78 116 894 (1978).
4 Y. Kurimura and K. Soda, Jpn. Pat., 79 66 887 (1979).
5 F. Holz, Landwirtsch. Forsch., 33 (1980) 272.
6 W. Vervack, M. Vanbelle and M. Foulon, Rev. Ferment. Ind. Aliment., 31 (1976) 143.
7 Z.M. Tiller and D.L. Bloxam, Anal. Biochem., 131 (1983) 426.
8 R.B. Roy, J. Food Sci., 44 (1979) 480.
9 M. Jasuda, K. Tamizawa, S. Toyama and K. Soda, J. Appl. Biochem., 2 (1980) 510.
10 H. Kusakabe, K. Kodama, A. Kuninaka, H. Yoshino and K. Soda, Agric. Biol. Chem., 43 (1979) 1749.
11 L. Macholán, Collect. Czech. Chem. Commun., 43 (1978) 1811.
12 D. Skogberg and T. Richardson, Cereal Chem., 56 (1979) 147.
13 J.L. Romette, P. Durand, L. Konate, D. Tran and J.P. Kernevez, Util. Enzymes Technol. Aliment., Symp. Int., (1982) 17.
14 N.D. Thran, J.L. Romette and D. Thomas, Biotechnol. Bioeng., 25 (1983) 329.
15 J.L. Romette, in H.U. Bergmeyer (Ed.), Methods of Enzymatic Analysis, Vol. 8, Verlag Chemie, Weinheim, 1985, p. 393.
16 Ajinomoto Co., Jpn. Pat., 80 98 349 (1980).
17 Ajinomoto Co., Jpn. Pat., 58 05 199 (1983).
18 P. Michele, B. Rittich and L. Macholán, Biol. Chem. Živočisné Výroby Vet., 18 (1982) 319.
19 J.L. Romette, J.S. Jang, H. Kusakabe and D. Thomas, Biotechnol. Bioeng., 25 (1983) 2557.
20 J.S. Jang, Han'guk Saenghwa Hakhoechi, 19 (1986) 17.
21 H. Kusakabe, K. Kodama, A. Kuninaka, H. Yoshino, H. Misono and K. Soda, J. Biol. Chem., 255 (1980) 976.
22 E. Vrbová and M. Marek, Anal. Chim. Acta, 239 (1990) 263.
23 E. Vrbová and M. Marek, Collect. Czech. Chem. Commun., 55 (1990) 2568.
24 H. Havlíčková, Rostl. Výroba, 32 (1986) 1313.
25 O. Valentová, M. Marek, I. Albrechtová, J. Albrecht and J. Káš, J. Sci. Food Agric., 34 (1983) 748.
26 I.P. Smirnova, S.P. Syatkin and T.T. Berezov, Vopr. Med. Khim., 30 (1984) 133.
27 S. Konstantinidou-Doltsini, H. Buchenauer and F. Grossmand, Z. Pflanzenkrank. Pflanzenschutz, 94 (1987) 614.
28 A. Ciepiela and S. Niraz, Rocz. Nauk Roln., Ser. E, 17 (1987) 237.

Analytica Chimica Acta, 270 (1992) 137–141
Elsevier Science Publishers B.V., Amsterdam

Trace measurements of beryllium by adsorptive stripping voltammetry and potentiometry

Joseph Wang and Baomin Tian

Department of Chemistry, New Mexico State University, Las Cruces, NM 88003 (USA)

(Received 29th April 1992; revised manuscript received 30th June 1992)

Abstract

A highly sensitive electrochemical stripping procedure for ultratrace measurements of beryllium, in which preconcentration is achieved by the adsorption of the beryllium–thorin complex onto a stationary mercury electrode is described. Both voltammetric and potentiometric stripping modes are used to follow the reduction of the adsorbed complex. Optimal conditions were found to be a stirred ammonium buffer (pH 9.1) solution containing 1×10^{-7} M thorin, a preconcentration potential of -0.48 V and a differential pulse scan. For a 2-min preconcentration time, the detection limit found was 30 ng l^{-1} (3×10^{-9} M). The relative standard deviation (at 2 μg l^{-1}) is 1.9%; most metal ions do not interfere.

Keywords: Potentiometry; Stripping voltammetry; Beryllium; Trace measurement

Because of the high toxicity of beryllium, a highly sensitive method for its determination is required. Spectroscopic techniques are commonly used to determine low concentrations of beryllium [1–3]. Atomic absorption spectroscopy is preferred for this task, despite numerous interferences in flame and graphite furnace operations [2]. The electrochemical behavior of beryllium makes its voltammetric quantitation very difficult. Only indirect polarographic procedures (in the presence of various organic ligands) have been developed for measuring micromolar concentrations of beryllium [4–6].

The present paper describes a highly sensitive adsorptive stripping procedure for determining beryllium by adsorptive accumulation and reduction of its complex with thorin. Adsorptive stripping procedures, utilizing the interfacial accumulation of various metal–ligand complexes, have been developed in recent years for extending the scope of stripping analysis toward numerous metals [7,8]. As illustrated in the following sections, an analogous adsorptive stripping scheme for trace beryllium can be developed by coupling the electrochemical and surface-active properties of the beryllium–thorin complex and carefully optimizing the operational conditions. Hence, detection limits can be improved by several orders of magnitude compared to previous polarographic procedures for beryllium. While thorin has not been used before in adsorptive stripping work, it has been shown useful for spectroscopic measurements of metals, including beryllium [9,10].

Correspondence to: J. Wang, Department of Chemistry, New Mexico State University, Las Cruces, NM 88003 (USA).

EXPERIMENTAL

Apparatus

An EG & G PAR Model 264A voltammetric analyzer, a PAR 303A static mercury drop electrode and a PAR Model 0073 X–Y recorder were

used to obtain the voltammograms. A medium-size hanging mercury drop electrode, with an area of 0.016 cm^2, was employed. A TraceLab™ potentiometric stripping unit (PSU 20, Radiometer), with a SAM20 sample station (containing a glassy carbon disk), and an IBM PS/2 55SX computer were used to obtain the potentiograms.

Reagents

All solutions were prepared with doubly-distilled waters. Chemicals used were of analytical grade. Stock solutions of beryllium (1000 mg l^{-1}) were purchased from Aldrich and diluted daily as required. The supporting electrolyte was an ammonium buffer solution (pH 9.1).

Procedures

Adsorptive stripping voltammetry. Ten ml of the supporting electrolyte solution, containing 1×10^{-7} M thorin, was pipetted into the cell and purged with nitrogen for 8 min. An accumulation potential of −0.48 V was applied to a fresh mercury drop, while the solution was stirred, for a predetermined period of time. Following the accumulation step, the stirring was stopped, and after 15 s the background voltammogram was obtained by applying a differential pulse negative-going scan terminating at −0.90 V. A scan rate of 10 mV s^{-1} and 25-mV pulse amplitude were used. A known volume of the beryllium standard was then added and the accumulation–stripping cycle was repeated with a new mercury drop.

Constant current stripping potentiometry. A beryllium analysis program was written on the computer utilizing the TAP2 Trace Talk Method Builder for complete control of the TraceLab and SAM 20 system. Potentiometric measurements were made on a mercury film electrode (MFE). The preplated MFE was obtained by plating mercury from an 80 mg l^{-1} Hg^{2+} in 0.025 M HCl solution at −0.9 V for 15 min on a diamond-paste-prepolished glassy carbon electrode. The resulting film was rinsed with doubly distilled water.

Twenty ml of the sample solution was pipetted into the cell and purged with nitrogen for 8 min (while the electrode was held at open circuit). An accumulation potential of −0.2 V was applied to the electrode, while the solution was stirred for a predetermined period of time. Following the accumulation step, the stirring was stopped and after 10 s the potentiogram was obtained by applying a constant current of −4.0 μA terminating at −0.80 V.

RESULTS AND DISCUSSION

Figure 1 shows cyclic voltammograms for 2×10^{-7} M thorin recorded in the absence (A) and presence (B) of 10 μg l^{-1} (ppb) beryllium, after 0 (a) and 90 (b) sec stirring at −0.30 V. The stirring period results in a substantial increase of the cathodic peak ($E_p = -0.57$ V) of the ligand (a vs. b (A)). When the same experiment is repeated in the presence of beryllium, an additional peak, associated with the reduction of the adsorbed complex is observed ($E_p = -0.65$ V). The complex peak increases substantially after the

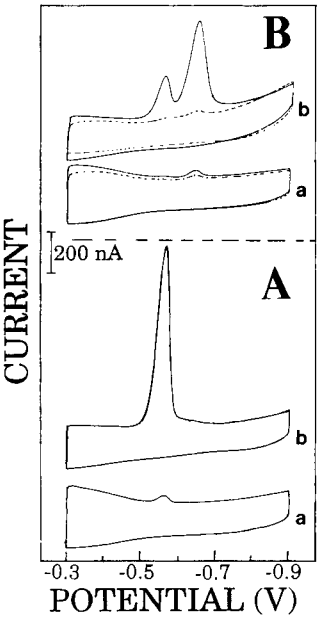

Fig. 1. Cyclic voltammograms obtained following (a) 0 and (b) 90 s stirring at −0.3 V. (A) Response to 2×10^{-7} M thorin; (B) same as A but after addition of 10 μg l^{-1} (ppb) beryllium. Electrolyte, 0.05 M ammonium buffer (pH 9.1). Scan rate, 50 mV s^{-1}.

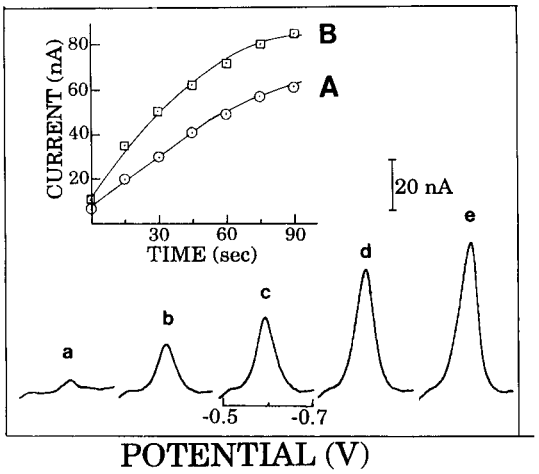

Fig. 2. Differential pulse voltammograms for 2.5 $\mu g\ l^{-1}$ beryllium after different preconcentration periods: (a) 0, (b) 15, (c) 30, (d) 60 and (e) 90 s. Preconcentration at −0.48 V with 400 r.p.m. stirring. Scan rate, 10 mV s^{-1}; amplitude, 25 mV. Solution, ammonium buffer (0.05 M, pH 9.1), containing 1×10^{-7} M thorin. Also shown, current vs. preconcentration time plots for (A) 2.5 and (B) 5.0 $\mu g\ l^{-1}$ beryllium.

stirring period, indicating a strong interfacial accumulation. Note also the simultaneous decrease of the thorin peak (associated with the lower level of the free ligand and the competition of the complex and ligand for adsorption sites). The significantly small complex peak observed in subsequent scans (dotted line) indicates desorption of the product from the surface. The distinct complex peak is attributed to the shift in the reduction potential of the azo group that is involved in the coordination (compared to the peak of the free ligand).

The interfacial behavior of the beryllium–thorin complex can be exploited for effective preconcentration, prior to the voltammetric measurement. By performing the accumulation at a potential region (in the "valley") between the ligand and complex, only a single complex peak is observed. For example, Fig. 2 shows differential pulse voltammograms for 2.5 $\mu g\ l^{-1}$ beryllium, after different preconcentration periods ((a–e) 0–90 s). The Be–thorin stripping peaks are well defined, with a peak potential of −0.60 V and peak half-width of 49 mV. A rapid increase of the complex peak is observed with increasing preconcentration time, reflecting the enhancement of the complex concentration on the mercury surface. For example, 30- and 60-sec preconcentration periods yielded 9- and 12-fold enhancement of the peak current, respectively, relative to that observed without preconcentration (compare curves a, c and d). As a result, beryllium can be conveniently determined at the low $\mu g\ l^{-1}$ level. Also shown in Fig. 2 are current vs. preconcentration-time plots for 2.5 (A) and 5.0 (B) $\mu g\ l^{-1}$ beryllium. In both cases, the initial linear increase of the current with the time is coupled with a curvature at long (> 60 s) periods.

Figure 3 illustrates the effect of various experimental variables upon the response to beryllium. The solution pH has a profound effect on the magnitude of the chelate peak (curve A). The peak increases rapidly upon increasing the pH from 8.0 to 8.6, and then decreases above a pH of 9.2. The effect of the accumulation potential was explored over the range from −0.05 to −0.50 V (curve B). Larger peaks are observed for accumulation around −0.10 to −0.20 V. However, preconcentration at −0.48 V yielded the most favor-

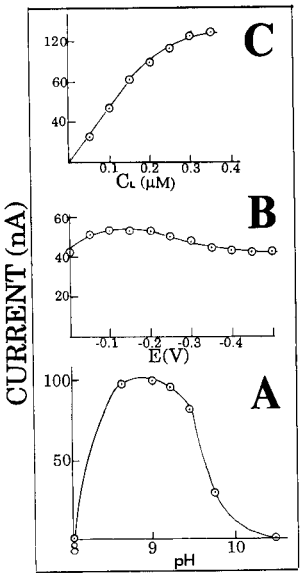

Fig. 3. Effect of (A) pH, (B) preconcentration potential, and (C) thorin concentration, on the adsorptive stripping current. Beryllium concentration, 2 $\mu g\ l^{-1}$. Preconcentration time, 45 s. Thorin concentration, (A) 2×10^{-7} M and (B) 1×10^{-7} M. Other conditions, as in Fig. 2.

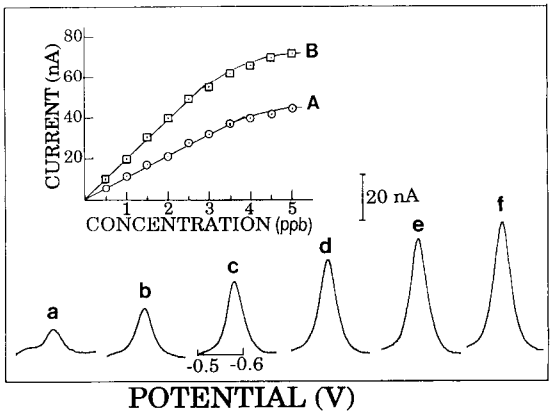

Fig. 4. Voltammograms obtained for solutions of increasing beryllium concentration, (a–f) 0.5–3.0 μg l^{-1}. Preconcentration for 90 s. Other conditions as for Fig. 2. Also shown are calibration plots for (A) 30 and (B) 90 s preconcentration.

able signal-to-background characteristics (due to the minimization of the background response associated with the free ligand peak). Similarly, while the Be–thorin peak increases rapidly upon increasing the thorin concentration (curve C), a 1×10^{-7} M thorin level offered the best signal-to-background characteristics.

Figure 4 shows voltammograms obtained after increasing the beryllium concentration in 0.5 μg l^{-1} (5.5×10^{-8} M) steps (a–f). Well-defined stripping peaks are observed following a 90-s accumulation. These six measurements are from a series of ten concentration increments, up to 5.0 μg l^{-1}. Also shown in Fig. 4 are the resulting calibration plots for (A) 30 and (B) 90 s preconcentration. As expected for measurements of surface-confined species, linearity prevails up to 3.0 (B) and 3.5 (A) μg l^{-1} (slopes, 19.6 and 10.4 nA l μg^{-1}, respectively). The interfacial accumulation of the beryllium–thorin complex results in extremely low detection limits. For example, a well-defined voltammetric peak was obtained for 100 ng l^{-1} beryllium following a 2-min preconcentration (not shown). A detection limit near 30 ng l^{-1} (3.3×10^{-9} M) was estimated from the signal-to-noise characteristics ($S/N = 3$) of these data. This concentration corresponds to 300 pg in the 10-ml sample used

The precision was estimated by twenty repetitive measurements of 2 μg l^{-1} beryllium (conditions, as in Fig. 2 with 45 s accumulation). The mean peak current was 44.7 nA, with a range of 43–46 nA, and a relative standard deviation of 1.9%. The high precision is coupled with good selectivity. Possible interferences from coexisting metal ions were evaluated. For example, measurements of 2 μg l^{-1} beryllium were not affected by the addition of 5 μg l^{-1} Fe(III), Zn(II), Cu(II), Pd(II), Cd(II), Tl(I), Ni(II), Co(II), Sb(III), Bi(III), Hg(II), Ti(IV), Cr(VI), Mn(II), Ga(III), Sn(IV), V(V) or In(III). In contrast, a similar addition of Pb(II) caused a 40% depression of the 2 μg l^{-1} beryllium response. Other species, including carbonate, halide ions and alkali metals (at 1 mM) did not affect the beryllium peak.

Besides voltammetric scanning, it is possible to employ a potentiometric stripping approach to follow the reduction of the adsorbed complex. For example, the potentiograms displayed in Fig. 5 illustrate the precision (A), time-dependence (B) and concentration-dependence (C) of the

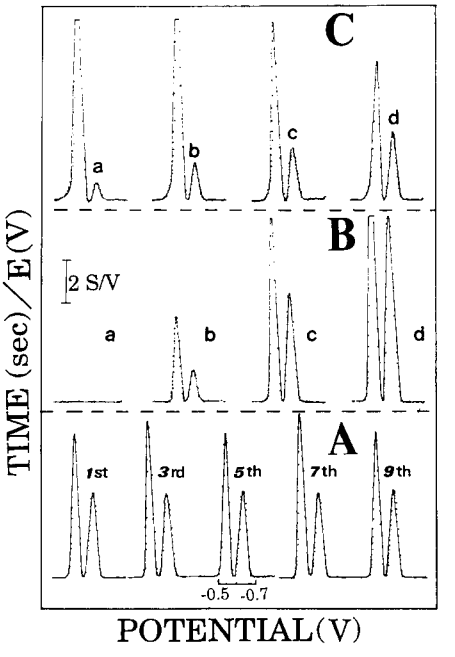

Fig. 5. Adsorptive stripping potentiometry of beryllium: (A) precision, (B) time dependence, and (C) calibration data. Beryllium concentration (A, B) 2 and (C (a–d)) 0.5–2.0 μg l^{-1}. Preconcentration time, (A, C) 90 and (a) 0, (b) 60, (c) 120 and (d) (B) 180 sec. Preconcentration potential, −0.20 V; constant-current (−4 μA) stripping.

Be–thorin system. Similar to its voltammetric counterpart, the constant-current potentiometric stripping operation exhibits two peaks corresponding to the reduction of the accumulated ligand and complex. The complex peak is very reproducible, with a relative standard deviation of 2.4% for ten repetitive measurements (A). The peak also increases linearly with the adsorption time (B) and the beryllium concentration (C). Convenient quantitation of sub-μg l^{-1} beryllium concentrations is indicated (e.g., C (a)). A preconcentration potential of -0.20 V yielded the best signal-to-background characteristics in potentiometric stripping measurements (since the free ligand peak did not affect the complex response).

In conclusion, the method described provides a highly sensitive approach to the determination of beryllium. The adsorption approach results in a substantial lowering of the detection limit compared to previously reported polarographic schemes. Hence, the scope of stripping analysis is extended towards an additional, highly toxic element.

This work was supported by the Lawrence Livermore Laboratory. B.T. acknowledges a fellowship from Sichuan University (P.R. China).

REFERENCES

1 L. Haraldsen and M. Pougnet, Analyst, 114 (1989) 1331.
2 L. Robles, C. Garcia-Ololla, M. Alemany and A. Allert, Analyst, 116 (1991) 735.
3 X. Shan, Z. Yian and Z. Ni, Anal. Chim. Acta, 217 (1989) 271.
4 V. Gutzmann, M. Michlmay and G. Pcychal-Heiling, J. Electroanal. Chem., 17 (1968) 153.
5 E. Blasius, K. Janzen and W. Fallot-Burghardt, Talanta, 18 (1971) 273.
6 E. Blasius and K. Janzen, Fresenius' Z. Anal. Chem., 258 (1972) 257.
7 J. Wang in A.J. Bard (Ed.), Electroanalytical Chemistry, Vol. 16, Marcel Dekker, New York, 1989, pp. 1–89.
8 C.M.G. van den Berg, Anal. Chim. Acta, 250 (1991) 265.
9 O. Nietzel, B. Wessling and M. Desasa, Anal. Chem., 30 (1958) 1182.
10 K. Iyer, K. Prakash, S. Iyer and U. Vekateswar, Indian J. Chem., 24A (1985) 168.

Analytica Chimica Acta, 270 (1992) 143–152
Elsevier Science Publishers B.V., Amsterdam

Determination of ultra-trace concentrations of tin by adsorptive cathodic stripping voltammetry on a glassy carbon mercury film electrode

Samuel B.O. Adeloju and Fleurdelis Pablo

Centre for Electrochemical Research and Analytical Technology, Department of Chemistry, University of Western Sydney, Nepean, P.O. Box 10, Kingswood, NSW 2747 (Australia)

(Received 31st March 1992; revised manuscript received 2nd July 1992)

Abstract

A sensitive and selective method is described for the determination of ultra-trace concentrations of tin by adsorptive cathodic stripping voltammetry on a glassy carbon mercury film electrode. The method involves a controlled preconcentration by accumulation of tin–catechol complexes on the electrode followed by stripping voltammetric measurement in the cathodic direction. The optimum conditions for the determination of tin by this method include the use of a rotated electrode at 1920 rpm, 0.10 M acetate buffer electrolyte (pH 4.2–4.7), 5×10^{-4} M catechol and an accumulation potential of -0.20 V vs. Ag/AgCl. A linear concentration range is obtained from 0 to 35 $\mu g\ l^{-1}$ and the limit of detection is 0.5 $\mu g\ l^{-1}$ for an accumulation period of 300 s. An interference study with various metal ions indicated that these substances generally do not interfere with the tin determination, except for Cu, Cd and Cr. The interference of Cu and Cd is eliminated by the addition of 1×10^{-6} M EDTA into the solution. The interference of surface-active organic substances, e.g., Triton X-100, is overcome by UV irradiation of the sample for at least 2 h. The method was successfully employed for the determination of tin in fruit juices. Comparison of the results obtained for the juices demonstrated reasonable agreement with those obtained by atomic absorption spectrometry.

Keywords: Stripping voltammetry; Fruit juices; Tin

Tin is one of the essential trace elements which are involved in various metabolic processes in plants, animals and man [1]. Besides ingestion from food, it is introduced into the human environment both as inorganic tin and as organotin compounds, through their use in food packaging, as fungicides in crops, in some veterinary formulations, in wood preservation, in marine anti-fouling paints, as stabilizer for poly(vinyl chloride) and as electrochemical catalysts [2]. Consequently, there has been growing concern about the significance and toxicity of this element and this, in turn, has encouraged the development of methods for its determination in various sample materials. The most commonly used methods include atomic absorption spectrometry (AAS) with hydride generation [3–5], electrothermal AAS [6–8] and electrochemical analysis, based on polarography or stripping voltammetry [9–29]. Of these, the electrochemical methods are capable of better sensitivity and selectivity.

In particular, the anodic stripping voltammetry of tin has been well studied and it is often considered for the determination of tin in various media

Correspondence to: S.B.O. Adeloju, Centre for Electrochemical and Analytical Technology, Department of Chemistry, University of Western Sydney, Nepean, P.O. Box 10, Kingswood, NSW 2747 (Australia).

and in different sample materials. However, the use of this technique for the determination of tin is limited by the overlap of tin stripping peak with that of lead. This is of major concern in the determination of tin because of these two elements, lead is usually present at higher concentrations in most samples. Several approaches have been used to reduce or overcome this problem and hence to permit the adequate determination of tin in the presence of lead. These include selective complexation of either metal [9–11], separation of tin by distillation as tin bromide [12], separation of tin by liquid–liquid extraction [13], use of flow or matrix-exchange methods [9,14], addition of surfactants [15,16], use of a suitable electrolyte [17] or use of methanolic hydrochloric acid as solvent at low temperatures [18]. However, the approaches requiring separation steps prior to determination are tedious and may result in the contamination of samples or incomplete recovery of tin. In other cases, the use of some of the approaches makes the voltammetric determination of tin more complex.

In recent years, the direct determination of tin by adsorptive cathodic stripping voltammetry (CSV) on a hanging mercury drop electrode has been reported [23,28,29]. The two approaches that have been reported so far employed catechol and tropolone to form the adsorbable tin complexes, and both methods were capable of determining the element down to sub-μg l^{-1} levels. However, as part of our interest in determining tin in a continuous flow system, the use of the hanging mercury drop electrode was undesirable. For this purpose, the use of a glassy carbon mercury film electrode was considered in this study for the reliable determination of tin by adsorptive CSV. As the use of this electrode is not common for adsorptive stripping analysis, its consideration in this study required careful characterization of the electrode processes, optimization of the analytical conditions and verification of the involvement of adsorption in the electrode process. Further, the effect of organic and inorganic interferents on the determination of tin by this approach was investigated. Also, the application of the method to the determination of tin in some fruit juices was considered.

EXPERIMENTAL

Apparatus

Cathodic stripping voltammograms were obtained using a Metrohm 646 VA processor with a 647 VA stand. A 3-mm diameter rotating glassy carbon electrode filmed with mercury in situ was employed as the working electrode; an Ag/AgCl ([KCl] = 3 mol l^{-1}) and a platinum rod 2 mm in diameter were employed as reference and auxiliary electrodes, respectively. pH measurements were made with an Activon Basic Digital pH meter. Cyclic voltammograms were obtained using an Amel Model 433 polarographic analyser. UV irradiation experiments were done using a Raytech Model LS-7 UV instrument (0.2 A, 50 Hz) in the shortwave UV region (2800–100 Å). Dry ashing of samples was carried out using a Heraeus M110 laboratory muffle furnace. AAS measurements were performed using a GBC 902 double-beam atomic absorption spectrometer (with deuterium arc background correction).

Reagents

Analytical-reagent grade chemicals were used unless indicated otherwise. All solutions were prepared from deionized water purified using a Milli-Q system (Millipore).

A 1000 mg l^{-1} stock standard tin solution was prepared from tin metal (Ajax Chemicals) dissolved in concentrated hydrochloric acid (BDH) and subsequently made up to the final solution (1.6 M in HCl). Dilute working standard tin solutions in the range 1–100 mg l^{-1} were prepared weekly from the stock standard solution by dilution with 1 M HCl. Catechol (Ajax Chemicals, laboratory reagent grade) solution (0.1 M) was prepared daily and always kept in the dark to prevent decomposition. Stock acetate buffer solutions (2 M) of different pH were prepared from glacial acetic acid (Ajax Chemicals) and anhydrous sodium acetate (BDH). Appropriate dilutions of the stock acetate buffer were made as required. A 1000 mg l^{-1} stock Hg(II) solution was prepared from $HgCl_2$ (Ajax Chemicals) dissolved in 0.10 M HCl. The solutions used for the interference studies were prepared by dissolving metals in either hydrochloric acid or nitric acid

(BDH). A stock aqueous EDTA solution (0.02 M) was prepared from ethylenediaminetetraacetic acid disodium salt (Ajax Chemicals, laboratory reagent grade).

Procedure

Volumes of 20 ml of the acetate buffer solution, 200 μl of stock 1000 mg l^{-1} Hg(II) solution and 100 μl of catechol solution are placed in the polarographic cell. The required amount of the dilute standard tin solution is also transferred into the cell. The solution is deaerated with nitrogen for 5 min while rotating the working electrode at 1920 rpm, and after which a nitrogen flow is maintained over the solution throughout the measurement. The accumulation potential (−0.20 V) is applied to the rotated glassy carbon mercury film electrode (GCMFE) for a required period to effect adsorption of tin–catechol complexes on it. The working electrode rotation is stopped and 15 s are allowed for the solution to attain equilibrium. The voltammogram is recorded as the adsorbed complexes are stripped off from the GCMFE by scanning the potential in the differential-pulse mode (pulse amplitude 50 mV, duration between pulses 600 ms, potential step between pulses 6 mV) over the range −0.200 to −0.800 V vs. Ag/AgCl at a scan rate of 10 mV s^{-1}.

The charge passed in the adsorptive process is determined by the "cut and weigh" method, which is used to integrate the stripping peaks.

Fruit juice samples (peach nectar, tomato juice, pineapple juice, grapefruit juice and apricot nectar) are analysed for tin after initial dry ashing treatment. This involves slow heating of a volume of the juice in a crucible on a hot-plate nearly to dryness and subsequent transfer of the crucible into a muffle furnace for dry ashing at 400°C for at least 24 h or until only a white residue is left. The resulting residue is then transferred into a volumetric flask and made up to the final volume with 1 M HCl. To determine the recovery of tin, appropriate volumes of standard tin solution are added to some samples and then treated by the same procedure. Both spiked and unspiked samples are prepared in triplicate. The samples are analysed by adsorptive CSV and flame AAS and

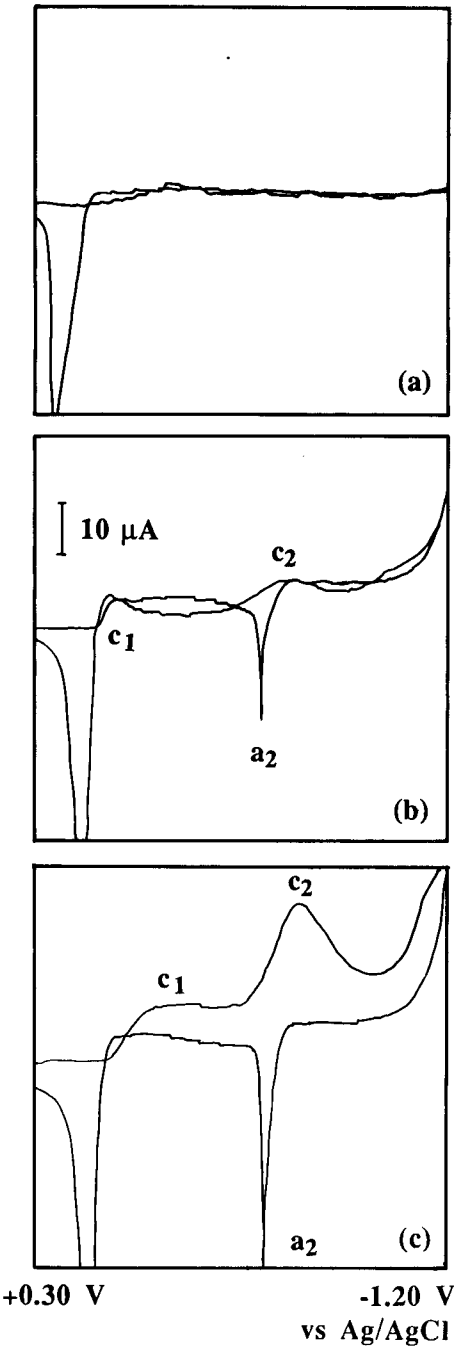

Fig. 1. Cyclic voltammetric curves obtained on a GCMFE at a voltage scan of 30 mV s^{-1}. (a) 0.10 M acetate buffer supporting electrolyte only; (b) 25 mg l^{-1} tin(IV) in the electrolyte (no catechol); (c) 25 mg l^{-1} tin(IV) and 4.7×10^{-3} M catechol in the electrolyte.

the amount of tin is determined in the former by the standard additions method.

RESULTS AND DISCUSSION

Characterization of the electrode reaction

Figure 1 shows the cyclic voltammograms obtained for tin in acetate buffer on the glassy carbon mercury film electrode. In the absence of tin and catechol (Fig. 1a), the blank electrolyte only gave an anodic peak due to the oxidation of mercury. With the addition of tin (Fig. 1b), a new cathodic peak c_1 corresponding to the reduction of Sn(IV) to Sn(II) and the pair of peaks c_2–a_2 corresponding to the Sn(II)–Sn(0) couple were obtained. The addition of catechol to the solution resulted in a considerable enhancement of the cathodic and anodic peaks, as shown in Fig. 1c. In addition to enhancing the tin peaks, the presence of catechol resulted in a shift of the peak potentials to more negative values, indicating that an interfacial process is involved. The peak widths at half-height [$w_{1/2}(c_1) = 149$ mV; $w_{1/2}(c_2) = 203$ mV; $w_{1/2}(a_2) = 43$ mV], the separation of c_2 and a_2 ($\Delta E_p = 245$ mV) and the absence of the anodic counterpart of c_1 (which is beyond the oxidation peak of Hg) indicate that the electrode processes for the Sn(IV)–Sn(II) and Sn(II)–Sn(0) couples are irreversible.

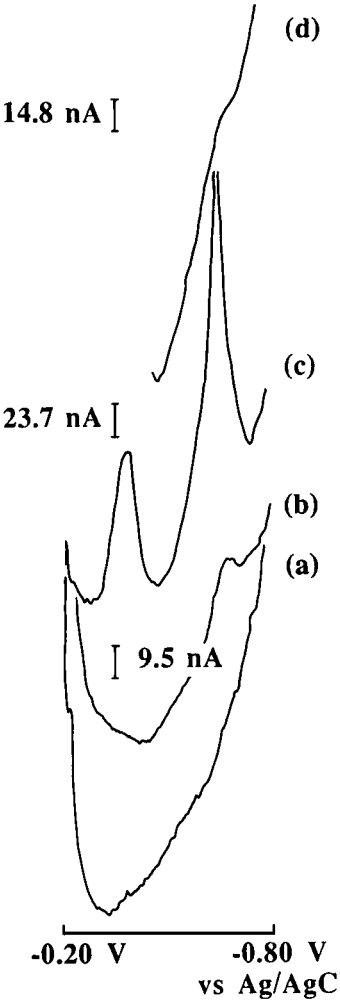

Fig. 2. Cathodic stripping voltammetric curves obtained on the GCMFE for an accumulation time of 300 s to demonstrate the influence of catechol and accumulation potential on the reduction of tin. (a) Blank; (b) 30 $\mu g\ l^{-1}$ tin(IV) without catechol, $E_{acc} = -0.20$ V vs. Ag/AgCl; (c) 30 $\mu g\ l^{-1}$ tin(IV) with 5×10^{-4} M catechol, $E_{acc} = -0.20$ V vs. Ag/AgCl; (d) 30 $\mu g\ l^{-1}$ tin(IV) with catechol, $E_{acc} = -0.45$ V.

Figure 2 illustrates the influence of catechol on the cathodic stripping behaviour of tin on the GCMFE in acetate buffer, following an initial accumulation for 300 s. It is clearly evident that in the absence of catechol (Fig. 2b) only a small peak due to the reduction of Sn(II) at -0.57 V was obtained. The addition of small amount of catechol to the solution gave, as shown in Fig. 2c, two well resolved peaks whose potentials shifted to more negative values. The enhancement of the cathodic peaks by catechol clearly indicates that the in situ formation and accumulation of tin as the tin–catechol complexes on the electrode surface is involved. The formation and accumulation of the complexes during the preconcentration step can be represented by

$$Sn^{4+}(aq) + n\mathrm{Cat}_{(aq)} \rightarrow \mathrm{SnCat}_{n(aq)} + 2nH^+$$

$$\mathrm{SnCat}_{n(aq)} \rightarrow \mathrm{SnCat}_{n(ads)}$$

where Cat represents catechol and n represents the number of complexing agent moieties reacting with Sn(IV). And the resulting peaks during the measurement correspond to the following reduction reactions:

$$\mathrm{SnCat}_{n(ads)} + 2nH^+ + 2e^- \rightarrow \mathrm{Sn(II)}_{(aq)} + n\mathrm{Cat}$$

$$E_p = -0.39 \text{ V}$$

and

$$Sn(II)_{(ads)} + 2e^- \rightarrow Sn(0)_{(aq)} \quad E_p = -0.66 \text{ V}$$

For the two peaks which appeared at −0.39 and −0.66 V, the peak widths at half-height ($w_{1/2}$) were 75 and 59 mV, respectively. This implies that the Sn(IV) reduction deviates from reversibility, whereas the Sn(II) reduction appeared to be reversible for a differential-pulse cathodic stripping on the GCMFE [30].

Unlike previous observations [28,29], the stripping current corresponding to the reduction of the Sn(IV)–catechol complex on the GCMFE is less than that corresponding to the Sn(II) reduction. However, it is well known that tin exists in most aqueous media almost exclusively in the Sn(IV) form [19]. Tin(II) is easily oxidized in air to Sn(IV), but the conversion of Sn(IV) to Sn(II) requires a reduction step by either chemical or electrochemical means, and the retention of the Sn(II) form requires a non-oxidizing condition. Figure 2d demonstrates the significance of the electrochemical reduction of the Sn(IV)–catechol complex in generating Sn(II) and, hence, in obtaining its response. By applying a potential of −0.45 V, but without initial accumulation of the Sn(IV)–catechol complexes, the sensitivity of the Sn(II) reduction is considerably reduced in comparison with that obtained when the accumulation of the Sn(IV) complex was involved. This indicates that the enhanced response obtained for the Sn(II) observed in the cathodic stripping measurement is generated from the reduction of the Sn(IV)–catechol complex during the stripping step. Evidently, the electrode processes for tin on the GCMFE in the presence of catechol is different to those previously observed on a hanging mercury drop electrode [28,29].

Optimization of conditions for tin analysis

Influence of rate of electrode rotation and accumulation potential. A convective mode of transfer of the tin–catechol complexes to the GCMFE during the preconcentration step is provided by the rotation of the electrode. The first tin peak which appeared at −0.39 V increased gradually with the increasing rate of rotation, whereas the second tin peak which appeared at −0.66 V increased significantly up to 1920 rpm, but showed little variation thereafter. Hence, it was established that a rate of rotation of 1920 rpm is adequate and this was used for all other measurements in this study.

The choice of accumulation potential is critical for the adsorptive accumulation of tin–catechol complexes on the GCMFE. The optimum potential established for the determination of tin on this electrode was −0.200 V vs. Ag/AgCl. The use of more positive accumulation potentials resulted in a very high initial current response, low sensitivity for the tin peaks and very noisy voltammograms. Normally, an accumulation potential of 300–400 mV less negative than the characteristic potential of the analyte is used [30]. However, the use of an accumulation potential of 0.00 or −0.10 V resulted in the appearance of the voltammetric peak response of catechol around −0.12 V and the sensitivity of the tin peaks was reduced. This implies that the initial reduction of catechol may somehow affect the extent of accumulation of the tin–catechol complexes. To overcome this problem, an accumulation potential of −0.200 V vs. Ag/AgCl was used for all subsequent work.

Dependence on catechol concentration. The influence of increasing concentration of catechol on the peak currents for tin on the GCMFE is shown in Fig. 3. The first tin peak current did not increase appreciably with increasing catechol concentration up to 5×10^{-4} M, but decreased thereafter with further increase in the concentra-

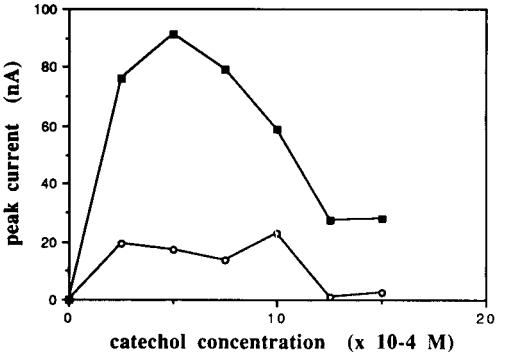

Fig. 3. Influence of concentration of catechol on the stripping peak currents of 10 $\mu g\, l^{-1}$ tin(IV) for an accumulation period of 300 s. ○ = Peak at −0.39 V; ■ = peak at −0.66 V.

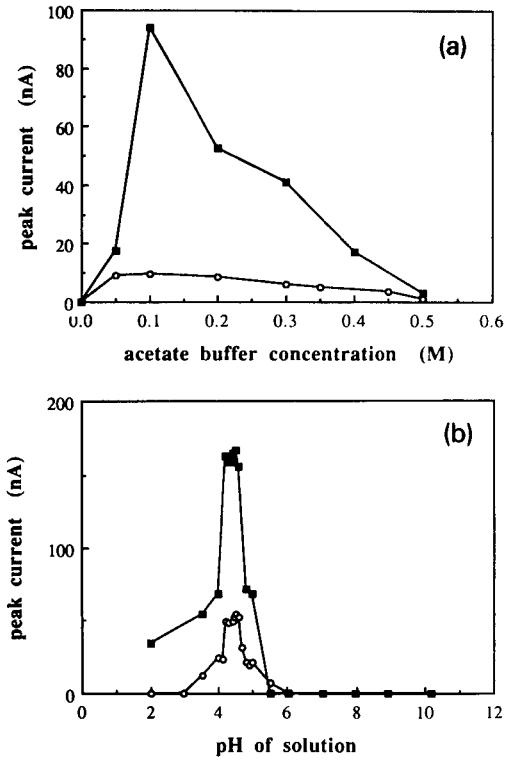

Fig. 4. Effect of (a) concentration of acetate buffer and (b) pH of the solution on the stripping peak currents of 25 $\mu g\ l^{-1}$ tin(IV) for an accumulation period of 300 s. ○ = Peak at −0.39 V; ■ = peak at −0.66 V.

tion of the complexing agent. Also, the peaks were broadened with increase in concentration of catechol. The sensitivity of the second tin peak increased slightly with increasing catechol concentration up to 5×10^{-4} M, but again decreased thereafter with further increase in catechol concentration. It appears that at the higher concentrations of catechol, there is a strong competition between the excess catechol and the tin–catechol complexes for adsorption on the electrode surface, resulting in a decrease in the sensitivity of the stripping peaks. However, it is apparent that the optimum catechol concentration was 5×10^{-4} M and this was used for all other work reported.

Influence of buffer concentration and pH. Figure 4(a) shows the dependence of the first stripping peak on the acetate buffer concentration. No voltammetric response was obtained for tin in the absence of the buffer. The use of acetate buffer electrolyte of concentration up to 0.10 M caused a considerable increase in the current for the second peak, but only a slight variation for the first peak. However, buffer concentration less than 0.10 M have a low buffering capacity and are inadequate. With further increase in acetate buffer concentration above 0.10 M, both stripping peak currents decreased, the measurements became less reproducible and the potentials shifted slightly towards less negative values. Hence the optimum acetate buffer concentration of 0.10 M was used for all subsequent measurements.

The influence of the resulting pH of the solution on the two stripping peaks for tin is shown in Fig. 4(b). The optimum pH for the tin measurement is 4.2–4.7; at higher and lower pH, the tin peaks were considerably less sensitive. At very low pH, the catechol may be unable to form complexes, whereas at very high pH, tin ions hydrolyse. The peak potentials shifted towards more negative values with increase in the solution pH, indicating that the electrode process is pH dependent.

Choice of accumulation time and linear concentration range

The influence of the accumulation period on the tin stripping peak currents is shown in Fig. 5. The peak currents increased linearly with increase in the accumulation period from 0 to 900 s, with correlation coefficients of 0.996 and 0.951

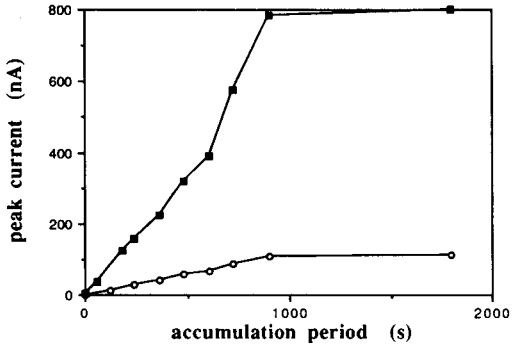

Fig. 5. Dependence of the stripping peak currents on the accumulation period for 20 $\mu g\ l^{-1}$ tin(IV) solution. □ = peak at −0.39 V; ◆ = peak at −0.66 V.

TABLE 1

Detection limit, linear concentration range and calculated maximum charge for different accumulation periods (t_{acc})

t_{acc} (s)	Linear concentration range [a] ($\mu g\ l^{-1}$)	Peak at −0.39 V			Peak at −0.66 V			Detection limit [a] ($\mu g\ l^{-1}$)
		Correlation coefficient [b]	Slope	Maximum charge ($\times 10^{-7}$ C)	Correlation coefficient [b]	Slope	Maximum charge ($\times 10^{-7}$ C)	
120	5–55	0.965	0.864	4.03	0.983	2.575	8.17	1.0
300	0–35	0.984	2.119	6.20	0.960	7.064	14.2	0.5
600	0–20	0.944	2.286	19.3	0.984	12.24	45.3	0.08

[a] Based on the use of second peak. [b] $n = 12$.

($n = 15$) for the two peaks respectively. The peak currents showed very little variation at accumulation periods longer than 900 s. As expected for adsorption processes, the dependence of the peak current on the accumulation period is limited by the saturation of the electrode surface, hence confirming that adsorption is involved in the electrode processes.

The influence of varying tin concentration on the two stripping peaks at various accumulation periods showed that the peak currents generally increased linearly with increase in tin concentration within a low concentration range, but deviated from linearity at higher concentrations. Table 1 summarizes the linear concentration range obtained with the different accumulation periods. The slope of the peak current–tin concentration plot increased and the linear concentration range decreased with increasing accumulation period. Evidently, the degree of saturation on the

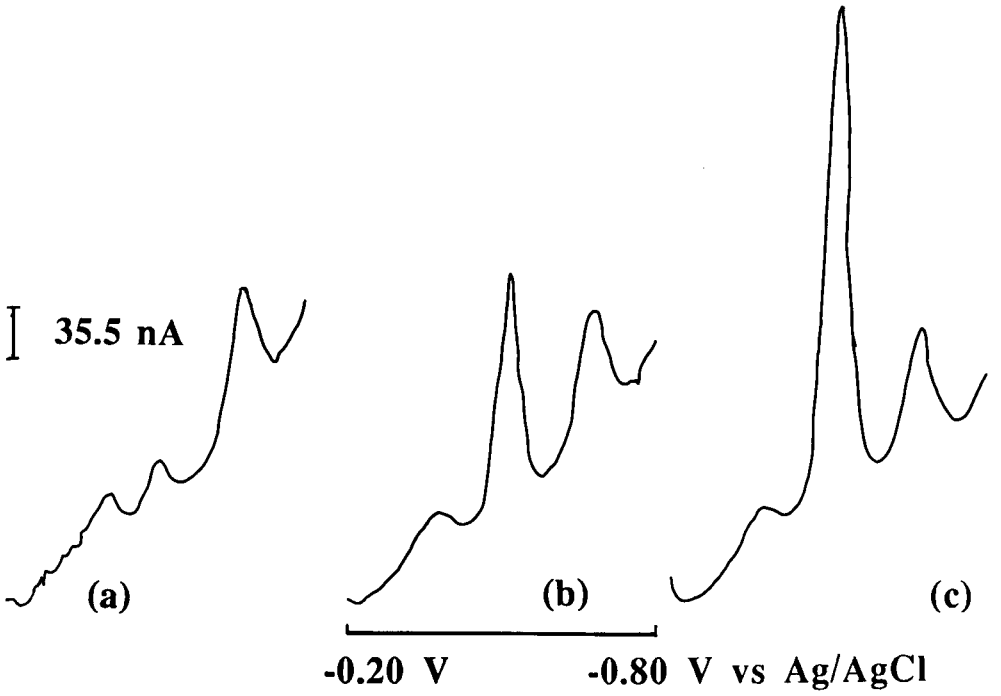

Fig. 6. Cathodic stripping voltammetric curves of 10 $\mu g\ l^{-1}$ tin(IV) for an accumulation period of 300 s in the presence of (a) 10, (b) 50 and (c) 100 $\mu g\ l^{-1}$ lead solution.

GCMFE increased with increasing accumulation of the tin–catechol complex. Hence it can be concluded that the linear dependence of the peak current on the tin concentration is limited by the saturation of the electrode surface. This also confirms that adsorption is involved in the electrode process. The total charge corresponding to the saturation of the electrode surface depends both on the bulk concentration of the analyte and the accumulation period. The use of a shorter accumulation period is useful in obtaining an extended linear concentration range, whereas a longer accumulation period is beneficial in lowering the limit of detection. Both of these aspects are useful in analysing samples of varying tin concentrations.

Interference of metal ions and Triton X-100

The interference effect of different metal ions on the adsorptive cathodic stripping voltammetric determination of tin on GCMFE was investigated. Calcium, zinc, iron, nickel, magnesium and lead did not cause appreciable changes in the stripping peak currents of tin when present at the same or 5–10 times higher concentrations than the tin concentration. For lead, a peak corresponding to its reduction appeared at −0.50 V vs. Ag/AgCl and this was separated by 110 and 160 mV from the two tin peaks. Figure 6 shows the stripping voltammograms obtained for tin in the presence of various concentrations of lead. The lead reduction peak current increased proportionately with increasing lead concentration and did not affect the tin peaks. The peaks are well resolved and, hence, indicate that tin and lead can be determined simultaneously. Large concentrations of cobalt, aluminium and arsenic (ten or more times the tin weight concentration) interfered slightly with the tin peaks, causing 2–10% suppresion. Large amounts of chromium (five or more times the tin concentration) caused the two tin peaks to overlap by shifting the potential of the second tin peak towards less negative values. Copper at five times the tin concentration suppressed the tin peaks by as much as 50%, possibly owing to its reaction with the catechol, which may consequently reduce the amount available for the formation of the tin(IV) complex. Cadmium resulted in a positive interference with the tin stripping peak at −0.66 V. The same concentration of cadmium increased the tin peak current by about 20%. However, with the use of 1×10^{-6} M EDTA, the copper and cadmium interferences were successfully overcome, without affecting the tin peak currents.

The interference of Triton X-100, as typical of surface-active organic substances, was investigated. It was found that the tin stripping peaks

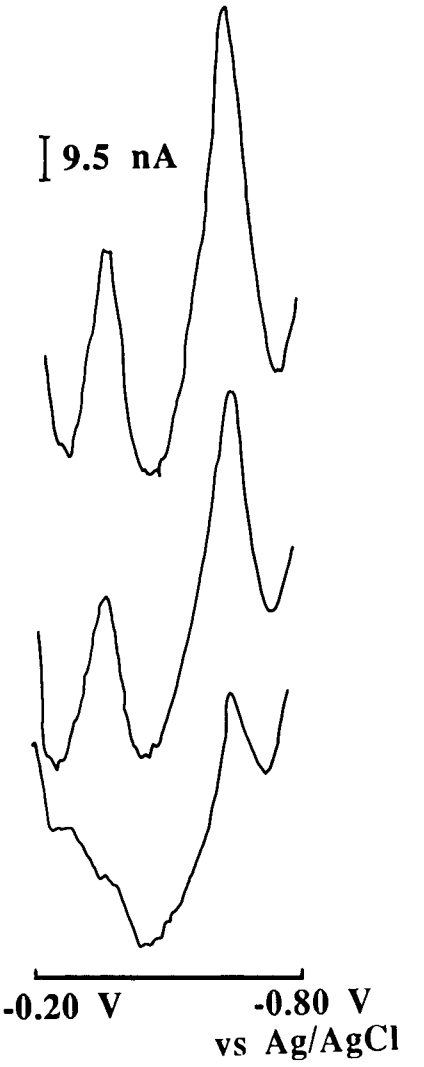

Fig. 7. Measurement of tin in canned apricot nectar by standard addition. (a) Sample only (4000-fold dilution); (b) sample with 5 $\mu g\ l^{-1}$ tin(IV) standard; (c) sample with 10 $\mu g\ l^{-1}$ tin(IV) standard.

TABLE 2

Analysis of fruit juice samples

Sample	Concentration of tin obtained from unspiked samples ($mg\ l^{-1}$) [a]		Recovery studies with spiked samples		
	Adsorptive CSV	AAS	Tin added ($mg\ l^{-1}$)	Tin found ($mg\ l^{-1}$)	Recovery (%)
Pineapple juice	100.3 ± 10.9	96.9 ± 3.4	10.00	10.83	108.3
Apricot nectar	7.7 ± 2.5	7.16 ± 1.14	5.00	3.18	63.6
Grapefruit juice	54.2 ± 5.4	67.56 ± 1.53	10.00	9.46	94.6
Tomato juice	51.0 ± 5.1	58.17 ± 1.46	5.00	3.23	64.5
Peach nectar	173.5 ± 14.1	201.8 ± 6.6	10.00	10.19	101.9

[a] Mean ± S.D. ($n = 3$).

were suppressed by 50–90% with the addition of the same level and 5–10 times more Triton X-100. This results from a competitive adsorption of Triton X-100 and the tin–catechol complexes on the GCMFE. The suppression of the tin peak currents indicates that the organic substance was more strongly adsorbed on the GCMFE. However, UV irradiation of the solution, without using hydrogen peroxide [31], for at least 2 h improved the sensitivity of the tin stripping peaks. The use of hydrogen peroxide should be avoided because of its tendency to oxidize the mercury film and develop a poor background.

Analytical utility

The enhancement of the cathodic stripping peaks of tin by the addition of catechol and the prior accumulation of tin–catechol complexes on the GCMFE results in low detection limits. The limits of detection for tin by this approach using the second stripping peak, which is at −0.66 V, based on a signal-to-noise ratio of 3 were 1.0, 0.5 and 0.08 $\mu g\ l^{-1}$ for accumulation periods of 120, 300 and 600 s, respectively. Generally, lower limits of detection were achieved with longer accumulation periods, but accumulation for longer than 600 s for very dilute solutions is not recommended because of increasing matrix effects on the adsorption-process. The achievable linear concentration ranges for the various accumulation periods are given in Table 1.

The application of the method to the determination of tin in five canned fruit juice samples was explored, as it is usually expected that the acidity of the fruit juices stored in tin cans may cause the dissolution and introduction of the element into the juices. Figure 7 shows typical voltammograms obtained for tin in the dry-ashed apricot nectar sample. The determination of tin in this sample was by the standard addition method with two successive additions of 5 $\mu g\ l^{-1}$ tin. Table 2 summarizes the results obtained for the determination of tin and recovery studies in the fruit juice samples. The recovery of tin in pineapple, grapefruit and peach nectar juices was good. However, the recovery of tin in tomato and apricot nectar juices was not very successful, probably because of adsorption of tin on components in the samples which could not be ashed completely at the chosen temperature, in spite of prolonged heating in the furnace. Table 2 also shows good agreement between the amount of tin obtained by AAS and by the proposed method.

Conclusion

The determination of ultra-trace amounts of tin by adsorptive CSV on a glassy carbon mercury film electrode has been successfully demonstrated. Unlike a previous approach which employed a hanging mercury drop electrode and demonstrated that catechol enhanced the reduction of Sn(IV), the reduction of Sn(II) was substantially more sensitized by the same complexing agent on the GCMFE. The limit of detection of 0.08 $g\ l^{-1}$ achievable under this condition with a 10-min accumulation period is adequate for the determination of tin in biological and environmental materials. The use of this approach for

the determination of tin in fruit juices proved to be adequate. Further, the successful use of the GCMFE in this study will permit the continuous flow determination of tin by adsorptive CSV.

We thank Mr. Bert Aarts for his assistance with the AAS determination of tin and Mr. Curt Stocksiek for help with the drawings. The provision of a Nepean postgraduate research scholarship for this work is gratefully acknowledged.

REFERENCES

1 D. Purves, Fundamental Aspects of Pollution Control and Environmental Science 7: Trace-Element Contamination of the Environment, Elsevier, Amsterdam, 1985.
2 G. Weber, Fresenius' Z. Anal. Chem., 321 (1985) 217.
3 A. D'Ulivo, Talanta, 35 (1988) 499.
4 P.W. Balls, Anal. Chim. Acta, 197 (1987) 309.
5 J.S. Han and J.H. Weber, Anal. Chem., 60 (1988) 316.
6 K.S. Subramanian, Talanta, 36 (1989) 1075.
7 T. Ferri, E. Cardarelli and B.M. Petronio, Talanta, 36 (1989) 513.
8 A. Brzezinska-Paudyn and J.C. Van Loon, Fresenius' Z. Anal. Chem., 331 (1988) 707.
9 E. Desimoni, F. Palsimano and L. Sabbatini, Anal. Chem., 52 (1980) 1889.
10 S. Glodowski and Z. Kublik, Anal. Chim. Acta, 104 (1979) 55.
11 G. Weber, Anal. Chim. Acta, 186 (1986) 49.
12 T.M. Florence and Y.J. Farrar, J. Electroanal. Chem., 51 (1974) 191.
13 T.V. Nghi and F. Vydra, J. Electroanal. Chem., 71 (1976) 333.
14 S. Mannino, Analyst, 109 (1984) 905.
15 J. Georges and M. Mermet, Anal. Chim. Acta, 185 (1986) 363.
16 J. Hernandez Mendez, R. Carabias Martinez, M.E. Gonzales Lopez, Anal. Chim. Acta, 138 (1982) 47.
17 S. Dogan, G. Nembrini and W. Haerdi, Anal. Chim. Acta, 130 (1981) 385.
18 L. Metzger, G.G. Willems and R. Neeb, Fresenius' Z. Anal. Chem., 288 (1977) 35; 292 (1978) 20; 293 (1978) 16.
19 A.M. Bond, Anal. Chem., 42 (1970) 1165.
20 A.M. Bond, T.A. O'Donnell, A.B. Waugh, R.J.W. McLaughlin, Anal. Chem., 42 (1970) 1169.
21 A.J. Bard, Anal. Chem., 34 (1962) 266.
22 S.L. Phillips and I. Shain, Anal. Chem., 34 (1962) 262.
23 J. Wang and J. Zadeii, Talanta, 34 (1987) 909.
24 R.C. Rooney, Analyst, 88 (1963) 959.
25 S. Glodowski and Z. Kublik, Anal. Chim. Acta, 115 (1980) 51.
26 C.M.G. van den Berg, S.K. Khan and J.P. Riley, Anal. Chim. Acta, 222 (1989) 43.
27 P. Kiekens, R.M.H. Verbeeck, H. Donche and E. Temmerman, Anal. Chim. Acta, 127 (1981) 251.
28 S.B. Adeloju, in T. Tran and M. Skyllas-Kazacos (Eds.), Electrochemistry: Current and Potential Applications, Proceedings of the Seventh Australian Electrochemistry Conference, Electrochemical Division, Royal Australian Chemical Institute, Sydney, 1988, pp. 330–333.
29 S.B. Adeloju, Anal. Sci., 7 (1991) 1099.
30 A.M. Bond, Modern Polarographic Methods in Analytical Chemistry, Dekker, New York, 1980.
31 A.M. Bond and D.L. Luscombe, J. Electroanal. Chem., 214 (1986) 21.

Analytica Chimica Acta, 270 (1992) 153–159
Elsevier Science Publishers B.V., Amsterdam

Effect of sodium dodecyl sulphate on the measurement of labile copper(II) species by anodic stripping voltammetry in the presence of humic acid

Masami Fukushima, Kiyoshi Hasebe and Mitsuhiko Taga

Department of Chemistry, Faculty of Science, Hokkaido University, 060 Sapporo (Japan)

(Received 7th April 1992; revised manuscript received 7th July 1992)

Abstract

The addition of sodium dodecyl sulphate (SDS) was found to be advantageous in measuring uncomplexed labile copper(II) species in the presence of humic acid (HA) by anodic stripping voltammetry with a thin mercury film glassy carbon electrode. If HA is present in the solution, the anodic peak of labile copper(II) species is broadened because of the adsorption of HA on the electrode. However, by adding SDS, a sharp peak was obtained and the peak area increased by about 30% because the adsorption of HA on the electrode was prevented. This was verified by electrocapillary curves in which SDS rather than HA become strongly adsorbed on the electrode. Moreover, this method was applied to the evaluation of copper(II) complexing abilities (conditional stability constants and complexing capacities) of HA by copper(II) titration. The copper(II) complexing capacities of HA evaluated in the presence of SDS were 16% smaller values than those in the absence of SDS.

Keywords: Stripping voltammetry; Copper; Humic acids; Sodium dodecyl sulphate

Complexation of humic acid (HA) with heavy metal ions has been investigated from environmental and geochemical points of view [1–4]. Especially anodic stripping voltammetry (ASV) has been applied to the speciation analysis of heavy metal ions in the presence of natural organic ligands such as HA, in which uncomplexed species were measured as "ASV-labile" species [5–8]. This method is sensitive, simple and flexible.

Generally, in the presence of organic matter such as HA, it was recognized that a high concentration of organic matter brings about adsorption on the electrode and this adsorption leads to broadening of the anodic waves of labile heavy metal species [9,10]. Therefore, the adsorption of organic matter would interfere in the determination of labile heavy metal species [11]. Moreover, dissociation of the metal complex in the diffusion layer occurs during the deposition time [12]. This leads to positive errors for the labile metal species.

Recently, in order to eliminate such interferences, glassy carbon electrodes with permselective membranes and polymer coatings have been developed, e.g., using a dialysis membrane [13,14], a cellulose acetate membrane [15] or a coating with Nafion [16]. These membranes and coatings could eliminate the adsorption of organic matter and prevent the dissociation of complexed species in the diffusion layer during the deposition time. Especially a Nafion-coated thin mercury film electrode [17] has been conveniently used for the measurement of labile species of heavy metal ions

Correspondence to: M. Taga, Department of Chemistry, Faculty of Science, Hokkaido University, 060 Sapporo (Japan).

in the presence of natural organic ligands such as HA [18–20].

On the other hand, in spite of their organic character, surfactants have been shown to accelerate the electrode reactions of analytes [21,22]. If the surfactant can be more strongly adsorbed on the electrode surface than HA and the surfactant does not interfere with the electron-transfer reaction of the heavy metal ions, a reduction of the broadening of the anodic peak can be expected. The addition of surfactant is a simple method and a new approach for the measurement of labile heavy metal species in the presence of organic matter such as HA by ASV. Also, it has been reported that the addition of sodium dodecyl sulphate (SDS) can improve the end-point in the copper(II) titration of EDTA or nitrilotriacetic acid (NTA) by ASV with a hanging mercury drop electrode [23].

In this work, the effects of SDS on the anodic waves of labile copper(II) species in the presence of HA were investigated by ASV with a thin mercury film glassy carbon electrode (TMFGCE). Moreover, this method was applied to the evaluation of the copper(II) complexing abilities [conditioning stability constant and copper(II) complexing capacity] of HA.

EXPERIMENTAL

Reagents and materials

HA was prepared from peat, according to previous work [24]; elemental analysis gave C 51.0, H 4.72, N 1.74% and an ash content of 2.44%. The amount of the acidic functional groups was 82.1 meq per gram of carbon in HA.

A stock solution of 0.1 M copper(II) was prepared by dissolving electrolytic copper (99.999% purity, Mitsuwa Pure Chemicals) in nitric acid. Surfactants (analytical-reagent grade, Wako) were as follows: cationic type, dodecyltrimethylammonium chloride (DTAC); anionic type, sodium dodecyl sulphate and sodium dodecyl benzenesulphonate (SDBS); non-ionic type, poly(vinyl alcohol) (PVA) and Triton X-100.

NTA (Wako) was used as a model ligand. The water used was doubly deionized.

Apparatus

A rotating ring-disc electrode system (RRDE-1, Nikko Keisoku) and a potentiostat (HA-501, Hokuto Denko) with a function generator (HB-105, Hokuto Denko) were used. A three-electrode system was used: the working electrode was a glassy carbon rotating disc electrode with plated mercury film, the reference electrode was a saturated calomel electrode (SCE) and the counter electrode was a platinum wire. Voltammograms were recorded with an X–Y plotter (RY-101, Rika Denki). A polarographic analyser (P-1100, Yanagimoto) with a dropping mercury electrode (DME) was used to measure the electrocapillary curve. All the measurements were made at 25 ± 0.3°C.

Preparation of thin mercury film glassy carbon electrode

A glassy carbon disc electrode was polished using a polishing cloth with an alumina slurry (particle size 1 μm) and rinsed with ethanol, 0.1 M nitric acid and 0.1 M hydrochloric acid and then distilled water. Potential cycling between +0.2 and −2 V vs. SCE at 0.5 V s^{-1} was performed in 0.02 M hydrochloric acid. The TMFGCE was prepared by plating a mercury film at 750 rpm in 2 mM $Hg(NO_3)_2$ solution containing 0.02 M nitric acid at −0.5 V. The surface area and the thickness of mercury film of the electrode were 0.2 cm^2 and 0.4 μm, respectively.

Procedure

A 50-ml volume of supporting electrolyte (0.1 M KNO_3 containing 0.01 M HOAc–KOAc buffer of pH 6) and 2 mg of HA was pipetted into a glass cell and deaerated with nitrogen for 15 min. A 25-μl volume of 1 mM copper(II) standard solution was added to the supporting electrolyte with a micro-pipette and then the solution was stirred by rotating the TMFGCE (750 rpm) for 3 min. The conditioning potential (+0.05 V) was applied for 30 s, then the deposition potential at −0.5 V was applied for 150 s with rotation of the TMFGCE at 750 rpm. After the rest time (30 s at deposition potential, no rotation of the electrode), the potential was linearly scanned at 75 mV s^{-1}

to 0.2 V and the anodic wave of copper(II) was recorded.

Electrocapillary curve

From the electrocapillary curve, the interfacial tension, γ, was calculated according to the following equation:

$$\gamma = (\rho_{Hg} - \rho_{soln}) m\tau / 2\pi r \rho_{Hg} \quad (1)$$

where m is the flow-rate (mg s^{-1}) of Hg from the capillary, ρ_{Hg} and ρ_{soln} are the densities of Hg and the solution, respectively, τ is the drop time of the mercury drop (s), and r is the radius of the capillary (0.052 mm). The mercury column height was 70 cm.

RESULTS AND DISCUSSION

Stripping voltammograms of labile copper(II) species in the presence of HA

The effect of various surfactants on the anodic waves of copper(II) by cyclic voltammetry was investigated in the absence and presence of HA. From Table 1, it appears that the addition of SDS is useful, because (i) no interference with the electrode reaction of copper(II), (ii) no complexation with copper(II) and (iii) no interaction with HA is observed.

The stripping voltammograms of labile copper(II) species in the presence of HA are shown in Fig. 1. A broad anodic wave was obtained in the absence of SDS (Fig. 1c). This was due to the adsorption of HA on the electrode and then the electrode reaction of copper(II) was interfered with by the adsorption of HA. However, a sharp anodic wave was obtained in the presence of SDS (Fig. 1d) together with an increase in peak area of about 30%. Therefore, adding SDS seems to be useful in eliminating the negative effect of HA on the measurement of labile copper(II) by ASV.

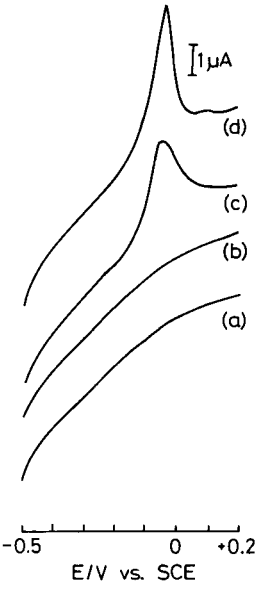

Fig. 1. Stripping voltammograms. Cu(II), 5 μM; HA, 40 mg l^{-1}; SDS, 2×10^{-3}%; deposition time, 150 s, 75 mV s^{-1}; supporting electrolyte, 0.1 M KNO_3 + 0.01 M HOAc–KOAc buffer (pH 6). (a) Supporting electrolyte + HA; (b) (a) + SDS; (c) (a) + Cu(II); (d) (c) + SDS.

TABLE 1

Effect of various surfactants on the anodic peak of 0.1 mM copper(II)

Surfactant	i_p [a] (μA)	Anodic wave with HA [b]	Interaction with HA [c]	Complexation with Cu(II)
None	14	Broad	–	–
SDS	14	Sharp	No	No
SDBS	12	Broad	No	No
DTAC	10	Broad	Yes	No
Trition X-100	9.3	Broad	No	Yes [20]
PVA	13	Broad	No	Yes [25]

[a] Anodic peak currents in the absence of HA; surfactants, 0.01%. [b] HA, 0.2 g l^{-1}; surfactants, 0.01%. [c] Identified by comparing the absorbance of HA (at 400 nm) in the presence of surfactants with the absorbance in the absence of surfactants; HA, 40 or 200 mg l^{-1}; surfactants, 0.01%.

The anodic peak current for ASV with a rotating disc electrode, i_p, is represented as follows [26]:

$$i_p = k\omega^{1/2} t v C_B \quad (2)$$

where k, ω, t, v and C_B are a constant, rotation speed, deposition time, scan rate and bulk concentration of analyte, respectively. When the peak currents were measured in the absence or presence of HA, the anodic peak current was proportional to the scan rate (v = 10–100 mV s^{-1}) and square root of the rotation speed (ω = 200–2000 rpm), as expected from Eqn. 2. Therefore, the

peak current is based on a diffusion-controlled process. In the present work, a rotation speed of 750 rpm was chosen because of the stability of the mercury film. Also, in the absence of HA, the peak current was proportional to concentration of copper(II) (0.1–10 μM) even if SDS was added. The concentration of labile copper(II) species was calculated by using this calibration graph.

Pseudo-polarograms of copper(II)

The pseudo-polarograms of copper(II) in the absence of HA (Fig. 2a and b) and in the presence of HA (Fig. 2c and d) are shown. From the limiting current, it can be calculated that about 20–30% of copper(II) exists as ASV-labile species in the presence of HA.

In the absence of HA (Fig. 2a and b), the half-wave potential without SDS is in good agreement with that with SDS. From this result, it can be concluded that the adsorption of SDS on the TMFGCE does not interfere with the electron-transfer reaction of copper(II). However, in the presence of HA the half-wave potential without SDS was 31 mV more negative than that with SDS. This suggests that the electron-transfer reaction of copper(II) was interfered with by the adsorption of HA on the TMFGCE.

Moreover, in the presence of HA, the limiting current with SDS (Fig. 2d) was higher than that without SDS (Fig. 2c). The decrease in the limiting current without SDS would cause the amount of the copper(II) plated on the TMFGCE to decrease during the deposition time because of

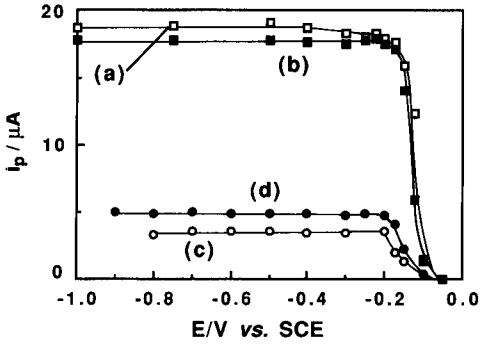

Fig. 2. Pseudo-polarograms of copper(II). HA, 40 mg l^{-1}; SDS, 1×10^{-3}%; deposition time, 150 s. (a) 5 μM Cu(II); (b) (a) + SDS; (c) (a) + HA; (d) (b) + HA.

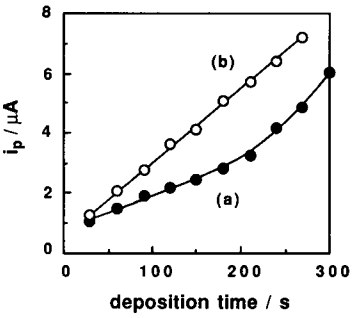

Fig. 3. Effect of deposition time. Cu(II), 5 μM; HA, 40 mg l^{-1}; pH, 6; SDS, 1×10^{-3}%; deposition potential, −0.5 V. (a) Without SDS; (b) with SDS.

the adsorption of HA on the TMFGCE. These observations suggest that the adsorption of HA on the electrode could be eliminated by the addition of SDS.

Effect of deposition time

The relationship between deposition time and peak current was investigated in the presence of HA, as shown in Fig. 3. A non-linear relationship was obtained in the absence of SDS, contrary to Eqn. 2. This may be caused by less adsorption of HA with increasing deposition time. Moreover, Shuman and Woodward [12] pointed out that chemical dissociation of the metal–ligand complex during the deposition time contributed to the stripping current. Therefore, the non-linear relationship in Fig. 3a may also be due to the dissociation of copper(II)–HA complex during the deposition time. However, a linear relationship was obtained in the presence of SDS (Fig. 3b). Therefore, addition of SDS seems to eliminate the interference of HA.

Electrocapillary curves

As already pointed out, problems due to adsorption of HA on the electrode were encountered. The addition of SDS seems to eliminate these interferences. To verify the effect of SDS, electrocapillary curves were investigated with a dropping mercury electrode (Fig. 4). The electrocapillary maximum (ecm) in the presence of SDS (Fig. 4c) was almost the same as that in the presence of HA and SDS (Fig. 4d), showing that

SDS could adsorb more strongly than HA on the electrode. Therefore, the adsorption of HA on the mercury electrode could be eliminated by adding SDS.

Further, the differential coefficient of the electrocapillary curve, $\partial\gamma/\partial E$, which is equivalent to the electrode surface charge density, q, as given by Lippmann's law, $\partial\gamma/\partial E = -q$, was calculated. In the positive potential region with respect to the ecm, $\partial\gamma/\partial E$ is usually negative. Hence q was positive, and anionic species in the solution are apparently collected in the diffusion layer. The higher is $\partial\gamma/\partial E$, the more anionic species are present in the diffusion layer. $\partial\gamma/\partial E$ in the presence of SDS (Fig. 4c and d) was lower than that in the absence of SDS (Fig. 4a and b) beyond the ecm. This suggests that the amounts of anionic species such as HA in the diffusion layer decreased on addition of SDS. Hence it was found that SDS adsorbed on the electrode had an anion-exclusion effect. This effect of SDS would be useful in preventing the adsorption of anionic species such as the copper(II)–HA complex or HA on the electrode during the deposition time.

Effect of SDS concentration

The effect of the concentration of SDS on the peak currents was investigated in the range of $0–2 \times 10^{-2}$% (Fig. 5). The anodic peak currents remained constant in the range $5 \times 10^{-4}–2 \times 10^{-2}$% (Fig. 5a). Figure 5b shows that the peak currents increase with increasing SDS concentration. This result suggests that the amounts of HA adsorbed on the electrode decrease with increasing SDS.

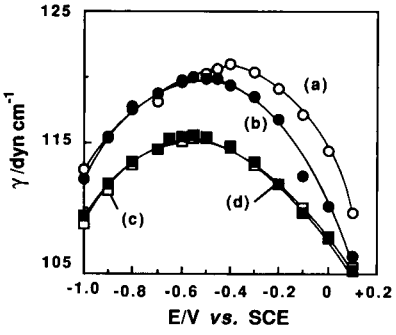

Fig. 4. Electrocapillary curves. HA, 40 mg l^{-1}; SDS, 1×10^{-3}%; supporting electrolyte, 0.1 M KNO_3 + 0.01 M HOAc–KOAc buffer (pH 6). (a) Supporting electrolyte only; (b) (a) + HA; (c) (a) + SDS; (d) (c) + HA.

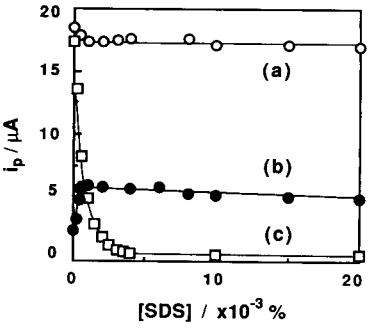

Fig. 5. Effect of SDS concentration. Deposition time, 150 s; deposition potential, −0.5 V. (a) 5 μM Cu(II); (b) (a) + 40 mg l^{-1} HA; (c) (a) + 5 μM NTA.

The effect of SDS was also studied by use of NTA as a model ligand. Figure 5c shows that the peak currents decrease with increasing SDS concentration. This can be attributed to the dissociation of the copper(II)–NTA complex in the diffusion layer at the lower SDS concentration [23]. Moreover, from the pseudo-polarograms of the copper(II)–NTA complex it can be seen that the half-wave potential shifted about 0.5 V in the negative direction in the presence of SDS. Therefore, it was concluded that SDS adsorbed on the electrode could prevent the direct reduction of the copper(II)–NTA complex.

Further, measurements of labile copper(II) species were made with 1×10^{-3}% SDS in the presence of HA and with 5×10^{-3}% SDS in the presence of NTA (Fig. 5b and c).

Copper(II) titration curves of NTA

The copper(II) titration curves of NTA are shown in Fig. 6. The titration curve in Fig. 6a is linear and does not show an end-point. In this case, most of the copper(II) was ASV labile because of the dissociation of the copper(II)–NTA complex in the electrode diffusion layer. However, in the presence of SDS, the titration curve shows a clear end-point (Fig. 6b). Moreover, the concentration of NTA added, 10 μM, was in good agreement with the concentration evaluated from the titration curve, 9.7 ± 0.4 μM ($n = 3$).

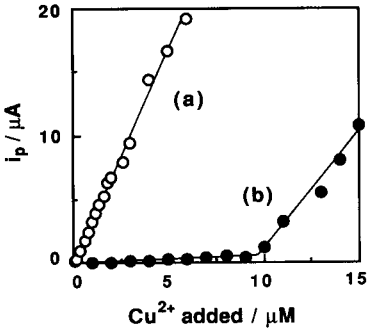

Fig. 6. Copper(II) titration curves of NTA. NTA, 10 μM; pH, 6; deposition time, 150 s; deposition potential, −0.5 V. (a) Without SDS; (b) with 5×10^{-3}% SDS.

Therefore, the addition of SDS is useful for the copper(II) titration of NTA in the presence of HA.

Evaluation of copper(II) complexing abilities of HA

The copper(II) complexing abilities of HA were evaluated by the copper(II) titration method. The conditional stability constants of the copper(II)–HA complex and the copper(II) complexing capacities were evaluated by a Scatchard approach as described in previous papers [24,27]. The relationship between the conditional stability constant, K', and copper(II) complexing capacity, N, can be written as

$$([Cu^{2+}]_t - [Cu^{2+}]_{labile})/[Cu^{2+}]_{labile} = -K'([Cu^{2+}]_t - [Cu^{2+}]_{labile}) + K'N \quad [HA\ added\ (g\ l^{-1})] \qquad (3)$$

where $[Cu^{2+}]_t$ and $[Cu^{2+}]_{labile}$ represent total and labile copper(II) concentration, respectively.

TABLE 2

Copper(II) complexing abilities at pH 6

Parameter	Without SDS	With SDS
Log K_1'	6.6	6.1
Log K_2'	5.8	5.4
N_1 [a]	160± 8	135±5
N_2	118± 6	85±3
N_1+N_2	278±14	220±8

[a] Cu(II), μmol per g HA.

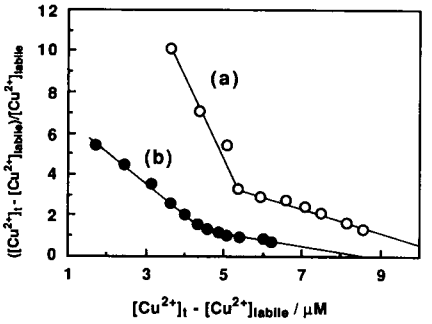

Fig. 7. Scatchard plot of HA. HA, 40 mg l^{-1}; pH, 6. (a) Without SDS; (b) With 1×10^{-3}% SDS.

From the linear relationship between $([Cu^{2+}]_t - [Cu^{2+}]_{labile})/[Cu^{2+}]_{labile}$ and $([Cu^{2+}]_t - [Cu^{2+}]_{labile})$, K' and N can be evaluated.

A Scatchard plot for HA is shown in Fig. 7. The Scatchard plot could be divided into two linear sections. Therefore, a two-site model was adopted, and then the conditional stability constants (K_1', K_2') and the complexing capacities (N_1, N_2) for each site were calculated by Eqn. 3 (Table 2). In the absence of SDS, the log K' values were higher than those with SDS and the total complexing capacity, N_1+N_2, was about 16% higher than that with SDS. Therefore, the values in the absence of SDS are overestimated.

In conclusion, addition of SDS could prevent the adsorption of HA on the electrode and is therefore a useful method for measuring the labile copper(II) species and subsequently for evaluating the copper(II) complexing ability of HA by ASV with a mercury electrode. Moreover, the amount of HA (2 mg) consumed in the copper(II) titration when using ASV detection was much lower than that in other methods (about 20 mg) [24,27]. Also, the copper(II) titration by ASV will be useful for the evaluation of copper(II) complexing abilities of small amounts of HAs.

REFERENCES

1 T.M. Florence, Talanta, 29 (1982) 345.
2 E.S. Nielsen and S. Wium-Anderson, Mar. Biol., 6 (1972) 93.
3 E.W. Davey, M.J. Morgan and S.J. Erickson, Limnol. Oceanogr., 18 (1973) 993.

4 M. Fukushima, S. Tanaka and M. Taga, Nikkashi, (1991) 556.
5 K.W. Hanck and J.W. Dillard, Anal. Chim. Acta, 89 (1977) 329.
6 T.M. Florence, Anal. Chim. Acta, 119 (1980) 217.
7 A. Nelson, Anal. Chim. Acta, 169 (1985) 273.
8 A. Nelson, Anal. Chim. Acta, 169 (1985) 287.
9 T.M. Florence and G.E. Batley, Anal. Chem., 52 (1980) 1962.
10 J.E. Gregor and K.J. Powell, Anal. Chim. Acta, 211 (1988) 141.
11 J. Wang, Stripping Analysis, VCH, New York, 1985, pp. 104–106.
12 M.S. Shuman and G.P. Woodward, Anal. Chem., 45 (1973) 2032.
13 E.E. Stewart and R.B. Smart, Anal. Chem., 56 (1984) 1131.
14 R.B. Smart and E.E. Smart, Environ. Sci. Technol., 19 (1985) 137.
15 J. Wang and L.D. Hutchins-Kumar, Anal. Chem., 58 (1986) 402.
16 B. Hoyer, T.M. Florence and G.E. Batley, Anal. Chem., 59 (1987) 1608.
17 G.M.P. Morrison and T.M. Florence, Anal. Chim. Acta, 209 (1988) 97.
18 G.M.P. Morrison and T.M. Florence, Electroanalysis, 1 (1989) 107.
19 G.M.P. Morrison and T.M. Florence, Electroanalysis, 1 (1989) 485.
20 G.M.P. Morrison, T.M. Florence and J.L. Sauber, Electroanalysis, 2 (1990) 9.
21 T. Ohsaka, H. Yamamoto and T. Yoshida, Bull. Chem. Soc. Jpn., 46 (1973) 1320.
22 T. Ohsaka, K. Nagasawa and T. Yoshida, Denki Kagaku, 44 (1976) 674.
23 S. Tanaka, Y. Morimoto, M. Taga and H. Yoshida, Talanta, 30 (1983) 867.
24 M. Taga, S. Tanaka and M. Fukushima, Anal. Sci., 5 (1989) 597.
25 W. Lund and M. Salberg, Anal. Chim. Acta, 76 (1975) 131.
26 N. Hojo and H. Shirai, Nikkashi, (1972) 1316.
27 M. Taga, S. Tanaka and M. Fukushima, Anal. Chim. Acta, 244 (1991) 281.

Analytica Chimica Acta, 270 (1992) 161–171
Elsevier Science Publishers B.V., Amsterdam

Cobalt-based glassy carbon chemically modified electrode for constant-potential amperometric detection of carbohydrates in flow-injection analysis and liquid chromatography

Tommaso R.I. Cataldi, Innocenzo G. Casella and Elio Desimoni

Dipartimento di Chimica, Università degli Studi della Basilicata, Via N. Sauro 85, 85100 Potenza (Italy)

Taddeo Rotunno

Dipartimento di Chimica, Università degli Studi di Bari, Via Re David Trav. 200, 70126 Bari (Italy)

(Received 2nd January 1992; revised manuscript received 8th June 1992)

Abstract

A cobalt-based glassy carbon (Co/GC) chemically modified electrode (CME) is described for use as an amperometric detector in the flow analysis of mono-, di- and trisaccharides. The preparation of the electrode is very easy and rapid. As with copper- and nickel-based glassy carbon electrodes, the Co/GC CME allows the electrocatalytic oxidation of scarcely electroactive compounds without recourse to pulsed waveform potentials. Hence, constant-potential amperometric detection is feasible and it has been applied successfully to reducing and non-reducing sugars. The chemical nature of cobalt species on glassy carbon was investigated using x-ray photoelectron spectroscopy and the results indicate that a Co(III) oxide hydroxide is present on the glassy carbon surface. However, electrochemical detection in an alkaline mobile phase of aliphatic organic compounds seems to take place through mediation of Co(IV) species produced from the oxidation of Co(III) during anodic polarization. Carbohydrates and related polyhydroxy compounds were determined at the micromolar level with an operating potential of 0.50 V vs. Ag/AgCl after anion-exchange chromatographic separation. The detector responds linearly to an increase in glucose concentration with a linear dynamic range that extends over three orders of magnitude (0.5 μM–0.5 mM).

Keywords: Amperometry; Flow injection; Liquid chromatography; Carbohydrates; Chemically modified electrodes; Cobalt-based electrodes

Generally, several schemes for the detection of carbohydrates after separation by liquid chromatography (LC) with an anion-exchange stationary phase can be adopted. However, refractive index detectors lack sensitivity and UV–visible photometric detection, following postcolumn derivatization, is more tedious and scarcely appealing. In the last few years, a detection scheme based on double- and triple-step potential waveforms, pioneered by Johnson and co-workers [1,2], has increased in popularity. Pulsed amperometric detection at platinum and gold electrodes has

Correspondence to: T.R.I. Cataldi, Dipartimento di Chimica, Università degli Studi della Basilicata, Via N. Sauro 85, 85100 Potenza (Italy).

been applied to several classes of organic compounds [3–5], showing good detection limits and long-term stability. The major disadvantage, however, is the need to dedicated instrumentation not commonly available in all laboratories.

Recently, the development of chemically modified electrodes (CMEs) to be used as amperometric detectors in flow-injection analysis (FIA) and LC has received growing attention [6–16]. Such electrodes permit the direct detection of non- or weakly chromophoric compounds operating at a constant applied potential. Significant efforts have been made to obtain modified substrates able to mediate electron reactions kinetically unfavourable at unmodified electrodes and/or hindered by gradual fouling of the surface. In the first reports [6–8] on modified glassy carbon electrodes, the catalytic activity towards polyhydroxy compounds was obtained with copper CME in basic media. Recently, a nickel-based glassy carbon (Ni/GC) CME [10,11] was successfully applied in LC with electrochemical detection (ED) of carbohydrates in real samples (milk and fruit juices). The catalytic oxidation process of scarcely electroactive compounds at a Ni/GC CME occurs on electrooxidation of the Ni(II) oxide to Ni(III) oxide hydroxide (NiOOH) and takes place at 0.4–0.5 V vs. Ag/AgCl. This is in agreement with previous reports [17,18] that metal(III) species in alkaline solution act as an electron-transfer mediator between the electrode surface and substrate molecules.

Pletcher et al. [19] reported that cobalt metal shows catalytic properties similar to those of nickel electrodes towards the electrooxidation of organic compounds in alkaline media. Recently, Luo et al. [16] reviewed the use of several electrode materials for amperometric detection, showing that cobalt electrodeposited on a glassy carbon substrate can also be used in flow-injection experiments. However, the low detection limit reported for glucose in FIA was accomplished with short-term electrode stability only. This paper reports the use of a cobalt-based glassy carbon electrode (Co/GC), obtained by modifying the surface of a conventional glassy carbon with a film of cobalt oxides and/or hydroxides formed after casting a cobalt(II) nitrate solution, drying, and subsequent electrooxidation in alkaline solution (0.20 M NaOH). Glassy carbon represents a very suitable substrate for metal oxides and hydroxides because it allows the incorporation of the catalytic deposit. X-ray photoelectron spectroscopy (XPS) of the Ni/GC CME [11] demonstrated that the deposit of nickel oxide hydroxide is either present on the surface or mechanically entrapped in the first few layers. Additionally, glassy carbon retains most of its advantages as an electrode material, including increased reversibility for several redox couples, a large anodic window and a short stabilization time compared with many metal electrodes.

In this work, the cyclic voltammetric behaviour in the presence of mono- di- and trisaccharides and the XPS results on the Co/GC CME indicated that Co(IV) is present on the electrode surface under conditions of electrochemical detection and it is responsible for the electrocatalytic oxidation of carbohydrates.

The Co/GC CMEs exhibit a stable response towards mono-, di- and trisaccharides, and represent a new example of a modified electrode requiring an alkaline medium for maximum sensitivity. Its analytical usefulness as an amperometric detector is demonstrated after anion-exchange separations of carbohydrates with an alkaline mobile phase. The cobalt high oxidation state surface oxide acts as an electrocatalytic sensing species of scarcely electractive compounds so, as in the case of copper- and nickel-based glassy carbon CMEs, it is capable of oxidizing several groups of analytes such as polyhydroxy compounds, reducing and non-reducing sugars, amino acids [20] and many other organic compounds.

EXPERIMENTAL

Reagents

All the solutions were prepared from deionized, doubly distiled water. Carbohydrate samples were purchased from Aldrich and used as received. A solution of 0.20 M sodium hydroxide was prepared from carbonate-free 50% NaOH and was used for all cyclic voltammetric (CV), FIA and LC experiments. Owing to the slow

decomposition of carbohydrates in alkaline media, stock solutions were prepared daily just prior to measurement. Test solutions of carbohydrates were prepared by diluting with 0.20 M NaOH appropriate volumes of the stock solutions. $Co(NO_3)_2 \cdot 6H_2O$ from Carlo Erba was used as received. Cobalt foil (Gold Label, 99.99 + %) and cobalt(II) oxide were purchased from Aldrich and cobalt(II,III) oxide was obtained from Fluka. All other chemicals were of analytical-reagent grade and were used as received. Where applicable, dissolved oxygen was removed by purging with reagent-grade nitrogen (99.99%). Glassy carbon plates (Sigradur K), used for XPS investigations, were obtained from HTW Hochtemperatur-Werkstoffe (Meitingen, Germany).

Instrumentation

An EG & G Princeton Applied Research Model 273 potentiostat/galvanostat was used for CV coupled to an Ericsson WS286 IBM-compatible personal computer. The 270 electrochemical analysis software (EG&G PAR) was used for data acquisition. The constant-potential detection system used consisted of an EG&G PAR Model 400 electrochemical detector. The current signal of the electrochemical detector was output to an Amel Model 868 strip-chart recorder.

Glassy carbon electrodes used for CV (MF-2012) and flow experiments (MF-1000) were purchased from Bioanalytical Systems (West Lafayette, IN). A conventional three-electrode cell was used for the batch experiments. The cell assembly consisted of a Co/GC CME, a silver chloride reference electrode and a platinum auxiliary electrode. The potentials were measured and are quoted with respect to the Ag/AgCl (4 M Cl^-). The thin-layer electrochemical flow cell consisted of a dual glassy carbon working electrode assembled in a parallel configuration, an Ag/AgCl reference electrode and a stainless-steel auxiliary electrode.

The flow-injection and chromatographic systems consisted of a Varian Model 2510 pump equipped with a Rheodyne (Berkeley, CA) Model 7125 sample injection valve with a 10-μl sample loop. All chromatographic separations were performed with a Carbopac PA1 (Dionex, Sunnyvale, CA) anion-exchange column (250 mm × 4 mm i.d., particle size 10 μm). The mobile phase was 0.20 M NaOH and the flow-rate was 1.0 ml min^{-1}. All experiments were run at 22 ± 1°C.

XPS measurements

X-ray photoelectron spectra were collected with a Leybold LH X1 spectrometer interfaced to an Olivetti M240 personal computer for data acquisition [21]. Spectra were obtained using the $K\alpha_1,\alpha_2$ radiation (1486.6 eV) operating at 180 W (12 kV, 15 mA). All the spectra were recorded under similar conditions: pressure always $< 10^{-8}$ mbar, FAT mode of operation with 50 eV pass energy, 0.1 eV channel width and 0.5 s dwell time. Co $2p$ regions were averaged over at least sixteen scans in order to improve the signal-to-noise ratio. The binding energy (*BE*) scale of the spectrometer was calibrated with respect to the Cu $2p_{3/2}$ (932.7 eV, FWHM 1.75 eV) and Au $4f_{7/2}$ (84.0 eV, FWHM 1.20 eV) signals using spectroscopically pure metals (Johnson Matthey, Royston, UK). The *BE* of Co species were calibrated with reference to the graphite C $1s$ peak after setting its *BE* to 284.6 eV. CoO and Co(II,III) oxide powder samples were mounted on conductive copper tape and corrections to the *BE* values for charging were made using the carbon C $1s$ peak at 285.2 eV (i.e., the peak due to adventitious carbon). XPS data were analysed with an in-house data-processing program [21].

Working electrodes

Cobalt-modified electrodes were prepared by casting 5 μl of 50 mM Co(II) nitrate solution on a clean glassy carbon surface. The electrode (face up) was dried in an air oven at ca. 60°C for ca. 30 min and was ready for use after rinsing thoroughly with deionized water. In flowing stream experiments, the Co/GC CME was assembled in the thin-layer flow cell. After a potential of +0.5 V vs. Ag/AgCl under flow conditions had been applied in order to reach a stable baseline current, the system was ready to serve as an electrochemical detector. Prior to each electrode modification, traces of cobalt deposit were removed from the glassy carbon surface by sonication in

concentrated ammonia and polishing with alumina powder on a polishing micro-cloth.

RESULTS AND DISCUSSION

Voltammetry

Figure 1 shows (A) the first and (B) the third cyclic voltammogram obtained with the Co/GC electrode in 0.20 M NaOH and at a scan rate of 50 mV s^{-1}. The main feature of the Fig. 1 is that the large anodic peak at about 0.3 V decreased on consecutive cycling. There is a corresponding cathodic wave but it is always lower and smaller. At potentials more positive than 0.6 V a large anodic current is present due to evolution of oxygen gas.

On the first scan towards positive potentials, the cobalt species on the GC underwent a redox process between −0.05 and +0.30 V vs. Ag/AgCl. During continued cycling the peak separation of the redox couple (curve C in Fig. 1) increased owing to the progressive shift of the anodic peak towards more positive values. Moreover, anodic and cathodic peaks became smaller, reaching a steady-state condition after about 50 cycles performed between −0.3 and +0.7 V. Unless the actual conditions of the glassy carbon surface were carefully controlled by thorough polishing and sonication pretreatment in concentrated ammonia, the peak intensities and peak separation during the initial scans were not very reproducible. Behl and Toni [22] reported four anodic peak potentials at cobalt metal electrodes referenced with respect to Hg/HgO in 0.2 M KOH solution. Using CV at stationary disc electrodes, they attributed the first peak (E_{pA} = −0.50 V) to the oxidation of cobalt to cobalt(II) hydroxide, the second (E_{pA} = +0.10 V) to the formation of an intermediate oxide, Co_3O_4, the third to cobalt(III) oxide hydroxide formation (E_{pA} = +0.34 V) and the final transition to the conversion Co(III) → Co(IV) (E_{pA} = +0.50 V). Apart from the first electrochemical oxidation, Co(0) → Co(II), the last three processes can be written as follows:

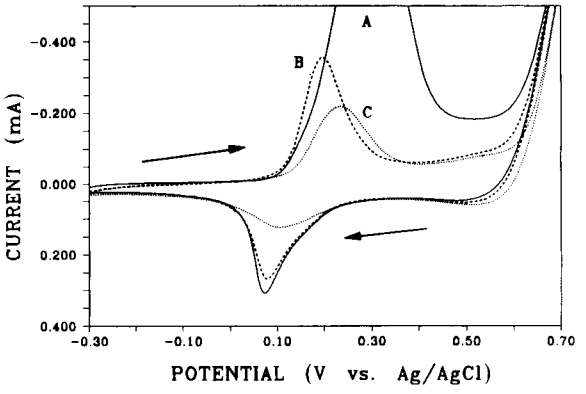

Fig. 1. Cyclic voltammograms at a Co/GC CME in 0.20 M NaOH blank solution at 22°C: (A) 1st cycle, (B) 3rd cycle and (C) steady-state condition, after about 50 cycles. Scan rate, 50 mV s^{-1}.

$$3Co(OH)_2\,(s) + 2OH^- \rightarrow Co_3O_4\,(s) + 4H_2O + 2e^- \quad (1)$$

$$Co_3O_4\,(s) + H_2O + OH^- \rightarrow 3CoO(OH)\,(s) + e^- \quad (2a)$$

$$Co(OH)_2\,(s) + OH^- \rightarrow CoO(OH)\,(s) + H_2O + e^- \quad (2b)$$

and/or

$$CoO\,(s) + OH^- \rightarrow CoO(OH)\,(s) + e^- \quad (2c)$$

and

$$CoO(OH)\,(s) + OH^- \rightarrow CoO_2\,(s) + H_2O + e^- \quad (3)$$

On the basis of the Co/GC electrode behaviour in CV, the anodic peak at about 0.2 V vs. Ag/AgCl may well be due to the formation of cobalt oxide hydroxide, CoO(OH), through oxidation either of the Co_3O_4 (Eqn. 2a) and/or cobalt(II) hydroxide (Eqn. 2b) or cobalt(II) oxide (Eqn. 2c), or both. The slow peak potential shift observed during electrochemical cycling suggests a gradual conversion of Co(II) to black Co(III), as is also indicated by visible inspection of the cobalt deposit. From the XPS results (see below), it seems most likely that reactions 2a and 2b com-

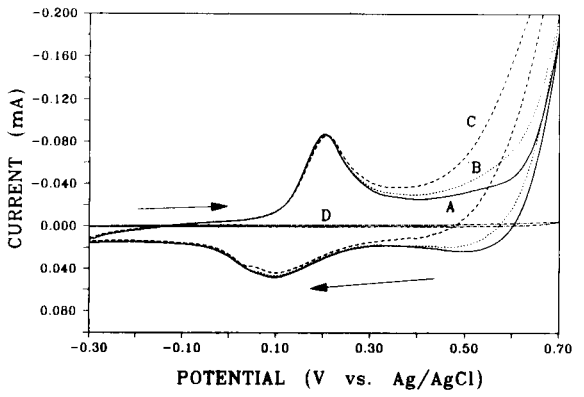

Fig. 2. Cyclic voltammograms at a Co/GC CME: (A) blank; (B) 2.0 mM fructose; (C) 4.0 mM fructose. Curve D represents the response at an unmodified glassy carbon electrode in the presence of 8 mM fructose. Scan rate, 50 mV s^{-1}.

pared with reaction 2c are of major importance for CoO(OH) formation, even though their extent is difficult to evaluate and is outside the scope of this work.

The final anodic transition which appeared prior to evolution of oxygen can be interpreted as being due to the oxidation of CoO(OH) to CoO_2 according to reaction 3. Previous studies by CV in alkaline media [23,24] have suggested that before oxygen evolution the surface of cobalt oxides is oxidized to Co(IV). On the Co-based GC electrode most of the anodic wave due the oxidation of carbohydrates and polyhydroxy compounds (i.e. sorbitol) is located just in the same potential range as the Co(III) → Co(IV) conversion. Examples of cyclic voltammograms obtained at a Co/GC CME in 0.20 M NaOH after additions of fructose at millimolar concentrations are shown in Fig. 2. Usually, stable voltammograms were observed after the third scan between −0.3 and +0.7 V (vs. Ag/AgCl) with the anodic waves starting at potentials more positive than that attributed to Co(III) oxide hydroxide formation. Also shown is the oxidation of fructose (curve D) at an unmodified glassy carbon electrode in the same alkaline solution; no CV peaks were observed for an 8 mM fructose concentration. The comparison of voltammograms A and D highlights the catalytic effect of the surface-confined high-valent cobalt oxides. Several other sugars and related compounds exhibited similar qualitative behaviour in CV to that described for fructose: a drawn-out wave instead of a peak. The compounds investigated included arabinose, glucose, lactose, sucrose, maltose, maltothreose and sorbitol. Figure 3(A) and (B) shows representative voltammetric responses in alkaline solution of a disaccharide [sucrose (5.0 mM)] and a trisaccharide [maltothreose (3.7 mM)], respectively. Reducing and non-reducing sugars yielded similar responses.

The dependence of the anodic peak potential (E_p) on pH was evaluated over the 0.003–0.5 M NaOH range using scan rate of 50 mV s^{-1} (Fig. 4). The ionic strength of solutions was kept constant ($I = 1.0$) by appropriate addition of $NaNO_3$. The slope of the E_p vs. pH plot is about 90 mV per pH unit. This value is higher than that ex-

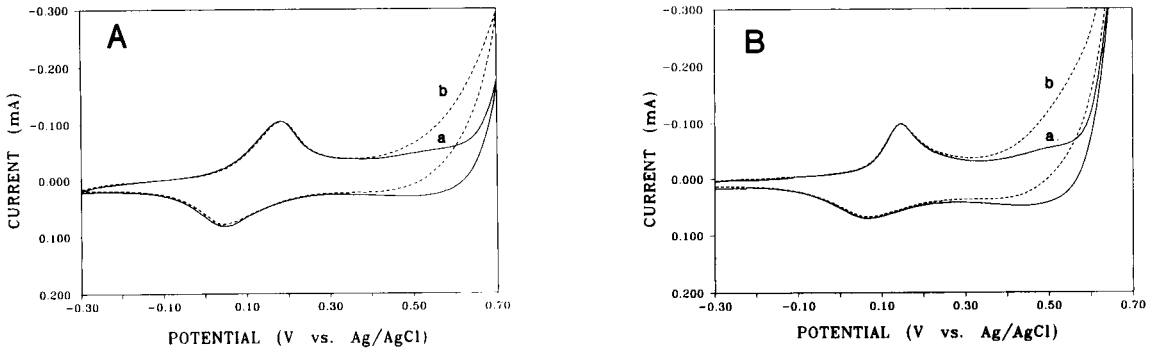

Fig. 3. Cyclic voltammograms at a Co/GC CME: (A) (a) blank and (b) 5.0 mM sucrose; (B) (a) blank and (b) 3.7 mM maltothreose. Scan rate, 50 mV s^{-1}.

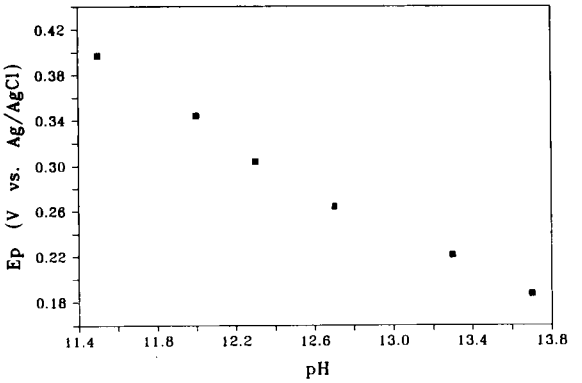

Fig. 4. Plot of anodic peak potential at a Co/GC CME as function of the solution pH. Constant ionic strength NaOH + $NaNO_3$ ($I = 1.0$); scan rate, 50 mV s^{-1}.

pected from reactions 2a–c but similar slopes are common when surface processes are involved [25]. They have been interpreted in terms of adsorption of intermediate hydroxyl radicals on the electrode surface [26]. Such an adsorption is pH dependent and should be responsible for the observed deviation from the classic Nernstian response. The shift of anodic peak potential is also accompanied by a decrease in peak current. At pH < 11.5 no signal was observed. Current values recorded at 0.50 V by CV in the presence of carbohydrates such as glucose, lactose and maltothreose (not shown) showed the same behaviour. Therefore, the carbohydrate oxidation mechanism is consistent with an electrocatalytic process [19] that mainly occurs at high pH and takes place in the potential range where high oxidation states of cobalt [i.e. Co(III) and Co(IV)] surface oxides and hydroxides are formed. To a great extent, the Co(IV) is most likely to be generated at 0.5 V vs. Ag/AgCl during electrochemical detection in flow analysis and is responsible for the catalytic process. This interpretation is also substantiated by observations in flow-injection experiments and XPS investigations, as will be discussed in more detail below.

X-Ray photoelectron spectroscopy

The examination of the chemical nature of cobalt species present on the electrode surface was accomplished by XPS. Figure 5 shows some representative Co $2p$ photoelectron spectra of Co_3O_4 oxide and of cobalt deposited on glassy carbon. Table 1 gives the binding energies (*BE*) of Co $2p_{3/2}$, $2p_{1/2}$ and $3s_{1/2}$ levels. In the same table are also reported the kinetic energies (*KE*) of the L_3VV Auger peak excited by x-rays and the relevant modified Auger parameter (α') ob-

TABLE 1

XPS data for cobalt species

	Binding energy (*BE*) [a] (eV ± 0.2)			*KE*(L_3VV) [b]	α' [c]
	Co $2p_{3/2}$	Co $2p_{1/2}$	Co $3s_{1/2}$		
Co foil (after sputtering)	778.2 (2.6) [d]	793.2	101.3 (4.3)	774.1	1552.3
Co(II,III) oxide [e]	780.2 (3.8)	795.6	102.9 (5.0)	772.3	1552.5
CoO [e]	779.8 (4.0)	795.3	102.5 (5.1)	772.5	1552.3
Co/GC, sample A [f]	781.4 (5.4)	796.9	102.5 (5.3)	770.4	1551.8
Co/GC, sample B [g]	780.9 (4.3)	796.8	103.2 (4.3)	770.8	1551.7
Co/GC, sample C [h]	780.0 (3.1)	795.1	102.6 (4.0)	772.6	1552.6

[a] Referenced to the graphitic C 1*s* 284.6 eV, Al $K\alpha_1,\alpha_2$ 1486.6 eV. [b] Auger line excited by x-rays (eV). [c] Modified Auger parameter: $\alpha' = KE(L_3VV) + BE(2p_{3/2})$. [d] The values in parentheses are the full width at half-maximum. [e] Referenced to the adventious carbon (C 1*s*, 285.2 eV). [f] Co/GC CME dried at 50°C and rinsed with water. [g] As sample A followed by immersion for 15 h in NaOH solution. [h] Co/GC CME after ca. 10 h of anodic polarization, 0.50 v (vs. Ag/AgCl) in 0.2 M NaOH.

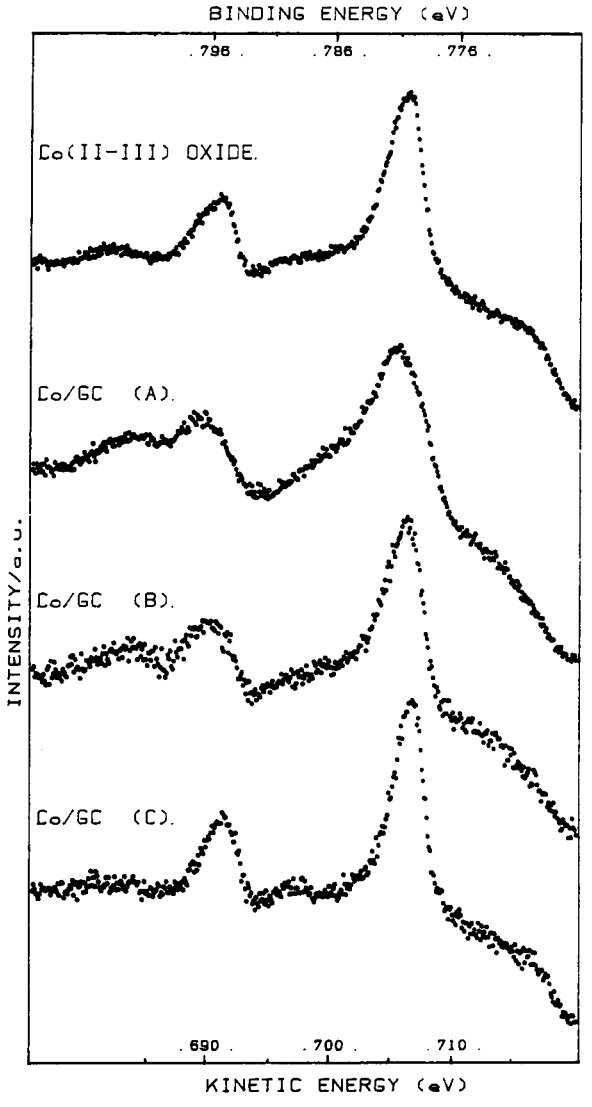

Fig. 5. X-ray photoelectron spectra of the Co $2p_{3/2}$ level for the following samples: top, Co(II,III) oxide powder; (A) Co CME dried at 50°C and thoroughly rinsed with distilled water; (B) Co CME, as sample A followed by immersion for 15 h in NaOH solution; (C) Co CME, anodic polarization at 0.50 V (vs. Ag/AgCl) for 10 h in 0.2 M NaOH.

tained by adding the *KE* of the L_3VV Auger level to the *BE* of Co $2p_{3/2}$ [27]. The XPS signal of nitrogen (N 1*s*) was always absent, suggesting that nitrate ions were completely removed during rinsing with distilled water.

As evidenced from the *BE* of the Co 2*p* and 3*s* levels, the assignment of cobalt chemical states is very difficult. Unfortunately, very similar binding energies are known [28] for most of cobalt oxides and hydroxides [i.e., Co_3O_4, CoO(OH), and CoO]. The Co $2p_{3/2}$ binding energies of CoO (779.8 eV) and Co(II,III) oxide (780.2 eV), in good agreement with values reported by McIntyre and Cook [28] and Schenck et al. [29], are indistinguishable from that of the Co/GC sample (C) (780.0 eV) which was held at applied potential of 0.50 V for ca. 10 h (see Table 1). In addition, either the Co $2p_{1/2}$–Co $2p_{3/2}$ spin–orbit splitting and the modified Auger parameter do not help much in identifying the chemical status of cobalt on GC. However, a detailed analysis of the Co 2*p* shake-up structure should allow the assignment of cobalt oxidation states [28–30]. In fact, the Co 2*p* X-ray photoelectron spectra of $Co(OH)_2$ and CoO are characterized by a satellite structure at high binding energies adjacent to the main photoelectronic peak. In contrast, Co(II,III) oxide shows only a very weak shape-up satellite structure at about 9 eV higher than the main Co(II) peak [30,31]. This is comparable to the very weak satellite peak observed in this study (Fig. 5).

After droplet evaporation of cobalt solution on the glassy carbon surface, drying and rinsing with purified water (sample A), the binding energies of Co $2p_{3/2}$ (781.4 eV) and Co $3s_{1/2}$ (103.5 eV) together with the satellite structure associated with the main peak indicate the presence of $Co(OH)_2$, as cobalt hydroxide (not shown) has a broad satellite structure centred at ca. 6 eV from the main peak. A noticeable decrease in the intensity of the satellite structure relative to the main photoelectric peak is evident for Co CME sample C (see Fig. 5). Early XPS studies on the cobalt oxides and hydroxides [28] indicated that Co(III) oxides exhibit a sharp Co 2*p* peak and absence of satellite structure compared with the pronounced tail observed for Co(II) samples. This XPS finding, even if not giving an ultimate answer on the chemical state of cobalt, supports the hypothesis that Co(III) is present on the glassy carbon substrate after anodic polarization (sample C). Notably, the full width at half maximum of Co $2p_{3/2}$ (3.1 eV) compares very well with the value of 3 eV reported by Schenck et al. [29].

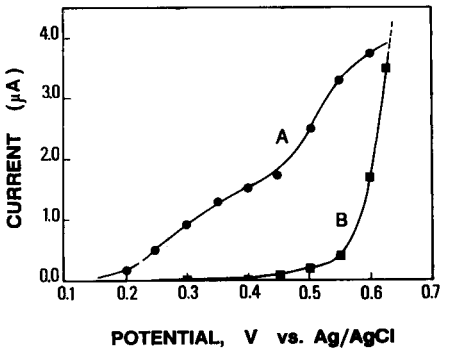

Fig. 6. (A) Hydrodynamic voltammogram in FIA at a Co/GC CME for 2 nmol of glucose injected. (B) Background current. Thin-layer cell with parallel-adjacent electrodes configuration. The injection volume was 10 μl and the electrolyte/carrier was 0.2 M NaOH; flow-rate, 1.0 ml min^{-1}.

Furthermore the Co(III) species is most likely present as the oxide hydroxide, CoO(OH), since its Co $2p_{3/2}$ line width is narrow whereas the peak of Co_2O_3 is as broad as those of the high-spin compounds CoO and $Co(OH)_2$ and should therefore be discounted.

FIA- and LC-electrochemical detection

The Co/GC CME was tested as an amperometric detector in flowing streams by using a conventional thin-layer cell configuration ordinarily employed in LC with electrochemical detection. Figure 6 shows the hydrodynamic voltammogram obtained under flow-injection conditions for 2 nmol of glucose injected. As expected from the CV data described above, an increasing electrocatalytic response was observed at oxidation potentials close to +0.25 V. In agreement with CV data, the hydrodynamic voltammogram further delineates the response of the cobalt-sensing electrode. Judging from this voltammogram (curve A in Fig. 6), a potential in the range +0.30–0.55 V is suitable for amperometric detection of glucose. On the basis of previous amperometric applications using Co–phthalocyanine (Co–PC)-containing carbon paste electrodes [12], one would have expected to see a decrease in catalytic response under constant potential operation. Surprisingly, very stable flow-injection signals were observed at the Co/GC electrode in the potential range +0.30–0.55 V vs. Ag/AgCl. This suggests that the Co–PC complex itself was most likely responsible for the passivation and subsequent decrease in catalytic activity. Although larger currents were obtained at potentials more positive than +0.55 V, the background current also increased (see curve B in Fig. 6) and the optimum signal-to-noise ratio was obtained at ca. 0.5 V. Interestingly, lower detection potentials can be used in flow-through analysis so to enhance the selectivity of the detector without significantly reducing the electrode sensitivity. This electrode behaviour is different from that previously observed at Ni/GC CMEs [11], where the electrocatalytic oxidation of carbohydrates appeared only at potentials more positive than 0.45 V vs. Ag/AgCl, i.e. in the potential region corresponding to Ni(II) oxidation. It is also important to note that the noise level at the glassy carbon electrode modified with Co or Ni oxide or hydroxide species remains essentially the same as that seen at the bare glassy carbon electrode.

In addition to the operating potential, the dependence of the Co/GC CME response on the flow-rate was evaluated by flow-injection analysis of glucose. The peak area decreased on increasing the flow-rate of the alkaline carrier (0.20 M NaOH) to 2.0 ml min^{-1}, after which it remained almost constant. Figure 7 illustrates such an effect for flow-rates ranging from 0.50 to 4.00 ml min^{-1} using 10 nmol of glucose injected into the

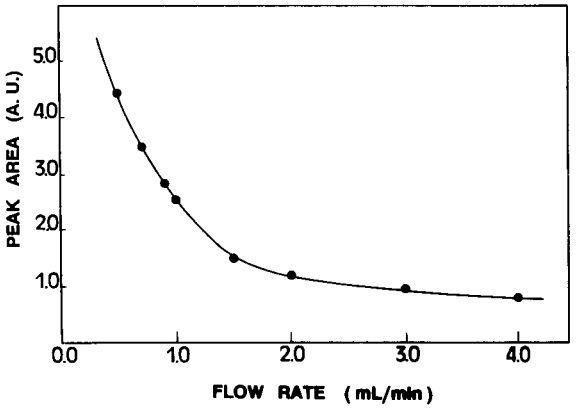

Fig. 7. Dependence of the peak area (arbitrary units) on the carrier flow-rate at Co/GC CME in flow-injection operation. E_{app}, +0.50 V vs. Ag/AgCl; 10 nmol of glucose injected; carrier, 0.2 M NaOH.

flow stream; a sharp decrease (ca. 60%) in peak area was observed between 0.50 and 1.50 ml min^{-1}. Probably, as with other catalytic electrodes, such as the nickel metal–oxide [18], ruthenium dioxide carbon paste [13], Cu-based GC [7] and Ni-based GC electrodes [11], the relatively slow catalytic reaction between the substrate and the Co-based GC electrode controls the overall process, so at high flow-rates the chemical step accounts for the observed decrease in peak area.

The Co/GC CME maintained its catalytic stability with repeated glucose exposures; representative responses for a set of flow injections of a test solution containing 200 μM glucose are shown in Fig. 8. Although only nine injections are presented, a stable response was maintained with subsequent injections. The average peak current and relative standard deviation for a series of fourteen injections were 2.23 μA and 1.6%, respectively. The long-term electrode stability and its applicability were studied during continuous chromatographic runs using a mixture of five sugars: arabinose (50 μM), fructose (100 μM), glucose (100 μM), lactose (200 μM) and sucrose (500 μM). The peaks heights for these analytes

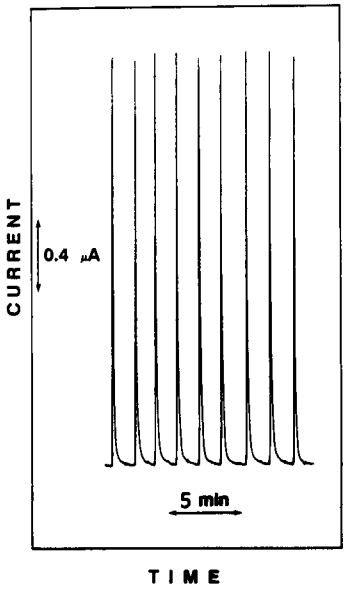

Fig. 8. Multiple flow-injection peaks of 2 nmol of glucose at a Co/GC CME: E_{app}, +0.50 V vs. Ag/AgCl; other experimental conditions as in Fig. 6.

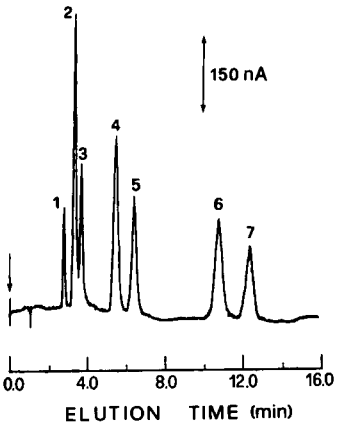

Fig. 9. Chromatogram of a mixture containing (1) 80 pmol of arabinose, (2) 160 pmol of glucose, (3) 160 pmol of fructose, (4) 320 pmol of lactose, (5) 400 pmol of sucrose, (6) 400 pmol of raffinose and (7) 400 pmol of maltose at a Co/GC CME (E_{app}, +0.50 V vs. Ag/AgCl). Column, Dionex Carbopac PA1 (250×4 mm i.d.); isocratic elution with 0.2 M NaOH; other experimental conditions as in Fig. 6.

yielded an average 7 ± 3% decrease in electrode response after more than 4 h of operating time, corresponding to twenty sample injections. Slight decreases in response are common with similar catalytic sensing electrodes. At a Cu CME electrode, a less than 10% decrease in activity was reported [6] after about 1 h and corresponding to 80 injections under flow-through conditions, whereas in earlier work with a Ni/GC CME [10] a comparable 5% was found after 4 h of operating time. It is assumed that the active catalyst is slowly lost from the electrode surface, thus accounting for the decrease in sensitivity during flowing stream operations. Accordingly, the CME was usually renewed after ca. 2 days of working time, during which, however, micromolar determinations of carbohydrates were normally accomplished.

The highest sensitivity for Co/GC CMEs is observed in alkaline media (see below) and ion chromatography can be conveniently used for carbohydrate separation [32–34]. Figure 9 shows the chromatogram obtained for a sample mixture containing monosaccharides (arabinose, glucose and fructose), disaccharides (lactose, sucrose and maltose) and a trisaccharide (raffinose). The capability of Co/GC amperometric detection and

TABLE 2

LC–ED of carbohydrates at the Co/GC CME [a]

Analyte	Capacity factor [b], k'	Linear range (μM) (10-μl loop)	n [c]	Slope (nA μM^{-1})	r^2 [c]	LOD [d] (ng)
Arabinose	1.6	0.4–500	6	11.3	0.999	0.6
Glucose	2.1	0.5–500	6	10.1	0.999	0.9
Lactose	4.0	0.8–250	4	4.6	0.998	2.7
Sucrose	4.9	1.4–250	4	2.4	0.998	4.8

[a] Amperometric detection at +0.50 V vs. Ag/AgCl. [b] Mobile phase, isocratic elution with 0.2 NaOH; column, Dionex Carbopac PA1 (250 4 × mm i.d., 10 μm). [c] n and r^2 represent the number of data points used for the least-squares analysis and the correlation coefficient, respectively. [d] LOD (limit of detection) is the amount that yields a signal current three times the background noise.

the effectiveness of the chromatographic separation are demonstrated by the high sensitivity and good resolution obtained with 13 min of elution time at +0.5 V vs. Ag/AgCl. The separation was effected with an anion-exchange stationary phase column and under isocratic elution with 0.20 M NaOH.

Tests were carried out in order to determine the dynamic range of concentrations over which the detector response is linear. This was evaluated by successive injections of a sample mixture of sugars containing arabinose, glucose, lactose and sucrose with an operating potential of +0.50 V vs. reference electrode. With glucose, for example, the electrocatalytic peak current increased linearly with concentration up to 0.5 mM; the slope of the resulting calibration plot ($n = 6$) corresponded to a sensitivity of 10.1 nA μM^{-1} (correlation coefficient 0.999). The signal-to-noise ratio of 3 indicated a detection limit for glucose of 0.5 μM, i.e., 0.9 ng in the 10-μl sample loop. Hence the Co/GC CME offers sensitivities comparable to that of the Cu CME [6] (0.22 ng) and better than that of the RuO_2 carbon paste [13] (2.8 ng) and Ni CME [11] (4 ng) types. Table 2 summarizes the results obtained for the other carbohydrates tested in this study.

Conclusion

The suitability of Co/GC CMEs as amperometric detectors of carbohydrates in flowing streams, including flow injection and liquid chromatography, has been explored. The electrocatalytic oxidation of carbohydrates in alkaline media resembles that demonstrated for metal nickel and copper- and nickel-based CME's. However, it is possible that in the present instance Co(IV) species are involved in the electrocatalytic oxidation process along with the oxide hydroxide of Co(III). The GC modification is very easy to make and should allow the use of other transition metal catalytic systems and/or various combination of metals such as Ni and Co.

The Co/CME shows excellent sensitivity towards reducing and non-reducing sugars, a wide linear dynamic range for all the compounds examined and appreciable time stability. Further, the Co/GC CME provides increased selectivity, as lower and constant-potential amperometric detection can be applied when interference problems arise. Because of its electrocatalytic capability towards a wide variety of scarcely electroactive compounds (sugars and sugar-related compounds), the determination of these substances in real samples is currently being investigated. The possibility of enhancing the long-term stability and means of gaining a deeper insight into the catalytic mechanism are under study.

This work was supported by the Italian National Research Council (CNR, Rome) and by the Ministero dell'Università e della Ricerca Scientifica e Technologica (MURST, Rome). Part of this work was presented at the 1991 Congresso dei Gruppi Interdivisionali della Società Chimica Italiana (CISCI), Chianciano Terme, October, 1991.

REFERENCES

1 S. Hughes, P.L. Meschi and D.C. Johnson, Anal. Chim. Acta, 132 (1981) 1.
2 D.C. Johnson and W.R. LaCourse, Anal. Chem., 62 (1990) 589A, and references cited therein.
3 J.A. Polta, D.C. Johnson and K.E. Merkel, J. Chromatogr., 324 (1985) 407.
4 G.G. Neuburger and D.C. Johnson, Anal. Chem., 59 (1987) 150.
5 W.R. LaCourse, D.C. Johnson, M.A. Rey and R.W. Slingsby, Anal. Chem., 63 (1991) 134.
6 S.V. Prabhu and R.P. Baldwin, Anal. Chem., 61 (1989) 852.
7 S.V. Prabhu and R.P. Baldwin, Anal. Chem., 61 (1989) 2258.
8 P. Luo, S.V. Prabhu and R.P. Baldwin, Anal. Chem., 62 (1990) 752.
9 J.M. Zadeii, J. Marioli and T. Kuwana, Anal. Chem., 63 (1991) 649.
10 I.G. Casella, E. Desimoni and A.M. Salvi, Anal. Chim. Acta, 243 (1991) 61.
11 I.G. Casella, E. Desimoni and T.R.I. Cataldi, Anal. Chim. Acta, 248 (1991) 117.
12 L.M. Santos and R.P. Baldwin, Anal. Chem., 59 (1987) 1766.
13 J. Wang and Z. Taha, Anal. Chem., 62 (1990) 1413.
14 Y. Yie and C.O. Huber, Anal. Chem., 63 (1991) 1714.
15 R.P. Baldwin and K.N. Thomsen, Talanta, 38 (1991) 1.
16 P. Luo, F. Zhang and R.P. Baldwin, Anal. Chim. Acta, 244 (1991) 169.
17 M. Fleischmann, K. Korinek and D. Pletcher, J. Electronanal. Chem., 31 (1971) 39.
18 R.E. Reim and R.M. Van Effen, Anal. Chem., 58 (1986) 3203.
19 D. Pletcher, K. Korinek and M. Fleischmann, J. Electroanal. Chem., 33 (1971) 478.
20 T.R.I. Cataldi, I.G. Casella and E. Desimoni, in preparation.
21 E. Desimoni and U. Biader Ceipidor, J. Electron Spectrosc. Relat. Phenom., 56 (1991) 189.
22 W.K. Behl and J.E. Toni, J. Electroanal. Chem., 31 (1971) 63.
23 R. Boggio, A. Carugati and S. Trasatti, J. Appl. Electrochem., 17 (1987) 828.
24 P. Rasiyah and A.C.C. Tseung, J. Electrochem. Soc., 129 (1982) 1724.
25 L.D. Burke, M.E. Lyons, E.J.M. O' Sullivan and D.P. Whelan, J. Electroanal. Chem., 122 (1981) 403.
26 G. Lodi, A. Daghetti and S. Trasatti, Mater. Chem. Phys., 8 (1983) 1.
27 C.D. Wagner, in D. Briggs and M.P. Seah (Eds.), Practical Surface Analysis, Vol. 1, Wiley, Chichester, 2nd edn., 1990, App. 5, p. 595.
28 N.S. McIntyre and M.G. Cook, Anal. Chem., 47 (1974) 2208.
29 C.V. Schenck, J.G. Dillard and J.W. Murray, J. Colloid Interface Sci., 95 (1983) 398.
30 R.B. Moyes and M.W. Roberts, J. Catal., 49 (1977) 216.
31 D.C. Frost, C.A. MacDowell and I.S. Woolsey, Mol. Phys., 27 (1974) 1473.
32 R.D. Rocklin and C.A. Pohl, J. Liq. Chromatogr., 6 (1983) 1577.
33 S.V. Prabhu and R.P. Baldwin, J. Chromatogr., 503 (1990) 227.
34 Y.C. Lee, Anal. Biochem., 189 (1990) 151.

Analytica Chimica Acta, 270 (1992) 173–179
Elsevier Science Publishers B.V., Amsterdam

Differential-pulse polarographic study of nicotinamide adenine dinucleotide at a dropping mercury electrode

Weiyuan Zhu

Chemistry Department, Southeast University, Nanjing 210018 (China)

Yingying Chen

Grain and Oil Sciences Department, Nanjing Food and Oil Economics Institute, Nanjing 210003 (China)

(Received 31st May 1991; revised manuscript received 8th July 1992)

Abstract

Differential-pulse polarography was applied in studies of the polarographic behaviour of nicotinamide adenine dinucleotide (NAD^+). The properties of the current of NAD^+ on a dropping mercury electrode are discussed and a CEC kinetic reduction process of NAD^+ on the electrode is proposed. It is recommended that the peak obtained under certain conditions could be used for the trace determination of this compound, with a detection limit of 5.0×10^{-7} mol l^{-1} in simple aqueous solution. In a solution containing 0.1 mol l^{-1} malonic acid (pH 2.30), a hydrogen catalytic current is observed with a peak potential of -1166 mV (vs. SCE). The electrode reduction occurs after protonation but before charge transfer. NAD^+ acts as a catalyst in the process

Keywords: Polarography; Nicotinamide adenine dinucleotide

The redox properties of nicotinamide adenine dinucleotide (NAD^+) and its reduced form (NADH) are very important in both biochemistry and clinical chemistry. The currents of this redox process with square-wave voltammetry and with polarography using a static mercury drop electrode as an indicator electrode have been well characterized [1–7]. Webber et al. [6] had studied NADH by differential-pulse polarography (DPP), but they obtained no response using a pulse amplitude of 25 mV. Sulaiman and Najeeb [8] detected NADH indirectly by DPP but they did not discuss the current properties. Webber and Osteryoung [7] investigated NAD^+ in acidic media with square-wave voltammetry and proposed a mechanism with a four-electron reduction of the adenine group being responsible for the wave at ca. -1.3 V. They proposed that the peak current corresponds to a diffusion-controlled adsorption process and the reduction process presumably to the reduction of the protonated adenine ring. However, they obtained a much smaller current peak at ca. -1.0 V than that for the four-electron reduction of the protonated adenine ring. They considered this one-electron reduction to be less useful for quantitative purposes.

In this work, DPP was used in the direct investigation of the reducing behaviour of NAD^+ on a dropping mercury electrode (DME). In a solution containing 0.1 mol l^{-1} malonic acid (pH 2.30), a reproducible and sensitive one-electron single peak was acquired at -1166 mV (vs. SCE). This peak corresponds to a hydrogen catalytic reduction process. The peak current is greater than that of a DPP reduction controlled by diffu-

Correspondence to: Weiyuan Zhu, Chemistry Department, Southeast University, Nanjing 210008 (China).

sion and adsorption processes, and is directly proportional to the concentration of NAD^+ in the range 5.0×10^{-7}–1.0×10^{-4} mol l^{-1}. This paper discusses the mode of reduction of NAD^+ in given electrode processes and puts forward a sensitive method for the detection of NAD^+ directly in aqueous solution.

EXPERIMENTAL

Apparatus

In all instances, a transistor integrated circuit polarograph (Model F-78, Fudan University) was used for the measurement of polarographic currents. Polarograms were recorded with a functional recorder (XWT-264) and potentials were monitored with a digital voltmeter (PZ-8). The values of the polarographic currents were calibrated by the DPP current (25°C) of Cd^{2+} ion under the same experimental conditions. The diffusivity of Cd^{2+} was assumed to be 7.15×10^{-6} cm^2 s^{-1} [9]. All pH measurements were made with a digital pH/mV meter (Yamei Model pHS-4). All measurements were made at 0°C in a system with an ice–water thermostat. The average of four successive scans (each recorded under the same conditions) was taken. A microcomputer (IBM-PC 386) was used as a data processor.

The differential-pulse mode was used with a three-electrode system with pulse amplitude (ΔE) 20 mV, drop time (t) 2 s, scan rate 2 mV s^{-1} and pulse width 60 ms with a 40-ms time delay, except where indicated otherwise. The indicator electrode was a glass capillary dropping mercury electrode, the reference electrode was a saturated calomel electrode (SCE) and the auxiliary electrode was a platinum wire. The solution was degasified by passing through it a slow stream of helium for 15 min.

Reagents

NAD^+ was purchased from Sigma. The reagent was checked by UV–visible spectrophotometry at 258 nm and 232 nm in an aqueous solution of pH

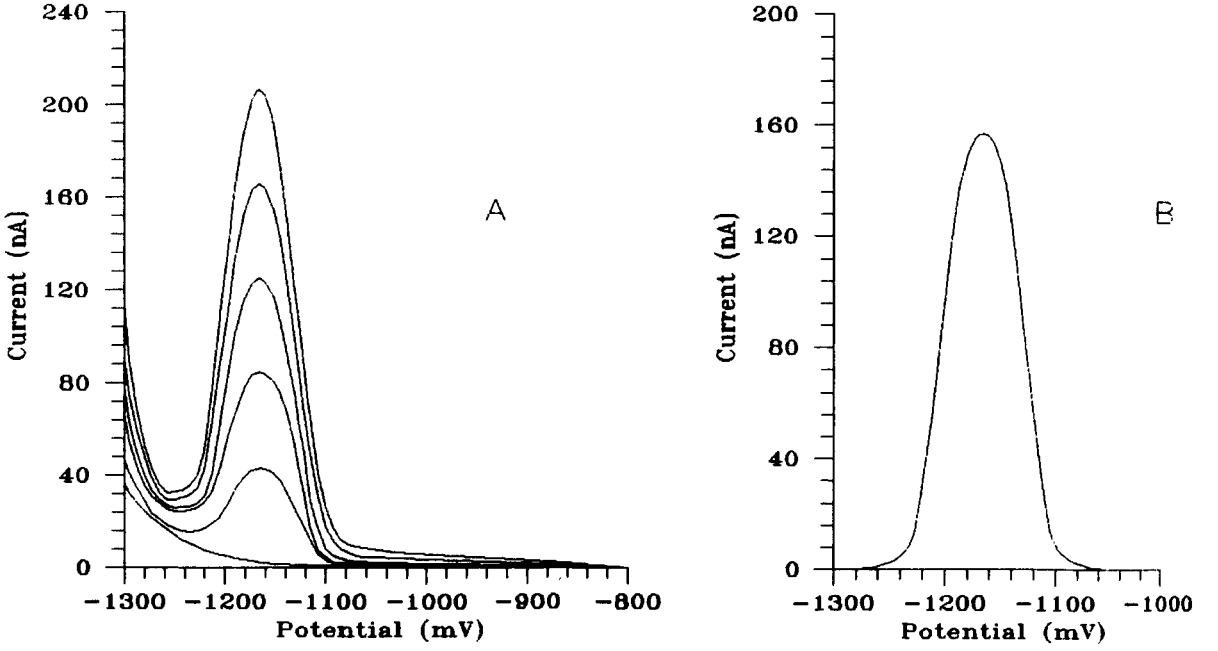

Fig. 1. Differential-pulse polarograms for NAD^+ in 0.1 mol l^{-1} malonic acid. Concentrations of NAD^+ were (A) 0, 2.0×10^{-6}, 4.0×10^{-6}, 6.0×10^{-6}, 8.0×10^{-6} and 10.0×10^{-6} mol l^{-1} from the lowest to the highest curve and (B) 8.0×10^{-6} mol l^{-1}. The curve in (B) was produced from (A) by background correction.

2.00. The $\lambda_{258}:\lambda_{232}$ and $\epsilon_{258}:\epsilon_{232}$ values were in agreement with literature values [10] and no additional purification was needed. Malonic acid and other chemicals were of analytical-reagent grade. Solutions were prepared from distilled water and further purified by quartz sub-boiling distillation (SYZ-A apparatus).

RESULTS AND DISCUSSION

Differential-pulse polarographic behaviour

Differential-pulse polarograms were run on a solution (25 ml) containing 0.1 mol l^{-1} malonic acid (pH 2.30) (Fig. 1A). As the concentration of NAD^+ increased, the second portion of the curves increased gradually. This indicated the direct reduction of hydrogen ions in solution. The background current was recorded and subtracted from the current observed after the addition of NAD^+. Figure 1B displays the DP polarogram of NAD^+ under the given conditions; it indicates a single symmetrical peak at -1166 mV (vs. SCE).

Parry and Osteryoung [11] noted that the peak half-width ($W_{1/2}$) for DPP is $3.52RT/nF$ when ΔE is smaller than RT/nF (23.5/n mV at 0°C). Hence the theoretical value of $W_{1/2}$ will be 82.8 and 41.4 mV for one- and two-electron reduction, respectively, at 0°C. Figure 1B indicates a $W_{1/2}$ = 78.4 mV when $\Delta E = 20$ mV. This value is very close to that for a one-electron reduction. The total peak current, $(i_t)_p$, is greater than might be expected for a diffusion- and adsorption-controlled one-electron reduction. According to the literature [12], the $(i_t)_p$ value for a diffusion- and adsorption-controlled one-electron reduction for a solution containing 6.0×10^{-6} mol l^{-1} NAD^+ would be ca. 6 nA under these conditions, using a value of 3.3×10^{-6} cm^2 s^{-1} [13] for the diffusion coefficient of NAD^+. However, the value for $(i_t)_p$ obtained was ≤ 120 nA, much greater than the expected value.

The peak potential (E_p) for DPP curves was proposed by Parry and Osteryoung [11] as

$$E_p = E_{1/2} - \Delta E/2 \quad (1)$$

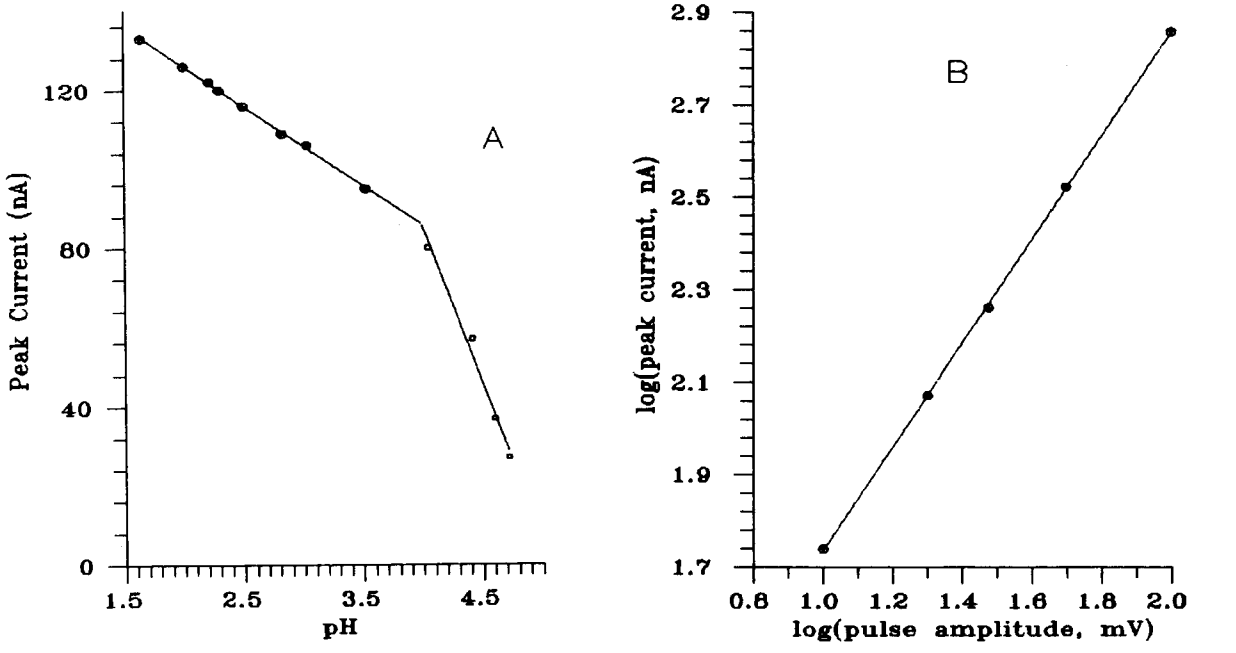

Fig. 2. Correlations of peak current versus (A) pH of solution and (B) pulse amplitude for 6.0×10^{-6} mol l^{-1} NAD^+ in 0.1 mol l^{-1} malonic acid.

Accordingly, $E_{1/2}$ of NAD^+ will be -1156 mV. Experimental results showed a linear relationship between E_p and ΔE, with a slope of -0.548 and an intercept of -1155 mV. The results for the slope and intercept agree with Eqn. 1 to within 1–2 mV, which is about the accuracy with which the peak potential could be read under these experimental conditions.

Effect of pH

An increase in the pH of solution results in a decrease in the peak potential. It is well known that E_p is related to pH for the DPP current with the participation of H^+ and is due to a CEC kinetic process [12,14]. The relationship is

$$dE_p/dpH = -3RT/2nF \quad (2)$$

For one- and two-electron reactions, this value will be -35.3 and -17.7 mV (0°C), respectively. Such a linear dependence of E_p on pH was found in the pH range 1.5–4.5. The slope (-35.5 mV) accords well with the theoretical value for a one-electron reaction.

$(i_t)_p$ is also related to the pH of the solution. Figure 2A shows that $(i_t)_p$ increases as the pH of solution decreases in the pH range 1.6–4.7. The peak current decreases more dramatically when the pH is >4. The reason is that the lower concentration of H^+ will result in a sharp decrease in the concentration of protonated NAD^+. As will be shown below, protonated adenine must be formed before a one-electron reduction of NAD^+ will take place under the experimental conditions. From Fig. 2A we obtained

$$(i_t)_p = -20.2pH + 166.4 \text{ nA}$$

$$(pH < 4,\ 6.0 \times 10^{-6} \text{ mol } l^{-1} NAD^+) \quad (3)$$

and

$$(i_t)_p = -78.3pH + 398.0 \text{ nA}$$

$$(pH > 4,\ 6.0 \times 10^{-6} \text{ mol } l^{-1} NAD^+) \quad (4)$$

Two linear parts of the graph intersect at pH 4.0. This value agrees with the pK_a of 4.1 (25°C) for protonation at N-1 in the adenine moiety [15–17]. When $pH > pK_a$, the concentration of NAD^+ in the double layer is greater than that of the protonated NAD^+, and unprotonated NAD^+ will seriously prevent the one-electron reduction of the protonated NAD^+ at the DME.

Contribution of adsorption to total current

On the basis of the study of Zhang and Shen [14], we have under the experimental conditions

$$(i_t)_p = 0.480nFm^{2/3}t^{2/3}D_o^{1/2}C_o^* \times [nF\,\Delta E/(4RT)]^{1+\alpha}/[(1+0.1655\alpha)\delta^{1/2}] \quad (5)$$

where n is the number of electrons transferred, m is the velocity of mercury flow, t is the drop time of mercury, D_o is the diffusion coefficient of the reactant, C_o^* is the concentration of the reactant, δ is the time interval between when the pulse is applied and the current is measured; $1+\alpha$ is the slope of curve of $\log(i_t)_p$ vs. $\log \Delta E$ and

$$X = \frac{\alpha}{0.858 + 0.142\alpha} \quad (6)$$

where X is the percentage of adsorption current in total current.

Figure 2B shows the relationship between $(i_t)_p$ and ΔE. The slope of the straight line is 1.122. Substituting this value for $1+\alpha$, gave $\alpha = 0.122$ and $X = 0.139$. Hence the fractions of current caused by adsorption and by diffusion are 13.9% and 86.1%, respectively.

Mercury column height

In order to elucidate the variation of $(i_t)_p$ with the column height above the DME, the dependence of $(i_t)_p$ on the drop time (t) and the velocity of mercury flow (m) was investigated. By means of curve fitting, it was found that $(i_t)_p$ is proportional to $m^{2/3}$ and $t^{2/3}$. Because m and t are proportional and inversely proportional to the mercury column height (h_{Hg}), respectively,

$$(i_t)_p \propto m^{2/3}t^{2/3} = h_{Hg}^{2/3}h_{Hg}^{-2/3} = h_{Hg}^{\circ} \quad (7)$$

that is, $(i_t)_p$ is not related to the mercury column height. This result conforms with the property of a catalytic current.

Determination of NAD^+

The addition of aqueous NAD^+ solution to the polarographic cell containing 0.1 mol l^{-1} mal-

TABLE 1

Selected base solutions for the study of NAD^+ reduction on DME

Base solution [a]	pH	E_p (mV) [b]	Peak [c]
Acetic acid	2.89	−1188	++
Acetic acid–sodium acetate	4.41	−1236	+
Citric acid	1.74	−1145	++
Dimethyl sulphoxide	5.71	–	–
Formic acid	2.14	−1160	++
Lactic acid	1.98	−1154	++
Oxalic acid	1.10	–	–
Succinic acid	2.33	−1168	++
Tris buffer	11.17	–	–

[a] The concentrations in the polarographic cell are $NAD^+ = 2.0\times10^{-5}$ mol l^{-1} and buffer = 0.1 mol l^{-1}. [b] Scan range: −800 to −1350 mV. [c] ++ represents $(i_t)_p$ which agrees with Eqn. 3, and + represents $(i_t)_p$ which agrees with Eqn. 4, when the NAD^+ concentration was 6.0×10^{-6} M.

onic acid at pH 2.30 caused a linear increase in the peak current of the hydrogen catalytic reduction at −1166 mV. It was determined that the linear range is 5.0×10^{-7}–1.0×10^{-4} mol l^{-1} NAD^+ with a slope of 20 mV per 10^{-6} mol l^{-1}. This is a sensitive way to determine the concentration of NAD^+ in acidic aqueous solution.

Other media

In addition to malonic acid, some other compounds were used as buffers to investigate the reduction behaviour of NAD^+ (Table 1). Table 1 shows that the one-electron reduction takes place from ca. −1145 to −1236 mV in the pH range 1.74–4.41, and indicates that the nature of the buffers does not affect the pathways significantly. The results not only give an illustration of the existence of a hydrogen catalytic process, but also show that the process is dependent merely on the pH of the solution in a certain pH range. The peak potentials accord well with the slope obtained above, and the peak currents agree with Eqns. 3 and 4 when the NAD^+ concentration was 6.0×10^{-6} M. Because of the low concentration of H^+ ions in solution, no reduction peaks of NAD^+ in the experimental potential range were obtained when dimethyl sulphoxide or Tris buffer was used. This conforms with the appearance of Fig. 2A. The reason why NAD^+ had no reduction response when oxalic acid buffer was used is due to the direct reduction of H^+ ions on the dropping mercury electrode. Under this condition, the hydrogen wave occurs at ca. −1000 mV.

Conclusion

On the basis of the structure of NAD^+:

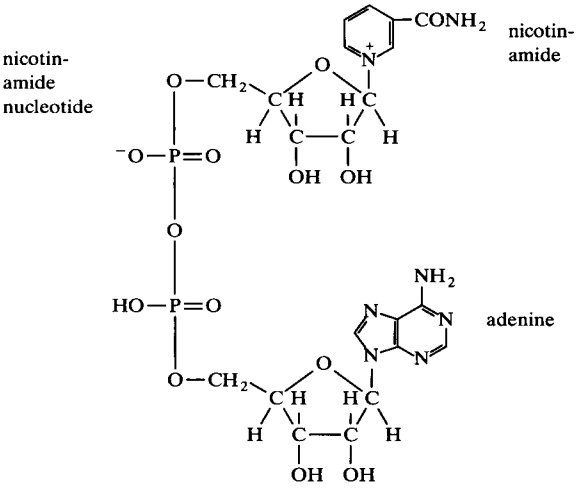

the molecule exists in a folded conformation [18], i.e., the nicotinamide and adenine rings in NAD^+ are in close proximity to each other and can therefore influence each other. No matter whether the adenine and nicotinamide rings in NAD^+ are parallel or perpendicular to each other, NAD^+ adsorbs strongly on mercury surfaces [1,19]. According to the literature [8], the wave peak for NAD^+ at ca. −1.0 V is probably due to the one-electron reduction of the nicotinamide ring, and consequently NAD^+ is reduced to $NAD^{\cdot}$. NAD^+ is adsorbed at the electrode/solution interface with the adenine ring lying flat on the electrode surface and the nicotinamide ring parallel and close to the adenine ring. Hence the electron should transfer from the electrode through the adenine ring to the nicotinamide moiety [2,18–20].

Both $(i_t)_p$ and E_p are strongly dependent on pH, which indicates that there exists at least one protonation process before one-electron reduction takes place. In the solution containing 0.1 mol l^{-1} malonic acid, NAD^+ combines with H^+ at N-1 in adenine ring and forms a protonated, electroactive molecule [15–17,21–23].

The conjugated electronic structure of the pyridine aromatic ring (conforming to the $4m + 2$

Hückel rule) makes NAD^+ fairly stable in acidic media [8]. An unstable $NAD^{\cdot}$ species was formed after the nicotinamide ring of the protonated NAD^+ had obtained an electron from DME through the adenine ring. As $NAD^{\cdot}$ is strongly adsorbed on the DME, whereas $(NAD)_2$ cannot be adsorbed on the surface in the experimental potential range [19], it can be expected that the dimer of $NAD^{\cdot}$ will not be formed after one-electron reduction takes place under given conditions. Also, NADH could not be the product of the reduction, because it is not stable in acidic medium, in which NADH will reduce H^+ and be converted into the starting molecule NAD^+ [24]. From the literature [25], the heat of formation (ΔH_f) of the reduced pyridine ring in $NAD^{\cdot}$ is 6.4 kcal mol^{-1}, whereas that of the pyridine ring in NAD^+ is 157.1 kcal mol^{-1}. Hence NAD^+ is much more stable than $NAD^{\cdot}$ under the experimental conditions. Therefore, the single electron of the pyridine ring must transfer back to the adenine ring quickly, which makes H^+ on N-1 of adenine be reduced to a hydrogen atom and $NAD^{\cdot}$ is changed into the original NAD^+. Two hydrogen atoms consequently combine to form one hydrogen molecule. It is proposed that a possible reduction process of NAD^+ on a DME under the given conditions could be

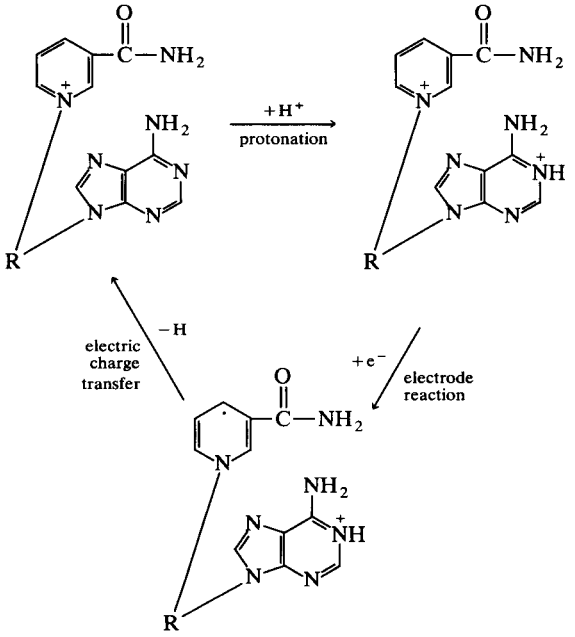

R = dinucleotide

The electrode reaction takes place after one chemical reaction (protonation) but before another chemical reaction (charge transfer), i.e., this is a CEC process. The net result is a hydrogen catalytic reduction. NAD^+ acts as a catalyst in the process. This is the reason why a large $(i_t)_p$ is obtained.

The state of the DME surface was inspected by a microscope during the recording of DPP curves. A few small bubbles were found on the surface of the DME when each current peak was reached. This phenomenon is also in keeping with the conclusion of the existence of a hydrogen catalytic wave.

This work was supported by the Youth Science Foundation of Southeast University, China.

REFERENCES

1 C.O. Schmakel, K.S.V. Santhanam and P.J. Elving, J. Am. Chem. Soc., 97 (1975) 5083.
2 C.O. Schmakel, M.A. Jensen and P.J. Elving, Bioelectrochem. Bioenerg., 5 (1978) 625.
3 M. Shah and J. Osteryoung, Anal. Chem., 54 (1982) 586.
4 D. Thevenot and R. Buvet, J. Electroanal. Chem., 39 (1972) 426.
5 D. Thevenot and R. Buvet, J. Electroanal. Chem., 40 (1972) 197.
6 A. Webber, M. Shah and J. Osteryoung, Anal. Chim. Acta, 157 (1984) 1.
7 A. Webber and J. Osteryoung, Anal. Chim. Acta, 157 (1984) 17.
8 S.T. Sulaiman and M.M. Najeeb, Microchem. J., 31 (1985) 37.
9 J. Heyrovsky and J. Kuta, Zaklady Polarografie, Nakladatelstvi Ceskoslovenske Akademie Ved, Prague, 1962.
10 R.A. Morton, Biochemical Spectroscopy, Vol. 12, Hilger, London, 1975.
11 E.P. Parry and R.A. Osteryoung, Anal. Chem., 37 (1965) 1634.
12 Z. Zhang and Z. Shen, Acta Chim. Sin., 43 (1985) 346.
13 Z. Samec, W.T. Bresnahan and P.J. Elving, J. Electronal. Chem., 133 (1982) 1.
14 Z. Zhang and Z. Shen, Acta Chim. Sin., 42 (1984) 529.
15 B. Janik and P.J. Elving, J. Electrochem. Soc., 116 (1969) 1087.
16 D. Krznaric, P. Valenta and H.W. Nürnberg, J. Electroanal. Chem., 65 (1975) 863.
17 H. Kinoshita, S.D. Christian and G. Dryhurst, J. Electroanal. Chem., 83 (1977) 151.
18 P.J. Elving, W.T. Bresnahan, J. Moiroux and Z. Samec, J. Electroanal. Chem., 141 (1982) 365.

19 W.T. Bresnahan and P.J. Elving, J. Am. Chem. Soc., 103 (1981) 2379.
20 W.T. Bresnahan, J. Moiroux, Z. Samec and P.J. Elving, J. Electroanal. Chem., 116 (1980) 125.
21 J.W. Webb, B. Janik and P.J. Elving, J. Am. Chem. Soc., 95 (1973) 8495.
22 T.E. Cummings, M.A. Jensen and P.J. Elving, Bioelectrochem. Bioenergy., 4 (1977) 425.
23 W.T. Bresnahan, J. Moiroux, Z. Samec and P.J. Elving, Bioelectrochem. Bioenerg., 7 (1980) 125.
24 J.C. Lepretre, D. Limosin, G. Pierre, P. Chautemps, G. Gellon and J.L. Pierre, J. Electroanal. Chem., 286 (1990) 63.
25 M.E. Brewster, J.J. Kaminski and N. Bodor, J. Am. Chem. Soc., 110 (1988) 6337.

Analytica Chimica Acta, 270 (1992) 181–186
Elsevier Science Publishers B.V., Amsterdam

On-line determination of iodine in nuclear fuel reprocessing off-gas streams by a combination of laser-induced fluorimetry and laser photoacoustic spectroscopy

Yusuke Kuno, Souichi Sato and Jinichi Masui

Power Reactor and Nuclear Fuel Development Corporation, Muramatsu, Tokai-mura, Ibaraki 319-11 (Japan)

(Received 7th April 1992; revised manuscript received 17th July 1992)

Abstract

The on-line determination of molecular iodine and organic iodides in nuclear fuel reprocessing off-gas streams containing high concentrations of NO_x gas was studied. Ultraviolet radiation is used to convert organic iodides into molecular iodine. The approximate concentration of iodine before and after the photochemical conversion in the presence of NO_x gas was first determined by laser-induced fluorimetry. NO_2 was determined by photoacoustic spectroscopy, correcting the acoustic signal due to iodine by using the approximate iodine concentration. NO was determined from the concentrations of NO_2 before and after the photoirradiation based on the photochemical fraction changes of NO and NO_2. The quenching of the fluorimetry due to NO and NO_2 was finally corrected with the NO and NO_2 concentrations obtained. The detection limit of the proposed method is 10 nl l^{-1}.

Keywords: Acoustic methods; Fluorimetry; Iodine; Lasers; Nitrogen oxides; Nuclear fuel reprocessing off-gas

There is environmental concern regarding radioactive iodine-129 owing to its long half-life and its biological effect. High recoveries of iodine evolved from Purex reprocessing plants have been achieved with cleaning systems such as an alkaline scrubber and AgX filter [1] prior to the release of off-gas to the atmosphere. Real-time monitoring equipment is required to ensure that such systems perform satisfactorily. It has been difficult to detect iodine-129 directly by radiometric analysis, however, because of its extremely low concentration and its low specific activity (6 MBq g^{-1}).

Spectrophotometry using a laser was selected for the determination of iodine because of its ultrasensitive detection. A ^3He–^{22}Ne laser was applied to detect $^{129}I_2$, providing a detection limit of about 10^{-7} mg ml^{-1} [2,3]. Hohimer and Hargis [4] and Goles et al. [5] used a continuous-wave dye laser, resulting in more sensitive detection. A certain fraction of iodine-129 in the off-gas stream, however, may statistically be present in the form of the $^{127}I^{129}I$ molecule. The selective induction for $^{127}I^{129}I$ requiring a stable laser and narrower band does not suit practical in situ measurements. The use of 514.5-nm radiation from an argon ion laser to induce the total I_2 was chosen based on the fact that the ratio of natural to radioactive iodine (^{129}I) is almost constant for a certain range of nuclear fuel burn-up in the off-gas of commercial reprocessing facilities. In the process of interest, the off-gas stream located just after the filtration and before the dilution with a large volume of air, where the I_2 concen-

Correspondence to: Y. Kuno, Power Reactor and Nuclear Fuel Development Corporation, Muramatsu, Tokai-mura, Ibaraki 319-11 (Japan).

tration is expected to be barely detected, contains high concentrations (several thousand $\mu l\ l^{-1}$) of NO_x gas, which is not negligible in fluorimetry. Matsui et al. [6] reported a correction for the influence of NO_2 on the laser-induced I_2 fluorescence with two different wavelengths using a pulsed dye laser. However, a large amount of NO arising from denitration may also be present in the off-gas stream, which significantly acts as a quencher of I_2 fluorescence just like NO_2. It is also known that the off-gas stream includes a certain fraction of organic iodides. In this paper, on-line detection of molecular iodine and organic iodides with a correction for NO and NO_2 using laser-induced fluorimetry combined with laser photoacoustic spectroscopy is described.

EXPERIMENTAL

A schematic diagram of the experimental apparatus, consisting of a UV irradiation vessel, a laser-induced fluorimetric detection system and a laser photoacoustic detection system, is presented in Fig. 1. A high-pressure mercury lamp (Ushio Electric UM-452, 450 W), surrounded by a 300-ml

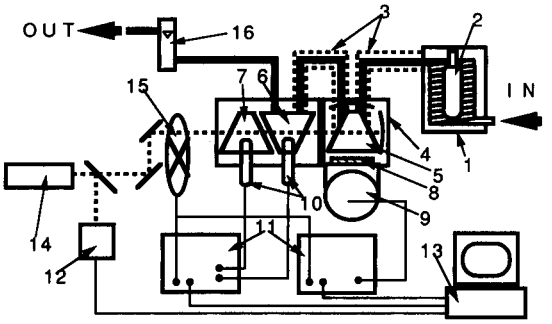

Fig. 1. Schematic diagram of laser-induced fluorimetry and photoacoustic spectroscopy for measurement of molecular iodine and organic iodides in the presence of NO_x. 1 = UV irradiation vessel; 2 = high-pressure mercury lamp; 3 = heated gas transfer tube; 4 = cell cover; 5 = fluorescence cell; 6 = acoustic sample cell; 7 = acoustic reference cell; 8 = filters, interference filter (available between 559 and 547 nm) and sharp cut filter (available above 540 nm; 9 = photomultiplier; 10 = microphone; 11 = lock-in amplifier; 12 = power meter; 13 = CPU; 14 = argon ion laser; 15 = chopper; 16 = flow meter.

volume photo-reaction spiral tube (7 mm diameter, quartz) was used as the light source. Photolysis in the UV irradiation vessel was monitored by detecting the decrease in methyl iodide level with a gas chromatograph (Shimadzu GC-14A with a flame ionization detector). The 554-nm radiation, at a total output power of 150 mW, from a 5-W all-line argon ion laser (Spectra-Physics 2020) was used as the excitation source. The lock-in amplifier employed was a Model 5600A (NF Electric Instruments) with an appropriate chopper and chopper reference. The intensity of the laser beam was monitored by introducing 1% of the beam to the power meter. A low-scatter external quartz sample cell with Brewster angle windows was installed. Sample gas was introduced into the cell through a heated tube, preventing the deposition of I_2. The fluorescence signal of I_2 was detected by means of the lock-in amplifier after isolating the emission with an interference filter (JASCO 554BP10). The light scattering of the laser was rejected by an interference filter (Sigma KOKI SCF-50S-540). The photoacoustic signal was detected with a B & K Type 4166 microphone and Type 2639 preamplifier that was connected to another Model 5600A lock-in amplifier. The photoacoustic cell, also made of quartz, is evacuable just like the fluorimetric cell so that it can be easily filled with gas along with carrier air. The microphone was coated with a thin Mylar film to prevent its corrosion.

Molecular iodine, methyl iodide and other reagents used were of analytical-reagent grade. Various concentrations of I_2 gas were prepared by the photolysis of known concentrations of methyl iodide with another photolysis cell, based on the experimental result shown in the next section. Some concentrations of I_2 were also prepared by taking and diluting I_2 gas from the gas phase after establishing gas–solid equilibrium. Good agreement of the observed fluorescence intensities of the same concentration of I_2 prepared by the two methods indicates the validity of the procedure for the preparation of I_2 concentrations.

NO_x gas was obtained by mixing sodium nitrite and nitric acid. Different fractions of NO and NO_2 were prepared by changes in their standing

time under the condition of photoirradiation. The concentration of NO_2 was determined by ion chromatography after NO_2 had been absorbed in 10% of triethanolamine–0.01% sodium hydroxide solution [7]. NO was calculated by subtraction of NO_2 from the total amount of NO and NO_2, which was determined by a direct photometric method [8].

RESULTS AND DISCUSSION

Photolysis of organic iodide

The photochemical method using UV radiation is based on the conversion of organic iodides into molecular iodine (I_2). Methyl iodide was chosen for this study because it has the largest C–I binding energy of the major organic iodides present in the reprocessing off-gas [9]. Vikis and McFarlane [3,10] reported a satisfactory result for the photolysis of methyl iodide with a high-pressure mercury lamp. The high-pressure mercury lamp was employed as a light source in this work. The irradiation period was adjusted by changing the flow-rate of methyl iodide gas.

Figure 2 shows the decomposition rate of methyl iodide on irradiation. It was found that irradiation for 6 min provides more than 95% decomposition/oxidation of methyl iodide, where the flow-rate in the proposed vessel was 50 ml $min.^{-1}$. The decomposition of I_2 by the argon ion laser was experimentally found to be negligible.

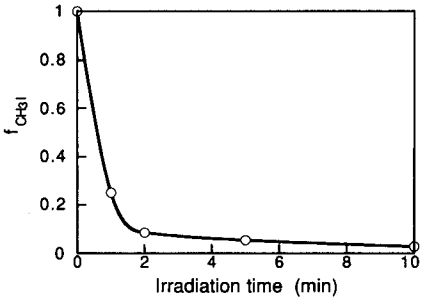

Fig. 2. Rate of decomposition methyl iodide by UV irradiation in the proposed vessel. f_{CH_3I} represents the fraction of CH_3I in the mixture of CH_3I and I_2.

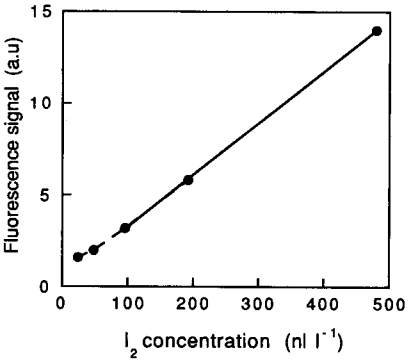

Fig. 3. Fluorescence analytical calibration graph for molecular iodine. Laser power, 150 mW; chopping frequency, 170 Hz; emission wavelength, 559–547 nm.

Laser-induced fluorimetry

The fluorescence of I_2 excited by 514.5-nm radiation from the argon ion laser was observed. Figure 3 shows the fluorescence signal as a function of I_2 concentration in air–nitrogen at ambient temperature. The calibration graph was linear down to 100 nl l^{-1}. The fluorescence detection limit was calculated to be 10 nl l^{-1}. The following calibration equation was experimentally obtained in the proposed cell:

$$[I_2](\text{nl } l^{-1}) = f(F) = 35.5F - 15.9 \qquad (1)$$

where F is the intensity (μV) of the fluorimeter. The error due to the cell-wall absorptive effect of I_2 cannot be neglected when determining less than a few μl l^{-1} of I_2. It was found that a volume of carrier gas (air) as large as 100 times the volume of the fluorimetric cell, combined with the heating system, lowered the fluorescence signal of I_2 to nearly the background level.

Determination of I_2 and NO_2 by laser photoacoustic spectroscopy

The photoacoustic signal of I_2 and/or NO_2 was detected in gas flowing at a rate of 50 ml min^{-1}. To minimize the environmental acoustic disturbances, the entire cell sytem was assembled in a cell cover. Another microphone also connected to the lock-in amplifier was installed between the cover and the acoustic cell in order to eliminate environmental disturbances. It was

found that the acoustic signal of I_2 gas varied linearly with the I_2 concentration (Fig. 4). The specific graph obtained with the proposed cell is represented by

$$A_{I_2} = g([I_2]) = 3.73[I_2] + 25.0 \quad (2)$$

where A_{I_2} (μV) is the intensity of acoustic signals due to I_2 (μl l^{-1}). The sensitivity of the method was calculated to be 2 μl l^{-1}. It was noted that photoacoustic spectroscopy can also be applied to the determination of high concentrations of NO_2. This is based on the absorption of 554-nm radiation from an argon ion laser by NO_2. A linear calibration graph for the NO_2 photoacoustic response was obtained (Fig. 4):

$$[NO_2] = h(A_{NO_2}) = 4.50A_{NO_2} - 85.7 \quad (3)$$

where A_{NO_2} is the intensity of acoustic signal due to NO_2. It is obvious that the concentration of NO_2 can be determined below about 5000 μl l^{-1}. It may be concluded that the calibration graph for $g([I_2])$ should rather be used for the I_2 interference correction to the NO_2 photoacoustic determination.

Quenching correction in I_2 fluorimetry

Assuming that the following dynamic quenching represents the effects of NO and NO_2 on I_2 fluorimetry, the quantitative effect of the quenching may be expressed by the Stern–Volmer equation[11], in which the effect is independent of the concentration of I_2:

$$Q = F_o/F = 1 + k[q] \quad (4)$$

where F and F_o are the intensity of I_2 fluorescence with and without a quencher (q) of NO or NO_2, respectively, F_o/F for I_2 is plotted against the NO or NO_2 concentration in Fig. 5, the concentration of I_2 being held constant at 30 μl l^{-1}. The following linear relationships were obtained:

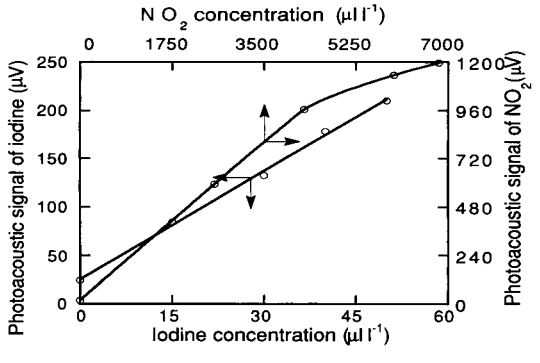

Fig. 4. Photoacoustic calibration graphs for iodine and NO_2. Laser power, 150 mW; chopping frequency, 170 Hz.

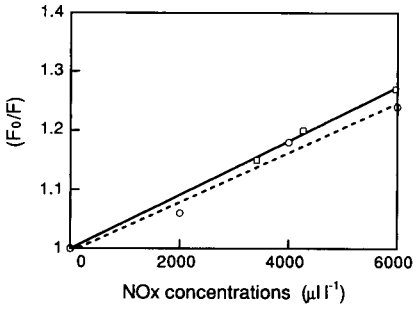

Fig. 5. Stern–Volmer plots, F and F_o are the intensity of I_2 fluorescence with and without quencher of NO or NO_2, respectively. Solid line (□), NO; dashed line (○), NO_2.

$$Q_{NO} = (F_o/F)_{NO} = 4.7 \times 10^{-5}[NO] + 1.0 \quad (5)$$

$$Q_{NO_2} = (F_o/F)_{NO_2} = 4.2 \times 10^{-5}[NO_2] + 1.0 \quad (6)$$

These equations indicate the validity of the above assumption that dynamic quenching is predominant in this system.

The reprocessing off-gas of interest initially contains both NO and NO_2. It is known that NO_2 is converted into NO by photolysis, whereas NO is oxidized in air, as given below:

$$NO_2 + h\nu(< 420 \text{ nm}) \rightarrow NO + O(O + O_2 \rightarrow O_3)$$

$$2NO + O_2 \rightarrow 2NO_2$$

$$NO + O_3 \rightarrow NO_2 + O$$

$$2NO + O_2 = 2NO_2 \text{ (net)}$$

$$K = [NO_2]^2/[NO]^2[O_2] \quad (7)$$

The ratio of equilibrium constants with and without photolysis, K_2 and K_1, is given by

$$K_1/K_2 = \exp(-h\nu/RT) \quad (8)$$

K_1/K_2 should be constant under the condition of fixed irradiation time. Assuming that $[O_2]$ before and after the photolysis is almost the same,

$$(K_1/K_2)^{1/2} = 1/k \approx ([NO_2]_1[NO]_2)/([NO_2]_2[NO]_1)$$

where the subscripts 1 and 2 represent the states of NO or NO_2 before and after the irradiation, respectively. The sum of the concentrations of NO and NO_2 at any time is constant, i.e., $[NO]_1 + [NO_2]_1 = [NO]_2 + [NO_2]_2$. Hence

$$[NO_2]_2/[NO_2]_1 = k([NO]_1 + [NO_2]_1 - [NO_2]_2)/[NO]_1$$

When the initial fraction of NO, $[NO]_1/([NO]_1 + [NO_2]_1)$, is replaced with f_{NO}, this leads to

$$[NO_2]_2/[NO_2]_1 = (k/f_{NO}) - k[(1-f_{NO})/f_{NO}]([NO_2]_2/[NO_2]_1)$$

$$[NO_2]_1/[NO_2]_2 = 1 + f_{NO}[(1/k) - 1] \quad (9)$$

Equation 9 implies that the fraction of NO initially present can be calculated by measuring the concentrations of NO_2 before and after photoirradiation. On the other hand, it was found in Table 1 that the composition of NO and NO_2 after the irradiation was independent of the initial NO/NO_2 concentration ratio. Estimates of the concentrations of NO and NO_2 concentrations in the mixture of gas before and after the irradiation were examined. The initial fractions of NO in various compositions of gas are plotted in Fig. 6 against the concentration ratios, $[NO_2]_1/[NO_2]_2$, for the corresponding gas. The result obtained (Eqn. 10) is almost consistent with Eqn. 9, although certain errors due to the small fraction values of $(NO_2)_2$ were observed in the result:

$$f_{NO} = (1/85.3)([NO_2]_1/[NO_2]_2 - 0.084) \quad (10)$$

It is concluded that the concentrations of NO and NO_2 with and without the photoirradiation can

TABLE 1

Effect of photoirradiation on NO–NO_2 mixed gas [a]

Compound	Initial concentration (μl l^{-1})	Initial NO fraction	NO fraction after irradiation
NO_2	5.7×10^3	0.53	0.011
NO	6.3×10^3		
NO_2	1.5×10^4	0.65	0.006
NO	2.8×10^4		
NO_2	3.4×10^4	0.43	0.015
NO	2.6×10^4		
NO_2	6.7×10^4	0.073	0.11
NO	5.3×10^3		
NO_2	5.7×10^5	0.24	0.041
NO	1.8×10^5		

[a] Observed in the proposed vessel with a gas flow-rate of 50 ml min^{-1}.

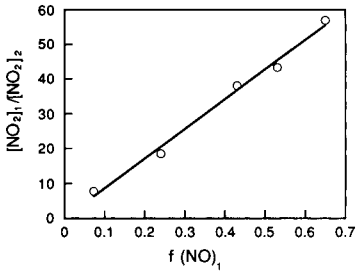

Fig. 6. Relationship between the initial fraction of NO and the concentration ratio, $[NO_2]_1/[NO_2]_2$, of the corresponding gas. Subscripts 1 and 2, represent the initial state and the state after irradiation, respectively; $f(NO)_1$ refers to the initial fraction of NO.

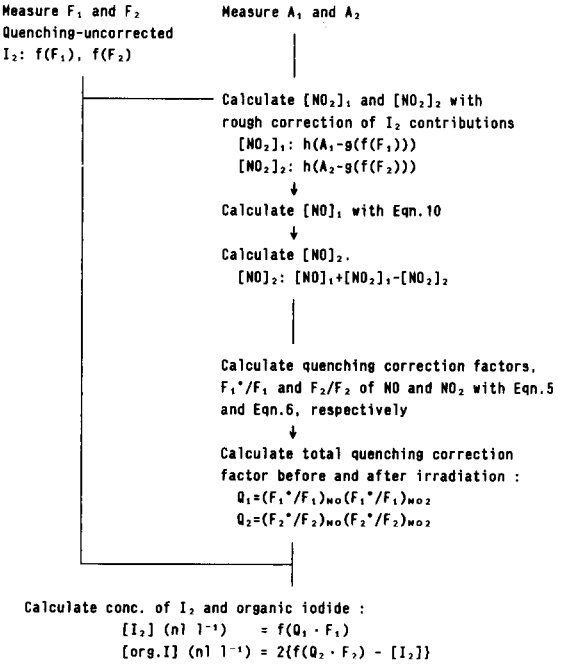

Fig. 7. Scheme for determination of I_2 and organic iodide in the presence of NO_x gas; F and F_0 refer to fluorescence intensity with and without NO_x quenching correction and subscripts 2 and 1 represent the initial state and the state after photoirradiation, respectively. A is photoacoustic intensity; functions, f, g and h refer to Eqns. 1, 2 and 3, respectively.

TABLE 2

Determination of molecular iodine and organic iodide in the presence of NO_x gas

I_2 taken ($\mu l\,l^{-1}$)	CH_3I taken ($\mu l\,l^{-1}$)	NO_x taken ($\mu l\,l^{-1}$)	F_1 (μV)	F_2 (μV)	A_1 (μV)	A_2 (μV)	NO_2 found ($\mu l\,l^{-1}$)	NO found ($\mu l\,l^{-1}$)	I_2 found ($\mu l\,l^{-1}$)	CH_3I found ($\mu l\,l^{-1}$)
10	20	2400	243	478	580	310	2270	70	9.5	18.7
0.25	0.25	4300	5.5	8.3	780	86	3310	880	0.22	0.24

be calculated by Eqn. 10 with only NO_2 concentrations determined by the laser photoacoustic spectroscopy before and after the irradiation.

A calculation scheme is given in Fig. 7. Mixtures of known concentrations of I_2 and CH_3I gas in the presence of NO and NO_2 were analysed. The results calculated using the proposed scheme based on the values measured by fluorescence and photoacoustic spectroscopy are in good agreement with the values of the prepared samples, as shown in Table 2.

Conclusions

The proposed method based on detection by laser-induced fluorimetry and photoacoustic spectroscopy combined with photolysis was found to be useful for the determination of molecular iodine and organic iodides in reprocessing off-gas in the presence of high concentrations of NO_x gas. The detection limit of the fluorimetric determination of iodine is 10 nl l^{-1}. The influence of quenching due to NO_x on the fluorimetric determination of iodine should be independent of the iodine concentration because the results satisfied the Stern–Volmer equation. The proposed method may therefore be valid for the determination of very low concentrations of iodine even in the presence of high concentrations of NO_x.

REFERENCES

1 S. Inami, M. Kawasaki, T. Tachihara and H. Okamoto, in Proceedings of the Third International Conference on Nuclear Fuel Reprocessing and Waste Management, RECOD'91, Japan Atomic Industrial Forum, Sendai, 1991, Vol. 1, p. 230.
2 A.P. Baronavski and J.R. McDonald, in Proceedings of the 15th DOE Air Cleaning Conference, Boston, 1979, Vol. 1, p. 901.
3 A.C. Vikis and R. Macfarlane, Advanced Methods for Abatement and Monitoring of Radioiodines, EUR10580, Whiteshell Nuclear Research Establishment, Manitoba, Canada, 1986, p. 686.
4 J.P. Hohimer and P.J. Hargis, Jr., Anal. Chem., 51 (1979) 930.
5 R.W. Goles, R.C. Fukuda, M.W. Cole and F.P. Brauer, Anal. Chem., 53 (1981) 776.
6 T. Matsui, H. Fujimori, S. Izumi, K. Yoshida and Y. Takimoto, in Proceedings of the Annual Meeting of the Atomic Energy Society of Japan, Kinki Univ., 1991, M18, p. 620.
7 National Research Council, Nitrogen Oxides, in Medical and Biologic Effect of Environmental Pollutants, National Academy of Sciences, Washington, DC, 1977, Chap. 4.
8 G.A. Norwitz, Analyst, 91 (1966) 553.
9 Chemical Society of Japan, Kagaku Benran (Handbook of Chemistry), Kiso-hen(II), Maruzen, Tokyo, 1975, p. 977.
10 A.C. Vikis, Photochemical Method for Radioiodine Abatement, AECL-7819, Whiteshell Nuclear Research Establishment, Manitoba, Canada, 1984.
11 P. Suppan, Principles of Photochemistry, Chemical Society, London, 1972, Chap. 3.

Analytica Chimica Acta, 270 (1992) 187–193
Elsevier Science Publishers B.V., Amsterdam

Diode-array ultraviolet detector for continuous monitoring of water quality

E. Naffrechoux, C. Fachinger and J. Suptil

Laboratoire Chimie et Ingénierie de l'Environnement, Université de Savoie, ESIGEC, 73376 Le Bourget du Lac Cedex (France)

(Received 7th April 1992; revised manuscript received 7th July 1992)

Abstract

UV spectrophotometry was applied to the continuous monitoring of water quality, allowing the direct determination of specific components in natural waters and treated waste waters and the determination of oxidizable material in natural and waste waters. A diode-array UV detector with an auto-cleaning cell and sample line was developed. The processing of the absorption spectrum and the control of the whole system are performed with a computer. A description and the characteristics and performance of the device are presented. Results are given for an automatic survey of waste-water quality (oxidizable material concentration) of a 300 000 eq. inhab. treatment plant.

Keywords: UV–Visible spectrophotometry; Waters

Continuous monitoring of natural and waste waters is essential in improving water treatment and avoiding accidental pollution. Spectrophotometry is often used for laboratory analysis but its application to field work concerns only suspended matter and organic matter measurement. UV absorption spectrophotometry has been used for about 30 years for water quality characterization; early work dealt with dissolved organic matter in sea water [1], natural waters [2] and sewage [3]. Some apparatus using absorbance at 254 nm has been developed [4]; the use of statistical relationships between UV absorbance (corrected or not to reduce interferences from suspended matter) and the values of reference methods [biological oxygen demand (BOD), chemical oxygen demand (COD) or total organic carbon (TOC)] gives estimates of the organic pollution of natural or waste waters. Because of the complex composition of the water, absorbance measurements at one or two wavelengths can give only very poor information. Moreover, some technical difficulties related to the use of such devices (clogging of the sampling line, fouling of the measurement cell, etc.), have limited their use. However, one of the interesting aspects of UV spectrophotometry is its low cost and its ease of use, allowing many measurements in a short time. Finally, as was shown recently, the exploitation of the whole UV absorption spectrum can give interesting information about water quality [5].

The aim of this work was to optimize the application of UV spectrophotometry to continuous oxidizable pollution monitoring via the development of a fully automated diode-array UV detector.

Correspondence to: E. Naffrechoux, Laboratoire Chimie et Ingénierie de l'Environnement, Université de Savoie, ESIGEC, 73376 Le Bourget du Lac Cedex (France).

EXPERIMENTAL

Diode-array UV detector

Signal treatment required an adapted measurement and acquisition system. As both con-

ventional and commercially available diode-array spectrophotometers are not convenient for many reasons, such as acquisition time and complexity, a multi-wavelength absorptiometric detector has been developed. Figure 1 shows the scheme of the computer-controlled device with the sampling line and UV detector (260 × 160 × 60 mm), which measures the light intensity transmitted through the sample from 200 to 800 nm. The different parts of the system are the light source unit, an auto-cleaning cell (virtual double-beam system), and the dispersion and detection part of the transmitted light. The stand-cover is made of a high-resistance aluminium alloy for maximum stiffness.

The UV source is a deuterium lamp of 30 W power with a spectral distribution in the range 160–400 nm; its maximum fluctuation is 0.5% after a 15-min warm-up and the long-term drift is 1%. The self-cleaning cell is described later.

The optical unit is completely dissociated from the diode-array electronics and was designed to allow a further adaptation of a visible source. The beam is bent back to 90° after the holographic diffraction grating, for easier access to detector adjustments and limitation of interfering light. A MOS linear image sensor (Hamamatsu S3901) with 512 photodiodes (50 μm × 2.5 mm) is used for measurement of light intensity. The signal detection method consists of a pixel addressing technique. The address signal, which is sent sequentially from the shift register synchronized with the clock pulses, is used to scan the photodiodes, so that a signal is immediately formed at the output terminal (video line); the charge stored in the photodiodes is a function of the incident light intensity and is read out as a collector current that forms the signal, which represents a spatial image. This signal is then multiplexed, amplified and delivered as a voltage varying from

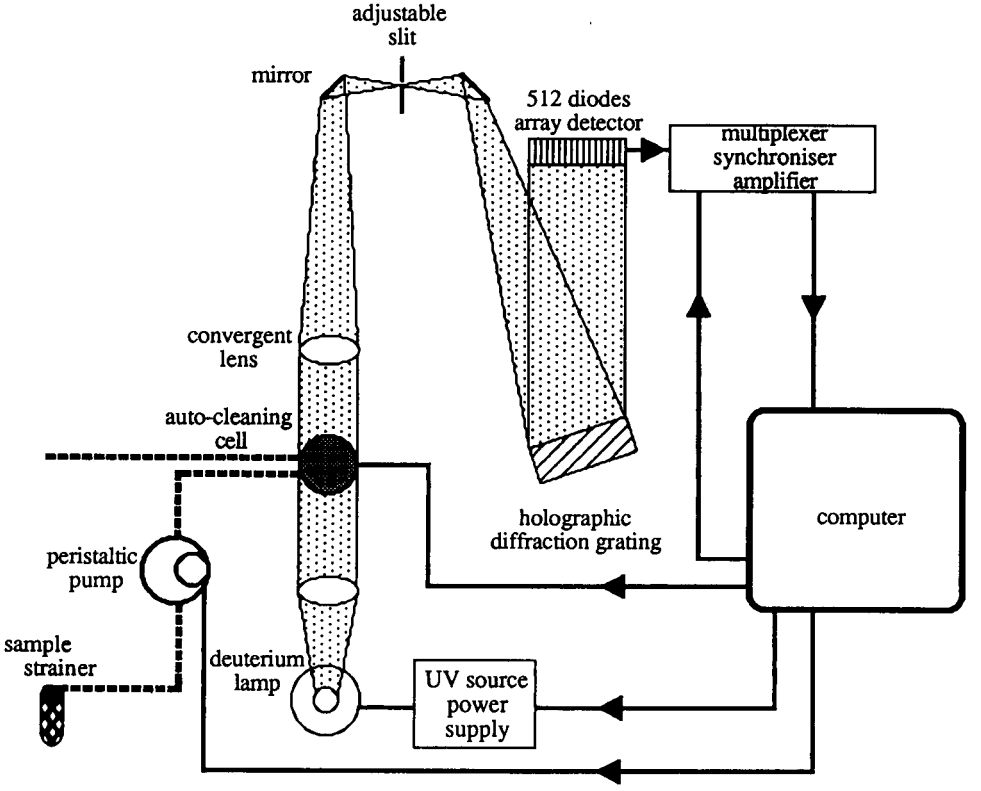

Fig. 1. Scheme of the device (UV detector and sample line).

0 to 10 V for each of the 512 diodes. The acquisition on the computer is made through an interface board (National Instrument Lab PC), with a 12-bit, 50-kHz analog-to-digital converter. An amplification and driving circuit is connected to the diode array; the acquisition procedure is initiated with a 10-μs length pulse, applied on the "start" gate; this acquisition is done at the frequency of the "clock" line (50 kHz). When the acquisition of the 512 data diodes has ended, a pulse signal is generated from the "end of scan" terminal to stop the operation. The output signal of the diode array is stored in the computer (Toshiba T3200SX) in 50 ms. The integration time of the whole sensor is 164 ms (time between two start signals). The maximum noise is 40 mV at 200 nm and it is doubled for an increase of 7°C; it is possible to reduce it with a Peltier effect [6]. For wavelengths higher than 225 nm, this noise is reduced to 7 mV. The blank signal intensity (resulting from the combination of the sensor sensitivity and of the UV source spectral distribution) increases from 5 V at 200 nm to 9 V at 250 nm, where it is continuous up to 350 nm. Therefore, the dynamic range is limited for wavelengths lower than 225 nm; the maximum absorbance measured in this region is 2.09 and increases to 3.95 for the upper wavelengths. The reproducibility of intensity measurement is fairly good, the relative error for ten values at 258 nm being about 0.1%. The sensor resolution, defined as the ratio of spectral range to diode number, is 1.17 nm; consequently, it is impossible to estimate the signal variation in wavelength.

The program, written in Quick-BASIC, performs the analogue signal acquisition, its conversion into numerical data, the calculation of absorbances, their graphic display and the mathematical processing for the computation of the concentrations of nitrate, hexavalent chromium and oxidizable matter.

Signal treatment method

The exploitation of the whole spectrum between 200 and 380 nm allows the direct determination of nitrate and hexavalent chromium concentrations without the use of reagents or preliminary treatment, with an optimized matrix resolution method using the orthogonal polynomial method [7–9]. The principle of this procedure is to model the absorbance function as the sum of two signals. The first is an estimation function of the background signal due to both suspended matter and dissolved organic compounds (which are the main factors of the featureless shape of the UV spectra of waters); the best adjustment was achieved with a polynomial function. The second signal comes from components whose spectral characteristics and concentration can significantly disturb the background spectrum. After the acquisition of absorbance values of the whole UV spectrum, UVMA (ultraviolet multi-wavelength absorptiometry) software simultaneously computes the unknown concentrations of the above specific absorbing components and the parameters of the background signal. For each specific component, the choice of the wavelength interval and the estimation function type is of great importance. The concentration of oxidizable matter is calculated by computation of the mean slope of the spectrum between 270 and 320 nm according to the equation

$$\mathrm{MOX} = 10^3 \left\{ \frac{\sum_{i=270}^{320} \lambda(i) \sum_{j=270}^{320} A(j) - 51 \sum_{i=270}^{320} A(i)}{51 \sum_{i=270}^{320} \lambda^2(i) - \left[\sum_{i=270}^{320} \lambda(i) \right]^2} \right\}$$

where $A(j)$ is the absorbance at the specified wavelength j and $\lambda(i)$ the value of the wavelength in nm. As the absorbance is measured at each nanometre, the number of values used for MOX calculation is 51.

The criterion obtained gives a value which in most instances is closely related to TOC or COD for a given waste-water type [10]. Because of the variability of the composition of samples, there is no universal relationship between UV and classical parameters, so a "calibration slope" is necessary for each kind of waste water (domestic, chemical industry, paper mill, sewage, etc.). The general procedure of this method is obviously less sensitive to interferences than absorbance measurement at one or two wavelengths. The charac-

teristics of the method using this multi-wavelength procedure are presented in Table 1. The limit of detection is the concentration corresponding to a signal of three times the standard deviation of the blank (distilled water).

Automation

Automatic control of the system is necessary for continuous monitoring. First, the warm-up of the deuterium lamp is ordered by the computer 10 min before the measurement, in order to obtain a stable UV source. Then, the peristaltic pump works backwards for a few seconds to clean the strainer and the line, and forwards for 2 s per metre of sampling tube in order to renew the sample (note that the tube material prevents fouling). After pumping, the measurement of the UV absorbance spectrum of the sample is initiated by the computer.

The absorbance of a solution is given by the logarithm of the ratio of the incident light intensity to the transmitted light intensity. For classical spectrophotometers, the incident light, or reference, is measured either with two different optical paths (double-beam spectrophotometer) or sequentially with the same optical line (single-beam apparatus). The latter method was used for the present UV detector because it seems better to keep the same optical components for both reference and sample measurements. Reference measurement is made automatically with a self-cleaning cell, in the reference position. The

TABLE 1

Characteristics of the method

Parameter	Typical sample	Range (mg l^{-1})	Detection limit [a] (mg l^{-1})
Nitrate	Natural water, treated waste water	Up to 180	0.2
Chromium(VI)	Natural water	Up to 5	0.05
Oxidizable materials (TOC estimation)	Natural water, waste water, industrial effluent	Up to 150	–

[a] Experimentally estimated values.

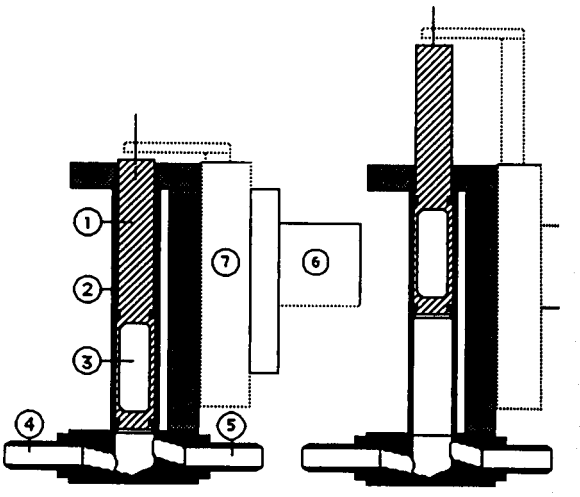

Fig. 2. Scheme of the auto-cleaning cell. 1 = Piston; 2 = quartz tube; 3 = reference window; 4 = sample inlet; 5 = sample outlet; 6 = reduction gear motor; 7 = piston motion device.

scheme of the cell is shown in Fig. 2; it is made of a 12 mm i.d. quartz tube with a scraper piston containing the reference chamber, hence sample and reference measurements are performed when the piston is up or down, respectively. Moreover, the possible effect of clogging of the cell and the optical evolution of the lamp or detector are equal for each spectrum acquisition; indeed, the measurement of the reference is made through the same part of the tube as the sample measurement. When the piston is down, the light passes through the reference chamber (a hole in the piston) of such a size that the measured light intensity is equivalent to that transmitted by pure water in the quartz tube. The inlet pipe of the sample is connected to a chamber located at the bottom of the quartz tube, where turbulence is created by the fluid circulation in order to prevent sedimentation of particles and to purge air bubbles whatever the cell position may be. The piston is shifted by a reduction gear motor driven by the computer, with a check of the piston position after every movement. The UV source signal is also tested for each spectrum acquisition.

After acquisition of the absorbance spectrum and mathematical computation, results are stored on hard disk and can be transmitted to a central

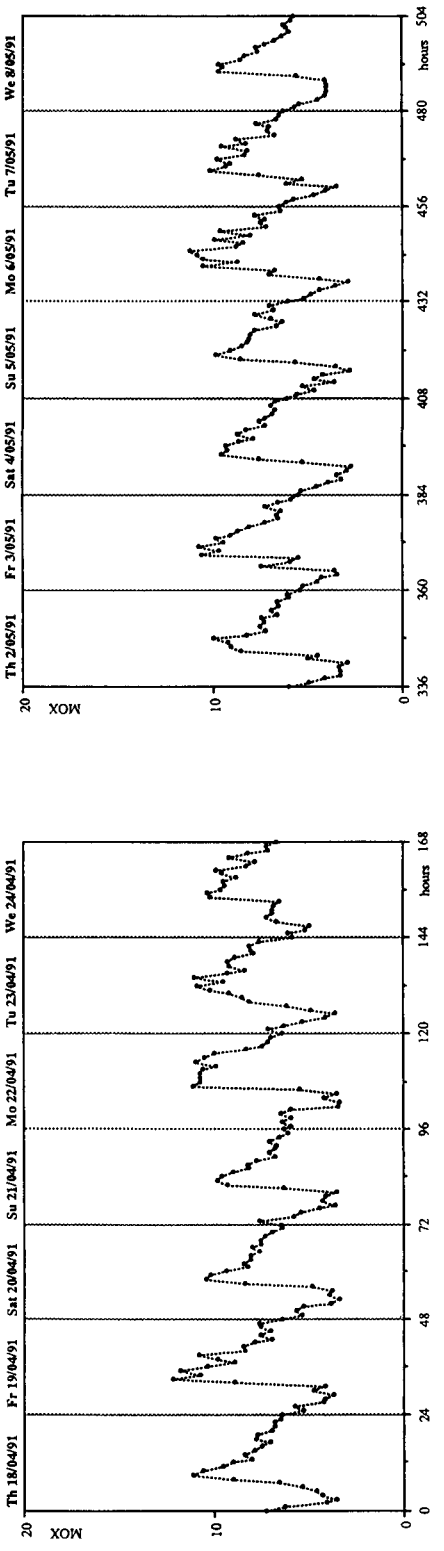

Fig. 3. Evolution of the oxidizable material concentration (UV estimated) at the entry of the Chambéry treatment plant.

computer by the serial port. Less than 3 s are needed for the measurement of the sample spectrum; this very short time allows raw samples to be used because it reduces the chance of changes in the sample (sedimentation of particles or photochemical reaction).

RESULTS AND DISCUSSION

Application to continous monitoring of natural or waste-water quality

The device can be used as a fixed monitoring or an alarm system, a portable analytical instrument or a process control station. The monitoring of the quality of natural waters is the most obvious application because it is useful both for a basic knowledge of the chemical characteristics of the waters and for the survey of the impact of any perturbations of the receiving medium such as waste-water outfall. When it is used for the control of drinking water treatment plants and of distribution systems, this UV detector can protect the pumping line from accidental pollution and can be used to control the different steps of the treatment (decantation, filtration, etc.).

The use of such an instrument for the control of waste-water collection system and treatment plant can be of great help for industrial discharge regulation and for the prevention of accidental shock load. Above biological treatment plants, an alarm function can also be useful to prevent sludge accidents caused by inflow of toxic organic material by automatically diverting the suspicious flow to a buffer tank. Therefore, the UV detector was located at the entry of the Chambery treatment plant (300 000 eq. inhab.); the polluting load variations were monitored every hour for 4 weeks. As described earlier, the MOX criterion is useful for characterizing the total organic pollution of sewage effluent. An automatic sampler was installed with the UV detector in order to proceed to further laboratory analysis. For the samples, COD and dissolved organic carbon (DOC) (peroxodisulphate–UV oxidation method) were determined (on a 24-h sample for COD determination) and the UV absorption spectrum was also been recorded with a Shimadzu UV 240 spectrophotometer. A comparison between the optical characteristics of the sensor and the reference spectrophotometer was made, which gave a linear relationship ($y = 1.002x - 0.002$ with a correlation coefficient of 1.000) between the absorbance values measured with the two systems for a raw waste-water sample.

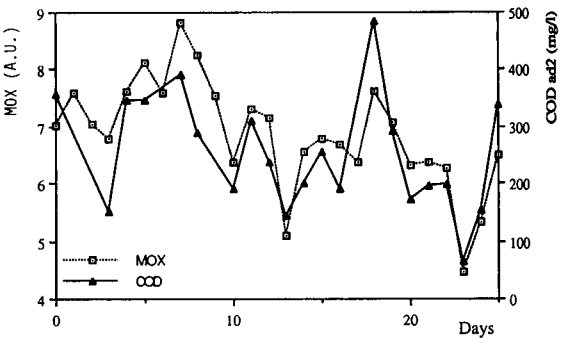

Fig. 4. (▲) COD and (□) MOX variations at the entry of the Chambéry treatment plant.

Figure 3 shows the evolution of the UV criterion at the treatment plant entry for 27 days. Similar variations were obtained for the different days; the lowest value was obtained at 3 a.m., then MOX quickly increased to a maximum at about 9 a.m. and subsequently decreased during the day. Some particular dates can be noted; e.g., at weekends and official holidays (May 1st and 8th) the MOX values were lower and variations were smoother because of the lack of industrial activity.

Figure 4 presents the COD and MOX variation [median MOX values were calculated (from 8 a.m. to 8 p.m. for each day)]. The correlation between COD and MOX values and DOC and MOX values can be calculated if needed. The correlation coefficients are not very good (0.793 for COD–MOX and 0.854 for DOC–MOX) because the COD and DOC determinations were made on a 2-h decantated sample and so did not take account of particular and colloidal fractions of organic matter whereas the MOX criterion was computed from a raw sample. Of course, the correlation is better if laboratory measurements are also made with the same sample quality. Despite this, similar variations of both the COD and MOX measurements can be noted, showing

the possibility of continuous automatic control of the different treatment steps. Moreover, some qualitative information can be obtained from the absorbance spectrum, such as the occurrence of blood or typical organic material. Hence, the treatment plant can be protected and its operation can be controlled and optimized with the UV detector system. The quality of the treated waste waters can also be monitored in order to minimize the impact of effluent on the natural medium.

Conclusion

UV absorptiometry is a useful approach for the direct determination of various components and for the study of organic pollution of waters. The exploitation of the absorption spectrum of natural or waste waters, obtained with the use of a fully automated diode-array UV detector system, is helpful for continuous control of their quality. At present, this device can only be used with a power-electric line, because of the energy requirement of the deuterium lamp and of the computer. However, the rapid evolution of electronics and computer science should allow the realization of low energy comsumption industrial boards. The need for electric power will also be reduced by using a flash lamp as the UV source. These developments will allow the design of a self-contained sensor (battery and solar cell), and will extend its field application to monitoring in remote locations (lakes, rivers, etc.). Research is in progress to increase the number of measurements (phenolic compounds, metals, etc.).

REFERENCES

1 F.A. Armstrong and G.T. Boalch, J. Mar. Biol. Ann. (UK), 41 (1961) 561.
2 M. Mrkva, J. Water Pollut. Control Fed., 41 (1969) 1923.
3 R.A. Dobbs, R.H. Wise and R.B. Dean, Water Res., 6 (1972) 1173.
4 R. Briggs, J.W. Shofield and P.A. Gotron, Water Pollut. Control Fed., 75 (1976) 47.
5 E. Naffrechoux, N. Mazas and O. Thomas, Environ. Technol., 12 (1991) 325.
6 M. Ryan-Hotchkiss and J.D. Ingle, Talanta, 34 (1987) 619.
7 O. Thomas and S. Gallot, Fresenius' J. Anal. Chem., 338 (1990) 234.
8 O. Thomas, S. Gallot and N. Mazas, Fresenius' J. Anal. Chem., 338 (1990) 238.
9 O. Thomas, S. Gallot and E. Naffrechoux, Fresenius' J. Anal. Chem., 338 (1990) 241.
10 E. Naffrechoux, Thèse de Doctorat, Laboratoire CIE, Université de Savoie, 1990.

Analytica Chimica Acta, 270 (1992) 195–204
Elsevier Science Publishers B.V., Amsterdam

Experimental evaluation of theoretical response equations for an unsegmented flow system with a well-stirred mixing chamber

James M. Jordan [1] and Harry L. Pardue

Department of Chemistry, 1393 Brown Building, Purdue University, West Lafayette, IN 47907-1393 (USA)

(Received 6th April 1992; revised manuscript received 7th July 1992)

Abstract

This paper describes results of an experimental study of theoretical equations developed to describe time-dependent responses of a flow-based sample-processing system that includes a well-stirred mixing chamber. It also describes an alternative approach to the sample-introduction step that improves agreement between experimental and theoretical results. The study confirms the validity of the theoretical equations for situations in which the assumptions on which they are based are met. The most serious deviations occur for situations in which chemical reactions are slow.

Keywords: Flow system; Response equations

Sample processing is one of the critical functions in any quantitative determination [1]. Flow-based sample-processors can be grouped into two general categories, namely segmented [2] and unsegmented [3] systems. One variant of the unsegmented approach involves the combination of sample with reagent in a well-stirred mixing chamber [4]. In a variant of this latter approach, the sample is intercalated into a flowing stream that carries it into the mixing chamber [5,6].

In the more recent version of this latter approach, the flow rate is relatively low and the volume of the mixing chamber is of the same order of magnitude as the volume of sample [6]. The result is that the transient processes in the mixing chamber occur over periods of several seconds. In the original [6] and most subsequent applications [7,8] of this latter approach, the measurement objective has been the time interval required for processes in the mixing chamber to change from one predetermined set of conditions to another. Accordingly, most mathematical treatments of such systems have focused on the relationships between the measured time interval and initial analyte concentration. However, this is just one of several ways that quantitative information can be obtained from such a sample-processing system. To take maximal advantage of such a system, a mathematical treatment is needed that describes the response for a wide variety of conditions.

In the initial study [6] the approach was perceived to be a titration and the mathematical treatment involved assumptions that resulted in equations that were valid only for a very limited

Correspondence to: H.L. Pardue, Department of Chemistry, 1393 Brown Building, Purdue University, West Lafayette, IN 47907-1393 (USA).

[1] Present address: The Procter & Gamble Company, International Technology Coordination–Laundry & Cleaning Products, 6060 Center Hill Road, Cincinnati, OH 45224 (USA).

set of conditions. Subsequent papers from this laboratory described a more complete model for the system and to a mathematical treatment that yielded response equations for a wide variety of conditions for 1:1:1 stoichiometry among reactant, analyte and product [9–12]. A subsequent paper [13] criticized conclusions in our earlier studies [9,10] suggesting that unnecessary approximations were made. Except for the use of different symbols for parameters such as flow-rate, sample volume, etc., the development of time-dependent response equations in the latter study [13] was identical to that described earlier [9,10]. It was argued in a later paper [14] that mathematical expressions and subjective conclusions that appeared to support the criticisms of our earlier work were really based on the use of hidden assumptions that restricted the validity of resulting expressions and conclusions [13] to a much more limited set of conditions than was considered in our origninal treatment [9,10]. However, these arguments have been based primarily on mathematical treatments. Although the general forms of the simpler calibration equations have been tested for a limited set of operating conditons [13], the validity of proposed response and calibration equations [13,14] has not been tested rigorously by comparing effects of a wide range of experiment variables on measured results and theoretical expections.

The present study was inspired partly by those criticisms of our earlier work and partly by our interest in alternative data-processing methods for this flow system. We believe that further studies will show that the criticisms were unjustified and we also believe that alternative data-processing approaches will complement the time-interval method used most frequently with this flow system. Both these issues are best served by a thorough understanding of the time-dependent responses of the system. The primary goal of this part of the study was to evaluate the degree to which the theoretical equations could predict experimental responses accurately for a wide range of experimental conditions. The present paper focuses on the validity of response equations for both tracer studies and reactions with complex stoichiometry. The latter part of the study required the extension of the mathematical treatment to include complex stoichiometries among analyte, reactants and product. Also, the study resulted in an alternative approach to sample introduction that could offer benefits in other types of flow systems. Subsequent papers will describe the use of these reponse equations to develop and understand alternative data-processing approaches.

EXPERIMENTAL

Triiodide ion was used for tracer studies. The reaction between iodate, iodide and hydronium ion to produce triiodide

$$IO_3^- + 8I^- + 6H_3O^+ \rightarrow 3I_3^- + 9H_2O \qquad (1)$$

was used to test response equations developed for reactions with complex stoichiometry. In each case, the triiodide was detected amperometrically in a thin-layer flow cell.

Instrumentation

Figure 1 is a block diagram of the instrumentation. The system included a reagent reservoir, RR, two peristaltic pumps, P1 and P2, used to pump reagent, R, and sample, S, three 4-port slider valves, V1–V3, operated synchronously in both directions by two pneumatic actuators, PA, a well-stirred mixing chamber, MC, a thin-layer electrochemical detector, D, a flow meter, FM, electronic circuitry, EC, to measure electrolysis current and a computer, CPU. Each of these

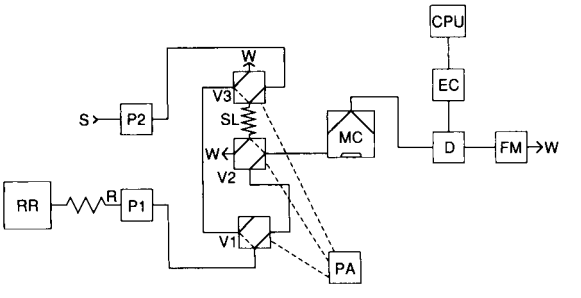

Fig. 1. Block diagram of the instrument system. RR = reagent reservoir; R = reagent; S = sample; P1, P2 = peristaltic pumps; V1, V2, V3 = 4-way slider valves; PA = pneumatic actuators; MC = mixing chamber; D = amperometric detector; FM = flow meter; EC = electronic circuitry; CPU = computer.

components is discussed below and elsewhere [15].

Reagent delivery system. Reagent was delivered from a 1-l mobile-phase reservoir system (Kontes, Vineland, NJ 08630) connected to a reagent pump (Minipuls 2A, Gilson Medical Electronics, Middleton, WI 53562) by polyvinyl tubing (1.52 mm i.d.). Segments of Teflon (35 cm, 1.5 mm i.d.) and C-Flex tubing (125 cm, C-Flex, Fisher Scientific, Pittsburg, PA) were used to connect the pump to a debubbler (Kontes), which was connected to the sampling valve by 15 m of coiled Teflon tubing (0.8 mm i.d.)

Sampling system. Two different sampling modes were evaluated. In one mode a sample loop is filled with a fixed volume of sample and switched in line with the reagent stream so that all the sample in the sample loop is flushed into the mixing chamber. In the other mode the sample loop is filled with sample and switched into the reagent stream for a fixed time period so that only the front portion of the sample in the sample loop is flushed into the mixing chamber.

Both modes can be described with the aid of Fig. 1. With the valves (Tefzel, 0.8 mm i.d., Chromatronics, Inc., Berkeley CA 94710) in the position shown by solid lines, sample is pumped through the sample-loop by pump P2 (Minipuls 2A, Gilson Medical Electronics, Middleton WI 53562) while reagent is pumped through the mixing chamber by pump P1 (Minipuls 2A). When the sample loop is flushed and filled with sample solution, valves are switched to positions represented by dashed lines inside the valve blocks. In this configuration, reagent is directed to flow through the sample loop forcing sample into the mixing chamber. In the first mode, the valves are left in this position for the duration of the experiment so that all sample in the sample loop is flushed into the mixing chamber. In the second mode, the valves are left in the position represented by dashed lines for a fixed period of time that is long enough to flush the desired volume of sample into the mixing chamber but short enough that all the sample is not flushed from the sample loop. At the end of the fixed time period, the valves are switched back to the initial positions represented by the solid lines so that reagent continues to flow through the mixing chamber and the sample loop can be filled with the next sample if desired.

The pneumatic actuators were driven by compressed air that was switched automatically to improve timing control. The sampling valve was connected to the mixing chamber by 3.8 cm of Teflon tubing (0.5 mm i.d., 1.5 mm o.d., Alltech Assoc., Inc., Applied Science Laboratories, Deerfield, IL 60015).

Mixing chambers. Mixing chambers were machined from Plexiglas as described earlier [9]. One design consisted of a flat surface sealed over a hemispherical indention in the bottom half; the other consisted of two hemispherical sections sealed together. The latter design resulted in better stirring and was used in most of the studies reported below. Stirring was achieved by a small magnetic bar inside the chamber driven by a motor-driven magnetic stirrer placed close to the chamber. The volume of the mixing chamber for all these studies was 0.7017 ml. The mixing chamber was connected to the flow-through detector by 3.8 cm of Teflon tubing (0.5 mm i.d., 1.5 mm o.d., Alltech).

Detector. Two thin-layer detectors (Bioanalytical Systems, West Lafayette, IN), both with internal volumes of about 30 μl, were evaluated for the detection of triiodide. One consisted of one glassy carbon and one platinum electrode and the other consisted of two platinum electrodes. The two platinum electrodes worked best because there was less adsorption of iodine to platinum than to the glassy carbon.

Best results were obtained when the platinum electrodes were polished and pretreated chemically prior to use. Before chemical pretreatment, electrodes were cleaned by using 6-μm diamond polish followed by 1-μm diamond polish (both on Texmet pads) and 0.5-μm alumina on microcloth disks. Electrodes were washed with water followed by methanol after each of the first two polishing steps and were washed with water and sonicated briefly in water after the third polishing step. The first step in the chemical pretreatment was to insert the electrodes in sulfuric acid (1 mol l^{-1}) and cycle the voltage twice between 1.3 and -0.3 V vs. Ag/AgCl (3 mol l^{-1} NaCl) reference

electrode at a rate of 5 mV s^{-1}. Each cycle was begun at +0.4 V and scanned anodically using a cyclic voltammograph (Bioanalytical Systems, BAS CV-27). Then the potential was held constant at +0.4 V vs. the Ag/AgCl reference electrode for 3 min after which the electrodes were immersed in 10 mmol l^{-1} triiodide solution (0.15 mol l^{-1} iodide, 0.12 mol l^{-1} dibasic potassium phosphate, 0.03 mol l^{-1} monobasic sodium phosphate heptahydrate) for 5 min.

A polarizing voltage of 200 mV was used for the amperometric detection of triiodide in the flow system. Electrolysis current varied linearly with triiodide concentration up to at least 2 mmol l^{-1}. A typical least-squares fit of current, I, vs. concentration, C, yielded $I(\text{mA}) = (5.56 \pm 0.05)C(\text{mmol } l^{-1}) - (0.09 \pm 0.05)\text{mA}$ with $S_{yx} = 0.087$ mA.

Flow meter. The electrochemical detector was connected to a digital flow meter (Phase Separations, Inc., Norwalk, CT) by 15 m of Teflon tubing (0.5 mm i.d.). This long length of tubing served to isolate the flow meter from the detector.

Measurement / data processing. Measurement circuitry is described in detail elsewhere [15]. Briefly, it consisted of a fast JFET-input operational amplifier in the current-to-voltage mode with appropriate offset and gain controls followed by a voltage amplification stage with variable gain.

Output signals were digitized and collected on-line by using an IBM-compatible microcomputer (AT&T PC-6300, AT&T Information Systems). A public domain transfer program (KERMIT) was used to transfer data files from the microcomputer to a supermicrocomputer workstation (MASSCOMP MC-5500, Massachusetts Computer Corp., Westford, MA) for further processing and long-term storage.

Theoretical equations were programmed in C-language for both DOS and UNIX operating systems. These programs were used to compare experimental and theoretical responses.

Reagents

All reagents were prepared in distilled deionized water and reagent-grade chemicals were used throughout. In most cases, water was degassed with helium. Critical concentrations were standardized by conventional titration procedures.

Buffer / iodide solution. This solution contained 0.1218 mol l^{-1} dibasic potassium phosphate, 0.02605 mol l^{-1} monobasic sodium phosphate heptahydrate and 0.15 mol l^{-1} potassium iodide. When necessary, the pH was adjusted to 6.0 by using strong acid or base. The solution was vacuum filtered by using 0.2 μm Nylon-66 membrane filters (Rainin Instrument Co., Woburn, MA 01801) and stored in brown glass bottles at 4°C.

Triiodide. Stock solutions of triiodide were prepared by dissolving approximately 10.2 mmol iodine in the buffered iodide solution. This solution was vacuum filtered as described above and stored in brown glass bottles at 4°C.

Other concentrations were prepared by dilution with the buffered iodide solution.

Iodide. Iodide solutions (0.15 mol l^{-1}) were prepared in water from which oxygen had been removed by passing helium gas through it. This solution was prepared immediately before use and was used to prepare the iodate and acid solutions described below.

Iodate. Iodate solutions (0.1500 mol l^{-1}) were prepared in 0.15 mol l^{-1} iodide immediately before use.

Hydrochloric acid. Hydrochloric acid solutions were prepared in 0.15 mol l^{-1} iodide. Working standards of 0.10 to 10 mmol l^{-1} were prepared by dilution with 0.15 mol l^{-1} iodide solution.

MATHEMATICAL TREATMENT

Symbols used are summarized in Table A1; assumptions are the same as those described earlier [14]. The mathematical treatment is the same except that the stoichiometry among analyte, A, reactant, B, and product, P, is as follows

$$xA + yB \rightarrow zP \quad (2)$$

Only those equations that are not the same or intuitively obvious from the previous paper [14] are presented here.

Mass-balance equations

The mass-balance equations define the instantaneous relationships among analyte, reactant and product in the mixing chamber (see Table A1 in [14]).

Mass-balance equations for analyte concentration differ in only one respect from those described earlier. The expression, $-(C_{ag} + C_b^0)$, for the third stage with excess sample is changed to $-(C_{ag} + (x/y)C_b^0)$. Mass-balance equations for reactant concentration are the same as reported earlier except that each term involving analyte concentration should be changed to $(y/x)C_{as}^0$. Similarly, mass-balance equations for product concentrations are the same except that all terms for analyte concentration should be changed to $(z/x)C_{as}^0$ and all terms for reactant concentration should be changed to $(z/y)C_b^0$.

All boundary conditions remain the same as reported earlier [14].

Response equations

All equations for tracer studies (no reaction) are the same as those reported earlier (Table A2 in [14]).

Unfortunately, changes in response equations for situations involving reactions are neither intuitively obvious nor easily summarized in text. Accordingly, detailed response equations are reported in Tables A2 through A4 in the appendix. These equations reduce to those in Tables A3 through A5 reported earlier [14] if the ratios of coefficients (y/x, x/z, etc) are replaced by unity.

Criteria for excess analyte or reactant

Procedures used to develop an equation to differentiate between conditions resulting in excess analyte or reactant were described earlier [14]. The resulting equation for a single-channel system with the stoichiometry in Eqn. 1 is given by

$$C_{bg}^0 = (y/x)C_{as}^0\left[\exp(V_s/V_g) - 1\right] \quad (3)$$

This equation describes the situation for which the combined effects of mass transport and chemical reaction are just sufficient to remove all reactant from the mixing chamber when all the sample has entered the chamber. Although some authors have confused points of equal concentration with equivalence points, it is important to note that this is not an equivalence point because some reactant will have been lost via mass transport.

For situations in which the initial reactant concentration in the gradient chamber, C_{bg}^0, is larger than the right side of Eqn. 3, reactant will be in excess. For situations in which initial reactant concentration in the gradient chamber is less than the right side of the equation, analyte will be in excess.

Unique points in time

As discussed earlier [9,10], processes in the mixing chamber take place in distinct phases. Accordingly, there are unique points in time that mark separations between these phases. Some unique points in time for a single-channel system are summarized in Table 1. Briefly, t_1 represents the time when all reactant is removed from the mixing chamber, t_2 is the time when all sample has entered the chamber and t_3 is the time when all analyte is removed from the chamber. These times and their significance are discussed in more detail elsewhere [14].

TABLE 1

Equations for unique points in time for a single-channel flow system

Symbol	Equation	Eqn. No.
t_1	$(V_g/f)\ \ln\{[(y/x)C_{as}^0 + C_{bg}^0]/(y/x)C_{as}^0\}$	4
t_2	V_s/f	5
t_3	$(V_g/f)\ \ln\{[C_{as}^0 + (x/y)(C_b^0)\ \exp(V_s/V_g) - (C_{as}^0 + (x/y)C_{bg}^0)]/[(x/y)C_b^0]\}$	6

RESULTS AND DISCUSSION

All results reported here were obtained by using the amperometric detection of triiodide. Response equations were tested both with triiodide used as a tracer and with triiodide produced by reaction among iodide, iodate and hydronium ion (Eqn. 1).

Tracer studies

Analyte profiles. Initial tracer studies were done with fixed volumes of triiodide solutions intercalated into the flowing stream in the conventional manner as described earlier [6–9]. As shown in Fig. 2, there were significant differences among experimental and theoretical response curves (Eqns. A1–A3 in [14]). Experimental results tended to lag behind predicted responses and to have lower and more rounded peak shapes than expected. After considerable efforts to resolve the problem were unsuccessful [15], we concluded there was a fundamental problem either with the mathematical treatment or the experimental design.

Because the largest deviations occurred during the time that the final portions of the sample were entering the chamber, we reasoned that the problem likely resulted from mixing between the trailing edge of the sample plug and the leading edge of the reagent stream. To test this idea we tried an alternative mode of sample introduction, namely timed control of sample volume.

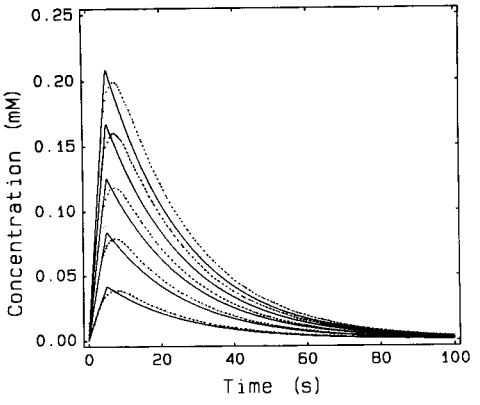

Fig. 2. Concentration vs. time profiles for triiodide tracer with fixed-mode of sample introduction. Experimental (·····), theoretical (———); $f = 0.0326$ ml s^{-1}; $V_g = 0.7017$ ml; $V_s = 0.655$ ml; C_{as}^0 (bottom to top) = 0.2, 0.4, 0.6, 0.8 and 1.0 mmol l^{-1}.

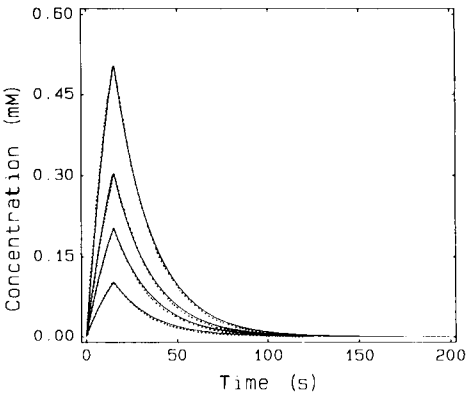

Fig. 3. Concentration vs. time profiles for triiodide tracer with time-controlled sample introduction. Experimental (·····), theoretical (———); $f = 0.0333$ ml s^{-1}; $V_g = 0.7017$ ml; $V_s = 0.5$ ml; C_{as}^0 (bottom to top) = 0.2, 0.4, 0.6 and 1.0 mmol l^{-1}.

Rather than using the total sample volume that is intercalated into the flow stream as is usually done, a timed introduction is used such that only a portion of the sample plug is used. In this way, the tailing portion of the sample plug which mixes with the leading edge of the reagent stream is not used. Thus, the sample introduction process should approach the assumption of plug flow more closely with this approach than with the more traditional approach to sample introduction.

As shown in Fig. 3, this approach to sample introduction gave very good agreement between experimental and theoretical results for a fixed volume of different concentrations of tracer. Results in Figs. 4 and 5 illustrate the ability of the theoretical equations (Eqns. A1–A3 in [14]) to account for changes in sample volume and flow-rate. This approach to sample introduction was used for all subsequent studies.

Reagent profiles. To test equations for reagent profiles, triiodide solution (1.0 mmol l^{-1}) was used as the carrier stream and aliquots of buffer solution were intercalated into the stream. As shown in Fig. 5, agreement between experimental and theoretical responses (Eqns. A4–A6 in [14]) is reasonable but is somewhat degraded relative

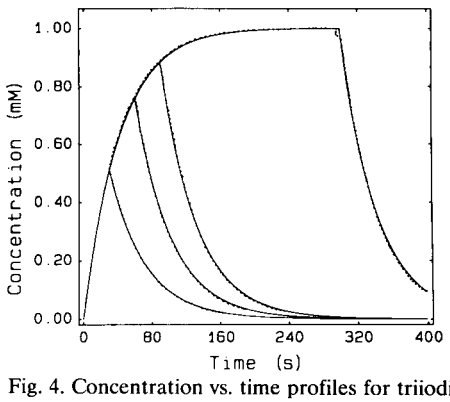

Fig. 4. Concentration vs. time profiles for triiodide tracer with time-controlled sample introduction. Experimental (· · · · · ·), theoretical (———); $f = 0.0250$ ml s^{-1}, $V_g = 0.7017$ ml, V_s (bottom to top) = 0.5, 1.0, 1.5, 5.0 ml, $C_{as}^0 = 1.0$ mmol l^{-1}.

to results for the tracer studies. Although the deviations are not large they are worrisome. They occur primarily along the leading edge and just beyond the valley and experimental values of tracer are consistently lower than expected. Also, the deviations are larger for larger volumes of buffer.

It was expected that the most probable source of error along the leading edge would be mixing of the sample plug with reagent in the flow stream between the sample loop and the mixing chamber. However, because the tracer was in the flow stream, mixing between the sample loop and the

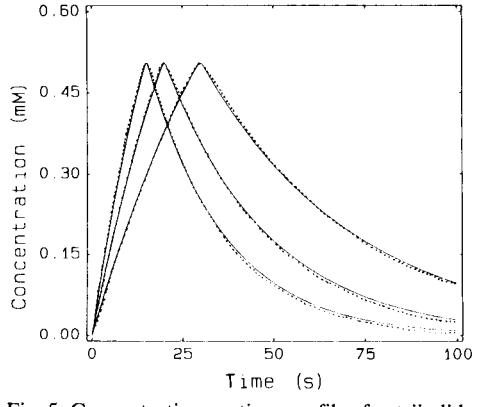

Fig. 5. Concentration vs. time profiles for triiodide tracer with time-controlled sample introduction. f (left to right) = 0.0333, 0.0250, 0.0166 ml s^{-1}; $V_g = 0.7017$ ml, $V_s = 0.5$ ml; $C_{as}^0 = 1.0$ mmol l^{-1}.

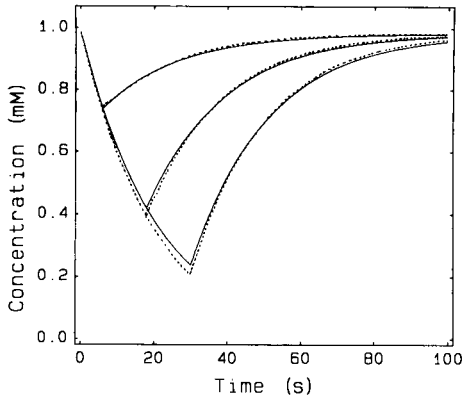

Fig. 6. Concentration vs. time profiles for triiodide tracer in flow stream with time-controlled introduction of buffer as sample. Experimental (· · · · · ·), theoretical (———); $f = 0.0333$ ml s^{-1}, $V_g = 0.7017$ ml, V_s (bottom to top) = 0.2, 0.6, 1.0 ml; $C_b^0 = 1.0$ mmol l^{-1}.

mixing chamber would cause tracer concentrations to be higher than predicted. Accordingly, there probably is some other source of the problem. Other possible sources of the deviations are errors in fixed parameters such as the flow-rate, sample volume or volume of the mixing chamber. However, if these were the sources of the deviations we would have expected similar problems when the tracer was used as the sample. Other possible sources of the deviations would be changes in electrode response, adsorption of triiodide on surfaces, incomplete return of tracer concentration to its steady-state value in the reagent line or mixing chamber. However, we were unable to confirm any single source of the deviations observed in Fig. 6.

For the record, the deviations correspond to flow-rates and sample volumes approximately 10% higher than the values used.

Chemical reaction

The reaction of iodate with iodide in acid solution was used to test equations for situations involving complex stoichiometry (Tables A2–A4). As in an earlier study [16], we chose the acid, HCl, as the analyte to be quantified. Preliminary studies showed that the reaction was quite fast with 150 mmol l^{-1} iodate in the flow stream and small volumes (0.1 to 1.0 ml) of low concentra-

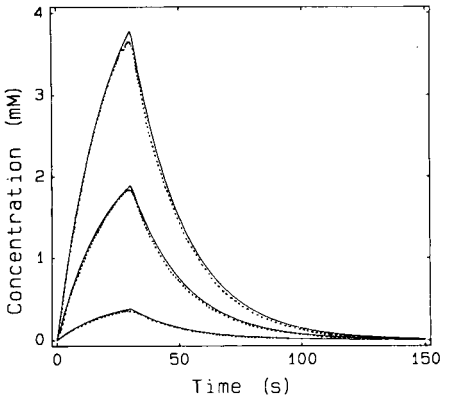

Fig. 7. Concentration vs. time profiles for reaction of acid with excess iodide and iodate with time-controlled sample introduction. Experimental (· · · · · ·), theoretical (———); f = 0.0333 ml s^{-1}, V_g = 0.7017 ml, V_s = 1.0 ml, C_{as}^0 (bottom to top) = 1.0, 5.0, 10.0 mmol l^{-1}.

tions (0.5 to 10 mmol l^{-1}) of hydrochloric acid in a 150 mmol l^{-1} iodide solution.

Excess reactant (product monitored). Figure 7 shows plots of experimental and theoretical responses (Eqns. A10–A12) for three different concentrations of hydrochloric acid. Good agreement is observed between experimental and predicted results. Similar agreement was observed for a 20-fold range of acid concentrations (0.5–10 mmol l^{-1}) and for a 10-fold range of sample volumes (0.1, 0.5 and 1.0 ml).

Excess analyte (product monitored). To test conditions of excess analyte, the same conditions described in the previous subsection were used except that volumes of analyte (HCl in iodide solution) were increased to 5.0 ml for initial experiments.

Figure 8A shows a comparison of experimental and theoretical (Eqns. A13–A19) results for the same volume of different concentrations of hydrochloric acid. There is good agreement between experimental and theoretical responses for the lowest concentration but the deviations become larger with higher concentrations. The deviations at high analyte concentrations are not surprising because the low iodate concentrations in the mixing chamber result in slow reaction rates. Reaction rates are too slow for all analyte to react during the measurement period and the amount of product is less than predicted by equations based on assumptions that reactions are instantaneous in the mixing chamber [14].

Analogous behavior is observed in Fig. 8B for different volumes of a fixed concentration of acid. This figure shows good agreement for different sample volumes up to about 1.0 ml, after which iodate is no longer in sufficient excess to ensure fast reaction in the mixing chamber.

Effects of flow-rate were not examined. It is expected that faster flow-rates would result in deviations at somewhat smaller amounts of analyte because there would be less time for reactions to go to completion and that slower flow-rates would give better agreement at higher ana-

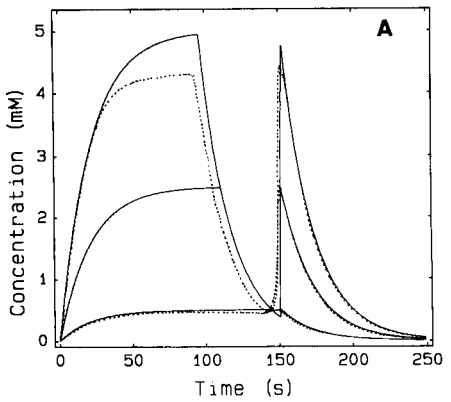

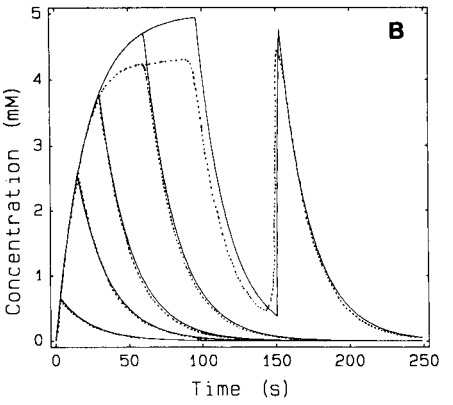

Fig. 8. Concentration vs. time profiles for reaction of excess acid and iodide with iodate, with time-controlled sample introduction. Both frames: experimental (· · · · · ·), theoretical (———); f = 0.0333 ml s^{-1}, V_g = 0.7017 ml; C_b^0 = 150 mmol l^{-1}. (A) V_s = 5.0 ml; C_{as}^0 (bottom to top) = 1.0, 5.0, 10.0 mmol l^{-1}. (B) V_s (botton to top) = 0.1, 0.5, 1.0, 2.0 and 5.0 ml, C_{as}^0 = 10 mmol l^{-1}.

lyte concentrations because there would be more time for reactions to go to completion.

Conclusions

Although many other combinations of variables and operational approaches could be studied, we believe the present study is sufficient to confirm the validity of the response equations when assumptions on which they are based are met. The study also identifies the types of circumstances that can cause deviations from expected behavior and introduces an approach to the sample-introduction step that can lead to improved performance. Finally, we conclude that these response equations can be used to develop improved understanding and alternative approaches to quantitative methods that include this approach to sample processing.

This work was supported by Grants No. GM-13326-23,24 from the National Institutes of Health.

APPENDIX

TABLE A1

Description of symbols used in the mathematical treatment

Symbol	Meaning
C_{as}^0	Analyte concentration in undiluted sample
C_{ag}	Analyte concentration in gradient chamber
C_b^0	Reactant concentration in undiluted reagent
C_{bg}^0	Initial reactant concentration in gradient chamber
C_{pg}	Product concentration in gradient chamber
C^{sn}	Concentration during nth stage ($n = 1, 2, 3 \ldots$)
C^P	Concentration at a peak response
C^v	Concentration at valley response
V_s	Volume of sample
V_g	Volume of gradient chamber
f	Flow-rate
t_1	Time for all reagent to be removed from the gradient chamber
t_2	Time for all sample to enter the gradient chamber
t_3	Time for all analyte to be removed from the gradient chamber
x, y, z	Stoichiometric coefficients (see Eqn. 2)

TABLE A2

Concentration profiles for analyte in a single-channel system with reaction

Excess reactant		
All stages [a].	$C_{ag} = 0$	
Excess analyte		
First stage [b]:	$C_{ag}^{s1} = 0$	
Second stage [c]:	$C_{ag}^{s2} = C_{as}^0 - [(C_{as}^0 + (x/y)C_{bg}^0) \exp(-ft/V_g)]$	(A1)
Peak [d]:	$C_{ag}^P = C_{as}^0 - [(C_{as}^0 + (x/y)C_{bg}^0) \exp(-V_s/V_g)]$	(A2)
Third stage [e]:	$C_{ag}^{s3} = \{[(C_{as}^0 + (x/y)C_b^0) \exp(V_s/V_g) - (C_{as}^0 + (x/y)C_b^0)][\exp(-ft/V_g)]\} - (x/y)C_b^0$	(A3)
Fourth stage [f]:	$C_{ag}^{s4} = 0$	

[a] $0 \le t < \infty$. [b] $0 \le t \le t_1$. [c] $t_1 \le t \le t_2$. [d] $t_2 = V_s/f$, [e] $t_2 \le t \le t_3$. [f] $t_3 \le t < \infty$.

TABLE A3

Concentration profiles for reactant in a single-channel system with reaction

Excess reactant		
First stage [a]:	$C_{bg}^{s1} = [(C_{bg}^0 + (y/x)C_{as}^0)\exp(-ft/V_g)] - (y/x)C_{as}^0$	(A4)
Valley [b]:	$C_{bg}^{v} = [(C_{bg}^0 + (y/x)C_{as}^0)\exp(-V_s/V_g)] - (y/x)C_{as}^0$	(A5)
Second stage [c]:	$C_{bg}^{s2} = C_{bg}^0 - \{[((y/x)C_{as}^0 + C_b^0)\exp(V_s/V_g) - ((y/x)C_{as}^0 + C_{bg}^0)]\exp(-ft/V_g)\}$	(A6)
Excess analyte		
First stage [d]:	$C_{bg}^{s1} = [(C_{bg}^0 + (y/x)C_{as}^0)\exp(-ft/V_g)] - (y/x)C_{as}^0$	(A7)
Second stage [e]:	$C_{bg}^{s2} = 0$	(A8)
Third stage [f]:	$C_{bg}^{s3} = C_b^0 - (y/x)\{[((x/y)C_{as}^0 + C_b^0)\exp(V_s/V_g) - ((x/y)C_{as}^0 + C_{bg}^0)]\exp(-ft/V_g)\}$	(A9)

[a] $0 \le t \le t_2$. [b] $t = t_2 = V_s/f$. [c] $t_2 \le t < \infty$. [d] $0 \le t \le t_1$. [e] $t_1 \le t \le t_3$. [f] $t_3 \le t < \infty$.

TABLE A4

Concentration profiles for product in single-channel system with reaction

Excess reactant		
First stage [a]:	$C_{pg}^{s1} = (z/x)C_{as}^0[1 - \exp(-ft/V_g)]$	(A10)
Peak [b]:	$C_{pg}^{p} = (z/x)C_{as}^0[1 - \exp(-V_s/V_g)]$	(A11)
Second stage [c]:	$C_{pg}^{s2} = (z/x)C_{as}^0[\exp(V_s/V_g) - 1]\exp(-ft/V_g)$	(A12)
Excess analyte		
First stage [d]:	$C_{pg}^{s1} = (z/x)C_{as}^0[1 - \exp(-ft/V_g)]$	(A13)
First peak [e]:	$C_{pg}^{p1} = ((z/x)C_{as}^0C_{bg}^0)/((y/x)C_{as}^0 + C_{bg}^0)$	(A14)
Second stage [f]:	$C_{pg}^{s2} = (z/y)C_{bg}^0\exp(-ft/V_g)$	(A15)
Valley [g]:	$C_{pg}^{v} = (z/y)C_{bg}^0\exp(-V_s/V_g)$	(A16)
Third stage [h]:	$C_{pg}^{s3} = C_b^0 - (z/y)\{[C_b^0\exp(V_s/V_g) - C_{bg}^0][\exp(-ft/V_g)]\}$	(A17)
Second peak [i]:	$C_{pg}^{p2} = (z/y)C_b^0\{C_{as}^0[\exp(V_s/V_g) - 1]\}/[(C_{as}^0 + (x/y)C_b^0)\exp(V_s/V_g) - (C_{as}^0 + (x/y)C_{bg}^0)]$	(A18)
Fourth stage [j]:	$C_{pg}^{s4} = (z/x)C_{as}^0[\exp(V_s/V_g) - 1]\exp(-ft/V_g)$	(A19)

[a] $0 \le t \le t_2$. [b] $bt_2 = V_s/f$. [c] $t_2 \le t < \infty$. [d] $0 \le t \le t_1$. [e] $t = t_1$. [f] $t_1 \le t \le t_2$. [g] $t_1 \le t \le t_2$. [h] $t_2 < t < t_3$. [i] $t = t_3$. [j] $t_3 \le t < \infty$.

REFERENCES

1 H.L. Pardue and J. Woo, J. Chem, Ed., 61 (1984) 409.
2 L.T. Skeggs, Anal. Chem., 38 (1966) 31A.
3 W.J. Blaedel and G.P. Hicks, Anal. Chem., 34 (1962) 388.
4 K.E. Hallikainen and D.J. Pompeo, Instruments, 25 (1952) 335.
5 D. Sanderson, J.A. Bittikofer and H.L. Pardue, Anal. Chem., 44 (1972) 1934.
6 J. Ruzicka, E.H. Hansen and H. Mosbaek, Anal. Chim. Acta, 92 (1977) 235.
7 K.K. Stewart, Anal. Chem., 55 (1983) 931A.
8 J.F. Tyson, Analyst (London), 109 (1984) 319.
9 H.L. Pardue and B. Fields, Anal. Chim. Acta, 124 (1981) 39.
10 H.L. Pardue and B. Fields, Anal. Chim. Acta, 124 (1981) 65.
11 H.L. Pardue and P. Jager, Anal. Chim. Acta, 179 (1986) 169.
12 P. Jager and H.L. Pardue, Anal. Chim. Acta, 187 (1986) 343.
13 J.F. Tyson, Anal. Chim. Acta, 179 (1986) 131.
14 H.L. Pardue and J.M. Jordan, Anal. Chim. Acta, 220 (1989) 23.
15 J.M. Jordan, Ph.D. Thesis, Purdue University, West Lafayette, IN, 1991.
16 W. Matuszewski, A. Hulanicki and M. Trojanowicz, Anal. Chim. Acta, 194 (1987) 269.

Analytica Chimica Acta, 270 (1992) 205–211
Elsevier Science Publishers B.V., Amsterdam

Flow-injection on-line fibre column separation and preconcentration system for efficient determination of trace gold in ores and metallurgical samples by flame atomic absorption spectrometry [1]

Weiyi Qi, Xing Wu, Chun Zhou, Haizhou Wu and Yingqi Gao

Department of Analytical Chemistry, General Research Institute for Non-ferrous Metals, Beijing 100088 (China)

(Received 2nd August 1991; revised manuscript received 24th February 1992)

Abstract

A flow-injection on-line 8531 fibre column separation and preconcentration system is proposed for the efficient flame atomic absorption spectrometric determination of trace gold in ores and metallurgical samples. A flow manifold with a pump and two valves was assembled to conduct the operating cycle of equilibration–preconcentration–washing–elution automatically in sequence. It was found that 8531 fibre is selective for gold and possesses good flow properties. A 40 mm long column is recommended. The detection limit (3σ) of the proposed method was 0.2 ng ml^{-1} gold and the relative standard deviation was 6% ($n = 11$) for 1 ng ml^{-1} and 2.2% ($n = 7$) for 80 ng ml^{-1} gold. About 40–60 injections can be performed per hour. The method was proved to be suitable for the routine determination of trace gold above 0.01 g t^{-1} in ores and metallurgical samples with satisfactory accuracy and precision.

Keywords: Atomic absorption spectrometry; Flow injection; Fibre column; Gold; Metallurgical samples; Ores

The flow-injection on-line column preconcentration technique, distinguished by its important characteristics of high preconcentration efficiency and great savings of time and sample consumption, demonstrates significant advantages over batch procedures [1,2]. In spite of the attraction of this technique, in routine practice its applications are limited [3]. Fang and Welz [3] made a detailed study of this limitation and, for practical considerations, proposed a modified design with advantages of sufficient enrichment factors, lower consumption of sample solution, lower susceptibility to interferences and higher sample throughput. Apart from these hardware improvements, Ruzicka and Arndal [4] pointed out that the key to a successful separation and preconcentration of an analyte is to choose a suitable separation system for each specific determination. They introduced sorbent extraction into a flow-injection analysis (FIA) on-line column preconcentration system so that the advantage of the single-stage solvent extraction principle of "all or nothing" was combined with the convenience of flow-injection on-line microcolumn operation.

For chemical analyses for trace elements in ores and metallurgical samples, many determinations can hardly be performed directly unless the analyte is previously isolated from the sample matrix and interfering ions. Separation and pre-

Correspondence to: Weiyi Qi, Department of Analytical Chemistry, General Research Institute for Non-ferrous Metals, Beijing 100088 (China).

[1] Originally submitted for the *Fifth International Conference on Flow Analysis, Kumamoto, August 21–24, 1991.* The majority of the papers presented at this conference have been published in *Anal. Chim. Acta*, Vol. 261 (1992).

concentration are in certain instances an indispensable step even for some instrumental analyses. The developments mentioned above stimulated the investigation of efficient flow-injection methods with on-line separation and preconcentration techniques for routine practice so that the labour- and time-consuming batch procedure could be discarded. Obviously, this can be achieved as long as a selective separation system can be found for a desired determinant in a given matrix.

In addition to sorbent extraction, another type of extraction adapted to column operation is reversed-phase extraction chromatography. Here the extractant is immobilized on the support as functional groups and the separation is carried out when the extracted materials on the stationary phase are "back-extracted" one by one during the elution process, according to the differences in their distribution coefficients (D). It has been successfully applied in separations of elements such as rare earth and radioactive elements. Although the D values of these elements are very similar, the method provides good separations in terms of the multi-step extraction principle. For elements that have large differences in D values, it is possible to realize the "all or nothing" principle in FIA on-line column operation. A flow-injection method using CL-5209 neutral phosphine resin for the on-line separation and preconcentration of uranium from geological samples followed by spectrophotometric determination has been reported [5]. In this work, a rapid analysis for trace gold in ores and metallurgical samples was achieved by inserting a microcolumn containing a similar type of extraction fibre (8531) in a flow-injection manifold for on-line separation and preconcentration prior to determination by flame atomic absorption spectrometry (AAS).

Several FIA methods have been reported for the determination of gold but the separations that preceded it were carried out off-line [6,7]. A chemiluminescence method for the determination of gold features a high sensitivity compared with most methods, but it does not have selectivity, and therefore it required a previous strict separation technique. Moreover, the determination can only be achieved when gold is present as gold(III), which poses obstacles for on-line separation because most eluents are reductants and gold is eluted only when it is reduced to gold(I). Spectrophotometry suffers similar problems, although not so seriously. In contrast, flame AAS is less prone to interferences, but the sensitivity for gold seems insufficient for the determination of < 0.2 $\mu g\ ml^{-1}$ gold. However, some improvements have been reported recently for enhancing the detection ability of the instrument [8]. Optimized AAS working conditions can be obtained by combining all these achievements in one system. In this work, the following components were used in combination to make up an efficient flame AAS system: a high-performance concentric pneumatic nebulizer to increase the efficiency of nebulization, a high-performance hollow-cathode lamp to increase the intensity and stability of the light source and an atom-trapping quartz tube to lengthen the retention time of the determined atoms in the flame and to stabilize the flame. The experiments showed that with this optimized combination the detection limit for the determination of gold was improved by an order of magnitude and can reach as low as 2 ng ml^{-1}. The method was shown to meet the requirements for the determination of trace gold in the process of ore dressing and metallurgy.

EXPERIMENTAL

Apparatus

The detector used was a Model WFX-1B atomic absorption spectrometer (Beijing Second Optical Instrument Factory), equipped with a high-performance concentric pneumatic nebulizer, a high-performance gold hollow-cathode lamp operated at 3 mA and 242.8 nm, a power supply to provide a booster current of 4 mA (all from Beijing General Research Institute for Non-ferrous Metals) and a 5-cm burner with a single-slot atom-trapping quartz tube. The detector was connected with a Hitachi Model 056 recorder.

The FIA system, composed of a peristaltic pump and two injection valves with an electronic controller, was laboratory made and designed to

(a)

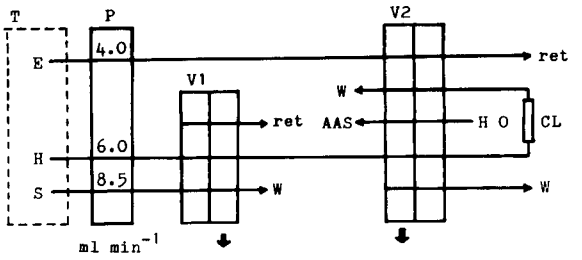

(b)

	Washing	Preconcentration	Washing	Elution
V1	A	B	A	B
V2	A			B
	5	15-40	15	25 s

Fig. 1. Schematic diagrams of (a) the manifold and (b) the operation of the valves. P = pump; V1, V2 = valves; T = thermostat; S = sample solution; H = washing solution; E = eluent; CL = column; W = waste; ret = returned solution. A is the position of the valves illustrated in (a), and B is the position of the valves directed by the arrows.

be especially suitable for column separation and preconcentration operation involving a washing process.

A small thermostat was used to maintain the working solution at a suitable temperature.

Reagents

All chemicals were of analytical-reagent grade.

A gold stock standard solution of 1 mg ml^{-1} was prepared from US NBS Gold Standard Reference Material (SRM 3121, spectrometric solution). Working standard solutions ranging from 1 to 100 ng ml^{-1} were prepared by serial dilution of the stock standard solution with 10% aqua regia.

The 8531 fibre was prepared by the Department of Applied Chemistry, Institute of Costume, as requested by the authors.

A 5 g l^{-1} thiourea solution was prepared for elution and 2% aqua regia as washing solution.

Procedure

The manifold was set up as shown in Fig. 1a with the flow-rates of sample, washing solution and eluent as shown. The microcolumn was made by inserting 80 mg of 8531 fibre into a PTFE tube (40 mm × 2 mm i.d.) and was connected to the system with silicone-rubber tubing of suitable i.d.. The two valves were controlled by an electronic timer and the intervals of each period were as given in Fig. 1b.

A general method was used for sample decomposition [9]. The sample solutions were prepared by dissolving 10 g of ore or metallurgical sample, previously ignited at 650°C, in aqua regia. The dissolved samples were then transferred into a 100-ml volumetric flask and diluted to volume with aqua regia to give a final acidity of 10%. After the precipitates had settled, the supernatant layer was aspirated into the flow injection system.

RESULTS AND DISCUSSION

Manifold design

A washing process is generally considered to be unnecessary in FIA column operation [1], so previous manifold designs omitted this manipulation in order to increase the rate of analysis. However, it was found when dealing with complex samples with a high concentration of a matrix of heavy metal ions, although the separation system was selective and the dead volume of the column was small, the coexisting ions remaining inside the column could still cause distortion of the detected signals of trace determinants. Moreover, certain ions in the matrix remaining inside the column could react with the eluent and cause problems. For example, a precipitate could form and block the connecting tube, as happened in the present instance when a high concentration of copper ions in the sample solution formed an insoluble complex with thiourea. Therefore, in this work, a washing step was considered to be essential to rinse away the coexisting ions remaining inside the column.

Similarly, it was also considered to be necessary to equilibrate the column before the next cycle so as to prevent entirely the possibility that the sample solution could come into contact with the eluent. A fixed-volume injection into a carrier stream which also served for washing purposes was employed previously in a method for the FIA

on-line column separation and preconcentration of uranium prior to spectrophotometric determination [5]. There, sample filling and sample injection/preconcentration were carried out in two steps, and sample dispersion occurred during the injection process, so the working efficiencies were evidently reduced. In this work, a time-based injection was employed and a flow-injection system with dual valves was designed, one to commutate the streams of washing solution and sample solution and the other to alternate the washing solution and eluent. The switching of the valves was controlled by an electronic timer so as to conduct the operating cycle of equilibration–adsorption–washing–elution automatically in sequence. Although the lengthening of the analytical period and the decrease in the concentration efficiencies are unfortunate to some extent, the technique was expected to benefit from its enhanced reliability owing to the interference-free treatment, as is confirmed in the following sections on investigations of interferences and sample analyses.

Preconcentration system and conditions

Gold does not lack separation systems, but many of those available experience technical obstacles to on-line operation. Gold in its chloride form can be strongly adsorbed on an anion exchanger, but is very difficult to elute back into the solution. Foam adsorption of gold is a comparatively simple method for the separation but the completeness and the stability of the adsorption were suspect. Considering the separation methods for gold, the selectivities of neutral phosphine oxide extractants (trioctylphosphine oxide and its derivatives) for gold in hydrochloric or nitric acid are so high that their extraction constants are even several orders of magnitude higher than those of the most of the common elements [10]. Therefore, this type of extractant was recommended as the stationary phase in the present work.

Another factor carefully considered was the material of the support. It is known [11] that the flow dynamic properties are greatly improved for an ion-exchange fibre compared with an ion-exchange resin. This dynamic advantage is essential

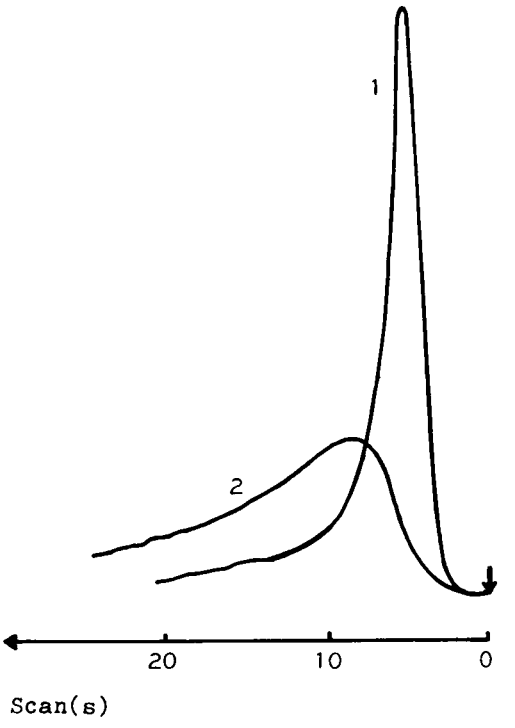

Fig. 2. Rapid scan of flow-injection curve for elution from (1) 8531 fibre and (2) 8531 resin.

for on-line FIA separation and preconcentration, as the concentration efficiency (CE) [12] mainly depends on the rates of both loading and elution. The synthesis of 8531 fibre involves linking the functional group of a neutral phosphine oxide extractant to an inert fibre. The capacity of the fibre for gold was 0.17 mmol g^{-1}. The flow elution curve illustrated in Fig. 2 shows the much more rapid and discrete elution from the fibre, compared with the resin. Therefore, 8531 fibre was used in the subsequent work.

Some of the factors governing the performance of separation and preconcentration were investigated and the optimized operating conditions were selected, some of which are shown in Fig. 3. Experiments showed that gold was adsorbed on 8531 fibre over a wide range of aqua regia concentrations; the signals were almost constant from 5% to 25% aqua regia. The flow properties of 8531 fibre for adsorption of gold were so good that when the pumping rate for loading was increased from 5 to 10 ml min^{-1}, the corresponding

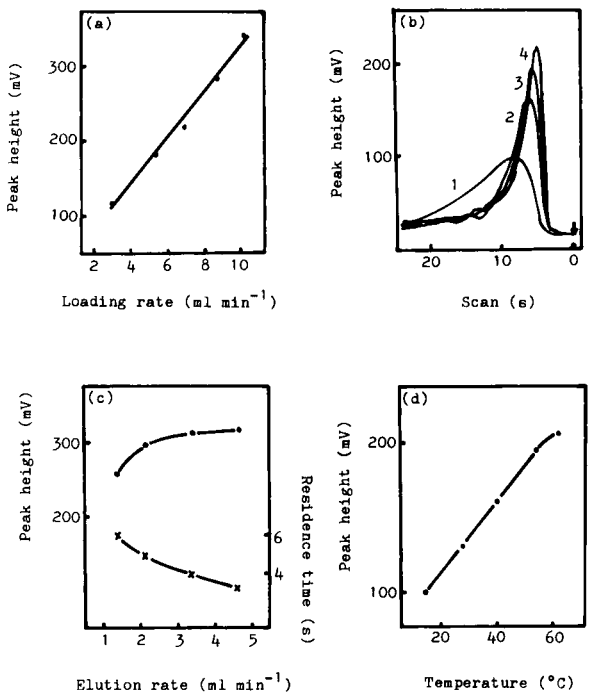

Fig. 3. Influence of (a) loading flow-rate, (b) eluent concentrations of (1) 1, (2) 3, (3) 5 and (4) 8 g l^{-1} thiourea, (c) elution flow-rate on (●) peak height and (×) residence time and (d) temperature.

signals increased almost linearly (Fig. 3a). As time-based injection was used in this work, such rapid adsorption made it possible to retain a greater amount of analyte on the column by passing a larger volumn of sample solution in the fixed time by increasing the flow-rate.

The FIA signals were recorded just after the elution cycle started, so the FIA curve is actually an elution curve. As only the peak maxima were collected for the determination, instantaneous elution with a sharp and narrow profile of the elution curve became a critical factor for the preconcentration efficiency. Gold had a strong affinity with the neutral phosphine extractant, so it was assumed that there would be some difficulty in eluting it back into the solution. Experiments demonstrated that a high thiourea concentration was required to ensure that the elution took place completely in a small volume (Fig. 3b). A 5 g l^{-1} thiourea solution was employed in subsequent work for the release of gold. Concentrations higher than 5 g l^{-1} could produce a slightly better sensitivity, but the background absorbance from thiourea increased so that the detection limit was degraded.

With the manual method, it was found that gold was adsorbed on 8531 fibre quantitatively at 16–70°C, but the desorption efficiency was decreased below 40°C. It was difficult to investigate the effect of temperature on adsorption and desorption separately in the FIA system, so the experiments were done by varying the temperature for all the solutions in the FIA system. The peak heights were almost doubled when the temperature was increased from 10 to 60°C (Fig. 3d); 50°C was preferred and used throughout the experiments.

The column parameters were investigated thoroughly. It was found that the retention behaviour of gold in the complex sample matrix differred from that in pure solution. In the latter instance, a shorter, thinner column was superior, with faster elution and better sensitivity. However, when gold in real samples was tested with such a shorter column, lower recoveries were found. Therefore, the waste solutions were collected and re-examined, and the results are shown in Fig. 4. It can be seen that when an 80 ng ml^{-1} gold standard was injected and the length of column was changed from 40 to 20 mm, only the background absorption of thiourea was recorded and the concentration of gold in the waste was lower than the detection limit. This means that for the standard solutions only, even with a column as short as 20 mm, more than 99% of

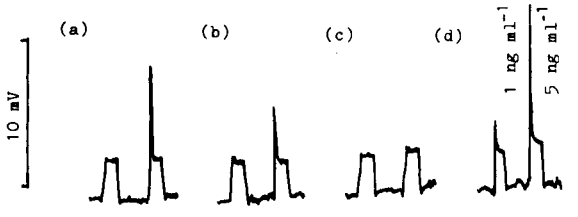

Fig. 4. Detection of gold concentration in the waste through columns of length (a) 20, (b) 30 and (c) 40 mm compared with (d) gold standards. For each pair of curves, the left-hand one was the record collected from the waste when 80 ng ml^{-1} gold standards were injected and the right-hand one represents the corresponding concentration of gold in the sample matrix.

retention efficiency was still able to be achieved. Nevertheless, when the same level of gold in the sample matrix was injected, the gold concentration detected in the waste solution increased as the column length decreased. The high ionic strength and the viscosity of sample solutions can be considered as the predominant factors affecting the mass transport efficiency during the extraction process. Therefore, a column of 40 mm $\times$ 2 mm i.d. was recommended to ensure accurate and reliable results.

Under the optimized conditions, a concentration factor of ten-fold was achieved when a loading period of 20 s was employed and it increased proportionally with the loading period. The column can be used at least 200 times before it needs to be changed.

Interference studies

It is known [10] that gold possesses high separation factors with most of the common ions in a neutral phosphine oxide extraction system. It can be predicted that it would also be selective on 8531 fibre. Experiments on interference studies were carried out which proved this prediction. More than 40 species were tested at the concentration levels corresponding to the real samples listed in Table 1 when gold was determined at 10 ng ml^{-1}. The experiments were conducted under the optimized conditions suggested above; no species affected the peak height by $> \pm 10\%$. However, as gold can only be adsorbed on 8531 fibre as gold(III), coexisting ions must be present in their oxidized state; the recovery could be decreased if gold is reduced to gold(I).

Sample analyses

Under the recommended conditions with a preconcentration period of 40 s, the slope of the calibration graph was 0.0033 peak-height absorbance for 1 ng ml^{-1} gold and the correlation coefficient was better than 0.999 for up to 100 ng ml^{-1} gold. The 3σ detection limit was 0.2 ng ml^{-1}. The relative standard deviation was 6% ($n = 11$) for 1 ng ml^{-1} and 2.2% ($n = 7$) for 80 ng ml^{-1} gold (Fig. 5). About 40–60 injections can be achieved per hour according to the variation of the preconcentration period.

Gold in standard materials was determined using the proposed method and the results were coincident with the certified values (Table 2). The method was used in routine applications for the determination of trace gold above 0.01 g t^{-1} in ores and metallurgical samples, e.g., in pyrite

TABLE 1

Effect of co-existing species on the determination of gold (10 ng ml^{-1})

Species	Added (mg ml^{-1})	Change in peak height (%)	Species	Added (mg ml^{-1})	Change in peak height (%)
Ag(I)	0.1 [a]	−5	Ni(II)	1	−6
Al(III)	1	−6	Pt/Pd/Rh/Ir	0.004	+5
As(V)	0.1	0	Pb(II)	1 [a]	0
Bi(III)	0.1	−8	RE(III) [b]	0.01	−3
Ca(II)	1	+6	Sb(V)	0.1 [a]	+5
Cd(II)	0.1	−3	Sc(III)	0.01	+5
Co(II)	0.1	0	Se(IV)	0.01	+2
Cr(III)	0.1	+4	Ti(IV)	0.1	−4
Cu(II)	1	−4	V(V)	0.1	+2
Fe(III)	20	+6	Zn(II)	1	−6
Hg(II)	0.1	+2	SiO_4^{4-}	1.3	−3
K(I)	1	+4	H_2SO_4	4%	−2
Mg(II)	1	−4	HF	5%	−4
Mn(II)	0.1	0	H_3PO_4	4%	−4
Na(I)	1	−3			

[a] The actual concentration was lower than the value given because of hydrolysis. [b] Rare earths.

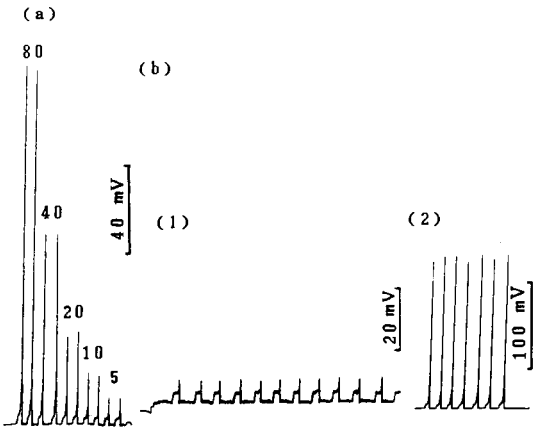

Fig. 5. (a) Calibration output for gold standards injected in duplicate (ng ml^{-1}); (b) repetitive records of preconcentrations and flame AAS determination of (1) 1 ng ml^{-1} gold (loading period 40 s) and (2) 80 ng ml^{-1} gold (loading period 20 s).

TABLE 2

Comparison of results obtained for standard materials by the proposed method with the certified values (g t^{-1})

Standard	Certified		Proposed method	
	Certified value	Standard deviation	Result obtained	Standard deviation ($n = 11$)
GBW 07208 [a]	0.051	0.002	0.053	0.002
GBW 07209 [a]	0.421	0.012	0.405	0.011
GBW(E) 070002 [a]	0.99	0.04	1.05	0.055
GRD-7 [b]	0.022		0.020	0.003

[a] Certified reference materials for gold and silver in ores approved by the State Bureau of Technical Supervision China (1991 catalogue). [b] Provided by the National Center of Analysis and Testing for Non Ferrous Metals and Electronic Materials (China).

with a 40% iron matrix and in copper concentrates, and the results were satisfactory. The method displayed great potential for replacing the batch method.

Using the fibre as support proved very advantageous owing to its excellent flow dynamic properties, lower back-pressure inside the column and easy packing of the column, which is especially suitable for FIA system. By preparing different fibres by linking certain groups to them and choosing suitable operating conditions, many selective systems for different components could be found for FIA system. Such work is in progress.

REFERENCES

1 Z. Fang, J. Ruzicka and E.H. Hansen, Anal. Chim. Acta, 164 (1984) 23.
2 S.D. Hartenstein, J. Ruzicka and G.D. Christian, Anal. Chem., 57 (1985) 21.
3 Z. Fang and B. Welz, J. Anal. At. Spectrom., 4 (1989) 543.
4 J. Ruzicka and A. Arndal, Anal. Chim. Acta, 216 (1989) 243.
5 X. Wu and W. Qi, Anal. Chim. Acta, 214 (1988) 279.
6 J. Lu, X. Zhang and Z. Zhang, Fenxi Huaxue, 15 (1987) 1120; Anal. Abstr., 50 (1988) 8B43.
7 S. Liu and B. Xia, Youkuangye, 7(4) (1988) 24.
8 Y. Gao, Fenxi Shiyanshi, 8(4) (1989) 105; Anal. Abstr., 52 (1990) 1J42.
9 F.E. Beamish and J.C. Vanloon, Analysis of Noble Metals, Academic Press, New York, 1977.
10 J.C. White and W.J. Ross, US At. Energy Comm. Rep., NAS-NS 3102, 1961.
11 N.I. Shcherbinina, G.V. Myasoedova and S.B. Savvin, Zh. Anal. Khim., 43 (1988) 2117.
12 Z. Fang, S. Xu and S. Zhang, Anal. Chim. Acta, 200 (1987) 35.

Analytica Chimica Acta, 270 (1992) 213–215
Elsevier Science Publishers B.V., Amsterdam

Flow-injection extraction–spectrophotometric determination of manganese(VII) with benzyltributylammonium cations

D. Thorburn Burns, S.A. Barakat, M. Harriott and M.S. El-Shahawi [1]

Department of Analytical Chemistry, The Queen's University of Belfast, Belfast BT9 5AG (UK)

(Received 14th April 1992)

Abstract

A flow-injection manifold has been developed for the spectrophotometric determination of manganese(VII) at 548 nm after extraction into chloroform of the ion-associate, benzyltributylammonium permanganate. The carrier stream was a pH 6 buffer containing 10% (w/v) ammonium fluoride and the reagent stream was 0.10% (w/v) benzyltributylammonium chloride. The injection rate was 20 h^{-1}. The calibration graph is linear up to 25 $\mu g\ ml^{-1}$ and the detection limit (3 × baseline noise) is 0.91 $\mu g\ ml^{-1}$ Mn(VII), based on 250-μl injection volumes. The system has been applied to the determination of manganese in steels and a cupro-nickel alloy.

Keywords: Flow injection; Spectrophotometry; Benzyltributylammonium cations; Cupro-nickel alloy; Extraction; Liquid–liquid extraction; Manganese

The oxo anions are amongst the least studied group of species which form liquid–liquid extractable ion-pairs with onium cations [1–2]. Permanganate has been monitored to determine manganese in high-quality calcium carbonate [3] and in iron, steel and non-ferrous metals [4] after extraction with the tetraphenylarsonium cation. Extraction with the tetraphenylphosphonium cation has been applied similarly in the analysis of ferrous alloys [5], as has the ethylenebis(triphenylphosphonium) cation to steels using both liquid–liquid [6] and adsorptive ion-pair extraction with microcrystalline naphthalene [7].

The present communication reports the development of a flow-injection manifold using benzyltributylammonium chloride as an ion-pairing extractant for permanganate, and the application of the system to the spectrophotometric determination of manganese in steels etc., after oxidation of manganese(II) to manganese(VII) by potassium periodate.

Correspondence to: D.T. Burns, Department of Analytical Chemistry, The Queen's University of Belfast, Belfast BT9 5AG (UK).

[1] Department of Chemistry, UAE University, Al-Ain P.O. Box 17551 (United Arab Emirates).

EXPERIMENTAL

Apparatus

Absorbances were measured at 548 nm with a Pye Unicam SP-6550 ultraviolet–visible spectrophotometer fitted with a 30-μl 10 mm path length optical quartz flow cell (Hellma) and recorded with a Philips 825 chart recorder. Solutions were pumped using a fixed proportioning pump (Technicon) fitted with Acidflex pump tubes for the organic phase and Tygon pump tubes for the aqueous phases. Samples were injected using a four-way Rheodyne valve fitted

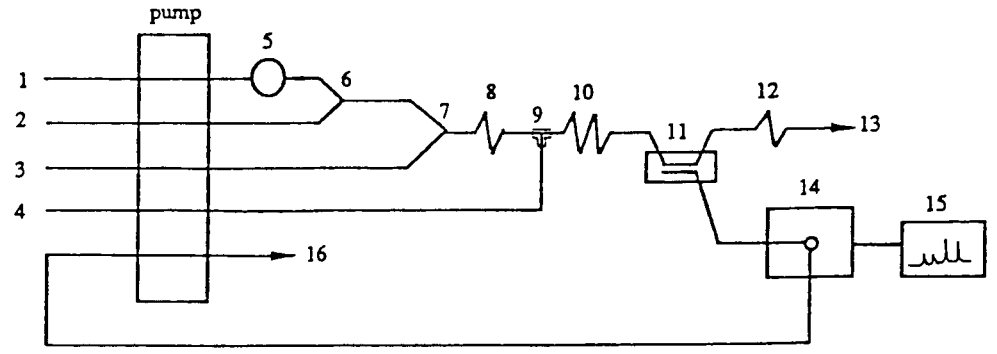

Fig. 1. Schematic diagram of the flow-injection system: (1) buffer solution pH 6 at 0.70 ml min^{-1}; (2) aqueous 10% (w/v) ammonium fluoride solution at 0.70 ml min^{-1}; (3) aqueous 0.10% (w/v) benzyltributylammonium chloride solution at 0.67 ml min^{-1}; (4) chloroform at 0.70 ml min^{-1}; (5, 7) mixing points ("Hex"); (6) sample solution (250 μl); (8) mixing coil (25 cm, 0.5 mm i.d.); (9) segmenter ("Tee"); (10) extraction coil (150 cm, 0.5 mm i.d.); (11) phase separator; (12) restrictor coil; (13) aqueous waste; (14) spectrophotometer; (15) recorder; (16) organic waste pumped at 0.68 ml min^{-1}.

with a by-pass coil. Flow lines were PTFE tubing (0.5 or 0.8 mm i.d.). The flow system is shown diagramatically in Fig. 1. Omnifit three-way connectors were used at the mixing points "Hex" for mixing aqueous phases and "Tee" for mixing organic and aqueous phase (segmenter). The phase separator was constructed following the design reported by Al-Wehaid [8] and fitted with a 1-μm pore size PTFE membrane (Zefluor, Gelman Sciences).

Reagents and solutions

All reagents, unless ortherwise specified, were of analytical grade; twice distilled water was used throughout.

Benzyltributylammonium chloride 0.10% (w/v) solution was prepared by dissolving the salt (Fluka, purum > 98%Cl) in water.

A stock solution of 500 μg ml^{-1} manganese (VII) was prepared by dissolving 1.438 g of potassium permanganate (AnalaR, BDH) in 500 ml of water, boiling the solution gently for 1 h, cooling, filtering through a sintered glass filter (porosity G2) to remove any manganese(IV) oxide formed, and diluting to exactly 1 l [9]. This solution was standardised against sodium oxalate and stored in a dark brown bottle.

A stock solution of 500 μg ml^{-1} manganese(II) was prepared by dissolving 1.438 g of potassium permanganate (AnalaR, BDH) in water and carefully adding to it a saturated solution of sulphur dioxide until the permanganate colour was just discharged; the solution was then diluted to exactly 1 l [10]. More of the dilute solutions were prepared daily as required.

A pH 6 buffer solution was prepared by mixing 61.5 ml of 0.2 M disodium hydrogenphosphate with 438.5 ml of 0.2 M sodium dihydrogenphosphate and diluting to 1 l with water. A sulphuric–phosphoric acid solution was prepared by mixing

TABLE 1

Determination of manganese in steels

Sample	Sample weight (g)	Manganese content (% w/w)	
		Certified [a]	Found [b]
BCS 459 "Mild" Steel	1.5	0.088 (0.085–0.090)	0.087 ± 0.005
E.C.R.M. 081-1 unalloyed steel	0.30	0.769 (s = 0.008) [c]	0.766 ± 0.006
BCS 457 mild steel	1.0	0.28 (0.28–0.29)	0.28 ± 0.002
BCS 180/1 cupro-nickel	0.50	0.81 (0.79–0.81)	0.808 ± 0.005

[a] Certified range in parantheses. [b] Mean ± 95% confidence limits for 4 replicates. [c] Standard deviation of 10 samples.

150 ml of concentrated sulphuric acid and 150 ml of 85% (w/w) orthophosphoric acid, and carefully adding the mixture to 600 ml of water, cooling, and then diluting to 1 l.

Ammonium fluoride solution 10% (w/v) solution was made by dissolving 10 g of ammonium fluoride (AnalaR BDH) in 100 ml of water. A 0.5% (w/w) potassium periodate solution was made by dissolving 2.5 g potassium periodate in a mixture of 500 ml of water and 100 ml of concentrated nitric acid by gentle warming; after cooling, the solution was diluted to 500 ml with water.

Procedure for steel samples

Dissolve accurately weighed samples (see Table 1, to contain 500 to 2000 μg Mn) in 35 ml sulphuric/phosphoric acid mixture in 250-ml conical flasks. Oxidise with 2 ml of concentrated nitric acid and boil to expel nitrous fumes. If any carbides remain evaporate to fumes and cool. Add 50 ml of water and 5 ml of concentrated nitric acid. Boil for 2 min, add 10 ml of 0.5% (w/v) potassium periodate solution and boil for a further 4 min. Cool, transfer to a 100-ml volumetric flask and make up to volume with distilled water [10]. Measure the peak-height absorbance using the flow system and the conditions given in Fig. 1. Evaluate the amount of manganese present from a calibration graph prepared from the results obtained from aliquots of manganese(II) solution proceeding as for the steel samples.

RESULTS AND DISCUSSION

The peak heights were found to be independent of the length of the extraction coil from 0.5 to 4.0 m; 1.5 m was chosen for routine use because this gave a convenient resistance to flow and reduced the risk of leakages in the phase-separator block. The effect of pH was investigated and the peak heights were found to be independent of pH over the range 2–12. A pH 6 buffer solution was used for the rest of the experiments.

The interferences of diverse ions were also investigated and were as for the manual method [11], chromium(VI) being the only ion which interfered significantly. In ratios up to 30:1, there was no significant effect at 548 nm provided that the extracts were protected from daylight, in which the absorbance slowly decreased.

A linear calibration graph was obtained over the range 0–25 μg ml^{-1} Mn(VII) at 548 nm. The detection limit (3 $\times$ base line noise) was 0.91 g ml^{-1} Mn. The results for the determination of manganese in metallurgical samples (Table 1) are in good agreement with certificate values. The method is simple in its operation and faster (20 injections h^{-1}) than conventional manual liquid–liquid extractions [11]. It was also noticed that this method works well over a wider range of pH values using benzyl-tributyl-ammonium chloride as an ion-pairing reagent than for other methods, which is an extra advantage.

REFERENCES

1 A.J. Bowd, D.T. Burns and A.G. Fogg, Talanta, 16 (1969) 719.
2 D.T. Burns, Anal. Proc., 19 (1982) 355.
3 M.L. Richardson, Analyst, 87 (1962) 435.
4 H. Goto and Y. Kakita, Fresenius' Z. Anal. Chem., 254 (1971) 18.
5 Deputy Minister of the Romanian Ministry of Petroleum Industry and Chemistry, Brit. Pat., 1,094,778, 23.65. See Anal. Abstr., 15 (1968) 4681.
6 D.T. Burns and D. Chimpalee, Anal. Chim. Acta, 199 (1987) 241.
7 D.T. Burns, D. Chimpalee and N. Chimpalee, Fresenius' Z. Anal. Chem., 332 (1988) 453.
8 A. Al-Wehaid, Ph.D. Thesis, University of Hull, (1987).
9 H.A. Laitinen, Chemical Analysis, McGraw Hill, New York, 1960, pp. 359–377.
10 Methods of thermal analysis of steel, British Steel Corporation, Sheffield, 1974, pp. 82–85.
11 D.T. Burns, M. Harriott and S.A. Barakat, Anal. Chim. Acta, 258 (1992) 325.

Analytica Chimica Acta, 270 (1992) 217–221
Elsevier Science Publishers B.V., Amsterdam

Determination of chloride ion concentration in natural and waste waters by flow-injection analysis with a silver chloranilate reaction column

Fumio Sagara, Tetsuya Tsuji, Isao Yoshida, Daido Ishii and Keihei Ueno

Department of Industrial Chemistry, Kumamoto Institute of Technology, 4–22–1 Ikeda, Kumamoto 860 (Japan)

(Received 27th May 1992; revised manuscript received 31st July 1992)

Abstract

The concentration of chloride ions in natural and waste waters was determined by a flow-injection method using a column packed with silver chloranilate powder. Ethanol–water–0.1 M sodium acetate buffer (pH 5.57) (5 + 4 + 1, v/v/v) was used as the carrier at a flow-rate of 2 ml min^{-1}. The chloranilate ion concentration, which corresponds to the chloride ion concentration, in the carrier from the reaction column was monitored by a spectrophotometric detector at 530 nm. Interferences from multi-charged cations were eliminated with the combined use of a cation-exchange column inserted in the upper stream of the reaction column. Interferences from anions were found to be negligible. The concentration of chloride ions in natural and waste waters (1–20 $\mu g\ ml^{-1}$) could be determined rapidly (one sample per 2 min) with high reproducibility. The results agreed well with those obtained by the standard manual method.

Keywords: Flow injection; UV–Visible spectrophotometry; Chloride; Silver chloranilate; Waters

The concentration of chloride ion in natural and waste waters has usually been determined by the volumetric method using silver nitrate or mercury(II) nitrate [1] or spectrophotometry using mercury(II) thiocyanate and iron(III) ion [2,3], the latter being applied to the flow-injection analysis of natural water [4]. Although the procedure developed by Ruzicka et al. [4] has been widely accepted for the analysis of natural water [4], it has the drawback of using a mercury(II) compound.

This paper reports the application of a flow-injection method for the spectrophotometric determination of $\mu g\ ml^{-1}$ levels of chloride ion in natural and waste waters, using a manifold in which a reaction column packed with solid silver chloranilate is incorporated. The proposed procedure is very simple and does not employ any environmentally undesirable reagents; one sample per 2 min can be treated in determining chloride ion concentrations down to 1 $\mu g\ ml^{-1}$.

The principle of the chloride ion determination using silver chloranilate (Ag_2Ch) is based on the following metathetical reaction:

$$2Cl^- + \underset{\text{solid}}{Ag_2Ch} \rightleftharpoons \underset{\text{solid}}{2AgCl} + \underset{\text{violet colour}}{Ch^{2-}}$$

where Ch^{2-} represents the chloranilate anion.

Although the use of silver chloranilate for the spectrophotometric determination of chloride ion has already been investigated, its practical application was not successful owing to the formation of colloidal silver chloride [5]. Hence Barney and Bertolacini [6] suggested the use of mercury(II)

Correspondence to: F. Sagara, Department of Industrial Chemistry, Kumamoto Institute of Technology, 4–22–1 Ikeda, Kumamoto 860 (Japan).

chloranilate for this purpose. In preliminary experiments, however, the effluent from the reaction column packed with silver chloranilate was very clear, indicating that the formation of colloidal silver chloride can be prevented in the flow-injection system. It is likely that silver chloride was trapped in the reaction column.

Also, as stated in a paper [7], as various multicharged cations strongly interfere with the reaction, samples must be pretreated with a cation-exchange resin to remove such interfering cations. For this purpose, a cation-exchange column was incorporated upstream of the reaction column.

EXPERIMENTAL

Reagents

All reagents were of analytical-reagent grade. All solutions were prepared with ultra-pure water (11.0–18.3 MΩ cm, 25°C), which was prepared using a Puric R water purifier (Organo, Tokyo).

Silver chloranilate was prepared by dropwise addition of 100 ml of an aqueous solution containing 2.57 g (0.015 mol) of silver nitrate to 1.5 l of an aqueous solution containing 2.0 g (0.01 mol) of chloranilic acid (Dojindo Labs., Kumamoto), followed by continuous stirring for 24 h. The resulting precipitate was collected on a glass filter, washed with water and dried under vacuum. A dark violet–brown powder was obtained (yield 2.7 g). The result of silver analysis after wet digestion of silver chloranilate, followed by titration with sodium chloride solution, indicated that the composition was Ag_2Ch. These procedures were carried out in a dark room.

Apparatus

A flow diagram is shown in Fig. 1. The carrier solution was pumped into the Teflon tube (0.5 mm i.d.) of the flow system using a Sanuki double-plunger pump (DM3M-2042).

Immediately after the injection valve (six-way loop type), a cation-exchange column (50 mm × 4.61 mm i.d., 0.83 ml) packed with Muromac 50W-X 4, 100–200 mesh cation-exchange resin (NH_4^+ form), and a reaction column (same size as the cation-exchange column) packed with silver chloranilate powder (0.4 g) were connected in series. The reaction column was covered with black tape to prevent the decomposition of silver chloranilate by light. The end of the reaction column was connected to a spectrophotometric detector (Shimadzu SPD 6AV; cell volume 8 μl; 10 mm × 1 mm i.d.) with a wavelength setting of 530 nm.

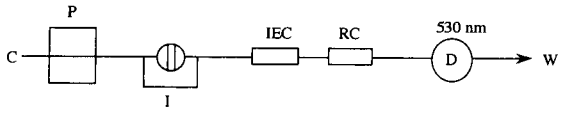

Fig. 1. Schematic diagram of the flow system. C = carrier solution; P = pump; I = injection valve; IEC = cation-exchange column; RC = reaction column; D = detector; W = waste.

Empty columns for ion chromatography (Tosoh, Tokyo) were employed as the ion-exchange column and the reaction column.

Recommended procedure

Pump the carrier solution [ethanol–water–0.1 M sodium acetate buffer (pH 5.57) (5 + 4 + 1, v/v/v)] into the flow system (Fig. 1) at a rate of 2.0 ml min^{-1}. After the baseline has stabilized on the recorder, inject 100 μl of an injection solution prepared by mixing a sample water, ethanol and 0.1 M acetate buffer (pH 5.57) in volume proportions of 4 + 5 + 1. Determine the chloride ion concentration from a calibration graph prepared using the same procedure and a standard sample solution containing a known concentration of chloride ion. A throughput of one sample per 2 min can easily be attained with this procedure.

RESULTS AND DISCUSSION

Silver chloranilate

Dark violet–brown crystals of silver chloranilate can be readily obtained by mixing aqueous solutions of silver nitrate (0.1 M) and chloranilic acid (0.007 M) at room temperature in a dark room. In repeated runs with various molar mixing ratios from 1 : 3 to 1 : 1.5 (chloranilic acid to silver nitrate), all the products obtained had the com-

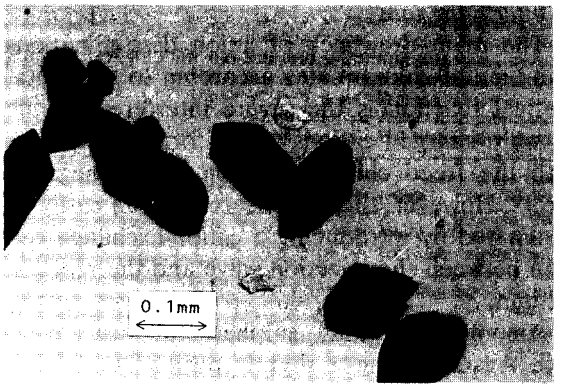

Fig. 2. Microphotograph of Ag_2Ch crystals.

position Ag_2Ch. The crystals thus prepared were of fairly uniform diameter of a few hundred μm, as shown in Fig. 2, and were used without grinding or sieving.

Composition of the carrier solution

Before the application of Ag_2Ch in the flow-injection method, the reaction conditions of Ag_2Ch with chloride ion were optimized by batch absorption spectrophotometry.

The solubility of Ag_2Ch in water and in 50% aqueous ethanol was investigated over the pH range 3–7 (acetate buffer) by observing the absorbance of the supernatant solution at 530 nm after shaking 10 mg of Ag_2Ch with 10 ml of water or aqueous ethanol for 20 min, then centrifuging. The results indicated that the blank absorption was lowest at pH 5.5–6, and the addition of ethanol further suppressed the absorption. At still higher pH, however, Ag_2Ch tended to hydrolyse.

The reaction of chloride ion with Ag_2Ch was investigated using a solution of this composition (50% ethanol with 0.1 M acetate buffer). The sample solution (40 ml) containing a known amount of chloride ion was mixed with 50 ml of ethanol and 10 ml of 0.1 M acetate buffer (pH 5.57) and the mixture was shaken with 15 mg of Ag_2Ch powder for 20 min on a mechanical shaker. The mixture was then centrifuged at 4000 rpm (2700 *g*) for 5 min to give a clear supernatant for absorption measurement at 530 nm.

The calibration graph for chloride ion by the batch procedure was linear over the concentration range 10–100 μg ml^{-1}, indicating the possibility of the application of Ag_2Ch in the flow-injection analysis of chloride ion using a carrier solution consisting of water–ethanol–0.1 M acetate buffer (pH 5.57) (4 + 5 + 1, v/v/v).

Flow-rate

The effect of flow-rate and sample volume were investigated using the flow system without or with the ion-exchange column. The peak heights obtained by injecting 100 μl of 12 μg ml^{-1} Cl^- at flow-rate from 1 to 2 ml min^{-1} were almost constant, while the peak width increased with increasing flow-rate. Introduction of the ion-exchange column also broadened the peak. Therefore, considering the sample throughput, the flow-rate was set at 2 ml min^{-1} in subsequent experiments.

Injection volume

The effect of sample size was investigated by injecting various volumes (100–140 μl) of samples containing different concentrations of chloride ion (2–20 μg ml^{-1}). As shown in Fig. 3, linear calibration graphs were obtained with sample volumes of 100–140 μl.

Although the peak height increased with increasing sample volume, detectable signals were observed on injection of 100 μl of 2 μg ml^{-1}. A volume of 100 μl [40 μl of sample water plus 50 μl of ethanol and 10 μl of 0.1 M acetate buffer (pH 5.57)] was sufficient to give a sharp signal,

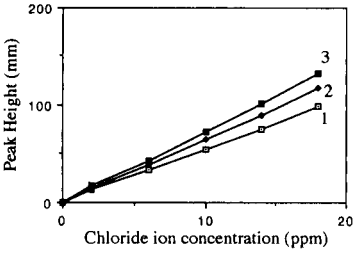

Fig. 3. Effect of sample volume on peak height. The injected solution was a mixture of chloride ion solution (2–18 μg ml^{-1} Cl^-), ethanol and 0.1 M acetate buffer (4+5+1, v/v/v). Injection volume: curve 1, 100 μl; $y = 10.6_5x + 1.17$ ($r = 0.999$, $n = 25$); curve 2, 120 μl; $y = 12.8_7x + 0.35_0$ ($r = 0.999$, $n = 25$); curve 3, 140 μl; $y = 14.4_4x + 0.70_0$ ($r = 0.999$, $n = 25$).

and this sample volume was employed as a standard sample size.

Packing of the reaction column

The conditions of packing the Ag_2Ch powder into the empty reaction column were found to be important for obtaining reproducible results. The procedure for packing of the reaction column was essentially the same as that described previously [7]. Dry Ag_2Ch powder (0.40 g) was placed in an empty plastic column (50 mm × 4.6 mm i.d., 0.83 ml) with one end plugged with a ball of glass-wool. Although the dimensions of the reaction colum were not optimized, the empty column employed in this work was an empty plastic column used in a commercial ion chromatography instrument (Tosoh). This column has also been successfully used in previous work. After filling the column with the reagent, it was subjected to centrifugation at 4000 rpm (2700 *g*) for 3 min in order to pack the reagent particles into the column uniformly. Finally, the open end (the carrier inlet) was plugged with another ball of glass-wool. The columns thus prepared were found to give reproducible results after the injection of 500 samples.

Interfering ions

The main drawback of anion determinations using metal chloranilates according to the metathetical reaction is the severe interferences due to multi-charged cations which form precipitates with the freed chloranilate ion, giving negative errors. However, these interferences can easily be eliminated by introducing a cation-exchange column between the injection valve and the reaction column.

Among the anions, sulphate ion also reacts with Ag_2Cl, giving a slightly positive error, but 100 μg ml^{-1} SO_4^{2-} gives a signal corresponding to only 1–2 μg ml^{-1} Cl^-. Other anions did not give any significant errors.

A typical result for calibration runs with the model sample solution is illustrated in Fig. 4. A linear calibration graph was obtained for sample solutions containing 2–10 μg ml^{-1} Cl^-.

Application to natural and waste waters

Some natural and waste waters from the local area were analysed for their chloride ion concentration using the proposed method; the results were compared with those obtained by the offi-

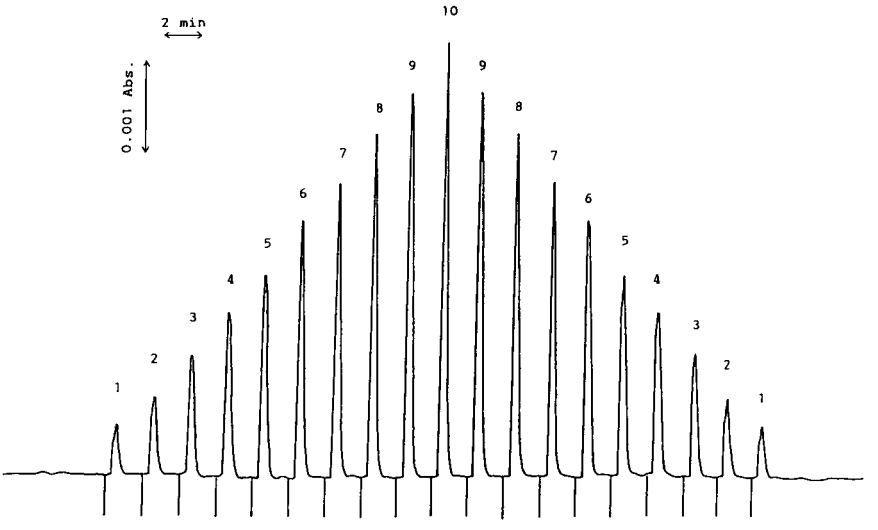

Fig. 4. Typical calibration run on the standard samples. The sample solutions were prepared by mixing the model solution with ethanol and 0.1 M acetate buffer in the proportions 4 + 5 + 1 (v/v/v). Peak numbers 1–10 correspond to chloride ion concentrations in the original model solution of 2, 4, 6, 8, 10, 12, 14, 16, 18 and 20 μg ml^{-1}, respectively. The linear regression equation for the signal heights is $y = 6.95x + 0.83_3$ ($r = 0.999$, $n = 40$).

TABLE 1

Analytical results for natural and waster waters [a]

Sample	Cl^- ($\mu g\ ml^{-1}$)		
	This work [b]		JIS official method [c]
Underground water:			
No. 1	9.5_2	(4.8)	10.3
No. 2	9.4_0	(2.6)	10.0
No. 3	9.6_6	(2.7)	10.1
No. 4	10.1_2	(3.6)	10.1
No. 5	8.9_6	(3.0)	9.4
No. 6	8.9_0	(3.1)	9.3
Industrial waste water (after tenfold dilution)	11.3_7	(3.9)	11.1
Sewage waste water (after 50-fold dilution)	12.2	(2.7)	11.7

[a] Determinations of chloride ion concentrations were carried out at Dojin Glocal. [b] Relative standard deviations (%) ($n = 4$) are given in parentheses. [c] A modified Fajans titration [8].

cial standard method [8]. The results of the two methods (Table 1) agree fairly well. Hence the proposed method is very useful for the rapid determination of chloride ion in natural and waste waters, as one sample can be analysed every 2 min in the repeated runs. A further advantage of the proposed method over the conventional flow-injection method using mercury(II) thiocyanate is that no environmentally undesirable reagent is employed.

The authors thank Dojindo Labs. for partial financial support of this work and Dojin Glocal for supplying natural and waste water samples of known chloride ion concentrations.

REFERENCES

1 R.A. Day, Jr., and A.L. Underwood, Quantitative Analysis, Prentice-Hall, Englewood Cliffs, NJ, 1958, p. 172.
2 S. Utsumi, Nippon Kagaku Zasshi, 73 (1952) 835.
3 I. Iwasaki, S. Utsumi and T. Ozawa, Bull. Chem. Soc. Jpn., 25 (1952) 226.
4 J. Ruzicka, J.W.B. Stewart and E.A.G. Zagatto, Anal. Chim. Acta, 81 (1976) 387.
5 A.B. Coutinho and M.D. Almeda, An. Assoc. Bras. Quim., 10 (1951) 83.
6 J.E. Barney and R.J. Bertolacini, Anal. Chem., 29 (1957) 1187.
7 K. Yakata, F. Sagara, Y. Yoshida and K. Ueno, Anal. Sci., 6 (1990) 711.
8 JIS K 0102 (1986), Testing Methods for Industrial Wastewater, Japanese Standards Association, Tokyo.

Analytica Chimica Acta, 270 (1992) 223–230
Elsevier Science Publishers B.V., Amsterdam

Determination of nanogram levels of boron in milligram-sized tissue samples by inductively coupled plasma–atomic emission spectroscopy

D.A. Johnson

Idaho National Engineering Laboratory, EG&G Idaho, Inc., INEL BNCT Program, Idaho Falls, ID 83415-2208 (USA)

D.D. Siemer

Westinghouse Idaho Nuclear Company, Inc., Idaho Falls, ID 83403-4000 (USA)

W.F. Bauer

Idaho National Engineering Laboratory, EG&G Idaho, Inc., INEL BNCT Program, Idaho Falls, ID 83415-2208 (USA)

(Received 3rd April 1992; revised manuscript received 22nd June 1992)

Abstract

This paper describes a simple modification to the sample introduction system of a standard inductively coupled plasma–atomic emission spectroscopy (ICP–AES) spectrometer that allows the determination of nanogram quantities of boron. This modification was applied to the part-per-million quantitation of boron in tissue samples in the range of 1–30 mg. Boron is converted to the volatile methoxyborate ester, which is immediately swept/aspirated into the torch with argon carrier gas. These small tissue samples are prepared by first moistening them with a drop or two of sodium hydroxide solution and then dry ashing them in small platinum crucibles. After cooling, 100 μl of concentrated sulfuric acid are weighed into these crucibles to dissolve the ash. The first step of the actual determination involves weighing aliquots of this acid into the plastic test tubes that subsequently serve as the esterification reaction vessel. A simple adaptor inserted into these tubes permits the suction generated by a standard concentric flow ICP–AES nebulizer to pull an argon carrier gas stream through the headspace volume of the tube. When methanol is added, the gaseous boron ester forms and is immediately swept into the torch. The absolute detection limit is on the order of 0.2 ng.

Keywords: Atomic absorption spectrometry; Inductively coupled plasma spectrometry; Boron

The ability to accurately determine boron in biological tissue samples of all sizes is important in evaluating the tumor specificity of the boron compounds being studied in boron neutron capture therapy (BNCT) research [1] (most often applied to brain tumors and metastatic melanoma). The analytical literature having to do with determining boron in biological specimens includes techniques based on prompt-gamma ray spectroscopy [2–4], various colorimetric procedures [5–8], atomic spectroscopy [9–12], and, most recently, inductively coupled plasma-mass spectrometry (ICP–MS) [13]. Unfortunately, all of

Correspondence to: D.A. Johnson, Idaho National Engineering Laboratory, EG&G Idaho, Inc., INEL BNCT Program, P.O. Box 1625, Idaho Falls, ID 83403-4000 (USA).

these papers describe bulk sample analysis techniques that lack the absolute sensitivity needed to determine low $\mu g\ g^{-1}$ levels of boron in milligram-sized samples. The capability to analyze very small samples is important because researchers find it desirable to be able to do boron concentration-mapping within and around specific structures, and physicians would like to be able to use biopsy-needle sampling techniques to determine if the drugs are actually localizing before they expose the patient to neutron sources. While it is possible to roughly quantitate boron in small samples with ion microscopy [14] or track-etch autoradiography [15], both of these techniques suffer from poor precision and require expensive and rather specialized instrumentation.

ICP–AES has supplanted other methods of determining boron in many applications [9–12]. The primary reasons for this are that ICP–AES has excellent solution–concentration sensitivity, is reasonably free from matrix effects, and the equipment has become widely available at a reasonable cost. Unfortunately, the absolute sensitivity of conventional ICP–AES is marginal for small sample applications. For example, a typical traditional approach to analyzing a 5-mg tissue sample would first involve dissolving it into a minimum of 5 ml of solution (1000 : 1 dilution). This degree of dilution is required because 5 ml is about the minimum volume needed to do an analysis and possibly reserve sufficient sample for a duplicate measurement. A typical ICP–AES instrument has detection limits for boron of about 5 $\mu g\ l^{-1}$ for the 249.68 and 208.96 nm lines in the absence of matrix effects. The detection limit for the 249.77 nm line is about 3 $\mu g\ l^{-1}$; however, this line is significantly overlapped by an iron emission line and often cannot be used to quantify boron in most samples. The practical detection limit for tissue sample analysis is about 8 $\mu g\ l^{-1}$ and practical quantitation limits are about 20–30 $\mu g\ l^{-1}$. The practical detection limit for boron in the 5-mg sample would therefore be ca. 8 $\mu g\ g^{-1}$ and practical quantitation limit would be about 20–30 $\mu g\ g^{-1}$. Since the tissue boron concentrations used in BNCT therapy are typically only 15–30 $\mu g\ g^{-1}$, conventional ICP–AES is quite marginal for such small sample work.

Accurate quantitation of low ppm levels of boron in small tissue samples requires an efficient way of getting the analyte into the plasma. The method described in this paper accomplishes this with a cold-vapor generation approach that is roughly analogous to those applied for determining both the hydride-forming elements and mercury. The reaction used to volatilize the boron is acid-catalyzed formation of volatile methoxyborate. This approach is not only more efficient at transporting analyte to the plasma, it also eliminates the iron emission line interference that often contraindicates use of boron's most sensitive emission line (249.779 nm) in traditional analyses.

The basic idea of interfacing a borate ester volatilization system directly to an atomic spectrometer was first reported by Siemer in 1982 [16]. A commercial AAS spectrometer was used in its emission mode to integrate the transient green BO_2 band responses generated when the methoxyborate was introduced into an air–acetylene flame. A few years later, Castilo et al. [17] performed basically the same experiment, but recorded the atomic absorption signal instead. Unfortunately, flames are not hot enough to efficiently atomize boron, which means that flame-based atomic spectrometric methods lack the sensitivity needed for BNCT research.

Methods that combine some type of borate ester volatilization step with ICP–AES detection have already been reported. Novozamsky et al.'s technique [18] generates a continuous, steady-state signal by pumping aqueous sample, sulfuric acid, and methanol streams into a gas–liquid separator and then introducing a portion of the gas phase into the torch. Unfortunately, the volume of carrier gas used is too small to carry more than a small fraction of the boron ester into the plasma; so little, in fact, that the method's detection limit (50 ng ml^{-1}) is considerably worse than that normally associated with strictly conventional pneumatic nebulization. Hosoya et al.'s approach [19] simply combines collection of the methoxyborate volatilized from a sample in water with a conventional ICP–AES analysis of the collecting solution. Since the actual determination is strictly conventional, the only thing gained by the esteri-

fication/distillation steps is freedom from line overlap problems.

Kumamaru and Matsuo [20] describe a technique involving two separate volatilizations of the ester: the first separates the methoxyborate and the bulk of the methanol from the sample matrix and condenses the two out together. The second step involves a gradual heating of the condensate to volatilize a portion of the ester into the argon stream going to the torch. Since methanol and methoxyborate form an azeotrope with a boiling point of ca. 53°C, the azeotrope reaches the torch before the bulk of the methanol, even though the methoxyborate and methanol have boiling points within one degree of each other. Introducing all of the ester would have simultaneously put enough methanol into the plasma to extinguish the discharge. The detection limit was equally unimpressive (approximately 40 ng ml^{-1}).

The technique described in this paper uses a carefully miniaturized version of the simple apparatus that Siemer originally developed for boron detection by flame emission. In common with the earlier approach, it combines convenient one-step operational simplicity with quantitative transfer of analyte from the sample aliquot to the excitation source. Even though most of the methanol accompanies the boron into the plasma, the amount of methanol used per analysis is so small that the plasma is not seriously perturbed. Consequently, the method features the best absolute detection limits ever reported by ICP–AES for boron.

EXPERIMENTAL

Instrumentation

An Applied Research Laboratories, Model ARL-3520, ICP–AES apparatus was used for the development of this method. The sample introduction system was modified as shown in Fig. 1. Argon plasma flow, coolant flow, and other ICP instrument settings are listed in Table 1 and are quite similar to those used by the same instrument for conventional analyses. The sample pick-up tube (0.5 mm i.d. PTFE) of a standard pneumatic nebulizer (Meinhard TR-30-A3) was inserted through the rubber stopper-tube adaptor used to seal the top of the polypropylene test-tube reaction vessel. Two other small PTFE tubes were also inserted through this stopper. One of these was connected to a syringe pump (Sage Instruments, Model 341A) used to deliver methanol and the other (0.8 mm i.d.) to vent the bottom of the stoppered reaction vessel to an atmospheric-pressure argon reservoir. A Y inserted into the nebulizer's argon line directed a small fraction of this argon first through a flow restrictor and then into this reservoir. The reaction vessels were 74 × 9.5 mm polypropylene test tubes cut to a length of 32 mm. The nebulizer was connected directly to the bottom of the torch with a short piece of surgical rubber tubing. The reaction test tubes were kept as short a possible and the spray chamber was removed to minimize severe "tailing" of the signals that would otherwise occur as the methoxyborate would absorb/desorb from the excess surface area on its way to the torch.

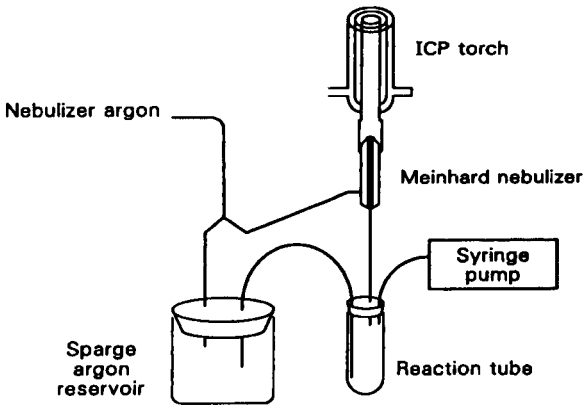

Fig. 1. Schematic of modification to ICP–AES sample introduction system for the in situ generation of methoxyborate.

TABLE 1

ICP–AES parameters

Coolant flow (l/min)	11
Plasma flow (l/min)	1
Carrier flow (l/min)	1.1
Incident power (kW)	1.2
Viewing height (mm)	15
Boron wavelength (nm)	249.776
Meinhard nebulizer	TR-30-A3
Radio frequency (MHz)	27

The nebulizer's natural suction was used to provide the force necessary to sparge the argon carrier flow through the solution in the reaction vessel and then aspirate the resulting gas mix into the torch. The aspiration rate of the selected nebulizer was ca. 40 ml min^{-1} of gas. Using the standard nebulizer to do this is not only convenient, but a negative-pressure sample introduction system also prevents any inadvertent leaks from causing loss of analyte.

Plastics are used wherever possible because they are both readily available and chemically compatible with the reagents. Glass is to be avoided wherever possible because most types of glass seem to have sufficient acid-leachable boron in them that background signal is overwhelming.

The instrument's tuning system was adjusted so the plasma would not be extinguished, since the gas being aspirated into the torch's sample introduction tube changes during the various stages of an individual analysis. The three different gases introduced during an analysis include argon only, argon with a combination of methanol and methoxyborate vapors, and air only. In the case of the ARL-3520, adjusting the tunable air-capacitor to give minimum reflected power when the nebulizer was freely aspirating air meets this requirement. With this adjustment, the reflected power ranges between 0 and 15 W as the gas composition varies during analyses.

For developmental/diagnostic work, a standard laboratory integrator recorder (Perkin-Elmer LCI-100) was used to record/display the raw photomultiplier-tube signal. The ARL-3520 with A-type electronics already has test jacks suitable for this. These jacks are not normally active, but can be activated using software commands in the TEST mode of operation. A previous report [21] describing use of the ARL-3520 as a chromatographic detector made similar use of those jacks. For routine analytical work, the spectrometer's standard read-out system was used to integrate the peak response for 60 s.

Calibration

Calibration was performed using standards prepared from 1000 μg ml^{-1} commercial boron standards for atomic spectroscopy (Fisher Scientific) that contain the boron as boric acid. At each boron concentration, 5 μl of the standard were placed into the bottom of the reaction vessel, 25 μl of concentrated sulfuric acid (approximately 0.04 g) were added, and the reaction vessel was stoppered with the modified stopper. Methanol was added via the syringe pump for five seconds (70 μl). The signal integration period was initiated at the beginning of the methanol addition. The boron response was integrated for 60 s, enough time for the signal to essentially return to baseline. Calibration was generally done, in triplicate, with standards containing 0, 5, 15, and 50 ng of boron (i.e. 5 μl of 0, 1, 3, and 10 μg boron ml^{-1} aqueous standards). Linearity is excellent. A typical calibration curve would give a line slope of 31.9 ± 0.3 mV ng^{-1}, y-intercept of 159 ± 8 mV, standard error of the y estimate of 16 mV and regression coefficients (r^2) greater than 0.998. Typical detection limits, expressed as three times the standard deviation of a blank, are about 0.2 ng.

Tissue sample preparation

Tissue samples were acquired from a dog that had been administered $Na_2B_{12}H_{11}SH$ (disodium mercaptoundodecahydro*closo*dodecaborate; commonly referred to as borocaptate sodium or BSH), a compound being investigated as a boron delivery agent for BNCT, intravenously at a rate of 1 mg boron kg^{-1} body weight min^{-1} with a total dose equal to 55 mg boron kg^{-1} body weight. The 1–2-g samples were homogenized to a paste with a mortar and pestle prior to the subsampling for analysis. To create a more homogeneous sample that would provide more reliable subsampling, a separate reference tissue was prepared by adding BSH to raw beef liver. The beef liver was then homogenized in a blender, lyophilized, and ground to a powder.

Samples were prepared for methoxyborate ICP–AES analysis by a caustic ashing technique. This technique involved weighing the sample (1–30 mg) into a tared 5-ml platinum crucible and wetting it with two drops of a dilute sodium hydroxide solution (ca. 0.2 M). The crucibles were then placed onto a cold hot-plate, gently heated to dry the samples, and the hot plate was turned

to its maximum setting to char the samples. Final decomposition was performed by heating the crucibles to a bright orange color over an open air–propane flame. When a crucible had cooled, it was placed onto an electronic balance, tared, and 100 μl (0.18 g) of concentrated sulfuric acid were weighed into it. An Eppendorf pipette was then used to rinse this acid repeatedly down the sides of the crucible to assure both complete dissolution and thorough mixing. The crucibles were then stored in a desiccator until the actual analysis was to be performed.

Sample analysis

One of the reaction vessels was tared onto a top-loading electronic balance and a 25-μl aliquot of the sulfuric acid solution from a sample crucible was weighed into it. The vessel was capped with the stopper-adaptor and the remainder of the analysis was performed exactly as described previously with the calibration standards.

RESULTS AND DISCUSSION

The argon carrier gas flow-rate affects the rate at which the generated methoxyborate is sparged from the reaction mixture and carried to the torch, the height of maximum boron emission intensity above the torch's load coil, and the residence time of individual boron atoms within the viewing area of the plasma. Low sparge and total carrier gas flow-rates generally give larger responses, peak and area, but the time necessary to integrate them becomes inconveniently long. For this work, the total carrier flow was kept at 1.1 l min^{-1} (ca. 20 p.s.i.), which kept the nebulizer uptake rate at about 40 ml min^{-1}. These values represent an acceptable trade-off of sensitivity and analysis time. Figure 2 shows both peak widths (at 20% of peak maximum) and cut and weigh integrals of signals generated by 5 ng of boron at various argon carrier flow-rates/pressures. For routine analytical work, carrier gas flow-rate is usually adjusted to force practically all of the boron through the torch within a convenient 60-s integration period. The previously quoted detection limit of 0.2 ng absolute was

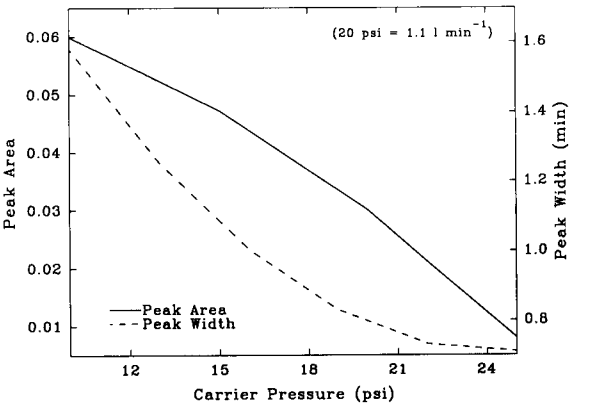

Fig. 2. Effect of the carrier flow-rate (represented as p.s.i. of backpressure) on the peak area and peak width at 20% of the maximum height.

generated with this sensitivity-compromised flow rate.

The amounts, both relative and absolute, of water, sulfuric acid, and methanol also affect the peak shape and/or sensitivity of the response. Table 2 shows the effect of varying the amount of sulfuric acid while keeping the amounts of boron (5 ng), water (5 μl), and methanol (70 μl) constant. If insufficient acid is used, the responses are both small and drawn out. Presumably, this is because of water's inhibitory effect on the esterification process; sufficient concentrated sulfuric acid can absorb this water and keep its activity low. As more acid is added, the response passes through a rather broad maximum and then starts decreasing. Presumably, the reason for this is that if there is too much sulfuric acid, its own reac-

TABLE 2

The dependence of the quantity of the water and sulfuric acid content on the measurable boron from the in situ formation of methoxyborate

Sulfuric acid [a]		Water [b]	
Volume (μl)	Area	Volume (μl)	Area
20	17.5	5	24.7
40	15.3	10	23.3
60	8.3	15	15.8
80	3.0	20	4.6

[a] Methanol, boron, and water are constant. [b] Methanol, boron and H_2SO_4 are constant.

tions with the alcohol do not leave enough free alcohol left over to esterify the boron. As less boron is transported to the torch per unit of time, it becomes difficult to distinguish the boron signal from the baseline and the peak areas drop significantly. The ratio of sulfuric acid to methanol appears to be the important feature in this case, since the addition of more methanol will restore the signal.

As can be seen from Table 2, excess water added to the reaction mixture in the test tube also affects the peak shape and should be kept constant and to a minimum. Less than 5–10 μl of water does not have a significant effect on the peak shape or area, but as the amount of water increases the peaks again become shorter and broader and generally less well defined.

In our laboratory, boron carryover has been noted during standard ICP–AES boron analysis. To limit the carryover, a rather lengthy time between the sample rinse procedures has been implemented for routine boron analysis. This rinse procedure reduces boron carryover, but does not completely eliminate boron accumulation in the torch. Boron accumulation in the torch can be easily demonstrated when the same torch used for standard analyses is also used for the methoxyborate technique. With each succeeding blank analysis a significant, but decreasing, boron background signal can be observed. Therefore, torches previously used to analyze solutions containing any significant boron concentrations should be avoided. A clean, boron-free torch must be used with the methoxyborate technique to achieve good background stability and to prevent drift during sample analysis.

The recorder tracings in Fig. 3 demonstrate a typical peak shape and give an idea of the reproducibility of the method. The reproducibility of 60-s electronically integrated responses are somewhat better than those of peak height measurements of the same signals. The reproducibility of signal integrals seen with triplicate analyses of either standards or blanks is typically less than 2.5% R.S.D. and often less than 1.5% R.S.D. A representative mean integral response value for series of blanks would be 135 mV ($s = 2.5$) and the corresponding integrals for a series of 50-ng

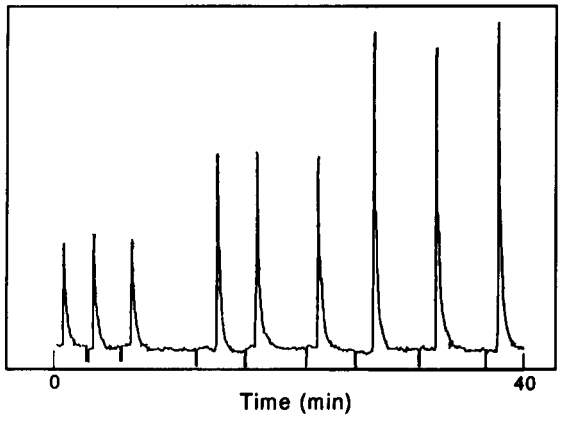

Fig. 3. Representative peak shapes obtained from repeated anaysis of 5, 10, and 15-ng boron standards.

standards would be 1700 mV ($s = 22.3$). Linearity extends from the detection limits to well beyond 250 ng boron. When the boron level exceeds the latter level, this technique would offer no advantage over conventional ICP–AES, unless there was a significant matrix interference. Many different sample decomposition methods were investigated. These methods include nitric acid digestions in Parr bombs, test tube digestions using sulfuric acid–potassium permanganate or nitric acid–hydrogen peroxide, and caustic ashing with both flames and furnaces. Apparent boron recoveries from BSH after Parr bomb acid digestions were typically twice as high when the determination was done by standard ICP–AES than when the same solution was analyzed with the esterification process. The problem was not tissue decomposition, but conversion of the very stable $Na_2B_{12}H_{11}SH$ to borate. None of the previously mentioned wet digestion techniques reproducibly and quantitatively decomposed this compound. Dry ashing methods with sodium hydroxide in high-temperature furnaces (ca. 500°C) were unsuccessful because all of the available furnaces had previously been used for borate fusions and boron recoveries were much greater than 100%. To prevent the external boron from entering, the crucibles were covered, but after 1.5 h, only ca. 36% of BSH boron could be recovered. The quickest and most satisfactory sample preparation technique for dealing with samples contain-

TABLE 3

Comparison of tissue sample analysis results from standard ICP–AES and ICP–AES with methoxyborate generation

Tissue	Direct aspiration ICP–AES (μg B/g)	Methoxyborate generation ICP–AES (μg B/g)	Difference
Spinal cord	5.6	4.1	1.5
Liver	81.9	87.8	−6.1
Spleen	20.4	22.9	−2.5
Adrenal gland	44.3	49.0	−4.7
Thyroid	22.0	22.7	−0.7
Lyophilized beef liver [a]	7.8	7.4	0.4
Mean difference			−2.0
Standard deviation			3.0
t_{calc}			1.63
t_{tab} at $p = 0.05$			2.57

[a] Spiked with boron as $Na_2B_{12}H_{11}SH$.

ing boron as BSH has been caustic ashing at high temperatures over a burner.

Comparison of samples analyzed with the caustic ashing/methoxyborate technique and acid digestion/standard ICP–AES demonstrates reasonable agreement. Five individual tissue samples of different organs acquired from a dog that had been treated with the BSH compound were analyzed by the methoxyborate technique and by a standard ICP–AES method. In both methods all analyses were done in duplicate. The results of this comparison are presented in Table 3. A paired t-test indicates that there is no significant difference between methods at $p = 0.05$. An F-test shows no difference in the precision of the method. The precision of the two analysis methods is similar as reflected by the relative percent differences between two measurements of the same sample digest, which ranged from 0 to 5% for the standard ICP–AES analysis technique and from 0 to 6% for the methoxyborate technique.

Also included in Table 3 is the lyophilized beef liver sample. The boron concentration in the beef liver was again determined by both the standard ICP–AES and the methoxyborate techniques. The standard ICP–AES analysis determined the concentration to be 7.8 ± 0.3 μg boron g^{-1} ($n = 6$). The determination by the methoxyborate technique found the tissue concentration to be 7.4 ± 0.2 μg boron g^{-1} ($n = 5$). Boron in an aqueous BSH standard was recovered at ca. 90%.

Overall, there is good agreement between standard ICP–AES and ICP–AES with methoxyborate sample introduction for tissue samples. Absolute detection limits on the order of 0.2 ng boron with the methoxyborate sample introduction will allow this technique to easily quantitate boron at ng mg^{-1} levels in samples as small as 1–10 mg. With this technique, detectability of boron in a 5-mg sample is now approximately 0.2 ng boron mg^{-1} with practical quantitation limits near 0.6 ng boron mg^{-1}. This represents a minimum of a tenfold decrease in the detection limit of boron in small tissue samples over the best conventional ICP–AES procedures. This work has described a relatively simple modification of the sample introduction system of a standard ICP–AES instrument so it can be used to reliably quantitate boron in small samples. The introduction of boron into the ICP torch as methoxyborate in the vapor phase allows the most sensitive boron emission line to be used for quantitation, since the boron is removed effectively from the sample matrix. The primary limitation of this technique is that all boron in the sample must be converted to boric acid to acquire quantitative generation of the methoxyborate. The conversion of boron containing compounds, including BSH, in tissues to boric acid can be done effectively with a caustic ashing procedure followed by dissolution in concentrated sulfuric acid. The methodology described here may potentially be used to determine both therapeutic and dietary boron at ppm levels in a variety of small biological sample types.

This study was performed under the auspices of the U.S. Department of Energy, Office of Energy Research, under DOE Field Office, Idaho, Contract No. DE-AC07-76ID01570.

REFERENCES

1 R.F. Barth, A.H. Soloway and R.G. Fairchild, Cancer Res., 50 (1990) 1061.

2 T. Kobayashi and K. Kanda, Nucl. Instrum. Methods, 204 (1983) 525.
3 R.G. Fairchild, D. Gabel, B.H. Laster, D. Greenberg, W. Kiszenick and P.L. Micca, Physics, 13 (1986) 50.
4 T. Matsumoto and O. Aizawa, Appl. Radioactive Isotop., 41 (1990) 897.
5 A. Kaczmarczyk, J.R. Messer and C.E. Peirce, Anal. Chem., 43 (1971) 217.
6 I. Ikeuchi and T. Amano, Chem. Pharm. Bull., 26 (1978) 2619.
7 K. Yoshino, M. Okamoto, H. Kakihana, T. Nakanishi, M. Ichihaski and Y. Mishima, Anal. Chem., 56 (1984) 839.
8 M.A.Z. Arruda and E.A.G. Zagatto, Anal. Chim. Acta, 199 (1987) 137.
9 S.R. Tamat, D.E. Moore and B.J. Allen, Anal. Chem., 59 (1987) 2161.
10 D.L. Mann, Spectrosc., 3 (1988) 37.
11 W.F. Bauer, D.A. Johnson, S.M. Steele, K. Messick, D.L. Miller and W.A. Propp, Strahlentherapie und Unkologie, 165 (2/3) (1989) 176.
12 R.F. Barth, D.M. Adams, A.H. Soloway, E.B. Mechetner, F. Alam and A.K.M. Anisuzzaman, Anal. Chem., 63 (1991) 890.
13 A. Anderson et al., in B.J. Allen et al. (Eds.), Progress in Neutron Capture Therapy of Cancer, Plenum Press, New York, 1992, p. 48.
14 W.A. Ausserer, Y. Ling, S. Chandra and G.H. Morrison, Anal. Chem., 61 (1989) 2690.
15 T.E. Blue, C.F. Roberts, R.F. Barth, J.W. Talnagi and F. Alam, Nucl. Technol., 77 (1987) 220.
16 D.D. Siemer, Anal. Chem., 54 (1982) 1321.
17 J.R. Castillo, J.M. Mir, C. Bendicho and C. Martinez, At. Spectrosc., 6 (1985) 152.
18 I. Novozamsky, R. van Eck, J.J. van der Lee, V.J.G. Houba and G.O. Ayaga, At. Spectrosc., 9 (1988) 97.
19 M. Hosoya, K. Tozawa and K. Takada, Talanta, 33 (1986) 691.
20 T. Kumamaru and H. Matsuo, Anal. Chim. Acta, 186 (1986) 267.
21 D.R. Migneault, Anal. Chem., 61 (1989) 272.

Analytica Chimica Acta, 270 (1992) 231–238
Elsevier Science Publishers B.V., Amsterdam

Determination of arsenic and selenium in environmental samples by flow-injection hydride generation atomic absorption spectrometry

Chris C.Y. Chan and Ram S. Sadana

Laboratory Services Branch, Ministry of the Environment, 125 Resources Road, Rexdale, Ontario M9W 5LI (Canada)

(Received 17th April 1992; revised manuscript received 27th July 1992)

Abstract

Flow-injection analysis is applied to sample introduction in conjunction with automated hydride generation and AAS for the determination of As and Se in environmental samples such as soil, vegetation, waters, sediments, and industrial wastes. A large sample loop was used to provide high sensitivities with an absorbance of 0.4 for 10 ng ml^{-1} for both As and Se. The samples, except waters, are digested with a mixture of nitric, sulfuric, and perchloric acids. Se^{6+} in the digested solutions is pre-reduced to Se^{4+} by exothermic reaction in 6–8 M HCl solution, and As^{5+} to As^{3+} by reacting with KI. The analyte is then converted to hydride by $NaBH_4$ in an automated hydride generation system. The evolved hydride is carried through to a heated quartz tube by a stream of argon, and the atomic absorption of the analyte is measured. 1,10-Phenanthroline is used as masking agent to control interferences from Cu and Ni on Se. The detection limits for both As and Se are 0.3 ng ml^{-1}, equivalent to 75 ng g^{-1} in solid sample. Precision is 2.6% R.S.D. Results for standard reference materials agree closely with the certified values.

Keywords: Atomic absorption spectrometry; Flow injection; Arsenic; Hydride generation; Selenium

Hydride generation atomic absorption spectrometry (HG–AAS) coupled with flow-injection analysis (FIA) technique has been used for the determination of As and Se [1–3]. A common advantage of these methods is high sample throughput. However, none of the approaches has achieved a high degree of sensitivity. Yamamoto et al. [1] used FIA combined with gas-segmentation and on-line prereduction techniques for determination of As, and a 0.2 absorbance was obtained on a 10 ng ml^{-1} As solution; Welz et al. [2] optimized the Perkin-Elmer FIAS-200 flow injection system with the aid of an electrodeless discharge lamp, and achieved a sensitivity of 0.5 absorbance for a 10 ng ml^{-1} As solution; Marshall [3,4] designed a HG–AAS and FIA system with an ion-exchange column installed to overcome chemical interferences from geological samples, which operates at high working ranges of 40 to 500 ng ml^{-1} for As and 30 to 300 ng ml^{-1} for Se. In determination of As and Se in environmental samples, particularly in waters, low detection limits are desirable because of low background levels of the analytes in these samples.

This paper describes a method using HG–AAS and FIA techniques with a different manifold arrangement and large sample loop to provide high sensitivity which can be applied to the determination of As and Se in environmental samples such as soil, vegetation, sediments, waters, and the biological samples. An absorbance of about

Correspondence to: C.C.Y. Chan, Laboratory Services Branch, Ministry of the Environment, 125 Resources Road, Rexdale, Ontario M9W 5LI (Canada).

0.4 on a 10 ng ml^{-1} of either As or Se solution can be obtained. The method enables one to determine more accurately the concentrations of analytes in samples at near background levels, and hence to distinguish more effectively between samples from environmental contamination and those with background levels. The system is simple, utilizing one peristaltic pump with one speed to propel both the carrier solution and the sample and reagent solutions, unlike that of Welz [2] using two computer controlled pumps with high speeds such as in the Perkin-Elmer FIAS-200 system. The analytical throughput of this method maintains a rate of about 50 samples per hour, a substantial improvement compared with about 25 samples per hour with our current continuous flow HG–AAS method.

EXPERIMENTAL

Instrumentation

A Varian Model AA-5 atomic absorption spectrometer. A flow-injection module (Model 1600-000, Lachat Instruments, Milwaukee, WI) for sample injection with six ports. The tubing connecting the ports is made of PTFE. A Gilson (Middleton, WI) sampler (Model 222) and a Gilson peristaltic pump (Model Minipuls II) were used to sample and propel the sample and reagent solutions. A timer, built by EG&G Labserco (Oakville) was interfaced with the sampler and the flow-injection valve to control the sampling time and synchronize the switching of the injection valve. A strip-chart recorder (Linear 1800, Reno, NV) was used to capture analog atomic absorption signals. A computer system (DP-1000) supplied by Labtronics (Guelph) was interfaced with the AA spectrometer to digitize the signal and automate the calculation step. The schematic of various components and the FIA manifold are shown in Fig. 1. A gas–liquid separator was installed to separate the gaseous hydrides of interest from the solution. An impinger partly filled with concentrated sulphuric acid served to remove moisture and to homogenize the hydride–argon mixture. The quartz tube, 10 cm × 1 cm i.d. with an inlet tube fused into the centre, was used as a flow through cell. It was wound with a 22-gauge Chromel wire and insulated with a wrapping of Thermofab™ (an asbestos substitute) string. This electrically heated quartz tube acts as an atomizer. It was mounted on the burner head of the spectrometer. The gaseous hydrides were transported from the gas–liquid separator to the impinger through 15 cm × 3 mm i.d. Tygon tubing and to the atomizer through tubing 5 cm long. The temperature of the quartz tube atomizer was controlled by a variable transformer.

Reagents

All chemicals used were reagent grade and water was distilled. Mineral acids used were nitric acid (70%, w/w), sulphuric acid (96%, w/w),

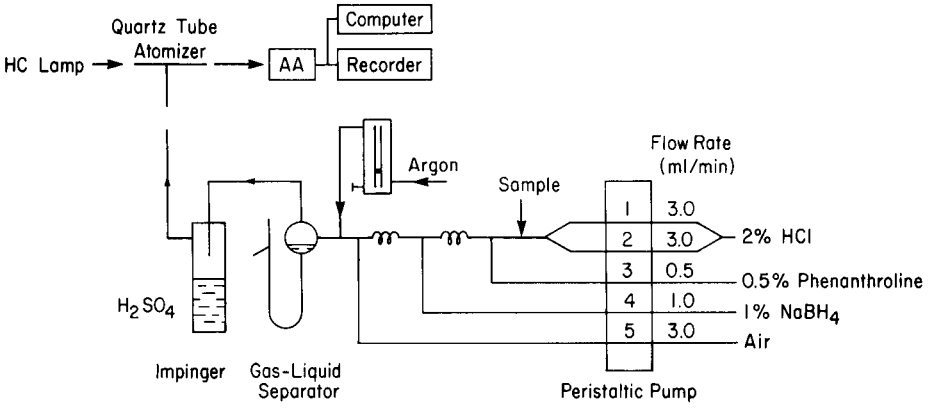

Fig. 1. Analytical system for determination of hydrides by automated FIA and hydride AAS.

perchloric acid (60%, w/w), and hydrochloric acid (38%, w/w).

Acid mixture was prepared by mixing nitric acid, sulphuric acid, and perchloric acid in a volume ratio of 6:3:1 in a bottle. One litre or 500 ml is normally prepared. Care should be taken during the mixing process to avoid generation of excessive heat.

1% $NaBH_4$ solution was prepared by dissolving 5 g of sodium borohydride and approximately 0.5 g (5 pellets) of sodium hydroxide in 500 ml of water. The solution was stored in a refrigerator when not in use. It is stable for at least a month at 4°C.

Reducing solution (10% KI and 1% ascorbic acid) was made by dissolving 50 g of potassium iodide and 5 g of ascorbic acid in 500 ml of water.

The masking reagent was prepared by dissolving 0.5 g of 1,10-phenanthroline in 100 ml of 0.1 M HCl solution.

Carrier solution: 2% HCl (v/v) was used. Two litres of solution is normally prepared at a time.

The diluent was 20% (v/v) HCl.

Arsenic and selenium stock solutions (1000 μg ml^{-1}) were obtained commercially from Fisher Scientific (Union-ville).

Working standard solutions for As: 100 ml each of 2.5, 5.0, and 10.0 ng ml^{-1} standard solutions in 20% (v/v) HCl was prepared by serial dilution of the arsenic stock solution. 10 ml of the reducing solution was added to each of the working standard solutions before it was made up to 100 ml, so that the final working standard solutions contain 1% KI and 0.1% ascorbic acid.

Working standard solutions for Se: 100 ml each of 2.5, 5.0, and 10.0 ng ml^{-1} standard solutions in 20% (v/v) HCl was prepared by serial dilution of the selenium stock solution.

Procedure

Preparation of sample solutions. About 0.06 g of sample was weighed out accurately and transferred to a test tube. 3 ml of acid mixture was added. The test tube was placed in an aluminum heating block on a hot plate which was turned on at low heat for approximately 3 h. The temperature was increased to 200°C and the sample was digested overnight. A batch of 40 samples in test tubes can be digested at the same time. When the digestion was complete, the sample tubes were removed from the heating block and were placed into racks to cool in a fume hood. 3 ml of concentrated HCl was then added to each sample tube. The sample was mixed and allowed to stand for 20 min. The heat generated in the process facilitates the reduction of Se^{6+} to Se^{4+} under high acidity of HCl. The sample was diluted to the 15 ml mark with water and was mixed well by bubbling air through for approximately one minute. A reagent blank was prepared simultaneously for each run. The solution was ready for Se analysis. For As analysis, an aliquot of 9 ml of the sample solution was pipetted into a test tube followed by adding 1 ml of the reducing solution. The solution was mixed well, and allowed to stand for at least 10 min before analysis. If digestate was found to contain concentrations of analyte beyond the usual calibration range, the digestate was diluted with the diluent to an appropriate concentration.

In the determination of As and Se in water samples, a pretreatment was required. For As analysis, a 7-ml aliquot of sample was pipetted into a test tube, and 2 ml of concentrated HCl was added followed by 1 ml of reducing solution. The solution was mixed and allowed to stand for at least 10 min before analysis. For Se analysis, a 7 ml aliquot of sample was pipetted into a sample tube, followed by 3 ml of concentrated HCl. The solution was mixed well prior to analysis.

Determination of As and Se. The instrumental parameters as given in Table 1 were selected. The quartz tube atomizer was aligned in the light beam to allow maximum radiation to reach the detector. The preset variable transformer was switched on to provide the desired temperature in the atomizer. The peristaltic pump was turned on with all the reagent tubes dipped in water. The argon was introduced immediately with its flow-rate regulated at 100 ml min^{-1}. The timer, which was interfaced with the sampler and the flow-injection valve, was turned on, and the desired sampling time and washing time were set. The reagent tubes were inserted into the corresponding solutions (see arrangement in Fig. 1). As soon as the system had stabilized and the

TABLE 1

Optimum instrumental parameters

Atomic absorption spectrometer	
Wavelength	193.7 nm (As)
	196.0 nm (Se)
Lamp current	7 mA
Slit width	300 μm
Damping	*D*
Flow injection module	
Sampling time	34 s
Washing time	46 s
Recorder	
Span	10 mV
Chart speed	1 cm min^{-1}

baseline established, which normally takes 5–10 min, the standard and sample solutions which had been loaded in the sampler were run sequentially.

When the analysis was complete, the concentrations of the analyte were calculated by a computer from a standard curve of peak height vs. concentration. The typical concentrations selected were 2.5, 5, and 10 ng ml^{-1}. The curve is linear. The use of a chart recorder assisted in the interpretation of the results and diagnoses of possible interference problems by visual examination of the peak shapes. Typical recorder tracings on series of As and Se standards are depicted in Figs. 2 and 3.

RESULTS AND DISCUSSION

A manifold was initially designed for the determination of As by on-line pre-reduction of As^{5+} to As^{3+} by KI. However, the system requires the introduction of large quantities of high concentration HCl (1:1) and KI (30%) and the use of long glass mixing coils to allow more time for the reduction of As^{5+}. The efficiency of pre-reduction is nearly 100% with the above setup. Since the flow path is long, the dispersion of the analyte in the stream becomes significant. The FIA technique is unable to offer high sensitivity with the above manifold arrangement. The corrosive properties of highly concentrated acid is a nuisance in operation and maintenance of the system. Furthermore, the manifold is too cumbersome for the application of Se analysis which requires neither pre-reduction of the analyte by KI nor a high concentration of HCl. Since we

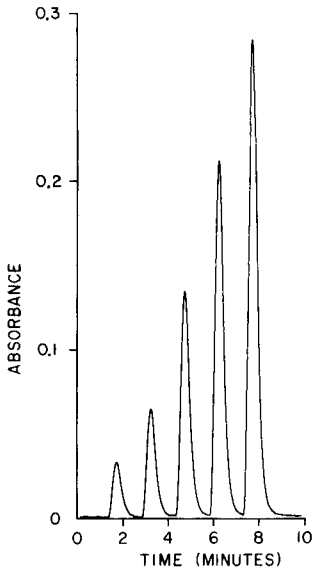

Fig. 2. Typical recorder tracings for As standard solutions of 1, 2, 4, 6, and 8 ng ml^{-1}.

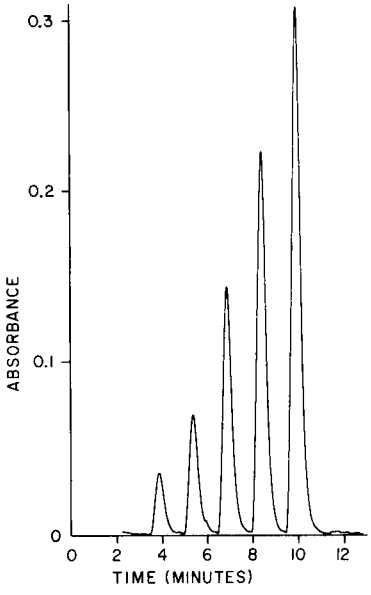

Fig. 3. Typical recorder tracings for Se standard solutions of 1, 2, 4, 6, and 8 ng ml^{-1}.

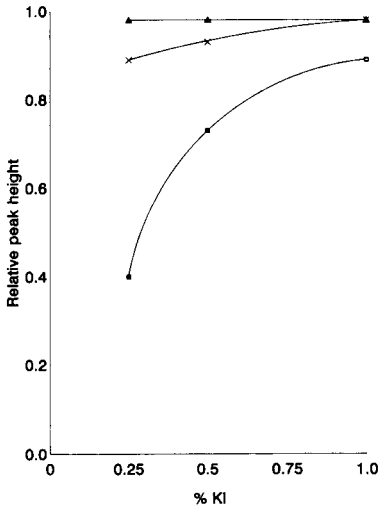

Fig. 4. Effect of concentration of HCl and KI on As (10 ng ml^{-1}) absorption signals: (a) 30% HCl, (b) 20% HCl; (c) 10% HCl.

analyse both As and Se on a routine basis, a universal manifold is desirable, which can serve both analyses without having to switch parts or add tubings. To fulfil this requirement, a modified manifold was designed (see Fig. 1). The pre-reduction of As^{5+} is carried out manually. The sample is introduced into the system, and finally, As^{3+} is determined as total arsenic. This manifold can also be used for the determination of Se, and potentially for Sb, Bi, and Te.

Effects of concentrations of HCl and KI for pre-reduction

The acidity and the KI concentration are critical for complete pre-reduction of As^{5+} to As^{3+}. The solutions of 10 ng ml^{-1} As^{5+} were prepared with various concentrations of HCl and KI. They were allowed to stand for a minimum of 10 min and analyzed. The absorbance signals were recorded. The relationship between absorbance and the concentrations of HCl and KI is shown in Fig. 4. The minimum requirements for complete reduction appear to be 20% HCl and 1% KI. Without KI, As^{5+} was found only one fourth as sensitive as As^{3+}. The inclusion of ascorbic acid in both the standard and sample solutions helps to prevent the oxidation of iodide to tri-iodide by air or oxidants in the solution. The brown coloured tri-iodide ion is unstable and decomposes with time to iodide ion and iodine. The iodine deposits on the container walls and it may also adsorb analyte. It was found that 1 ml of 1% ascorbic acid solution per 10 ml of sample solution is sufficient to keep the iodide containing solution stable.

Effect of type and concentration of acids in sample solutions

Signal response is independent of the type and concentration of the common acids (HCl, H_2SO_4, HNO_3, $HClO_4$), provided the acidity is greater than 5% (v/v). In the sample preparation, an acidity of more than 13% has been provided, therefore a small variation of acidity in samples after digestion does not impose any effect on the response.

Effect of flow-rate of carrier solution (2% HCl)

The flow-rate of the 2% HCl solution (lines 1 and 2 in Fig. 1) which carries the sample into the reacting stream has an effect on the sensitivity of the method. A standard solution was run at various carrier flow-rates, and the peak heights were recorded. The analytical signal increases with flow-rate. Many workers [1–3] used a very high flow-rate, up to 25 ml min^{-1} in one case [2], to achieve good sensitivity. However, too high a flow-rate would increase internal flow pressure and therefore increase the chance of loosening the tubing connections. A flow-rate of about 6 ml min^{-1} was found to be safe and convenient in terms of maintenance of the FIA manifold, while providing adequate sensitivity. The main function of the carrier is to propel the sample slug. It seems that water alone can act as a carrier; however, a slightly acidic carrier is preferred in practice, since it helps to clean the flow path by keeping any less soluble materials from depositing on the wall of the tubing. A concentration of 2 to 5% (v/v) of HCl is sufficient. In addition, an acidic carrier reacts with $NaBH_4$ and generates hydrogen. An uninterrupted supply of hydrogen to the atomizer helps to maintain a steady background and baseline.

Effect of sample volume (loop volume)

Sample solution is pumped into and collected in the sample loop (made of 1.35 mm i.d. PTFE tubing) before it is released into the reacting stream. A standard solution was run with various lengths (proportional to volume) of sample loop and the absorption signals compared. In the system described here, the instrument response at a given concentration of analyte is affected by the amount of analyte introduced. The relationship between the absorbance and sample volume (loop volume) is shown in Fig. 5. Thus, if a volume of sample injected is less than required to achieve the steady-state signal, a peak thus generated is not the maximum peak. In general, sensitivity increases with increasing sample volume. The minimum sample volume that gives maximum sensitivity appears to be about 2 ml which can be pumped in about 30 s. This volume was chosen for use in the method. Reduction of sample volume results in decrease of sensitivity, but it increases sample throughput.

Effect of air in the carrier gas stream

It is known [5] that oxygen is essential in facilitating the reduction of the hydrides. Oxygen first reacts with the hydrogen to produce hydrogen atoms which in turn reduce the arsine successively into arsenic atoms. The possible reactions progress according to the following equations:

$$O_2 + 3H_2 \rightarrow 2H_2O + 2H^{\cdot}$$

$$AsH_3 + H^{\cdot} \rightarrow AsH_2^{\cdot} + H_2$$

$$AsH_2^{\cdot} + H^{\cdot} \rightarrow AsH + H_2$$

$$AsH + H^{\cdot} \rightarrow As + H_2$$

It is then expected that introduction of air into the reaction phase through the argon carrier would increase the signal response. A pump tube was used to introduce air (line 5 in Fig. 1) into the system. The signal response of a 10 ng ml^{-1} As solution was compared with and without introducing air. A difference of 30% was observed in favour of air introduction. The amount of air introduced in the system was optimised. Signal responses are equal from the air flow-rates of 1 ml min^{-1} to 5 ml min^{-1}. A flow-rate of 3 ml min^{-1} was adopted arbitrarily.

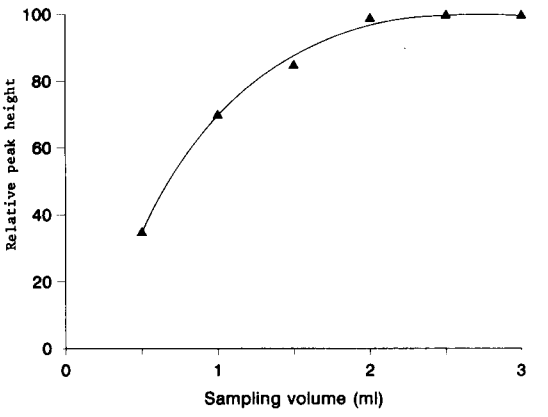

Fig. 5. Effect of sample volume on signal (As, Se) response.

Effect of length of reaction tube

Length of reaction tube refers to the length of tubing between the mixing coil of the $NaBH_4$ and the entrance of the gas–liquid separator. Although the hydride-generation reaction is fast, it still needs a definite time for the reaction to be completed. Various lengths of reaction tube, 1 mm i.d., were chosen to test the signal response on a 10 ng ml^{-1} As solution. A 20-cm tube length was found to give maximum signal, thus indicating completion of reaction.

Effect of concentration of $NaBH_4$

There are no appreciable differences in signal response with either 1% or 2% $NaBH_4$ solutions. The signal decreases if a lower concentration is used. Use of a 0.5% solution results in loss of sensitivity of 15%. A greater than 2% solution does not produce better sensitivity. To ensure that there is sufficient strength for hydrides formation and to keep the consumption of reagent to a minimum, 1% $NaBH_4$ was used. The solution was made slightly alkaline to inhibit decomposition. One pellet of sodium hydroxide dissolved in each 100 ml of $NaBH_4$ solution was sufficient. No appreciable difference in stability of signal response was found from solutions whether filtered or not.

Interferences

The method is free of interference from the common anions, such as chloride, nitrate, sul-

TABLE 2

Tolerance limits of interferents

Interferent	Tolerance limit for As		Tolerance limit for Se	
	$\mu g\ ml^{-1}$ in solution	% in sample [a]	$\mu g\ ml^{-1}$ in solution [b]	% in sample [a,b]
Ni	500	12.5	500 (40)	12.5 (1)
Cu	> 500	> 12.5	50 (1)	1.25 (250 $\mu g\ g^{-1}$)
Co	> 500	> 12.5	200	5

[a] Based on 0.06 g of sample in 15 ml of solution. [b] Values in parentheses are tolerance limits in the absence of masking agent.

phate, perchlorate, and phosphate. The most well known interfering cations encountered in hydride determination are nickel, copper, and cobalt. An attempt to reduce the transition-metal interferences by shortening the length of the reaction tube resulted in decrease of sensitivity. A chemical study of the effect of these metals on the analytes was carried out and the tolerance limits established. The results are shown in Table 2.

The masking effects of thiosemicarbazide on Cu and of 1,10-phenanthroline on Ni have long been known [6]. Kirkbright et al. [7] successfully used these compounds to minimize interferences from Cu and Ni in the determination of As by flame AAS after hydride generation; Chan et al. [8] applied the same masking agents to control these interferences on the determination of Bi in geological materials by flow injection and hydride generation AAS. Although we did not find appreciable interferences from these heavy metals with the As analysis by this method, their interferences with that of Se were significant. Use of the same treatment for controlling these interferences was attempted and tests for their effectiveness on a 10 ng ml^{-1} Se solution under the acidic conditions of the procedure were carried out. Unexpectedly, thiosemicarbazide was found to suppress the Se signal, acting as an interferent itself, and its use was abandoned. However, 1,10-phenanthroline works effectively. In the absence of 1,10-phenanthroline, the tolerance limit of Cu is only 1 $\mu g\ ml^{-1}$, while that of Ni is 40 $\mu g\ ml^{-1}$. With the use of this masking agent, the interferences are reduced substantially, as the tolerance limits of Cu and Ni increase to 50 and 500 $\mu g\ ml^{-1}$ respectively. Such high concentrations are normally not to be expected in environmental samples.

Precision, accuracy, and detection limits

The precision of the method for both As and Se was determined on the sample solutions at concentrations near 10 ng ml^{-1}. The R.S.D. of ten replicate analyses on a typical sample, BCSS-1, a sediment, is 2.6% for As. For water samples, precision for As analysis is better than 2% R.S.D.

TABLE 3

Analytical results of SRMs ($\mu g\ g^{-1}$)

Sample	Matrix	Arsenic			Selenium		
		Certified value	Found		Certified value	Found	
			HG–AAS FIA [a]	HG–AAS		HG–AAS FIA [a]	HG–AAS
NIST 2704	Sediment	23.4 ± 0.8	21.5	20.7	(1.1) [b]	1.02	1.14
NIST 1646	Sediment	11.6 ± 1.3	10.4	10.4	(0.6) [b]	0.61	[d]
NIST 1571	Orchard leaves	10.0 ± 2.0	10.4	9.9	0.08 ± 0.01	0.06 [c]	[d]
NIST 1572	Citrus leaves	3.1 ± 0.3	3.24	2.8	(0.025) [b]	0.025 [c]	[d]
MESS-1	Sediment	10.6 ± 1.2	10.3	10.1	0.34 ± 0.06	0.37	[d]
BCSS-1	Sediment	11.1 ± 1.4	11.0	10.7	0.43 ± 0.06	0.44	[d]
TORT-1	Lobster hepato	24.6 ± 2.2	24.9	23.6	6.88 ± 0.47	5.79	6.10
DORM-1	Dogfish liver	17.7 ± 2.1	16.2	16.7	1.62 ± 0.12	1.45	1.67
EPA WS378	Water	25.0 [e]	25.0	26.0	6.0 [e]	5.0	5.0

[a] Values in this column are means of two to five determinations. [b] Values in the brackets are uncertified. [c] Results obtained by using 0.2 g sample weight. [d] Below method detection limit. [e] Values for EPA WS378 are in ng ml^{-1}.

based on five replicate analyses on the SRM sample, EPA WS378. For Se analysis, similar precisions were found.

The accuracy of the method was validated by the close agreement of the analytical results with the certified values or reference values of a number of environmental and biological samples, as shown in Table 3. The samples were also analyzed for As and Se by a continuous flow HG–AAS method without the use of FIA, and the results are included in Table 3 for comparison. As expected, the results from the two methods are in good agreement.

The detection limit is defined as three times the S.D. (3σ) from replicate analysis on a sample with low concentration of the analyte. A sediment sample, BCSS-1, containing 0.43 $\mu g\ g^{-1}$ Se, was chosen for replicate analysis (ten times). The S.D. was found to be 0.1 ng ml^{-1} in solution. The detection limit (3σ) for Se thus calculated is 0.3 ng ml^{-1} in solution and 75 ng g^{-1} in solid sample. The practical detection limit, arbitrarily expressed as three times the overall blank value, is also 0.3 ng ml^{-1} for both As and Se in solution, equivalent to 75 ng g^{-1} in solid sample, based on 0.06 g of sample in 15 ml. The detection limits for both As and Se can further be lowered by increasing sample weight, e.g., 0.1 g or 0.2 g, if so desired.

GENERAL REMARKS

The temperature of the quartz tube was set to about 850°C, which is indicated with the appearance of a dull red glow emitted in the quartz tube. Optimum temperature can be obtained by trial and error method by varying the setting of the transformer until the maximum absorbance is reached. The temperature can be measured with a pyrometer. The absorbance varies considerably with the flow-rate of the argon carrier gas. Strict regulation of the argon flow is required. 100 ml min^{-1} was found to be optimum in this system. The volume of the gas–liquid separator is approximately 8 ml, and was found to be not critical. The solution transmission lines including the mixing coils were 0.56 mm i.d. PTFE tubing designed to minimize the dead volume. Up to 5% loss of As in digestion process was not uncommon. To minimize analytical error, the absorbance signals from a set of digested As standards were used for construction of a standard curve. A minimum HCl concentration of 30% was required for Se analysis in water samples to prevent Cu interference. The masking agent was not required in performing the As analysis; therefore, the phenanthroline line (line 3 in Fig. 1) could be placed into the 2% HCl carrier solution.

We thank Sasan Bina for preparing the sample solutions of the standard reference materials and the graphic work for this manuscript.

REFERENCES

1 M. Yamamoto, M. Yasuda and Y. Yamamoto, Anal. Chem., 57 (1985) 1382.
2 B. Welz and M. Schubert-Jacobs, At. Spectrosc., 12 (1991) 91.
3 G.D. Marshall, Mintek Report No. M388, Laboratory Method No. 33/13, Geological Survey of South Africa, 1990.
4 G.D. Marshall and J.F. van Staden, J. Anal. At. Spectrom., 5 (1990) 681.
5 Narsito, J. Agterdenbos and S.J. Santosa, Anal. Chim. Acta, 237 (1990) 189.
6 D.D. Perrin, Masking and Demasking of Chemical Reactions, Wiley–Interscience, New York, 1970, pp. 35, 37.
7 G.F. Kirkbright and M. Taddia, Anal. Chim. Acta, 100 (1978) 145.
8 C.Y. Chan, M.W.A. Baig and P.A. Lichti, Anal. Lett. 23 (1990) 2259.

Analytica Chimica Acta, 270 (1992) 239–245
Elsevier Science Publishers B.V., Amsterdam

Solid surface room-temperature phosphorescence analysis of banned substances in sport

L.M. Cabalín and J.J. Laserna

Department of Analytical Chemistry, Faculty of Sciences, University of Málaga, E-29071 Málaga (Spain)

A. Rupérez

Department of Physical Chemistry, Faculty of Sciences, University of Málaga, E-29071 Málaga (Spain)

(Received 28th May 1992; revised manuscript received 23rd July 1992)

Abstract

Room-temperature phosphorescence (RTP) characteristics of 27 banned drugs in sport on Whatman No. 1 filter paper were studied. Several heavy-atom perturbers, including I^-, Tl^+ and Pb^{2+}, and the effect of pH were investigated. Optimum experimental conditions for every case were evaluated. The phase plane method was applied to the determination of phosphorescence lifetimes on a filter-paper substrate. Compared with RTP, laser-induced phosphorescence spectrometry provides lower limits of detection.

Keywords: Phosphorimetry; Doping; Laser-induced phosphoresence; Pharmaceuticals; Room-temperature phosphorescence

According to the IOC Medical Commission, the most recent doping classes in sport include five main categories: stimulants, narcotics, anabolic steroids, β-blockers and diuretics. The qualitative identification of drugs, usually in urine specimens, is needed for the effective control of their illegal use in sport. The finding of a drug or metabolite in a sample must be confirmed by a different analytical method of measurement. The methods currently approved for doping control include gas chromatography (GC), gas chromatography–mass spectrometry (GC–MS), liquid chromatography (LC) and radioimmunoassay.

Solid substrate room-temperature phosphorimetry (SSRTP) is a technique that has been growing in recent years as a promising tool for the trace level detection and determination of various organic compounds such as pharmaceutical products [1,2], pesticides [3,4], polycyclic aromatic hydrocarbons [5–7] and drugs [8,9]. The advantages of RTP derive from its simplicity, good sensitivity and selectivity and the possibility of automation [10,11]. Cellulose filter-papers are considered to be the most suitable RTP supports to date [12]. Boutilier and Winefordner [13] reported analytical figures of merit for laser-induced phosphorescence of drugs at 88 K and compared the use of two different lasers as excitation sources. Recently, other workers have reported on the applicability of laser-induced phosphorescence spectrometry of cryogenic temperatures [14,15]. Vo-Dinh [16] provided an overview of laser-induced luminescence spectroscopy on solid substrates and applications of laser-based

Correspondence to: J.J. Laserna, Department of Analytical Chemistry, Faculty of Sciences, University of Málaga, E-29071 Málaga (Spain).

techniques in fluorescence and phosphorescence analysis. Very little has been reported on the use of lasers in solid-substrate RTP.

In this paper, the RTP spectral characteristics of 27 doping drugs (stimulants, diuretics, narcotic analgesics and β-blockers) on Whatman No. 1 filter-paper are reported. Three heavy atoms (I^-, Tl^+ and Pb^{2+}) and the effect of pH were evaluated. Radiative lifetimes of the drugs were calculated using the phase plane method for RTP decay analysis [17,18]. Room-temperature phosphorimetry and laser-induced phosphorescence spectroscopy (LIP) were compared in terms of analytical figures of merit.

EXPERIMENTAL

Apparatus

RTP was conducted on a Perkin-Elmer Model 650-10S spectrofluorimeter fitted with a phosphorescence accessory. The excitation source was a 150-W xenon lamp. The sample compartment includes a rotating disc chopper which permits non-calibrated chopping of the excitation beam in the range 0–3600 rotations per minute. A Model UV-12 pulsed nitrogen laser (Laser Photonics) was also used to induce room-temperature phosphorescence. It had a peak out power of 2.5 mJ and a pulse width of 10 ns at 337.1 nm. A

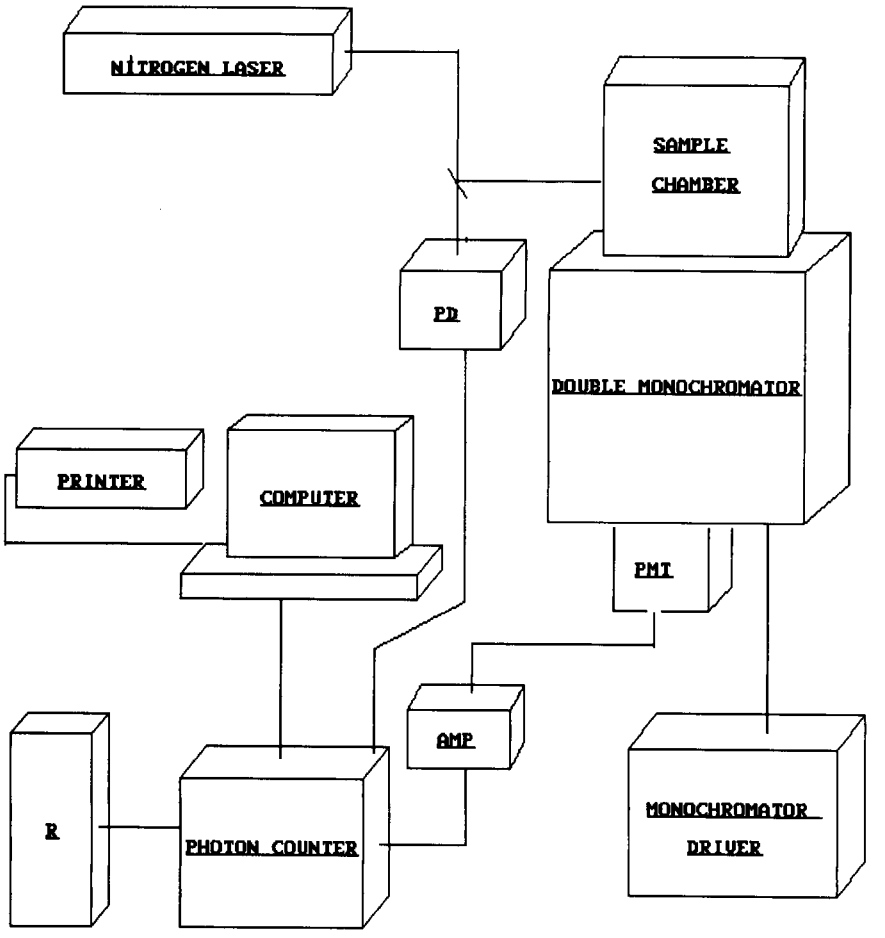

Fig. 1. Schematic diagram of the spectrometer. Pd = fast photodiode; PMT = photomultiplier tube and cooled housing; AMP = fast preamplifier; R = recorder.

TABLE 1

RTP spectral characteristics of banned drugs in sport

Compound [a]	λ_{ex} (nm)	λ_{em} (nm)	P [b]	Exp. conditions
Acebutolol (B)	340	516	Strong	Pb^{2+}, neutral
	290	496	Weak	I^-, basic
Acetazolamide (D)	312	504	Weak	I^-, basic
	320	514	Weak	Tl^+, basic
	316	508	Strong	Pb^{2+}, basic
Alprenolol (B)	296	504	Weak	I^-, basic
	346	530	Weak	Tl^+, basic
Amiloride (D)	342	532	Weak	Tl^+, basic
Atenolol (B)	344	532	Weak	Tl^+, basic
Bendroflumethiazide (D)	308	504	Weak	Tl^+, neutral
	300, 348	500	Strong	Pb^{2+}, neutral
	344	528	Weak	Tl^+, basic
	330	500	Weak	Pb^{2+}, basic
Caffeine (S)	310	520	Weak	Pb^{2+}, neutral
	292	450	Strong	I^-, basic
Chlorthalidone (D)	320	528	Weak	Tl^+, neutral
	310	506	Weak	I^-, basic
	340	530	Weak	Tl^+, basic
Cocaine (N)	308	520	Weak	Tl^+, neutral
	300	500	Weak	I^-, basic
	348	536	Weak	Tl^+, basic
	335	524	Weak	Pb^{2+}, basic
Codeine (N)	300	510	Weak	Tl^+, neutral
	326	524	Weak	I^-, basic
	350	536	Weak	Tl^+, basic
Ethacrinic acid (D)	322	512	Weak	I^+, basic
	344	540	Weak	Tl^+, basic
Furosemide (D)	320	512	Weak	I^-, basic
Hydrochlorothiazide (D)	320	510	Moderate	I^-, basic
	342	532	Weak	Tl^+, basic
Methadone (N)	320	528	Weak	Pb^{2+}, neutral
	342	532	Weak	Tl^+, basic
Methamphetamine (S)	–	–	None	–
Methoxamine (S)	–	–	None	–
Nadolol (B)	300	522	Weak	Tl^+, neutral
	340	530	Weak	Tl^+, basic
Oxprenolol (B)	320	528	Weak	Pb^{2+}, neutral
	340	540	Weak	Tl^+, basic
Pemoline (S)	310	524	Weak	Tl^+, neutral
	344	528	Weak	Tl^+, basic
	340	522	Weak	Pb^{2+}, basic
Pentazocine (N)	338	500	Weak	I^-, basic
Pentylenetetrazole (S)	310	524	Weak	Tl^+, neutral
	306	514	Weak	I^-, basic
	346	534	Weak	Tl^+, basic
Phenylephrine (S)	350	528	Weak	Tl^+, basic
	336	515	Weak	Pb^{2+}, basic
Probenecid (D)	320	530	Weak	Pb^{2+}, neutral
	310	516	Weak	I^-, basic
	340	528	Weak	Tl^+, basic
Propranolol (B)	306	494, 526	Moderate	I^-, neutral
	308	496, 524	Strong	Tl^-, neutral
	306	498, 528	Strong	Pb^{2+}, neutral
Theobromine (S)	290	450	Strong	I^-, basic
Theophylline (S)	296	508	Weak	Pb^{2+}, neutral
	298	456	Strong	I^-, basic
Triamterene (D)	–	–	None	–

[a] Compound: 3 μl of 100 μg ml^{-1} solution + 3 μl of 1 M NaOH solution. Drug class: B = β-blockers, D = diuretics, N = narcotics and S = stimulants. [b] Phosphorescence intensity: weak, $< 2 \times$ blank intensity: moderate, $\geq 2 \times$ blank intensity; strong, $> 4 \times$ blank intensity.

schematic diagram of the experimental apparatus used for LIP is shown in Fig. 1. Spectra were obtained with a Model 1680B 0.22-m double-grating spectrometer (Spex Industries). Phosphorescence was collected at right-angle and detected with a thermoelectrically cooled photomultiplier tube (Hamamatsu Model R928) and a photon-counting system (Stanford Research Model SR400). Operation of the photon counter was controlled by an AT personal computer with Stanford Research SR465 software. The photon counter was discharged externally by a trigger, which consisted in a photodiode sustained with 9 V.

Paper discs of 1 cm were used as the substrate for RTP. A laboratory-constructed sample holder was used. Right-angle geometry was used for collection of phosphorescence but, owing to the geometry of the sample holder, the angle of incidence of the exciting light into the substrate was 45°. A 50 mm^2 circular window limited the exposed paper area. During the measurements, a flow of dry nitrogen was directed to the front of the paper surface by means of a glass capillary (1 mm i.d.). The nitrogen flow-rate was adjusted for the maximum RTP signal, and was 9 l min^{-1}.

Reagents

The drugs studied were of analytical-reagent grade (Sigma) and were used as received. Stock solutions of 100 μg ml^{-1} were prepared in methanol. The heavy atoms utilized were in the form of solutions of 1 M potassium iodide, 0.1 M thallium(I) nitrate and 0.1 M lead(II) acetate (all from Panreac). Sodium hydroxide solution (1 M) was used (Panreac). The solvent used to prepare solutions were absolute methanol and demineralized water. All chemicals used were of analytical-reagent grade or equivalent and were used as received. Whatman No. 1 filter-paper was obtained from Whatman International.

Sample preparation

In RTP, batches of Whatman No. 1 filter-paper were submerged in a heavy atom solution [1 M potassium iodide, 0.1 M thallium(I) nitrate or 0.1 M lead(II) acetate] and dried under a stream of hot air for 1 min. Subsequently the filter-paper was successively spotted with 3 μl of the drug solution and 3 μl of 1 M NaOH solution. The sample holder was then placed in the sample compartment of the spectrofluorimeter where the samples were allowed to dry for 3 min under a flow of dry nitrogen.

RESULTS AND DISCUSSION

Phosphorescence spectral properties

The RTP spectra characteristics of 27 drugs spotted on Whatman No. 1 filter-paper pretreated with sodium iodide, thallium(I) nitrate or lead(II) acetate are presented in Table 1. As the RTP spectra of most aromatic compounds containing acidic or basic functional groups are very sensitive to pH in relation to the hydrogen-bonding ability of the substrate, the effect of pH was evaluated. pH can also be used as a parameter to reduce interferences by extraneous solutes or to cause stronger association in the analyte–heavy atom–substrate complex.

The results in Table 1 show that 24 of the 27 banned drugs exhibit an RTP signal. However, only for seven of these compounds was the signal strong or moderate. Phosphorescence emission was not observed for methamphetamine, methoxamine and triamterene. Sodium hydroxide is added to ionize the molecule, allowing favourable interactions (electrostatic or hydrogen bonding) of the molecule with the cellulose substrate material; this may be the reason why most of the compounds tested, with the exception of bendroflumethiazide and propranolol and depending on the heavy atom employed, are phosphorescent at room temperature in an alkaline medium. For most of the drugs the RTP excitation and emission bands were red shifted in a basic medium with respect to their positions in neutral medium. As shown in Fig. 2, the phosphorescence intensity of bendroflumethiazide decreased with addition of 1 M NaOH and the excitation peak at 300 nm was affected. Except for propranolol, the position of the phosphorescence excitation and emission maxima of the drugs changed significantly with the type of heavy atom employed. For instance, the phosphorescence excitation and emission

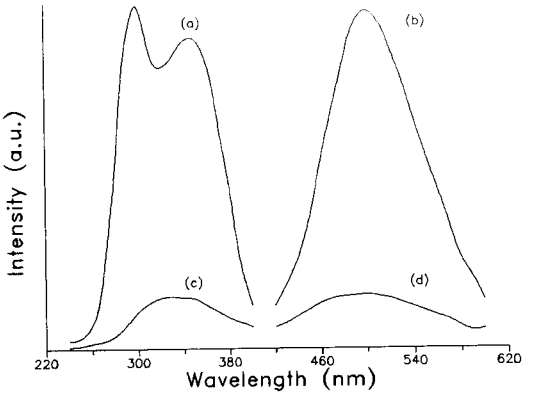

Fig. 2. RTP excitation and emission spectra of bendroflumethiazide (100 μg ml^{-1}) on Whatman No. 1 filter-paper pretreated (a), (b) with lead(II) acetate (0.1 M) in neutral medium and (c), (d) with lead(II) acetate (0.1 M) and NaOH (1 M).

spectra of acetazolamide with three heavy atom salts are shown in Fig. 3. The presence of lead(II) and thallium(I) results in significant red shifts of the phosphorescence excitation and emission maxima compared with the RTP spectra with iodide. This is in agreement with the results obtained in other studies [19,20].

The sensitivity can be improved by the use of different heavy atoms; certain heavy atoms preferentially increased or decreased the emission of drugs studied. For instance, the three methylxanthines (caffeine, theophylline and theobromine) emitted the highest RTP intensities in the presence of iodide [20]. The optimum combination of heavy atom and pH varies with the particular compound under examination.

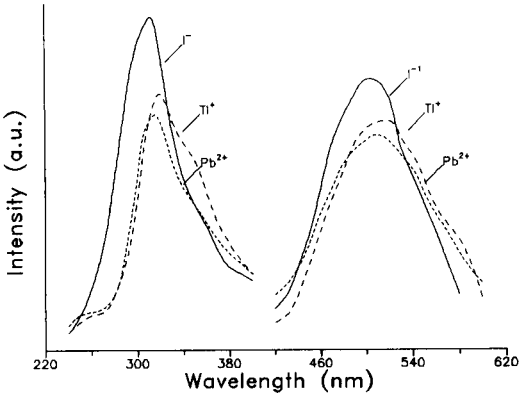

Fig. 3. Heavy atom effect on the RTP excitation and emission spectra of acetazolamide (100 μg ml^{-1}) on Whatman No. 1 filter-paper in basic medium. Solid line, with potassium iodide (1 M); dashed line, with thallium(I) nitrate (0.1 M); and dotted line, with lead(II) acetate (0.1 M).

Phosphorescence lifetimes

RTP lifetimes are extremely sensitive to the environmental conditions, such as the substrate and the heavy atom. In addition, the phosphorescence of the analyte and impurities in the paper, photochemical degradation of both of them and decay of the scattered stray source radiation can directly affect the observed RTP lifetimes. Among the different approaches for the analysis of the radiative decays, the phase plane method has been demonstrated to be well suited for RTP [17,18]. The advantages of the phase plane method over the conventional semi-logarithmic method include the ability to analyse decay curves with a high background phosphorescence and higher accuracy of the calculated lifetime values. The RTP lifetime values of selected drugs under the optimum experimental conditions are summarized in Table 2. Lifetimes were calculated over the ex-

TABLE 2

RTP lifetimes of the drugs examined

Analyte	Experimental conditions [a]	τ_1 [b] (ms)	τ_2 [c] (ms)	χ^2 [d]
Acebutolol	Pb^{2+}, neutral	0.28	–	1.11 (110)
Bendroflumethiazide	Pb^{2+}, neutral	0.26	–	0.61 (110)
Caffeine	I^-, basic	0.66	–	0.22 (159)
Hydrochlorothiazide	I^-, basic	0.08	–	0.15 (100)
Propranolol	Tl^+, neutral	2.09	9.05	0.93 (146)
Theobromine	I^-, basic	4.70	–	2.00 (150)
Theophylline	I^-, basic	0.84	–	1.30 (159)

[a] Whatman No. 1 filter-paper. [b] Lifetime of first component. [c] Lifetime of second component. [d] Value of chi-squared test. In parentheses, number of points used for calculation.

perimental curve for time interval of at least three lifetimes. The goodness of the fit between experimental and calculated values was calculated by a chi-squared test. Under the conditions examined, most of the drugs exhibited a single lifetime with values ranging between a 0.1 and 4.7 ms. Only propranolol showed a biexponential decay, with two lifetimes, 2.1 and 9.05 ms. The short values of the calculated lifetimes suggest that the heavy atom induced at strong substrate–analyte interaction.

Analytical figures of merit

Table 3 summarizes the analytical figures of merit for five drugs in RTP and LIP under the optimum experimental conditions. The calibration graphs were linear at least up to 100 μg ml^{-1} in both RTP and LIP. The background signal was measured by making ten measurements of the blank and the limits of detection (LOD) were calculated as the concentration of analyte giving rise to a signal equal to twice the standard deviation of the blank signal at the analyte wavelength. The LODs for acebutolol and bendroflumethiazide were about 2–3 times lower in LIP than in RTP. Unfortunately, this observation is not general. The lack of tunability of the nitrogen laser prevents effective excitation of some drugs (acetazolamide and caffeine), which is not compensated for by the high intensity provided by the laser source. As a result, the LODs observed are worse than those obtained with xenon lamp excitation. The LOD for propranolol in LIP was found to be 2.9 ng. This is interesting taking into account that the maximum excitation wavelength of propranolol is 306 nm and the wavelength of the nitrogen laser is about 30 nm longer. Caffeine cannot be analysed by laser-induced RTP as this does not absorb at 337.1 nm.

Conclusions

RTP at solid surfaces is of particular interest because of the simplicity of substrate preparation and the good sensitivity and selectivity. The screening of 27 banned drugs in sport resulted in seven strong and seventeen weak phosphorescing drugs. Optimum experimental conditions for RTP analysis depend on the particular compound being studied. RTP cannot supplant other analytical techniques used for screening for illegal drugs in sport, but some limited analyses with acceptable LODs can be performed for acebutolol, bendroflumethiazide and propranolol. The use of a nitrogen laser as an excitation source for RTP did not result in large enhancements in detectability as most drugs showed only residual excitation at the laser wavelength. The use of a shorter wavelength laser (excimer laser or frequency-doubled dye laser) will provide improved excitation efficiency. However, unless the background phosphorescence from the substrate is decreased, no large improvement in detectability will be achieved.

Financial support for this project (89/0441) was provided by the Fondo de Investigaciones Sanitarias de la Seguridad Social, Madrid.

TABLE 3

Analytical figures of merit for RTP and LIP of banned drugs in sport

Analyte	Substrate [a]	RTP				LIP			
		m [b]	Correlation coefficient	LOD [c] (μg ml^{-1})	LOD [d] (ng)	m [b]	Correlation coefficient	LOD [c] (μg ml^{-1})	LOD [d] (ng)
Acebutolol	W-1 + Pb^{2+}	0.128	0.991	15.57	46.5	0.284	0.996	7.02	21.1
Acetazolamide	W-1 + Pb^{2+}	0.114	0.998	17.40	52.2	0.057	0.993	21.60	64.8
Bendroflume-thiazide	W-1 + Pb^{2+}	0.048	0.999	41.10	123.3	0.171	0.985	11.66	34.9
Caffeine	W-1 + I^-	0.781	0.999	2.23	6.7	–	–	–	–
Propranolol	W-1 + Tl^+	3.154	0.978	0.99	3.0	2.021	0.998	0.98	2.9

[a] W-1 = Whatman No. 1 filter-paper. [b] Analytical sensitivity. m = slope/standard deviation. [c] Relative limit of detection. [d] Absolute limit of detection.

REFERENCES

1 M.M. Andino, C.G. de Lima and J.D. Winefordner, Spectrochim. Acta, Part A, 43 (1987) 427.
2 R.P. Bateh and J.D. Winefordner, J. Pharm. Biomed. Anal., 1 (1983) 113.
3 E.B. Asafu-Adjaye and S.Y. Su, Anal. Chem., 58 (1986) 539.
4 J.J. Vannelli and E.M. Schulman, Anal. Chem., 56 (1984) 1033.
5 V.P. Senthilnathan and R.J. Hurtubise, Anal. Chem., 57 (1985) 1227.
6 A.M. Alak and T. Vo-Dinh, Anal. Chem., 60 (1988) 596.
7 J.M. Bello and R.J. Hurtubise, Anal. Chem., 60 (1988) 1291.
8 L.J. Cline Love, M.L. Grayeski and R. Noroski, Anal. Chim. Acta, 170 (1985) 3.
9 K.J. Harbaugh, C.M. O'Donnell and J.D. Winefordner, Anal. Chem., 46 (1974) 1206.
10 T. Vo-Dinh, Room-Temperature Phosphorimetry for Chemical Analysis, Wiley, New York, 1984.
11 R.J. Hurtubise, Phosphorimetry: Theory, Instrumentation, Applications, Dekker, New York, 1990.
12 R.T. Parker, R.S. Freedlender and R.B. Dunlap, Anal. Chim. Acta, 120 (1980) 1.
13 G.D. Boutilier and J.D. Winefordner, Anal. Chem., 51 (1979) 1384.
14 C.F. Pace and J.R. Maple, Anal. Chem., 61 (1989) 872.
15 R.M. Wilson and T.L. Miller, Anal. Chem., 47 (1975) 256.
16 T. Vo-Dinh, in T. Vo-Dinh and D. Eastwood (Eds.), Laser Techniques in Luminescence Spectroscopy (ASTM 1066), ASTM, Philadelphia, 1990, p. 133.
17 A. Rupérez, L. Ayala and J.J. Laserna, Appl. Spectrosc., 44 (1990) 465.
18 A. Rupérez, L. Ayala and J.J. Laserna, Spectrochim. Acta, Part A, 48 (1992) 569.
19 J.J. Aaron, M. Andino and J.D. Winefordner, Anal. Chim. Acta, 160 (1984) 171.
20 A.D. Campiglia, J.J. Laserna, A. Berthod and J.D. Winefordner, Anal. Chim. Acta, 244 (1991) 215.

Analytica Chimica Acta, 270 (1992) 247–252
Elsevier Science Publishers B.V., Amsterdam

Effect of cavity surface on S_2 emission in molecular emission cavity analysis

Koichi Nakajima and Kyuji Ohta

Faculty of Liberal Arts, Hosei University, 2–17–1 Fujimi, Chiyoda-ku, Tokyo 102 (Japan)

Takeo Takada

Department of Chemistry, College of Science, Rikkyo University, 3–34–1 Nishi-Ikebukuro, Toshima-ku, Tokyo 171 (Japan)

(Received 29th May 1992; revised manuscript received 4th August 1992)

Abstract

Alkali metal salts present in distilled water as impurities change the surface of a silica cavity from smooth to rough and groovy surface. The multi-peaked responses observed with a new cavity change into a single peak when the cavity is treated with alkali metal salts compounds. It is concluded that the effect of the alkali metal salt-treated cavity is mainly attributable to the roughness of the surface; the peak splitting is caused by aggregate formation and the roughness of the cavity surface enhances good dispersion and volatility of samples and suppresses peak splitting.

Keywords: Cavity surface effect; Molecular emission cavity analysis; Sulphur compounds

Molecular emission cavity analysis (MECA) is applicable to the determination of many elements [1–3]. This method has several advantages over flame spectrophotometric techniques based on conventional nebulization [1]. The advantages are derived from use of a cavity for introduction of samples to a flame, because all the processes, including decomposition of samples, formation of emitting species and emission of radiation, occur within the cavity. Therefore, the size, shape and material of the cavity significantly influence the emission profile.

We have been studying S_2 emission with a silica cavity in MECA [4,5]. The typical emission response observed in conventional MECA is a single, sharp peak. When a certain amount of sample is applied, however, complex multi-peaked responses are obtained. The threshold amount to give multi-peaked responses is different for different compounds; some compounds show a single peak with 500 ng of S whereas the others give multi-peaked responses with 50 ng of S. The sensitivity for the compounds with low threshold amounts is poorer than that of the others.

In a previous paper [4], we reported that the addition of acids or the use of a cavity that had been repeatedly used for sulphur determination depresses the peak splitting even with a relatively large amount of sample. Evmiridis and Townshend [6] also observed a similar phenomenon using an aluminium cavity, but the cause of the peak splitting and the effect of the aged cavity remained obscure. It was therefore considered important to study the effect of aged cavities in order to clarify the cause of peak splitting.

Correspondence to: K. Nakajima, Faculty of Liberal Arts, Hosei University, 2–17–1 Fujimi, Chiyoda-ku, Tokyo 102 (Japan).

EXPERIMENTAL

Apparatus

The MECA system used was as described previously [4]. A silica cavity (8 or 5 mm deep, 6 mm diameter) was fixed at the end of a rod held in a sample holder assembly. The cavity was positioned reproducibly in a nitrogen sheath oxy–hydrogen flame in line with a detector by sliding the assembly on an optical bench. The rod was pitched at 8° below the horizontal with the centre of the cavity 20 mm above the top of the burner.

Hydrogen (5.0 l min^{-1}) and oxygen (0.15 l min^{-1}) were supplied to a total consumption burner through the fuel (outer) and nebulizer (inner) inlets, respectively. The burner was modified so that nitrogen (6.0 l min^{-1}) could flow around the oxy–hydrogen flame to prevent air entering the flame from its surrounding [5].

Sample solutions (10 μl) were placed in the cavity using a microsyringe. After the solvent had been evaporated to dryness with a heated air stream using a hot air blower, the cavity was introduced into the flame. The S_2 emission was measured through an interference filter (half band width 18 nm) at 394 nm using a photomultiplier tube (R268, HTV) connected with an amplifier (high-voltage supply; 800 V), and responses were recorded on a Shimadzu Chromatopack C-R3A recorder.

A Shimadzu TGA-30M instrument was used for thermogravimetric analysis of thiourea and 1,3-diethylthiourea. The sample weight loss was measured at a heating rate of 15°C min^{-1} in an atmosphere of nitrogen (40 ml min^{-1}) using a silica cell (2.5 mm deep, 5.5 mm diameter).

X-ray microprobe analysis was performed with a Jeol JCMA-733 instrument.

Reagents

All water used was distilled or ion-exchanged. Distilled water was prepared by distillation in two stages, first from a copper vessel and then from a silica vessel. Ion-exchanged water was prepared with an AS-90DF automatic still (Iwaki Glass) with dual ion exchangers, a carbon filter and a 0.2-μm membrane filter. All reagents were of guaranteed grade or analytical-reagent grade and used as received. Sample solutions were prepared in water unless stated otherwise. The ethanol used was 99.5% (v/v).

RESULTS AND DISCUSSION

Several emission profiles are shown in Fig. 1. Thiourea shows single peaks up to 500 ng of S, whereas 1,3-diethylthiourea and methionine give multi-peaked responses with smaller amounts (ca. 50 ng of S). As shown in Fig. 1, the peak splitting seems to be caused by portions of sample being volatilized or decomposed at intervals after introduction into the flame. Although it is not clear whether volatilization and/or decomposition of samples occur by a simple thermal process or in contact with flame gases, as a conventional cup cavity was used, it was thought that volatilization and/or decomposition of the samples which were deposited on a corner of the cavity would be delayed with either process. In order to examine the effect of the location of the samples and the shape of the cavity, a short silica tube (10 mm × 6 mm i.d., thickness 2 mm) was tested as a cavity.

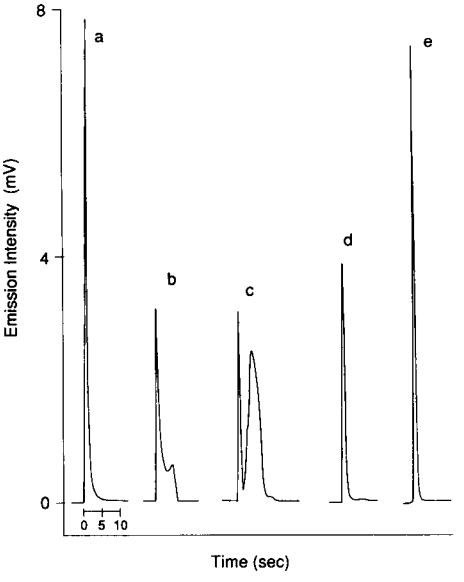

Fig. 1. Emission–time profiles for (a) thiourea (100 ng S), (b) 1,3-diethylthiourea (100 ng S), (c) methionine (250 ng S) with a new silica cavity, (d) 1,3-diethylthiourea and (e) methionine with an alkali cavity.

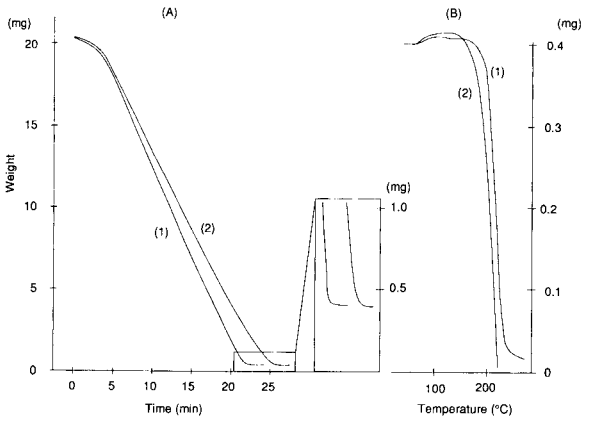

Fig. 2. (A) Weight loss for aqueous solutions of (1) thiourea and (2) 1,3-diethylthiourea owing to evaporation of water at 65°C. (B) Weight loss of the residues by thermogravimetry.

The samples were placed on the centre of the inside of the tube and the S_2 emissions were measured. The results were same as those from a cup cavity, i.e., 1,3-diethylthiourea gave a multi-peaked response and thiourea showed a single peak. Therefore, the location of sample in the cavity and the shape of the cavity are not responsible for the peak splitting.

As general practice in MECA, solvent water is removed before the cavity is introduced into the flame because the presence of water gives rise to multi-peaked responses [1]. As mentioned above, a hot air blower was used for the evaporation of the solvent, and it was examined whether the sample could be dried completely with the blower as follows. A 20-μl volume of a 2% aqueous solution of thiourea or 1,3-diethylthiourea was injected into the cell of the thermobalance and the weight loss was recorded with isothermal heating at 65°C in a stream of nitrogen. Although the amount of sample was much larger than that normally used in MECA, it was limited by the sensitivity of the thermobalance. The temperature of the hot air stream from the blower was applied to the measurement in the thermobalance. As shown in Fig. 2A, the weights of either solution decreased linearly and attained 0.4 mg, which corresponded to the dry weight of the sample, although the evaporation rates were different. After the solvent had been evaporated, the decrease in the weight of the residue was measured successively with increasing furnace temperature in order to confirm that the residue contains no water (Fig. 2B). The initial increase

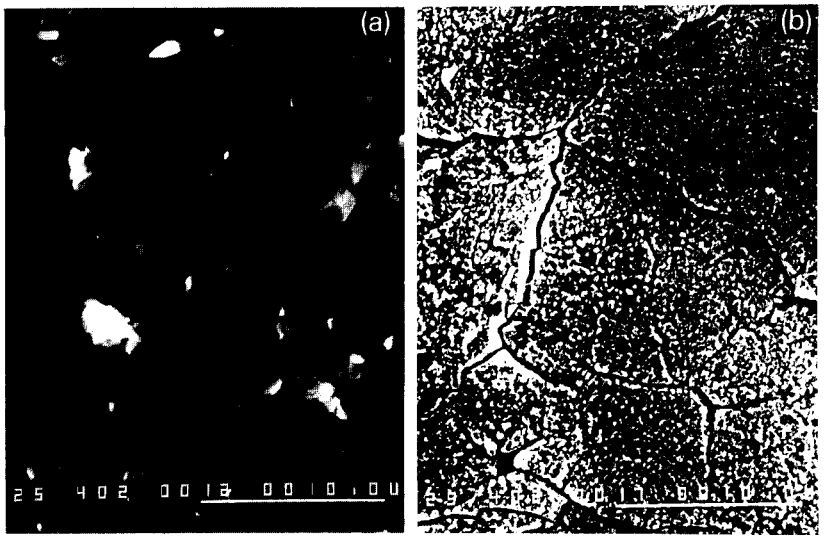

Fig. 3. SEM images of (A) an unused cavity and (B) an aged cavity. The scale bar corresponds to 10 μm. The small white pieces in the image of the unused cavity are small silica fragments that were formed when the cavity was prepared as a specimen for the x-ray microprobe analyser.

in weight is an apparent weight change owing to the changes in buoyancy [7]. The profile of the thermogravimetric curves did not show any signs of the presence of water on the residue. This evidence strongly supports the conclusion that samples in the cavity are sufficiently dried with the general drying procedure. It was consequently concluded that water is not responsible for the multi-peaked responses considered here.

It was reported previously [5] that a transparent silica cavity became frosted with prolonged use and multi-peaked responses obtained with a new cavity became single peaks on using the aged cavity. In order to clarify the cause of the change in the cavity, the surface of an aged cavity was characterized using an x-ray microprobe analyser. Electron probe microanalysis (EPMA) revealed that potassium, chlorine and sulphur had deposited on the surface, and a scanning electron micrograph (Fig. 3) showed the roughness of the surface with small cracks. As no potassium salts were used as the samples, it is most likely that the potassium was derived from the distilled water that was used to prepare the sample solutions. The distilled water would be expected to contain much more sodium than potassium. As EPMA has a low sensitivity for elements of low atomic number [8], sodium would escape detection. The effect of alkali metal chlorides on the response of S_2 emission was therefore investigated, and the following results were obtained.

When a new cavity containing a large amount of alkali metal chlorides (20 μl of 1 mol l^{-1} solution) was heated for a while in a flame of high oxygen content, the inner surface became frosted with small cracks, like the aged cavity, and the emission response obtained from the cavity showed higher and narrower peaks and no peak splitting (Fig. 1). The same results were obtained with other alkali metal compounds such as hydroxides, sulphates and sulphites. Without the cavity treatment at high temperature, the response from 1,3-diethylthiourea and methionine still showed split peaks, although the response from methionine increased slightly. These results suggest that alkali metal oxides penetrated into the silica crystal lattice at high temperature, and the surface of the cavity became rough and

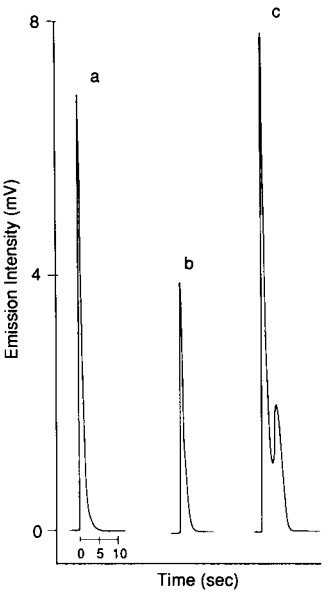

Fig. 4. Emission–time profiles with a ground cavity for (a) thiourea (100 ng S), (b) 1,3-diethylthiourea (100 ng S) and (c) methionine (250 ng S).

frosted as a result. This cavity is hereafter called an "alkali cavity".

As free alkali metal chlorides have no effect on the peak splitting, it is suggested that the roughness of the surface, rather than the chemical properties of the surface, is responsible for the enhancement of the aged cavity. Therefore, a cavity with a rough inner surface was prepared by grinding it roughly with abrasives (termed a "ground" cavity), and examined the effect on the emission responses. The profiles are shown in Fig. 4. 1,3-Diethylthiourea showed a single peak with the ground cavity, similar to that with the alkali cavity. It is clear that the roughness of the cavity surface enhances volatilization and/or decomposition of the samples. The response from methionine still remained split, which suggests that the origin of the splitting is different from that of 1,3-diethylthiourea.

When water evaporation and crystal deposition processes were observed on a glass slide under a microscope, difference in these processes was found between thiourea solution and 1,3-diethylthiourea solution. Volumes of 10 μl of solutions were dropped on a glass slide and were

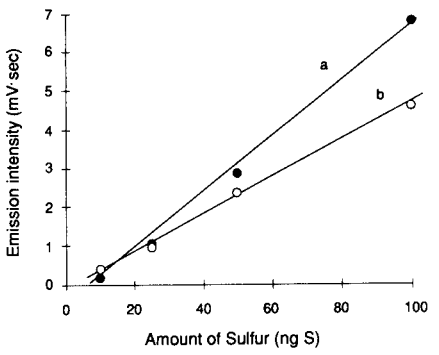

Fig. 5. Calibration graphs for (a) thiourea and (b) 1,3-diethylthiourea.

heated with a hot air blower according to general practice for drying. During evaporation of solvent water, the thiourea solution deposited crystals only on the edge of the solution while reducing the area of the solution droplet, and finally the crystals were deposited dispersedly. In contrast, 1,3-diethylthiourea solution did not deposit any crystals while reducing the area of the solution droplet until the solution became very concentrated, and finally the crystals formed with aggregation. These results suggest that the peak splitting is related to the degree of dispersion of the sample in the cavity; samples formed with aggregation do not volatilize or decompose all at once.

These results were well supported by the evidence that 1,3-diethylthiourea dissolved in ethanol showed a single peak response even with a new cavity. An ethanol solution has a lower surface tension than an aqueous solution, and the sample extensively disperses in the cavity. No difference was found in the emission responses between the ethanol and the aqueous solutions with a ground cavity.

Figure 5 shows the relationship between emission intensity (peak area) and amount of sulphur with a ground cavity. There is a slight difference in the emission intensities between thiourea and its derivative, but both showed good linearity.

Conclusion

The change in the cavity is therefore caused by alkali metal chlorides contained as impurities in the distilled water. These alkali metal chlorides penetrate into the silica quartz lattice and make the inner surface of the cavity rough. The roughness of the surface leads to good dispersion of the sample and suppresses the peak splitting, which results in an increase in the peak height and good linearity of the relationship between the intensity and the amount of sulphur.

Although methionine showed a single peak response with an alkali cavity, the use of this cavity offered several disadvantages. The conditions of the treatment with alkali metal chlorides require strict optimization; treatment with a small amount of alkali metal chlorides (20 μl of a 1 mmol l^{-1} solution) enhances the emission intensity from methionine but the peak is still split; for a large amount of the compounds (20 μl of a 1 mol l^{-1} solution) the second peak disappears but the first peak is not increased, and repetition of the treatment decreases the intensity of the remaining peak. These results show that treatment with a large amount of alkali metal chloride suppresses not only peak splitting but also the emission intensity. In addition, the cavity cannot be used so many times, because it is fragile owing to the cracks formed by the alkali metal salt treatment. It is difficult to judge whether or not the drying of the solvent in the cavity was completed, by visual observation, owing to the opacity of the cavity.

In contrast, the ground cavity provides easy visual observation of the drying of the solvent with a faster evaporation rate (twice that in a new cavity). Further, the emission intensity is higher than that with an alkali cavity. From these results, the ground cavity is recommended to use in MECA, although the response from methionine splits.

As the emission responses are also affected by the addition of acids, it would be of interest to relate the chemical effect on the surface to the effect of acids. Work is in progress to clarify the cause of multi-peaked responses with amino acids.

The authors thank Dr. Y. Tegawa and his co-workers (Nippon Mining) for the analyses of cavities with an x-ray microprobe analyser.

REFERENCES

1 M. Burguera, S.L. Bogdanski and A. Townshend, CRC Crit. Rev. Anal. Chem., 10 (1980) 185.
2 A.C. Calokerinos and A. Townshend, Prog. Anal. At. Spectrosc., 5 (1982) 63.
3 K. Dittrich, CRC Crit. Rev. Anal. Chem., 16 (1986) 223.
4 K. Nakajima and T. Takada, Anal. Chim. Acta, 199 (1987) 147.
5 K. Nakajima and T. Takada, Anal. Chim. Acta, 235 (1990) 413.
6 N.P. Evmiridis and A. Townshend, J. Anal. At. Spectrom., 2 (1987) 339.
7 T. Ozawa, J. Chem. Soc. Jpn., 87 (1966) 54.
8 D.M. Hercules, Anal. Chem., 42 (1970) 20A.

Analytica Chimica Acta, 270 (1992) 253–265
Elsevier Science Publishers B.V., Amsterdam

Evaluation and elimination of the "blank bias error" using the H-point standard addition method

Application to spectrophotometric determinations using absorbent blank

Pilar Campíns-Falcó, Francisco Bosch-Reig and Jorge Verdú-Andrés

Departamento de Química Analítica, Facultad de Química, Universidad de Valencia, c / Dr. Moliner 50, 46100-Burjassot, Valencia (Spain)

(Received 1st June 1992)

Abstract

The basis of the H-point standard addition method in the cases where the analyte determination requires the use of an absorbent reagent is considered. The method evaluates and eliminates the blank bias error present in such procedures by using the absorbance increment at two selected wavelengths as the analytical signal of the calibration graphs. Three different determinations were tested: the determination of proteins with the biuret method, thorium with thoron and of magnesium with Titan Yellow. These procedures are better described by the proposed method than by the traditional approach using absorbance values against reagent blank.

Keywords: UV–Visible spectrophotometry; Blank bias error; H-point method; Standard addition method

The reagent blank, chemical blank or analytical blank is the response obtained from an analyte-free sample solution. The blank is considered as an integral part of a measurement technique, and its response is physically cancelled or algebraically subtracted from the standard and sample responses.

In spectrophotometry, when the product formed and one of the reagents absorb at the same wavelength, the blank absorbance at the end of the reaction can be lower than that measured at the beginning, because of the reagent consumption. Therefore, the real absorbance of the formed product will be larger than the measured value. If we consider a calibration line, this difference will be greater the higher are the concentrations assayed, and it will affect the accuracy of the analytical results obtained.

This aspect appears to have received little attention. Zhou [1] studied the effect of excess reagents on spectrophotometric determinations. He deduced that if the blank absorbs near the absorbance maximum of the product formed, the molar absorptivities are modified, and the calibration line is distorted. All this causes the analytical results to be affected by systematic errors. Kroll and Ellin [2] proposed a blank correction factor (BCF) for such cases.

We previously suggested a modification of the standard addition method, called the H-point standard addition method (HPSAM) [3,4], where the in-corrigible error resulting from the presence of a direct interferent in the determination of an analyte is converted into a systematic constant error that can be evaluated and permits the determination of the analyte concentration free from

Correspondence to: P. Campíns-Falcó, Departamento de Química Analítica, Facultad de Química, Universidad de Valencia, c/Dr. Moliner 50, 46100-Burjassot, Valencia (Spain).

bias error. The basis of the method was established [3,4] and it was applied to the determination of two species with extensively or even coincident overlapping spectra [5]. It has also been applied to kinetic data, with time as an additional variable [6]. In cases in which only the analyte concentration was required, a variant of the method was developed in which the absorbance increment (ΔA) is used as the analytical signal [7]. This variant can be adapted to the calibration method with a unique standard. In addition, the method has been adapted to liquid chromatography [8].

The objective of this paper is to demonstrate the utility of this method in all instances where the analyte determination requires the use of an absorbent reagent.

THEORETICAL BASIS

The HPSAM applied to static procedures and spectrophotometric data allows the determination of two species, X and Y, in a mixture of two compounds, or only the analyte concentration free from bias error, when the spectrum of the sample matrix is known. The determination of the concentration of X by the HPSAM under these conditions entails selecting two wavelengths, λ_1 and λ_2, lying on both sides of the absorption maximum of Y in such a way that the absorbances of the latter component are the same at both wavelengths. Then, known amounts of X are successively added to the mixture, and the resulting absorbances are measured at the two aforesaid wavelengths.

The two straight lines obtained intersect at the so-called H-point ($-C_H$, A_H), where $-C_H = -C_X$ is the unknown concentration of X and $A_H = A_Y$ is the analytical signal of Y in the former instance, and represents the constant bias error of the sample in the latter [3–8].

As a calibration line can be considered as a standard addition line with an added sample portion equal to zero, the basis of the HPSAM is extendable to the calibration lines in determinations with absorbing blanks. The first point of the standard addition corresponds to the analytical signal of the solution that contains the blank. The theoretical basis in this case is as follows.

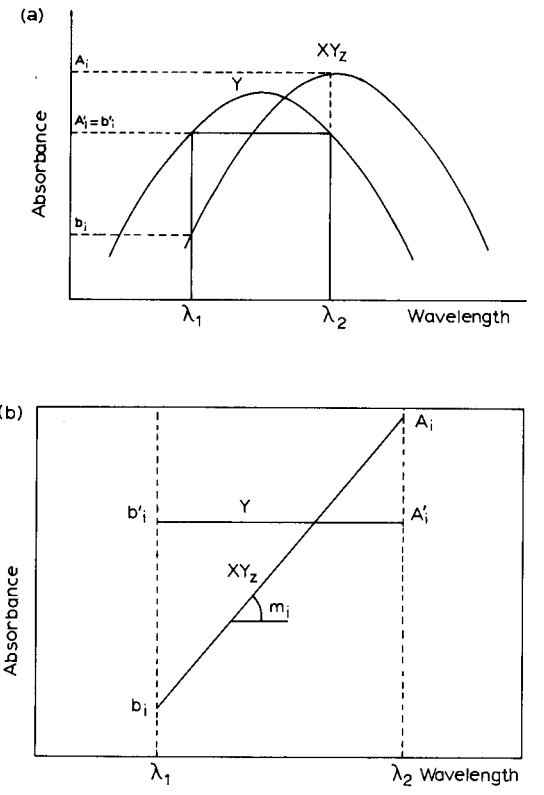

Fig. 1. (a) Absorption spectra of two compounds, Y being the absorbing reagent and XY_z the product formed. (b) Shape of the spectra of the absorbing reagent Y and the product formed XY_z in the wavelength interval λ_1–λ_2.

Consider X as the analyte to be determined and Y as the absorbing reagent used in the determination. The reaction between them is described by

$$X + zY \rightleftharpoons XY_z$$

Two wavelengths, λ_1 and λ_2, are selected, lying on both sides of the absorption maximum of Y in such a way that the absorbances of this component are the same, in accordance with the basis of the HPSAM (Fig. 1a). The absorbance of the species XY_z in the different calibration solutions at λ_1 and λ_2 will be b_i and A_i. The absorbance of the excess reagent Y in the same solutions will be b'_i and λ_1 and A'_i at λ_2, equal for each i solution (Fig. 1b).

Both absorbances, considering only the extreme points λ_1 and λ_2, can be described for each addition by the equations

XY_z: $A_i = b_i + m_i\lambda$

$(\lambda = \lambda_1, \lambda_2; i = 0, 1, \ldots, n)$

Y: $A'_i = b'_i + m\lambda$

$(\lambda = \lambda_1, \lambda_2; m = 0; i = 0, 1, \ldots, n)$

The subscript i denotes the different solutions for n additions of analyte X. When $i = 0$, then $C_{X\ added} = C_{XY_z\ formed} = 0$. b_i and m_i depend on the concentration of X, owing to the formation of XY_z, and b'_i depend of the excess concentration of Y present.

The overall absorbance of the Y–XY_z mixtures at λ_1 and λ_2 are

$$A(\lambda_1) = b'_i + b_i \quad (1)$$

$$A(\lambda_2) = A'_i + A_i \quad (2)$$

On the other hand, application of HPSAM at the two aforesaid wavelengths will yield

$$A(\lambda_1) = b'_i + b_0 + M(\lambda_1)C_i \quad (3)$$

$$A(\lambda_2) = A'_i + A_0 + M(\lambda_2)C_i \quad (4)$$

where C_i is the analyte concentration added, b_0 and A_0 are the absorbance values of the product formed at λ_1 and λ_2, measured when $i = 0$ (when the analyte added concentration is zero, and therefore, $C_X = C_{XY_z} = 0$), and $M(\lambda_1)$ and $M(\lambda_2)$ are the slopes of the straight lines obtained on applying the HPSAM at λ_1 and λ_2, respectively. Both straight lines intersect at the H-point $(-C_H, A_H) = (-C_{XY_z}, A_Y)$ (Fig. 2).

At the common point:

$$b'_i + b_0 + M(\lambda_1)(-C_H) = A'_i + A_0 + M(\lambda_2)(-C_H) \quad (5)$$

Hence

$$-C_H = \frac{(A'_i - b'_i) + (A_0 - b_0)}{M(\lambda_1) - M(\lambda_2)} \quad (6)$$

As the Y species show the same absorbance values at λ_1 and λ_2, then $A'_i = b'_i$, at each i. Moreover, the X species, for $i = 0$, is not present, and for this reason nor is the species XY_z. For all of this, $b_0 = A_0 = 0$. Hence,

$$-C_H = \frac{0}{M(\lambda_1) - M(\lambda_2)} = 0 \quad (7)$$

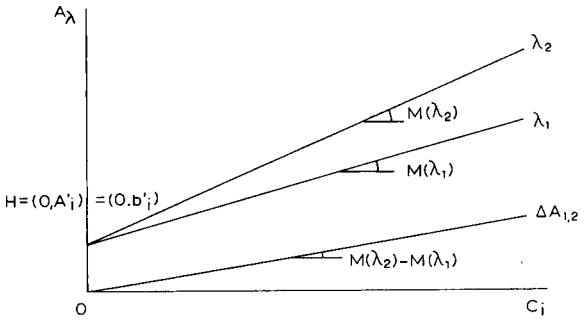

Fig. 2. Plot of the H-point standard addition method, using A_{λ_1}, A_{λ_2} and $\Delta A_{1,2}$ as the analytical signal.

The use of ΔA as the analytical signal, from Eqns. 3 and 4, and considering that $A_0 = b_0$ for $i = 0$, yields

$$A_2 - A_1 = \Delta A_{1,2} = A'_i - b'_i + [M(\lambda_2) - M(\lambda_1)]C_i \quad (8)$$

For every i, $b'_i = A'_i$, and therefore

$$\Delta A_{1,2} = [M(\lambda_2) - M(\lambda_1)]C_i$$

This expression shows that the absorbance increments depend exclusively on the analyte concentration. Plotting $\Delta A_{1,2}$ vs. C_i leads to a straight line with zero intercept and a slope of $M(\lambda_2) - M(\lambda_1)$ (Fig. 2). The excess of free absorbing reagent does not affect the straight line, because for each point its contribution is cancelled, although its absorbance values were different in each solution. The blank bias error can be considered as a variable and proportional interference, and the method can eliminate it because the absorbance increment is not dependent on the free absorbent reagent.

EXPERIMENTAL AND RESULTS

Examples

Three determinations using an absorbent blank were chosen, with different conditions: determi-

nation of proteins with the biuret method [9], of thorium with thoron [10] and of magnesium with Titan Yellow [11].

In the first case, the excess of reagent is sufficient to obtain results with no error from the calibration line, using a reagent blank. It will be demonstrated that the method leads to similar results to those when the usual procedure is followed.

The second case can be representative of all determinations of metal ions using a coloured organic compound as a complex former that reacts with the metal ion to form chelate complexes affected by the studied error.

In the third case, the studied reaction is the formation of a strongly coloured lake by adsorption of dye by the previously formed hydroxide in alkali metal hydroxide solution.

Apparatus and reagents

A Shimadzu UV-240 spectrophotometer and the OPI-2 data point program, which prints out absorbances values at selected wavelengths, were used.

Bovine serum albumin, fraction V, was obtained from Fluka. Biuret reagent was prepared by mixing 8.65 g of copper(II) sulphate ($CuSO_4 \cdot 5H_2O$) (Probus), 86.5 g of sodium citrate ($Na_3C_6H_5O_7 \cdot 2H_2O$) (Panreac) and 50 g of anhydrous sodium carbonate (Na_2CO_3) (Panreac) in 500 ml of water. Thorium(IV) stock solution was prepared from thorium(IV) nitrate [$Th(NO_3)_4 \cdot 4H_2O$] (Merck). Thoron was obtained from BDH. Mg^{2+} stock solution was prepared from magnesium nitrate [$Mg(NO_3)_2 \cdot 6H_2O$] (Probus). Titan Yellow was obtained from Riedel-de Haën. Poly(vinyl alcohol) (Probus) was used as a surfactant.

Determination of proteins with the biuret method

For the determination of proteins the experimental conditions established by Henry et al. [9] were used. The NaOH concentration was 0.625 M in all experiments.

The biuret reagent, under the experimental conditions used, shows a broad spectrum with a maximum at 670 nm (Fig. 3a). The blank is present at a concentration up to 200 times higher than the maximum albumin concentration assayed (0.070–0.42%, w/v).

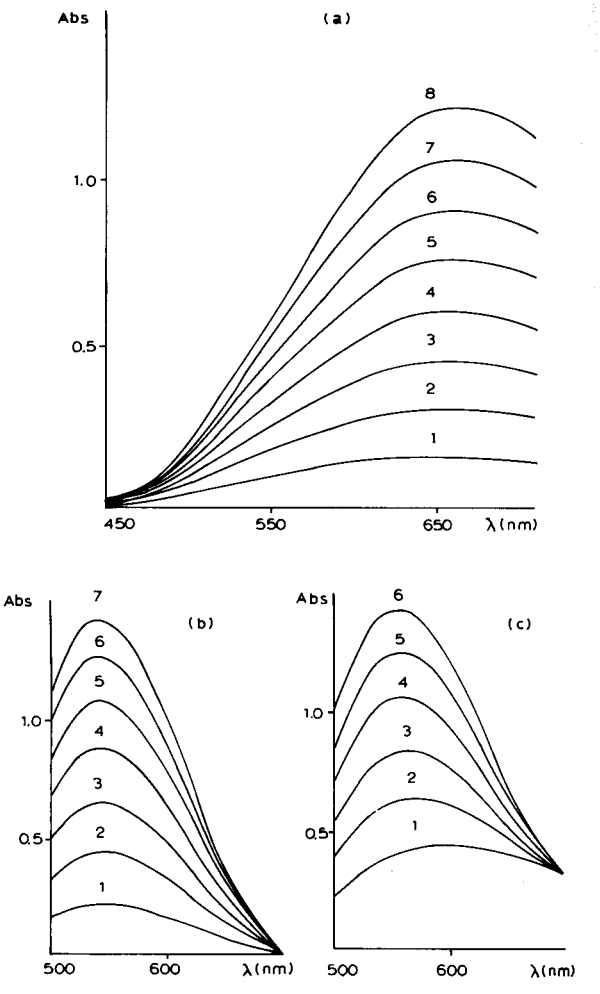

Fig. 3. (a) Absorption spectra for biuret reagent in 0.625 M NaOH for the following concentrations of Cu^{2+}: 1 = 4.93×10^{-3}; 2 = 9.87×10^{-3}; 3 = 1.48×10^{-2}; 4 = 1.97×10^{-2}; 5 = 2.47×10^{-2}; 6 = 2.96×10^{-2}; 7 = 3.45×10^{-2}; 8 = 3.95×10^{-2} M. (b) Spectra for solutions of biuret reagent containing 1.97×10^{-2} M Cu^{2+} and the following concentrations of albumin, measured against the reagent blank: 1 = 0.07; 2 = 0.14; 3 = 0.21; 4 = 0.28; 5 = 0.35%; 6 = 0.42; 7 = 0.49%. (c) Spectra for the solutions in (b), measured against a water blank.

The spectra of the different solutions prepared to obtain the calibration line by using a reagent blank and water blank are shown in Fig. 3b and c, respectively. The spectra against a water blank show a hypsochromic shift of the absorption maximum, in agreement with the overlapping of the

TABLE 1

Results obtained for the calibration lines in the determination of albumin with biuret reagent

Parameter	Replicate	λ measured (nm)			
		545 (r.b.) [a]	ΔA (700 − 636)	ΔA (690 − 644)	ΔA (679 − 653)
No. of	1	6	7	7	7
points	2	6	7	7	7
a	1	−0.00 ± 0.04	0.003 ± 0.009	0.002 ± 0.007	0.001 ± 0.005
	2	0.00 ± 0.03	0.003 ± 0.007	0.002 ± 0.007	0.002 ± 0.004
b	1	2.99 ± 0.13	1.15 ± 0.03	0.84 ± 0.03	0.482 ± 0.018
	2	2.94 ± 0.11	1.14 ± 0.03	0.83 ± 0.03	0.474 ± 0.017
r	1	0.99940	0.99964	0.99953	0.99937
	2	0.99958	0.99976	0.99959	0.99944
Detection	1	0.019	0.014	0.016	0.018
limit (%)	2	0.016	0.011	0.015	0.017
s_{yx}	1	0.015	0.005	0.004	0.003
	2	0.012	0.004	0.004	0.003

Parameter	Replicate	λ measured (nm)					
		700	636	690	644	679	653
No. of	1	6	6	6	6	6	6
points	2	6	6	6	6	6	6
a	1	0.348 ± 0.013	0.353 ± 0.025	0.355 ± 0.014	0.358 ± 0.025	0.359 ± 0.016	0.361 ± 0.023
	2	0.354 ± 0.011	0.359 ± 0.020	0.360 ± 0.011	0.363 ± 0.021	0.364 ± 0.014	0.368 ± 0.020
b	1	−0.01 ± 0.05	1.14 ± 0.09	0.10 ± 0.05	0.93 ± 0.09	0.24 ± 0.06	0.72 ± 0.09
	2	0.01 ± 0.04	1.14 ± 0.07	0.11 ± 0.04	0.93 ± 0.08	0.26 ± 0.05	0.72 ± 0.07
r	1	−0.18407	0.99801	0.92319	0.99718	0.98241	0.99574
	2	0.26093	0.99878	0.96020	0.99796	0.98780	0.99699

[a] Absorbance values against reagent blank.

TABLE 2

Results obtained for Bartlett and ANOVA tests for all of the pairs of lines studied in the determination of albumin with biuret reagent

Parameter	λ measured (nm)					
	700	636	690	644	679	653
No. of points	8	8	8	8	8	8
a	0.002 ± 0.009	0.002 ± 0.006	0.000 ± 0.009	−0.000 ± 0.007	−0.000 ± 0.009	−0.001 ± 0.007
b	29.4 ± 0.4	29.37 ± 0.25	30.0 ± 0.4	30.0 ± 0.3	30.4 ± 0.4	30.4 ± 0.3
r	0.99991	0.99996	0.99992	0.99996	0.99993	0.99995
Bartlett test:						
χ^2_{calc} [χ^2_{tab} ($P = 0.95$, $\nu = 1$) = 3.84]	0.98		0.48		0.20	
ANOVA test:						
F_{calc} [F_{tab} ($P = 0.95$, $\nu_1 = 2$, $\nu_2 = 12$) = 3.89]	0.004		0.17		0.002	

absorption maxima of the product formed (545 nm) and the free reagent in excess (670 nm).

The results obtained for the calibration line against the reagent blank for the two replicates assayed are shown in Table 1, where good linearity can be observed. The intercept is zero in this instance owing to the low variation of the analyte/reagent concentration ratio in the concentration range assayed, as has been mentioned before.

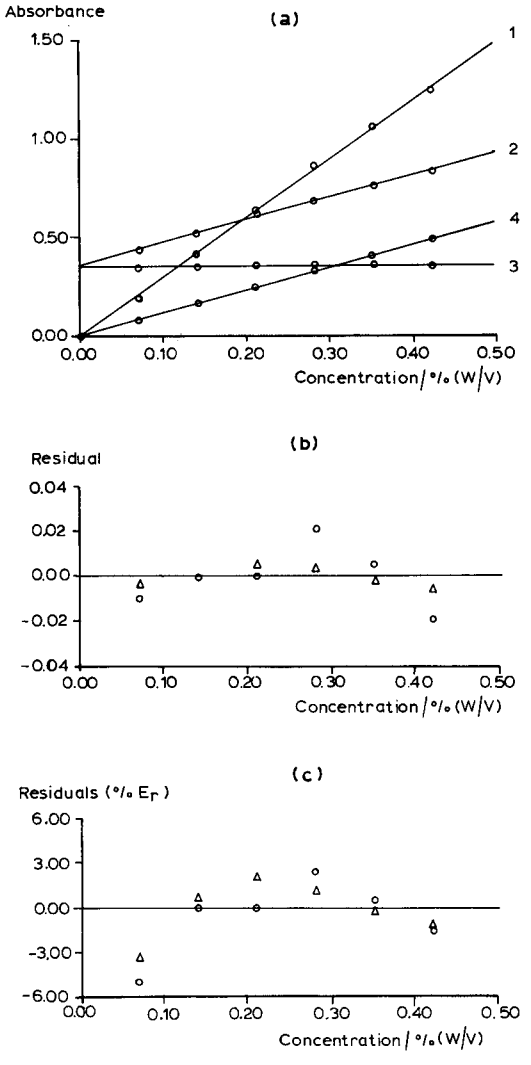

Fig. 4. (a) H-point standard addition method applied to the determination of albumin with biuret reagent: 1, using absorbance at 545 nm against reagent blank as the analytical signal; 2, using absorbance at 636 nm against water blank as the analytical signal; 3, using absorbance at 700 nm against water blank as the analytical signal; 4, using ΔA between 700 and 636 nm against water blank as the analytical signal. (b) Plot of residuals (absolute values) vs. concentration of albumin. ○ = 545 nm using reagent blank; △ = using ΔA (700–636 nm). (c) Plot of residuals (relative values) vs. concentration of albumin. Symbols as in (b).

In order to apply the method, and in agreement with the theoretical basis, two reagent wavelengths with the same absorbance were chosen. Three pairs were studied: 700/636, 690/644 and 679/653 nm. Table 2 gives the results obtained for the Bartlett and ANOVA tests for all the pairs studied, showing that the lines obtained for the reagent blank solutions tested are statistically identical. The absorbances were measured in biuret solutions, without analyte, against a water blank.

The results obtained for the calibration lines of albumin against a water blank are given in Table 1, using ΔA as the analytical signal. The low regression coefficients for the line at 700 nm can be explained because the slope of these lines is almost zero. At these wavelengths, the product formed and the reagent have the same absorbance, which is why the slope is almost zero.

From Table 1 it can be inferred that the traditional calibration method with a reagent blank is accurate enough to obtain good results. However, the use of ΔA as the analytical signal leads to similar detection limits at all of the studied wavelengths, except that the slopes are lower. Detection limits were obtained as explained in the Appendix.

Figure 4 shows the calibration lines obtained at 545 nm against a reagent blank and at 700–636 nm against a water blank, using ΔA as the analytical signal. The residuals vs. added analyte concentration are shown too, in absolute and relative values. In both cases, the lines obtained are similar, because the two models properly describe the experimental data.

Determination of thorium with thoron

The determination was carried out using the experimental conditions according to Sandell [10]. The HCl concentration was 0.5 M in all experiments.

Thoron, in a strongly acidic medium, shows the absorption spectrum in Fig. 5, with the maximum at 477 nm. In the experiments, the thoron concentration was constant at 1.50×10^{-4} M and the thorium concentration was in the range 8.05×10^{-6}–4.02×10^{-5} M.

The results obtained for the calibration line against a reagent blank are shown in Table 3, where it can be seen that the intercept is not zero, as in the determination of albumin with biuret, but positive. This is because the analyte/reagent concentration ratio (about 0.25 for the higher concentration assayed) is higher in this instance, and at those points where higher concentrations of analyte are registered the reagent blank subtracts from the solution an amount that is higher than the real reagent concentration, as mentioned under Theoretical Basis. This leads to a distorted calibration line, with a higher inter-

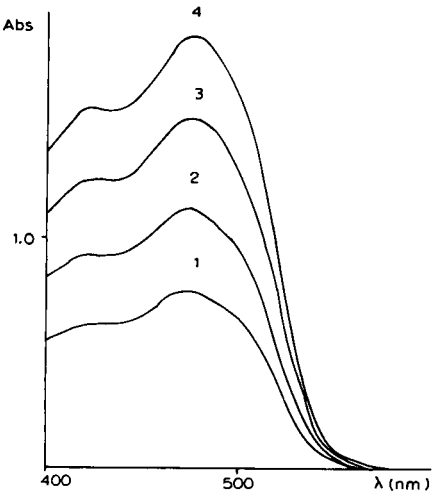

Fig. 5. Absorption spectra for thoron in 0.5 M HCl for the following concentrations: $1 = 7.5 \times 10^{-5}$; $2 = 11.3 \times 10^{-5}$; $3 = 15.0 \times 10^{-5}$; $4 = 18.8 \times 10^{-5}$ M.

TABLE 3

Results obtained for the calibration lines in the determination of thorium with thoron

Parameter	Replicate	λ measured (nm)		
		545 (r.b.) [a]	ΔA (487 − 466)	ΔA (495 − 457)
No. of	1	5	6	6
points	2	5	6	6
a	1	0.02 ± 0.03	0.000 ± 0.005	0.001 ± 0.004
	2	0.02 ± 0.03	0.003 ± 0.005	−0.000 ± 0.004
b	1	0.060 ± 0.005	$(2.29 \pm 0.09) \times 10^{-2}$	$(3.55 \pm 0.06) \times 10^{-2}$
	2	0.059 ± 0.005	$(2.23 \pm 0.09) \times 10^{-2}$	$(3.55 \pm 0.07) \times 10^{-2}$
r	1	0.99893	0.99961	0.99992
	2	0.99873	0.99955	0.99989
Detection	1	0.7	0.4	0.17
limit (mg l^{-1})	2	0.7	0.4	0.20
s_{yx}	1	0.010	0.025	0.0018
	2	0.010	0.003	0.0021

Parameter	Replicate	λ measured (nm)			
		487	466	495	457
No. of	1	5	5	5	5
points	2	5	5	5	5
a	1	1.43 ± 0.03	1.43 ± 0.04	1.343 ± 0.025	1.34 ± 0.03
	2	1.339 ± 0.015	1.333 ± 0.020	1.254 ± 0.015	1.255 ± 0.019
b	1	$(-2 \pm 5) \times 10^{-3}$	−0.025 ± 0.006	0.009 ± 0.004	$(-2.6 \pm 0.5) \times 10^{-2}$
	2	$(-2.0 \pm 2.5) \times 10^{-3}$	−0.024 ± 0.003	0.0102 ± 0.0025	$(-2.5 \pm 0.3) \times 10^{-2}$
r	1	−0.63167	−0.98975	0.96191	−0.99298
	2	−0.78474	−0.99648	0.98853	−0.99706

[a] Absorbance values against reagent blank.

cept and lower slope and regression coefficient. In Fig. 6 the calibration line against reagent blank is plotted, and the plot of residuals vs. thorium concentration added in absolute and relative values for each experimental point. The extreme points have the highest deviation (the highest error), as the theoretical basis predicted.

For the study of the proposed method, two wavelengths where the reagent has the same absorbance were chosen; two pairs were selected: 495/457 and 487/466 nm. The results of the Bartlett and ANOVA tests applied to those pairs of wavelengths are given in Table 4. In both instances, the lines were identical for the blank solutions.

The results obtained for the calibration lines using ΔA as the analytical signal are given in Table 3. All of the lines using ΔA have an intercept of zero and the slope is equal for the two replicates assayed. In Fig. 6 are plotted the calibration line and the residual plots obtained for the wavelengths 495/457 nm. The experimental points are better described by this model than by the calibration against reagent blank.

From Table 3, it can be seen that the proposed method is better than the traditional method, because of its lower detection limit and the fact that it does not introduce any error in the intercept value.

Determination of magnesium with Titan Yellow

The determination was made by following the method of Kenyon and Oplinger [11]. The NaOH concentration was 0.8 M in all instances. Titan Yellow, in alkaline medium, shows the spectrum given in Fig. 7, with a maximum at 499 nm. For the experiments, the range of Mg^{2+} concentration was 3.804×10^{-5}–1.902×10^{-4} M and the concentrations of Titan Yellow were 3.452×10^{-5} and 4.597×10^{-5} M. Two different concentrations of Titan Yellow were studied as we wanted to verify experimentally that the results obtained using ΔA were related only to the analyte concentration, and not to the reagent concentration.

The results obtained for the calibration line against reagent blank, measured at 545 nm, are given in Table 5. The slopes for both lines are similar; on the other hand, the reagent concen-

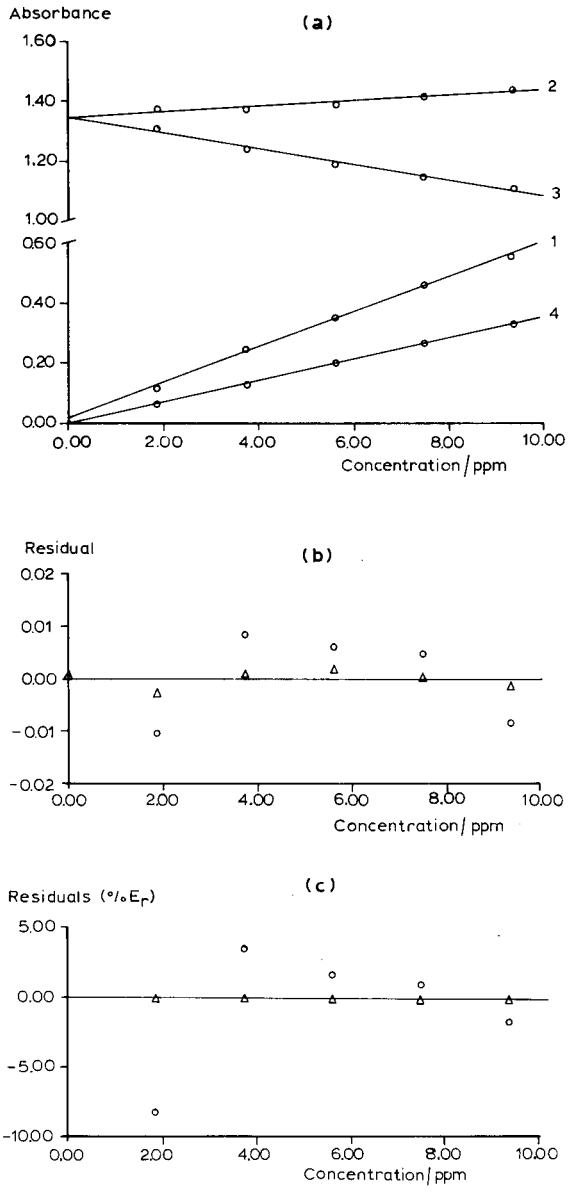

Fig. 6. (a) H-point standard addition method applied to the determination of thorium with thoron: 1, using absorbance at 545 nm against reagent blank as the analytical signal; 2, using absorbance at 495 nm against water blank as the analytical signal; 3, using absorbance at 457 nm against water blank as the analytical signal; 4, using ΔA between 495 and 457 nm against water blank as the analytical signal. (b) Plot of residuals (absolute values) vs. concentration of thorium. ○ = 545 nm using reagent blank; △ = ΔA (495 − 457 nm). (c) Plot of residuals (relative values) vs. concentration of thorium. Symbols as in (b).

TABLE 4

Results obtained for Bartlett and ANOVA tests for all of the pairs of lines studied in the determination of thorium with thoron

Parameter	λ measured (nm)			
	495	457	487	466
No. of points	4	4	4	4
a	0.02 ± 0.04	0.01 ± 0.04	0.02 ± 0.07	0.02 ± 0.06
b	0.091 ± 0.003	0.092 ± 0.003	0.097 ± 0.005	0.097 ± 0.004
r	0.99988	0.99991	0.99983	0.99988
Bartlett test:				
χ^2_{calc} [χ^2_{tab} ($P = 0.95$, $\nu = 1$) = 3.84]	0.028		0.046	
ANOVA test:				
F_{calc} [F_{tab} ($P = 0.95$, $\nu_1 = 2$, $\nu_2 = 4$) = 6.94]	0.10		0.017	

TABLE 5

Results obtained for the calibration lines in the determination of magnesium with Titan Yellow

Parameter	Replicate	λ measured (nm)			
		545 (r.b.) [a]	Δ*A* (523 − 475)	Δ*A* (529 − 470)	
No. of points	1	5	6	6	
	2	5	6	6	
a	1	0.00 ± 0.07	0.002 ± 0.011	−0.003 ± 0.012	
	2	0.01 ± 0.03	0.001 ± 0.008	−0.003 ± 0.011	
b	1	0.101 ± 0.023	0.095 ± 0.004	0.106 ± 0.004	
	2	0.096 ± 0.009	0.094 ± 0.003	0.104 ± 0.004	
r	1	0.99046	0.99942	0.99947	
	2	0.99802	0.99974	0.99958	
Detection limit (mg l^{-1})	1	0.9	0.22	0.21	
	2	0.5	0.15	0.19	
$s_{y/x}$	1	0.024	0.006	0.007	
	2	0.010	0.004	0.006	
Titan Yellow concentration (M)	1	3.452×10^{-5}	3.452×10^{-5}	3.452×10^{-5}	
	2	4.597×10^{-5}	4.597×10^{-5}	4.597×10^{-5}	
Parameter	Replicate	λ measured (nm)			
		523	475	529	470
No. of points	1	5	5	5	5
	2	5	5	5	5
a	1	0.852 ± 0.019	0.849 ± 0.021	0.776 ± 0.021	0.782 ± 0.020
	2	1.47 ± 0.04	1.46 ± 0.03	1.35 ± 0.04	1.35 ± 0.03
b	1	0.074 ± 0.006	−0.020 ± 0.007	0.083 ± 0.007	−0.024 ± 0.007
	2	0.054 ± 0.013	−0.039 ± 0.011	0.064 ± 0.013	−0.041 ± 0.010
r	1	0.99858	−0.97700	0.99868	−0.98580
	2	0.98856	−0.98512	0.99165	−0.98956
Titan Yellow concentration (M)	1	3.452×10^{-5}	3.452×10^{-5}	3.452×10^{-5}	3.452×10^{-5}
	2	4.597×10^{-5}	4.597×10^{-5}	4.597×10^{-5}	4.597×10^{-5}

[a] Absorbance values against reagent blank.

trations are different. However, the calibration graph obtained with the lowest Titan Yellow concentration is less precise, because the last point of the calibration line deviates from linearity by more than 5%. Under these conditions, this point should not be taken into account, and the dynamic range of concentrations is diminished. Owing to all these shortcomings, the application of the method with this reagent concentration to the determination of Mg^{2+} cannot be recommended.

Pairs of wavelengths where the reagent shows the same absorbance were chosen to study the proposed method. Two pairs were chosen, 523/475 and 529/470 nm. The results for the Bartlett and ANOVA tests for both pairs of wavelengths are given in Table 6. χ^2_{calc} and F_{calc} were lower than χ^2_{tab} and F_{tab}, and show that the lines are coincident for all the blank solutions tested.

The results obtained for the calibration lines using ΔA as the analytical signal are given in Table 5. For different reagent concentrations the results obtained are the same because, as has been proposed, ΔA is related only to the analyte concentration and not to the reagent concentration.

In this particular instance, and comparing Table 5, the calibration lines using ΔA show

TABLE 6

Results obtained for Bartlett and ANOVA tests for all of the pairs of lines studied in the determination of magnesium with Titan Yellow

Parameter	Replicate	λ measured (nm)			
		523	475	529	470
No. of points	1	5	5	5	5
a		0.02 ± 0.03	0.04 ± 0.03	0.02 ± 0.05	0.03 ± 0.03
b		$(246 \pm 15) \times 10^2$	$(245 \pm 12) \times 10^2$	$(226 \pm 21) \times 10^2$	$(226 \pm 11) \times 10^2$
r		0.99965	0.99976	0.99914	0.99975
Titan Yellow concentration (M)		3.452×10^{-5}	3.452×10^{-5}	3.452×10^{-5}	3.452×10^{-5}
Bartlett test:					
χ^2_{calc} [χ^2_{tab} ($P = 0.95$, $\nu = 1$) = 3.84]		0.08		0.62	
ANOVA test:					
F_{calc} [F_{tab} ($P = 0.95$, $\nu_1 = 2$, $\nu_2 = 6$) = 5.14]		1.98		3.09	
No. of points	2	5	5	5	5
a		0.03 ± 0.04	0.03 ± 0.05	0.02 ± 0.05	0.02 ± 0.05
b		$(317 \pm 12) \times 10^2$	$(317 \pm 15) \times 10^2$	$(292 \pm 16) \times 10^2$	$(294 \pm 16) \times 10^2$
r		0.99973	0.99956	0.99945	0.99944
Titan Yellow		4.597×10^{-5}	4.597×10^{-5}	4.597×10^{-5}	4.597×10^{-5}
Bartlett test:					
χ^2_{calc} [χ^2_{tab} ($P = 0.95$, $\nu = 1$) = 3.84]		0.19		0.001	
ANOVA test:					
F_{calc} [F_{tab} ($P = 0.95$, $\nu_1 = 2$, $\nu_2 = 6$) = 5.14]		0.001		0.42	

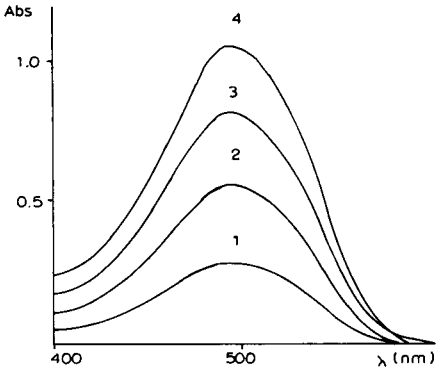

Fig. 7. Absorption spectra for Titan Yellow in 0.5 M NaOH for the following concentrations: $1 = 8.63 \times 10^{-6}$; $2 = 1.72 \times 10^{-5}$; $3 = 2.59 \times 10^{-5}$; $4 = 3.45 \times 10^{-5}$ M.

slopes equal to or greater than those for the calibration lines against reagent blank; they have a lower detection limit, so with the use of these lines more accurate and precise analytical results are obtained.

In Fig. 8 are plotted the calibration lines against reagent blank and using ΔA at 570–529 nm. The residual plots vs. concentration of analyte added are also shown. The proposed method describes the experimental points better.

Conclusions

The basis of the H-point standard addition method for the evaluation and elimination of the blank bias error has been established by using a calibration line for spectrophotometric determinations by means of an absorbent blank. The absorbance increments depend only on the analyte concentration [8], hence plotting $\Delta A_{1,2}$ vs. C_i leads to a straight line with zero intercept and a slope of $M_{\lambda_1} - M_{\lambda_2}$. This line shows no influence of the free reagent, because at each point its absorbance is cancelled, even when its contribution to the absorbance value differs from one solution to other.

It has been demonstrated that the use of ΔA, obtained according to the basis of the method, leads to better results in spectrophotometric determinations by using the absorbent blank than the traditional method, because this kind of situation is better described by the proposed method

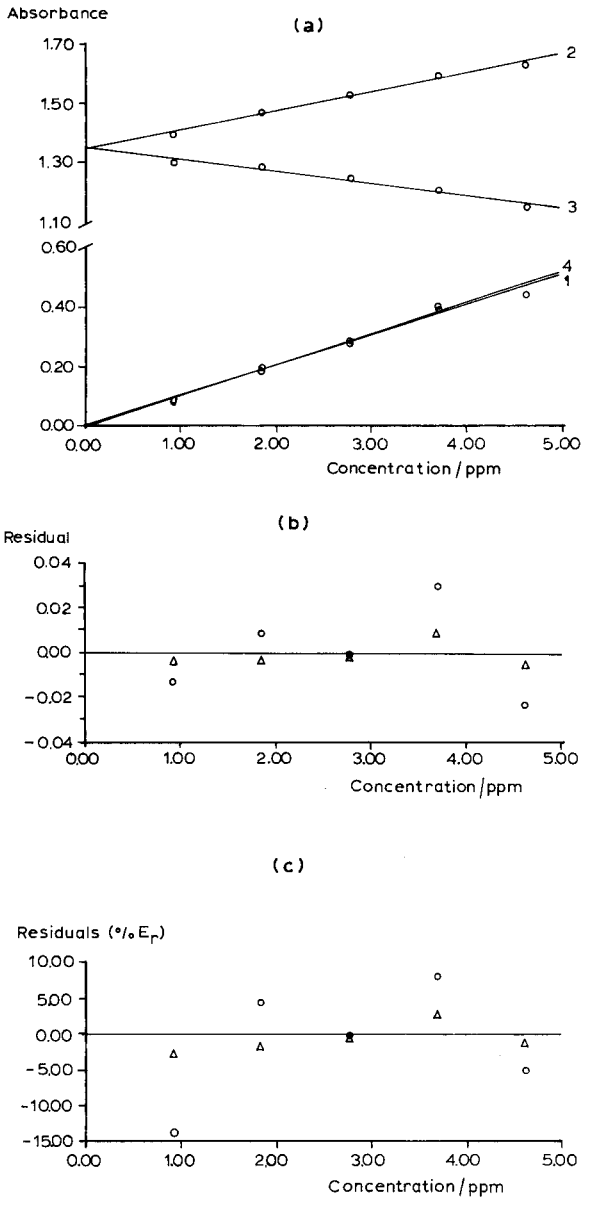

Fig. 8. (a) H-point standard addition method applied to the determination of magnesium with Titan Yellow: 1, using absorbance at 545 nm against reagent blank as the analytical signal; 2, using absorbance at 529 nm against water blank as the analytical signal; 3, using absorbance at 470 nm against water blank as the analytical signal; 4, using ΔA between 529 and 470 nm against water blank as the analytical signal. (b) Plot of residuals (absolute values) vs. concentration of magnesium. O = 545 nm using reagent blank; Δ = ΔA (529 − 470 nm). (c) Plot of residuals (relative values) vs. concentration of magnesium. symbols as in (b).

than by the usual method using absorbance values against reagent blank.

The authors are grateful to the DGICYT for financial support received for the realization of Project PB 88-0495. Jorge Verdú Andrés acknowledges a grant from the Conselleria de Cultura, Educació i Ciència de la Generalitat Valenciana for carrying out PhD studies.

APPENDIX [12,13]

Bartlett test

The statistic used is

$$\chi^2_{cal} = \left(\frac{1}{C}\right)\left(\nu \ln s^2 - \sum_{i=1}^{k} \nu_i \ln s_i^2\right)$$

where

K = number of straight lines that are compared;
N_i = number of x, y values employed for the determination of line i;
s_i^2 = estimate of the variance of line i;
$\nu_i = N_i - 2$, number of degrees of freedom of s_i^2;

$$\nu = \sum_{i=1}^{k} \nu_i = \sum_i N_i - 2K$$

$$S^2 = \frac{\left(\sum_i \nu_i s_i^2\right)}{\nu}$$

$$C = 1 + \frac{\sum_{i=1} \frac{1}{\nu_i} - \frac{1}{\nu}}{3(k-1)}$$

If $\chi^2_{cal} < \chi^2_{tab}$ $(\alpha, \nu_0 = k-1)$, then the variances are homogeneous.

ANOVA method

The statistic used is calculated by the expression

$$F_{cal} = \frac{\frac{Q_d}{\nu_d}}{\frac{Q}{\nu}} = \frac{Q_d}{2(k-1)s^2} = \frac{(Q_T - Q)}{2(k-1)s^2}$$

where

$$Q = \sum_i \left[\sum_j (y_{ij} - \bar{y}_i)^2\right] - \frac{\left[\sum_j (x_{ij} - \bar{x}_i)(y_{ij} - \bar{y}_i)\right]^2}{\sum_j (x_{ij} - \bar{x}_i)^2}$$

j is the number of points used for the determination of the calibrate line i and i is the number of straight lines to be compared.

$$Q_T = \sum_i \sum_j (y_{ij} - \bar{y})^2 - \frac{\left[\sum_j (x_{ij} - \bar{x})(y_{ij} - \bar{y})\right]^2}{\sum_j (x_{ij} - \bar{x})^2}$$

$$\bar{x} = \frac{\sum_i \sum_j x_{ij}}{\sum_i N_i}$$

$$\bar{y} = \frac{\sum_i \sum_j y_{ij}}{\sum_i N_i}$$

$$\nu = \sum_j N_j - 2K$$

$$\nu_d = \nu_T - \nu = 2(k-1)$$

If $F_{calc} < F^{tab}_{1-\alpha}$ (ν_d, ν), then the lines are coincident.

Detection limits

$$C_s = \bar{C} + \frac{b(y_s - \bar{y})}{K} \pm \frac{t_{1-\frac{\alpha}{2}, \nu} S'_R}{K} \times \left\{\frac{(y_s - \bar{y})^2}{\sum (C_i - \bar{C})^2} + \left(\frac{1}{n} + \frac{1}{m}\right)K\right\}^{1/2}$$

where

$\bar{C}$ = average concentration for the n observations;
b = slope of the calibration line;

y_s = instrumental response for the sample;
$\bar{y}$ = average response for the n observations;

$$K = b^2 - \left(t_{1-\frac{\alpha}{2},\nu}\right)^2 s_b^2;$$

$t_{1-\frac{\alpha}{2},\nu}$ = Student's t values for a confidence level $1-\alpha$ and $\nu = n + m - 3$ degrees of freedom;
s_b^2 = squared variance of the slope of the calibration line;

$$s_R'^2 = \frac{(n-2)s_R^2 + \sum_{i=1}^{m} (y_{s,i} - y_s)^2}{n + m - 3};$$

s_R^2 = squared pooled variance;
$y_{s,i}$ = response of the m samples assayed;
n = number of observations used for the determination of the calibration line;
m = number of responses obtained for the sample in the unknown sample; when $m \ll n$, then $s_r \approx s_r'$.

REFERENCES

1 F. Zhou, Fenxi Huaxue, 11 (1983) 398.
2 M.H. Kroll and R.J. Ellin, Clin. Chem., 31 (1985) 462.
3 F. Bosch Reig and P. Campíns Falcó, Analyst, 113 (1988) 1011.
4 F. Bosch Reig and P. Campíns Falcó, Analyst, 115 (1989), 111.
5 P. Campíns Falcó, F. Bosch Reig and A. Molina Benet, Fresenius' J. Anal. Chem., 338 (1990) 16.
6 F. Bosch Reig, P. Campíns Falcó, A. Sevillano Cabeza, R. Herráez Hernández and C. Molíns Legua, Anal. Chem., 63 (1991) 2424.
7 P. Campíns Falcó, F. Bosch Reig and J. Verdú Andrés, Talanta, 39 (1992) 1.
8 P. Campíns Falcó, F. Bosch Reig, R. Herráez Hernández and A. Sevillano Cabeza, Anal. Chim. Acta, 257 (1992) 89.
9 R.J. Henry, C. Sobel and S. Berckman, Anal. Chem., 29 (1957) 1491.
10 E.B. Sandell, Colorimetric Determination of Traces of Metals, Interscience, New York, 1959.
11 O.A. Kenyon and G. Oplinger, Anal. Chem., 27 (1955) 1125.
12 M.A. Sharaf, D.L. Illman and B.R. Kowalsky, Chemometrics, Wiley-Interscience, New York, 1986.
13 Commissariat a l'Energie Atomique, Statistique Appliquée a l'Exploitation des Mesures, Masson, Paris, 1978.

Analytica Chimica Acta, 270 (1992) 267–269
Elsevier Science Publishers B.V., Amsterdam

Sequential determination of molybdenum and tungsten in silicate rocks by a spectrophotometric method

Zhen-Hai Fan, Li-Xing Zhang and Hui-De Zhou

Northwest Institute of Nuclear Technology, P.O. Box 69, Xian 710000 (China)

(Received 18th February 1992)

Abstract

A spectrophotometric method has been proposed for the sequential determination of molybdenum and tungsten in silicate rocks. The procedure proposed has been successfully used to determine molybdenum and tungsten in granite. The results show that this method can accurately determine molybdenum and tungsten down to the $\mu g\ g^{-1}$ and sub-$\mu g\ g^{-1}$ level with relative standard deviations of 1% and 3.5%, respectively.

Keywords: Spectrophotometry; Molybdenum; Silicate rocks; Toluene-3,4-dithiol complexes; Tungsten

Toluene-3,4-dithiol, generally referred to as "dithiol", forms green complexes with both molybdenum and tungsten. These complexes are soluble in many organic solvents giving green solutions and have been used for the photometric determination of molybdenum and tungsten in silicate rocks. The wavelengths at which the maximum absorptions occur for the complexes of molybdenum and tungsten, are very close. Therefore a separation procedure is necessary for the quantitative determination of both elements. Earlier procedures [1] were based upon suppression of the formation of the tungsten complex by the addition of citric acid. Molybdenum was extracted into carbon tetrachloride and separated quantitatively from tungsten, which could be determined with dithiol after the destruction of the citric acid remaining in the solution. However, the destruction of the citric acid is troublesome and time-consuming. In the present paper we propose a procedure which is based upon the fact that the molybdenum complex is formed under conditions of high acidity, in contrast to the tungsten complex which is formed only in hot and weakly acid solutions. Therefore the molybdenum dithiol complex, which is formed in high acidity medium, can be extracted into carbon tetrachloride and quantitatively separated from tungsten, which is not extracted, but can be determined with dithiol after adjusting the pH of the solution to a value of 1.5. The procedure proposed has been successfully used to sequentially determine molybdenum and tungsten in granite.

Correspondence to: L.-X. Zhang, Northwest Institute of Nuclear Technology, P.O. Box 69, Xian 710000 (China).

EXPERIMENTAL

Reagents

To obtain the α-benzoinoxime solution (2%), dissolve 1.0 g of α-benzoinoxime in 50 ml ethanol. To obtain the standard stock solution of molybdenum (500 $\mu g\ ml^{-1}$), dissolve 0.9201 g of ammonium molybdate (G.R.) in 500 ml of 1% ammonium hydroxide. To obtain the standard stock solution of tungsten (500 $\mu g\ ml^{-1}$), dissolve 0.6305 g of tungsten oxide (S.P.) in 500 ml 1% sodium hydroxide. To obtain the toluene-3,4-dithiol solution (0.2%), dissolve 0.2 g of the reagent and 1 g of sodium hydroxide in 80 ml of water,

add 1 ml thioglycollic acid and dilute to 100 ml with water. This reagent is unstable, so the solution should be stored in a refrigerator and must be discarded after 14 days.

Apparatus

A Model 72 spectrophotometer (Shanghai Analytical Instruments Factory, China) was used for all absorbance measurements. One-centimeter matched cells were used, and all readings were made against a carbon tetrachloride blank. pH measurements were made with a Model PHS-2 pH meter (Shanghai Second Analytical Instruments Factory, China).

Procedure

Accurately weigh 1 g (−200 mesh) rock sample into a platinum dish, moisten with water and add 1 ml concentrated nitric acid and 10 ml concentrated hydrofluoric acid. Transfer the dish to a boiling-water bath and evaporate to near dryness. On cooling, add 5 ml of concentrated hydrofluoric acid and again evaporate to near dryness, repeat the treatment with another 5 ml of concentrated hydrofluoric acid. After cooling, add 2 ml of concentrated perchloric acid, evaporate on a hot plate to dryness, add another 2 ml of concentrated perchloric acid and repeat the treatment. Add 5 ml of concentrated hydrochloric acid and 20 ml of water, heat to dissolve the residue. Transfer the solution to a 100-ml beaker, adjust the pH of the solution to 1.5 with ammonia solution (1 + 1) and hydrochloric acid (1 + 3).

Transfer the solution obtained to a 100-ml separating funnel. Add 2 ml of the α-benzoinoxime solution and mix by shaking. Add 10 ml of chloroform, shake for about $1\frac{1}{2}$ min. Allow the phases to separate, collect the organic layer in a platinum crucible and repeat the extraction twice each with a 5 ml portion of chloroform. Add 50 mg of sodium carbonate to the organic solution obtained, evaporate the chloroform to dryness at a temperature < 60°C, ignite and fuse over a burner. After cooling, extract the melt with 5 ml of water, transfer the solution to a 100-ml separating funnel, wash the crucible with 5 ml of 10 M sulphuric acid, then wash the crucible twice with a 5-ml portion of water, combine the washings in the separating funnel. Add 5 ml of the dithiol solution, mix and stand for 20 min. Add 5 ml of carbon tetrachloride and shake for 1 min. Allow the phases to separate, remove the organic layer into a 1-ml cell, measure the absorbance of molybdenum complex at a wavelength of 670 nm. Repeat the extraction with 5 ml of carbon tetrachloride and discard the organic layer. Run the aqueous layer into a 100-ml beaker, adjust the pH of the solution to a value of 1.5 with ammonia solution, add 3 ml of the dithiol solution. Place the beaker on a hot plate and heat to just below boiling. On cooling, transfer the solution into a 100-ml separating funnel, add 5 ml of carbon tetrachloride and shake for 1 min. Allow the phases to separate, collect the organic layer into a 1-ml cell, measure the absorbance of tungsten complex at a wavelength of 650 nm.

Calibration

Transfer aliquots of the standard molybdenum working solution containing 0–10 μg Mo to a series of 100-ml separating funnels, add 5 ml of 10 M sulphuric acid, dilute to 20 ml with water. Add 5 ml of the dithiol solution, mix and stand for 20 min. Extract the molybdenum complex and measure the absorbance as described above. Plot the relation of absorbance to molybdenum concentration.

Transfer aliquots of standard tungsten working solution containing 0–10 μg W to a series of 100-ml beakers, dilute the solution to 25 ml with water, adjust the pH to 1.5 with dilute sulphuric acid, add 3 ml of the dithiol solution, form and extract tungsten complex, and measure the absorbance as described above. Plot the relation of absorbance to tungsten concentration.

RESULTS AND DISCUSSION

Absorption spectra of the dithiol complexes of molybdenum and tungsten show that the maximum absorption occurs at wavelengths of 650 nm (tungsten) and 670 nm (molybdenum), respectively. Straight line calibration graphs indicate that the Beer–Lambert law is followed up to at least 20 μg tungsten and molybdenum.

TABLE 1

Analytical results of No. 1 granite

Element	Content ($\mu g\ g^{-1}$)					Average ($\mu g\ g^{-1}$)	R.S.D. (%)	Standard recovery (%)
Mo	2.85	2.87	2.88	2.90	2.84	2.86	0.9	99.8
	2.90	2.89	2.85	2.82	2.84			
	2.85	2.84	2.85	2.86	2.87			
	2.90	2.85	2.90					
W	0.73	0.80	0.77	0.77	0.73	0.77	3.5	97.6
	0.77	0.80	0.73	0.80	0.73			
	0.75	0.75	0.80	0.80	0.75			
	0.78	0.78	0.75					

The effect of acidity on the formation of molybdenum and tungsten complexes with dithiol has been investigated in detail. The results shown in Fig. 1 indicate that molybdenum forms a stable complex with dithiol in 0.25–7.5 M sulphuric acid. Tungsten, however, forms a complex with dithiol when the acidity of solution is lower than 1.5 M, and the optimum acidity for the formation of tungsten dithiol complex is pH 1.5. The acidity of 2 M sulphuric acid is selected for the formation of molybdenum complex. Thus, after extraction of molybdenum complex with carbon tetrachloride, tungsten still remains in the aqueous layer. Therefore the molybdenum and tungsten are separated quantitatively.

Heating is necessary for the formation of tungsten dithiol complex, but boiling should be avoided as experiments have shown that prolonged boiling will destroy the complex and reduce the absorbance; heating to just below boiling is optimum.

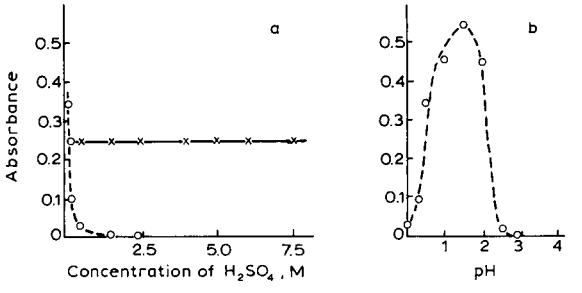

Fig. 1. Effect of acidity on the formation of complexes: Mo 5 μg, 670 nm (———); W 20 μg, 650 nm (- - - - -). For various sulphuric acid concentrations: 0.25–7.5 M (a), and for pH 0–4 (b).

Under the conditions selected, molybdenum and tungsten are separated and determined quantitatively. The standard recovery of molybdenum (5 μg) and tungsten (2 μg) is 99.8% and 97.6%, respectively.

For some silicate rocks it is possible to extract the molybdenum and tungsten complexes with dithiol directly after the acid decomposition procedure of samples. However, titanium, chromium, vanadium, iron etc. may interfere with the determinations. Therefore prior to the determination of molybdenum and tungsten for more complex rocks an extraction stage with α-benzoinoxime may be applied to separate these interference elements [2]. Thus, 5 mg chromium oxide, titanium oxide, vanadium pentoxide and 50 mg iron trioxide do not interfere with the determination of molybdenum and tungsten at the μg level.

The procedure proposed has been successfully used to sequentially determine molybdenum and tungsten in granites. Typical results are shown in Table 1. The results show that this method can accurately determine Mo and W down to the $\mu g\ g^{-1}$ and sub-$\mu g\ g^{-1}$ level, and relative standard deviations are 1% and 3.5%, respectively.

REFERENCES

1 P.G. Jeffery and D. Hutchison, Chemical Methods of Rock Analysis, 3rd edn., Pergamon Press, 1981, p. 325.
2 Hu Shi-Fu and Zhang Bao-Chuan, unpublished work.

ANALYTICA CHIMICA ACTA, VOL. 270 (1992)

AUTHOR INDEX

Erratum corrected 12 Mar. 93 /AP

Anal. Chim. Acta, 269 (1992) 59–64
p. 61, 12th line of the text in the right column: "bromide (DTAB)" should be deleted.

Multivariate Pattern Recognition in Chemometrics, Illustrated by Case Studies

edited by **R.G. Brereton**, University of Bristol, Bristol, UK

Data Handling in Science and Technology Volume 9

Chemometrics originated from multivariate statistics in chemistry, and this field is still the core of the subject. The increasing availability of user-friendly software in the laboratory has prompted the need to optimize it safely. This work comprises material presented in courses organized from 1987-1992, aimed mainly at professionals in industry.

The book covers approaches for pattern recognition as applied, primarily, to multivariate chemical data. These include data reduction and display techniques, principal components analysis and methods for classification and clustering. Comprehensive case studies illustrate the book, including numerical examples, and extensive problems are interspersed throughout the text. The book contains extensive cross-referencing between various chapters, comparing different notations and approaches, enabling readers from different backgrounds to benefit from it and to move around chapters at will. Worked examples and exercises are given, making the volume valuable for courses.

Tutorial versions of SPECTRAMAP and SIRIUS are optionally available as a Software Supplement, at a low price, to accompany the text.

Contents:

ELSEVIER

SCIENCE PUBLISHERS

1992 xii + 326 pages

Hardbound
Price: US $ 174.50 / Dfl. 305.00
ISBN 0-444-89783-6

Paperback
Price: US $ 85.50 / Dfl. 150.00
ISBN 0-444-89784-4

5 Pack Paperback + Software Supplement
Price: US $ 428.50 / Dfl. 750.00
ISBN 0-444-89786-0

Software Supplement
Price: US $ 100.00 / Dfl. 175.00
ISBN 0-444-89785-2

TO ORDER

Contact your regular supplier or:

ELSEVIER SCIENCE PUBLISHERS
P.O. Box 211
1000 AE Amsterdam
The Netherlands

Customers in the USA & Canada:

ELSEVIER SCIENCE PUBLISHERS
Attn. Judy Weislogel
P.O. Box 945
Madison Square Station
New York, NY 10160-0757, USA

No postage will be added to prepaid book orders. US $ book prices are valid only in the USA and Canada. In all other countries the Dutch guilder (Dfl.) price is definitive. Customers in The Netherlands please add 6% BTW. In New York State please add applicable sales tax. All prices are subject to change without prior notice.

Sampling of Heterogeneous and Dynamic Material Systems

Theories of Heterogeneity, Sampling and Homogenizing

by **P.M. Gy**, Sampling Consultant, Cannes, France

Data Handling in Science and Technology Volume 10

Although sampling errors inevitably lead to analytical errors, the importance of sampling is often overlooked. The main purpose of this book is to enable the reader to identify every possible source of sampling error in order to derive practical rules to (a) completely suppress avoidable errors, and (b) minimise and estimate the effect of unavoidable errors. In short, the degree of representativeness of the sample can be known by applying these rules.

The scope covers the derivation of theories of probabilistic sampling and of bed-blending from a complete theory of heterogeneity which is based on an original, very thorough, qualitative and quantitative analysis of the concepts of homogeneity and heterogeneity. All sampling errors result from the existence of one form or another of heterogeneity. Sampling theory is derived from the theory of heterogeneity by application of a probabilistic operator to a material whose heterogeneity has been characterized either by a simple scalar (a variance: zero-dimensional batches) or by a function (a variogram: one-dimensional batches). A theory of bed-blending (one-dimensional homogenizing) is then easily derived from the sampling theory.

The book should be of interest to all analysts and to those dealing with quality, process control and monitoring, either for technical or for commercial purposes, and mineral processing.

Although this book is primarily aimed at graduates, large portions of it are suitable for teaching sampling theory to undergraduates as it contains many practical examples provided by the author's 30-year experience as an international consultant. The book also contains useful source material for short courses in Industry.

ELSEVIER
SCIENCE PUBLISHERS

Contents:

1992 xxx + 654 pages
Price: Dfl. 425.00 / US$ 243.00
ISBN 0-444-89601-5

ORDER INFORMATION

For USA and Canada
ELSEVIER SCIENCE PUBLISHERS
Judy Weislogel
P.O. Box 945
Madison Square Station,
New York, NY 10160-0757
Tel: (212) 989 5800
Fax: (212) 633 3880

In all other countries
ELSEVIER SCIENCE PUBLISHERS
P.O. Box 211
1000 AE Amsterdam
The Netherlands
Tel: (+31-20) 5803 753
Fax: (+31-20) 5803 705

US$ prices are valid only for the USA & Canada and are subject to exchange fluctuations; in all other countries the Dutch guilder price (Dfl.) is definitive. Books are sent postfree if prepaid.

CATALOGUE 1993 ON CD-ROM

Elsevier Science Publishers - the world's largest scientific publisher - presents for the first time details of all its publications on CD-ROM

ADVANTAGES

- Easy to use.
- Get more comprehensive information than ever before.
- Make fast and effective searches.
- Find what you want even with incomplete information.
- Compile special lists of products without typing.
- Improve your control of scientific product information.
- Enhance service to clients.

PRODUCT DESCRIPTION

The CD-ROM contains descriptions of all Elsevier products.

- All the journals, with complete information about journal editors and editorial boards
- Listings of recently published papers for many journals
- Complete descriptions and contents lists of book titles
- Independent reviews of published books
- Forthcoming title information
- Book series
- All other products, e.g. software, CDs, dictionaries, wallcharts.

In addition, the CD-ROM features easy-to-use search tools, making the information accessible and useful. For example, searches can be made by subject area, by year of publication, by author/editor or title and by "free text" search.

Full book and journal information can be printed to initiate your order.

If you do not find what you need, or wish to know more about Elsevier's publishing programme, the CD-ROM can supply you with the name, address and fax number of the correct person to contact.

AUDIENCE

Librarians, booksellers, researchers, agents and information specialists.

SYSTEM REQUIREMENTS

The CD-ROM has been designed to run under Microsoft® Windows™ 3.0, on IBM PC-ATs and compatibles. The CD-ROM is Microsoft® Windows™ 3.1 compatible.

ELSEVIER
SCIENCE PUBLISHERS

The minimum requirements are:

- IBM or IBM-compatible PC with a 80286 or higher processor
- 2 MB or more RAM
- MS-DOS® 3.3 or higher installed
- Microsoft® Windows™ 3.0 (or 3.1) installed
- Microsoft® Windows™ compatible mouse or other pointing device
- VGA graphics adapter (colour or monochrome)
- Hard disk with at least 2 MB free disk space
- CD-ROM drive which is accessible from Microsoft® Windows™
- For faster operation a 80386SX or higher processor is recommended, as well as a fast CD-ROM drive (access time less than 0.4 seconds).

The CD-ROM can be installed in a local area network.

For further information please contact

ELSEVIER SCIENCE PUBLISHERS
Attn. Vivian Wong Swie San
Marketing Services Department
P.O. Box 211
1000 AE Amsterdam
The Netherlands
FAX: (020) 5862 425

In the USA & Canada
Journal Information Center
P.O. Box 882
Madison Square Station
New York, NY 10159, USA
FAX: (212) 633 3764

PUBLICATION SCHEDULE FOR 1993

	S'92	O'92	N'92	D'92	J	F
Analytica Chimica Acta	267/1 267/2	268/1 268/2	269/1 269/2	270/1 270/2	271/1 271/2	272/1 272/2
Vibrational Spectroscopy		4/1			4/2	

INFORMATION FOR AUTHORS

Manuscripts. The language of the journal is English. English linguistic improvement is provided as part of the normal editorial processing. Authors should submit three copies of the manuscript in clear double-spaced typing on one side of the paper only. *Vibrational Spectroscopy* also accepts papers in English only.

Abstract. All papers and reviews begin with an Abstract (50–250 words) which should comprise a factual account of the contents of the paper, with emphasis on new information.

Figures. Figures should be prepared in black waterproof drawing ink on drawing or tracing paper of the same size as that on which the manuscript is typed. One original (or sharp glossy print) and two photostat (or other) copies are required. Attention should be given to line thickness, lettering (which should be kept to a minimum) and spacing on axes of graphs, to ensure suitability for reduction in size on printing. Axes of a graph should be clearly labelled, along the axes, outside the graph itself. All figures should be numbered with Arabic numerals, and require descriptive legends which should be typed on a separate sheet of paper. Simple straight-line graphs are not acceptable, because they can readily be described in the text by means of an equation or a sentence. Claims of linearity should be supported by regression data that include slope, intercept, standard deviations of the slope and intercept, standard error and the number of data points; correlation coefficients are optional.

Photographs should be glossy prints and be as rich in contrast as possible; colour photographs cannot be accepted. Line diagrams are generally preferred to photographs of equipment.

Computer outputs for reproduction as figures must be good quality on blank paper, and should preferably be submitted as glossy prints.

Nomenclature, abbreviations and symbols. In general, the recommendations of the International Union of Pure and Applied Chemistry (IUPAC) should be followed, and attention should be given to the recommendations of the Analytical Chemistry Division in the journal *Pure and Applied Chemistry* (see also *IUPAC Compendium of Analytical Nomenclature, Definitive Rules*, 1987).

References. The references should be collected at the end of the paper, numbered in the order of their appearance in the text (*not* alphabetically) and typed on a separate sheet.

Reprints. Fifty reprints will be supplied free of charge. Additional reprints (minimum 100) can be ordered. An order form containing price quotations will be sent to the authors together with the proofs of their article.

Papers dealing with vibrational spectroscopy should be sent to: Dr J.G. Grasselli, 150 Greentree Road, Chagrin Falls, OH 44022, U.S.A. Telefax: (+1-216) 2473360 (Americas, Canada, Australia and New Zealand) or Dr J.H. van der Maas, Department of Analytical Molecule Spectrometry, Faculty of Chemistry, University of Utrecht, P.O. Box 80083, 3508 TB Utrecht, The Netherlands. Telefax: (+31-30) 518219 (all other countries).

0003-2670/92/$05.00

This issue is printed on acid-free paper.

PRINTED IN THE NETHERLANDS

CHEMOMETRICS TUTORIALS II

edited by **R.G. Brereton**, University of Bristol, Bristol, UK, **D.R. Scott**, U.S. Environmental Protection Agency, Research Triangle Park, NC, USA, **D.L. Massart**, Vrije Universiteit Brussel, Brussels, Belgium, **R.E. Dessy**, Virginia Polytechnic Institute, Blackburg, VA, USA, **P.K. Hopke**, Clarkson University, Potsdam, NY, USA, **C.H. Spiegelman**, Texas A&M University, College Station, TX, USA and **W. Wegscheider**, Universität Graz, Graz, Austria

The journal Chemometrics and Intelligent Laboratory Systems has a specific policy of publishing tutorial papers (i.e. articles aiming to discuss and illustrate the application of chemometric and other techniques) solicited from leading experts in the varied disciplines relating to this subject. This book comprises reprints of tutorials from Volumes 6-11 of this journal, covering the period from mid 1989 to late 1991. The authors of the papers include analytical, organic and environmental chemists, statisticians, pharmacologists, geologists, geochemists, computer scientists and biologists, which reflects the strong interdisciplinary communication. The papers have been reorganized into major themes, covering most of the main areas of chemometrics.

This book is intended both as a personal reference text and as a useful background for courses in chemometrics and laboratory computing.

1992 x + 314 pages
Paperback
Price: US $ 156.50 / Dfl. 250.00
ISBN 0-444-89858-1

ORDER INFORMATION

For USA and Canada
ELSEVIER SCIENCE PUBLISHERS
Judy Weislogel
P.O. Box 945
Madison Square Station,
New York, NY 10160-0757
Tel: (212) 989 5800
Fax: (212) 633 3880

In all other countries
ELSEVIER SCIENCE PUBLISHERS
P.O. Box 211
1000 AE Amsterdam
The Netherlands
Tel: (+31-20) 5803 753
Fax: (+31-20) 5803 705

US$ prices are valid only for the USA & Canada and are subject to exchange rate fluctuations; in all other countries the Dutch guilder price (Dfl.) is definitive. Books are sent postfree if prepaid.

ELSEVIER
SCIENCE PUBLISHERS